

Sulfur Polymers for the Environment and Human Health

by

Max Worthington

*Thesis
Submitted to Flinders University
for the degree of*

Doctor of Philosophy
College of Science and Engineering
6th February 2020

Sulfur Polymers for the Environment and Human Health

Max J. H. Worthington, BSc (Hon.) Chemistry

College of Science and Engineering

Flinders University

6th February 2020

CONTENTS

Summary.....	ii
Declaration	iii
Acknowledgements	iv
1. The Use of Sulfur in Mercury Remediation	1
Appendix: Green chemistry and polymers made from sulfur.....	20
2. Polysulfide Synthesis.....	21
2.1 Polysulfide Synthesis Experimental	43
3. Sulfur Polymers for Mercury Capture	119
Appendix: Laying Waste to Mercury: Inexpensive Sorbents Made from Sulfur and Recycled Cooking Oils	132
3.1 Sulfur Polymers for Mercury Capture Experimental.....	133
4. Sulfur Polymers for Oil Remediation	181
Appendix: Sustainable Polysulfides for Oil Spill Remediation: Repurposing Industrial Waste for Environmental Benefit	194
4.1 Sulfur Polymers for Oil Remediation Experimental.....	195
5. Sulfur Polymers for Gene and Drug Delivery	221
5.1 Sulfur Polymers for Gene and Drug Delivery Experimental	239

SUMMARY

With the rapid depletion of our most important chemical feedstock—crude oil—ever looming it is important to explore the possibility of alternate carbon sources for the production of polymers and other chemicals. Sulfur, a by-product of the petroleum industry, offers an incredibly cheap and accessible building block for the polymerisation of such materials. By reacting canola oil, an inexpensive and abundant plant extract with sulfur through inverse-vulcanisation, our lab has developed a new high-sulfur-content rubber from renewable and waste materials.

This rubber is able to remove various species of toxic mercury from air, water and soil, and inclusion of sodium chloride as a porogen in synthesis affords a porous version of this material with improved mercury binding capabilities and also the capacity to absorb crude oil and diesel; key pollutants in ocean oil spills.

The use of sulfur polymers as biomedical implants was also explored with the incorporation of therapeutic molecules for controlled and targeted delivery within the body.

DECLARATION

I certify that this thesis does not incorporate without acknowledgment any material previously submitted for a degree or diploma in any university; and that to the best of my knowledge and belief it does not contain any material previously published or written by another person except where due reference is made in the text.

Signed..... Max Worthington.....

Date..... 6th February 2020.....

ACKNOWLEDGEMENTS

Justin Chalker, my principal supervisor, for the many opportunities provided to me during my PhD to engage in research here and abroad, and for his mentorship in what it takes to be a great scientist.

Mike Perkins, my associate supervisor, for valuable contributions in group meetings and the organic synthesis seminar series.

Members of the Chalker research group for contributions to the various sulfur polymer projects.

Members of the Flinders Institute for Nanoscale Science and Technology, Flinders Analytical and the Bernardes research group for their help in experimental design, instrument training, time and effort.

My candidature was supported by a Research Training Program scholarship and the research visit to the Instituto de Medicina Molecular supported by traveling fellowships from Flinders University, the Royal Australian Chemical Institute and the Australian Nanotechnology Network.

1. THE USE OF SULFUR IN MERCURY REMEDIATION

Introduction

With the rapid depletion of fossil fuels, it is important to explore the possibility of alternate carbon sources for the production of polymers and other chemicals^{1,2}. Several recent advances have been made in producing functional polymeric materials from economical or renewable sources, particularly in the field of polysulfide materials³. Recent estimates put annual generation of excess sulfur at 7 million tons, produced primarily from the hydrodesulfurisation of crude oil. Since this largely untapped resource was recognised, research into novel high sulfur-content materials has picked up significantly³. From advanced Li-S batteries^{4,5} to advanced optical materials⁶ and other high-sulfur-content polymeric materials⁷. Inspired by these developments we looked to utilise sulfur to create new polymeric materials by combining organic monomers from renewable or waste sources with sulfur. Literature precedent suggested terpenes might be good candidates as monomers⁸⁻¹⁰ and so the citrus terpene limonene was used to form our first generation material: Sulfur Limonene Polysulfide. Affinity for heavy metals, a property conferred by the high content of sulfur, was hypothesised and demonstrated by the Chalker laboratory in 2016. This thesis follows from this initial work and encompasses the development of a subsequent generation of sulfur polymer and the exploration of its applications in environmental remediation and human health.

Mercury pollution

Mercury pollution is a global crisis that affects the lives of millions of people. Each year up to 9,100 tonnes of mercury are emitted into the atmosphere: approximately 500 from natural sources (depending on the frequency natural occurrences such as volcanic eruptions and geothermal activity), approximately 2,500 from anthropogenic sources and a significant contribution from re-emission of legacy mercury emissions from soils and oceans¹¹. Of the mercury emitted by human activity, the combustion of fossil fuels for domestic and industrial use, and metal and cement production makes up the majority of the output at 52 %, the highest output from any single sector however is from a practice that accounts for 38 % of all anthropogenic mercury emitted and is totalled from a large number of small, isolated locations around the world – artisanal gold mining.

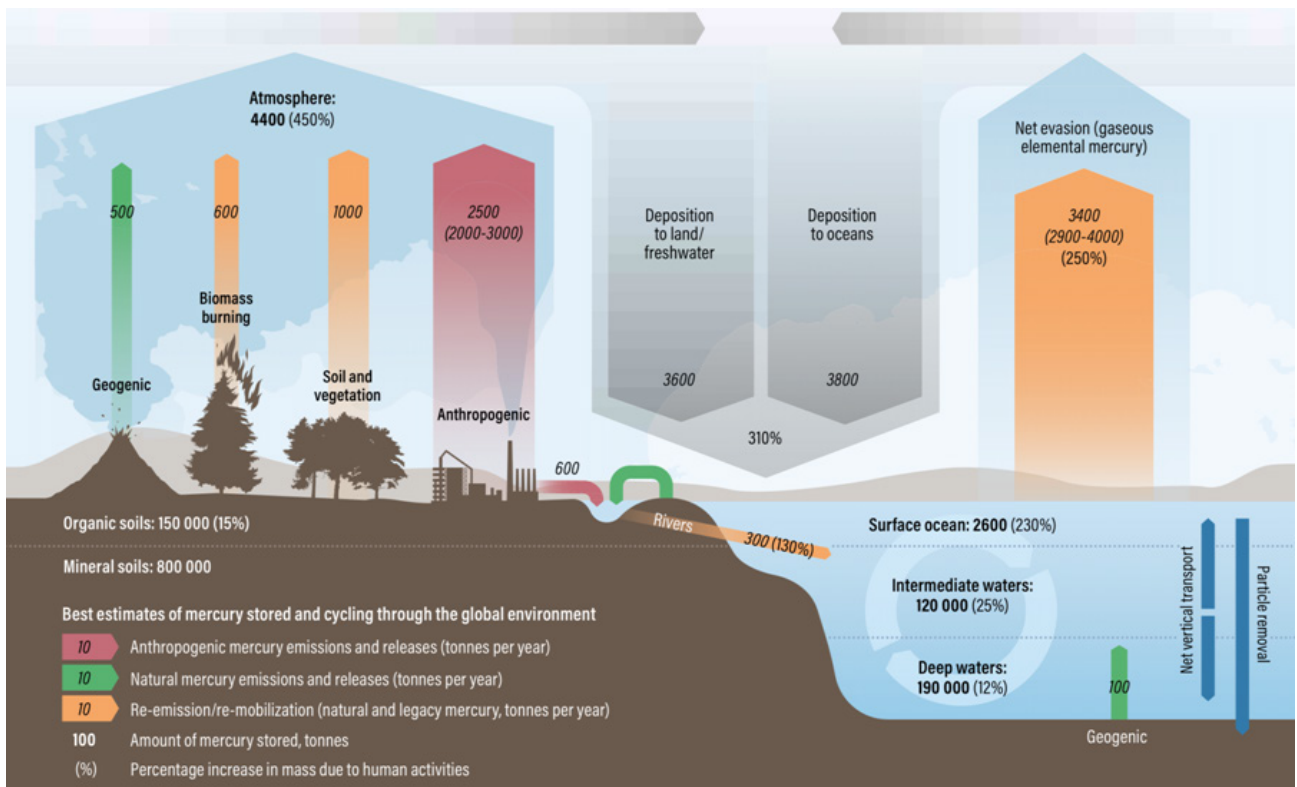


Figure 1.1 | Current estimates of annual mercury distribution in the atmospheric mercury cycle (reproduced under a creative commons attribution license¹¹). “Percentage increase in mass due to human activities” is totalled in consideration of the output of mining activities since the 16th century.

Artisanal and Small Scale Gold Mining (ASGM) occurs in over 70 countries across Africa, South America and South-East Asia¹², employing 10–19 million people, including millions of child labourers. This informal industry produces 15–25 % of the world’s gold supply¹³. The United Nations Environmental Programme (UNEP) estimates this practice introduces an average of 1,000 tonnes of mercury into the environment each year¹¹; 40 % as vapour emissions to the atmosphere and 60% as liquid elemental mercury released into the hydrosphere through rivers, lakes and soil. Exact numbers are difficult to define as in many cases the practice is outlawed¹³, directly or indirectly from the banning of mercury use, resulting in a mercury black market and an aversion to outside monitoring. ASGM involves the direct and intentional use of mercury to remove gold from its ore by first mixing the two together and then boiling off the mercury from the amalgam formed. This procedure, often carried out with a hand torch and in the miners’ homes or in gold shops in villages leads to serious harm to themselves, their families and communities. Mercury vapour is a powerful neurotoxin that results in irreversible brain damage and loss of motor function in those exposed directly and developmental defects in children exposed in-utero¹⁴⁻¹⁶. These dangers are not isolated to these communities, as emission into the global mercury cycle can result in deposition in an entirely different continent¹¹.

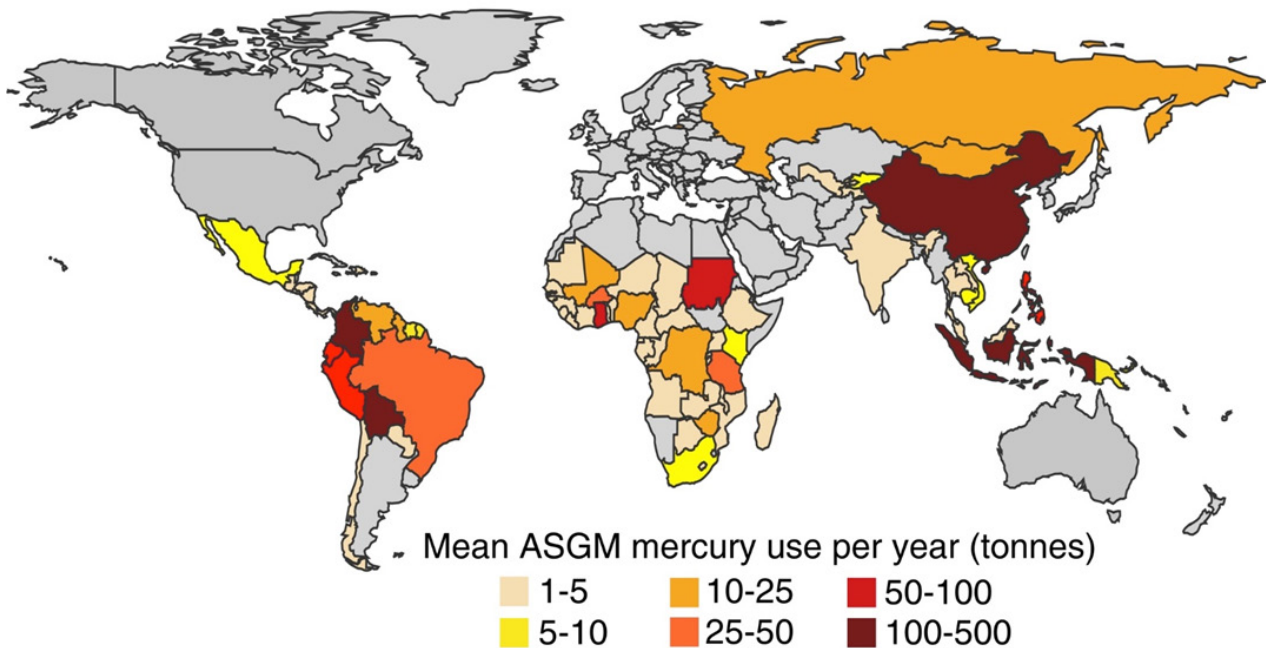


Figure 1.2 | Location and intensity of intentional mercury usage in artisanal and small scale gold mining, reproduced under a creative commons attribution license¹³

The effects of global mercury pollution arise in the developed world most notably as toxic seafood. Mercury emitted from fossil fuel combustion and refinement is deposited in soil and water where environmental forces act upon it to mobilise mercury through the surrounding ecosystem¹⁷. Mercury can range in mobilisation from a readily mobile chemical form to tightly bound in a soil matrix depending on mercury speciation and soil chemistry¹⁷. In general terms, these states can be categorised as: Dissolved, as a free ion or soluble complex. Non-specifically adsorbed, for example by electrostatic forces. Specifically adsorbed, by covalent or coordinative forces. Chelated, as an organo-mercury complex. Or precipitated, as a salt (sulfide, carbonate, hydroxide etc.).

Methylation and demethylation, and oxidation and reduction of mercury affect mercury mobility in the environment. These reactions are influenced by changes in pH and redox potential of soil, the presence of organic matter that binds to mercury, and minerals or bacteria that provoke reactions with mercury. Anaerobic bacteria are responsible for the methylation of mercury in soil or water. Methyl mercury is a highly toxic form of mercury that bioaccumulates through the aquatic food chain resulting in carnivorous fish that are harmful for human consumption^{18, 19}. Atmospheric deposition of mercury to surface soil and water can directly influence the concentration of mercury and methylmercury in fish¹⁹ and even with no local mercury emissions, 10–30 % of mercury deposition can come from intercontinental sources²⁰. A comprehensive approach of intercepting mercury before it enters the atmosphere (by primary emission or re-emission) is just as important as cleaning polluted water and soil directly for this reason.

Current remediation efforts

Current remediation efforts target both the removal of mercury from water and soil to clean contaminated areas and prevent re-emission and also the prevention of primary emission by intercepting flue streams in the coal and gas industries. An overview of techniques to combat contaminated soil are given in table 1²¹.

Technique	Description	Limitations	Waste stream
<i>Soil washing</i>	Physical separation of soil layers to concentrate Hg into a smaller volume followed by chemical extraction	Physical separation can be difficult in complex or viscous soil samples	Contaminated sludge/water
<i>Stabilisation and solidification</i>	Stabilisation of mercury as an insoluble form followed by entrapment in a rigid matrix	Increases volume of treated material, long term monitoring required	None
<i>Thermal treatment</i>	Use of heat and reduced pressure to volatise mercury followed by condensation and capture	High capital cost: Requires specialised facilities and chemical treatments.	Off gas, waste water if pre-treated (to assist melting)
<i>Biological and microbial</i>	Use of mercury-resistant microorganisms and plants to absorb mercury and reduce its bioavailability	Requires more studies to evaluate efficiency— infrastructure may require indefinite monitoring	Potential Hg emission from microbe/plant volatisation

Table 1 | Overview of current mercury remediation strategies

Stabilisation and solidification techniques rely primarily on the use of sulfur or selenium for their high affinity for mercury, and in the case of sulfur, polymerisation ability. This technique also has the benefit of not only producing no new waste but valorising a waste stream of the petroleum industry that produces over 70 million tonnes of sulfur each year as a by-product of the hydrodesulfurisation of crude oil⁷. As the Chalker research group focuses on the development of a novel class of sulfur polymers to tackle mercury pollution, this technique was evaluated as part of this thesis.

Sulfur-Based Solutions

Current methods see the stabilisation of mercury compounds achieved through one, or a combination of three methods: mercury sulfide or selenide formation, entrapment in an insoluble, specialised cement matrix or through amalgamation with other metals. The latter generally involves the solidification of liquid mercury with copper or zinc, though it is doubtful whether the solid product shows any advantage over elemental mercury in the areas of solubility or vaporisation characteristics²². Sulfur forms a strong bond with mercury to form mercury sulfide, HgS, known by its ore name cinnabar. Fortuitously HgS is classified as non-hazardous waste²³ making it an ideal target product in remediation efforts. Depending on reaction conditions HgS may form one of three crystal structures: Hexagonal (α -HgS), cubic (β -HgS) or trigonal (γ -HgS). The alpha form is the most ideal sulfur-stabilised form of mercury, but only seems to be prioritised by remediation efforts where the choice exists and is not a difficult priority to maintain: some stabilisation methods seem to favour the formation of one morphology over the other with seemingly little or no control and a working method is prioritised over investigations into the mechanics of HgS formation. Selenium reacts similarly, forming mercury selenide (tiemannite). If mercury is present in inorganic form, sulfide-containing agents are required to form mercury sulfide²².

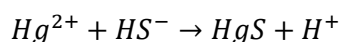
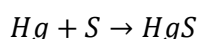
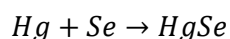


Figure 1.3 | General reaction mechanisms for reaction of mercury with selenium, sulfur and thiol compounds.

Technique	Description	Limitations	Scale
<i>DELA, Germany</i>	Sulfur is added to a modified cement mixer that is purged with N ₂ , kept under light vacuum and heated to >580 °C. Stoichiometric amount of Hg is added slowly and spontaneously reacts to form a both α and β-HgS.	Requires high temperature and nitrogen atmosphere	Pilot: 500 kg per day Full: Estimated 3–6 t per day in continuous or batch operation
<i>STMI, France</i>	Hg and Sulfur are mixed (1:1–1:3) in apparatus resembling a rotary evaporator and rotated at 50 rpm over 2 hours. Functions at 20 °C but 60–80 °C preferred. Produces β-HgS. Excess Hg can be cleared of volatiles, distilled and recovered in same apparatus.	Requires specialised apparatus, small scale	Semi-pilot: 1 kg per batch
<i>CENIM, Spain</i>	1:1 Sulfur and Hg mixed in a planetary ball mill containing stainless steel balls and milled at 400 rpm for approximately 1 hour.	Requires specialised apparatus	N/A
<i>Bethlehem Apparatus</i>	Elemental Hg is reacted with vapourised sulfur to form HgS, stored as pellets after blending with polymer.	Requires specialised apparatus and high temperature	300–1,000 t mercury per year (1 – 3 t per day)
<i>Wet Process</i>	Hg dissolved in strong acid, addition of aqueous sulfide solution results in precipitation of black cinnabar. For radioactively contaminated mercury, the product is then bound in a polysiloxane matrix	Produces Hg-contaminated water waste stream and gaseous H ₂ S	Radioactive samples max, 1 L—considered challenging to upscale
<i>HgS by shaking</i>	Finely powdered sulfur is beaten in a paint shaker with stainless steel milling balls for 1 hour. Hg is added and the mixture shaken longitudinally for 1 hour, then transversely for 1 hour. 99.96% mercury is converted to the final product.	May require specialised apparatus, demonstrated only on small scale	1 kg batches
<i>Sulfur Polymer Cement (Brookhaven National Lab)</i>	Hg contaminated waste or liquid Hg is mixed with a powdered sulfur cement (95 % sulfur, 5 % organic modifiers) in a 0.2:3.0 ratio and mixed at 120–150 °C for 4–8 hours. The molten product is cast and cooled, trapping mercury in a sulfur polymer matrix.	Requires elevated temperature	Pilot: 55 gallon drum of waste soil or 62 kg radioactive mercury per batch
<i>Shearing (Westinghouse Savannah River Co.)</i>	5:1 ratio of Hg and sulfur is blended with high shear. >5000 rpm produces more stable α-HgS, <5000 rpm produces β-HgS but with less danger of overheating.	Requires specialised apparatus	N/A

Table 2 | Current sulfur-based stabilisation and solidification methods for mercury remediation. Information provided by companies mentioned²². Procedures purely designed for dealing with radioactive mixed mercury waste excluded as they are all inherently more complex and costly to implement.

Several technologies are currently in place and in development that utilise sulfur and selenium's affinity for mercury to capture and stabilise mercury from contaminated water and soil. A brief overview of methods that utilise sulfur is given in table 2. Selenium stabilisation methods follow similar procedures but haven't been as widely adopted as selenium is generally a more expensive element to acquire²². A prevalent feature in these commonly used sulfur stabilisation methods is the requirement to process contaminated waste off-site. In general, specialised apparatus under controlled heating and/or pressure, are needed to combine the sulfur and mercury-contaminated waste to form and mould the final product. We identify these as two major drawbacks limiting application on a mass scale and in developing nations. A promising new direction has arisen in the emerging field of inverse vulcanised high-sulfur sulfur polymers.

Direct Processing of Sulfur

Direct use of sulfur generally follows one of two pathways: Melt-diffusion of molten sulfur, or vapour (or solution) dispersion³. The former has been widely used to diffuse sulfur through mesoporous carbon and carbon nanotube networks as well as metal-organic frameworks to impart sulfur-properties to an ordered and rigid system. Similarly vapour-phase diffusion has been used in an analogous process carried out under vacuum at higher temperatures. Sulfur's low cost and low enthalpies of vaporisation and sublimation pose little obstruction to the processing of these materials, the high cost and demanding requirements to produce nanostructured hosts are where difficulties arise³.

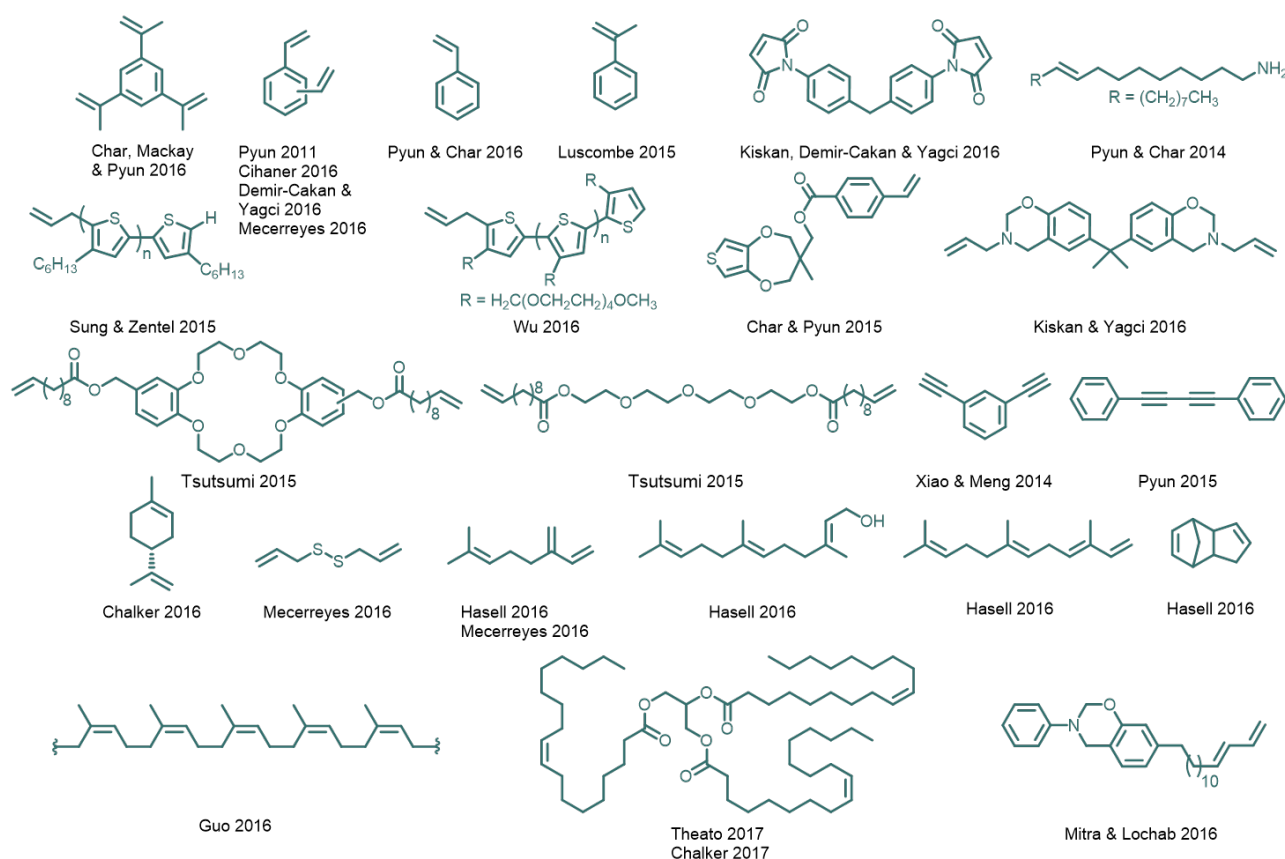


Figure 1.4 | A selection of monomers used in inverse vulcanisation reproduced under a creative commons attribution license²⁴

The discovery of inverse vulcanisation has triggered a resurgence in sulfur research, with promising applications in new materials. In this process large quantities of sulfur may be valorised into polymeric materials that contain up to 90 % sulfur by weight with only a small quantity of organic crosslinker, in contrast to classic vulcanisation in which sulfur is used as the crosslinker. Current uses of sulfur polymers, many prepared and published during the development of this thesis, include cathode materials for lithium-sulfur batteries²⁵⁻⁵³, IR-transparent lenses⁵⁴⁻⁶⁰, gas separation^{61, 62}, heavy metal remediation⁶³⁻⁷³, solar cell electrolytes⁷⁴⁻⁷⁶, water splitting⁷⁷, thermal insulation⁷⁸, dynamic and self-healing materials⁷⁹⁻⁸⁶, and platforms for nanoparticle synthesis^{87, 88}, among others. Instead of dispersing sulfur throughout a rigid matrix, cross-linking of polymeric sulfur with a diene co-monomer produces a rigid and stable polymer with high sulfur content. Sulfur exists as a multitude of allotropes, with the most abundant and stable being powdered octasulfur (α -S₈). S₈ has a melting point of 119.6 °C, however continued heating results in a second phase change at 159.4 °C, sulfur's "floor temperature". At this temperature, sulfur-sulfur bond scission occurs to produce a linear chain of sulfur atoms, with thiyl radicals at each terminus. These radicals are able to react further with sulfur, leading to ring-opening polymerisation. The resulting polymeric sulfur is not stable and backbiting leads to the regeneration of the S₈. In inverse vulcanisation, an alkene is used to react with the radical sulfur chains through a thiol-ene reaction, providing a stable polymer. The termination event is thought to occur through radical recombination²⁴.

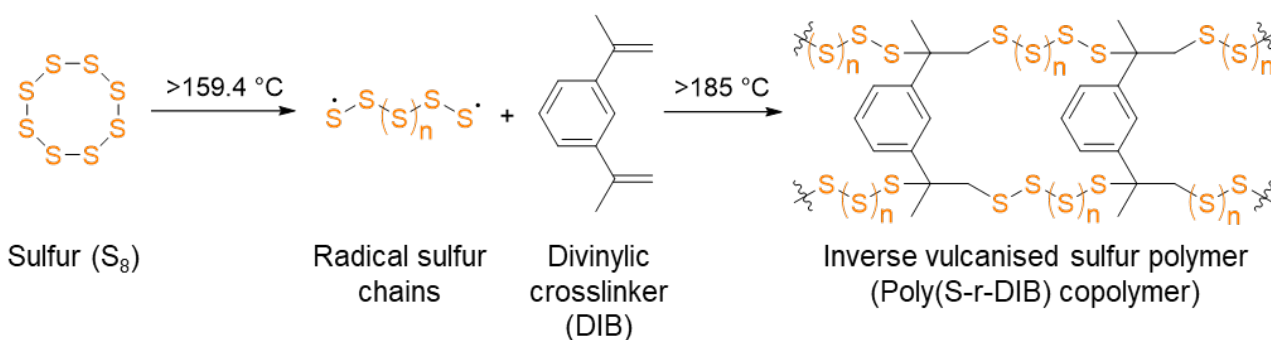


Figure 1.5 | Proposed inverse vulcanisation reaction procedure for Sulfur-random-DIB Copolymer

Inverse vulcanisation was first demonstrated by Pyun et al. in 2013⁷ with the co-polymerisation of molten sulfur with diisopropylbenzene (DIB) to create a glassy red plastic. Since then several groups have replicated this reaction with a variety of alkenes, alkynes and natural olefins resulting in a wide array of inverse vulcanised sulfur polymers to date (Fig. 1.4). Our first attempt to develop a new material by inverse vulcanisation resulted in a viscous red wax we termed sulfur-limonene polysulfide, prepared from only sulfur and the citrus terpene limonene⁶⁶.

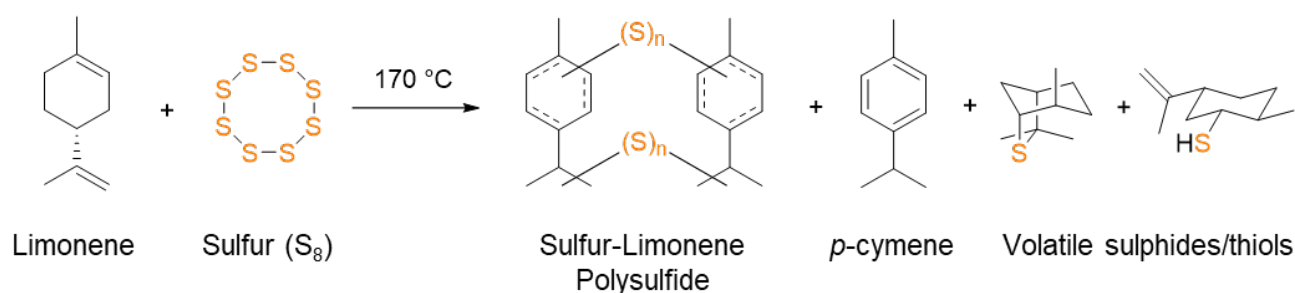


Figure 1.6 | Inverse vulcanisation reaction of sulfur (S_8) with limonene: 80 % of the product mixture is a mix of sulfur-limonene polysulfides ranging in molecular weight from 300–800 Da. Volatile materials that make up the remaining 20 % are removed by distillation.

Exploration of inverse vulcanisation has seen contributions from many groups but is still in its infancy with opportunities not just in optimisations to currently documented materials (seen already in foaming to tune surface area for mercury remediation efforts⁶⁵) but in the synthesis, characterisation and development into useful devices of entirely new materials.

By utilising inexpensive, renewable and waste materials to process sulfur into polymeric materials, we aimed to synthesise a material that will offer a scalable and widely applicable alternative for mercury remediation. During my Honours year we published our work on Sulfur-Limonene Polysulfide as proof of this concept: made from sulfur, a by-product of the petroleum industry, and limonene, a by-product of the citrus industry, Sulfur-Limonene Polysulfide is able to sequester inorganic mercury from water⁶⁶. The next step through my PhD was to extend this chemistry into several different areas, as well as to improve on this technology with the exploration of different chemical feedstocks to produce a mercury-sequestering material from inexpensive reagents through a facile and non-hazardous process, able to sequester different types of mercury (organic, inorganic,

elemental, liquid or vapour). Ideally the material would be applicable for use on-site to capture mercury pollution from a wide variety of pollution hotspots from contaminated water and soil to filtering the off-gases from coal-fired power plants and gold mines before it escapes to the atmosphere.

References

1. Nejad, E. H.; Paoniasari, A.; van Melis, C. G. W.; Koning, C. E.; Duchateau, R., Catalytic Ring-Opening Copolymerization of Limonene Oxide and Phthalic Anhydride: Toward Partially Renewable Polyesters. *Macromolecules*, **2013**, *46* (3), 631-637.
2. Gandini, A., Polymers from Renewable Resources: A Challenge for the Future of Macromolecular Materials. *Macromolecules*, **2008**, *41* (24), 9491-9504.
3. Lim, J.; Pyun, J.; Char, K., Recent Approaches for the Direct Use of Elemental Sulfur in the Synthesis and Processing of Advanced Materials. *Angew. Chem., Int. Ed.* **2015**, *54* (11), 3249-3258.
4. Ji, X.; Lee, K. T.; Nazar, L. F., A highly ordered nanostructured carbon-sulphur cathode for lithium-sulphur batteries. *Nat. Mater.* **2009**, *8* (6), 500-506.
5. Zhang, K.; Wang, L.; Hu, Z.; Cheng, F.; Chen, J., Ultrasmall Li₂S Nanoparticles Anchored in Graphene Nanosheets for High-Energy Lithium-Ion Batteries. *Sci. Rep.*, **2014**, *4*, 6467.
6. Griebel, J. J.; Nguyen, N. A.; Namnabat, S.; Anderson, L. E.; Glass, R. S.; Norwood, R. A.; Mackay, M. E.; Char, K.; Pyun, J., Dynamic Covalent Polymers via Inverse Vulcanization of Elemental Sulfur for Healable Infrared Optical Materials. *ACS Macro Letters* **2015**, *4* (9), 862-866.
7. Chung, W. J.; Griebel, J. J.; Kim, E. T.; Yoon, H.; Simmonds, A. G.; Ji, H. J.; Dirlam, P. T.; Glass, R. S.; Wie, J. J.; Nguyen, N. A.; Guralnick, B. W.; Park, J.; Somogyi, A.; Theato, P.; MacKay, M. E.; Sung, Y.-E.; Char, K.; Pyun, J., The use of elemental sulfur as an alternative feedstock for polymeric materials. *Nat. Chem.* **2013**, *5* (6), 518-524.
8. Weitkamp, A. W., The action of sulfur on terpenes. The limonene sulfides. *J. Am. Chem. Soc.* **1959**, *81*, 3430-3434.
9. Wilbon, P. A.; Chu, F.; Tang, C., Progress in Renewable Polymers from Natural Terpenes, Terpenoids, and Rosin. *Macromol. Rapid Commun.* **2013**, *34* (1), 8-37.
10. Firdaus, M.; Montero de Espinosa, L.; Meier, M. A. R., Terpene-Based Renewable Monomers and Polymers via Thiol-Ene Additions. *Macromolecules*, **2011**, *44* (18), 7253-7262.
11. United Nations Environment Programme, Global Mercury Assessment 2018. Geneva, Switzerland, **2018**. <<https://www.unenvironment.org/resources/publication/global-mercury-assessment-2018>> Accessed September 2019
12. Pirrone, N. and Mason, R. Mercury Fate and Transport in the Global Atmosphere: *Emissions, Measurements and Models*. **2009**. Springer, Boston, MA. DOI: 10.1007/978-0-387-93958-2

13. Esdaile, L. J.; Chalker, J. M., The Mercury Problem in Artisanal and Small-Scale Gold Mining. *Chem. Eur. J.* **2018**, *24* (27), 6905-6916.
14. World Health Organisation, Mercury and Health. **2016**. <<https://www.who.int/news-room/fact-sheets/detail/mercury-and-health>> Accessed October 2019
15. Nakazawa, K.; Nagafuchi, O.; Kawakami, T.; Inoue, T.; Yokota, K.; Serikawa, Y.; Cyio, B.; Elvince, R., Human health risk assessment of mercury vapor around artisanal small-scale gold mining area, Palu city, Central Sulawesi, Indonesia. *Ecotoxicol. Environ. Saf.* **2016**, *124*, 155-162.
16. Gonzalez-Merizalde, M. V.; Menezes-Filho, J. A.; Cruz-Erazo, C. T.; Bermeo-Flores, S. A.; Sanchez-Castillo, M. O.; Hernandez-Bonilla, D.; Mora, A., Manganese and Mercury Levels in Water, Sediments, and Children Living Near Gold-Mining Areas of the Nangaritza River Basin, Ecuadorian Amazon. *Arch. Environ. Contam. Toxicol.* **2016**, *71* (2), 171-182
17. Xu, J. Y.; Bravo, A. G.; Lagerkvist, A.; Bertilsson, S.; Sjoblom, R.; Kumpiene, J., Sources and remediation techniques for mercury contaminated soil. *Environ. Int.* **2015**, *74*, 42-53.
18. Mergler, D.; Anderson, H. A.; Chan, L. H. M.; Mahaffey, K. R.; Murray, M.; Sakamoto, M.; Stern, A. H., Methylmercury Exposure and Health Effects in Humans: A Worldwide Concern. *Ambio*. **2007**, *36* (1), 3-11.
19. Engstrom, D. R., Fish respond when the mercury rises. *Proc. Natl. Acad. Sci. U. S. A.* **2007**, *104* (42), 16394-16395.
20. United Nations Environment Programme, Global Mercury Assessment 2013. Geneva, Switzerland, **2013**. <<http://wedocs.unep.org/handle/20.500.11822/7984>> Accessed October 2019
21. Rodriguez, O.; Padilla, I.; Tayibi, H.; Lopez-Delgado, A., Concerns on liquid mercury and mercury-containing wastes: A review of the treatment technologies for the safe storage. *J. Environ. Manage.* **2012**, *101*, 197-205.
22. Hagemann, S., Technologies for the stabilization of elemental mercury and mercury-containing wastes. *GRS - Gesellschaft für Anlagen-und Reaktorsicherheit mbH* **2009**.
23. DELA, Mercury stabilisation - Stabilisation of mercury for final disposal by formation of mercury sulphide. **2009**.
24. Worthington, M. J. H.; Kucera, R. L.; Chalker, J. M., Green chemistry and polymers made from sulfur. *Green Chem.* **2017**, *19* (12), 2748-2761.

25. Bhargav, A.; Bell, M. E.; Cui, Y.; Fu, Y., Polyphenylene Tetrasulfide as an Inherently Flexible Cathode Material for Rechargeable Lithium Batteries. *ACS Appl. Energy Mater.* **2018**, *1* (11), 5859-5864
26. Dirlam, P. T.; Park, J.; Simmonds, A. G.; Domanik, K.; Arrington, C. B.; Schaefer, J. L.; Oleshko, V. P.; Kleine, T. S.; Char, K.; Glass, R. S.; Soles, C. L.; Kim, C.; Pinna, N.; Sung, Y.-E.; Pyun, J., Elemental Sulfur and Molybdenum Disulfide Composites for Li-S Batteries with Long Cycle Life and High-Rate Capability. *ACS Appl. Mater. Interfaces*, **2016**, *8* (21), 13437-13448.
27. Dong, P.; Han, K. S.; Lee, J.-I.; Zhang, X.; Cha, Y.; Song, M.-K., Controlled Synthesis of Sulfur-Rich Polymeric Selenium Sulfides as Promising Electrode Materials for Long-Life, High-Rate Lithium Metal Batteries. *ACS Appl. Mater. Interfaces*, **2018**, *10* (35), 29565-29573.
28. Chang, C.-H.; Manthiram, A., Covalently Grafted Polysulfur-Graphene Nanocomposites for Ultrahigh Sulfur-Loading Lithium-Polysulfur Batteries. *ACS Energy Lett.* **2018**, *3* (1), 72-77.
29. Fu, C.; Li, G.; Zhang, J.; Cornejo, B.; Piao, S. S.; Bozhilov, K. N.; Haddon, R. C.; Guo, J., Electrochemical Lithiation of Covalently Bonded Sulfur in Vulcanized Polyisoprene. *ACS Energy Lett.* **2016**, *1* (1), 115-120.
30. Je, S. H.; Hwang, T. H.; Talapaneni, S. N.; Buyukcakir, O.; Kim, H. J.; Yu, J.-S.; Woo, S.-G.; Jang, M. C.; Son, B. K.; Coskun, A.; Choi, J. W., Rational Sulfur Cathode Design for Lithium-Sulfur Batteries: Sulfur-Embedded Benzoxazine Polymers. *ACS Energy Lett.* **2016**, *1* (3), 566-572.
31. Dirlam, P. T.; Simmonds, A. G.; Shallcross, R. C.; Arrington, K. J.; Chung, W. J.; Griebel, J. J.; Hill, L. J.; Glass, R. S.; Char, K.; Pyun, J., Improving the Charge Conductance of Elemental Sulfur via Tandem Inverse Vulcanization and Electropolymerization. *ACS Macro Lett.* **2015**, *4* (1), 111-114.
32. Li, G.; Huang, Q.; He, X.; Gao, Y.; Wang, D.; Kim, S. H.; Wang, D., Self-Formed Hybrid Interphase Layer on Lithium Metal for High-Performance Lithium-Sulfur Batteries. *ACS Nano*, **2018**, *12* (2), 1500-1507.
33. Shen, K.; Mei, H.; Li, B.; Ding, J.; Yang, S., 3D Printing Sulfur Copolymer-Graphene Architectures for Li-S Batteries. *Adv. Energy Mater.* **2018**, *8* (4) 1701527.
34. Je, S. H.; Kim, H. J.; Kim, J.; Choi, J. W.; Coskun, A., Perfluoroaryl-Elemental Sulfur SNAr Chemistry in Covalent Triazine Frameworks with High Sulfur Contents for Lithium-Sulfur Batteries. *Adv. Funct. Mater.* **2017**, *27* (47), 1703947.

35. Hu, G.; Sun, Z.; Shi, C.; Fang, R.; Chen, J.; Hou, P.; Liu, C.; Cheng, H.-M.; Li, F., A Sulfur-Rich Copolymer@CNT Hybrid Cathode with Dual-Confinement of Polysulfides for High-Performance Lithium-Sulfur Batteries. *Adv. Mater.* **2017**, *29* (11), 1603835.
36. Wu, F.; Chen, S.; Srot, V.; Huang, Y.; Sinha, S. K.; van Aken, P. A.; Maier, J.; Yu, Y., Sulfur-limonene-based electrode for lithium-sulfur batteries: High-performance by self-protection. *Adv. Mater.* **2018**, *30* (13), 1706643.
37. Hoefling, A.; Nguyen, D. T.; Partovi-Azar, P.; Sebastiani, D.; Theato, P.; Song, S.-W.; Lee, Y. J., Mechanism for the Stable Performance of Sulfur-Copolymer Cathode in Lithium-Sulfur Battery Studied by Solid-State NMR Spectroscopy. *Chem. Mater.* **2018**, *30* (9), 2915-2923.
38. Gomez, I.; Mantione, D.; Leonet, O.; Blazquez, J. A.; Mecerreyes, D., Hybrid Sulfur-Selenium Co-polymers as Cathodic Materials for Lithium Batteries. *ChemElectroChem* **2018**, *5* (2), 260-265.
39. Gomez, I.; Leonet, O.; Blazquez, J. A.; Mecerreyes, D., Inverse Vulcanization of Sulfur using Natural Dienes as Sustainable Materials for Lithium-Sulfur Batteries. *ChemSusChem* **2016**, *9* (24), 3419-3425.
40. Zeng, S.; Li, L.; Xie, L.; Zhao, D.; Wang, N.; Chen, S., Conducting Polymers Crosslinked with Sulfur as Cathode Materials for High-Rate, Ultralong-Life Lithium-Sulfur Batteries. *ChemSusChem* **2017**, *10* (17), 3378-3386.
41. Zeng, S.; Li, L.; Yu, J.; Wang, N.; Chen, S., Highly crosslinked organosulfur copolymer nanosheets with abundant mesopores as cathode materials for efficient lithium-sulfur batteries. *Electrochim. Acta*, **2018**, *263*, 53-59.
42. Arslan, M.; Kiskan, B.; Cengiz, E. C.; Demir-Cakan, R.; Yagci, Y., Inverse vulcanization of bismaleimide and divinylbenzene by elemental sulfur for lithium sulfur batteries. *Eur. Polym. J.* **2016**, *80*, 70-77.
43. Almeida, C.; Costa, H.; Kadhirvel, P.; Queiroz, A. M.; Dias, R. C. S.; Costa, M. R. P. F. N., Electrochemical activity of sulfur networks synthesized through RAFT polymerization. *J. Appl. Polym. Sci.* **2016**, *133* (39), 43993.
44. Jiang, Q.; Li, Y.; Zhao, X.; Xiong, P.; Yu, X.; Xu, Y.; Chen, L., Inverse-vulcanization of vinyl functionalized covalent organic frameworks as efficient cathode materials for Li-S batteries. *J. Mater. Chem. A*, **2018**, *6* (37), 17977-17981.

45. Gracia, I.; Benyoucef, H.; Judez, X.; Oteo, U.; Zhang, H.; Li, C.; Rodriguez-Martinez, L. M.; Armand, M., S-containing copolymer as cathode material in poly(ethylene oxide)-based all-solid-state Li-S batteries. *J. Power Sources*, **2018**, *390*, 148-152.
46. Itaoka, K.; Kim, I.-T.; Yamabuki, K.; Yoshimoto, N.; Tsutsumi, H., Room temperature rechargeable magnesium batteries with sulfur-containing composite cathodes prepared from elemental sulfur and bis(alkenyl) compound having a cyclic or linear ether unit. *J. Power Sources* **2015**, *297*, 323-328.
47. Hoefling, A.; Nguyen, D. T.; Lee, Y. J.; Song, S.-W.; Theato, P., A sulfur-eugenol allyl ether copolymer: a material synthesized via inverse vulcanization from renewable resources and its application in Li-S batteries. *Mater. Chem. Front.* **2017**, *1* (9), 1818-1822.
48. Kim, H.; Lee, J.; Ahn, H.; Kim, O.; Park, M. J., Synthesis of three-dimensionally interconnected sulfur-rich polymers for cathode materials of high-rate lithium-sulfur batteries. *Nat. Commun.* **2015**, *6*, 7278.
49. Yamabuki, K.; Itaoka, K.; Shintchi, T.; Yoshimoto, N.; Ueno, K.; Tsutsumi, H., Soluble sulfur-based copolymers prepared from elemental sulfur and alkenyl alcohol as positive active material for lithium-sulfur batteries. *Polymer*, **2017**, *117*, 225-230.
50. Diez, S.; Hoefling, A.; Theato, P.; Pauer, W., Mechanical and electrical properties of sulfur-containing polymeric materials prepared via inverse vulcanization. *Polymers*, **2017**, *9* (2), 59.
51. Dirlam, P. T.; Simmonds, A. G.; Kleine, T. S.; Nguyen, N. A.; Anderson, L. E.; Klever, A. O.; Florian, A.; Costanzo, P. J.; Theato, P.; Mackay, M. E.; Glass, R. S.; Char, K.; Pyun, J., Inverse vulcanization of elemental sulfur with 1,4-diphenylbutadiyne for cathode materials in Li-S batteries. *RSC Adv.* **2015**, *5* (31), 24718-24722.
52. Zhao, F.; Li, Y.; Feng, W., Recent Advances in Applying Vulcanization/Inverse Vulcanization Methods to Achieve High-Performance Sulfur-Containing Polymer Cathode Materials for Li-S Batteries. *Small Methods*, **2018**, *2* (11).
53. Choudhury, S.; Srimuk, P.; Raju, K.; Tolosa, A.; Fleischmann, S.; Zeiger, M.; Ozoemena, K. I.; Borchardt, L.; Presser, V., Carbon onion/sulfur hybrid cathodes via inverse vulcanization for lithium-sulfur batteries. *Sustainable Energy Fuels*, **2018**, *2* (1), 133-146.
54. Anderson, L. E.; Kleine, T. S.; Zhang, Y.; Phan, D. D.; Namnabat, S.; LaVilla, E. A.; Konopka, K. M.; Ruiz Diaz, L.; Manchester, M. S.; Schwiegerling, J.; Glass, R. S.; Mackay, M. E.; Char, K.; Norwood, R. A.; Pyun, J., Chalcogenide Hybrid Inorganic/Organic Polymers: Ultrahigh Refractive Index Polymers for Infrared Imaging. *ACS Macro Lett.* **2017**, *6* (5), 500-504.

55. Griebel, J. J.; Nguyen, N. A.; Namnabat, S.; Anderson, L. E.; Glass, R. S.; Norwood, R. A.; MacKay, M. E.; Char, K.; Pyun, J., Dynamic Covalent Polymers via Inverse Vulcanization of Elemental Sulfur for Healable Infrared Optical Materials. *ACS Macro Lett.* **2015**, 4 (9), 862-866.
56. Kleine, T. S.; Diaz, L. R.; Konopka, K. M.; Anderson, L. E.; Pavlopolous, N. G.; Lyons, N. P.; Kim, E. T.; Kim, Y.; Glass, R. S.; Char, K.; Norwood, R. A.; Pyun, J., One Dimensional Photonic Crystals Using Ultrahigh Refractive Index Chalcogenide Hybrid Inorganic/Organic Polymers. *ACS Macro Lett.* **2018**, 7 (7), 875-880.
57. Griebel, J. J.; Namnabat, S.; Kim, E. T.; Himmelhuber, R.; Moronta, D. H.; Chung, W. J.; Simmonds, A. G.; Kim, K.-J.; van der Laan, J.; Nguyen, N. A.; Dereniak, E. L.; MacKay, M. E.; Char, K.; Glass, R. S.; Norwood, R. A.; Pyun, J., New Infrared Transmitting Material via Inverse Vulcanization of Elemental Sulfur to Prepare High Refractive Index Polymers. *Adv. Mater.* **2014**, 26 (19), 3014-3018.
58. Boyd, D. A.; Baker, C. C.; Myers, J. D.; Nguyen, V. Q.; Drake, G. A.; McClain, C. C.; Kung, F. H.; Bowman, S. R.; Kim, W.; Sanghera, J. S., Organically modified chalcogenide polymers for infrared optics. *Chem. Commun.* **2017**, 53 (1), 259-262.
59. Lim, J.; Cho, Y.; Kang, E.-H.; Yang, S.; Pyun, J.; Choi, T.-L.; Char, K., A one-pot synthesis of polysulfane-bearing block copolymer nanoparticles with tunable size and refractive index. *Chem. Commun.* **2016**, 52 (12), 2485-2488.
60. Tanaka, K.; Yamane, H.; Mitamura, K.; Watase, S.; Matsukawa, K.; Chujo, Y., Transformation of sulfur to organic-inorganic hybrids employed by networks and their application for the modulation of refractive indices. *J. Polym. Sci., Part A: Polym. Chem.* **2014**, 52 (18), 2588-2595.
61. Je, S. H.; Buyukcakir, O.; Kim, D.; Coskun, A., Direct Utilization of Elemental Sulfur in the Synthesis of Microporous Polymers for Natural Gas Sweetening. *Chem*, **2016**, 1 (3), 482-493.
62. Bear, J. C.; McGettrick, J. D.; Parkin, I. P.; Dunnill, C. W.; Hasell, T., Porous carbons from inverse vulcanised polymers. *Microporous Mesoporous Mater.* **2016**, 232, 189-195.
63. Crockett, M. P.; Evans, A. M.; Worthington, M. J. H.; Albuquerque, I. S.; Slattery, A. D.; Gibson, C. T.; Campbell, J. A.; Lewis, D. A.; Bernardes, G. J. L.; Chalker, J. M., Sulfur-Limonene Polysulfide: A Material Synthesized Entirely from Industrial By-Products and Its Use in Removing Toxic Metals from Water and Soil. *Angew. Chem. Int. Ed.* **2016**, 55, 1714-1718.
64. Lee, J.; Lee, S.; Kim, J.; Hanif, Z.; Han, S.; Hong, S.; Yoon, M.-H., Solution-based Sulfur-Polymer Coating on Nanofibrillar Films for Immobilization of Aqueous Mercury Ions. *Bull. Korean Chem. Soc.* **2018**, 39 (1), 84-89.

65. Hasell, T.; Parker, D. J.; Jones, H. A.; McAllister, T.; Howdle, S. M., Porous inverse vulcanised polymers for mercury capture. *Chem. Commun.* **2016**, 52, 5383-5386.
66. Worthington, M. J. H.; Kucera, R. L.; Albuquerque, I. S.; Gibson, C. T.; Sibley, A.; Slattery, A. D.; Campbell, J. A.; Alboajji, S. F. K.; Muller, K. A.; Young, J.; Adamson, N.; Gascooke, J. R.; Jampaiah, D.; Sabri, Y. M.; Bhargava, S. K.; Ippolito, S. J.; Lewis, D. A.; Quinton, J. S.; Ellis, A. V.; Johs, A.; Bernardes, G. J. L.; Chalker, J. M., Laying Waste to Mercury: Inexpensive Sorbents Made from Sulfur and Recycled Cooking Oils. *Chem. Eur. J.* **2017**, 23 (64), 16219-16230.
67. Xu, D.; Wu, W. D.; Qi, H.-J.; Yang, R.-X.; Deng, W.-Q., Sulfur rich microporous polymer enables rapid and efficient removal of mercury(II) from water. *Chemosphere* **2018**, 196, 174-181.
68. Akay, S.; Kayan, B.; Kalderis, D.; Arslan, M.; Yagci, Y.; Kiskan, B., Poly(benzoxazine-co-sulfur): An efficient sorbent for mercury removal from aqueous solution. *J. Appl. Polym. Sci.* **2017**, 134 (38), 45306.
69. Lee, J.-S. M.; Parker, D. J.; Cooper, A. I.; Hasell, T., High surface area sulfur-doped microporous carbons from inverse vulcanized polymers. *J. Mater. Chem. A* **2017**, 5 (35), 18603-18609.
70. Parker, D. J.; Jones, H. A.; Petcher, S.; Cervini, L.; Griffin, J. M.; Akhtar, R.; Hasell, T., Low cost and renewable sulfur-polymers by inverse vulcanization, and their potential for mercury capture. *J. Mater. Chem. A*, **2017**, 5 (23), 11682-11692.
71. Shin, H.; Kim, J.; Kim, D.; Nguyen, V. H.; Lee, S.; Han, S.; Lim, J.; Char, K., Aqueous "polysulfide-ene" polymerization for sulfur-rich nanoparticles and their use in heavy metal ion remediation. *J. Mater. Chem. A*, **2018**, 6 (46), 23542-23549.
72. Thielke, M. W.; Bultema, L. A.; Brauer, D. D.; Richter, B.; Fischer, M.; Theato, P., Rapid Mercury(II) Removal by Electrospun Sulfur Copolymers. *Polymers* **2016**, 8, 266.
73. Lundquist, N. A.; Worthington, M. J. H.; Adamson, N.; Gibson, C. T.; Johnston, M. R.; Ellis, A. V.; Chalker, J. M., Polysulfides made from re-purposed waste are sustainable materials for removing iron from water. *RSC Adv.* **2018**, 8 (3), 1232-1236.
74. Liu, P.; Gardner, J. M.; Kloo, L., Solution processable, cross-linked sulfur polymers as solid electrolytes in dye-sensitized solar cells. *Chem. Commun.* **2015**, 51 (78), 14660-14662.
75. Zhuo, S. F.; Huang, Y.; Liu, C. B.; Wang, H.; Zhang, B., Sulfur copolymer nanowires with enhanced visible-light photoresponse. *Chem. Commun.* **2014**, 50 (76), 11208-11210.

76. Liu, P.; Kloo, L.; Gardner, J. M., Cross-Linked Sulfur-Selenium Polymers as Hole-Transporting Materials in Dye-Sensitized Solar Cells and Perovskite Solar Cells. *ChemPhotoChem* **2017**, *1* (8), 363-368.
77. Cho, H.; Kim, S. M.; Kang, Y. S.; Kim, J.; Jang, S.; Kim, M.; Park, H.; Bang, J. W.; Seo, S.; Suh, K.-Y.; Sung, Y.-E.; Choi, M., Multiplex lithography for multilevel multiscale architectures and its application to polymer electrolyte membrane fuel cell. *Nat. Commun.* **2015**, *6*, 8484.
78. Abraham, A. M.; Kumar, S. V.; Alhassan, S. M., Porous sulphur copolymer for gas-phase mercury removal and thermal insulation. *Chem. Eng. J.* **2018**, *332*, 1-7.
79. Fortman, D. J.; Brutman, J. P.; De Hoe, G. X.; Snyder, R. L.; Dichtel, W. R.; Hillmyer, M. A., Approaches to Sustainable and Continually Recyclable Cross-Linked Polymers. *ACS Sustainable Chem. Eng.* **2018**, *6* (9), 11145-11159.
80. Zhang, Y.; Pavlopoulos, N. G.; Kleine, T. S.; Karayilan, M.; Glass, R. S.; Char, K.; Pyun, J., Nucleophilic Activation of Elemental Sulfur for Inverse Vulcanization and Dynamic Covalent Polymerizations. *J. Polym. Sci., Part A: Polym. Chem.* **2018**, *57* (1), 7-12
81. Lim, J.; Jung, U.; Joe, W. T.; Kim, E. T.; Pyun, J.; Char, K., High Sulfur Content Polymer Nanoparticles Obtained from Interfacial Polymerization of Sodium Polysulfide and 1,2,3-Trichloropropane in Water. *Macromol. Rapid Commun.* **2015**, *36* (11), 1103-1107.
82. Westerman, C. R.; Jenkins, C. L., Dynamic Sulfur Bonds Initiate Polymerization of Vinyl and Allyl Ethers at Mild Temperatures. *Macromolecules* **2018**, *51* (18), 7233-7238.
83. Naebpetch, W.; Junhasavasdikul, B.; Saetung, A.; Tulyapitak, T.; Nithi-Uthai, N., Influence of filler type and loading on cure characteristics and vulcanisate properties of SBR compounds with a novel mixed vulcanisation system. *Plast., Rubber Compos.* **2017**, *46* (3), 137-145.
84. Zhang, Y.; Konopka, K. M.; Glass, R. S.; Char, K.; Pyun, J., Chalcogenide hybrid inorganic/organic polymers (CHIPs) via inverse vulcanization and dynamic covalent polymerizations. *Polym. Chem.* **2017**, *8* (34), 5167-5173.
85. Zhang, Q.; Shi, C.-Y.; Qu, D.-H.; Long, Y.-T.; Feringa, B. L.; Tian, H.; Feringa, B. L., Exploring a naturally tailored small molecule for stretchable, self-healing, and adhesive supramolecular polymers. *Sci. Adv.* **2018**, *4* (7), eaat8192.
86. Arslan, M.; Kiskan, B.; Yagci, Y., Recycling and Self-Healing of Polybenzoxazines with Dynamic Sulfide Linkages. *Sci. Rep.* **2017**, *7* (1), 5207.

87. Bear, J. C.; Peveler, W. J.; McNaughter, P. D.; Parkin, I. P.; O'Brien, P.; Dunnill, C. W., Nanoparticle-sulphur "inverse vulcanisation" polymer composites. *Chem. Commun.* **2015**, 51 (52), 10467-10470.
88. Martin, T. R.; Mazzio, K. A.; Hillhouse, H. W.; Luscombe, C. K., Sulfur copolymer for the direct synthesis of ligand-free CdS nanoparticles. *Chem. Commun.* **2015**, 51 (56), 11244-11247.

APPENDICES

Publications that resulted from the research in this chapter:

Worthington, M. J. H.; Kucera, R. L. and Chalker, J. M. Green Chemistry and Polymers made from Sulfur. *Green Chem.* **2017**, 19, 2748-2761 published by The Royal Society of Chemistry and reproduced below under a Creative Commons Attribution License.



Cite this: *Green Chem.*, 2017, **19**, 2748

Received 3rd January 2017,
Accepted 27th February 2017

DOI: 10.1039/c7gc00014f

rsc.li/greenchem

Green chemistry and polymers made from sulfur

Max J. H. Worthington, Renata L. Kucera and Justin M. Chalker*

Polymers are among the most important mass-produced materials on the planet, yet they are largely derived from a finite supply of petrochemicals. To ensure the sustainable production of polymers and functional materials, alternative feedstocks are required. This Perspective examines this challenge in the context of an emerging class of polymers made from elemental sulfur. Because sulfur is a by-product of the petroleum industry, converting it into useful polymers and related materials is an advance in waste valorisation. Additionally, co-polymerisation of sulfur with renewable monomers represents an additional contribution to sustainability. These reactions are often solvent free and benefit from full atom economy, further augmenting their Green Chemistry credentials. Applications of these materials will be discussed, with a spotlight on environmental benefits. A forward looking assessment of the opportunities for using sulfur polymers in Green Chemistry is also included.

Introduction

The impact of synthetic polymers and functional materials on human life is profound. Such materials ensure access to clean air and water,^{1,2} medical devices that improve quality of life,^{3,4} sustainable power generation and energy storage,^{5,6} building materials for transportation and infrastructure,⁷ high-tech devices for communication and information processing,^{8,9} fibres for functional textiles,^{10,11} and a host of other far-reaching capabilities.^{12–14} Our everyday routines and economies

also rely heavily on synthetic polymers, especially plastics. With approximately 322 million tonnes of plastics produced in 2015,¹⁵ polymers are among the most widely produced synthetic materials on Earth. To ensure sustainable access to these materials, it is imperative that the synthesis of polymers aligns with the principles of Green Chemistry.^{16,17} Given that the vast majority of synthetic polymers are derived from finite resources such as petroleum feedstocks,¹⁸ a grand challenge in polymer chemistry is to identify sustainable building blocks that provide monomers already in use or polymers that are functional equivalents to existing macromolecules. To this end, the Green Chemistry and polymer communities have made some admirable gains. Through the use of safer solvents,¹⁹ greener and catalytic processing,^{16,20} starting materials

School of Chemical and Physical Sciences, Flinders University, Bedford Park, South Australia, 5042, Australia. E-mail: justin.chalker@flinders.edu.au



Max J. H. Worthington

Max J. H. Worthington completed his BSc in Chemistry with a first class Honours degree at Flinders University in 2015. He is currently a PhD student at Flinders University where he is investigating renewable polymers for applications in environmental remediation, biochemistry, and agriculture. His research in sulfur polymers that capture mercury pollution has garnered wide attention, with profiles in international news and documentaries, and several on-going collaborations with both industry and environmental agencies.



Renata L. Kucera

Renata L. Kucera is a third-year undergraduate at Flinders University. With the support of summer research scholarships from Flinders University and the National Environmental Science Programme, Renata has discovered several new polymers made by the co-polymerisation of sulfur and unsaturated industrial waste. Her current research interests span Green Chemistry, synthesis and sustainable polymers.

and several on-going collaborations with both industry and environmental agencies.



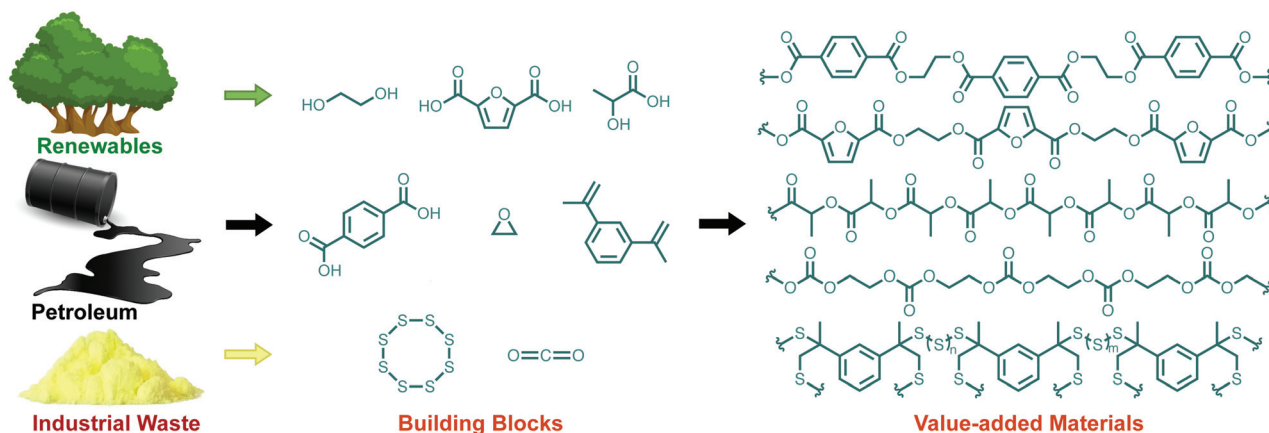
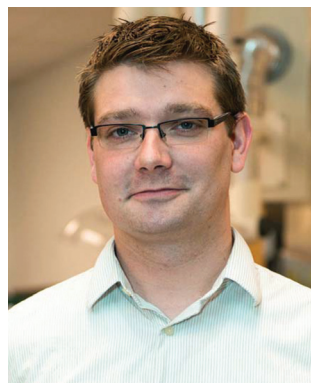


Fig. 1 Polymers are largely derived from a finite resource: petroleum. However, the future of polymer synthesis will depend on sourcing monomers from alternative feedstocks such as renewable biomass, agricultural waste, and industrial by-products such as CO₂ and sulfur. This Perspective examines the opportunities in Green Chemistry afforded by the use of sulfur as a building block for functional materials that benefit the environment. The tree and oil barrel graphics were licensed from 123RF.com with image credit to lilu330 and dvarg, respectively. Copyright 123RF.com.

derived from renewable biomass,^{21,22} re-purposing agricultural and industrial waste as a starting material,^{20,23,24} using CO₂ as a monomer¹⁸ or converting it into a traditional olefin monomer,²⁵ and designing new strategies for recycling and bio-degradation,^{26,27} the Green Chemistry metrics over the lifetime of synthetic macromolecules have improved. Simultaneously, the introduction of new polymers that address

these concerns also improves the outlook for sustainability and environmental benefit. In this Perspective, we discuss one of these classes of new materials—polymers made from sulfur—and the many ways in which they are green in their preparation and use. While this class of materials alone will not solve the problem of polymer sustainability, it may contribute in several important ways. Accordingly, this Perspective examines how polymers made from sulfur can be derived from waste and renewable sources, and how the resulting materials can be used in applications that benefit the environment (Fig. 1).



Justin M. Chalker

Dr Justin M. Chalker earned a B.S. in Chemistry and a B.A. in the History and Philosophy of Science at The University of Pittsburgh in 2006. At Pittsburgh, he contributed to the total synthesis of several natural products under the direction of Theodore Cohen. Supported by a Rhodes Scholarship and a National Science Foundation Graduate Research Fellowship, Justin then completed his D.Phil. at the University of Oxford under

the supervision of Prof. Benjamin Davis where he developed several tools for the site-selective modification of proteins. In 2012, Justin started his independent career as an assistant professor at The University of Tulsa where he established a diverse research program in organic chemistry, biochemistry and material science. In these projects, contributions to sustainability, environmental protection and human wellbeing are priorities. In 2015, Justin moved to Flinders University in Adelaide, Australia where he is a Lecturer in Synthetic Chemistry and recipient of an Australian Research Council Discovery Early Career Researcher Award. In 2016, Justin was named Tall Poppy of the Year for South Australia in recognition of his achievements in research, teaching and science communication.

Sulfur: a widely available and underused building block

Sulfur has been used for many centuries in applications as diverse as medicine, fabric bleaching, construction of lamp wicks, gun powder formulation and then more recently in the vulcanisation of latex.^{28,29} In these cases, sulfur was sourced largely through geological deposits.²⁸ With the growing concerns for acid rain, however, the desulfurisation of crude oil shifted the major share of sulfur production to the petroleum sector from 1970 to 1990.²⁹ By removing sulfur from crude oil and natural gas, SO₂ emissions from combustion of petroleum-derived fuels are curtailed, preventing acid rain.²⁹ In the desulfurisation process, the sulfur atoms in H₂S and organosulfur compounds are ultimately converted to elemental sulfur.³⁰ Although elemental sulfur is not toxic,³¹ it is a flammable solid³² so finding productive uses for this stockpiled material is important. With approximately 70 million tonnes produced each year from petroleum refining,^{28,33} elemental sulfur is widely available and inexpensive (~\$120 USD per tonne).³³ A significant portion of sulfur is used in the industrial production of sulfuric acid, and in the United States 90% of all sulfur consumption is tied to the synthesis of H₂SO₄.²⁹





Fig. 2 A stockpile of sulfur produced from the hydrodesulfurisation process in petroleum refining. Approximately 70 million tonnes of sulfur were produced in 2015 by the petroleum industry. Image credit: Gord McKenna, made available through a Creative Commons license: <https://www.flickr.com/photos/gord99/5170487123/>.

On a smaller scale, sulfur is used directly in the production of rubber³⁴ and fertiliser.²⁸ Modern synthetic chemistry has also benefitted from the versatile chemistry of elemental sulfur.^{35–37} Still, there is a net excess of several millions of tonnes of sulfur produced each year in petrochemical refining.²⁹ This excess sulfur is accumulated and stored in megaton deposits, often open to the environment (Fig. 2). Finding

large-scale uses for this sulfur, such as conversion to useful polymers, would be an important advance. And while any product made from this sulfur should rightly be classified as petroleum-derived, there are also well-established methods to access this abundant element directly from geological sources, should this prove necessary in the future.³⁸ In the first instance, however, it is best to take advantage of the excess waste sulfur generated by the petroleum industry. In doing so, this by-product is repurposed for value-added applications—a clear opportunity to develop novel sulfur chemistry.

Polymers and materials made from sulfur

Given the wide availability of sulfur, there has been a resurgence in using it as a starting material for polymers and materials.^{38–41} In order to make polymers directly from sulfur, however, there are several challenges. The main limitation has been the instability of polysulfides⁴² made by the ring-opening polymerisation (ROP) of sulfur (Fig. 3).^{35,43} When elemental sulfur is heated above its floor temperature (159 °C), S–S bond homolysis provides thiyl radicals that attack and open the ring of another molecule of S₈.^{43,44} The polymerisation is then pro-

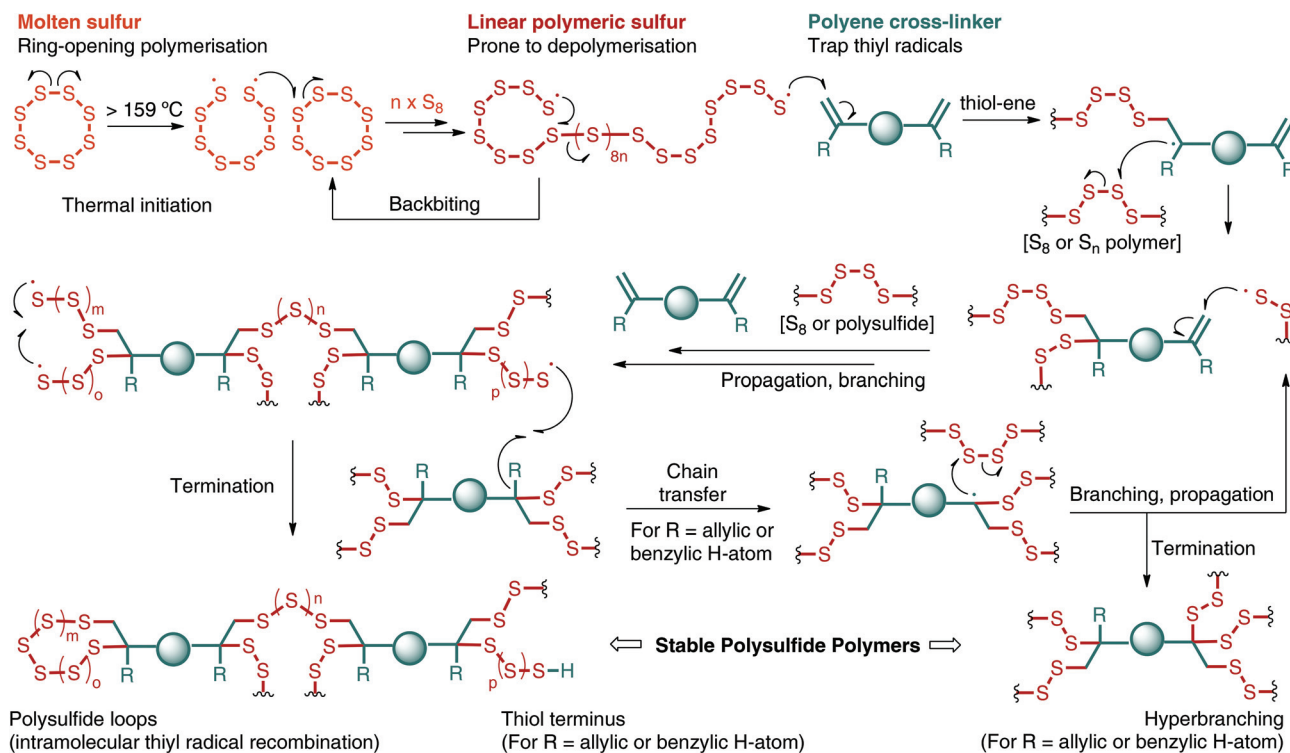


Fig. 3 Mechanistic aspects of inverse vulcanisation. Sulfur is heated to a temperature at which S–S bonds undergo homolysis and generate thiyl radicals. These thiyl radicals react with sulfur (S₈ or polysulfides) and alkene co-monomers. Without an alkene cross-linker, the terminal thiyl radicals are unstable and decompose (through backbiting, for instance) to reform S₈. Addition of the thiyl radical to the alkene, followed by radical termination, provides stable polysulfide polymers. The termination may result in polysulfide loops by intramolecular thiyl radical recombination. Where H-atoms are available (as allylic or benzylic H-atoms, for instance) thiyl groups can be converted into thiols and chain transfer results in increased branching.



pagated by repeated ring-opening and S–S bond formation between S_8 and the growing polysulfide chain (Fig. 3). However, the reaction is reversible and the terminal thiyl radicals of the polysulfide can depolymerise and expel S_8 or other cyclic sulfur species. Backbiting is one mechanism by which this depolymerisation may occur (Fig. 3), providing thermodynamically favoured S_8 in preference to terminal thiyl radicals.⁴³ To provide stable polysulfide polymers, the thiyl radicals must be quenched before depolymerisation. Pyun, Sung, Char and collaborators have shown that trapping the thiyl radicals with polyenes can provide a stable polymer made predominantly from elemental sulfur.⁴⁵ As outlined in Fig. 3, addition of the linear polymeric sulfur to polyenes results in branching of the polymeric chains. In the termination events, the thiyl radicals are thought to be quenched by at least two different mechanisms. In one case, intramolecular recombination of thiyl radicals would provide stable polysulfide loops (Fig. 3).⁴⁵ In cases where H-atoms are available (e.g. allylic and benzylic hydrogen atoms from the alkene co-monomer), H-atom abstraction may convert the thiyl radical to a thiol (Fig. 3).^{38,46} Notably, the H-atom abstraction pathway would result in chain transfer processes that ultimately lead to increased branching at the alkene co-monomer (Fig. 3). In any case, by quenching the thiyl radicals in the polysulfide polymer, the depolymerisation is suppressed and a stable macromolecule is obtained. In classic vulcanisation, elemental sulfur is used in relatively small quantities to cross-link latex or other preformed polymers. In the so-called inverse vulcanisation in Fig. 3 (coined by Pyun, Sung, Char and collaborators),⁴⁵ the alkene co-monomer is used in relatively small amounts and links together and branches the polysulfide polymers. Through inverse vulcanisation, polymers containing very high sulfur content can be obtained (typically 50–90% sulfur by mass). Of relevance to Green Chemistry, inverse vulcanisation does not require exogenous solvents or reagents in the synthesis. The sulfur and alkene are used as co-monomers and the reaction medium. Furthermore, the reaction is entirely atom economical, with all of the starting material incorporated into the product.

In Pyun's seminal report, he and his collaborators used 1,3-diisopropylbenzene (DIB, **1**) as the organic cross-linker. In the event, sulfur was heated to 185 °C to initiate ring-opening polymerisation. Addition of DIB (typically at a feed ratio of 10–50 wt%) resulted in cross-linking and vitrification within minutes (Fig. 4a). The resulting red polymeric glass is referred to as poly(sulfur-*random*-1,3-diisopropenylbenzene), or poly(*S-r*-DIB). Because of the high sulfur content (typically targeted at 50–90 wt% sulfur) and the polysulfide structure of the backbone of the polymer, poly(*S-r*-DIB) has several interesting chemical, material, and optical properties. For instance, the poly(*S-r*-DIB) polysulfides are redox active and useful as next generation cathode materials for lithium–sulfur batteries, as Pyun and co-workers demonstrated in their original⁴⁵ and subsequent studies.^{47–51} The high sulfur content also imparts a high refractive index and an IR region of transparency that is convenient for night vision, thermal imaging and other optical

applications.^{52–54} Furthermore, the S–S crosslinks of the polysulfide are dynamic, which allows for straightforward repair of the polysulfide by thermal annealing.^{53,55}

These creative contributions from Pyun and co-workers have since inspired further exploration of inverse vulcanisation with a variety of unsaturated cross-linkers to obtain polysulfides with complementary properties (Fig. 4). Pyun and associates showed, for instance, that inverse vulcanisation using triene **2**, provides a polysulfide with improved thermomechanical properties in the form of a higher glass transition temperature (over 100 °C) than the first generation poly(*S-r*-DIB) which possessed a T_g of 43–49 °C.⁵⁴ In other studies, inverse vulcanisation with divinylbenzene (DVB, **3**),^{56–58} styrene (**4**),⁴⁶ and α -methylstyrene (**5**),⁵⁹ demonstrated that traditional and widely available monomers for radical polymerisation can also be converted into polysulfides. In the case of DVB, the synthesis of the corresponding polysulfides was informed by early studies in the Pyun laboratory in 2011 when sulfur was used as a reaction medium to prepare gold nanoparticles and related composites. In this prescient study, sulfur was cross-linked with DVB.⁶⁰ The more recent DVB polysulfides, prepared by inverse vulcanisation, could be fashioned into a highly IR transparent thin film,⁵⁶ or used as a cathode material for Li–S batteries.⁵⁸ The co-polymerisation of sulfur, DVB, and bis-maleimide **6** also provided a novel cathode material for Li–S cells.⁵⁷ In the case of styrene, important mechanistic aspects of the polymerisation were revealed in the inverse vulcanisation. Specifically, chain transfer reactions can occur after thiyl radicals abstract the benzylic hydrogen atom available after styrene is incorporated into the polysulfide (see Fig. 3 for related processes). The chain transfer results in branching—despite styrene having only one alkene—and provides a stable polysulfide that is resistant to depolymerisation.⁴⁶ The resulting polymers were further tested for their potential as cathodes. For α -methylstyrene, the resulting polysulfide was used as a reaction medium for CdS nanoparticle synthesis. This was possible because the polysulfide derived from **5** was a liquid at the temperature of the CdS synthesis (200 °C). The CdS nanoparticles formed could then be isolated by centrifugation after dissolving the polysulfide in chloroform.⁵⁹ These studies by Luscombe built upon prior work in nanoparticle composite preparation by Pyun⁶⁰ and Char⁶¹ in which liquid sulfur and polysulfides formed from DVB⁶⁰ or oleylamine (**7**)⁶¹ provided a matrix for the synthesis of gold and PbS nanoparticles.

To improve the prospects of polysulfides as cathode materials, several polymers have been prepared by inverse vulcanisation that contain polythiophene cross-linkers that overcome the high resistivity of sulfur. For example, polythiophenes such as **8** and **9** contain alkene end groups that can be cross-linked by inverse vulcanisation.^{62,63} An alternative approach features monomer **10** in which the inverse vulcanisation is carried out first, with a second-stage electrochemical oxidation of the polysulfide providing the target polythiophene polymer.⁴⁸ This tandem and orthogonal polymerisation strategy is notable not only for its entry to polythiophenes after inverse vulcanisation, but also for the manner in which it



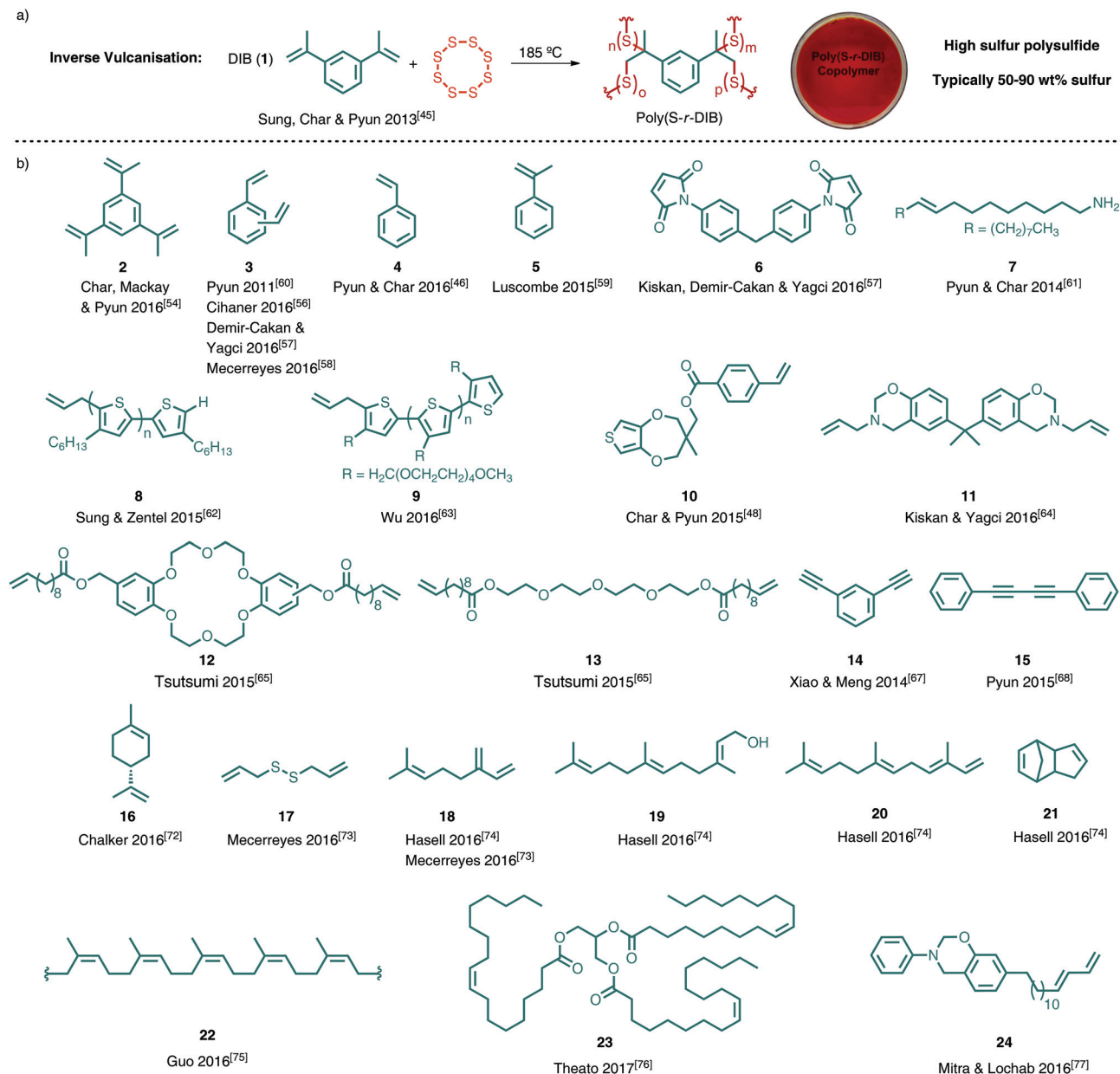


Fig. 4 (a) Inverse vulcanisation of 1,3-diisopropenylbenzene (DIB) provides the polysulfide poly(sulfur-*random*-1,3-diisopropenylbenzene), or poly(S-*r*-DIB).⁴⁵ The polymer can be processed, moulded and cured in a variety of architectures. The image of the poly(S-*r*-DIB), cured in a petri dish, was adapted with permission from ref. 55. Copyright 2014 American Chemical Society. (b) A selection of unsaturated cross-linkers used for inverse vulcanisation and related reactions used to access polysulfide polymers. The corresponding authors and the associated citations are indicated for reference.

installs complementary and distinct polymer backbones. Such sequential cross-linking has also been studied by Kiskan and Yagci using monomer **11**. In this report, inverse vulcanisation of **11** was followed by ring-opening polymerisation of the oxazine to provide polysulfide phenolic networks reinforced by both polysulfide branching and polybenzoxazine cross-linking.⁶⁴

Dienes **12** and **13** were also used to form polysulfides, with further testing as cathode materials in Mg-S and Li-S cells.^{65,66}

The polyether groups were proposed to increase ion mobility of the magnesium or lithium ions. Other studies toward novel cathode materials also revealed that poly-alkynes are suitable monomers for the synthesis of polysulfides. Alkyne **14** provides highly crosslinked polysulfides in which thiyl radicals of the growing polysulfide can add multiple times to the alkyne carbons.⁶⁷ In the case of di-yne **15**, addition of sulfur to the alkynes ultimately provides a thiophene derivative that is cross-linked through polysulfide linkages.⁶⁸



It should also be noted that while alkene and alkyne cross-linkers are highlighted in Fig. 4, other functional groups react with sulfur in which alternative mechanisms are operative in the inverse vulcanisation. For instance, Park has illustrated how polythiols such as trithiocyanuric acid can be used to prepare sulfur-rich polymers by reaction with elemental sulfur.⁶⁹ Coskun and Choi have also explored aromatic thiol cross-linkers in inverse vulcanisation.⁷⁰ The same laboratories also described a unique cross-linking mechanism in which thiyl radicals of the polysulfide chain insert into aromatic C–H bonds.^{70,71} These materials were tested further as cathodes for Li–S batteries.^{69–71}

In the survey of unsaturated cross-linkers for inverse vulcanisation discussed so far, many are relatively valuable fine chemicals. Other than the monomers 3–5, which are available in bulk quantities because of their use in traditional polymerisations, alkenes 1–15 in Fig. 4 are comparatively expensive, require multiple steps to prepare, or are simply not available in the multi-kilogram quantities required for bulk polymer synthesis. These features may be irrelevant for high-end applications where monomer cost and raw material supply are not primary considerations. Also, it is entirely possible that increasing demand for these cross-linkers, and their polysulfides, could lead to bulk production and lower cost. These future prospects aside, there is still a mismatch in scale and supply of these co-monomers when compared to sulfur, which is available in multi-million tonne quantities. It is therefore worthwhile to consider other co-monomers for inverse vulcanisation that are available on large scale as either industrial by- or co-products or renewable feedstocks from biological sources. In considering such co-monomers for inverse vulcanisation, the excess sulfur produced industrially can be productively consumed. This strategy also draws strong links to the principles of Green Chemistry by using industrial by-products and renewable feedstocks as the sole materials in the synthesis of valuable polymers. Monomers 16–24 were explicitly chosen for use in inverse vulcanisation because they address this overarching goal of sustainability.^{72–78} The resulting polysulfides have also been employed in applications that benefit the environment, such as environmental remediation and sustainable energy technologies. These polysulfides, and their applications in Green Chemistry, are discussed in more detail in the next two sections.

Polysulfides for environmental protection and remediation

Using sulfur as a monomer aligns with several principles of Green Chemistry in that its polymerisation benefits from excellent atom economy and does not require solvent. Furthermore, because sulfur is a by-product of the petroleum industry, using it as a starting material is an advance in waste valorisation. The environmental benefits are compounded when sulfur is co-polymerised with a renewable olefin and the resulting polymer is used in pollution monitoring and remediation.

Specifically, the high sulfur content of these polysulfides is expected to impart affinity for soft Lewis acids, such as certain heavy metals. But, in contrast to elemental sulfur, the polysulfide polymers have the capacity to be processed into forms that confer mechanical, chemical and thermal properties that are complementary or superior to elemental sulfur.

Our lab contributed in this regard with the development of a polysulfide made from elemental sulfur and *D*-limonene (Fig. 5a).⁷² The *D*-limonene monoterpene (**16**) is found in the zest of citrus fruit and is produced on the order of 70 000 tonnes per year in the citrus industry through steam distillation of the non-edible peel.⁷⁹ By simply reacting sulfur with *D*-limonene using an inverse vulcanisation protocol, a polysulfide wax was formed that was effective in capturing palladium and mercury salts.⁷²

Palladium is a valuable catalyst in a variety of organic transformations,^{80,81} and its recovery from waste streams is desirable. More recently palladium has been identified as a pollutant leached from catalytic converters by automobile exhaust.⁸² The capture of palladium therefore confers both economic and environmental benefits, so it is valuable to know that polysulfides can be used to recover this transition metal.

Mercury is a highly toxic metal that is encountered in a variety of industrial activities such as oil and gas refining, coal combustion and artisanal and small-scale gold mining.⁸³ Exposure to mercury can lead to serious health problems,

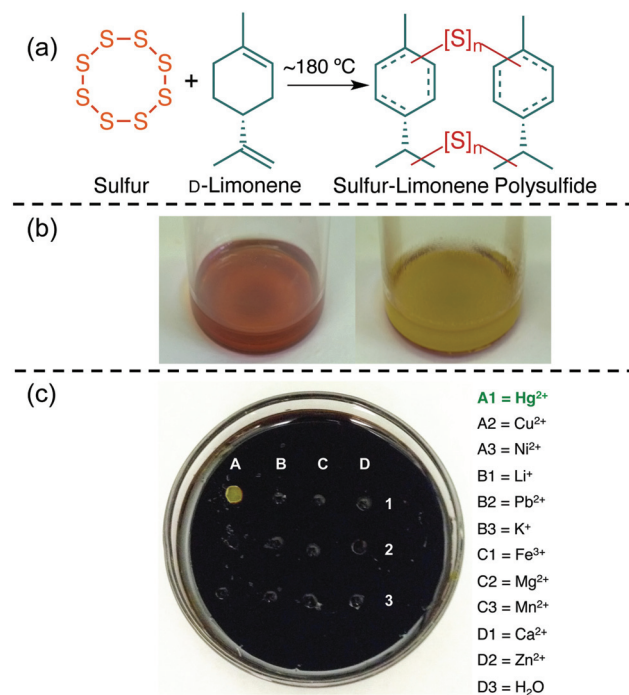


Fig. 5 (a) A polysulfide made from elemental sulfur and *D*-limonene. (b) The limonene polysulfide changes colour from dark red to yellow upon binding to mercury(II) and removing it from water. (c) The chromogenic response to mercury(II) is selective among the metals screened in the study. These images are reproduced with permission from the authors and ref. 72 under a Creative Common License.



including debilitating neurological and embryotoxic effects.⁸⁴ The remediation of mercury pollution is therefore essential in protecting the environment and human health. For these reasons, it was encouraging that the limonene polysulfide was effective in removing highly toxic mercury(II) from water.⁷² The mercury removal was even suitable for remediating pond water littered with silt and other debris.⁷² Upon capture of the mercury(II), the polysulfide underwent a colour change from dark red to yellow—revealing an additional (and unexpected) sensing capability of the material (Fig. 5b). The chromogenic response was selective for mercury(II) among the metals investigated in this report (Fig. 5c).⁷²

The Green Chemistry aspects in this limonene polysulfide synthesis are worth noting. The synthesis does not require exogenous reagents or solvents, it requires only limonene and sulfur.⁷² Like the majority of inverse vulcanisations, the synthesis of the limonene polysulfide is highly atom-economical, though some small molecule by-products such as *p*-cymene were produced.⁷² Furthermore, both co-monomers can be considered by- or co-products of industrial processes, so this is an example of a value-added material made entirely from re-purposed waste.

Building upon the use of polysulfides in mercury capture, Hasell and co-workers⁸⁵ studied both the limonene polysulfide⁷² and Pyun's poly(*S-r*-DIB) co-polymer⁴⁵ in the removal of mercury(II) chloride from water. Their team found the active surface of the limonene polysulfide, due to its soft waxy nature, can actually be regenerated by the mechanical force of stirring.⁸⁵ More impressively, the authors disclosed a method to form polysulfide foams from the polymers using supercritical carbon dioxide.⁸⁵ The foam dramatically increases the surface area and the polymer's ability to capture mercury(II) from water (Fig. 6). For instance, a foam prepared from Pyun's poly(*S-r*-DIB) was able to reduce the concentration of mercury(II) in water from 2000 ppb to ~80 ppb after a 3 hour incubation. Translation to a continuous process was also demonstrated where the polysulfide foam was packed into a column as a solid adsorbent for water purification.⁸⁵

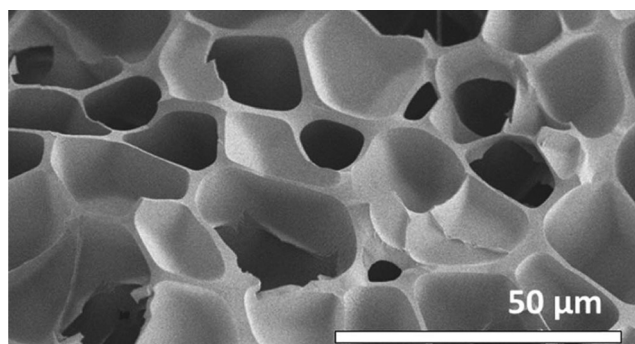


Fig. 6 A porous version of poly(*S-r*-DIB) was prepared by foaming with supercritical CO₂. This material was effective in removing mercury salts from water. The image was adapted from ref. 85 with permission from the Royal Society of Chemistry.

The Hasell laboratory has since extended these foams to polysulfides made from the reaction of sulfur with the low cost, industrially produced monomer dicyclopentadiene (21) and renewable terpenes such as myrcene (18), farnesol (19) and farnesene (20).⁷⁴ Again the high surface area imparted by supercritical carbon dioxide foaming or using sodium chloride as a porogen allowed efficient sequestration of inorganic mercury from water. In this study, the authors deliberately explored renewable alkene cross-linkers so the preparation of the polysulfides is imminently scalable and sustainable—a necessary requirement for applications in environmental protection and remediation.

Another effective method for imparting high surface area to polysulfide polymers is electrospinning.^{86,87} Theato and co-workers recently demonstrated for the first time that polysulfides prepared by inverse vulcanisation, such as poly(*S-r*-DIB), are compatible with electrospinning.⁸⁸ Using a carrier polymer such as high molecular weight poly(methyl methacrylate) proved important in accessing uniform fibres with diameters on the order of 1 micron (Fig. 7).⁸⁸

The high surface area of these fibres was beneficial in mercury uptake studies in which an impressive 98% of mercury(II) could be removed in just a few seconds from water containing 20 ppm HgCl₂. The authors also demonstrated a higher affinity of the polysulfide fibres for Hg²⁺ than for other metals ions examined (Cd²⁺, Co²⁺, Cu²⁺, Fe³⁺, Pb²⁺, and Zn²⁺).⁸⁸ The rapid binding to mercury and high distribution coefficients (*K_d*) on the order of 10⁵ mL g⁻¹ bode well for applications of electrospun polysulfides in water filtration devices.

The polysulfide polymers prepared by inverse vulcanisation can be further converted to porous carbon materials.⁸⁹ The Hasell laboratory showed that heating the polysulfides at 750 °C in a furnace under a flow of argon leads to the thermal extrusion of sulfur and sulfurous by-products—some of which, the authors note, could be recycled and re-used. The remaining carbonised product is porous and doped with between 7 and 14% sulfur—a value independent of the amount of sulfur in the original polysulfide.⁸⁹ The authors further characterised

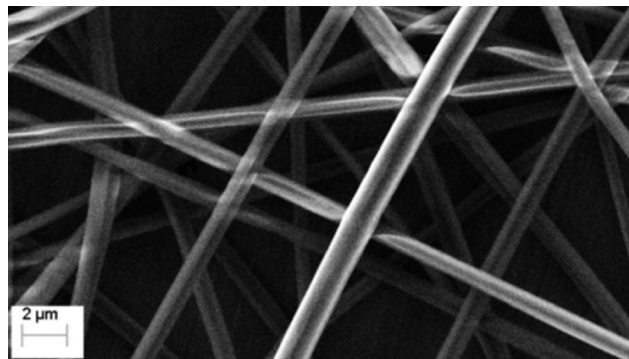


Fig. 7 Electrospinning a blend of poly(*S-r*-DIB) and poly(methyl methacrylate) provides uniform fibres with very high surface area. The fibres showed excellent performance in capturing water soluble mercury. Adapted from ref. 88 under a Creative Commons License.



the gas sorption properties for their porous carbonaceous materials made from both Pyun's poly(*S-r*-DIB) and Chalker's sulfur-limonene polysulfide.⁸⁹ Remarkably, these porous materials were complementary in their gas adsorption selectivity. The carbon derived from the poly(*S-r*-DIB), for instance, was microporous and readily adsorbed nitrogen and carbon dioxide. In contrast, the porous carbon derived from the sulfur-limonene polysulfide occluded nitrogen, but readily adsorbed hydrogen and carbon dioxide.⁸⁹ Porous materials are widely used in a variety of industrial separations and environmental applications,⁹⁰ such as gas separations,⁹¹ carbon dioxide sequestration,^{92,93} oil spill cleanup,⁹⁴ waste treatment,^{95,96} and water purification.⁹⁷ The authors also explicitly point out that the synthesis of polysulfides by inverse vulcanisation is atom-economical, solvent free, and makes use of industrial by-products such as sulfur and limonene.⁸⁹ Therefore, Hasell's work constitutes an important advance not only in waste valorisation and sustainable material synthesis, but also how such materials can be tailored for environmentally focussed end uses.

Polysulfides for sustainable energy production and storage

Sustainable energy production and storage are two of the greatest challenges facing our species.^{98,99} And while it is still an exploratory period for polysulfides, several studies using these high sulfur content materials have revealed promising results in energy generation and battery research.

Liu, Gardner and Kloo, for instance, recently demonstrated that polysulfides prepared by inverse vulcanisation work as hole-transport materials in solid-state dye-sensitised solar cells.¹⁰⁰ Using poly(*S-r*-DIB) at 50% sulfur by weight, the authors demonstrated a power conversion efficiency of 1.5%. While this result is modest in comparison to high-performance dye-sensitised solar cells, the very low cost of the sulfur polymer will likely lead to further studies to improve its performance in generating power from sunlight.

Polysulfides prepared by inverse vulcanisation have also been used in the photochemical generation of hydrogen fuel. Zhang and co-workers prepared poly(*S-r*-DIB) as nanowires and explored their use in the photochemical splitting of water with visible light to generate hydrogen, a clean-burning fuel.¹⁰¹ The nanowires were prepared using an anodic aluminium oxide membrane as a template, in which poly(*S-r*-DIB) was synthesised and cured. The template was removed by etching with sodium hydroxide, providing the polysulfide nanowires. The photocatalytic activity of these polysulfide nanowires was superior to bulk sulfur, a feature attributed in part to their high surface area. This study is an important report of the ways in which inexpensive sulfur can be converted into a valuable catalyst that can harness visible light for the generation of clean fuels.

In a third area of energy research featuring polysulfides, polymers prepared by inverse vulcanisation have been inten-

sely studied as next-generation cathode materials for batteries. Because many forms of sustainable energy production are intermittent (*e.g.* solar and wind power), high performance energy storage is required.⁹⁹ Because Li-S cells have a theoretical capacity and power density that exceeds current Li-ion technology, and sulfur is very inexpensive, there has been intense interest in developing practical Li-S cells.^{102,103} The original report on inverse vulcanisation by Pyun and associates explored, among other things, the use of their poly(*S-r*-DIB) polymers as cathode materials.⁴⁵ One of the main objectives was to determine if their sulfur-DIB co-polymers could address the rapid capacity loss and short cycle lifetimes of typical Li-S cells. Indeed the authors found that poly(*S-r*-DIB) at 90 wt% sulfur and 10 wt% DIB displayed superior capacity to sulfur over hundreds of cycles.^{38,45,47,49} Specific capacities on the order of 1000 mA h g⁻¹ over 100 cycles are especially encouraging.⁴⁷ A key to this success is the polysulfide's ability to suppress lithium sulfide deposits on the cathode and protect it against mechanical wear.³⁸

Since these reports,^{45,47,49} many more studies have emerged in which inverse vulcanisation and related processes are used to prepare cathode materials and other composites with high sulfur content.^{46,48,50,51,57,58,62,63,65-71,73,75-78,104-109} Rather than reiterate these achievements here, we instead highlight some recent efforts where renewable alkenes were used in the inverse vulcanisation. In this way, the cathode materials can be prepared entirely from waste and renewable resources, thereby raising their Green Chemistry profile. Theato, for example, prepared polysulfides from plant triglycerides (linseed oil, sunflower oil, and olive oil) and sulfur in an inverse vulcanisation procedure.⁷⁶ A simplified structure of the triglyceride monomer (**23**) is shown in Fig. 4. And while oleic acid is shown as the fatty acid in **23**, it should be noted that polyunsaturated linoleic acid is also a major component of these triglycerides.⁷⁶ The resulting material was a polysulfide rubber containing embedded particles of free sulfur. The materials were studied as cathode materials for "green Li-S batteries."⁷⁶ Encouragingly, the authors discovered high initial specific capacities (880 mA h g⁻¹) and established a benchmark in capacity retention for these green materials over 100 cycles (63%). In a similar effort, Mecerreyes and co-workers explored the inverse vulcanisation of the renewable alkenes diallyl disulfide and myrcene, derived from alliums and thyme, respectively.⁷³ Subsequent electrochemical tests demonstrated the use of the polysulfides as cathode materials for Li-S batteries.⁷³ Initial capacities of 770 mA h g⁻¹ and 790 mA h g⁻¹ were measured for the diallyl disulfide and myrcene polysulfides, respectively, with a capacity retention of about 80%.

Renewable monomers **22** and **24** have also been reported recently in inverse vulcanisation, with further electrochemical testing. Polyisoprene **22**, for instance, can be converted to a polysulfide very similar to vulcanised rubber, but with higher sulfur content necessary for use as a cathode.⁷⁵ Importantly **22** is a renewable polyene. Similarly, **24** is interesting in that it is derived in part from an agricultural waste material, cardanol,



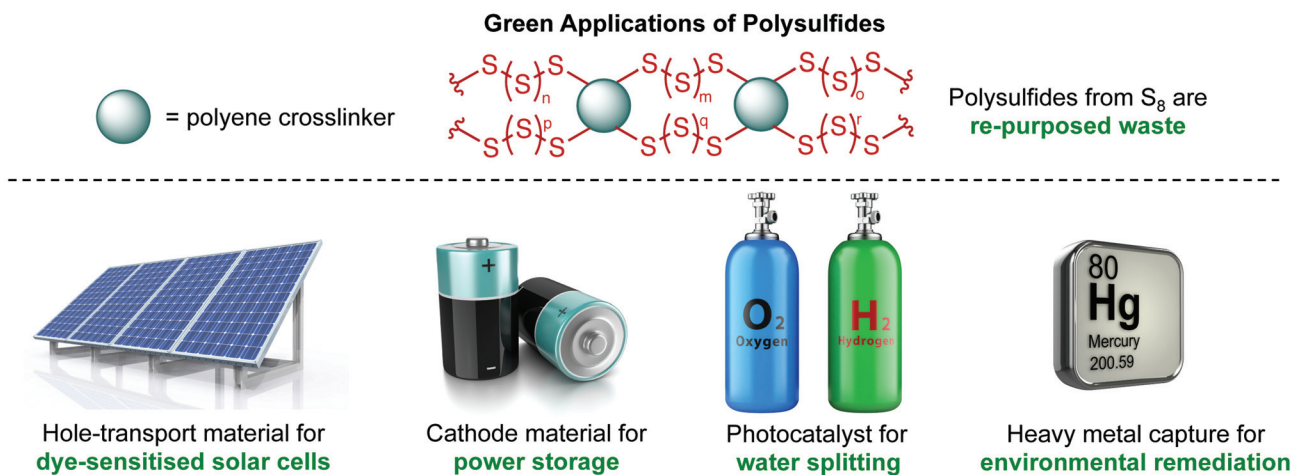


Fig. 8 Polysulfides prepared by inverse vulcanisation have been explored in diverse areas of sustainability including power generation, power storage, photocatalytic water splitting, and environmental remediation. Graphics of solar panels, batteries, gas cylinders, and mercury symbol were licensed from 123RF.com, with image credit to Michael Roskoth, mrgao, Oleksandr Marynchenko, and 3dalia, respectively. Copyright 123RF.com.

and therefore provides an advance in waste valorisation as well as a contribution to sustainable power storage materials.^{77,78}

The merger of waste sulfur and renewable plant oils to access polysulfides is an important effort in sustainable synthesis. Furthermore, the polysulfides are useful in a variety of applications that benefit the environment. In particular, these materials have been demonstrated to be effective in power generation and storage, photocatalysis for the production of clean fuels, and sequestration of heavy metal pollution. These green applications are summarised in Fig. 8.

Green chemistry outlook for sulfur polymers

The sustainable synthesis of polymers and functional materials is critical for our future. Among the diverse efforts toward this goal, polymers made from sulfur have emerged as a new class of materials useful in several applications. Because sulfur can be considered a by-product of the petroleum industry, the preparation of high sulfur polymers is an innovative example of waste valorisation. Furthermore, the syntheses of sulfur polymers typically benefit from high atom economy and often require no solvent—two ways in which they align with priorities of Green Chemistry. Further benefits to the environment come from preparing these polymers through the copolymerisation of sulfur and renewable alkenes such as terpenes and triglycerides. Additionally, several recent reports were discussed in which these polysulfide materials were used to capture heavy metal pollution, and generate and store power. In this way, the synthesis and application of polymers made from sulfur provides a broad platform for sustainable science and technology. In order to realise the full benefit of these features, however, there are several challenges on the horizon. We outline these challenges and opportunities to

help motivate future research in the Green Chemistry of polymers made from sulfur.

Controlled polymerisation of sulfur at low temperature

The microstructure of polysulfides prepared by inverse vulcanisation can be controlled in part by simply varying the feed ratio of sulfur to alkene.³⁸ Higher levels of sulfur result in longer stretches of catenated sulfur atoms (higher sulfur rank), while lower levels provide shorter stretches of sulfur atoms between the alkene co-monomer (lower sulfur rank). This feature allows some control over the level of crystallinity, as higher levels of sulfur in the polysulfide result in more crystalline polymers. Nonetheless, inverse vulcanisation still provides a statistical distribution of polysulfide microstructures. It could be advantageous, perhaps, to devise alternative polymerisation conditions in which the sulfur rank, cross-linking, molecular weight and polydispersity can be better controlled. Such control would benefit fundamental studies in how specific polysulfide structures affect their function. In Green Chemistry, for instance, control over the polysulfide structure would allow the preparation of materials with optimised electrochemical properties for power generation and storage, or optimal structures for binding a particular heavy metal pollutant. While devising methods for the controlled polymerisation of sulfur are a task for future research, there have been some notable efforts to use reversible addition–fragmentation chain transfer (RAFT) to control the rate of inverse vulcanisation.¹⁰⁸ This strategy also provides a polysulfide with dormant RAFT groups ligated to the polymer, presenting further opportunities for post-synthetic functionalisation.¹⁰⁸ These early steps in controlling the polymerisation of sulfur will help guide future efforts to exact more control of polysulfide structure.

Limited control of inverse vulcanisation is due, in part, to high temperatures employed in the polymerisation (typically



160 to 200 °C). These temperatures likely lead to random and equilibrated microstructures, due to thermal scission and recombination of S–S bonds in the polysulfide backbone. The high temperatures could also lead to side reactions such as undesired H-atom abstraction, chain transfer, or oxidation. When limonene is used as the alkene cross-linker, for instance, its oxidation by sulfur to *p*-cymene was an undesired side reaction.⁷² The high temperatures used for inverse vulcanisation also necessitate energy input that violates a principle of Green Chemistry. It is therefore worth identifying alternative methods for polymerising sulfur at lower temperatures. In doing so, energy input would be reduced, side reactions may be suppressed, and it is likely that more control could be exerted over the polymerisation. To achieve this aim in radical polymerisation of sulfur, it is likely that alternative methods of initiation will be required, as well as a suitable solvent or form of sulfur that is miscible with the co-monomer or reaction medium. It may be the case that entirely different mechanisms of polymerisation are required. For instance, ionic condensation polymerisation of polysulfides and haloalkanes proceeds efficiently at 30 °C.¹¹⁰

The ability to carry out polymerisations of sulfur at lower temperature will also allow a far greater range of alkene cross-linkers to be used in the reaction. Using the standard inverse vulcanisation protocol, the alkene typically requires a relatively high boiling point. In Fig. 4, for instance, most of the alkenes have a boiling point higher than 160 °C. Of these co-monomers, styrene has the lowest boiling point at 145 °C. If the radical polymerisation of sulfur can be carried out at lower temperatures, alkenes with lower boiling points could then be readily employed as co-monomers. As the material properties of the polysulfide also depend on the alkene, this is an important way in which complementary materials can be accessed. Even the relatively small panel of alkenes in Fig. 4 illustrate this point: inverse vulcanisation with **1** provides a glass,⁴⁵ while **16** provides a wax⁷² and **23** a rubber.⁷⁶

Green solvents for polysulfide synthesis and processing

While inverse vulcanisation can be executed under solvent free conditions (*i.e.* the unsaturated cross-linker is reacted with molten sulfur and polysulfide pre-polymers), it is worth considering what green solvents are available for both polysulfide synthesis and processing. In the relatively few solution-phase syntheses of polysulfides by inverse vulcanisation, non-green organic solvents such as *o*-dichlorobenzene,⁶³ pyridine¹¹¹ and carbon disulfide⁶⁷ have been used because of their relatively high boiling points and ability to solvate sulfur. Likewise, in experiments that required manipulation of polysulfide polymers in solution (such as casting polysulfides into thin films or electrospinning polysulfide solutions), non-green solvents such as dimethylformamide,^{69,88} acetonitrile,⁷⁷ tetrahydrofuran,^{61,77,88} and 1,2-dichlorobenzene,⁵² were used. It is therefore worthwhile to identify safe, sustainable and biodegradable solvents suitable for the synthesis and manipulation of sulfur polymers. The limited solubility of sulfur and sulfur-rich polymers, as well as the high reac-

tion temperatures typically used in inverse vulcanisation, make this a largely unmet challenge.

Notably, a few reports have integrated green solvents into the processes involving sulfur polymers. Pyun, Char and co-workers, for instance, have made progress in interfacial condensation polymerisations in water, studying inorganic polysulfides (NaS-[S]_{*n*}-SNa, derived from sodium sulfide and elemental sulfur) and their reaction with 1,2,3-trichloropropane.¹¹⁰ The polymer products presented as nanoparticles containing above 75% sulfur by mass. While this polymerisation is mechanistically distinct from inverse vulcanisation, it is a clear demonstration of converting elemental sulfur into polymers in a safe and relatively green aqueous solvent. Importantly, even though the polymer particles were not soluble in water, they could be processed as dispersions.

For polysulfide processing, super critical carbon dioxide has been explored by Hasell and co-workers in the preparation of polysulfide foams, as described previously and shown in Fig. 6.^{74,85} In addition to establishing a route to high surface area polysulfides, Hasell's work illustrated that super critical carbon dioxide can innervate and swell polysulfides—perhaps providing a lead for further studies in solvating polysulfide melts or pre-polymers. As supercritical carbon dioxide is recognised as a relatively green solvent for polymer processing,¹¹² its use in the manipulation of polysulfides is encouraging.

Outside of these few studies, the integration of green solvents with sulfur polymer synthesis and processing is limited. There is clearly an opportunity for further progress in identifying green solvents for sulfur polymer chemistry.

Toxicity of polysulfides

A central tenet of Green Chemistry is the design of safer chemicals. While elemental sulfur is non-toxic, little is known about the toxicity of polysulfide polymers. For the polysulfide prepared using sulfur and limonene,⁷² it was shown by our team and collaborators that nothing toxic was leached from the material into water, as indicated by cell viability assays of HepG2 and Huh7 liver cells. This result was used as motivation to explore these polysulfides for water purification in both natural waterways and in municipal water systems—research that is ongoing in our lab. Other than these relatively simple tests, there have not been additional toxicity studies on polymers prepared by inverse vulcanisation. It is likely that the toxicological profile will vary based on the organic cross-linker and its products of biodegradation. As this information becomes available, it will help guide the use of these polymers in environmental and biological applications.

Biodegradability of polysulfides

The persistence of polymers in the environment is cause for concern.¹¹³ A future line of research in the biodegradability of sulfur polymers is therefore worth considering. The mechanism of degradation will likely depend on both the polysulfide stability and the organic cross-linker. For instance, the S–S bonds of polysulfides are susceptible to reduction and photolysis, so polysulfide polymers might be degraded by reductases



found in living organisms or after long-term exposure to sunlight. Additionally, by using cross-linkers that contain labile groups, biodegradability can be programmed into polysulfides. Polyenes **10**, **12**, **13**, and **23**, for instance, contain esters that can hydrolyse—perhaps slowly upon exposure to water or at the provocation of esterases. It remains to be seen whether these reactions are efficient, and if the products of degradation are ecologically innocuous, but the chemical lability of polysulfides could potentially be leveraged in the preparation of polymers with programmed lifetimes and biodegradability.

Recycling polysulfides

Consideration of polymer lifetime also prompts investigation of recycling methods. Unlike traditional polyolefins, which contain a very stable backbone of carbon–carbon bonds, polysulfides are comprised of relatively labile S–S bonds. It is therefore intriguing to consider ways in which polysulfides produced on an industrial scale could be depolymerised back to re-usable monomers or oligomers. Such a process does not necessarily have to provide S₈ and the original alkene, but only a suitable precursor to other polysulfide polymers. Relatedly, polysulfides may be amendable to repair or restructuring by virtue of dynamic S–S bonds. Reports in thermal healing of fractured poly(S-*r*-DIB) bode well for such strategies.^{53,55}

Commercial use and scalability

Commercial and industrial uptake of polysulfide materials prepared by inverse vulcanisation is required for wide impact in Green Chemistry. Otherwise, the applications in Fig. 8 will be confined to the research laboratory. One technical hurdle that will need to be overcome is the large-scale preparation of high-sulfur polysulfides (>50% sulfur) by inverse vulcanisation. As classic vulcanisation has long been used for the commercial production of rubber, factice, ebonite, and other sulfur-rich materials (typically containing up to 30% sulfur by mass),³⁴ this challenge seems surmountable. Moreover, kilogram scale inverse vulcanisations have been reported.⁴⁹ Yet, it is possible that commercial applications in energy and environmental protection would require hundreds of kilograms or even tonnes of polymer. In meeting such demand, the complex thermodynamics and changes in viscosity during inverse vulcanisation would make even pilot-scale batch processing a challenge. Therefore, it may be necessary to develop continuous processes for polysulfide production in which the scale of the reaction at any given time is relatively small, but sustained or parallel operation provides several kilograms of polymer or pre-polymer per hour. In one form, this may involve the direct polymerisation of sulfur and the alkene in an extruder. This reactive extrusion process would provide the polysulfides on a large scale and likely benefit from a superior safety profile when compared to batch methods.

Targeting problems of scale

In several parts of this Perspective it was argued that making polymers from elemental sulfur constitutes waste valorisation. The excess sulfur produced from petroleum refining demands

such efforts. However, this excess sulfur problem will not be seriously addressed by inverse vulcanisation unless commercial production of polysulfides proves viable. It is therefore worthwhile considering sectors of the economy that would benefit from industrial production of polysulfides made from low-cost alkenes and elemental sulfur. Likewise, the potential benefits in Green Chemistry will only have impact if such polysulfides are deployed in applications and problems of immense scale. Several of these areas have been mentioned already, with power generation, power storage, water and air purification, and environmental remediation likely requiring industrial scale polysulfide production for serious impact. Other areas such as construction and agriculture may also benefit from an industrial supply of inexpensive polysulfides, so there are ample opportunities for future research to benefit these sectors. In our own efforts, we are aiming to devise new and versatile sulfur polymers—made entirely from renewables and industrial waste—that benefit the environment and align with values and priorities of Green Chemistry.

Acknowledgements

The authors thank Flinders University, the Australian Research Council, and the Australian National Environmental Science Program Emerging Priorities Funding for generous support of their research program.

References

- 1 M. Ulbricht, *Polymer*, 2006, **47**, 2217–2262.
- 2 M. T. M. Pendergast and E. M. V. Hoek, *Energy Environ. Sci.*, 2011, **4**, 1946–1971.
- 3 *Biomaterials Science: An Introduction to Materials in Medicine*, ed. B. D. Ratner, A. S. Hoffman, F. J. Schoen and J. E. Lemons, Elsevier, Amsterdam, 3rd edn, 2013.
- 4 S. Agarwal, J. H. Wendorff and A. Greiner, *Polymer*, 2008, **49**, 5603–5621.
- 5 F. Vilela, K. Zhang and M. Antonietti, *Energy Environ. Sci.*, 2012, **5**, 7819–7832.
- 6 E. Serrano, G. Rus and J. García-Martínez, *Renewable Sustainable Energy Rev.*, 2009, **13**, 2373–2384.
- 7 A. Correia Diogo, in *Materials for Construction and Civil Engineering: Science, Processing and Design*, ed. M. C. Gonçalves and F. Margarido, Springer International Publishing, Switzerland, New York, 2015, pp. 447–499.
- 8 P. Bujak, I. Kulszewicz-Bajer, M. Zagorska, V. Maurel, I. Wielgus and A. Pron, *Chem. Soc. Rev.*, 2013, **42**, 8895–8999.
- 9 E. P. Tomlinson, M. E. Hay and B. W. Boudouris, *Macromolecules*, 2014, **47**, 6145–6158.
- 10 W. Weng, P. Chen, S. He, X. Sun and H. Peng, *Angew. Chem., Int. Ed.*, 2016, **55**, 6140–6169.
- 11 P. J. Rivero, A. Urrutia, J. Goicoechea and F. J. Arregui, *Nanoscale Res. Lett.*, 2015, **10**, 1–22.



- 12 Z. L. Wang, *ACS Nano*, 2013, 7, 9533–9557.
- 13 I. Armentano, M. Dottori, E. Fortunati, S. Mattioli and J. M. Kenny, *Polym. Degrad. Stab.*, 2010, 95, 2126–2146.
- 14 E. A. Jackson and M. A. Hillmyer, *ACS Nano*, 2010, 4, 3548–3553.
- 15 Plastics—the Facts 2016. An analysis of European plastics, production, demand and waste data. PlasticsEurope and the European Association of Plastics Recycling and Recovery Organisations. 2016. http://www.plasticseurope.org/documents/document/20161014113313-plastics_the_facts_2016_final_version.pdf accessed 27 December 2016.
- 16 P. Anastas and N. Eghbali, *Chem. Soc. Rev.*, 2010, 39, 301–312.
- 17 M. A. R. Meier, J. O. Metzger and U. S. Schubert, *Chem. Soc. Rev.*, 2007, 36, 1788–1802.
- 18 Y. Zhu, C. Romain and C. K. Williams, *Nature*, 2016, 540, 354–362.
- 19 R. A. Sheldon, *Green Chem.*, 2005, 7, 267–278.
- 20 R. A. Sheldon, *J. Mol. Catal. A: Chem.*, 2016, 422, 3–12.
- 21 D. Esposito and M. Antonietti, *Chem. Soc. Rev.*, 2015, 44, 5821–5835.
- 22 A. Gandini, T. M. Lacerda, A. J. F. Carvalho and E. Trovatti, *Chem. Rev.*, 2016, 116, 1637–1669.
- 23 J. H. Clark and A. S. Matharu, in *Issues in Environmental Science and Technology: Waste as a Resource*, ed. R. E. Hester and R. M. Harrison, Royal Society of Chemistry, 2013, 37, pp. 66–82.
- 24 T. Mekonnen, P. Mussone and D. Bressler, *Crit. Rev. Biotechnol.*, 2016, 36, 120–131.
- 25 A. Goeppert, M. Czaun, J.-P. Jones, G. K. Surya Prakash and G. A. Olah, *Chem. Soc. Rev.*, 2014, 43, 7995–8048.
- 26 R. S. Boethling, E. Sommer and D. DiFiore, *Chem. Rev.*, 2007, 107, 2207–2227.
- 27 R. A. Gross and B. Kalra, *Science*, 2002, 297, 803–807.
- 28 G. Kutney, *Sulfur: History, Technology, Applications & Industry*, ChemTec Publishing, Toronto, 2nd edn, 2013.
- 29 J. A. Ober, Materials Flow of Sulfur, Open-File Report 02–298. 2003, U.S. Department of the Interior, U.S. Geological Survey. <https://pubs.usgs.gov/of/2002/of02-298/> accessed 27 December 2016.
- 30 E. Jüngst and W. Nehb, in *Handbook of Heterogeneous Catalysis*, ed. G. Ertl, H. Knozinger, F. Schüth and J. Weitkamp, Wiley-VCH Verlag GmbH & Co. KGaA, 2008, pp. 2609–2623.
- 31 Reregistration Eligibility Document Facts: Sulfur. U.S. Environmental Protection Agency, Pesticides and Toxic Substances. May 1991. <https://archive.epa.gov/pesticides/reregistration/web/pdf/0031fact.pdf> accessed 27 December 2016.
- 32 B. P. Kolodji, *Process Saf. Prog.*, 1993, 12, 127–131.
- 33 Mineral Commodity Summaries 2016. U.S. Department of the Interior, U.S. Geological Survey, 2016, 165–166. <https://minerals.usgs.gov/minerals/pubs/mcs/> accessed 27 December 2016.
- 34 *Rubber Basics*, ed. R. B. Simpson, Rapra Technology Ltd., Shawbury, UK, 2002.
- 35 R. Mayer, in *Organic Chemistry of Sulfur*, ed. S. Oae, Plenum Press, New York, 1977, pp. 33–69.
- 36 K. Wang, M. Groom, R. Sheridan, S. Zhang and E. Block, *J. Sulfur Chem.*, 2013, 34, 55–66.
- 37 O. Illa, M. Namutebi, C. Saha, M. Ostovar, C. C. Chen, M. F. Haddow, S. Nocquet-Thibault, M. Lusi, E. M. McGarrigle and V. K. Aggarwal, *J. Am. Chem. Soc.*, 2013, 135, 11951–11966.
- 38 J. J. Griebel, R. S. Glass, K. Char and J. Pyun, *Prog. Polym. Sci.*, 2016, 58, 90–125.
- 39 J. Lim, J. Pyun and K. Char, *Angew. Chem., Int. Ed.*, 2015, 54, 3249–3258.
- 40 A. Hoefling and P. Theato, *Nachr. Chem.*, 2016, 64, 9–12.
- 41 D. A. Boyd, *Angew. Chem., Int. Ed.*, 2016, 55, 15486–15502.
- 42 Here, we refer to polysulfides as materials that contain multiple stretches of sulfur atoms linked together through S–S bonds. We also take this definition to include materials where non-sulfur cross-linkers covalently connect networks of [S]*n* of various rank, where *n* ≥ 2. The key feature of polysulfide co-polymers in this context is the presence of multiple sulfur atoms that link together organic co-monomers.
- 43 B. Meyer, *Chem. Rev.*, 1976, 76, 367–388.
- 44 S. J. Kennedy, J. C. Wheeler, C. Osuch and E. Wasserman, *J. Phys. Chem.*, 1983, 87, 3961–3966.
- 45 W. J. Chung, J. J. Griebel, E. T. Kim, H. Yoon, A. G. Simmonds, H. J. Ji, P. T. Dirlam, R. S. Glass, J. J. Wie, N. A. Nguyen, B. W. Guralnick, J. Park, Á. Somogyi, P. Theato, M. E. Mackay, Y.-E. Sung, K. Char and J. Pyun, *Nat. Chem.*, 2013, 5, 518–524.
- 46 Y. Zhang, J. J. Griebel, P. T. Dirlam, N. A. Nguyen, R. S. Glass, M. E. Mackay, K. Char and J. Pyun, *J. Polym. Sci., Part A: Polym. Chem.*, 2016, 55, 107–116.
- 47 A. G. Simmonds, J. J. Griebel, J. Park, K. R. Kim, W. J. Chung, V. P. Oleshko, J. Kim, E. T. Kim, R. S. Glass, C. L. Soles, Y.-E. Sung, K. Char and J. Pyun, *ACS Macro Lett.*, 2014, 3, 229–232.
- 48 P. T. Dirlam, A. G. Simmonds, R. C. Shallcross, K. J. Arrington, W. J. Chung, J. J. Griebel, L. J. Hill, R. S. Glass, K. Char and J. Pyun, *ACS Macro Lett.*, 2015, 4, 111–114.
- 49 J. J. Griebel, G. Li, R. S. Glass, K. Char and J. Pyun, *J. Polym. Sci., Part A: Polym. Chem.*, 2015, 53, 173–177.
- 50 V. P. Oleshko, J. Kim, J. L. Schaefer, S. D. Hudson, C. L. Soles, A. G. Simmonds, J. J. Griebel, R. S. Glass, K. Char and J. Pyun, *MRS Commun.*, 2015, 5, 353–364.
- 51 P. T. Dirlam, J. Park, A. G. Simmonds, K. Domanik, C. B. Arrington, J. L. Schaefer, V. P. Oleshko, T. S. Kleine, K. Char, R. S. Glass, C. L. Soles, C. Kim, N. Pinna, Y.-E. Sung and J. Pyun, *ACS Appl. Mater. Interfaces*, 2016, 8, 13437–13448.
- 52 J. J. Griebel, S. Namnabat, E. T. Kim, R. Himmelhuber, D. H. Moronta, W. J. Chung, A. G. Simmonds, K.-J. Kim, J. van der Laan, N. A. Nguyen, E. L. Dereniak, M. E. Mackay, K. Char, R. S. Glass, R. A. Norwood and J. Pyun, *Adv. Mater.*, 2014, 26, 3014–3018.



- 53 J. J. Griebel, N. A. Nguyen, S. Namnabat, L. E. Anderson, R. S. Glass, R. A. Norwood, M. E. Mackay, K. Char and J. Pyun, *ACS Macro Lett.*, 2015, **4**, 862–866.
- 54 T. S. Kleine, N. A. Nguyen, L. E. Anderson, S. Namnabat, E. A. LaVilla, S. A. Showghi, P. T. Dirlam, C. B. Arrington, M. S. Manchester, J. Schwiegerling, R. S. Glass, K. Char, R. A. Norwood, M. E. Mackay and J. Pyun, *ACS Macro Lett.*, 2016, **5**, 1152–1156.
- 55 J. J. Griebel, N. A. Nguyen, A. V. Astashkin, R. S. Glass, M. E. MacKay, K. Char and J. Pyun, *ACS Macro Lett.*, 2014, **3**, 1258–1261.
- 56 M. K. Salman, B. Karabay, L. C. Karabay and A. Cihaner, *J. Appl. Polym. Sci.*, 2016, **133**, 43655.
- 57 M. Arslan, B. Kiskan, E. C. Cengiz, R. Demir-Cakan and Y. Yagci, *Eur. Polym. J.*, 2016, **80**, 70–77.
- 58 I. Gomez, D. Mecerreyes, J. A. Blazquez, O. Leonet, H. Ben Youcef, C. Li, J. L. Gómez-Cámer, O. Bundarchuk and L. Rodriguez-Martinez, *J. Power Sources*, 2016, **329**, 72–78.
- 59 T. R. Martin, K. A. Mazzio, H. W. Hillhouse and C. K. Luscombe, *Chem. Commun.*, 2015, **51**, 11244–11247.
- 60 W. J. Chung, A. G. Simmonds, J. J. Griebel, E. T. Kim, H. S. Suh, I.-B. Shim, R. S. Glass, D. A. Loy, P. Theato, Y.-E. Sung, K. Char and J. Pyun, *Angew. Chem., Int. Ed.*, 2011, **50**, 11409–11412.
- 61 E. T. Kim, W. J. Chung, J. Lim, P. Johe, R. S. Glass, J. Pyun and K. Char, *Polym. Chem.*, 2014, **5**, 3617–3623.
- 62 B. Oschmann, J. Park, C. Kim, K. Char, Y.-E. Sung and R. Zentel, *Chem. Mater.*, 2015, **27**, 7011–7017.
- 63 A. Chang, Q. Wu, X. Du, S. Chen, J. Shen, Q. Song, J. Xie and W. Wu, *Chem. Commun.*, 2016, **52**, 4525–4528.
- 64 M. Arslan, B. Kiskan and Y. Yagci, *Macromolecules*, 2016, **49**, 767–773.
- 65 K. Itaoka, I.-T. Kim, K. Yamabuki, N. Yoshimoto and H. Tsutsumi, *J. Power Sources*, 2015, **297**, 323–328.
- 66 K. Yamabuki, K. Itaoka, I.-t. Kim, N. Yoshimoto and H. Tsutsumi, *Polymer*, 2016, **91**, 1–6.
- 67 Z. Sun, M. Xiao, S. Wang, D. Han, S. Song, G. Chen and Y. Meng, *J. Mater. Chem. A*, 2014, **2**, 9280–9286.
- 68 P. T. Dirlam, A. G. Simmonds, T. S. Kleine, N. A. Nguyen, L. E. Anderson, A. O. Klever, A. Florian, P. J. Costanzo, P. Theato, M. E. Mackay, R. S. Glass, K. Char and J. Pyun, *RSC Adv.*, 2015, **5**, 24718–24722.
- 69 H. Kim, J. Lee, H. Ahn, O. Kim and M. J. Park, *Nat. Commun.*, 2015, **6**, 7278.
- 70 S. H. Je, T. H. Hwang, S. N. Talapaneni, O. Buyukcakir, H. J. Kim, J.-S. Yu, S.-G. Woo, M. C. Jang, B. K. Son, A. Coskun and J. W. Choi, *ACS Energy Lett.*, 2016, **1**, 566–572.
- 71 S. N. Talapaneni, T. H. Hwang, S. H. Je, O. Buyukcakir, J. W. Choi and A. Coskun, *Angew. Chem., Int. Ed.*, 2016, **55**, 3106–3111.
- 72 M. P. Crockett, A. M. Evans, M. J. H. Worthington, I. S. Albuquerque, A. D. Slattery, C. T. Gibson, J. A. Campbell, D. A. Lewis, G. J. L. Bernardes and J. M. Chalker, *Angew. Chem., Int. Ed.*, 2016, **55**, 1714–1718.
- 73 I. Gomez, O. Leonet, J. Alberto Blazquez and D. Mecerreyes, *ChemSusChem*, 2016, **9**, 3419–3425.
- 74 D. J. Parker, H. A. Jones, S. Petcher, L. Cervini, J. M. Griffin, R. Akhtar and T. Hasell, *J. Mater. Chem. A*, 2017, DOI: 10.1039/C6TA09862B, in press.
- 75 C. Fu, G. Li, J. Zhang, B. Cornejo, S. S. Piao, K. N. Bozhilov, R. C. Haddon and J. Guo, *ACS Energy Lett.*, 2016, **1**, 115–120.
- 76 A. Hoefling, Y. J. Lee and P. Theato, *Macromol. Chem. Phys.*, 2017, **218**, 1600303.
- 77 S. Shukla, A. Ghosh, P. K. Roy, S. Mitra and B. Lochab, *Polymer*, 2016, **99**, 349–357.
- 78 A. Ghosh, S. Shukla, G. S. Khosla, B. Lochab and S. Mitra, *Sci. Rep.*, 2016, **6**, 25207.
- 79 R. J. Braddock, *Handbook of Citrus By-Products and Processing Technology*, Wiley, New York, 1999.
- 80 K. C. Nicolaou, P. G. Bulger and D. Sarlah, *Angew. Chem., Int. Ed.*, 2005, **44**, 4442–4489.
- 81 C. Torborg and M. Beller, *Adv. Synth. Catal.*, 2009, **351**, 3027–3043.
- 82 C. Barbante, A. Veysseyre, C. Ferrari, K. van de Velde, C. Morel, G. Capodaglio, P. Cescon, G. Scarponi and C. Boutron, *Environ. Sci. Technol.*, 2001, **35**, 835–839.
- 83 Global Mercury Assessment 2013. Sources, Emissions, Releases and Environmental Transport. United Nations Environment Programme, Chemicals Branch, Geneva, Switzerland, 2013. accessed 24 Oct 2016 from <http://www.unep.org/PDF/PressReleases/GlobalMercuryAssessment2013.pdf>.
- 84 P. B. Tchounwou, W. K. Ayensu, N. Ninashvili and D. Sutton, *Environ. Toxicol.*, 2003, **18**, 149–175.
- 85 T. Hasell, D. J. Parker, H. A. Jones, T. McAllister and S. M. Howdle, *Chem. Commun.*, 2016, **52**, 5383–5386.
- 86 A. Greiner and J. H. Wendorff, *Angew. Chem., Int. Ed.*, 2007, **46**, 5670–5703.
- 87 S. Agarwal, A. Greiner and J. H. Wendorff, *Adv. Funct. Mater.*, 2009, **19**, 2863–2879.
- 88 M. W. Thielke, L. A. Bultema, D. D. Brauer, B. Richter, M. Fischer and P. Theato, *Polymers*, 2016, **8**, 266.
- 89 J. C. Bear, J. D. McGettrick, I. P. Parkin, C. W. Dunnill and T. Hasell, *Microporous Mesoporous Mater.*, 2016, **232**, 189–195.
- 90 M. E. Davis, *Nature*, 2002, **417**, 813–821.
- 91 K. M. Steel and W. J. Koros, *Carbon*, 2003, **2003**, 253–266.
- 92 Y.-S. Bae and R. Q. Snurr, *Angew. Chem., Int. Ed.*, 2011, **50**, 11586–11596.
- 93 P. Nugent, Y. Belmabkhout, S. D. Burd, A. J. Cairns, R. Luebke, K. Forrest, T. Pham, S. Ma, B. Space, L. Wojtas, M. Eddaoudi and M. J. Zaworotko, *Nature*, 2013, **495**, 80–84.
- 94 M. O. Adebajo, R. L. Frost, J. T. Klopogge, O. Carmody and S. Kokot, *J. Porous Mater.*, 2003, **10**, 159–170.



- 95 J. M. Dias, M. C. M. Alvim-Ferraz, M. F. Almeida, J. Rivera-Utrilla and M. Sánchez-Polo, *J. Environ. Manage.*, 2007, **85**, 833–846.
- 96 M. Hartmann, S. Kullmann and H. Keller, *J. Mater. Chem.*, 2010, **20**, 9002–9017.
- 97 M. A. Shannon, P. W. Bohn, M. Elimelech, J. G. Georgiadis, B. J. Mariñas and A. M. Mayes, *Nature*, 2008, **452**, 301–310.
- 98 S. Chu and A. Majumdar, *Nature*, 2012, **488**, 294–303.
- 99 M. Armand and J.-M. Tarascon, *Nature*, 2008, **451**, 652–657.
- 100 P. Liu, J. M. Gardner and L. Kloo, *Chem. Commun.*, 2015, **51**, 14660–14662.
- 101 S. Zhuo, Y. Huang, C. Liu, H. Wang and B. Zhang, *Chem. Commun.*, 2014, **50**, 11208–11210.
- 102 A. Manthiram, Y. Fu and Y.-S. Su, *Acc. Chem. Res.*, 2013, **46**, 1125–1134.
- 103 J. W. Choi and D. Aurbach, *Nat. Rev. Mater.*, 2016, **1**, 16013.
- 104 J. C. Bear, W. J. Peveler, P. D. McNaughten, I. P. Parkin, P. O'Brien and C. W. Dunnill, *Chem. Commun.*, 2015, **51**, 10467–10470.
- 105 B. Ding, Z. Chang, G. Xu, P. Nie, J. Wang, J. Pan, H. Dou and X. Zhang, *ACS Appl. Mater. Interfaces*, 2015, **7**, 11165–11171.
- 106 J. Li, L. Yang, S. Yang and J. Y. Lee, *Adv. Energy Mater.*, 2015, **5**, 1501808.
- 107 Y. Wei, X. Li, Z. Xu, H. Sun, Y. Zheng, L. Peng, Z. Liu, C. Gao and M. Gao, *Polym. Chem.*, 2015, **6**, 973–982.
- 108 C. Almeida, H. Costa, P. Kadhivel, A. M. Queiroz, R. C. S. Dias and M. R. P. F. N. Costa, *J. Appl. Polym. Sci.*, 2016, **133**, 43993.
- 109 B. Li, S. Li, J. Xu and S. Yang, *Energy Environ. Sci.*, 2016, **9**, 2025–2030.
- 110 J. Lim, U. Jung, W. T. Joe, E. T. Kim, J. Pyun and K. Char, *Macromol. Rapid Commun.*, 2015, **36**, 1103–1107.
- 111 S. Yu, H. Kwon, H. R. Noh, B.-I. Park, N. K. Park, H.-J. Choi, S.-C. Choi and G. D. Kim, *RSC Adv.*, 2015, **5**, 36030–36035.
- 112 S. P. Nalawade, F. Picchioni and L. P. B. M. Janssen, *Prog. Polym. Sci.*, 2006, **31**, 19–43.
- 113 A. A. Shah, F. Hasan, A. Hameed and S. Ahmed, *Biotechnol. Adv.*, 2008, **26**, 246–265.



2. POLYSULFIDE SYNTHESIS

Acknowledgements

Renata Kucera for performing forming a selection of experiments in this chapter (as detailed in the experimental section) as part of an undergraduate research project.

Louisa Esdaile for developing and optimising the up-scaling of polymer synthesis.

Christopher Gibson for Raman spectromicroscopy.

Alexander Sibley for Auger and XPS spectroscopy.

Jonathan Campbell for DMA analysis and instrument training.

Inês Albuquerque for toxicology studies of the polysulfide.

Jason Young for GPC training.

Synthesis and characterisation of a canola oil polysulfide

Sulfur-Limonene Polysulfide, useful as it was at demonstrating the capability of sulfur polymers to capture mercury, unfortunately required further processing to develop it into a useful device¹. The first goal in this project was to develop a material to overcome its shortcomings, including the strong odour and tendency to flow at room temperature. A sorbent that can be prepared in a solid form in a single step would be desirable. We theorised that vegetable oil triglycerides would make a suitable substitution for limonene as the fatty acid chains, though non-homogenous, could contain multiple points of unsaturation and the mobility to position favourably to bond to multiple sulfur chains. Our sulfur-limonene synthesis protocol needed some refining to adapt to the triglyceride crosslinker, but the result was a solid brown rubber with only a slight sulfurous odour—a great result for a first attempt at a second generation of polysulfide. First 20.0 g sulfur was heated above its floor temperature of 159 °C, the point at which sulfur bonds begin to cleave and form thiyl radicals. This is observable as a colour change from yellow to orange. If left above this temperature without interference the colour will continue to change to red and the sulfur will solidify, this indicates bonding of radical sulfur chains and formation of polymeric sulfur. Sulfur is not stable in this form and will eventually reform S₈ however. Once orange, the temperature was raised to 180 °C and an equal mass of canola oil dripped into the molten yellow liquid with stirring over ca. 5 minutes to ensure the temperature did not drop significantly and cause sulfur to crystallise. Over the following 10 minutes, the reaction mixture changes from two phases: orange, opaque molten sulfur and clear yellow canola oil, to a single phase that moves from orange to brown and darkens further as the reaction proceeds. At the end of this time, the mixture will suddenly increase in viscosity and requires careful control of magnetic stirring to keep moving, finally vitrifying to a brown friable polymer (Fig. 2.1). The product was left at temperature for a further 10 minutes to cure and then allowed to cool to room temperature to be removed from the reaction vessel. By blending the polysulfide in a food processor for a few minutes and passing through gradation sieves, material could be isolated at different particle sizes. In case of the formation of trace H₂S, all material after blending was washed for 90 minutes in 0.1 NaOH,

followed by a wash in water. The resulting material we define as a canola oil polysulfide, sieved to a series of particle diameters: >5.0 mm (large), 2.5–5.0 mm (medium), 1.0–2.5 mm (small) and <1.0 mm (fine). We initially began synthesising canola oil polysulfide at 40.0 g quantities in round bottom flasks with magnetic stirrers but have since optimised and upscaled to batches more than 10 times greater. For the experiments that follow it should be assumed the synthesis was carried out in flasks at the lower scale, different procedures will be detailed as they become relevant and the product given a different name to differentiate the synthetic process, though the materials remain chemically identical.

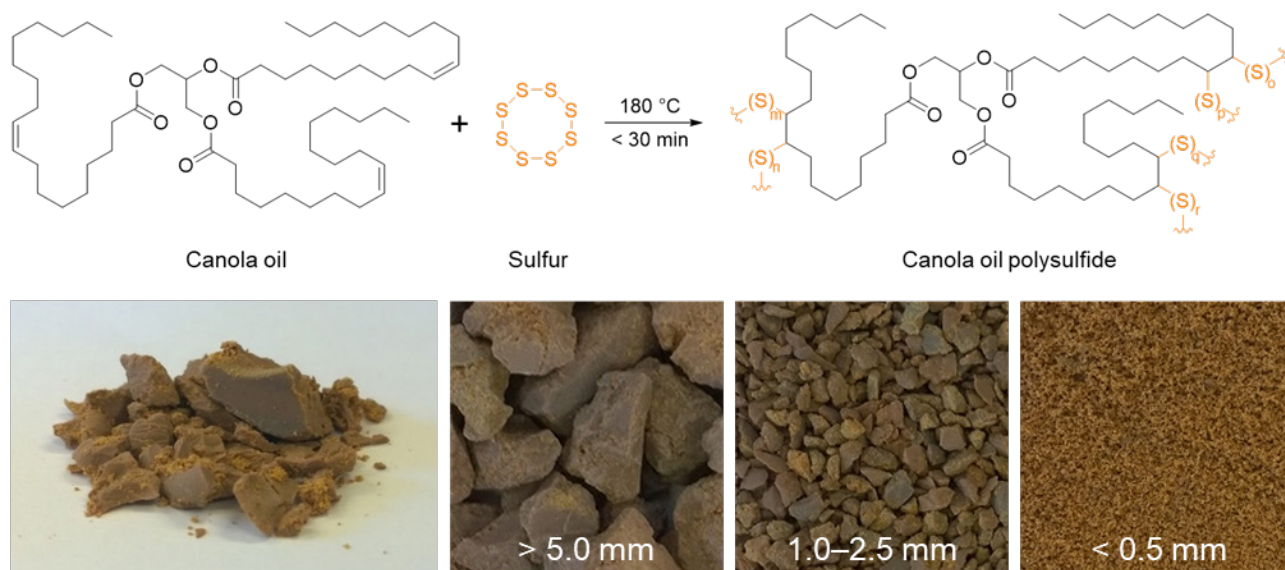


Figure 2.1 | Anticlockwise from top: Synthesis of canola oil polysulfide, simplified oleate-only triglyceride shown. Canola oil polysulfide as synthesised. Canola oil polysulfide milled to indicated particle size

Characterisation of the material was quite thorough: Scanning electron microscopy (SEM) revealed two distinct regions across the surface, amorphous polysulfide regions and microtextured crystalline regions (Fig. 2.2). Energy-dispersive X-ray spectroscopy (EDX) showed the former to contain both carbon and sulfur whereas the latter contained vastly more sulfur atoms. On the surface of the polysulfide the distribution of these two regions seemed quite even, however cutting open a particle and looking at a cross section revealed that within the polysulfide the amorphous region made up the bulk of the material and the crystalline regions of high sulfur were mostly present along the surface. Some sulfur was trapped inside, but not nearly as much as was on the outside. Auger spectroscopy of the polymer surface shows heterogenous distribution of sulfur and carbon that corroborate EDX observations (Fig. 2.2).

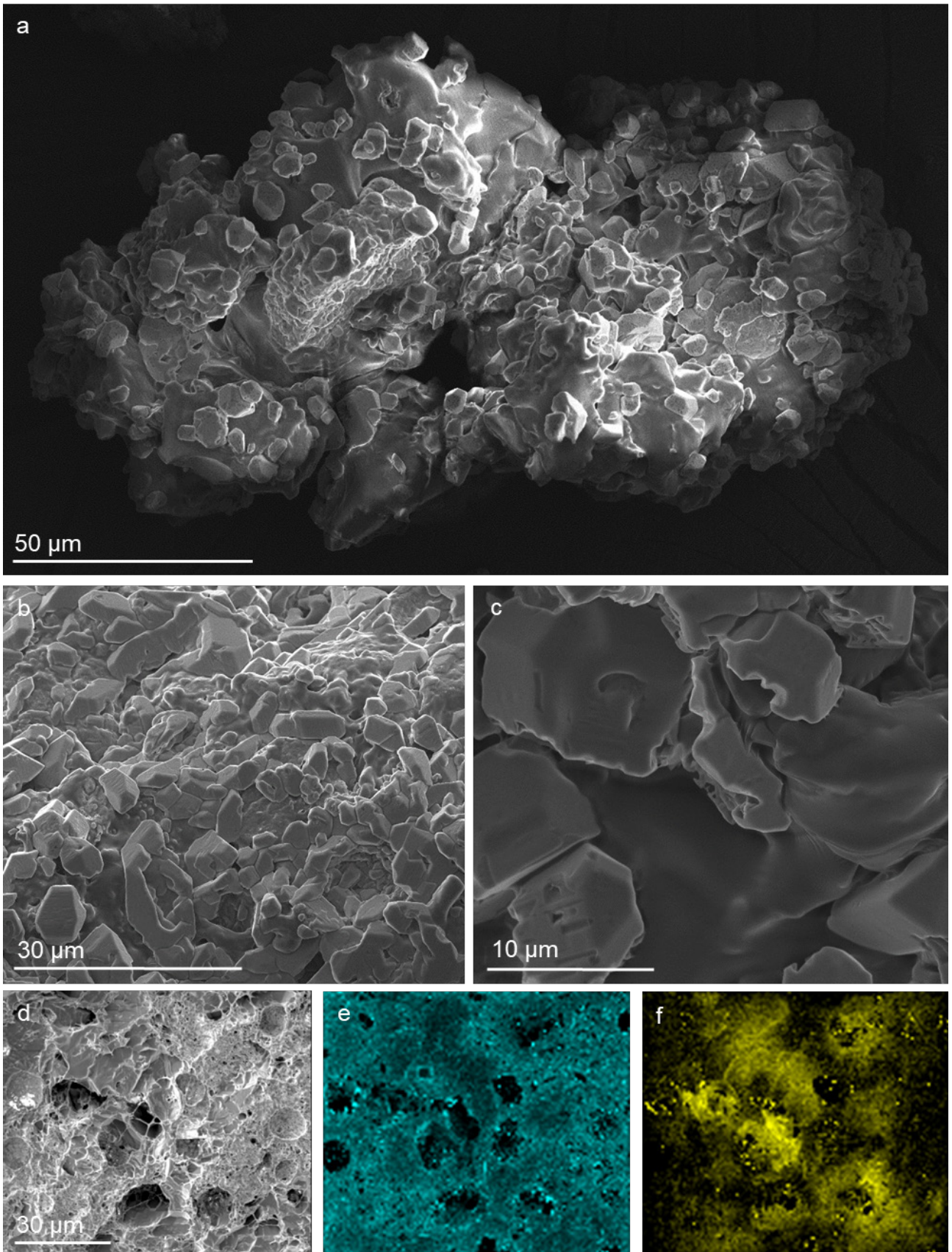


Figure 2.2 | a – c. SEM micrographs of canola oil polysulfide at increasing focus. d. SEM micrograph of polysulfide and corresponding Auger spectroscopy maps of carbon (e) and sulfur (f).

Raman analysis showed similar results. Depending on where the detector was pointed on the surface the spectra could shift between showing a spectrum near identical to orthorhombic sulfur, or a spectrum with peaks shared between sulfur and canola oil. In the spectra with more canola oil character the peaks at 450 cm^{-1} and 470 cm^{-1} see a change in peak height, with the latter diminished compared to the former and the presence of a new peak, shouldering at 505 cm^{-1} (Fig. 2.3). Other than that the sulfur seems to have reacted and its stretching modes altered, it is difficult to precisely determine what has changed in chemical structure. Perhaps the peak at 505 cm^{-1} is indicative of carbon-sulfur bonding, or perhaps the shift represents a change in sulfur rank from S_8 to a different number of sulfur atoms in crosslinked chains.

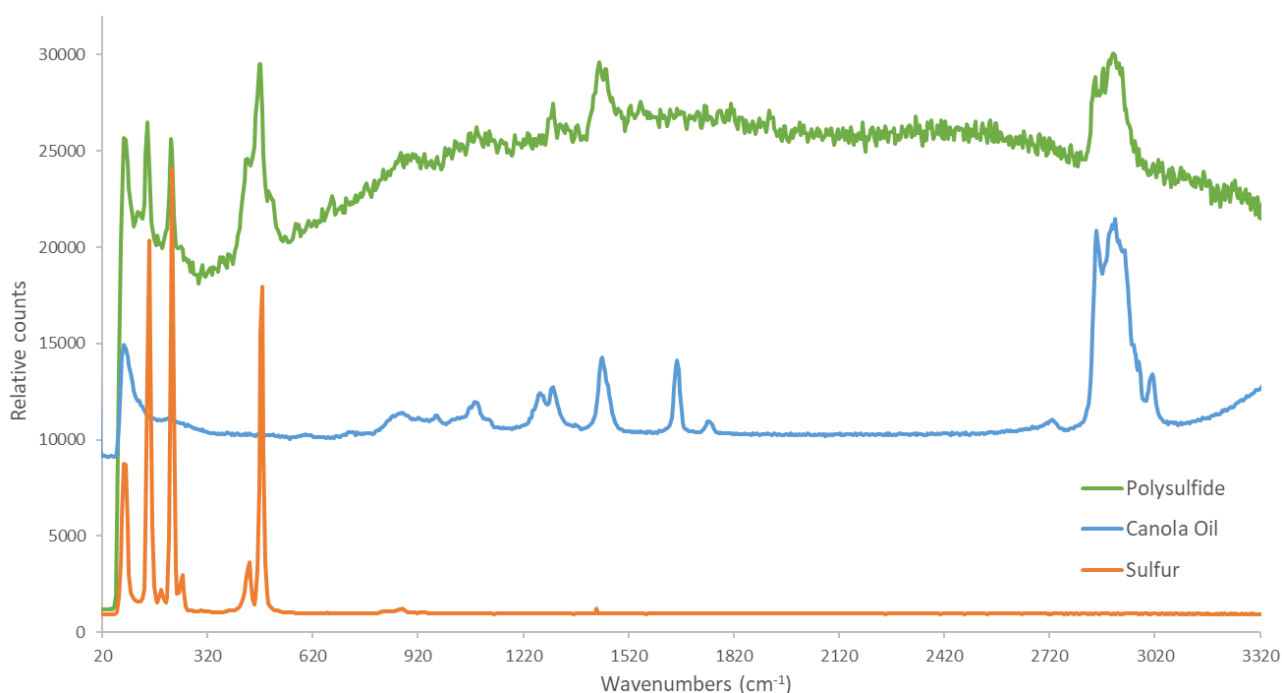


Figure 2.3 | Raman analysis of canola oil polysulfide and starting materials.

FTIR provided our earliest spectroscopic evidence of reactivity between the starting materials. A peak at 3000 cm^{-1} in canola oil was not present in the spectra after reaction, indicating consumption of the alkenes available in oleic (1), linoleic (2) and linolenic (3) fatty acid chains (Fig. 2.4). Beyond this there was very little changes in the spectra, so the triglyceride seems to remain intact throughout the process, with just the radical thiol-alkene reaction diminishing the carbon-carbon double bond stretching signal.

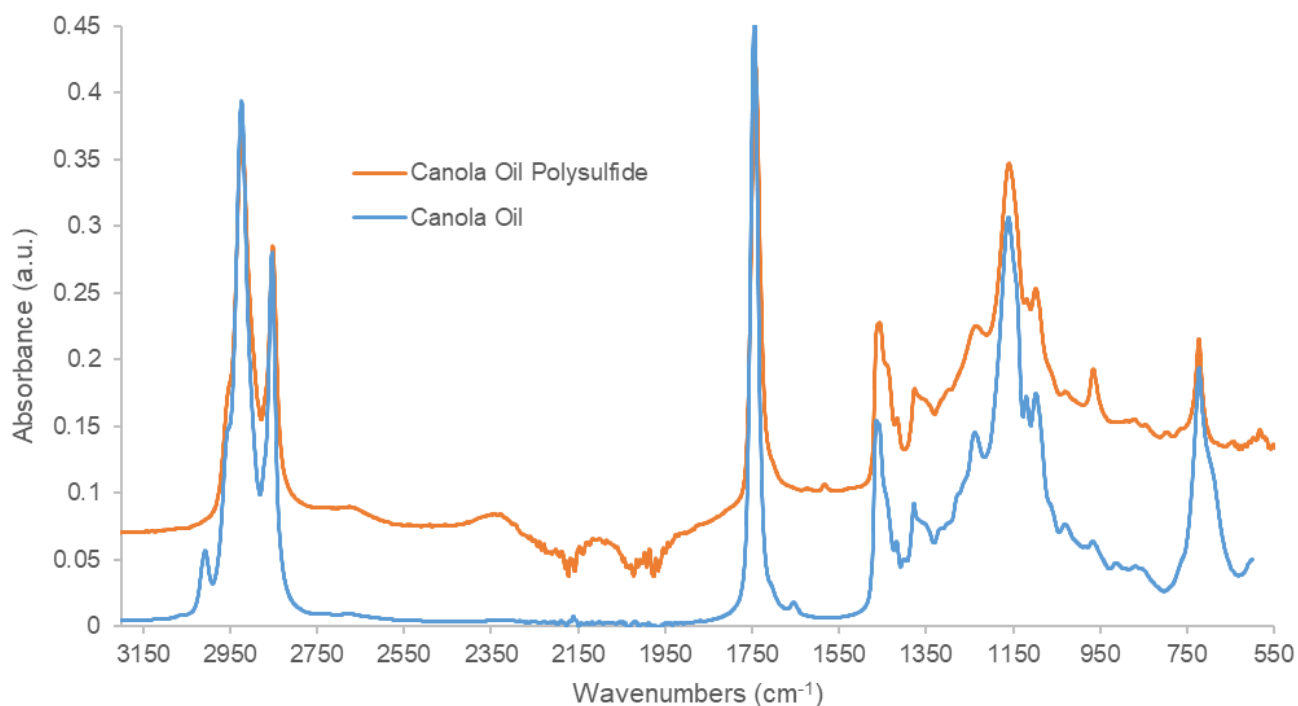


Figure 2.4 | ATR FTIR analysis of canola oil polysulfide and starting material. The alkene peak at 3000 cm^{-1} is diminished from the starting material to the polysulfide.

Thermomechanical analysis of the polysulfide began with simultaneous thermal analysis (STA): both thermal gravimetric analysis (TGA) and dynamic scanning calorimetry (DSC) data was acquired from a single instrument. Essentially the polysulfide is weighed and heated at a controlled temperature ramp and the mass change and energy required to maintain temperature recorded over time. This allows the analysis of phase changes and also sample purity. Monitoring began at $50\text{ }^{\circ}\text{C}$ and the temperature ramped to $700\text{ }^{\circ}\text{C}$ at $20\text{ }^{\circ}\text{C min}^{-1}$ under nitrogen. Over this temperature range it was observed that the polysulfide contains two forms, as it exhibited two thermal decomposition events, seen as mass losses in the TGA—first at $230\text{ }^{\circ}\text{C}$ and second at $380\text{ }^{\circ}\text{C}$ (Fig. 2.5). The first also coincides with a large endotherm in the DSC, where thermal decomposition of the polysulfide begins. STA analysis of sulfur and canola oil revealed the origin of these two decomposition steps, sulfur begins to degrade at $230\text{ }^{\circ}\text{C}$ with a mass loss onset of $290\text{ }^{\circ}\text{C}$, and canola oil $350\text{ }^{\circ}\text{C}$ with an onset of $380\text{ }^{\circ}\text{C}$. The mass losses displayed in the polysulfide essentially correspond to the sulfur and canola oil components individually, confirmed also by the fact that each loss accounts for approximately half of the analysed material and the reactant ratio used in synthesis was 1:1. Through more thorough DSC analysis made capable by the acquisition of a more accurate instrument, the glass transition temperature was determined to be $-12.2\text{ }^{\circ}\text{C}$. What this means is that below this temperature, the polysulfide is more rigid, whereas above it retains the rubbery properties observed at room temperature. Paired with the previous DSC results this affords an operating window of -12.2 to $230\text{ }^{\circ}\text{C}$ in which the polysulfide is thermally stable, below which its mechanical properties will change to become less flexible and above which it begins to degrade. Thinking forward to potential applications for the polysulfide, it can be inferred from this that anything involving water should not

pose a temperature issue. Also revealed by DSC analysis was the presence of free sulfur within the polysulfide. Utilising a 1:1 ratio of sulfur and canola oil, chosen just for simplicity and to maximise the use of both starting reagents, it appeared that though all sulfur seemed to be incorporated into the final product, some of it had not fully reacted. This was visible as a small endotherm in the DSC profile between 110 and 140 °C with a peak at 125 °C (Fig. 2.5).

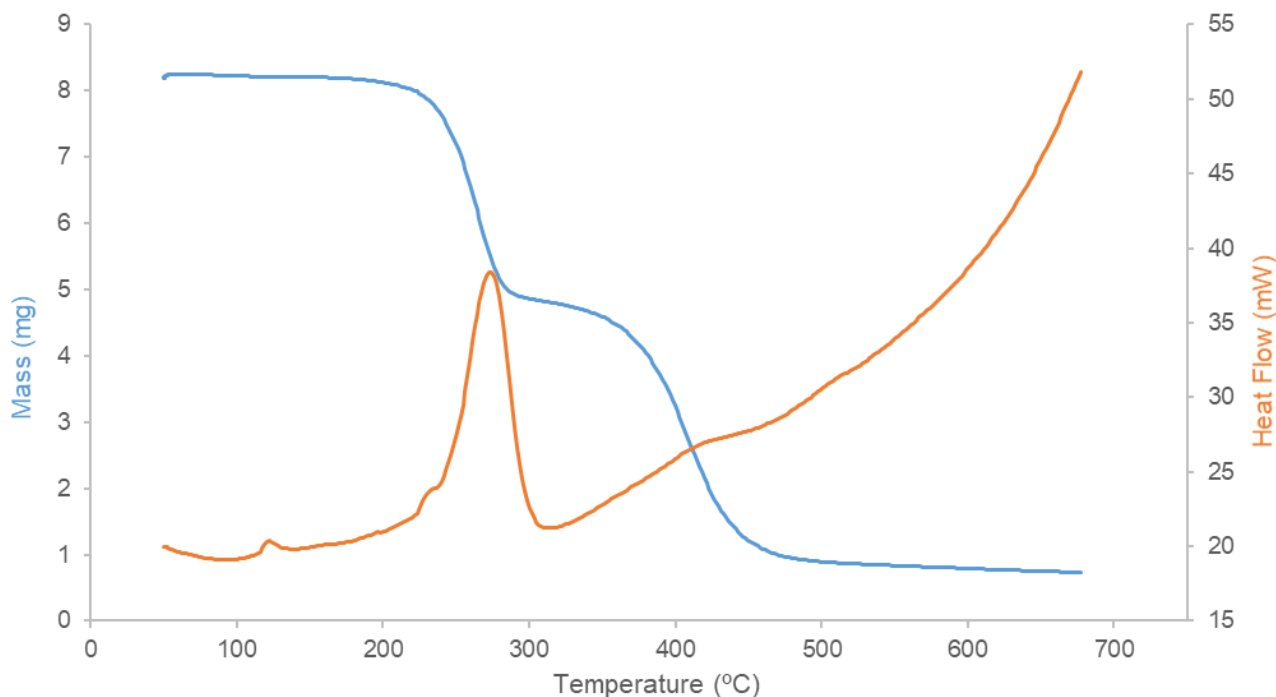


Figure 2.5 | STA analysis of canola oil polysulfide

To determine the precise amount of free sulfur, a calibration curve of sulfur mass against the energy released by its melting at ca. 125 °C was plotted. Polysulfides were prepared at different reactant ratios (30, 50, 60, and 70 wt. % sulfur) for comparison by STA (Fig. 2.6). As the amount of sulfur in the reaction increased, so too did the amount of free sulfur. Likely not just due to the increase in sulfur, but also less available triglyceride alkenes for the sulfur to bind to. Polysulfide prepared at 30 wt. % sulfur contained 3.8 % free sulfur, 50 wt. % contained 9.0 %, 60 wt. % contained 23.3 %, and 70 wt. % contained 38.1%. This data seems to correlate to an exponential relationship such that the percentage of total sulfur is proportional to the natural log of the percentage of free sulfur embedded in the polymer.

This seems to indicate that under the reaction conditions, all feed ratios tested will result in some amount of free sulfur embedded in the polymer. In order to maximise the use of both starting materials, and because many experiments that will appear in later chapters had been started using polymer of that ratio, and further for the sake of simplicity, a 1:1 ratio of sulfur and canola oil was continued with to form the polysulfide. It may be that not just the fully reacted sulfur, but the free sulfur embedded in the polysulfide may be responsible for some of the phenomena described in later chapters for example.

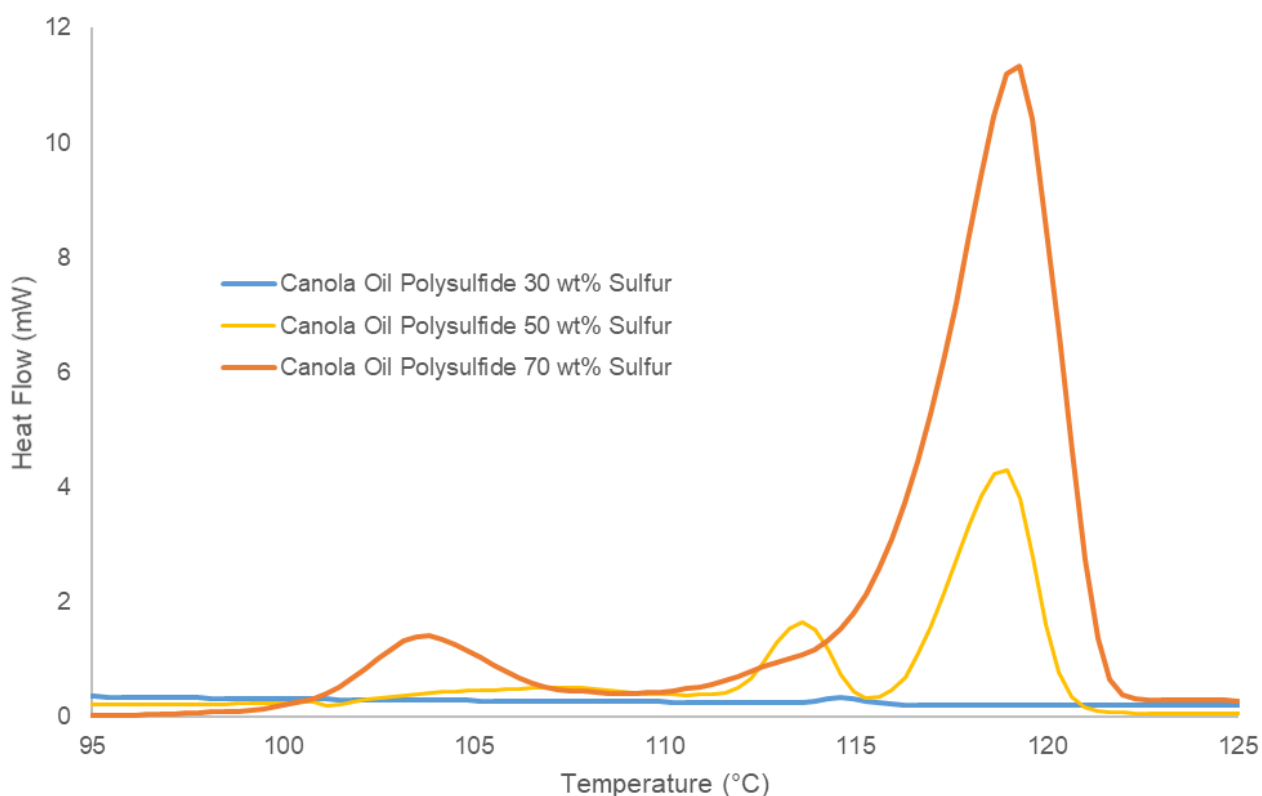


Figure 2.6 | Comparison of free sulfur by DSC of canola oil polysulfide prepared with different sulfur ratios.

On top of changing the sulfur ratio to see how it affected the material, the identity of the unsaturated fatty acids in the triglyceride was also considered. To determine if the triglyceride structure of canola oil was required to form a solid material, the vegetable oil was substituted for oleic acid. After 4 hours under the reaction conditions however, though the mixture thickened and formed one phase, no vitrification was observed. The mixture did change colour however, so the formation of short oleic acid-polysulfides seems possible. From this and other experiments varying ratios of canola oil and oleic acid compared to sulfur, it appears that the connecting of fatty acids into a triglyceride does aid in the inverse vulcanisation process by packing more reactive alkene handles into each individual molecule, resulting in increased crosslinking.

Further to this, different vegetable oils were also tested—olive and sunflower oils. Different vegetable oils contain different distributions of fatty acids among their triglycerides. To determine their composition, each oil was subject to a transesterification, and then the resulting methylated fatty acids analysed by gas chromatography-mass spectrometry (GC-MS). Each oil contained a small proportion of saturated fatty acids (stearic, palmitic, myristic), a higher proportion of monounsaturated (oleic, paullinic, palmitoleic), and then a small portion also of polyunsaturated (linoleic, linolenic). Except for the sunflower oil, which had a much greater deal of the polyunsaturated fats than the other two (Fig. 2.8). All oils were rendered into brown rubbers by the inverse vulcanisation procedure, similar to canola oil. Olive oil took the same amount of time as canola oil to vitrify, resulting in a light brown rubber after cooling, and sunflower oil with its increased alkene content from polyunsaturated fatty acids vitrified in nearly half the time to give a rubber of a

darker brown than canola oil (Fig. 2.7). In both cases a 1:1 mass ratio of sulfur and vegetable oils were used. By DSC analysis, the olive oil polysulfide contained 17.1 % free sulfur, and the sunflower oil polysulfide 15.2 %, both more than the 9.0 % of canola oil polysulfide. Increased alkene content along the same triglyceride might account for this observation: More alkenes for cross-linking results in faster cross-linking, which increases viscosity quicker and so decreases mobility and interaction opportunities, resulting in less reaction of sulfur overall.

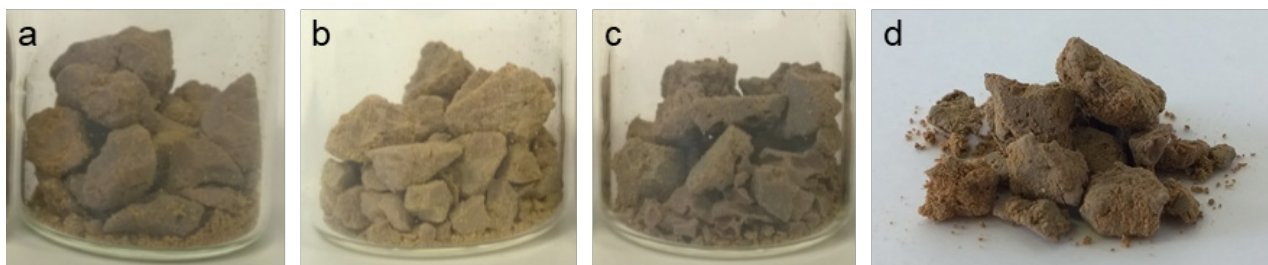


Figure 2.7 | Photograph of polysulfides prepared with different cooking oils. Canola oil (a), olive oil (b), sunflower oil (c) and waste cooking oil (d).

Also analysed and tested was a used vegetable oil sample from a campus café. This waste cooking oil, if viable as a replacement for pristine canola oil, would prove a crucial development, increasing the material's pertinence to green chemistry by deriving every atom in its structure from waste streams. Sulfur is by-product of a petroleum industry that has little use for it and is produced at a scale much greater than it is consumed by other industries, resulting in global megaton deposits. Using it in this capacity is not taking away from any other use, nor does it require the application of extraneous energy or chemicals to refine for synthesis. Analysis of the waste oil revealed a ratio very similar to sunflower oil: 53 % monounsaturated, 34 % polyunsaturated, and 13 % saturated fatty acid (Fig. 2.8). Despite this composition, the time for the material to vitrify was closer to canola oil than sunflower, perhaps due to interference by foodstuff impurities the oil was used to cook. Free sulfur was measured at 15.6 %, close to the ratio in sunflower oil polysulfide.

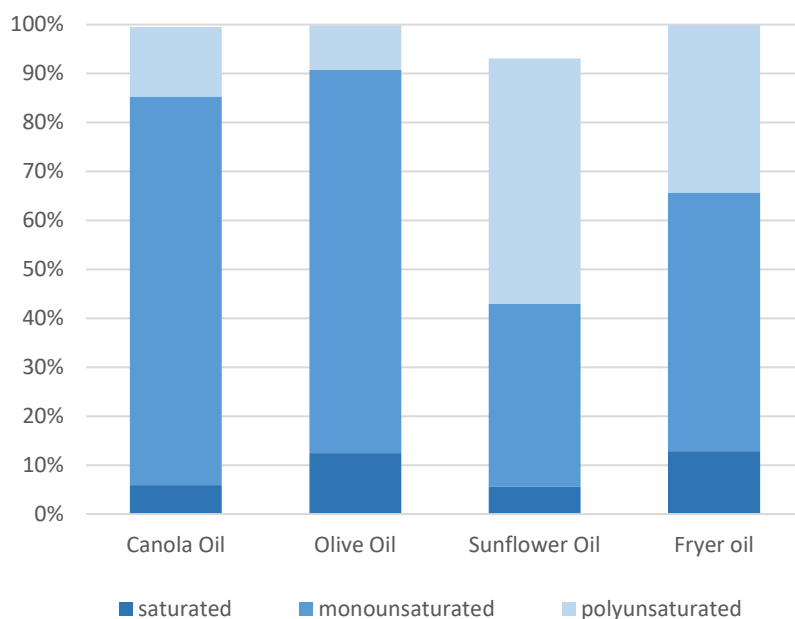


Figure 2.8 | Relative composition of cooking oils used to synthesise polysulfides.

STA analysis revealed little difference between vegetable oil polysulfides: All display two mass losses, the first at approximately 210 °C and the second at approximately 330 °C (Fig. 2.9). Each displays a similar heat flow profile with small peaks from free sulfur at 120 °C and a significant endotherm at 280 °C as the polysulfides decompose. A high-resolution scan through 100–125 °C reveals some slight differences in the free sulfur peaks however. All share a peak at 120 °C, but peaks of varying heights also appear at 106 °C and 114 °C (Fig. 2.9). This may relate simply to the packing of free sulfur within the polymer, or perhaps sulfur chains of different rank. With a faster temperature ramp these peaks all seem to be merged into one, as in the full DSC trace from 50 to 650 °C (Fig. 2.5). In determining free sulfur by DSC, the full range of peaks from 100 to 150 °C were considered.

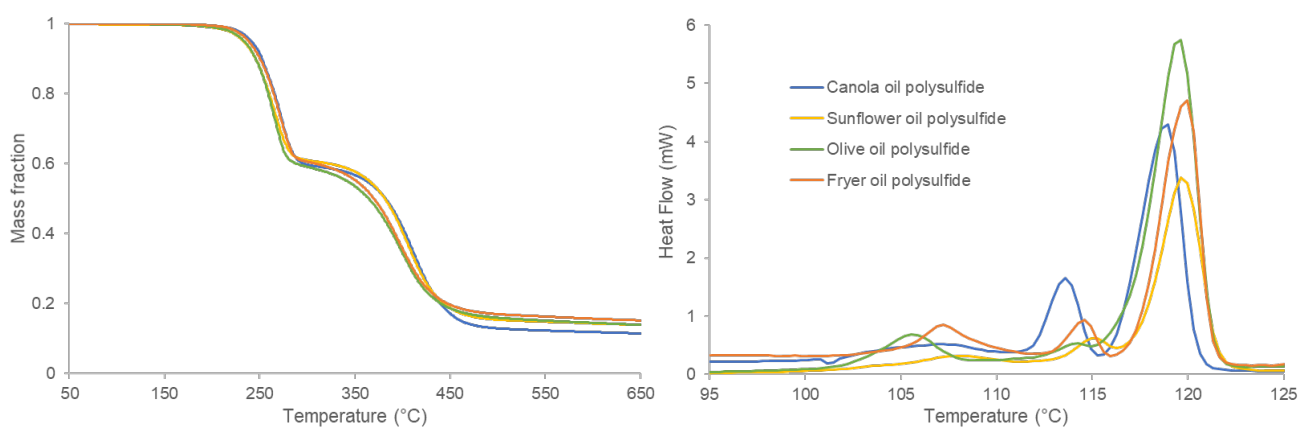


Figure 2.9 | TGA (left) and DSC (right) analysis of polysulfides prepared with different cooking oils.

It came to our attention early in the project that a material similar to canola oil polysulfide had been developed in the 1960s. Factice, produced industrially as a plasticising additive for polymer

manufacture, is formed from the vulcanisation of vegetable oil. Typically using lesser quantities of sulfur, such as 5–25 % sulfur by mass. Despite these differences in motivation however there was every chance factice could share the same properties as our canola oil polysulfide regarding the applications we were testing in, and so samples were purchased to compare. Three variants were acquired from Deutsche Oelfabrik Gesellschaft (D.O.G.): F10, F17 and F25 factices (Fig. 2.10), where the number after “F” corresponds to the targeted average percentage of sulfur in each (referred to as “sulfur grade” by D.O.G.).

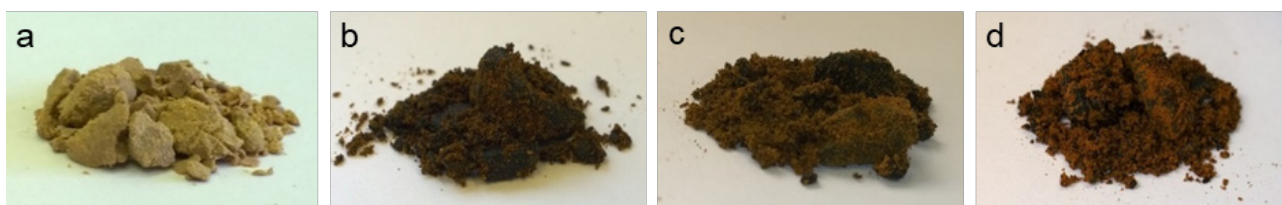


Figure 2.10 | Photographs of canola oil polysulfide (a) and F10 (b), F17 (c) and F25 (d) grade factice.

FTIR comparison to canola oil polysulfide showed identical peaks, unsurprisingly as the starting materials were the same and the synthetic procedure very similar. Raman analysis showed a decrease in sulfur signal (peaks at 432 and 470 cm^{-1}) in F25 (25 wt. % sulfur) compared to polysulfide (50 wt. % sulfur), even more so in F10 (10 wt. % sulfur). Peaks corresponding to the canola oil component however appear in all spectra unchanged, all in line with a polysulfide of lesser sulfur content. STA analysis reveals a similar trend to canola oil polysulfide – two mass losses occur separately, however two endotherms occur corresponding to both losses, rather than just the first (Fig. 2.11). It seems that in the polysulfide, this second endotherm is present (Fig. 2.11), but is simply small enough compared to the first that is masked by the baseline that tends to trend upwards sharply once all material has decomposed (Fig. 2.5). With less sulfur incorporated in factice, the first endotherm is weaker and the second becomes prominent. From this we can at least conclude that the sulfur component requires more energy per mass to decompose than the canola oil component as the latter is able to escape notice where sulfur content is significant.

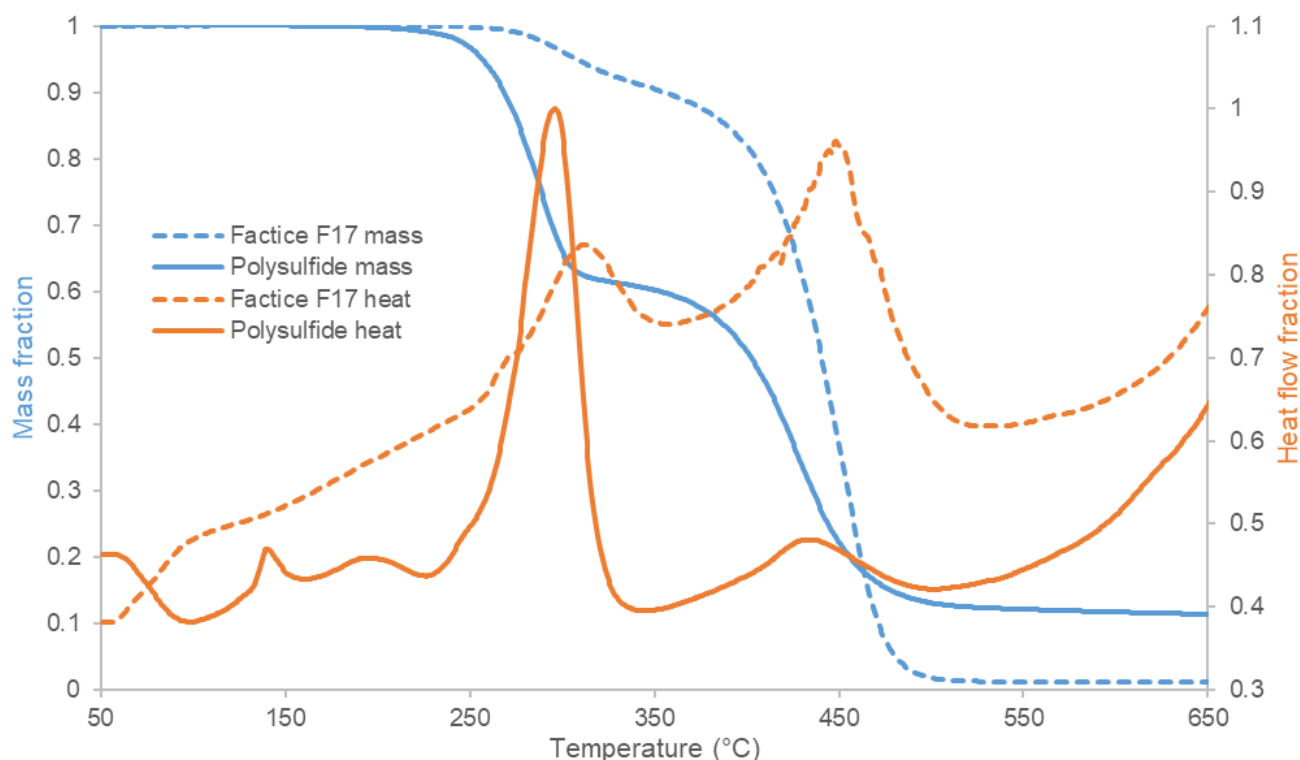


Figure 2.11 | Comparison by STA of canola oil polysulfide and F17 grade factice

To scrutinise the importance of the order of addition of reactants, that is, to see if classic or inverse vulcanisation are truly independent reactions in the context of polysulfide synthesis, polysulfide was prepared in two ways. One, following standard procedure, the other, by switching the order of addition of starting materials—canola oil was brought up to 180 °C, and then sulfur added slowly over 5 minutes. Both reactions proceeded through the formation of a single phase, then colour change through orange to brown, then vitrification to give a brown rubber. STA analysis showed no thermochemical differences between the two materials, except when focusing solely on the melting peak of free sulfur (Fig. 2.12). Classically vulcanised canola oil polysulfide exhibits a single peak at 120 °C, and inverse vulcanised two peaks: the same, with a very similar height and area at 120 °C, and a second lower intensity peak at 114 °C. By the DSC calibration for free sulfur mentioned earlier, the classically vulcanised polysulfide contained 8.8 wt. % free sulfur to the inverse vulcanised polysulfide's 9.0 wt. %, values within 0.2 % of one another. It is likely that canola oil polysulfide is not unique in this regard, as there is growing literature on the dynamic nature of S-S bonds within such polysulfides²⁻¹¹. During synthesis the scrambling of labile S-S bonds that can form, break back to radical chains and then reform occurs until crosslinking increases the viscosity, cuts mobility and forms a solid polymer.

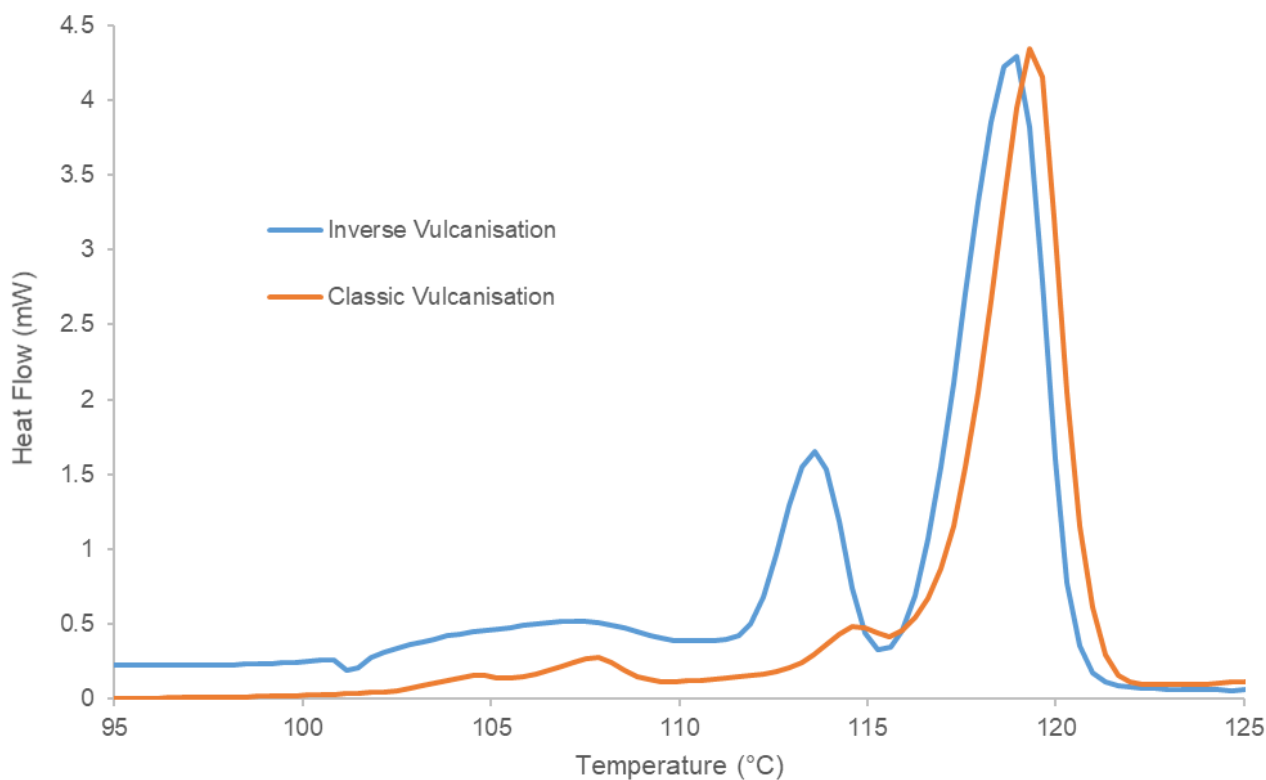


Figure 2.12 | Comparison of free sulfur by DSC of canola oil polysulfide prepared by classic or inverse vulcanisation.

Synthesis of a porous polysulfide

In 2016 and 2017, the Hassel group published works in which they took a series of inverse-vulcanised polysulfides and attempted to process them post-synthesis to enhance mercury-binding affinity¹²⁻¹⁴. One such technique was the templating of pre-polymers on a sodium chloride mould to cure mesoporous, mercury-sorbent materials. Inspired by this, we sought to simplify the process and apply it to canola oil polysulfide, to increase porosity with minimal extra steps or reagents. By simply including table salt (NaCl) in the synthesis of the polysulfide, followed by chopping and then washing with water, we were able to achieve our goal. The precise ratio of salt to include was informed by studying the product after synthesis: too much would hinder the reaction process, too little would limit pore and channel formation, without which removal of the salt would not be trivial. 70 wt. % of the reaction mixture as NaCl was found to be ideal, allowing for particles as large as 5.0 mm in diameter to be purged of salt by a simple washing step.

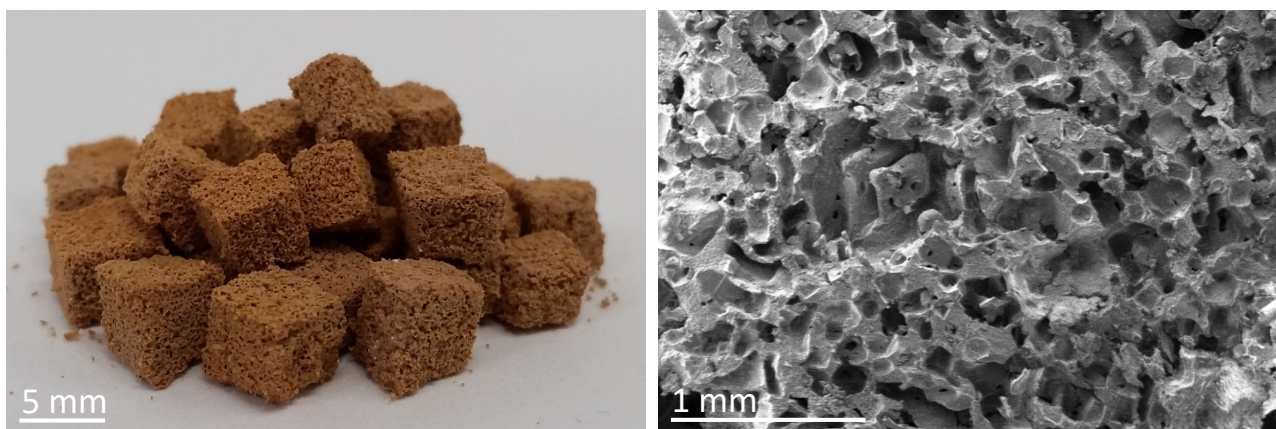


Figure 2.13 | Porous polysulfide prepared as 5.0 mm cubes (left) and an SEM micrograph of a cross-section of porous polysulfide showing pores and channels formed in synthesis (right).

Cubic NaCl crystals, ground in a mortar and pestle before use in polymer synthesis, were found to have an average side length of 289.7 microns with a standard deviation of ± 62.4 . After synthesis, pore size was measured as 119.2 ± 53.0 microns by the same method with an average distribution (distance between pores) of 57.8 ± 33.2 microns. Though in the same order of magnitude, pore diameter is less than half that of the salt template the polymer is forming around. It may be that after washing the polymer expands into this void space, or that the attrition from stirring the reaction mixture causes fracturing of the salt. More likely though is that crystals aggregate to form the larger pores and channels that are not easy to identify from a cross-section of the polysulfide and so the count is skewed towards smaller, more easily distinguishable pores. For this reason, the size of the salt crystals likely gives a more precise description of the void spaces within the polymer. Porous polysulfide density was measured by averaging that of 7 cubes with 5.0 mm sides and found to be 0.521 g/cm^3 with a standard deviation of ± 0.060 ; Purely from the difference in density measurements, with all salt washed out porous polysulfide has a theoretical void volume of 56.3 %, so has more than doubled in volume and greatly increased in surface area for the same mass of non-porous polysulfide. BET analysis for an accurate determination of surface area was attempted but unfortunately was not possible as surface area was too low for the instrument.

Thermal analysis revealed an identical DSC and TGA trace to non-porous canola oil polysulfide (Fig. 2.14), and T_g by DSC was very close at $-12.9 \text{ }^\circ\text{C}$ to the non-porous polysulfide's $-12.2 \text{ }^\circ\text{C}$.

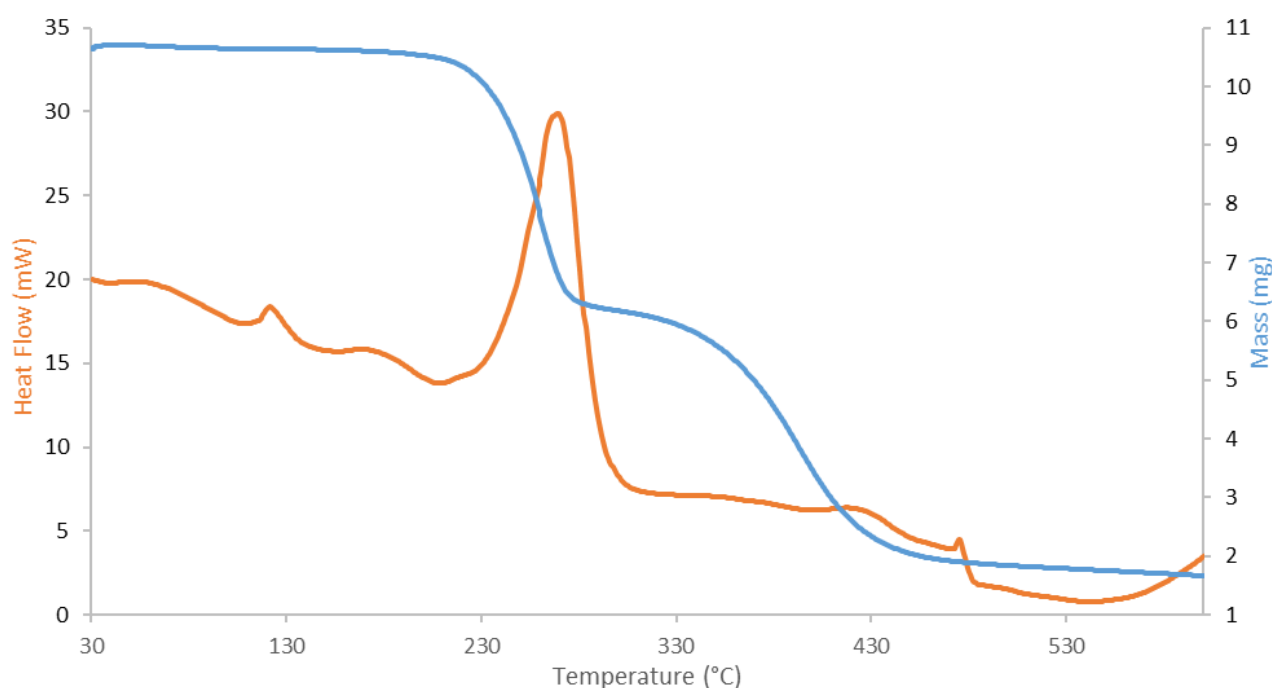


Figure 2.14 | STA analysis of porous polysulfide.

In an attempt to install thiol surface functionality, a change that might aid in mercury binding, porous polysulfide was treated with sodium borohydride to reduce sulfur-sulfur linkages. $\frac{1}{4}$ and 1 equivalent (in relation to incorporated S_8) $NaBH_4$ in methanol broke the polymer down slightly into smaller particles during the 1 hour incubation but did not result in any additional thiol functionality as tested for with Ellman's reagent. 4 molar equivalents $NaBH_4$ proved too harsh a reducing environment and caused the polysulfide particles to clump and darken in colour. A control of untreated polysulfide also showed no difference from an Ellman's control, indicating no reaction with Ellman's reagent and thus no reactive thiols present on the polysulfide's surface.

To truly exploit the abundant and inexpensive nature of canola oil polysulfide's starting materials, and to meet the needs of the applications we were discovering (see later chapters), it became evident we would need to significantly up-scale production. With the use of an overhead mechanical stirrer, we were able to accommodate and process a 2.5 kg reaction mixture in a 4.7 L steel vessel, for a yield of 750 g porous or "low density" polysulfide (full procedure in experimental section). To efficiently break this much material into smaller chunks a meat grinder was used, however the particle sizes achieved by this method were smaller than with the previous methods (0.5 to 3 mm, where our first synthesis afforded 0.2 to 12 mm particles and we aimed for a maximum 5 mm to aid with salt washing for the porous synthesis). Under SEM, porosity of these new particles was not immediately evident in the same way it was for larger particles produced by previous methods. For this reason, it seemed prudent to classify this product slightly differently, as we were not explicitly producing larger particles with high porosity but were breaking these particles down further into a low density powder. As with the porous polysulfide before it, thermal analysis showed an STA trace identical to the original, non-porous canola oil polysulfide.



Figure 2.15 | Illustrative diagram of porous and low-density polysulfide synthesis.

Pyridine was the only solvent able to dissolve the polysulfide, and even then, it is not clear if what is occurring is solvation or a chemical reaction to break down the polymer¹⁵. When canola oil polysulfide is submerged in pyridine, the solvent begins to change colour from clear to a cloudy brown as the polymer falls apart and dissolves. Often a yellow powder remains, sunken in solution. Initially it was thought that perhaps this was elemental sulfur, either free sulfur trapped within the polysulfide or released by a reaction to break it down. Collection and analysis by STA however confirmed this to just be canola oil polysulfide still, undissolved and broken down to a fine powder. Allowing the solvent to evaporate and drying the product results in reformation and recovery of the polymer. A proposed mechanism for the reaction of pyridine with the polysulfide is offered in Fig. 2.16. This allows for interesting applications in drop-casting of polymer coatings that will be explored in later chapters. As it is the only way to solvate the polymer, pyridine was the solvent used to obtain information where liquid samples were required.

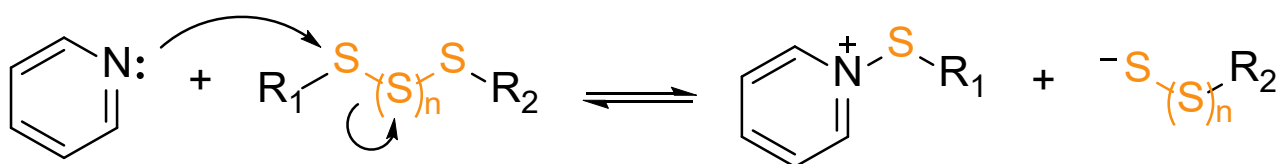


Figure 2.16 | Proposed mechanism for the reversible reaction of canola oil polysulfide with pyridine. A simplified structure of the polysulfide is shown where R groups correspond to the alkyl components of the polymer bonded to sulfur and $n \geq 1$ such that the minimum sulfur rank is 3. The reaction products dissolve in pyridine giving the appearance that the polysulfide itself dissolves in the solvent. The reaction is reversible in that evaporation of pyridine produces a modified canola oil polysulfide in which the sulfur-sulfur bonds have been scrambled.

In understanding the mechanism of synthesis several questions still need answering: How much of the sulfur is consumed? How long are the sulfur chains? Are they all the same length or are they present as a distribution? Also, to what extent are the canola oil molecules incorporated—are all points of unsaturation fully reacted or do some remain? The latter of these is the simplest to answer with NMR spectroscopy, as we are dealing with the monitoring of organic components. Fig. 2.17 contains the ^1H NMR spectra of canola oil and canola oil polysulfide, with integration of the alkene protons and fatty acid CH_3 end-groups shown. Over the course of the reaction, the alkene signal is diminished by 87 %, corresponding to an equal percentage consumption of alkene. For the other questions, the answer is not so simple to elucidate spectroscopically. An average sulfur rank can be determined theoretically if we assume full reactivity: At an equal mass ratio of sulfur to oil, canola oil polysulfide contains 8.42 sulfurs per alkene, olive contains 9.41 and sunflower 5.79. If we remove from the equation the sulfur that did not react (determined as free sulfur previously by DSC) and also the alkenes that did not react (determined just above by NMR), this estimate increases to an average of 8.81 sulfur atoms in each sulfur chain in canola oil polysulfide.

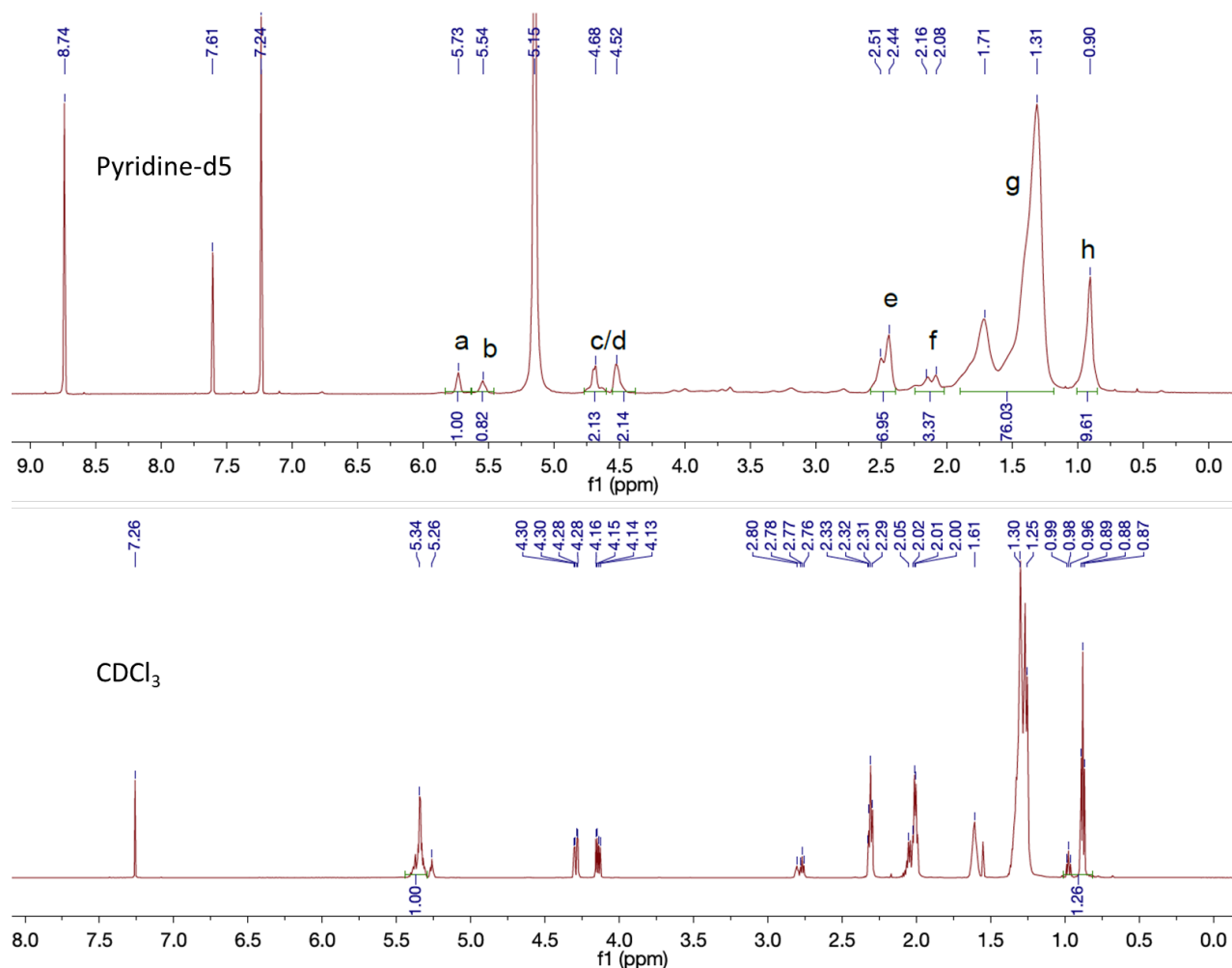
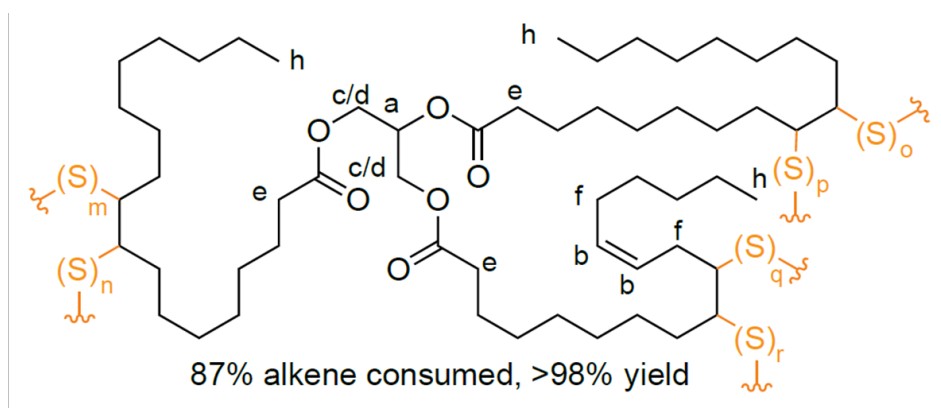


Figure 2.17 | ¹H NMR spectra of canola oil polysulfide with assignments (top) and canola oil (bottom)

Important for polymer analysis also is its molecular weight, obtainable usually by gel permeation chromatography (GPC). Canola oil polysulfide was dissolved in pyridine then diluted with THF to a solvent mix of 95% THF, 5% pyridine for a concentration of 3 mg mL⁻¹ polysulfide. The mobile phase for the experiment was the same solvent mixture: 95 % THF, 5 % pyridine. Compared to polystyrene standards prepared in the same solvent and to the same concentration, GPC revealed a very broad molecular weight distribution with two distinct peaks. The stretch runs through a polystyrene-equivalent weight average range of approximately 19,700 g mol⁻¹ down to approximately 800 g mol⁻¹, with peaks at 5,010 and 1,350 g mol⁻¹. GPC comparison is commonly made to linear polystyrene

standards; however, the canola oil polysulfide is likely not a linear molecule and so the molecular weight is only apparent and relative to polystyrene, not absolute. For comparison, canola oil was also dissolved in the same solvent mixture and analysed by GPC, eluting at a time corresponding to $1,362 \text{ g mol}^{-1}$. The canola oil used in polymer synthesis has an average molecular weight of 877.7 g mol^{-1} determined by addition of GC-MS fragments, 65% of the reported value. Depending on how canola oil polysulfide travels through the column, this could make the molecular weight quite different. Lacking known polysulfide GPC standards however, a polystyrene reference is the best available alternative.

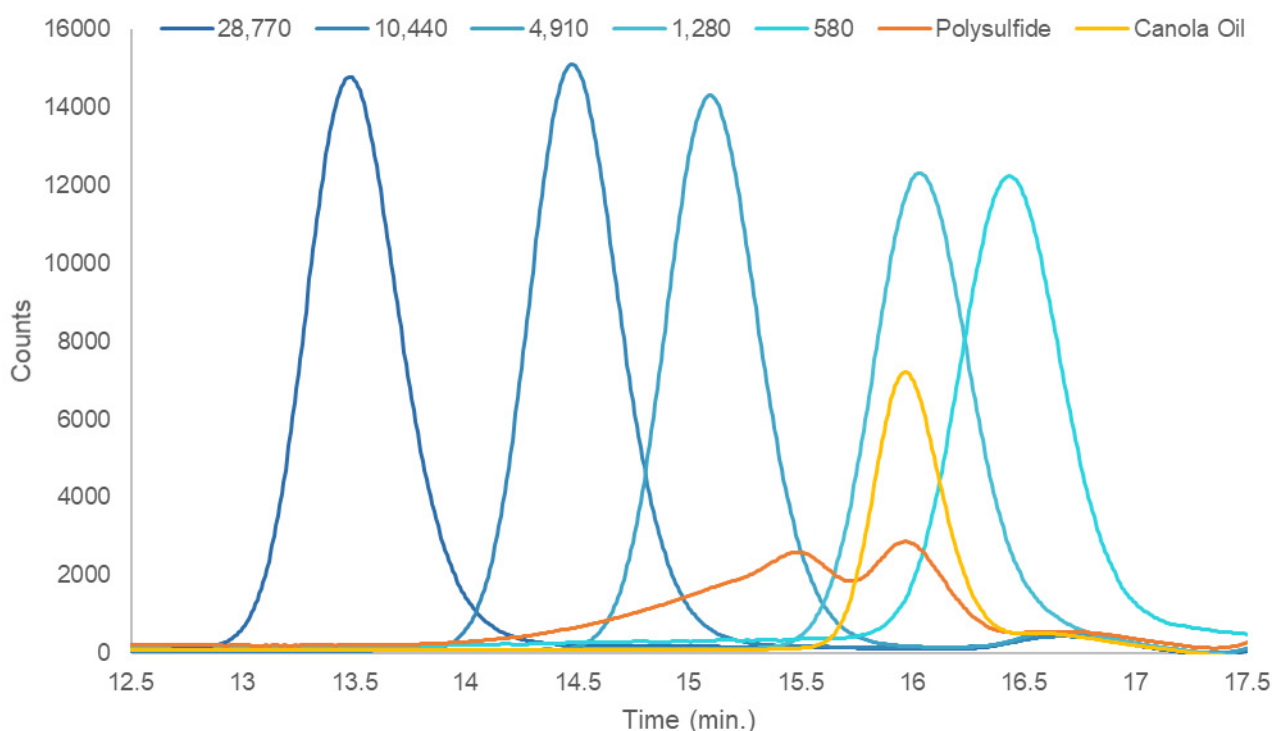


Figure 2.18 | GPC analysis of canola oil polysulfide (low density) and starting material. Spectra of relevant polystyrene standards (molecular weight in legend) are included for comparison.

By definition a fully crosslinked thermoset polymer should have an infinite molecular weight, as such these GPC results would indicate that canola oil polysulfide simply isn't fully crosslinked. This may be true, or it may be that the material analysed is not truly the polysulfide, but the result of the reaction of canola oil polysulfide with pyridine. It is likely the pyridine breaks down the polymer as in the proposed mechanism in Fig. 2.16, and so the molecular weights observed are the minimal mass and not of the intact polymer.

To review, canola oil polysulfide is prepared by the thorough mixing of sulfur and canola oil at $180 \text{ }^\circ\text{C}$ for 20 minutes. No exogenous solvents are required; molten sulfur is both a reactant and the solvent. Other vegetable oils may be supplemented, with sunflower, olive and vegetable oil previously used to fry food in a campus cafeteria all tested. The product is a friable brown rubber, with a different hue depending on the oil used. It remains elastic over its T_g of $-12 \text{ }^\circ\text{C}$ and stable under its first thermal

decomposition at 230 °C. All starting material is incorporated into the product, but not all is reacted, some sulfur remains free and embedded in the polysulfide structure. The polysulfide can be prepared with the inclusion and subsequent separation of NaCl by washing with water to make it porous, increasing surface area and reducing density. The reaction can be performed at a scale affording up to 750 g of product in one batch, milled to a low density, porous powder. In using used fryer oil and sulfur from the desulfurisation of crude oil, all starting materials can be sourced from waste streams. Sodium chloride used to install pores and channels can also be theoretically recovered and re-used to eliminate further waste generation.

References

1. Wu, X.; Smith, J. A.; Petcher, S.; Zhang, B.; Parker, D. J.; Hasell, T.; Griffin, J. M., Catalytic inverse vulcanization. *Nat. Commun.* **2019**, *10* (1), 647.
2. Griebel, J. J.; Nguyen, N. A.; Astashkin, A. V.; Glass, R. S.; MacKay, M. E.; Char, K.; Pyun, J., Preparation of Dynamic Covalent Polymers via Inverse Vulcanization of Elemental Sulfur. *ACS Macro Lett.* **2014**, *3* (12), 1258-1261.
3. Arslan, M.; Kiskan, B.; Yagci, Y., Recycling and Self-Healing of Polybenzoxazines with Dynamic Sulfide Linkages. *Sci. Rep.* **2017**, *7* (1), 5207.
4. Zhang, Y.; Konopka, K. M.; Glass, R. S.; Char, K.; Pyun, J., Chalcogenide hybrid inorganic/organic polymers (CHIPs) via inverse vulcanization and dynamic covalent polymerizations. *Polym. Chem.* **2017**, *8* (34), 5167-5173.
5. Lin, H.-K.; Lai, Y.-S.; Liu, Y.-L., Crosslinkable and Self-Foaming Polysulfide Materials for Repairable and Mercury Capture Applications. *ACS Sustainable Chem. Eng.* **2019**, *7* (4), 4515-4522
6. Lim, J.; Jung, U.; Joe, W. T.; Kim, E. T.; Pyun, J.; Char, K., High Sulfur Content Polymer Nanoparticles Obtained from Interfacial Polymerization of Sodium Polysulfide and 1,2,3-Trichloropropane in Water. *Macromol. Rapid Commun.* **2015**, *36* (11), 1103-1107.
7. Naebpetch, W.; Junhasavasdikul, B.; Saetung, A.; Tulyapitak, T.; Nithi-Uthai, N., Influence of filler type and loading on cure characteristics and vulcanisate properties of SBR compounds with a novel mixed vulcanisation system. *Plast. Rubber Compos.* **2017**, *46* (3), 137-145.
8. Fortman, D. J.; Brutman, J. P.; De Hoe, G. X.; Snyder, R. L.; Dichtel, W. R.; Hillmyer, M. A., Approaches to Sustainable and Continually Recyclable Cross-Linked Polymers. *ACS Sustainable Chem. Eng.* **2018**, *6* (9), 11145-11159.
9. Westerman, C. R.; Jenkins, C. L., Dynamic Sulfur Bonds Initiate Polymerization of Vinyl and Allyl Ethers at Mild Temperatures. *Macromolecules* **2018**, *51* (18), 7233-7238.
10. Zhang, Q.; Shi, C.-Y.; Qu, D.-H.; Long, Y.-T.; Feringa, B. L.; Tian, H.; Feringa, B. L., Exploring a naturally tailored small molecule for stretchable, self-healing, and adhesive supramolecular polymers. *Sci. Adv.* **2018**, *4* (7), eaat8192.
11. Zhang, Y.; Pavlopoulos, N. G.; Kleine, T. S.; Karayilan, M.; Glass, R. S.; Char, K.; Pyun, J., Nucleophilic Activation of Elemental Sulfur for Inverse Vulcanization and Dynamic Covalent Polymerizations. *J. Polym. Sci., Part A: Polym. Chem.* **2018**, *57* (1), 7-12

12. Hasell, T.; Parker, D. J.; Jones, H. A.; McAllister, T.; Howdle, S. M., Porous inverse vulcanised polymers for mercury capture. *Chem. Commun.* **2016**, *52*, 5383-5386.
13. Lee, J.-S. M.; Parker, D. J.; Cooper, A. I.; Hasell, T., High surface area sulfur-doped microporous carbons from inverse vulcanized polymers. *J. Mater. Chem. A* **2017**, *5* (35), 18603-18609.
14. Parker, D. J.; Jones, H. A.; Petcher, S.; Cervini, L.; Griffin, J. M.; Akhtar, R.; Hasell, T., Low cost and renewable sulfur-polymers by inverse vulcanization, and their potential for mercury capture. *J. Mater. Chem. A* **2017**, *5* (23), 11682-11692.
15. Davis, R. E.; Nakshbendi, H. F., Sulfur in Amine Solvents. *J. Am. Chem. Soc.* **1962**, *84* (11), 2085-2090.

APPENDICES

Publications that resulted from the research in this chapter:

Worthington, M. J. H.; Kucera, R. L.; Albuquerque, I. S.; Gibson, C. T.; Sibley, A.; Slattery, A. D.; Campbell, J. A.; Alboaiji, S. F. K.; Muller, K. A.; Young, J.; Adamson, N.; Gascooke, J. R.; Jampaiah, D.; Sabri, Y. M.; Bhargava, S. K.; Ippolito, S. J.; Lewis, D. A.; Quinton, J. S.; Ellis, A. V.; Johs, A.; Bernardes, G. J. L. and Chalker, J. M. Laying Waste to Mercury: Inexpensive Sorbents Made from Sulfur and Recycled Cooking Oils. *Chem. Eur. J.* **2017**, 23, 16219

2.1 POLYSULFIDE SYNTHESIS EXPERIMENTAL

General Experimental Considerations

IR Spectroscopy: Infrared (IR) spectra were recorded on a Fourier Transform spectrophotometer using the ATR method. Absorption maxima are reported in wavenumbers (cm^{-1}).

NMR Spectroscopy: Proton nuclear magnetic resonance (^1H NMR) were recorded on a 600 MHz spectrometer. All chemical shifts are quoted on the δ scale in ppm using residual solvent as the internal standard (^1H NMR: CDCl_3 $\delta = 7.26$).

GC-MS: Gas chromatography-mass spectrometry (GC-MS) was carried out on a Varian CP-3800 using a Phenomenex Zebron ZB5MS, 5 %-phenyl-arylene-95 %-dimethylpolysiloxane column (30 m long \times 25 mm film thickness \times 0.25 mm ID). The injection temperature was set at 220 $^\circ\text{C}$, the column temperature at 190 $^\circ\text{C}$, and the gas flow rate 1.2 mL min^{-1} . Electron ionization was used to obtain nominal masses.

Raman Spectroscopy and Microscopy: Raman spectra were acquired using a Witec alpha300R Raman microscope at an excitation laser wavelength of 532 nm with a 40 \times objective (numerical aperture 0.60). Typical integration times for single Raman spectra were between 20 to 60 s and averaged from 1 to 3 repetitions. Confocal Raman images were also acquired with integrations between 1 to 6 seconds per pixel. Each pixel in the Raman images represents a Raman spectrum with the number of pixels in a typical Raman image representing hundreds to thousands of spectra. Confocal Raman images are generated by plotting the intensity of a specified region of each Raman spectrum that corresponds to a material, versus the X-Y position of the excitation laser as it scans the sample surface.

Raman data were also obtained using an XplorRA Horiba Scientific Confocal Raman microscope. Spectra were acquired using a 50X objective (numerical aperture 0.6) at an excitation wavelength of 532 nm. Typical integrations times for the spectra were 20 to 60 s and averaged from 1 to 3 repetitions.

SEM and EDS: Scanning Electron Microscopy (SEM) images were obtained using an FEI F50 Inspect system, while corresponding EDS spectra were obtained using an EDAX Octane Pro detector.

XPS: X-Ray Photoelectron Spectroscopy was performed on a Leybold Heraeus LHS-10 with a SPECS XR-50 dual anode source operating at 250 W. Base vacuum pressure in the analysis chamber was better than 5×10^{-9} torr. All spectra were taken with the 1253.6 eV Mg-K α anode with the analyser pass energy set to 20 eV. Survey spectra were taken 'constant retarding ratio mode', while high resolution spectra were taken in fixed analyser transmission mode.

Auger Spectroscopy: Scanning Auger Electron Spectromicroscopy was performed on a PHI710 Scanning Auger Nanoprobe. Samples were sputter coated with 2 nm of platinum prior to analysis. The vacuum pressure in the analysis chamber during analysis was maintained below 10^{-9} Torr. Electron beam energies used for analysis ranged between 3 kV and 10 kV, with a beam current of between 3 and 10 nA.

Dynamic Mechanical Analysis: Dynamic Mechanical Analysis was performed on a TA Q800 DMA in tension mode. Samples were prepared as short bars with dimensions of 1.4 cm × 0.8 cm × 0.2 cm. The sample was cooled to -100 °C and then heated to 170 °C at 3.0 °C min⁻¹.

Simultaneous Thermal Analysis: Simultaneous Thermal Analysis (STA) was carried out on a Perkin Elmer STA8000 simultaneous thermal analyzer. A sample size between 11 and 15 mg was used in each experiment. The furnace was purged at 20 mL min⁻¹ with either nitrogen or air, as indicated, and equilibrated for 1 minute at 30 °C before each test. Heating was carried out up to 700 °C using either 5 °C min⁻¹ or 20 °C min⁻¹ heating rates, as indicated. The temperature was held isothermally at 700 °C at the end of each experiment to oxidize remaining organic matter.

Differential Scanning Calorimetry (DSC): Differential Scanning Calorimetry (DSC) was carried out using a Perkin Elmer DSC 8000 with nitrogen furnace purged at 20 mL min⁻¹. Samples were approximately 7 mg and sealed in aluminium sample pans. The sample was cooled to -80 °C, held for 5 minutes, and then heated to 300 °C at 10 °C min⁻¹.

Synthesis

20.0 g sulfur was melted above its floor temperature of 159 °C with stirring and then raised to 180 °C. The molten sulfur turned from yellow to orange as sulfur-sulfur bonds cleave to form thiyl radicals. 20.0 g canola oil was then added dropwise and stirred more vigorously to thoroughly blend the two layers together. After 10 minutes the product solidified. The solid was allowed to cure at this temperature for a further 10 minutes. The material was then blended for 3 minutes in a food processor achieving particle sizes from 0.2 to 12 mm in diameter with an average diameter of 2 mm. In case of H₂S formation the material was stirred with 0.1 M NaOH for 90 minutes followed by washing with 3 aliquots of 40 mL deionised water under vacuum filtration. The material was then left to dry in fumehood for 24 hours.

SEM Analysis

Canola Oil Polysulfide was prepared to standard procedure and then cut and filtered through a series of sieves to give particle sizes between 0.5 and 1.0 mm in diameter. Material was affixed to an SEM pin with carbon tape and sputter coated with platinum at 5 nm for analysis by SEM.

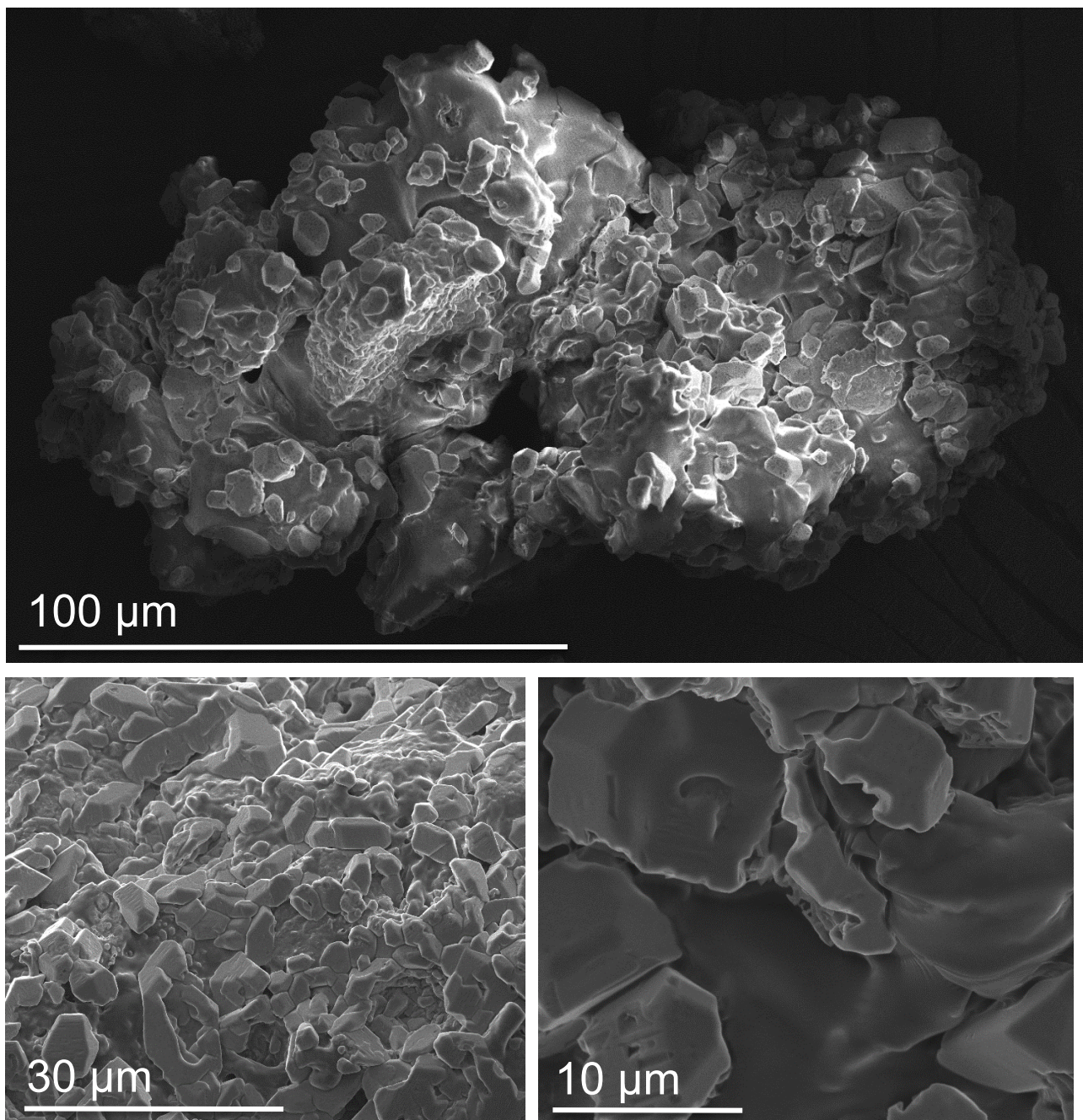


Figure 2.1.1 | SEM images of canola oil polysulfide at increasing magnitude. Top: a single particle of canola oil polysulfide approximately 200 microns in length. Bottom: Images taken at high magnitude, demonstrating both microtextured regions of high sulfur and amorphous polysulfide regions.

FTIR Analysis

No pre-treatment was required to examine canola oil polysulfide by ATR-FTIR. Canola oil was also analysed to determine functional differences before and after the reaction with sulfur.

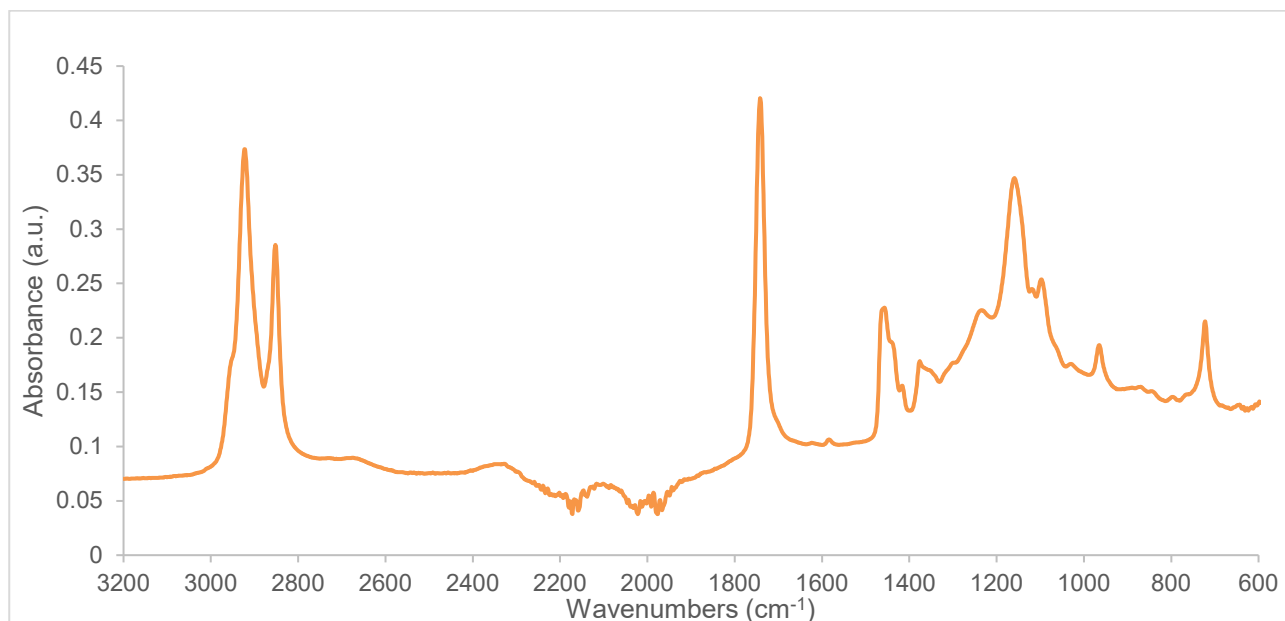


Figure 2.1.2 | Absorbance mode ATR-FTIR spectra of canola oil polysulfide

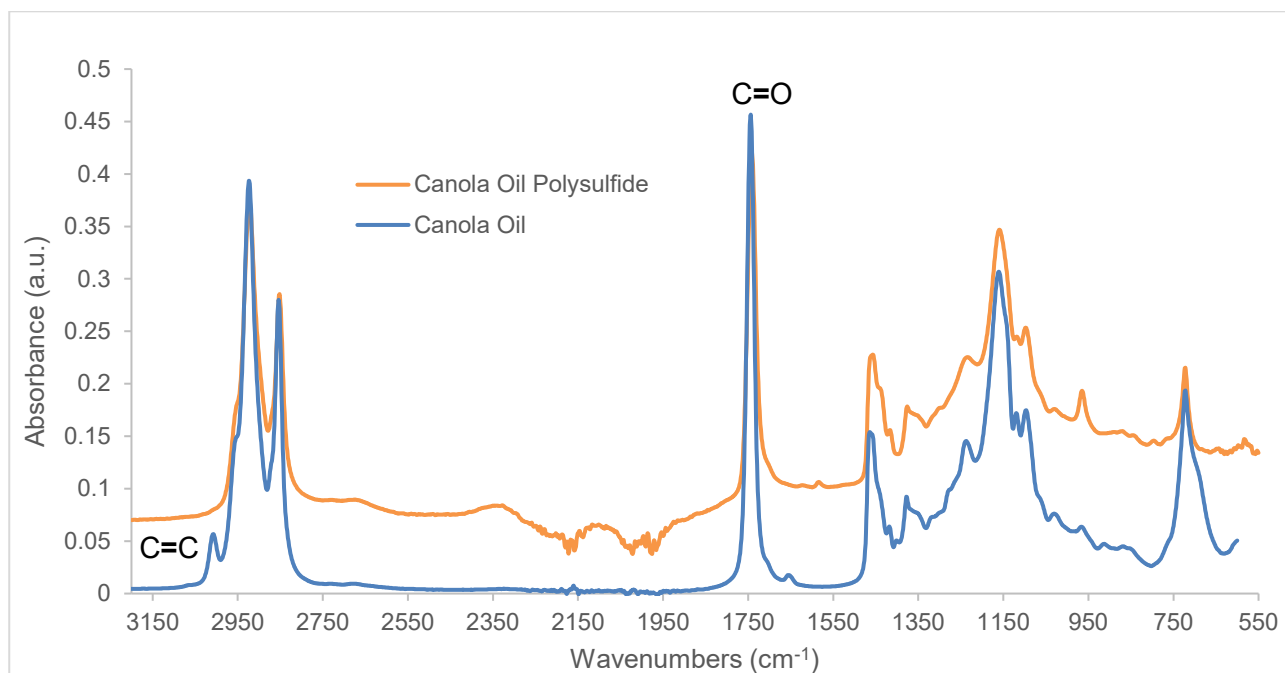


Figure 2.1.3 | Absorbance mode ATR-FTIR spectra of both canola oil polysulfide and canola oil, key stretches are indicated.

IR analysis shows the presence of carbonyls (1742 cm⁻¹), indicating the canola oil's triglyceride structure remains intact. The absence of alkene stretches (1600 cm⁻¹ and over 3000 cm⁻¹) in the polysulfide is consistent with reaction of sulfur with the alkenes of the triglyceride.

Raman Analysis

Raman analysis performed by Christopher Gibson

No pre-treatment was required to examine canola oil polysulfide by ATR-FTIR. Canola oil and sulfur were also analysed to determine differences in bonding before and after synthesis.

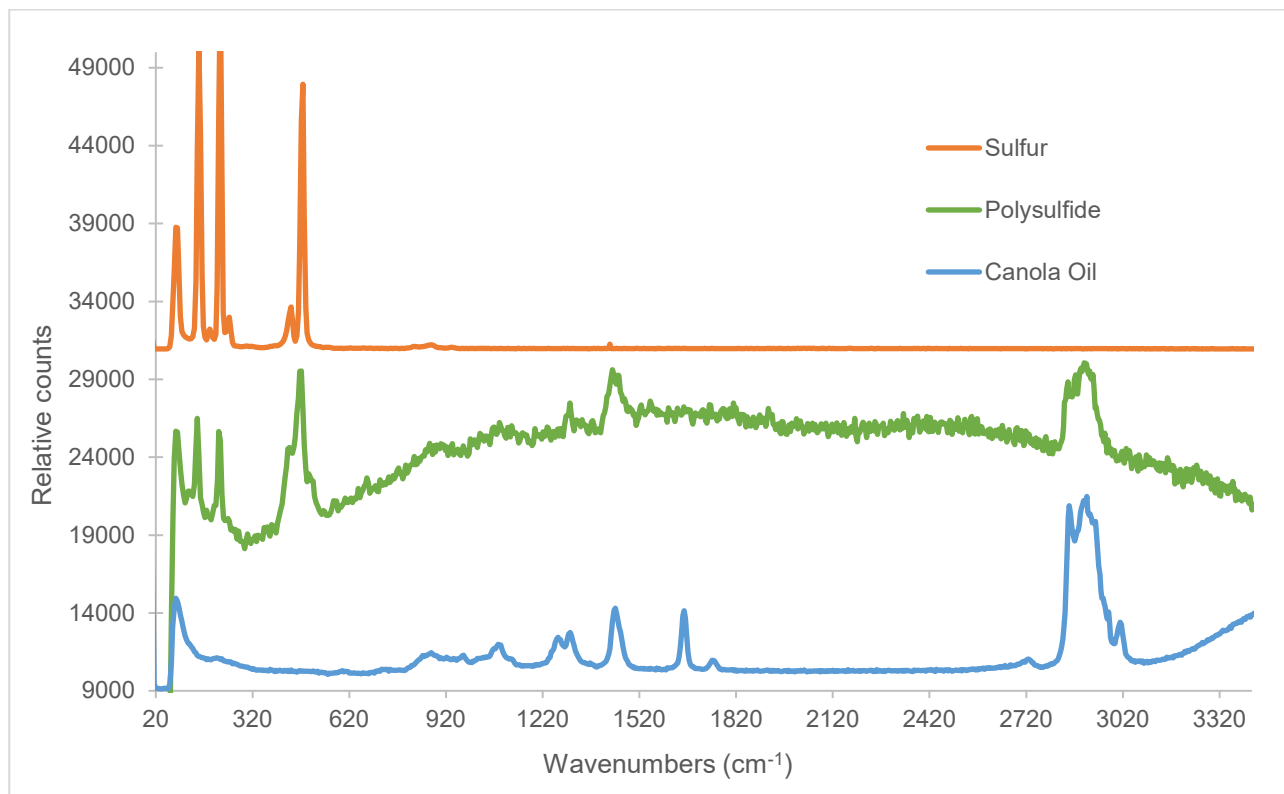


Figure 2.1.4 | Raman spectra of canola oil polysulfide against starting materials: canola oil and sulfur

Raman analysis shows stretches at 343 cm⁻¹ and 471 cm⁻¹, indicative of S-S stretching modes¹, consistent with a polysulfide material.

Simultaneous Thermal Analysis

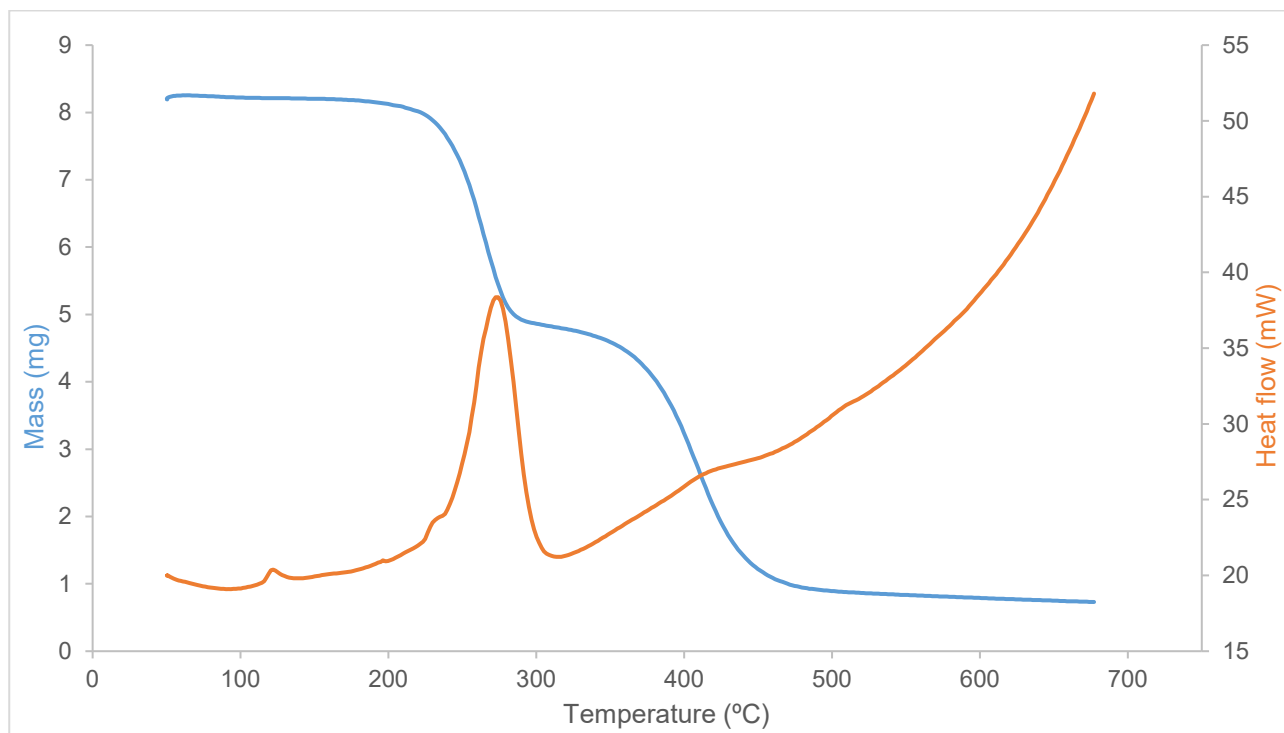


Figure 2.1.5 | STA (DSC and TGA) of canola oil polysulfide.

Simultaneous thermal analysis indicates degradation occurs over two steps: An initial 50% mass loss at 230 °C followed a second at 380 °C. This analysis also indicates the presence of a small amount of unreacted sulfur in the polysulfide by the peak in the DSC running through sulfur's melting point (ca. 115 °C, the use of technical grade sulfur may result in variation) from 110 °C to 140 °C with a peak maxima of 120 °C. The large endotherm beginning at 230 °C corresponds to the thermal decomposition of the polysulfide and coincides with the first mass loss event in the TGA.

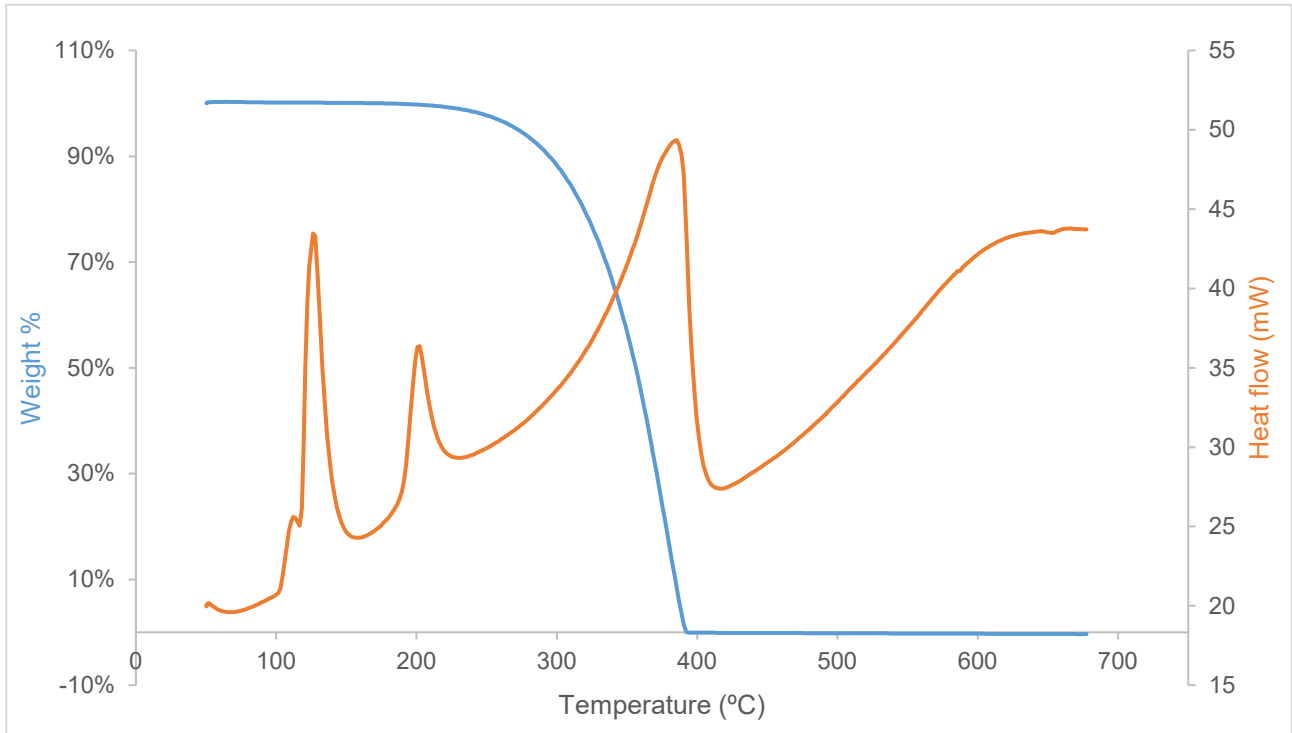


Figure 2.1.6 | STA (DSC and TGA) of elemental sulfur.

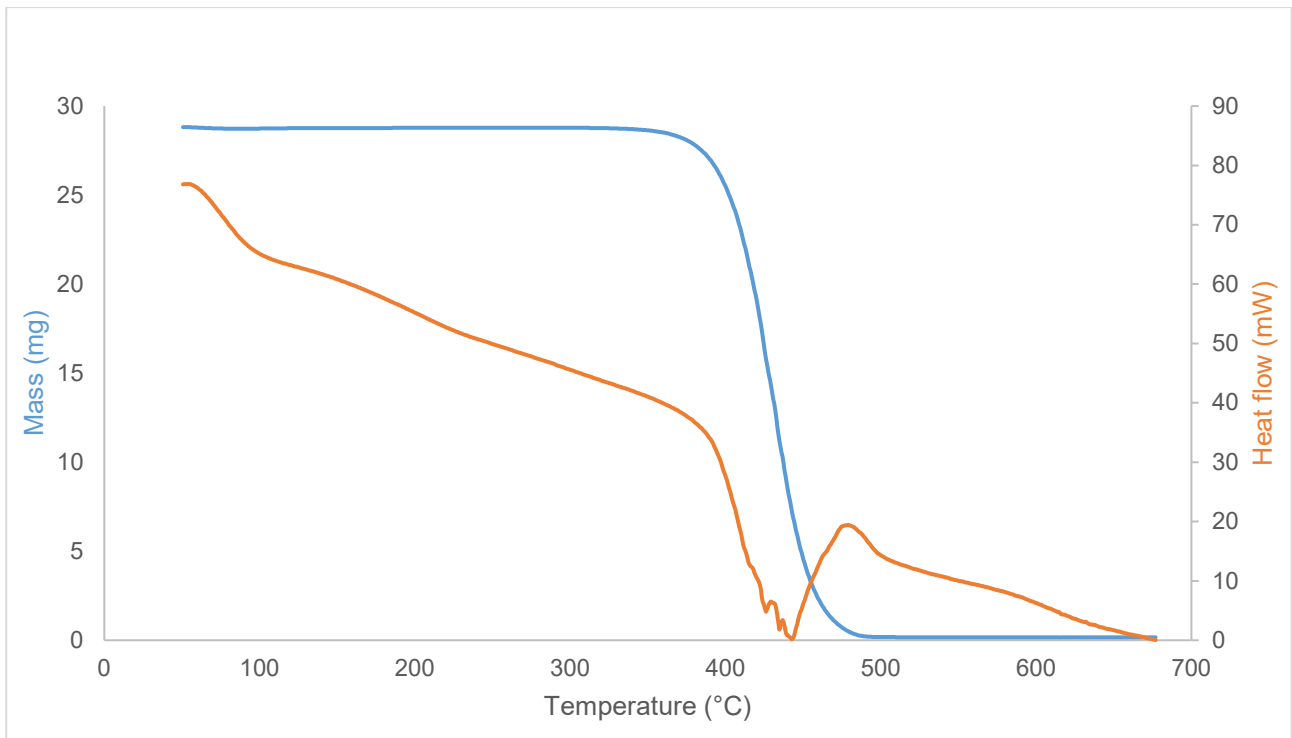


Figure 2.1.7 | STA (DSC and TGA) of canola oil.

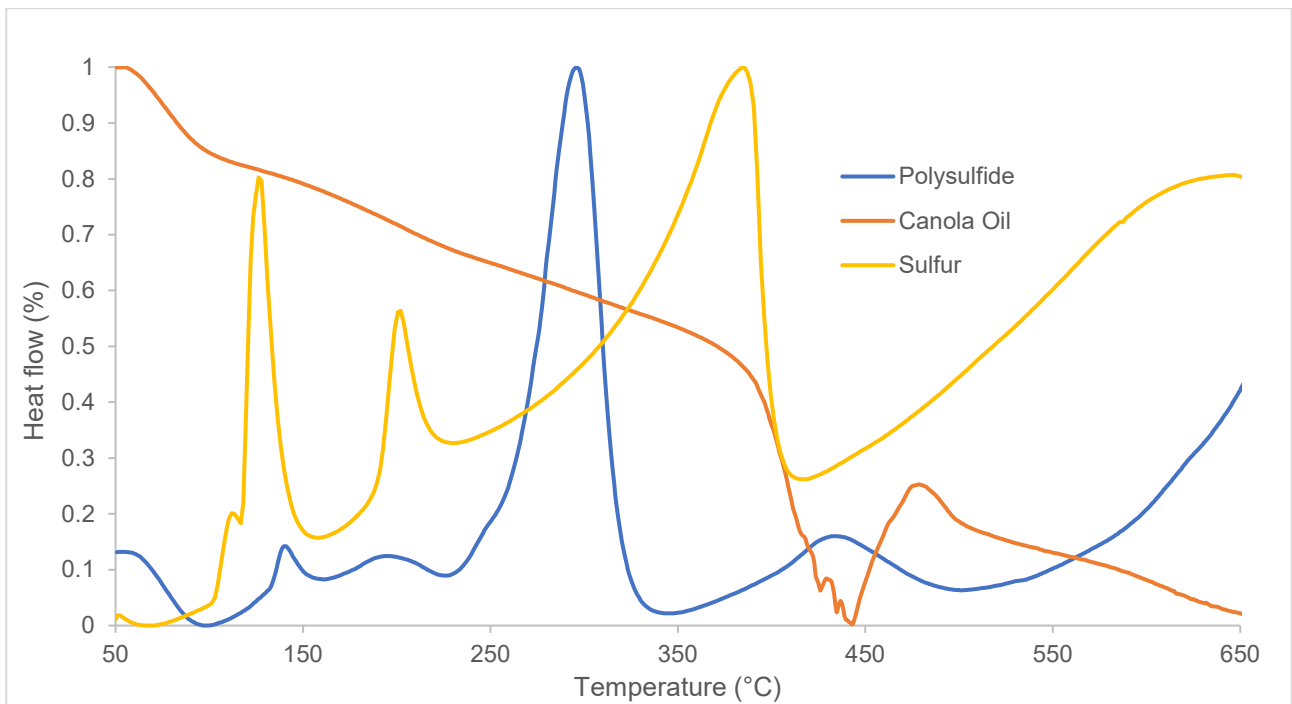


Figure 2.1.8 | DSC analysis of polysulfide and starting materials, canola oil and sulfur. The melting of elemental sulfur occurs at 125 °C, visible in both the sulfur and polysulfide spectra.

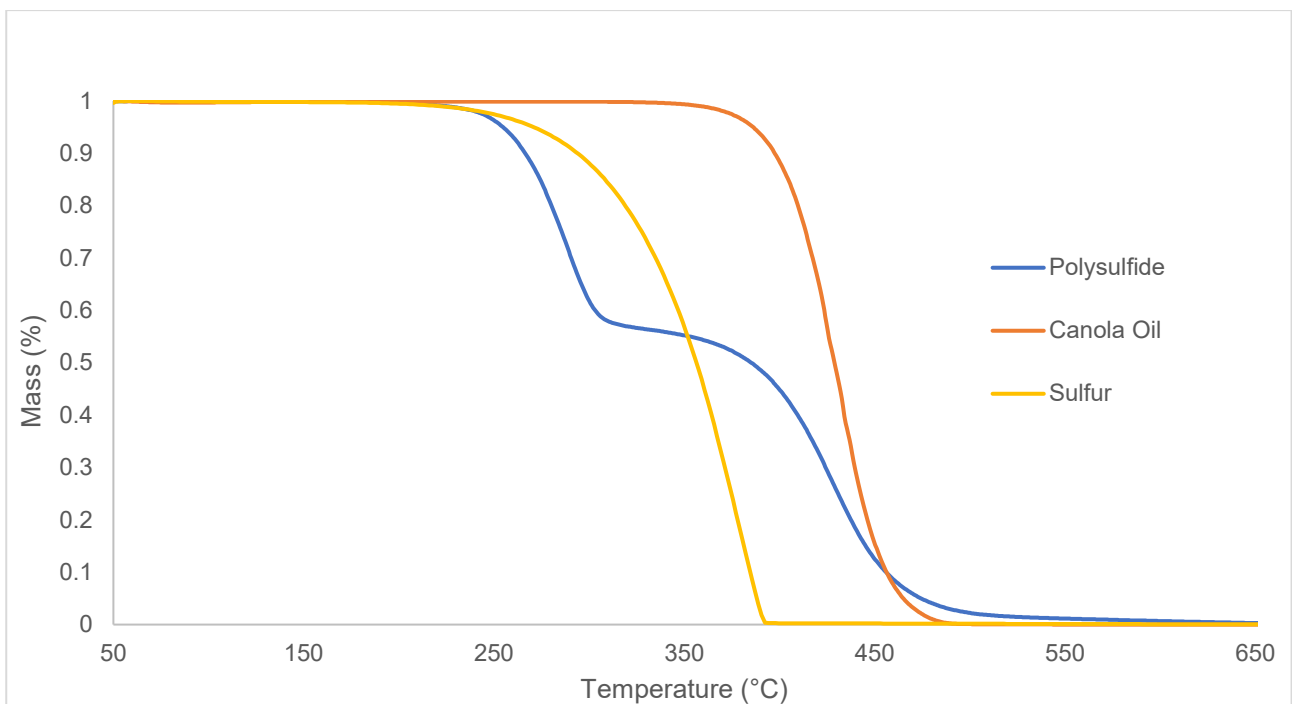


Figure 2.1.9 | TGA analysis of polysulfide and starting materials, canola oil and sulfur. Sulfur begins to boil and is lost to air at ca. 230 °C and canola oil at ca. 380 °C, matching the two distinct mass losses in the polysulfide's trace.

Dynamic Mechanical Analysis

DMA analysis performed with the help of Johnathan Campbell

Polysulfide (50 wt. % sulfur) was prepared to standard procedure within a beaker rather than a round bottom flask, and a bar of dimensions 1.4 cm × 0.8 cm × 0.2 cm cut out of the solid product to analyse mechanical properties by tension mode DMA.

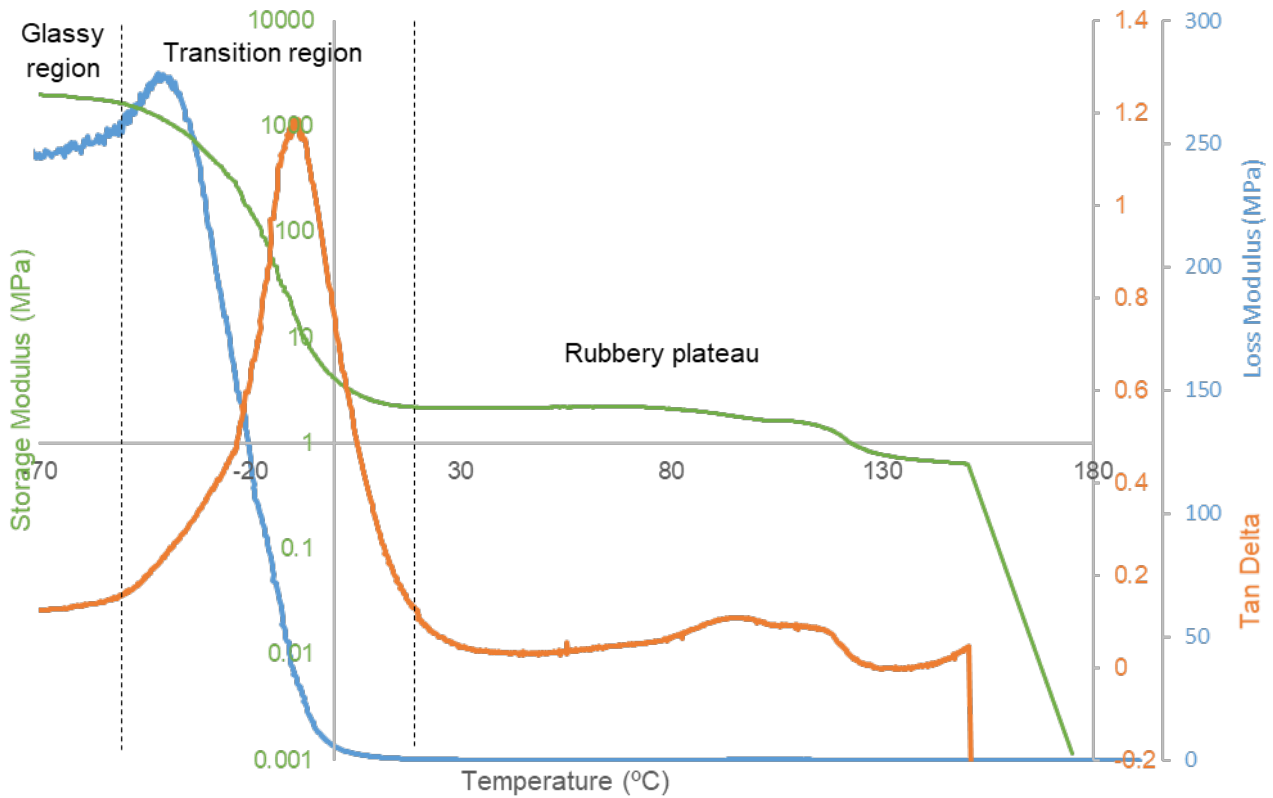


Figure 2.1.10 | Tension-mode DMA of canola oil polysulfide

Storage Modulus drop onset	Loss Modulus peak	Tan Delta (Loss/Storage) Peak
-32 °C	-42 °C	-9 °C

By the Tan Delta peak the canola oil polysulfide's T_g is -9 °C, below this temperature the material will be in the glassy region and brittle, above this (and at room temperature) the material will be in the rubbery plateau: elastic and malleable.

Solubility

500 mg Canola Oil Polysulfide was left to incubate for 24 hours with 5 mL various solvents in 20 mL glass vials. The liquid was then filtered by vacuum, washed with 3 × 5 mL aliquots of the dissolving solvent and transferred to pre-weighed 50 mL round-bottom flasks. The solvents were removed by rotary evaporation the precipitate weighed.

Solvent	Solubility (mg mL ⁻¹)	Mass dissolved polymer per mass solvent (w/w%)
Water	0.0	-
Acetonitrile	0.2	0.02
Methanol	0.6	0.08
Ethanol	1.5	0.19
Acetone	4.4	0.55
Ethyl Acetate	5.8	0.64
Hexane	7.9	1.21
THF	18.3	2.06
Dichloromethane	18.4	1.39

Canola oil polysulfide requires very harsh organic solvents to dissolve and is most soluble in DCM. In all solvents tested polysulfide is only sparingly soluble and in no case did all polysulfide dissolve.

Free (unreacted) sulfur content

Quantitative DSC was used to determine free sulfur content in Canola Oil Polysulfide. S_8 has a distinctive DSC peak at 125 °C that stretches from 100 °C to 150 °C (fig. 2.1.13). Further testing showed the area of this peak increases linearly with sulfur weight. On average 1 mg sulfur gave a response of 49.3 J g⁻¹ within the range tested. By taking the area of this same peak as it appears in a known mass of canola oil polysulfide tested under identical DSC parameters, the weight percent of free sulfur in the polysulfide can be determined: 8.19 mg of Canola Oil Polysulfide gave a response of 36.15 mJ, or 4.41 J g⁻¹, 8.96 % of the S_8 response. From this canola oil polysulfide would seem to contain 9.0 % free or unreacted sulfur.

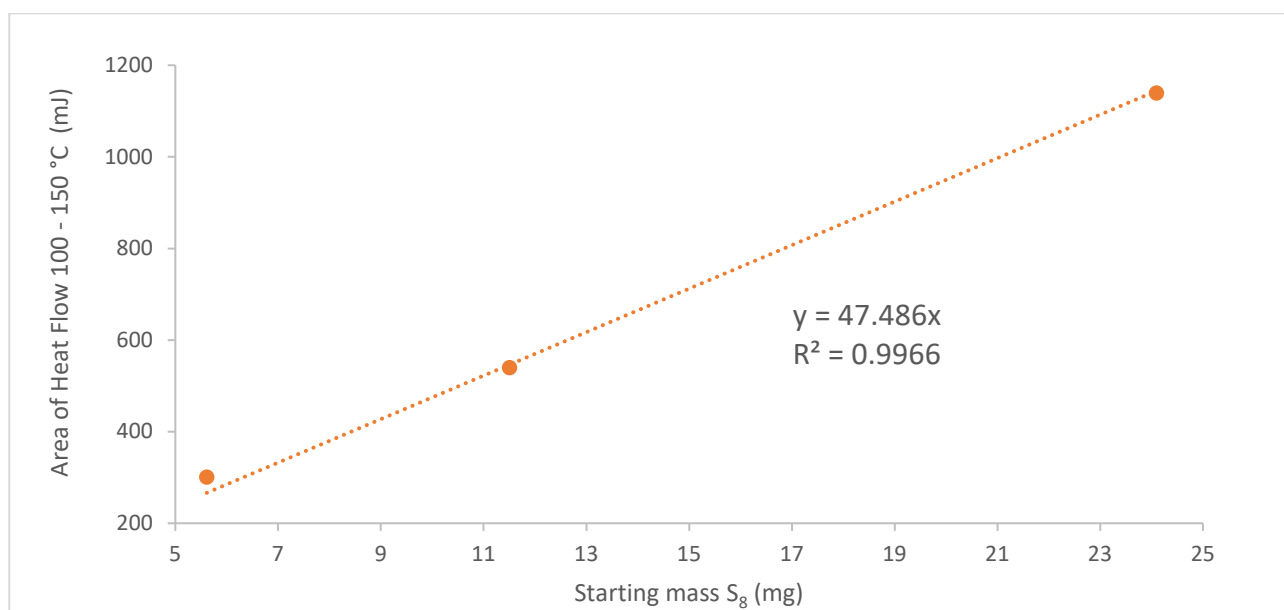


Figure 2.1.11 | S_8 mass versus heat flow response by dynamic scanning calorimetry (DSC)

Sample	ΔH (J g ⁻¹)	Free sulfur (wt. %)
Canola oil polysulfide (30 wt. % sulfur)	1.866	3.8%
Canola oil polysulfide (50 wt. % sulfur)	4.4079	9.0%
Canola oil polysulfide (60 wt. % sulfur)	11.467	23.3%
Canola oil polysulfide (70 wt. % sulfur)	18.721	38.1%
Olive oil polysulfide (50 wt. % sulfur)	8.43	17.1%
Sunflower oil polysulfide (50 wt. % sulfur)	7.4529	15.2%
Waste oil polysulfide (50 wt. % sulfur)	7.667	15.6%
Classically vulcanised "factice" (50 wt. % sulfur)	4.3174	8.8%

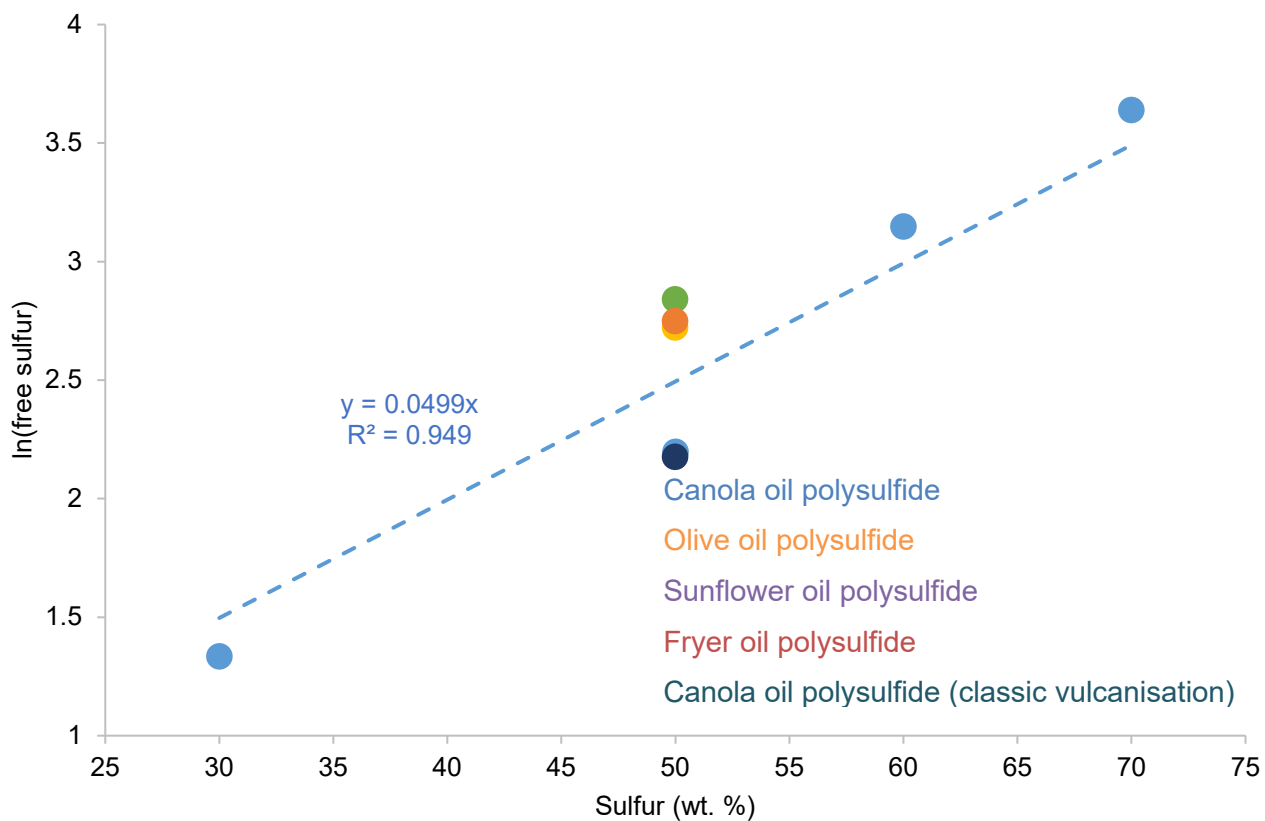


Figure 2.1.12 | Comparison of total sulfur in synthesis against the percentage of free sulfur in the product.

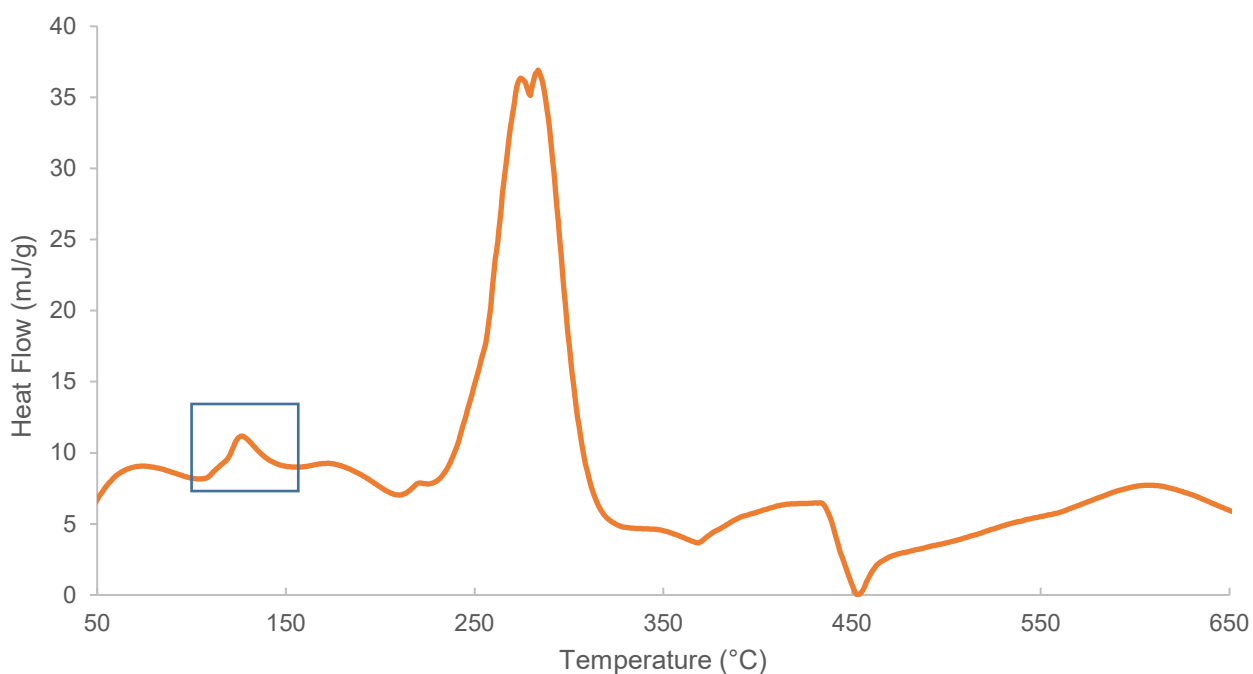


Figure 2.1.13 | DSC of polysulfide with region indicating the melting of free sulfur highlighted.

Alternative Sulfur-Canola Oil Ratios

Syntheses of oleic acid and vegetable oil (including canola oil of varying brands) polysulfides performed by Renata Kucera as part of an undergraduate research project. Note: "Sulfur" refers to analytical-grade sulfur purchased from Sigma-Aldrich, "crude sulfur" refers to technical grade sulfur acquired from industrial sources.

Sulfur and oleic acid

With stirring (at 1,000 rpm), sulfur (500 mg) was melted above its floor temperature (159 °C) and subsequently the temperature was raised to 180 °C. As the sulfur melted, its colour changed from yellow to orange as thiyl radicals were formed. 0.56 mL of oleic acid ($d = 0.895 \text{ g mL}^{-1}$) was added dropwise to the molten sulfur. Over a period of 2 hours, the mixture gradually changed colour from yellow/orange to dark brown/black. After 2 hours and a dark brown/black viscous product was seen.

Sulfur and canola oil (Black and Gold) (1:1 ratio)

With stirring (at 1,000 rpm), sulfur (500 mg) was melted above its floor temperature (159 °C) and subsequently the temperature was raised to 170 °C. As the sulfur melted, its colour changed from yellow to orange as thiyl radicals were formed. 0.56 mL of canola oil ($d = 0.88 \text{ g mL}^{-1}$) was added dropwise to the molten sulfur at 170 °C and the temperature was then raised to 180 °C. Within 15 minutes of the addition of canola oil, the mixture had solidified to form a brown/black solid product which was allowed to cure for a further 1 hour 45 minutes.

Sulfur and canola oil (Black and Gold) (2:1 ratio)

With stirring (at 1,000 rpm), sulfur (1 g) was melted above its floor temperature (159 °C) and subsequently the temperature was raised to 170 °C. As the sulfur melted, its colour changed from yellow to orange as thiyl radicals were formed. 0.56 mL of canola oil ($d = 0.88 \text{ g mL}^{-1}$) was added dropwise to the molten sulfur at 170 °C and the temperature was then raised to 180 °C. Within 25 minutes of the addition of canola oil, the mixture had solidified to form a brown/black solid product which was allowed to cure for a further 1 hour 35 minutes.

Sulfur and canola oil (Black and Gold) (1:2 ratio)

With stirring (at 1,000 rpm), sulfur (500 mg) was melted above its floor temperature (159 °C) and subsequently the temperature was raised to 170 °C. As the sulfur melted, its colour changed from yellow to orange as thiyl radicals were formed. 1.12 mL of canola oil ($d = 0.88 \text{ g mL}^{-1}$) was added dropwise to the molten sulfur at 170 °C and the temperature was then raised to 180 °C. Within 25 minutes of the addition of canola oil, the mixture had solidified to form a brown/black solid product which was allowed to cure for a further 1 hour 35 minutes.

Sulfur, oleic acid and canola oil (Black and Gold)

With stirring (at 1,000 rpm), sulfur (500 mg) was melted above its floor temperature (159 °C) and subsequently the temperature was raised to 170 °C. As the sulfur melted, its colour changed from yellow to orange as thiyl radicals were formed. 0.56 mL of oleic acid ($d = 0.895 \text{ g mL}^{-1}$) was added dropwise to the molten sulfur at 170 °C and the temperature was then raised to 180 °C. Over a period of 1 hour, the reaction mixture gradually darkened to a dark brown/black colour and remained liquid. After 1 hour, 0.8 mL of canola oil ($d = 0.88 \text{ g mL}^{-1}$) was added dropwise to the reaction mixture and no immediate change was observed. Next, a total of 3.2 mL canola oil was added in 4 aliquots at 20 minute intervals with no change being observed. After a further 20 minutes, a dark brown/black viscous product was seen.

Sulfur and pre-mixed oleic acid and canola oil (Black and Gold) (1:1:1 ratio)

With stirring (at 1,000 rpm), sulfur (500 mg) was melted above its floor temperature (159 °C) and subsequently the temperature was raised to 170 °C. As the sulfur melted, its colour changed from yellow to orange as thiyl radicals were formed. Oleic acid (0.56 mL) and canola oil (0.41 mL) (pre-mixed) were added dropwise to the molten sulfur at 170 °C and the temperature was then raised to 180 °C. Over a period of 2 hours, the mixture gradually changed colour from yellow/orange to dark brown/black. After 2 hours, a dark brown-black viscous product was seen.

Table of polysulfide products formed from alternate ratios of sulfur to canola oil—

Reactants with mass ratio	Product description
1:1 sulfur & oleic acid	Dark brown viscous liquid (did not vitrify)
1:1 sulfur & canola oil	Dark brown rubbery solid
2:1 sulfur & canola oil	Dark brown rubbery solid (took longer to solidify)
1:2 sulfur & canola oil	Dark brown rubbery solid (took longer to solidify)
1:1:1 sulfur, canola oil & oleic acid	Dark brown viscous liquid (did not vitrify)

Alternative Sulfur and Olefin Sources

Sulfur and sunflower oil (Black and Gold) (1:1 ratio)

With stirring, sulfur (500 mg) was melted above its floor temperature (159 °C) and subsequently the temperature was raised to 180 °C. As the sulfur melted, its colour changed from yellow to orange as thiyl radicals were formed. 0.5 mL of sunflower oil ($d = 1 \text{ g mL}^{-1}$) was added dropwise to the molten sulfur and the stirring was raised to 1,500 rpm. Over a period of 20 minutes, the mixture gradually changed colour from yellow/orange to dark brown. After 20 minutes, a dark brown solid product was seen.

Sulfur and extra virgin olive oil (Foodland) (1:1 ratio)

With stirring, sulfur (500 mg) was melted above its floor temperature (159 °C) and subsequently the temperature was raised to 180 °C. As the sulfur melted, its colour changed from yellow to orange as thiyl radicals were formed. 0.5 mL of olive oil ($d = 1 \text{ g mL}^{-1}$) was added dropwise to the molten sulfur and the stirring was raised to 1,500 rpm. Over a period of 20 minutes, the mixture gradually changed colour from yellow/orange to dark brown. After 20 minutes, a dark brown liquid product was seen with some crystallised sulfur.

Crude sulfur and canola oil (Black and Gold) (1:1 ratio)

With stirring, crude sulfur (500 mg) was melted above its floor temperature (159 °C) and subsequently the temperature was raised to 180 °C. As the crude sulfur melted, its colour changed from yellow to orange as thiyl radicals were formed. 0.56 mL of canola oil ($d = 0.88 \text{ g mL}^{-1}$) was added dropwise to the molten crude sulfur and the stirring was raised to 1,500 rpm. Over a period of 25 minutes, the mixture gradually changed colour from yellow/orange to dark brown. After 25 minutes, a dark brown solid product was seen.

Crude sulfur and canola oil (Foodland) (1:1 ratio)

With stirring, crude sulfur (500 mg) was melted above its floor temperature (159 °C) and subsequently the temperature was raised to 180 °C. As the crude sulfur melted, its colour changed from yellow to orange as thiyl radicals were formed. 0.55 mL of canola oil ($d = 0.9 \text{ g mL}^{-1}$) was added dropwise to the molten crude sulfur and the stirring was raised to 1,500 rpm. Over a period of 25 minutes, the mixture gradually changed colour from yellow/orange to dark brown. After 25 minutes, a dark brown solid product was seen.

Crude sulfur and canola oil (Gold'n Canola) (1:1 ratio)

With stirring, crude sulfur (500 mg) was melted above its floor temperature (159 °C) and subsequently the temperature was raised to 180 °C. As the crude sulfur melted, its colour changed from yellow to orange as thiyl radicals were formed. 0.5 mL of canola oil ($d = 1 \text{ g mL}^{-1}$) was added dropwise to the molten crude sulfur and the stirring was raised to 1,500 rpm. Over a period of 20 minutes, the mixture gradually changed colour from yellow/orange to dark brown. After 20 minutes, a dark brown solid product was seen.

Table of polysulfide products formed from alternate sulfur and olefin sources—

Reactants (1:1 mass ratio)	Product description
Sulfur & sunflower oil (Black & Gold)	Dark brown rubbery solid
Sulfur & extra virgin olive oil (Foodland)	Dark brown viscous liquid with crystal sulfur visible
Crude sulfur & canola oil (Black & Gold)	Dark brown rubbery solid (took longer to solidify)
Crude sulfur & canola oil (Foodland)	Dark brown rubbery solid (took longer to solidify)
Crude sulfur & canola oil (Gold'n Canola)	Dark brown rubbery solid (took slightly longer to solidify)

Comparison of canola oil polysulfide prepared by inverse- and classic-vulcanisation.

Canola oil polysulfide was prepared with 50 wt. % sulfur according to the standard inverse vulcanisation procedure. For classic vulcanisation, canola oil (10.0 g) was heated to 180 °C in a 250 mL round bottom flask with stirring. Sulfur (10.0 g) was then added in several portions over 5 minutes. The mixture was stirred vigorously for an additional 15 minutes, after which time the mixture reached its gel point and formed a brown rubber very similar in appearance to the product formed from inverse vulcanisation. STA of both samples revealed a similar decomposition and calorimetric profile.

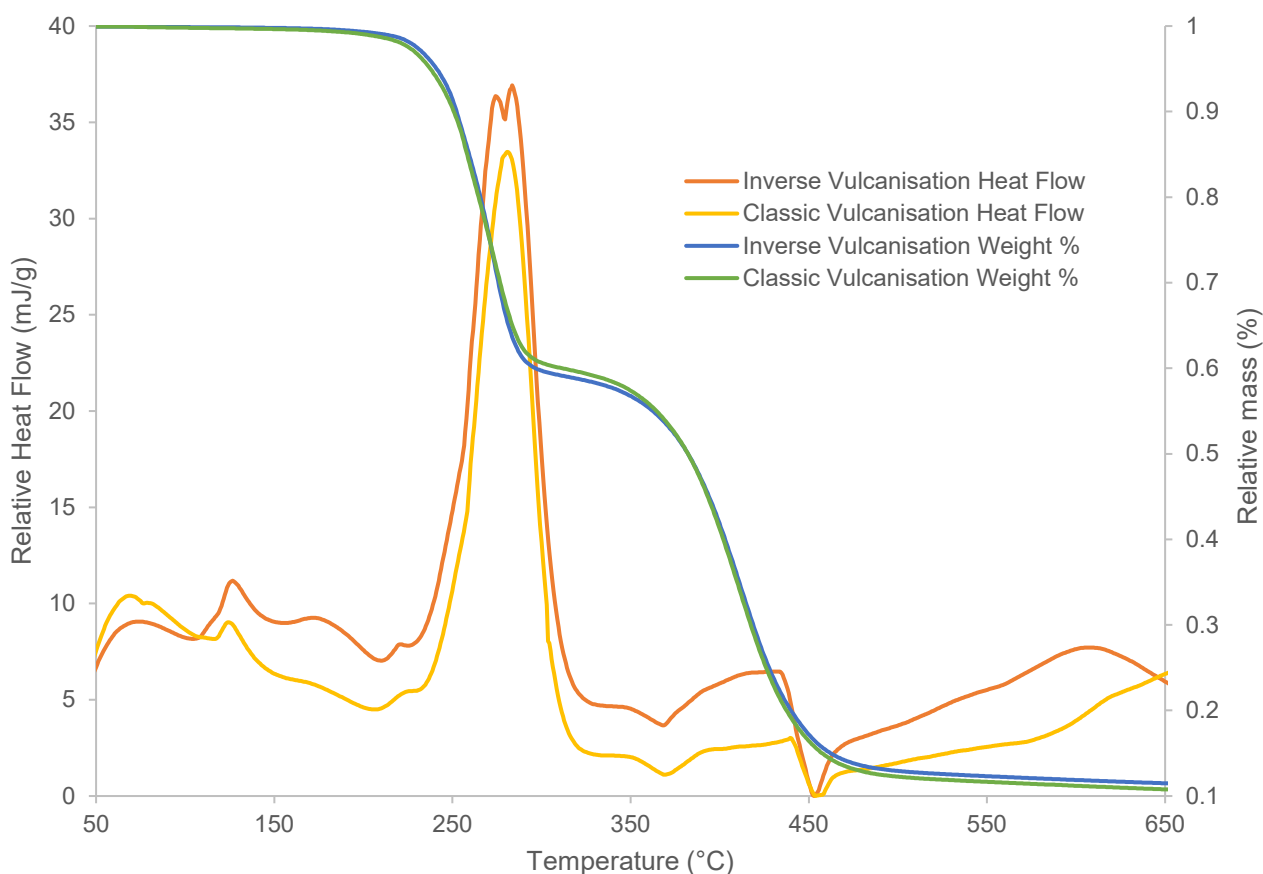


Figure 2.1.14 | Thermal gravimetric analysis and dynamic scanning calorimetry of the canola oil polysulfide prepared at 50 wt. % sulfur using inverse vulcanisation and classic vulcanisation. By STA analysis the method of synthesis does not seem to influence the thermal stability of the product.

DSC of canola oil polysulfide prepared by traditional vulcanisation and inverse vulcanisation

Dynamic scanning calorimetry was repeated, with a focus on the region where sulfur melts. Slightly more free sulfur was observed when using inverse vulcanisation (9 % free sulfur) compared to traditional vulcanisation (8 % free sulfur).

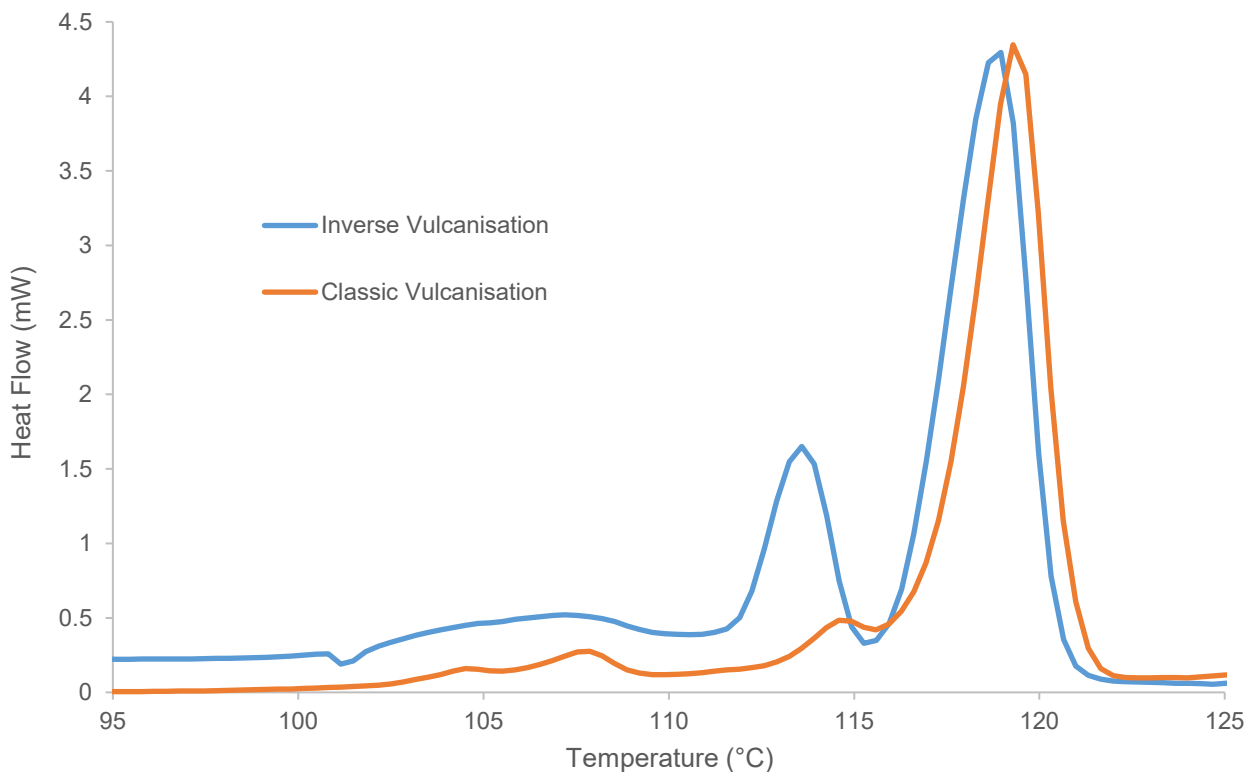


Figure 2.1.15 | Dynamic scanning calorimetry of canola oil polysulfide prepared at 50 wt. % sulfur using inverse vulcanisation and classic vulcanisation. The region of free sulfur is shown to illustrate a subtle difference in the materials.

Glass transition temperature by DSC for non-porous polysulfide (50 wt. % sulfur)

Glass transition temperature can also be determined by DSC as the onset of shift in the baseline. The glass transition temperature of the non-porous canola oil polysulfide was $-12.2\text{ }^{\circ}\text{C}$, as determined by DSC. This is very close to the T_g previously determined by DMA but is demonstrated to occur at the same temperature through multiple heating and cooling cycles for the same sample of polysulfide by DSC.

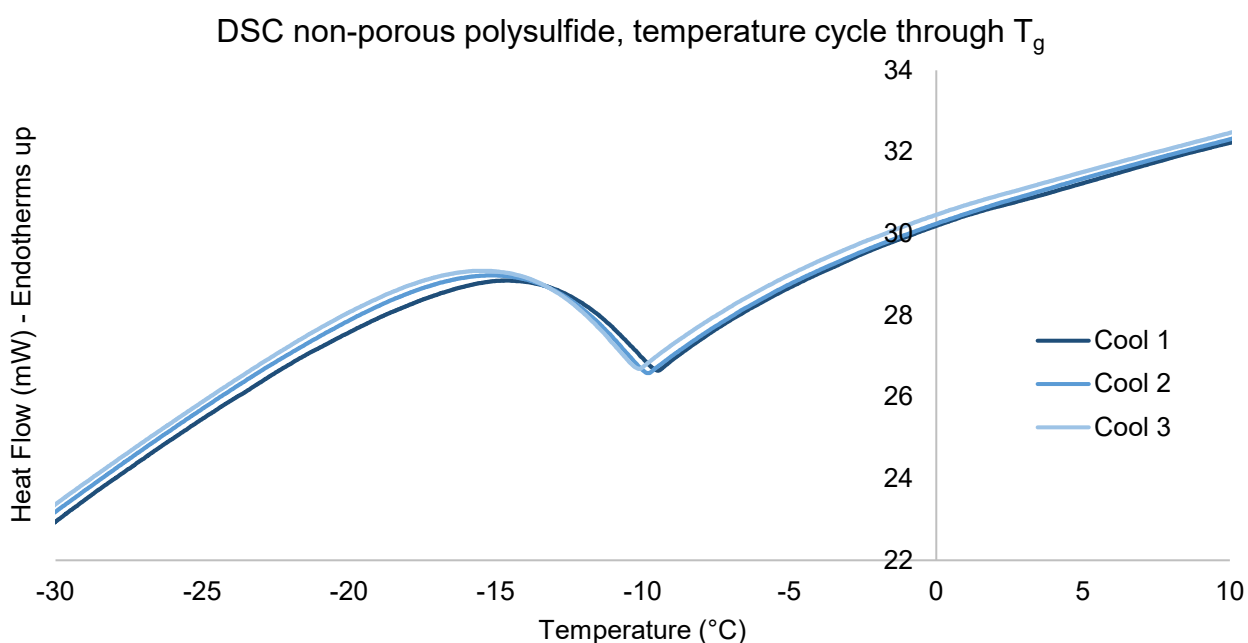
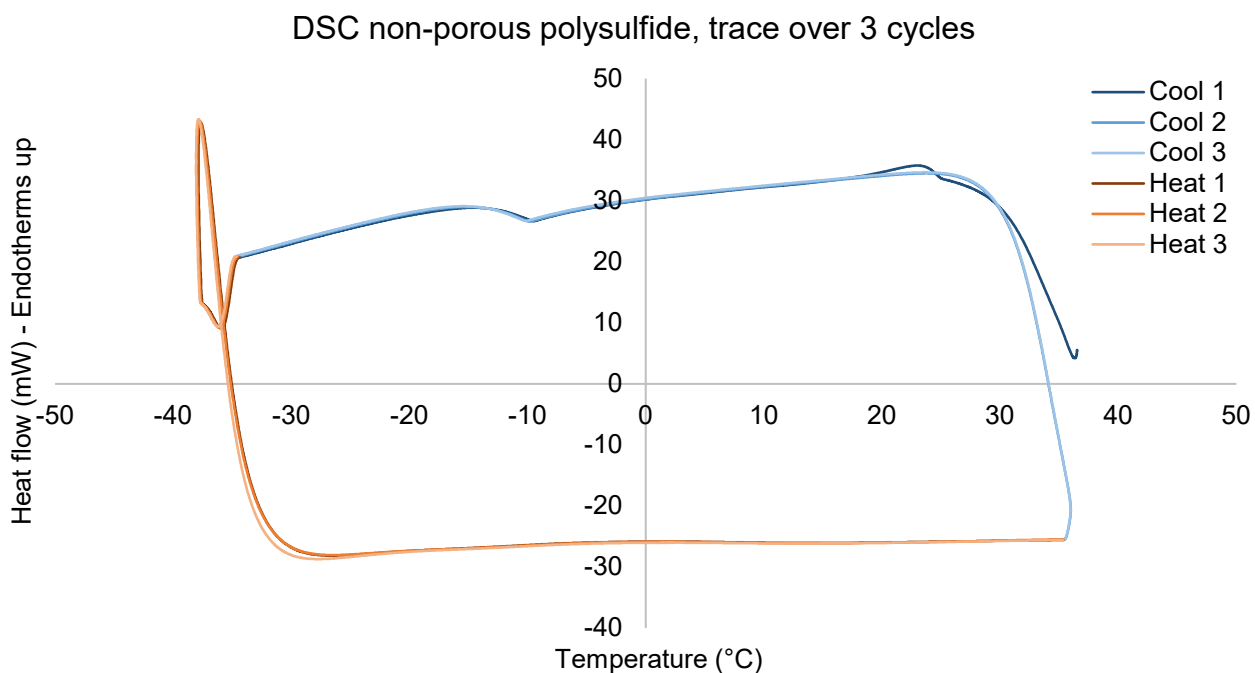


Figure 2.1.16 | Determination of T_g using DSC for the polysulfide prepared at 50 wt. % sulfur. Polysulfide was heated to $35\text{ }^{\circ}\text{C}$ and cooled to $-35\text{ }^{\circ}\text{C}$ for 3 cycles. Top: whole spectra, bottom: focus on the glass transition.

Canola Oil Polysulfide from Different Reactant Ratios

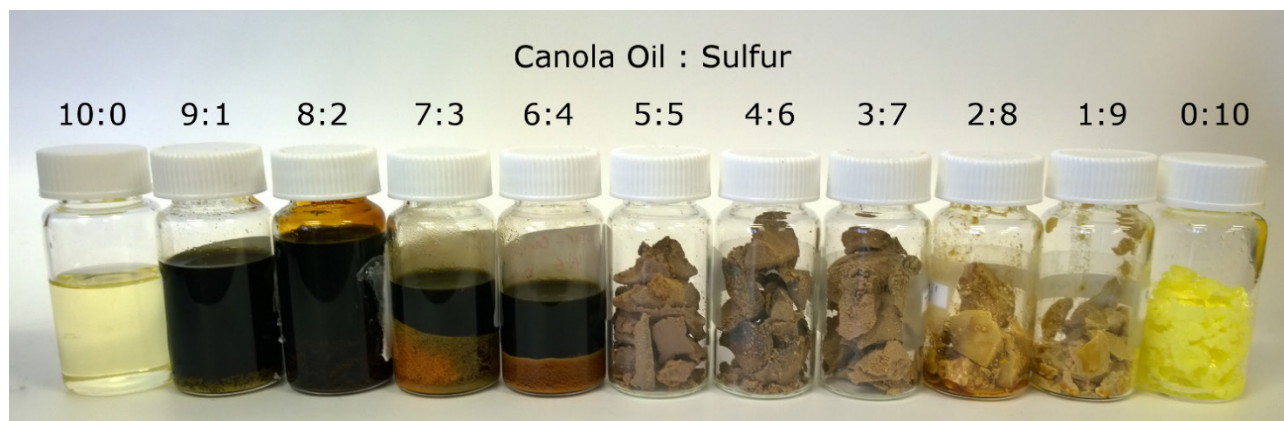


Figure 2.1.18 | 9:1 through to 1:9 produced from standard synthesis protocol. 10:0 unreacted canola oil and 0:10 unreacted crystal sulfur (powdered sulfur melted then cooled in water) for comparison. After some modification to the synthesis protocol, 30 wt. % sulfur was found to be feasible in forming a solid polymer.

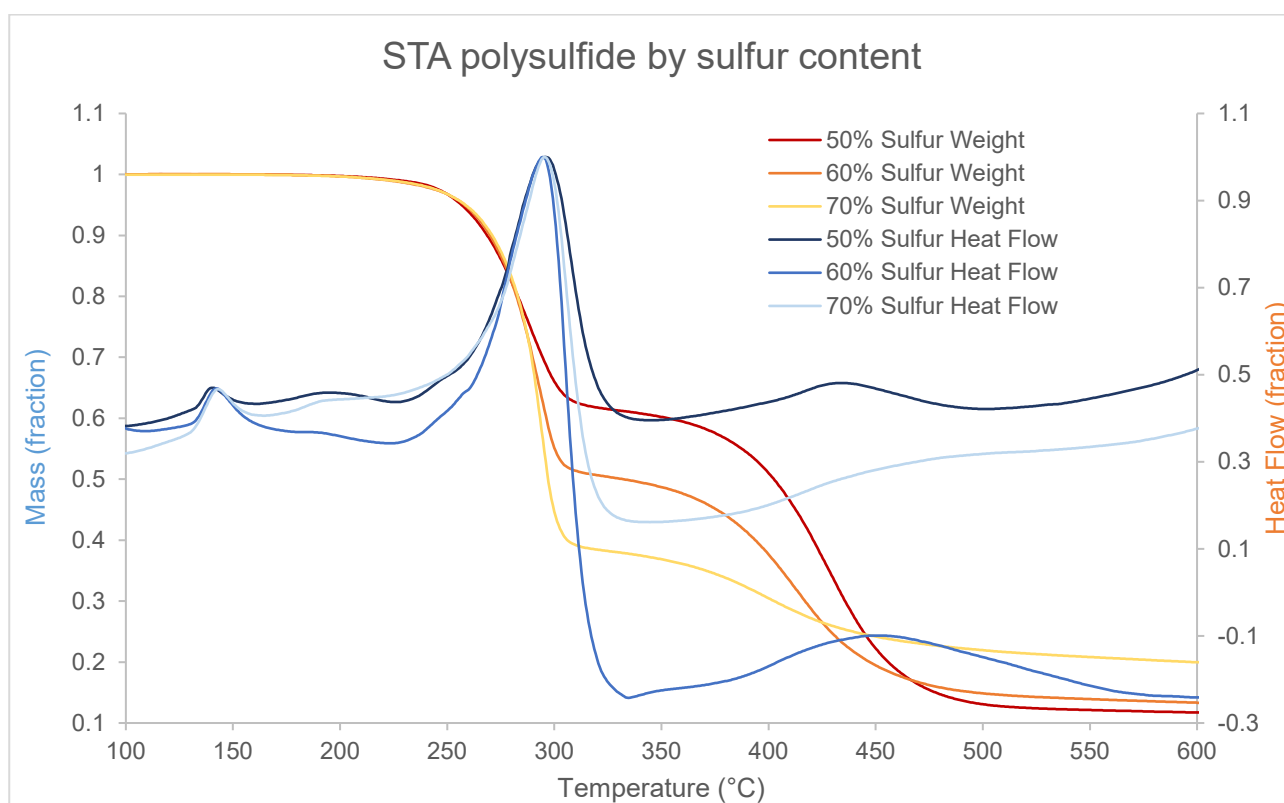


Figure 2.1.19 | STA analysis of polysulfides prepared at different reactant ratios. All polysulfide samples show very similar DSC and TGA profiles with an increased TGA onset at 260 °C with increasing sulfur content. This again indicates the first drop corresponds to the thermal decomposition of sulfur within the material. A second mass loss follows at ca. 400 °C corresponding to the loss of the canola oil component.

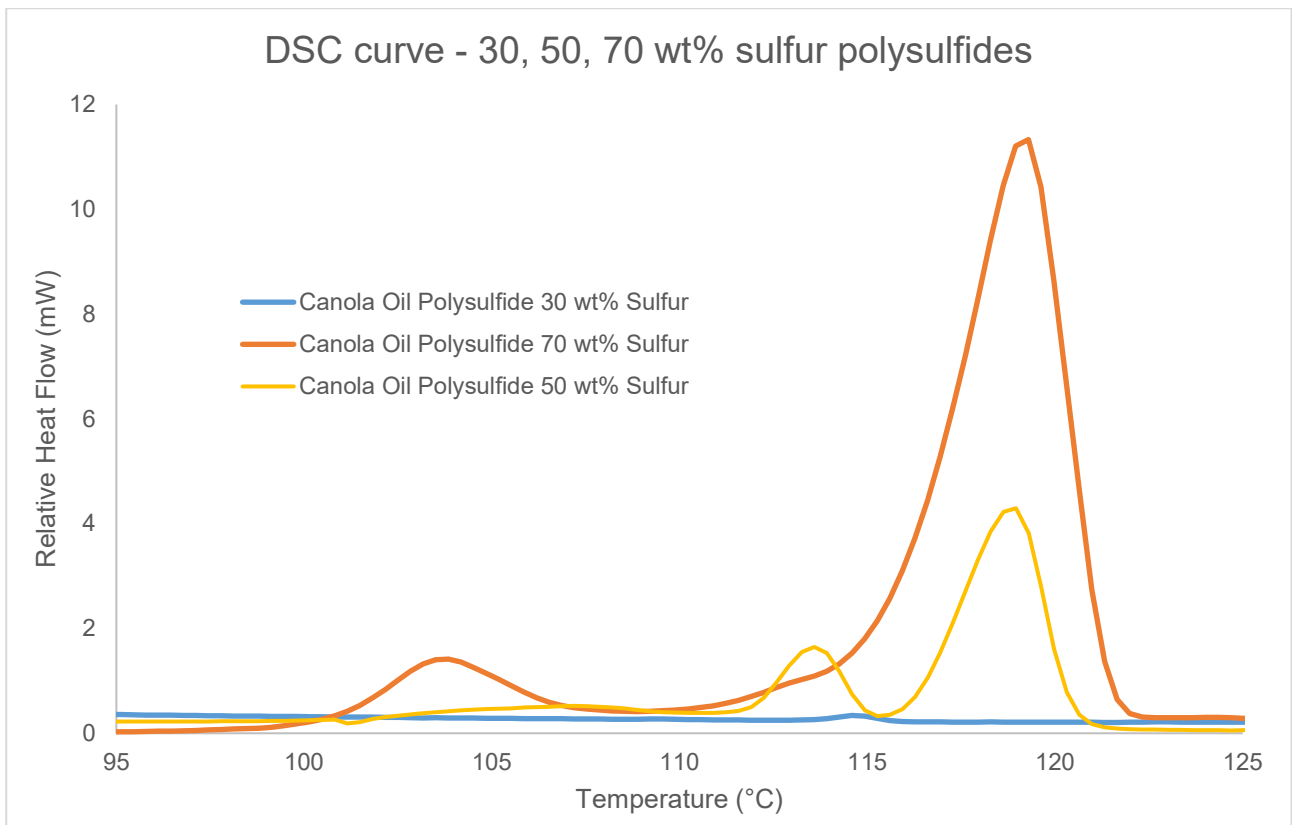


Figure 2.1.20 | DSC analysis of polysulfide prepared at different reactant ratios, focusing only on the melting point of free sulfur. With increasing sulfur content, the amount that is not incorporated into the polysulfide and instead remains as free sulfur also increases. At 30 wt. %, 4 % of the final material remains free sulfur. At 50 wt. % this rises to 9 % and 70 wt. % sulfur results in 38 % of the final product as free sulfur.

Other Inverse Vulcanised Vegetable Oils

Sunflower and olive oil polysulfides were prepared using the same procedure as canola oil polysulfide: Sulfur (20.0 g) was added to a 250 mL round bottom flask and heated, with stirring, to 180 °C. After 5 minutes of heating at this temperature the sulfur turned from a yellow to an orange liquid. At this point, the sunflower or olive oil (20.0 g) was added dropwise over 5 minutes. After 12 minutes, the reaction with sunflower oil reached its gel point and formed a rubber. The reaction with the olive oil reached its gel point after 21 minutes of reaction time. Both samples were left to cool for 15 minutes before removing from their flasks. A third reaction prepared with canola oil was carried out for comparison. All samples were independently washed by submerging in 0.1 M aqueous NaOH for 90 minutes followed by washing with DI water and drying in a fume hood. The samples have the same physical appearance, but are coloured in different shades of brown:

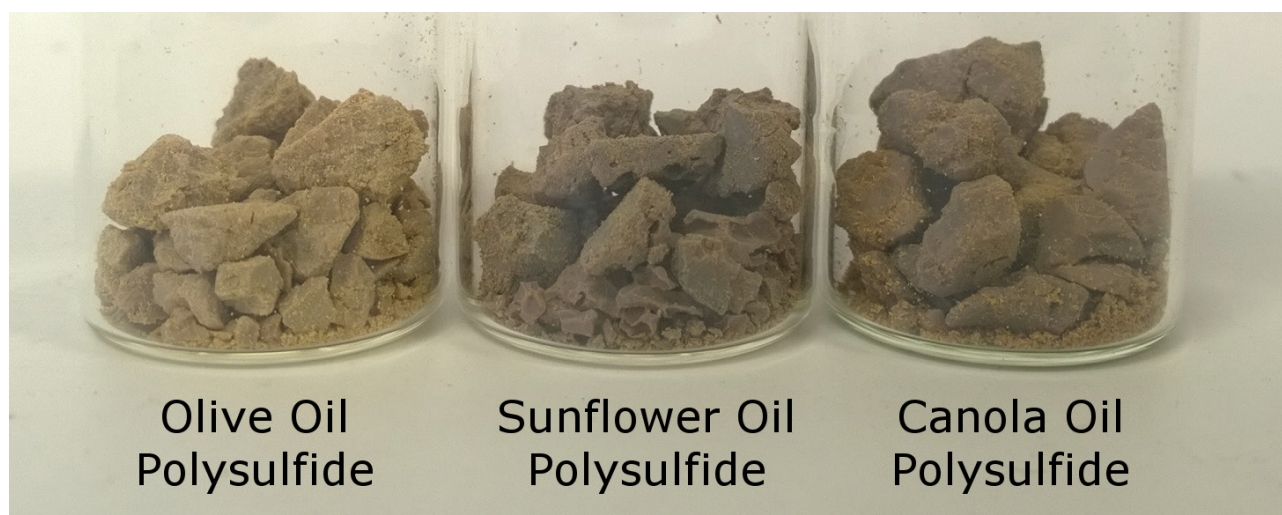


Figure 2.1.21 | A polysulfide rubber is obtained by the reaction of an equal mass of sulfur and olive oil, sunflower oil, or canola oil. The time to reach the gel point is shorter for sunflower oil, likely because of its higher polyunsaturated linoleic acid content in the triglyceride.

Vegetable Oil Composition

The fatty acid compositions of canola, olive and sunflower oils (used to produce inverse vulcanised vegetable oils) were deduced by transesterification of the triglycerides to form fatty acid methyl esters followed by GCMS analysis.

Method

Transesterification protocol performed by Renata Kucera as part of an undergraduate research project. GC-MS analysis was performed by the author.

Vegetable oil triglycerides were separated into individual long chain fatty acids and glycerol by transesterification, followed by GCMS analysis to identify the fatty acid methyl esters present. 1.0 g of each vegetable oil (canola, sunflower, olive) was placed in methanol (100 mL) and the mixture was subsequently cooled to 0°C in an ice bath followed by the addition of sodium methoxide (100 mg) to the mixture. The mixture was stoppered and stirred vigorously with a magnetic stirrer bar (~1000 rpm) at room temperature for 24 hours. An ice bath was used to cool the mixture to 0 °C and the reaction was quenched with 0.1 M HCl (10 mL). The mixture was diluted with ethyl acetate (150 mL) and water (150 mL) to separate and extract the aqueous and organic layers. Water (3 × 50 mL) and brine (3 × 50 mL) were then used to wash the ethyl acetate layer. The ethyl acetate layer was extracted, dried with sodium sulfate, filtered and dried under high vacuum. Samples were diluted (1 drop in 2 mL chloroform) for GC-MS analysis and run to a procedure adapted from literature for the determination of fatty acid methyl esters²: Hold at 50 °C for 1 min, ramp from 50 to 200 °C at 25 °C min⁻¹ (6 min), slow to a 3 °C min⁻¹ rate from 200 to 230 °C (10 min). Hold at 230 °C for 25 min. then ramp to 280 °C at 25 °C min⁻¹ (2 min) and hold at 280 °C for 10 min. Total run time 54 minutes. Injection temperature was 250 °C, flow rate 1.2 mL min⁻¹, stabilisation time 30 s.

Results

Fatty acids (as methyl esters)	Canola Oil (%)	Olive Oil (%)	Sunflower Oil (%)
oleic	78.7	77.7	37.3
linoleic	14.2	8.91	50.0
palmitic	4.01	9.89	0.064
stearic	1.82	2.26	5.40
paullinic	0.66	0	0
palmitoleic	0	0.63	0
arachidic	0	0.31	0.14
linolenic	0	0.16	0
2,4 di(methylethyl) phenol	0.075	0.092	0.050
myristic	0.036	0	0.040
margaric	0.028	0	0
unknown	0.44	0.073	6.86

Methyl ester molecular ions determined by comparison to major fragmentation product of M-31, indicating loss of OCH_3 (MW 31 Da)

Average sulfurs per alkene

With a thorough analysis of fatty acid composition, the average number of sulfur atoms per alkene can be calculated, a value that should indicate the sulfur rank (average polysulfide length) of the polymer.

	Canola oil	Olive oil	Sunflower oil
Calculated molecular weight (g mol^{-1})	877.69	875.68	822.92
Average number of alkenes per triglyceride	3.251	2.903	4.433
Average number of sulfur atoms per alkene	8.422	9.410	5.790

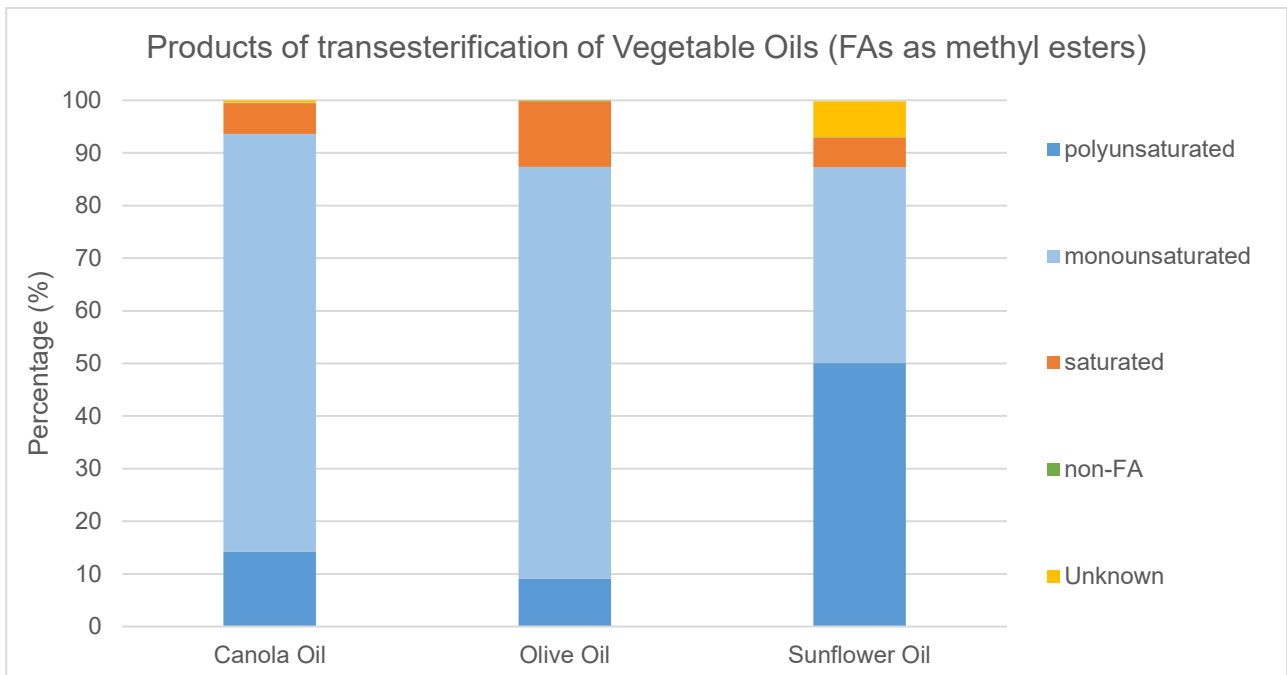
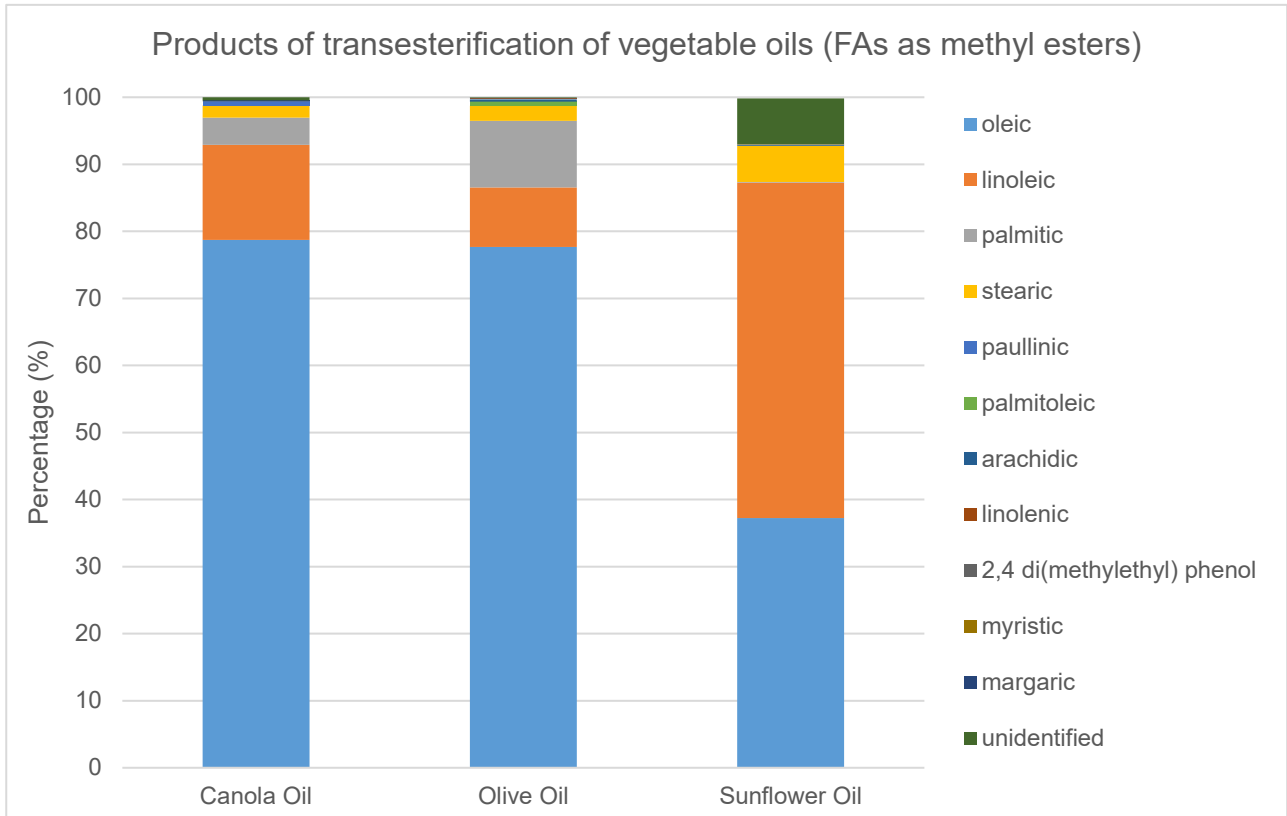


Figure 2.1.22 | Canola oil and olive oil show very similar fatty acid profiles containing comparable levels of oleic acid (the major monounsaturated fatty acid in both oils). Their main difference is in polyunsaturated fatty acid content, where canola oil contains 59 % more linoleic acid with the difference made up by palmitic acid (saturated) in olive oil. Sunflower oil differs quite greatly from canola and olive oil, containing half as much monounsaturated fatty acids (oleic acid) as either canola or olive oil with 3.5–5.5 times the amount of polyunsaturated fatty acids (linoleic).

GC-MS Traces

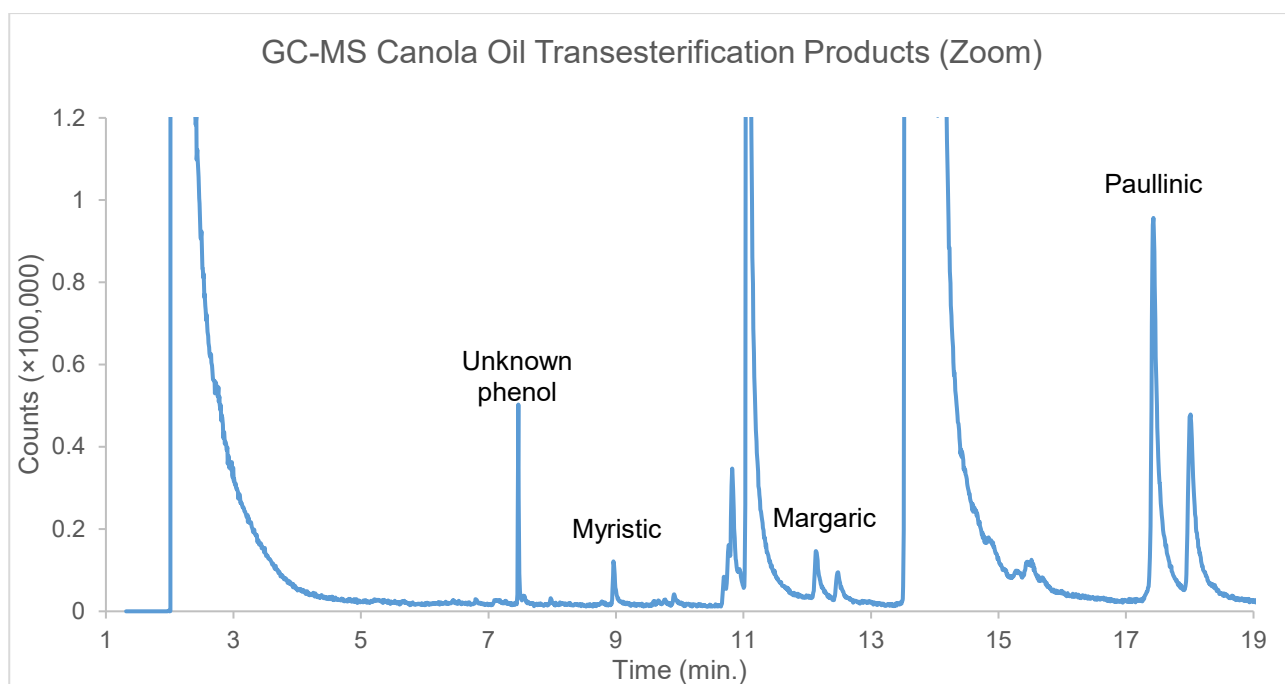
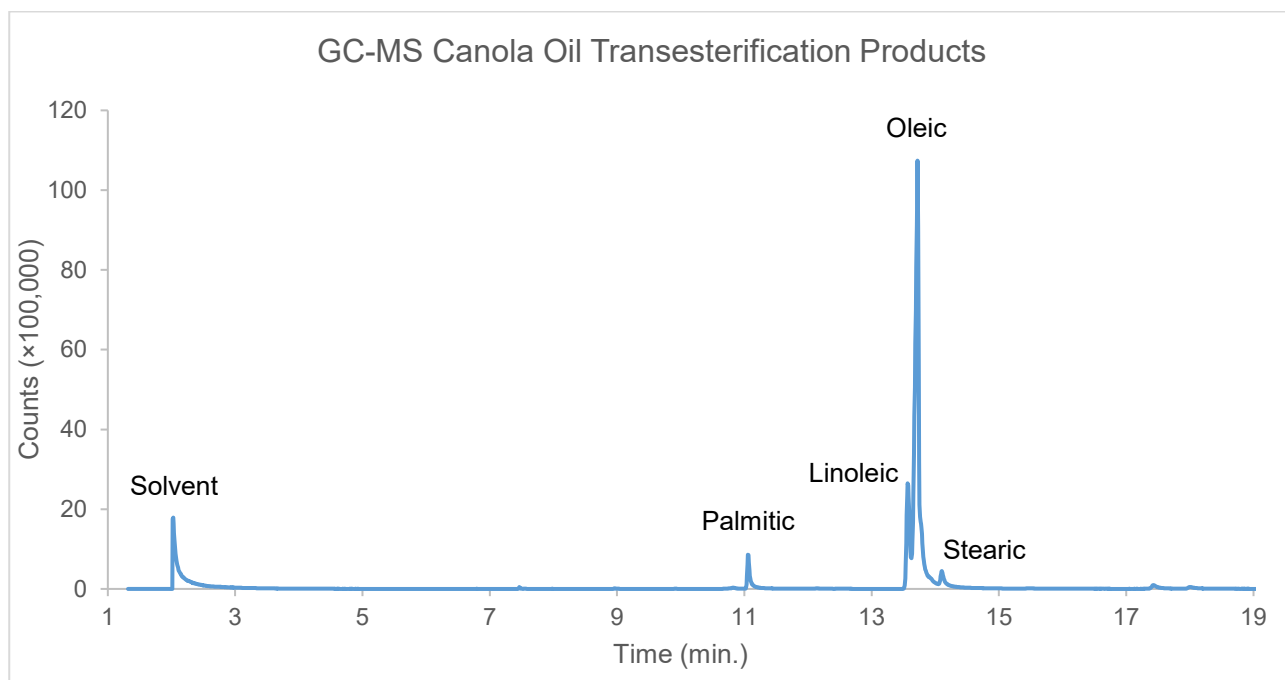


Figure 2.1.23 | GC-MS analysis of the products of transesterification of canola oil. Fatty acids are present as methyl esters. Top: Full spectra; Bottom: Region up to 120,000 counts only.

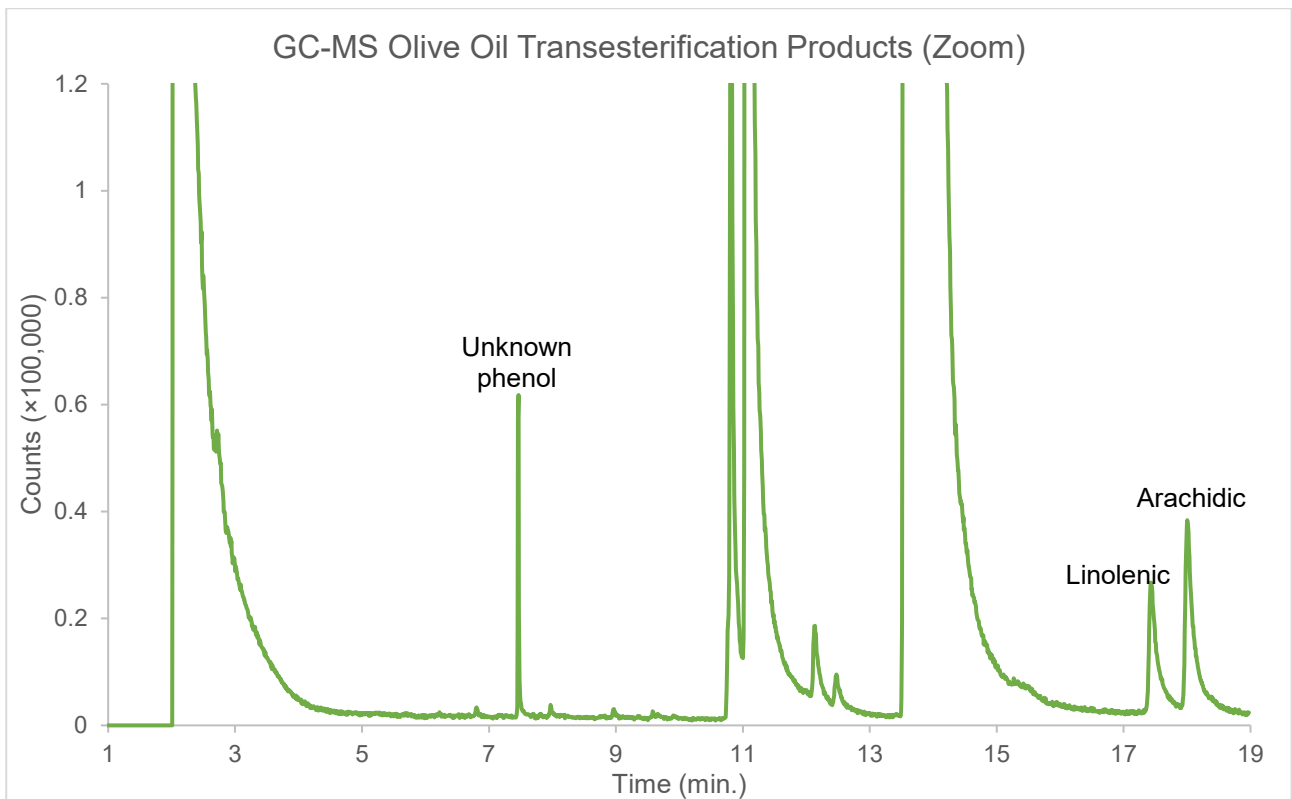
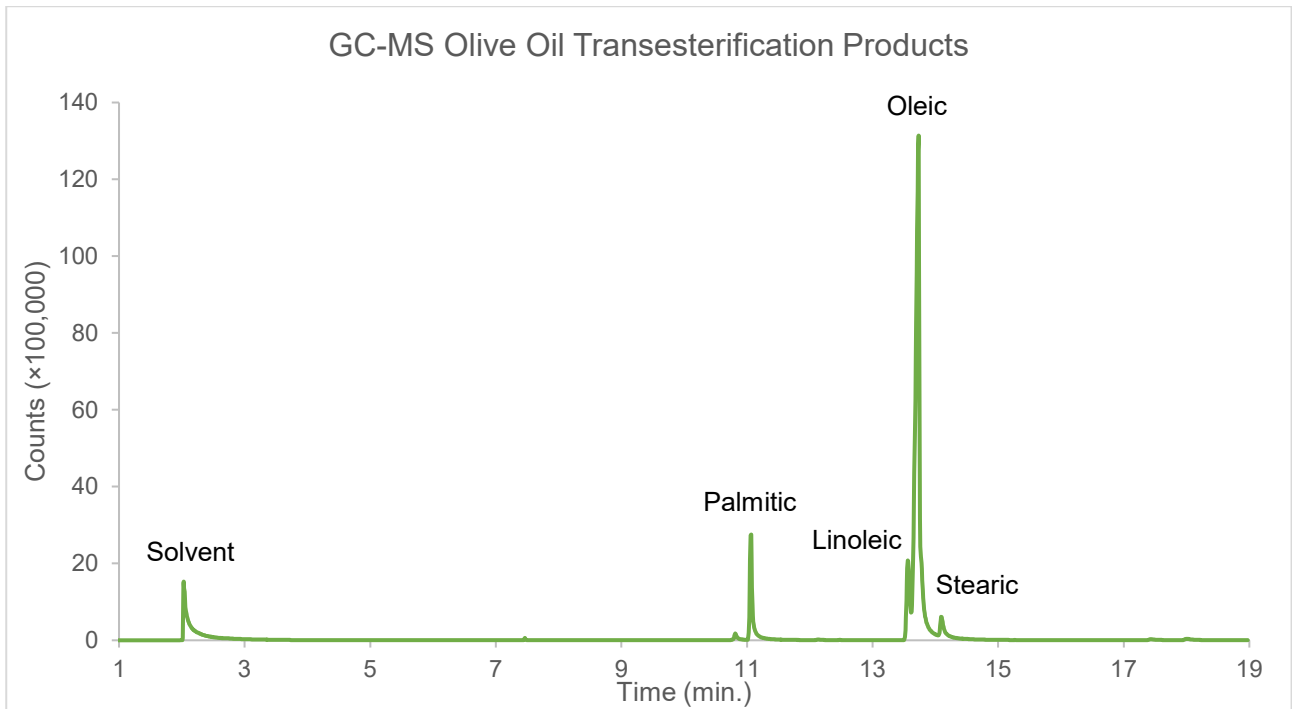


Figure 2.1.24 | GC-MS analysis of the products of transesterification of olive oil. Fatty acids are present as methyl esters. Top: Full spectra; Bottom: Region up to 120,000 counts only.

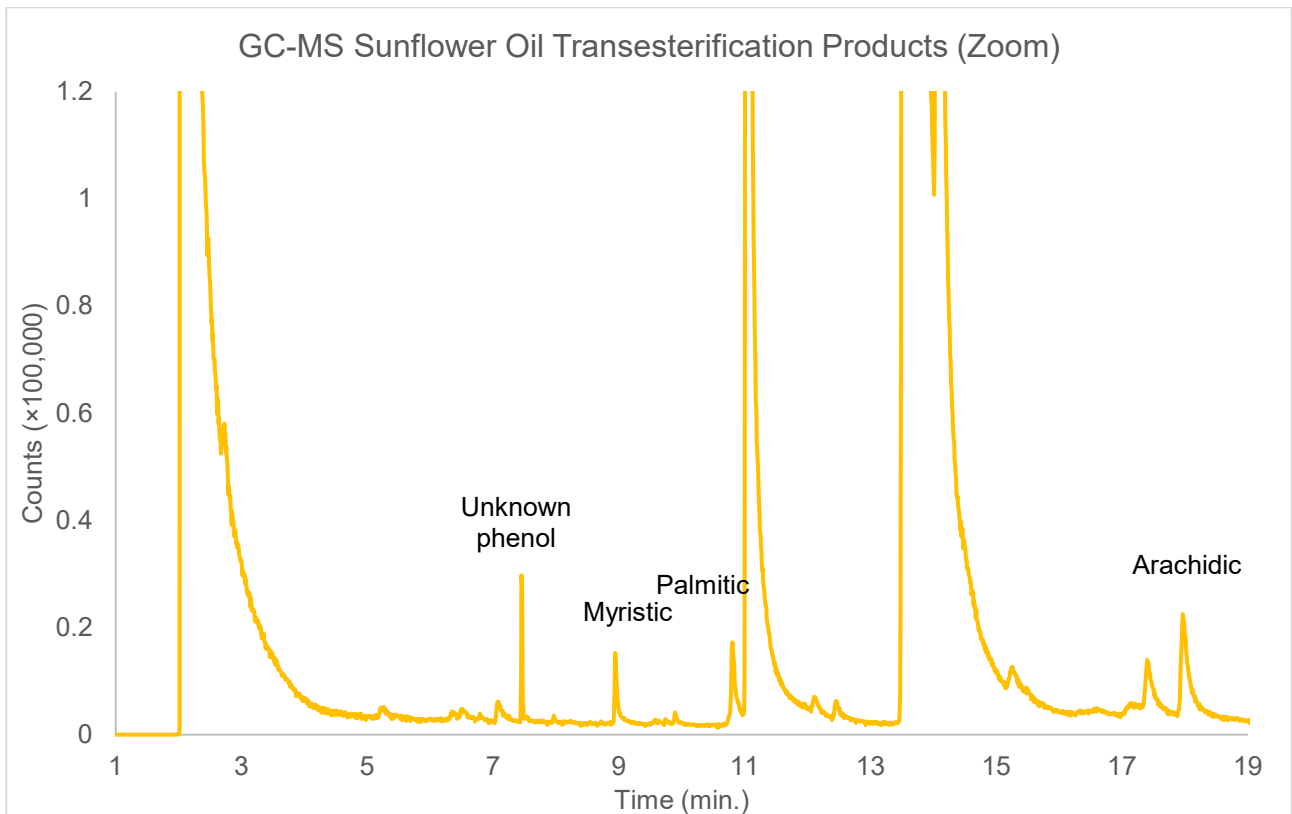
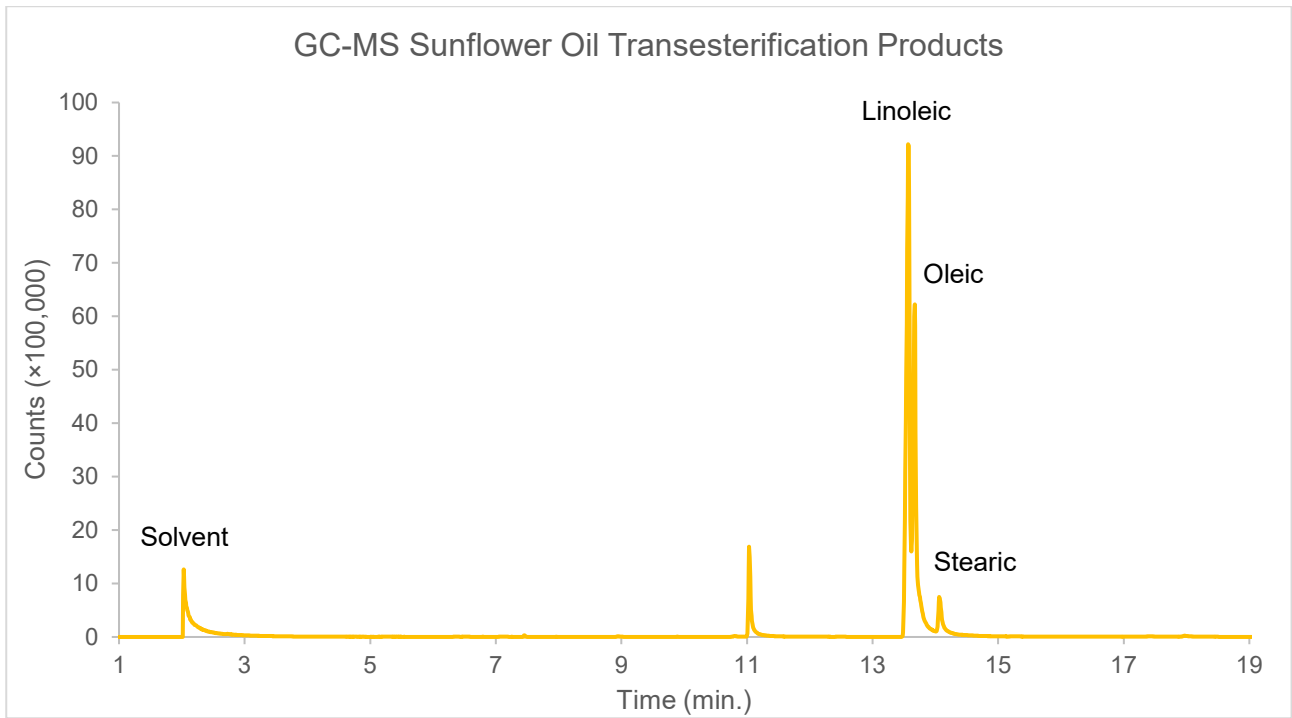


Figure 2.1.25 | GC-MS analysis of the products of transesterification of sunflower oil. Fatty acids are present as methyl esters. Top: Full spectra; Bottom: Region up to 120,000 counts only.

Characterisation of Waste Vegetable Oil (Fryer Oil)

Waste vegetable oil (1.00 g) was mixed with methanol (100 mL) in a 250 mL round bottom flask and cooled to 0 °C. Sodium methoxide (100 mg) was then added to the stirred mixture. The reaction mixture was stoppered and stirred vigorously at room temperature for 24 hours. Vigorous stirring is important to ensure effective mixing of the two phases present at the start of the reaction. After 24 hours, the reaction was cooled to 0 °C and quenched with 0.1 M HCl (10 mL). The mixture was transferred to a separatory funnel and then diluted with ethyl acetate (100 mL) and water (150 mL). The organic layer was isolated and then washed with water (3 x 50 mL) and brine (3 x 50 mL) before drying (sodium sulfate), filtering and concentrating under reduced pressure. Analysis by ¹H NMR and GC-MS following the protocol described above² revealed clean conversion to the fatty acid methyl esters. Yield for fatty acid methyl esters from 1.00 g vegetable oil: 970 mg.

GC-MS Fryer Oil Transesterification Products

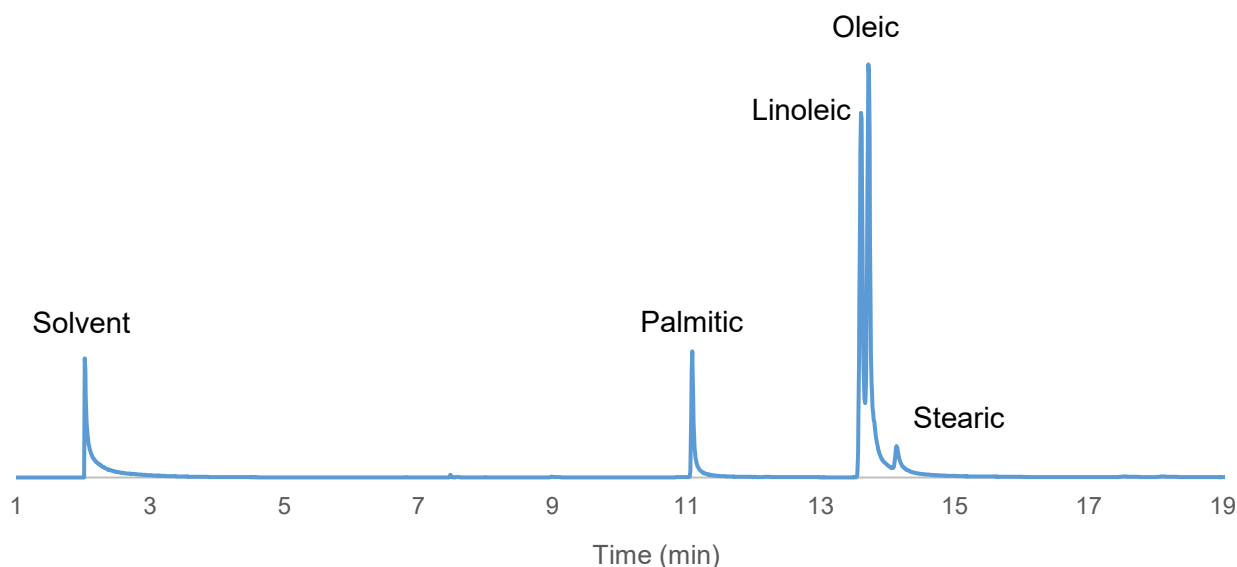


Figure 2.1.26 | GC-MS analysis of the products of transesterification of waste fryer oil from McHugh's cafe. Fatty acids are present as methyl esters.

Major products were fatty acid methyl esters of oleic (52.84 %), linoleic (34.14 %), palmitic (10.00 %), and stearic acids (2.87 %) with other unidentified materials comprising 0.15 % of the non-solvent peaks.

Products of transesterification of vegetable oils (fatty acids as methyl esters)

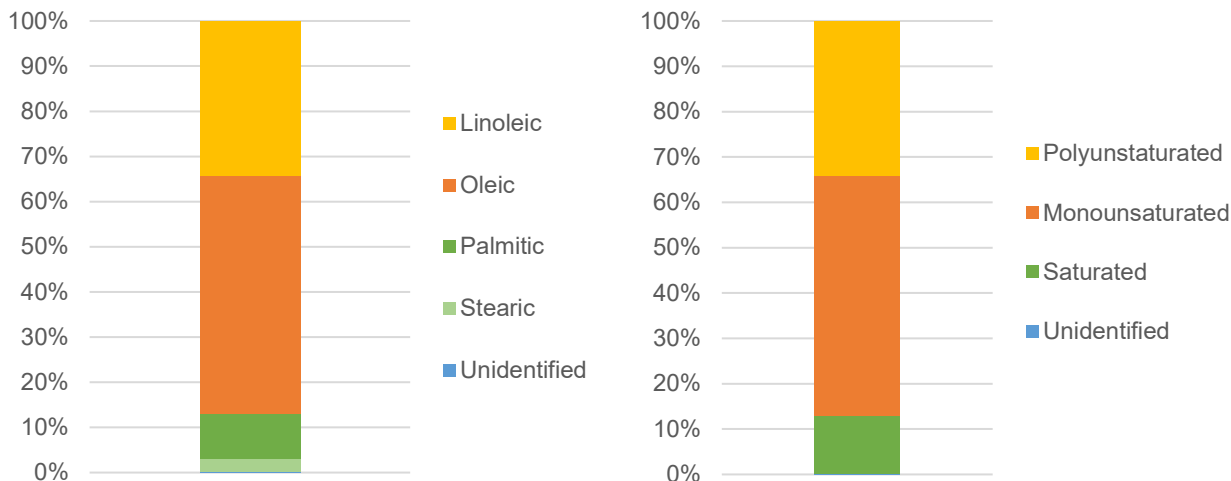


Figure 2.1.27 | Charts representing the relative composition of waste fryer oil. Left: Separated as individual fatty acids; Right: Grouped by degree of saturation.

Simultaneous thermal analysis of vegetable oils used in the synthesis of the polysulfides

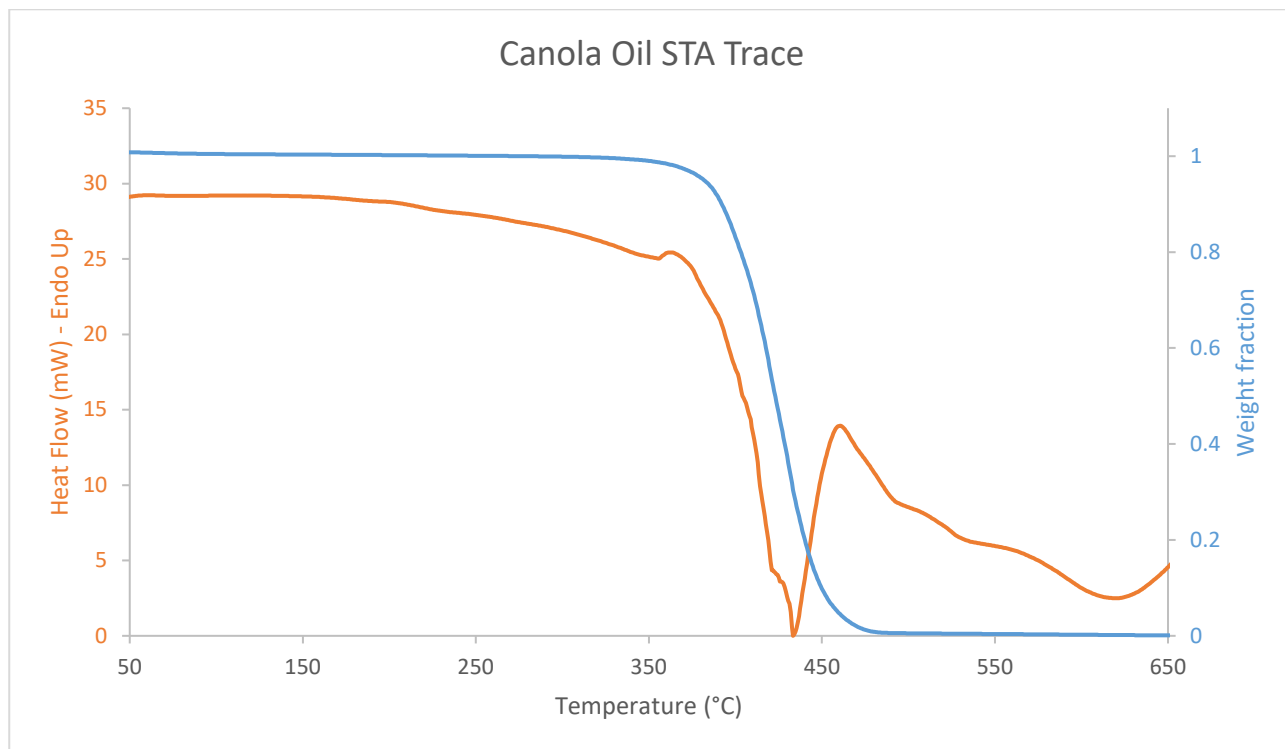


Figure 2.1.28 | STA of pristine canola oil. Endotherms are displayed upwards.

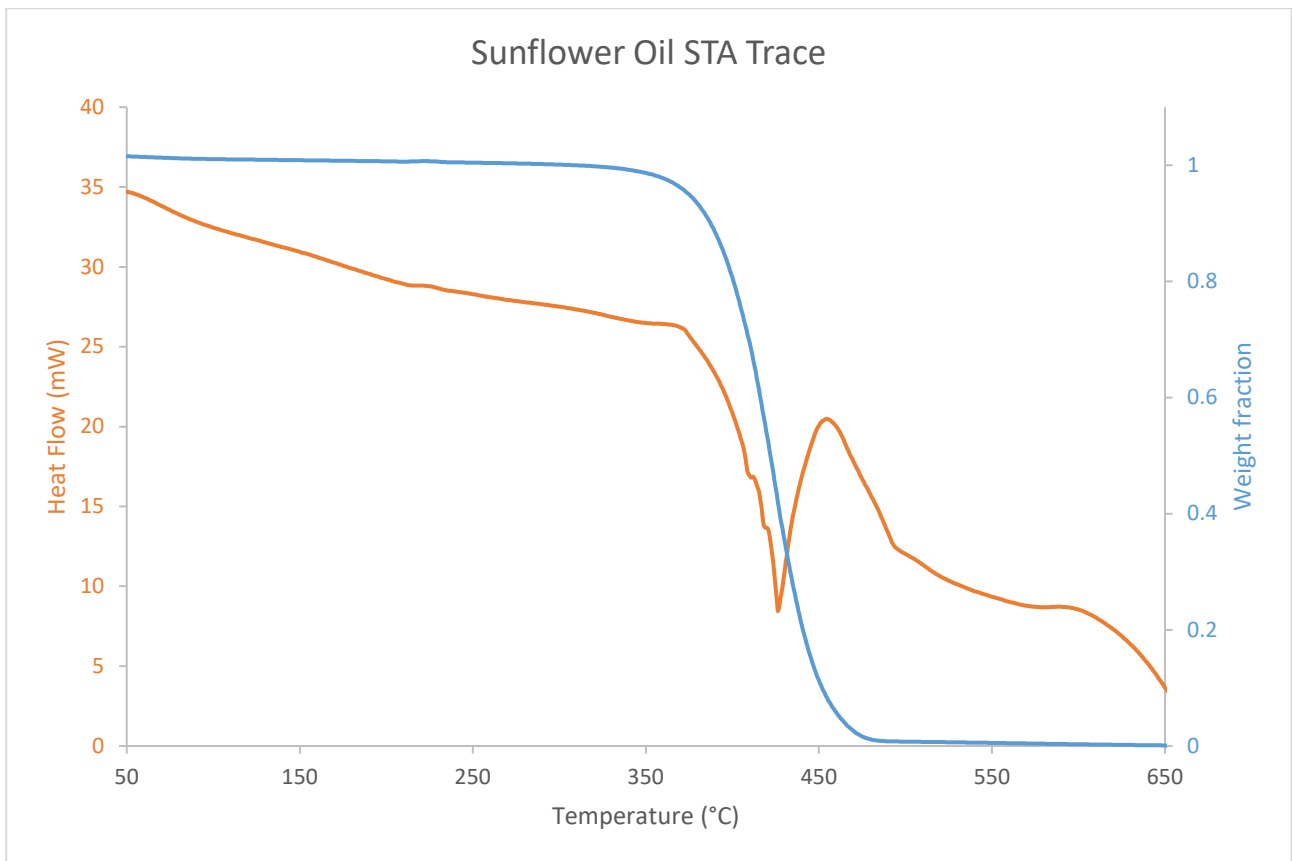


Figure 2.1.29 | STA of pristine sunflower oil. Endotherms are displayed upwards.

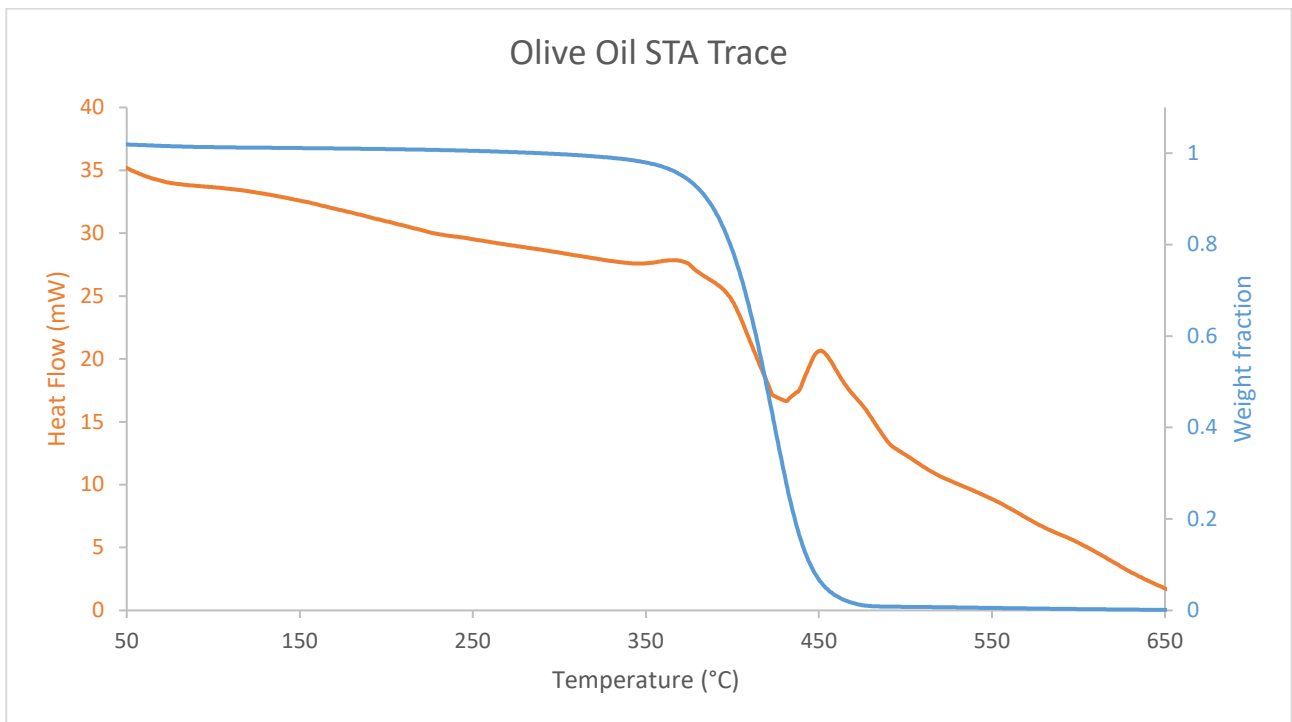


Figure 2.1.30 | STA of pristine olive oil. Endotherms are displayed upwards.

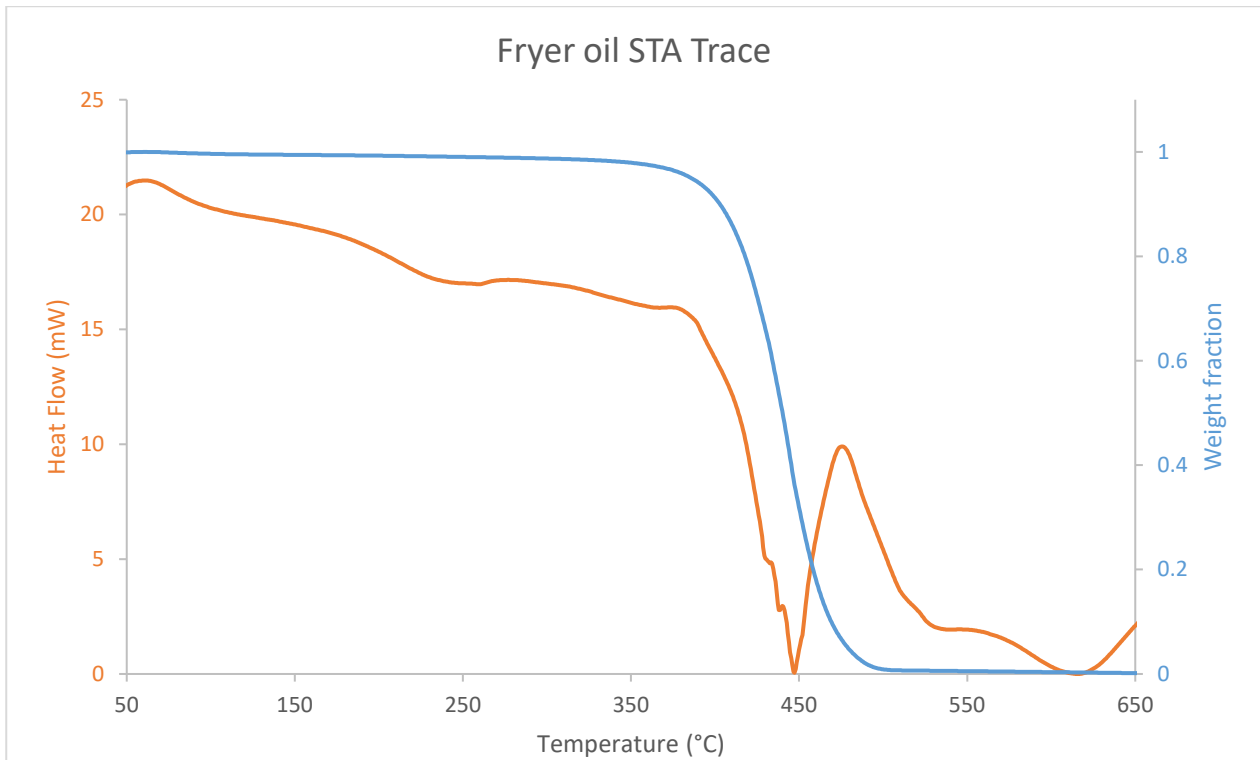


Figure 2.1.31 | STA of waste fryer oil. Endotherms are displayed upwards.

DSC of polysulfides prepared from canola, sunflower, olive and recycled cooking oils

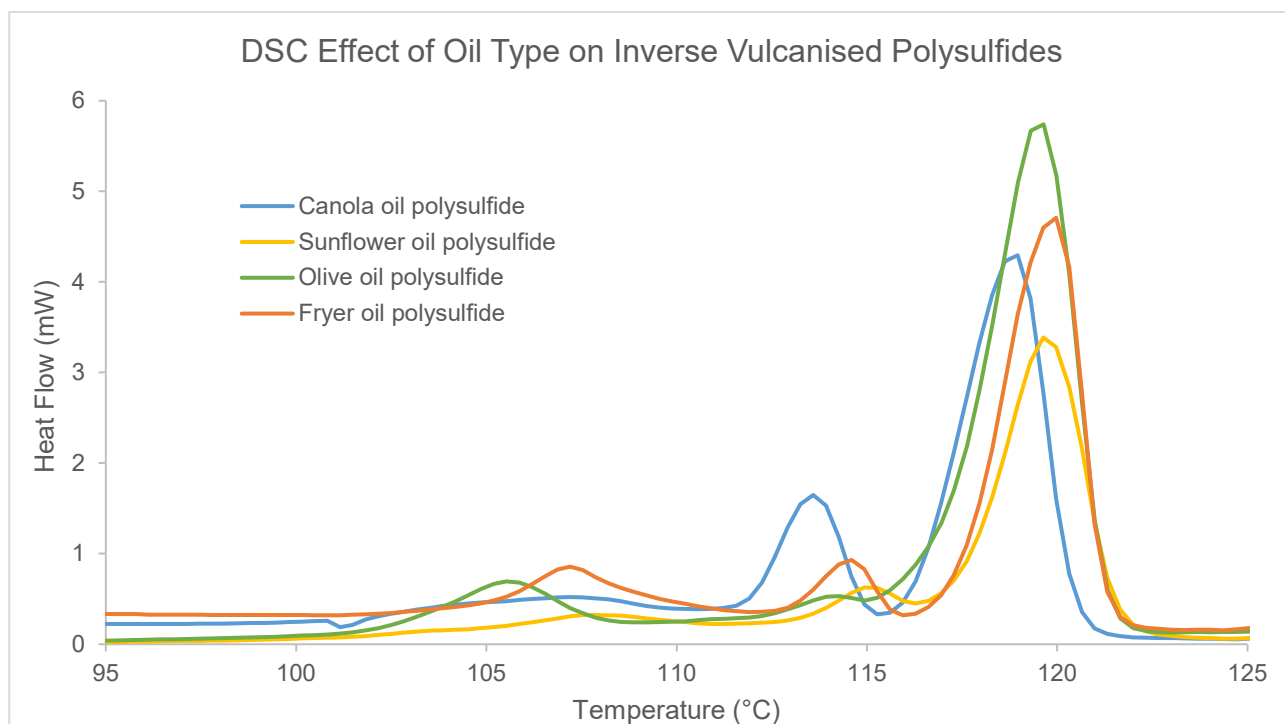


Figure 2.1.32 | Normalised DSC of polysulfides prepared from canola oil, sunflower oil, olive oil and recycled cooking oil (waste fryer oil) in the region in which unreacted/free sulfur results in a phase transition. While the TGA and DSC were largely the same (see below for full DSC) regardless of the oil source, subtle variations in the region between 100 and 125 °C were noted, as shown in the figure. These endotherms correspond to the melting of free sulfur.

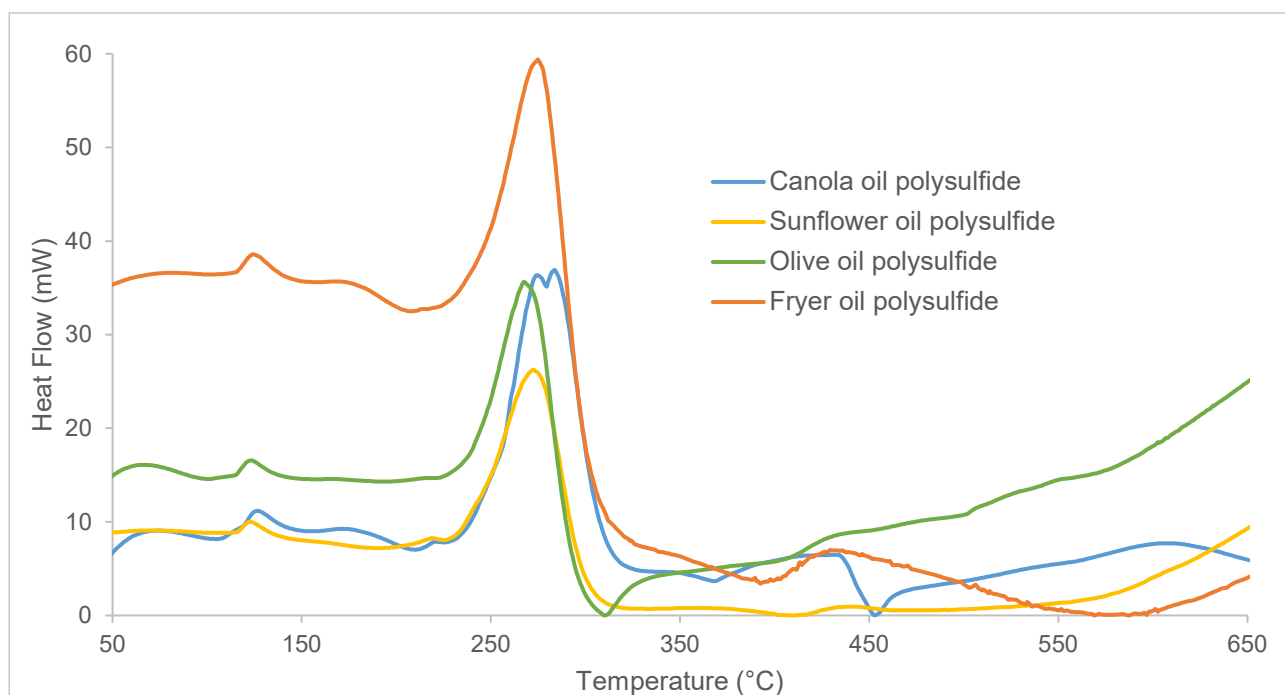


Figure 2.1.33 | Full DSC trace of polysulfides prepared from canola oil, sunflower oil, olive oil and recycled cooking oil.

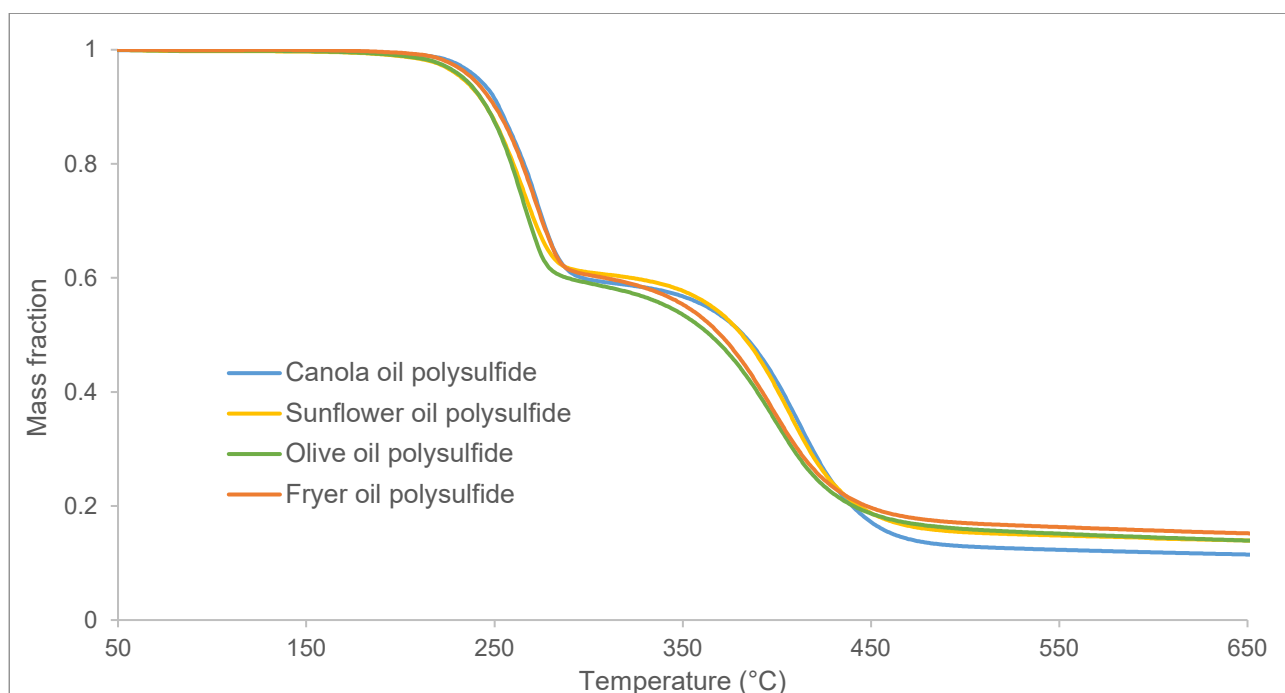


Figure 2.1.34 | TGA trace of polysulfides prepared from canola oil, sunflower oil, olive oil and recycled cooking oil.

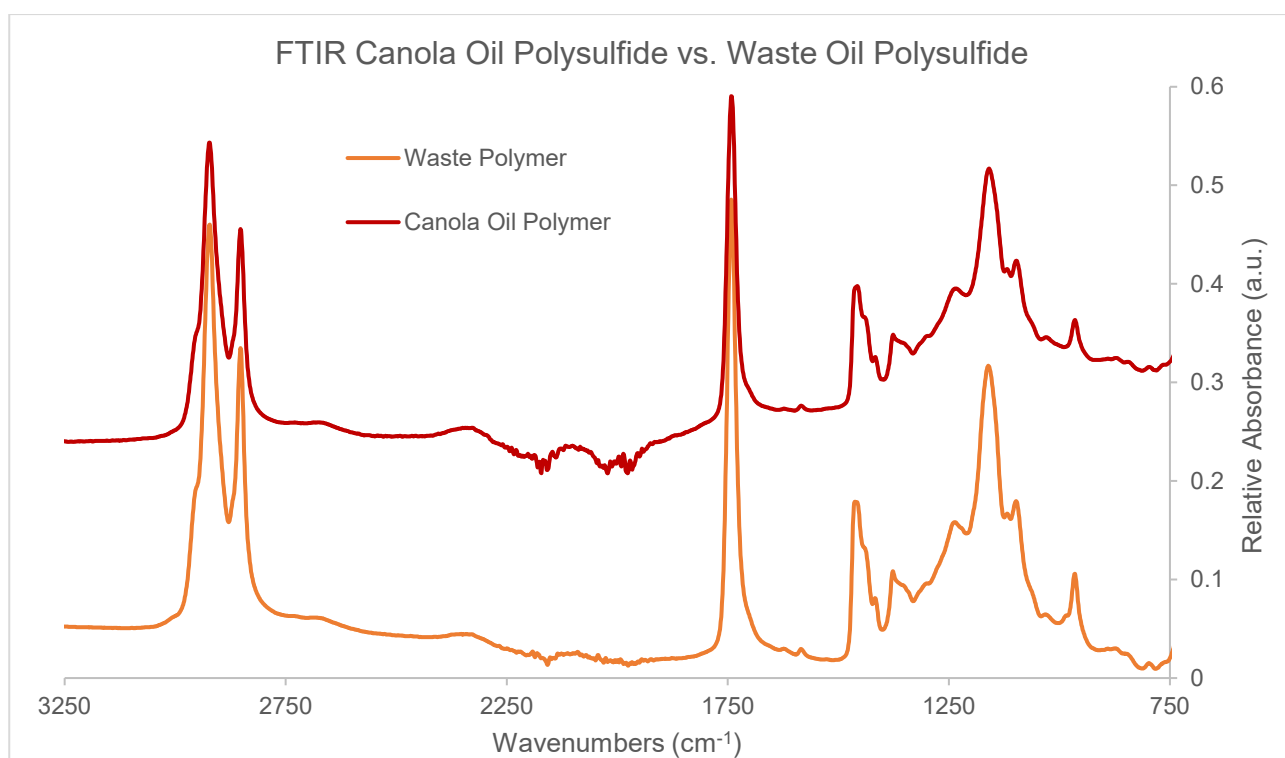


Figure 2.1.35 | FT-IR comparison of canola oil polysulfide and recycled cooking oil polysulfide. Traces are very similar. Noise from 2000 to 2200 cm⁻¹ is an artefact of the instrument and not due to the polysulfide.

Comparison to Factice

Factice is a commercially available rubber material and plasticiser used in the rubber industry. Similar to canola oil polysulfide, it is synthesised from only canola oil and sulfur with the key difference being the reaction process. The polysulfide is produced by the inverse vulcanisation of canola oil, where canola oil is added dropwise to molten sulfur to crosslink long sulfur chains. Factice is produced by the vulcanisation of canola oil, where sulfur is added dropwise to canola oil to crosslink triglyceride molecules. Factice is generally produced to a target weight % sulfur (denoted as the material's "grade"), where different grades offer slightly different physical properties. 3 grades were acquired from D.O.G. Chemie: F10, F17 and F25 where the number after F denotes the percentage sulfur content.



Canola oil polysulfide



F10 grade factice



F17 grade factice



F25 grade factice

Figure 2.1.36 | Photographs of canola oil polysulfide and D.O.G. factice of different grades for comparison.

FTIR

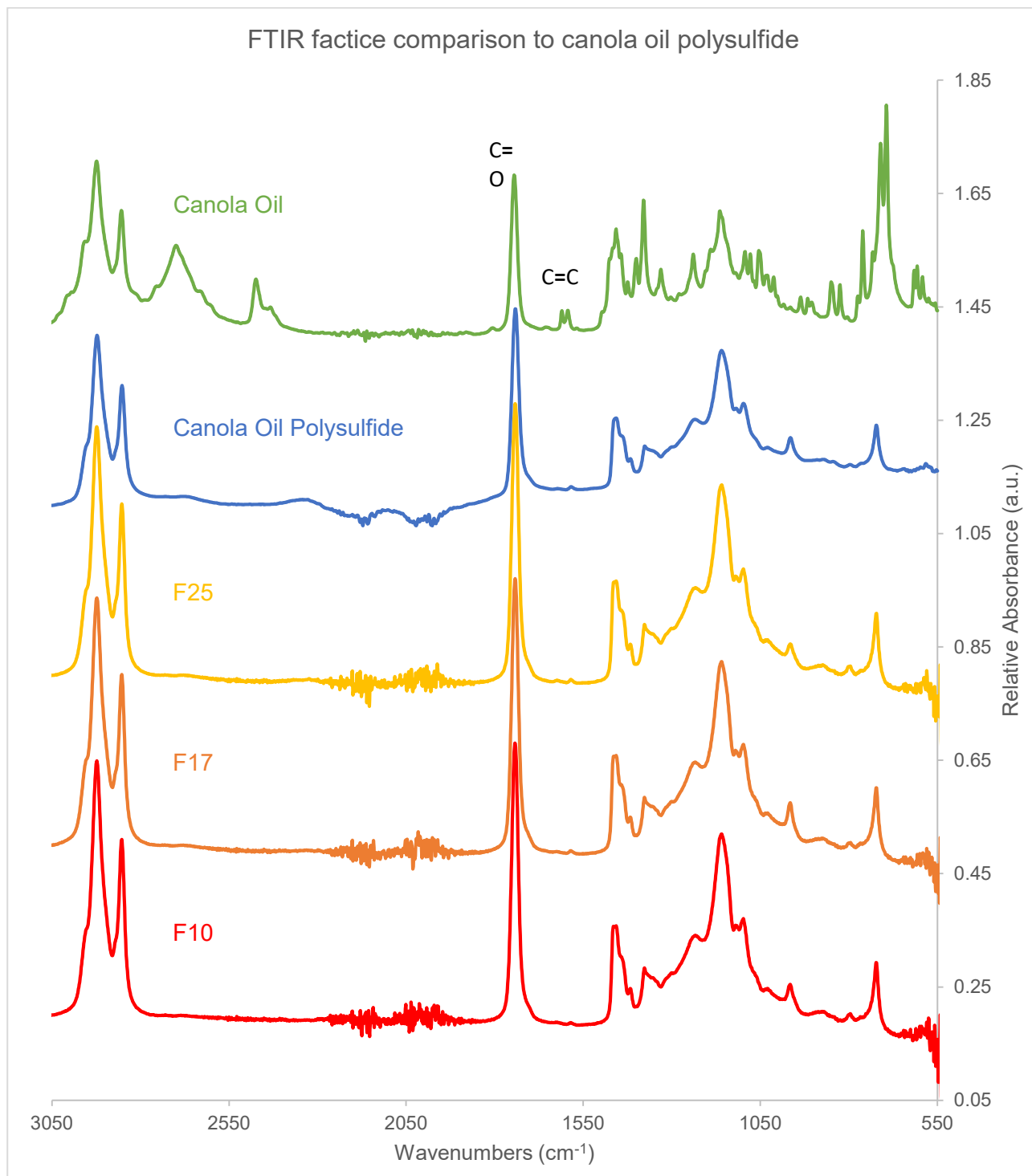


Figure 2.1.37 | Layered FTIR spectra canola oil polysulfide, pristine canola oil and D.O.G. factices. Noise in the spectra from 1900 - 2200 cm^{-1} is an artefact due to the instrument in solid phase analysis by ATR FTIR.

Raman

Raman analysis performed by Christopher Gibson

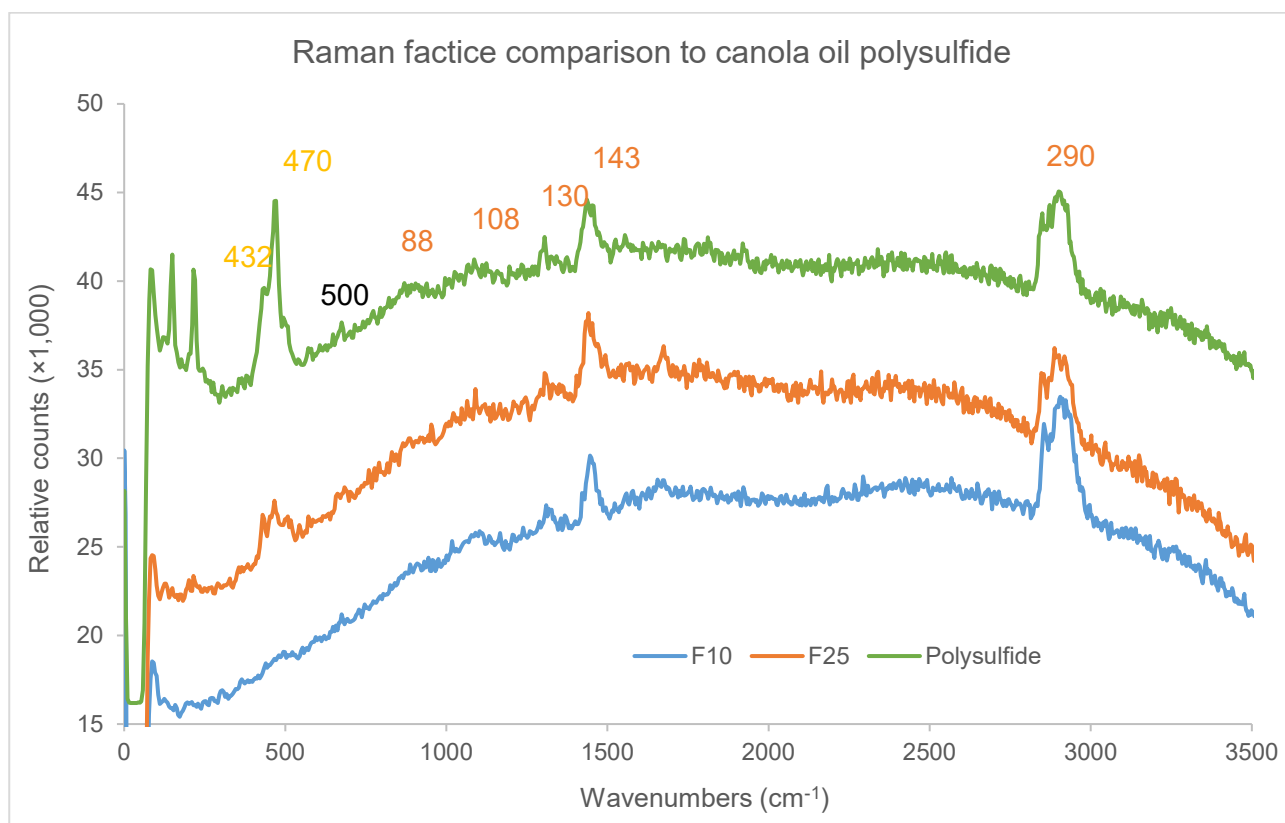


Figure 2.1.38 | Raman spectra of canola oil polysulfide and factice

Peaks highlighted in yellow have corresponding peaks in the S₈ control spectra, those in orange have corresponding peaks in the canola oil reference spectra. Both factice and canola oil polysulfide contain a new shoulder to the major sulfur peak at 500–505 cm⁻¹. It is currently unclear what this corresponds to; whether this indicates S-C bonds or perhaps sulfides present in the polymer.

STA

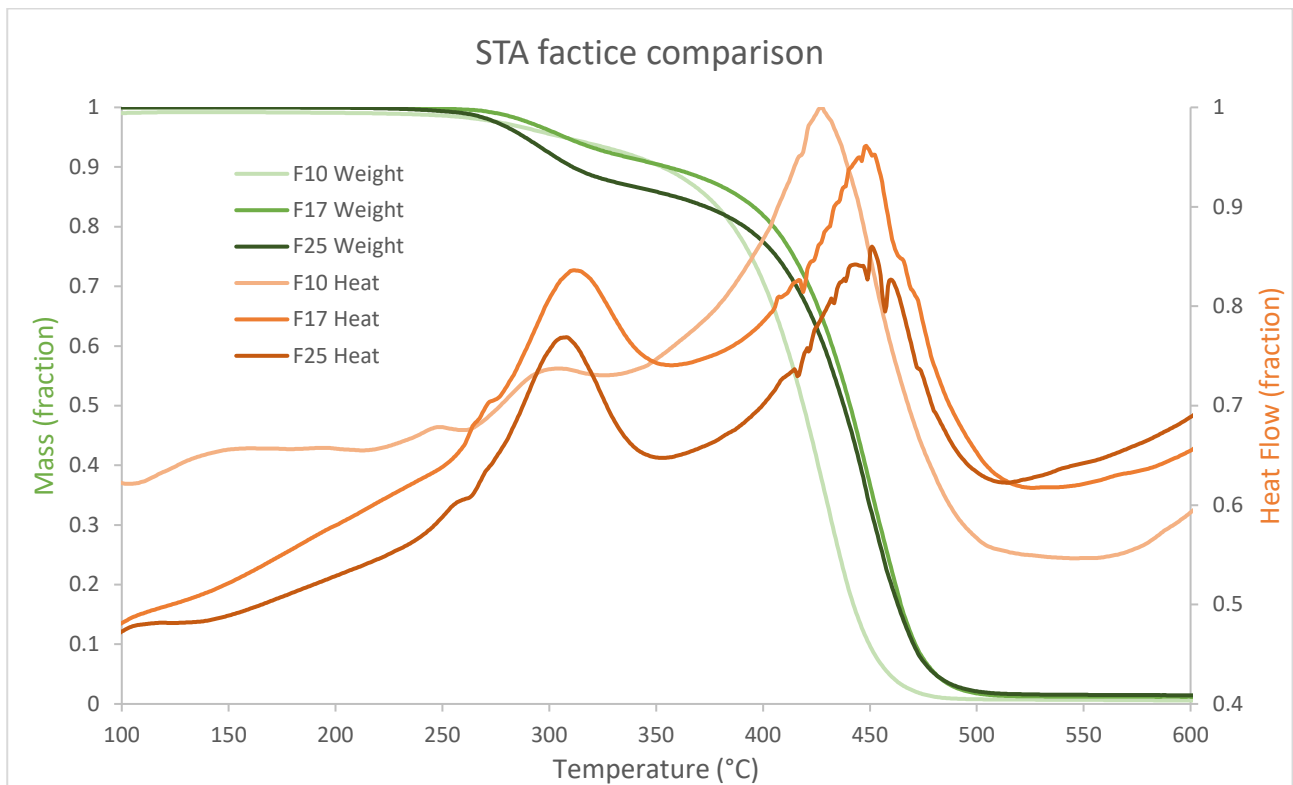


Figure 2.1.39 | Comparative STA (TGA in green, DSC in orange) spectra of three grades of factice.

All factice grades show very similar DSC and TGA profiles with an increased TGA onset beginning at 280 °C with increasing grade (sulfur content) followed by a second mass loss occurring sharply from 400 °C.

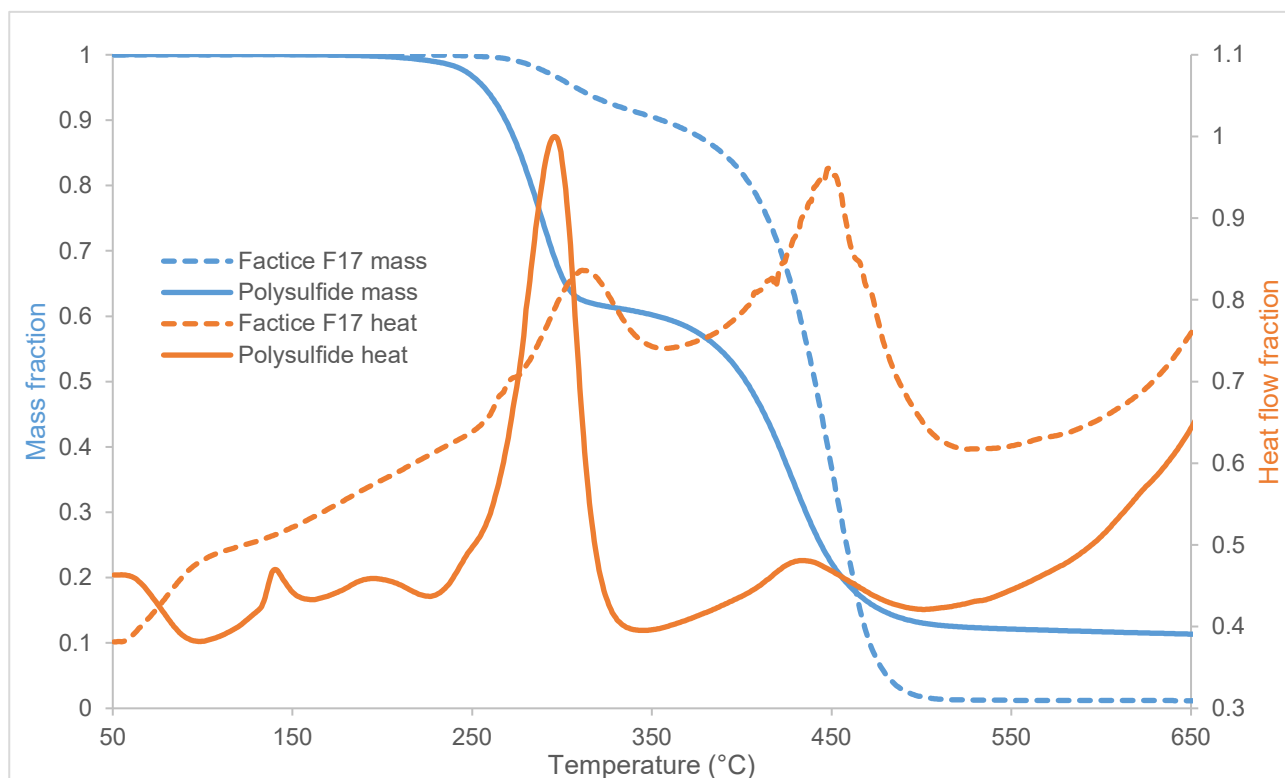


Figure 2.1.40 | Overlaid polysulfide and factice STA (TGA in blue, DSC in orange) spectra. Solid line: Polysulfide data; Spaced line: Factice data.

Canola oil polysulfide and factice at first glance seem quite dissimilar in their DSC and TGA profiles. By TGA we see two distinct drops in sample mass in canola oil polysulfide first at 280 °C, corresponding to loss of sulfur, then 400 °C corresponding to the loss of the canola oil component. A similar profile is seen in factice (F17 shown) with the first mass loss far less pronounced, presumably due to the decreased sulfur content. In DSC can be seen multiple peaks for the polysulfide and only 2 major peaks for factice. Peaks at 300 °C and 430 °C are present in both profiles, the first indicating sulfur sublimation and the second carbonaceous material sublimation. The third peak unique in the polysulfide spectrum occurs at 130 °C and corresponds to free, unreacted sulfur present in the polysulfide structure. Oddly this peak does not appear in factice despite the manufacturer's report claiming it to contain a similar percentage of free sulfur.

Porous Polymer synthesis

14.00 g NaCl was ground to a fine powder in a mortar and pestle and left until required in synthesis. 3.00 g sulfur powder was poured, using a powder funnel, into a 250 mL round bottom flask containing a 40 mm oval stirrer bar. The RBF was placed into an aluminium heating block preheated to 180 °C to melt the sulfur with slow (50 rpm) stirring as required. Once the heating block had reached 180 °C and the sulfur had melted into an orange liquid, 3.00 g canola oil was added dropwise over 2 minutes. After the addition of all canola oil, the ground NaCl was added portion-wise over 5 to 10 minutes. During this time the mixture thickened and stirring was reduced accordingly to ensure continued mixing. Approximately 15 to 20 minutes after the addition of all NaCl, the mixture vitrified to a brown solid. At this point the RBF was taken off the heat and allowed to cool to room temperature for 1 hour. Polymer was removed from the RBF by abrasion and then blended for 1 minute in a food processor.

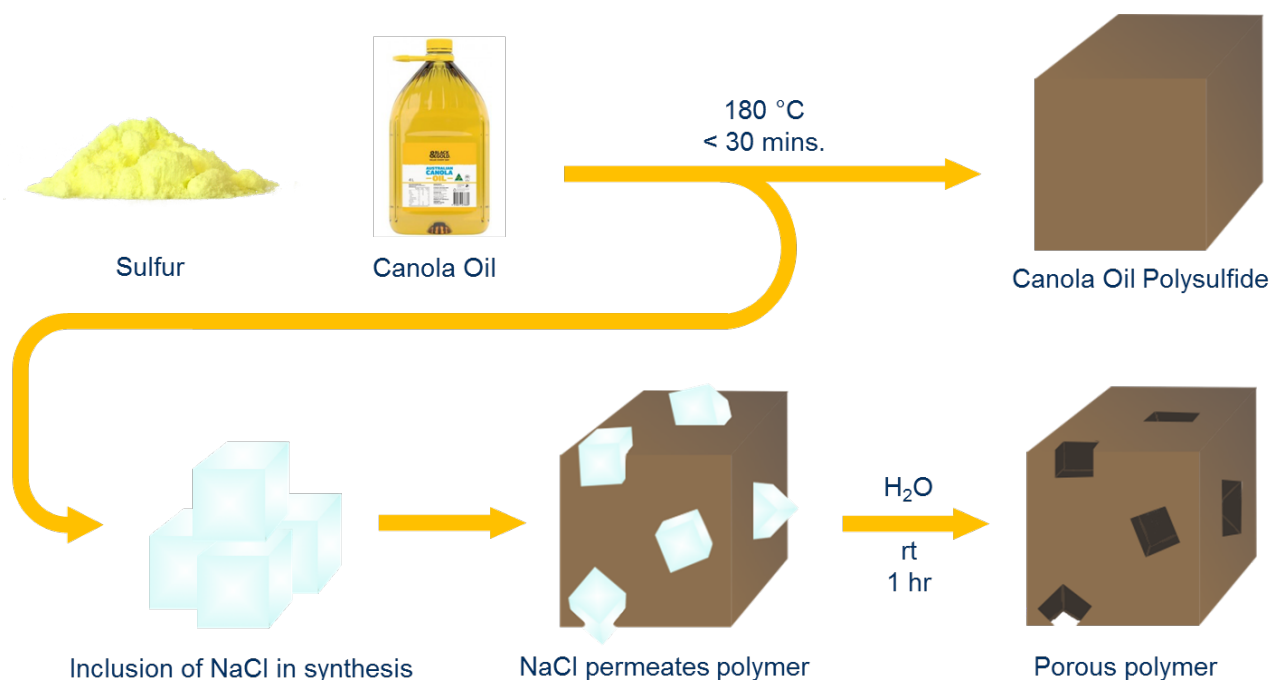


Figure 2.1.41 | Simplified diagram of porous polymer synthesis demonstrating introduction of porosity from salt crystals embedded in the polymer structure.

There were 2 washing steps. For the first, the blended material (20.0 g) was placed into a 250 mL beaker along with 150 mL DI water and a 30 mm straight stirrer bar and left for 1 hour with medium stirring (600 rpm). After vacuum filtering with a further 2 × 50 mL water and leaving to dry overnight, powdered salt became visible on the surface of the polymer. To remove this residual salt, a second wash was required. The polymer was placed in a plastic container with 100 mL water and shaken vigorously for 30 seconds. Vacuum filtration was repeated, and the polymer allowed to dry overnight once more. The material was now ready for use, final yield was 6.0 g.



Figure 2.1.42 | Left: polymer before wash procedure, right: polymer after wash procedure

It is recommended at least 20.0 g material be blended at any one time to ensure the effectiveness of this step. For washing more material in a single process – determine the amount of water required by noting the total amount of salt present (e.g. 42.0 g), determining the water saturation limit for this amount at room temp (359 g L^{-1} , so 117 mL for 42.0 g) and multiplying that amount by 4 ($117 \times 2 = 468 \text{ mL}$) to hasten the process. Use at least this much water in the first wash step, less can be used for the second wash.

STA porous polysulfide

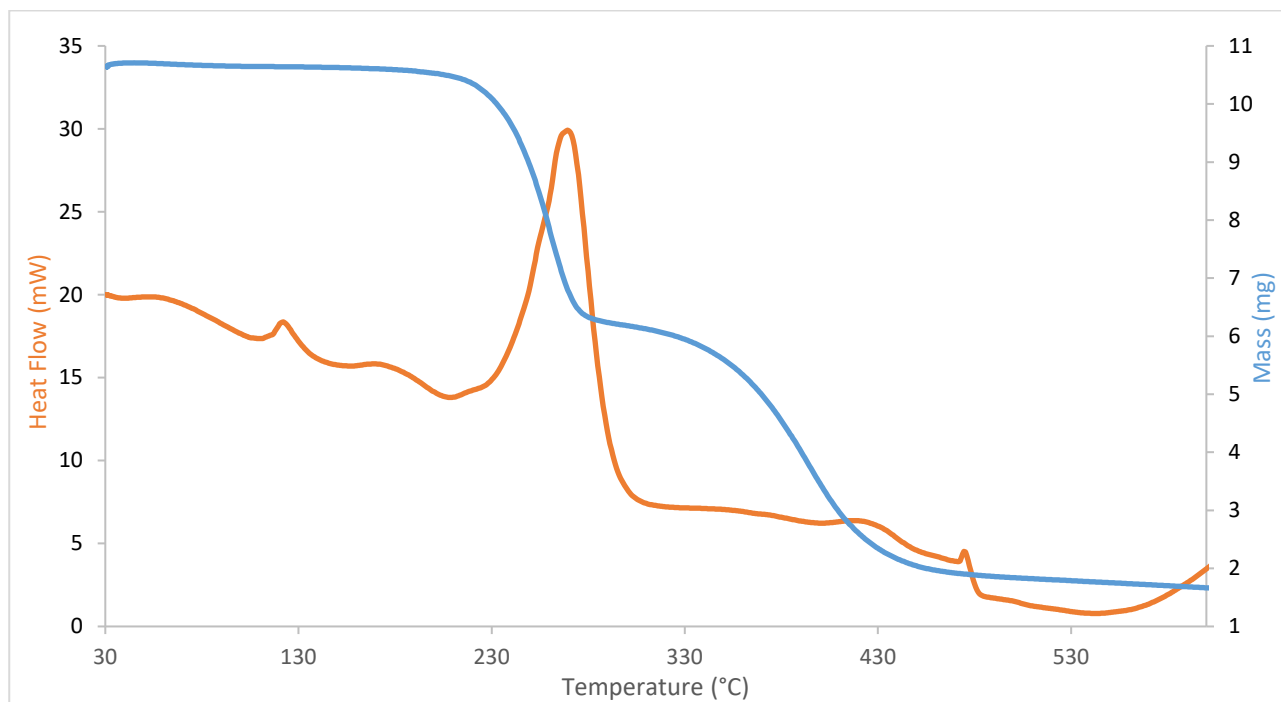


Figure 2.1.43 | STA trace of 9.13 mg porous (70 wt. % NaCl) polysulfide (1:1 sulfur - canola oil)

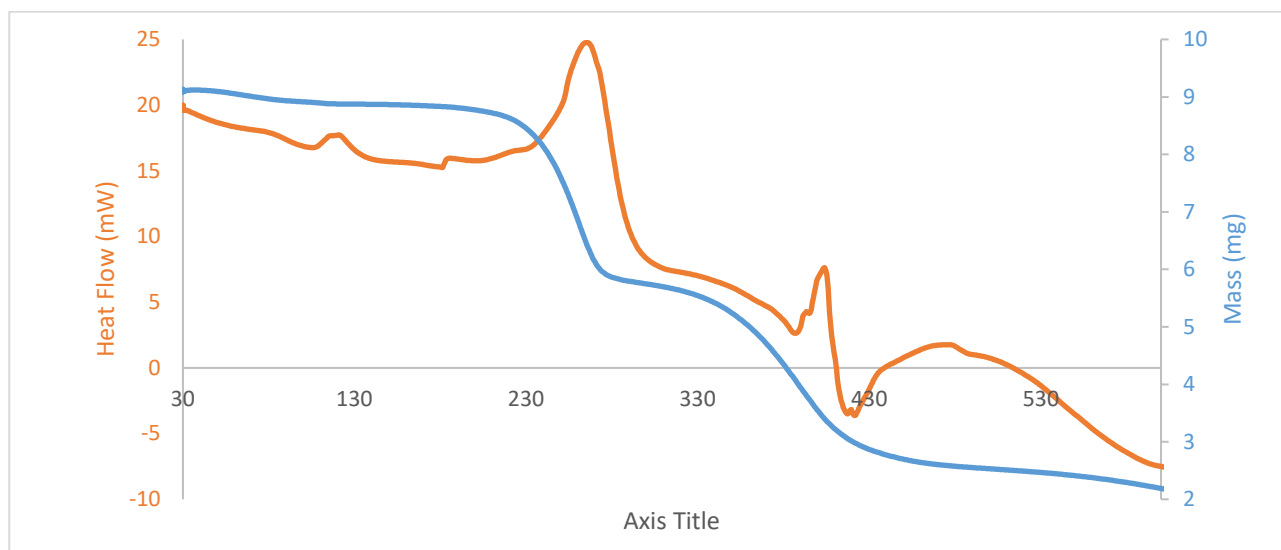


Figure 2.1.44 | STA trace of 10.64 mg porous (50wt. % NaCl) polysulfide (1:1 sulfur - canola oil)

	120 °C peak (100 - 150)	270 °C peak (200 - 300)	400 °C peak (380 - 420)
50% NaCl	67.524 mJ	1596.024 mJ	301.804 mJ
70% NaCl	63.913 mJ	2059.879 mJ	-16.264 mJ (no peak)

From previous sulfur testing, the area of the peaks at 120 °C corresponds to free sulfur content. In the 50 % salt polysulfide this equates to 12.9 % and in the 70 % salt 14.2 % free sulfur respectively. For comparison, non-porous canola oil polysulfide of the same sulfur - canola oil ratio has registered free sulfur levels of 8.96 % to 15.43 % previously. The peak at 400 °C we believe to be due to the presence of NaCl, this peak appears quite strongly in the 50 % NaCl polymer in which channels are not fully formed, but not in the 70 % variant. We attribute this to increased porosity, with channels formed throughout the polymer that allow more, if not all salt to be removed in the washing step.

Raman Analysis of 70 wt. % Salt Porous Canola Oil Polysulfide

Raman spectra acquired by Christopher Gibson and further processed by Jason Gascooke

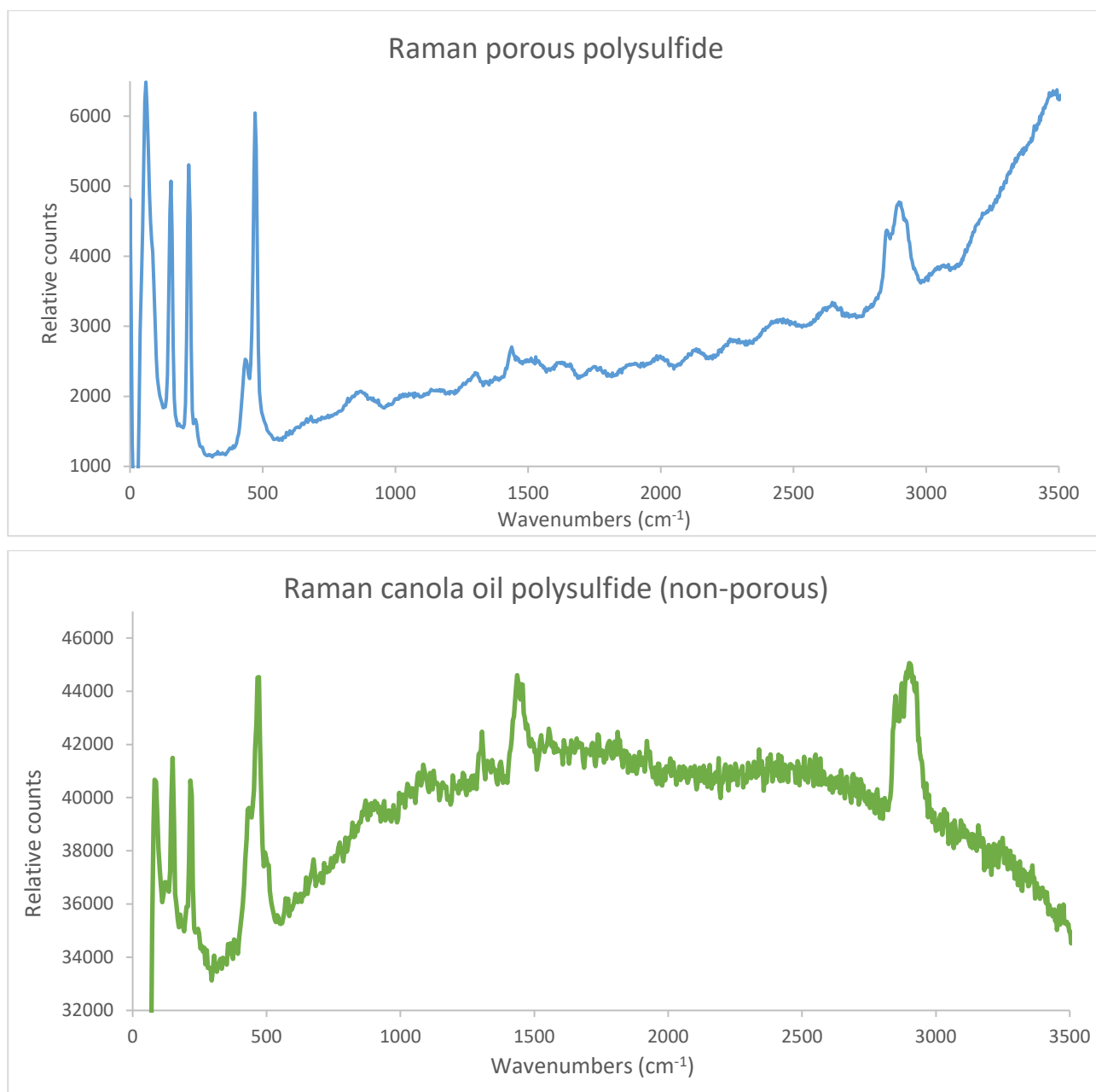


Figure 2.1.45 | Raman spectra of canola oil polysulfide. Top: porous polymer; Bottom: non-porous polymer for comparison.

By Raman spectroscopy, the porous material is identical to the non-porous material, sharing the same trace and major peaks. As in the analysis of the non-porous polysulfide, there was variation in the spectra acquired across the polysulfide surface, with some regions displaying strong sulfur stretching signals (<550 cm⁻¹) only and others, as above, showing varying signal intensities for the peaks related to carbon bonding. The spectra above was chosen as it displayed all present features.

SEM Analysis of 70 wt. % Salt Porous Canola Oil Polysulfide

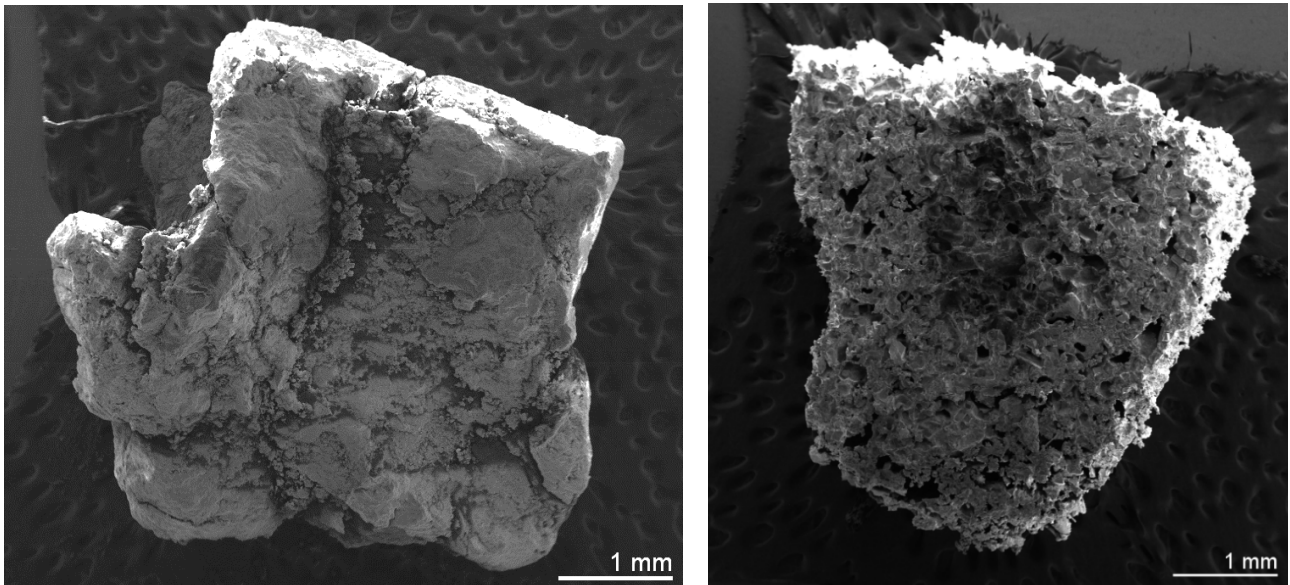


Figure 2.1.46 | Left: Canola oil polysulfide, right: porous polysulfide (70 wt. % NaCl). With the inclusion of NaCl in synthesis, the polymer vitrifies around the crystals, leaving pores in the material once the salt has been washed away.

Salt Crystal Analysis

Salt crystals, prepared for use in polymer synthesis, were sputter coated (Pt, 5.0 nm) and analysed by SEM spectroscopy. Analysis was performed on a Hitachi TM4000Plus tabletop SEM. Special thanks to Dr Martin Cole of NewSpec Pty Ltd, Myrtle Bank, South Australia for facilitating trial use of the instrument.

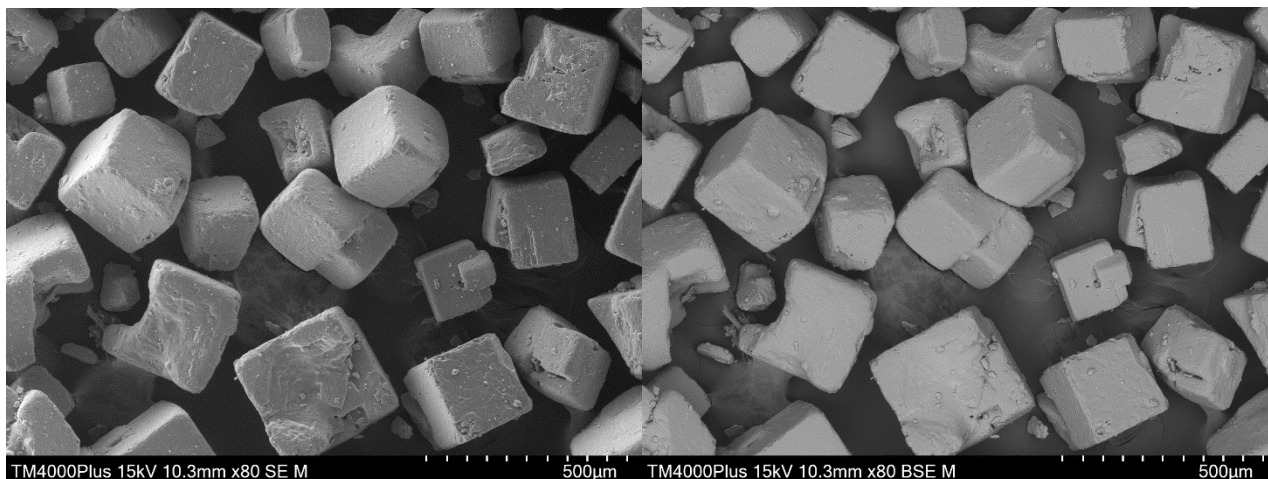


Figure 2.1.47 | SEM images of NaCl crystals as used in polymer synthesis. Left: SE, right: BSE. The side lengths of 38 cubes were measured using annotation tools within the SEM analysis software package. The average side length was found to be 289.7 microns with a standard deviation of ± 62.4 . The maximum size was 435 and the smallest 168, giving a range of 267 microns.

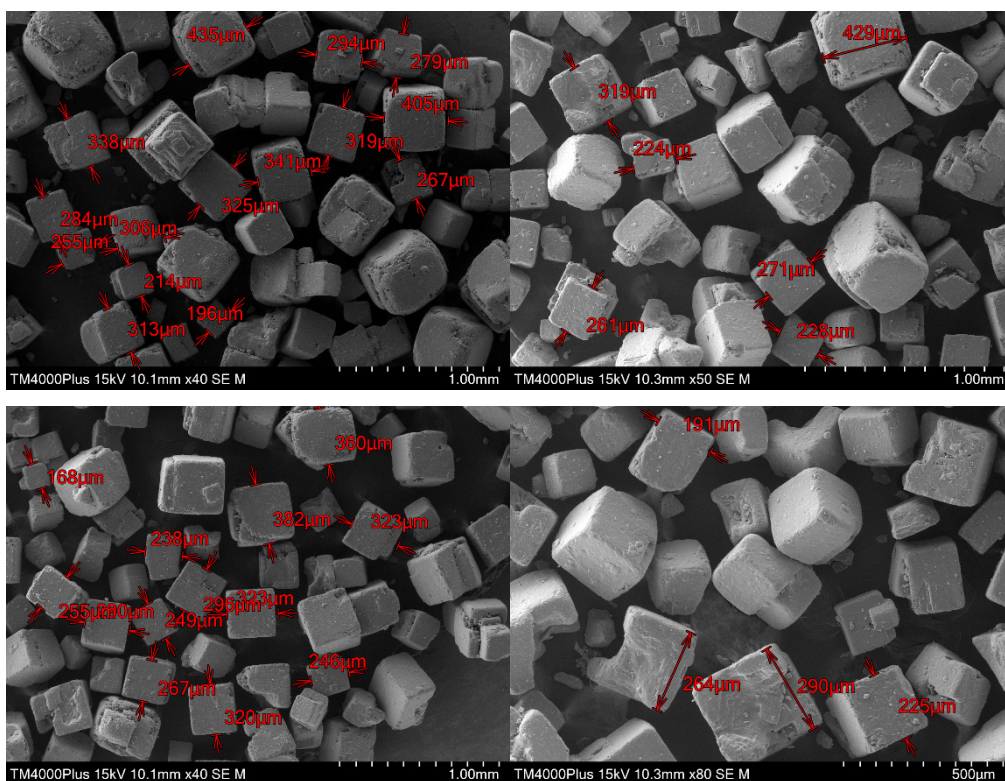


Figure 2.1.48 | Raw annotated images of salt crystals

Density Measurements of Porous Polymer

Porous polysulfide was cut into approximately 5.0 mm cubes during synthesis, before removal of salt. This was found over several syntheses to be the upper limit of sample thickness that would consistently result in complete removal of salt during the washing step. After purification (washing of salt and drying) actual sample dimensions were measured and the mass and volume correlated to determine density. From an average of 7 samples the density was determined to be 0.521 g cm^{-3} with a standard deviation of ± 0.060 (11.5 %). Large variations are due to inconsistency in pore and channel sizes throughout the material.



Figure 2.1.49 | Approximately 5.0 mm-side polysulfide cubes

Given 70 wt. % of the reaction was sodium chloride, with a density of 2.16 g cm^{-3} , any 1.0 g of material before washing should contain 0.7 g of salt with a volume of 0.324 cm^3 . During the washing step, the dimensions of the polysulfide remain the same with a reduction in mass down to just that of the sulfur and canola oil components (30 wt. %) to give porous polysulfide with the density measured above. So the resulting 0.3 g polymer has a void volume of 0.324 cm^3 , but a total volume of 0.576 cm^3 , resulting in a 56.3 % void volume.

NaBH₄ Reduction of Porous Canola Oil Polysulfide

In an effort to introduce thiol functional groups into the polysulfide, sodium borohydride was used to reduce surface sulfur-sulfur linkages.

2.00 g Porous Polysulfide (50:50 sulfur-canola oil prepared with 70 wt. % NaCl) was measured into a 100 mL RBF with 0.1546 g NaBH₄ (1 molar equivalent NaBH₄ to S₈ used in the syntheses of porous polymer). 10 mL methanol was added, and the solution stirred (20 mm oval stirrer, 200 rpm) for 1 hour. Initial addition of methanol resulted in evolution of H₂ gas, visible as violent bubbling of the mixture (now yellow) for the first 20 seconds. The solution was quenched with 10 % HCl and diluted with water (10 mL) before washing under vacuum filtration with 5 × 20 mL DI water. After leaving the washed polymer to dry overnight, the product was weighed to determine yield and thiol content tested by Ellman's reagent.

This procedure was repeated with 0.0341 g NaBH₄ and 0.5941 g NABH₄, representing ¼ and 4 molar equivalents respectfully.

Results

The polymer samples treated with ¼ and 1 equivalents NABH₄ were both broken down moderately to smaller sized particles. Some large particles remained in both cases. The samples treated with 4 equivalents NABH₄ resulted in a clumped, dark brown material—destroyed under the harsher conditions.



Figure 2.1.50 | Left: untreated porous polymer; Right: 1 eq. NaBH₄ treated porous polymer

Ellman's Test for thiol content

This experiment was performed by Renata Kucera as part of an undergraduate research project.

Method

500 mg porous polysulfide treated with $\frac{1}{4}$ eq. NaBH_4 and 500 mg porous polysulfide treated with 1 eq. NaBH_4 were prepared in a 50 ml centrifuge tubes with inclusion of 10 mg Ellman's reagent in 10 mL phosphate buffer (100 mM, pH 8) and mixed on the end-over-end mixer (25 rpm) for 2.5 hours. After this time, each sample was vacuum filtered and stored in a 15 mL centrifuge tube overnight. The following day, the Cary 60 UV-Vis was used to measure the absorbance of each sample (undiluted) in triplicate at 412 nm with phosphate buffer as the blank between measurements.

Results

Sample	Absorbance (A.U.)			
	Replicate 1	Replicate 2	Replicate 3	Average
Control (Ellman's + Buffer)	0.5259	0.5189	0.5253	0.5234
Porous polysulfide treated with $\frac{1}{4}$ eq. NaBH_4	0.8586	0.8546	0.8467	0.8533
Porous polysulfide treated with 1 eq. NaBH_4	0.5306	0.5269	0.5314	0.5296

Analysis of thiol-content on the canola oil polysulfide surface using Ellman's test

This experiment was performed by Renata Kucera as part of an undergraduate research project.

Method

A sample of canola oil polysulfide (1.00 g, 50 % sulfur) was placed into each of three 50 mL centrifuge tubes along with 8 mL phosphate buffer (100 mM, pH 8) and Ellman's reagent (8 mg, 0.020 mmol). As a control, Ellman's reagent was also added to three separate samples of buffer in the same way, except in the absence of polymer. All samples were mixed on a lab rotisserie for 1 hour at room temperature before filtering. The filtrates were then diluted 7-fold and analysed by UV-Vis spectroscopy. Absorbance at 412 nm are listed below. No reaction with Ellman's reagent was observed, as no significant increase in absorbance at 412 nm was observed (student t-test). Therefore, thiol content on the polymer is negligible and consistent with the proposed polysulfide structure.

Results

	Ellman's only control, absorbance (A.U.)	Polymer with Ellman's reagent, absorbance (A.U.)
Test 1	0.0720	0.0753
Test 2	0.0637	0.0762
Test 3	0.0822	0.0628
Average	0.0726	0.0714

Ellman's test for thiol content on the canola oil polysulfide (50 % sulfur). No thiols were detected.

Porous canola oil polysulfide pore size and distribution

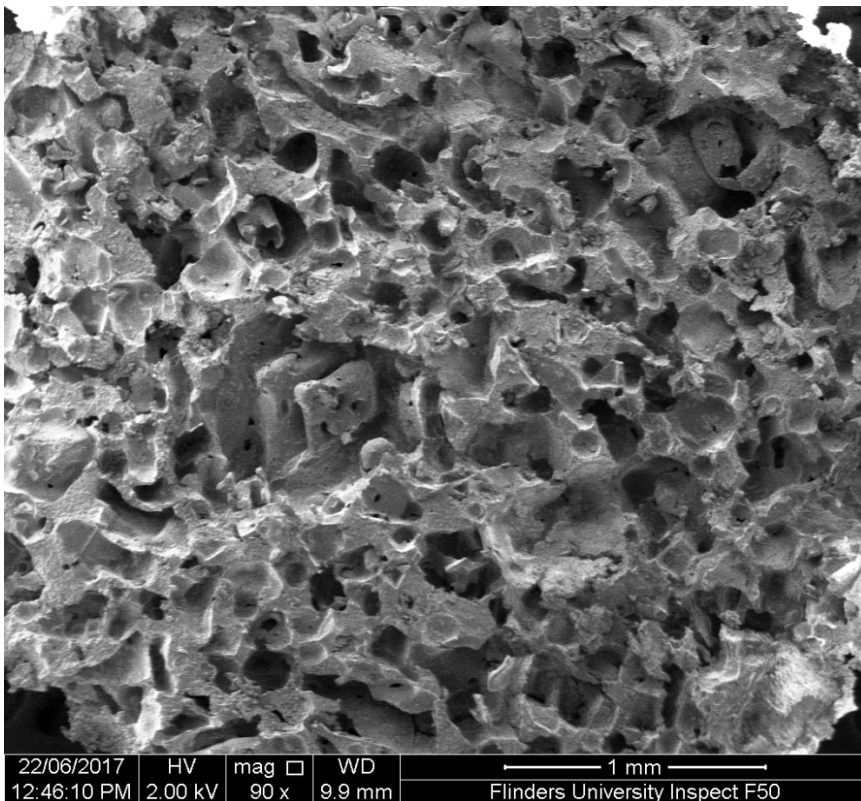


Figure 2.1.51 | Cross section of a particle of porous canola oil polysulfide

Pore diameter

Pore diameter was measured along the longest edge of 50 randomly selected pores in fig. 2.1.51

Average pore size \pm std. dev. = $119.2 \pm 53.0 \mu\text{m}$

Range = $160.5 \mu\text{m}$

Pore distribution

Pore distribution was measured as the shortest distance from 50 randomly selected pores in fig. 2.1.51 to the next closest in a random direction.

Average distance pore-to-pore \pm std. dev. = $57.8 \pm 33.2 \mu\text{m}$

Range = $138.0 \mu\text{m}$

Glass transition temperature by DSC for porous polysulfide (50 wt. % sulfur)

The glass transition temperature of the porous canola oil polysulfide was $-12.9\text{ }^{\circ}\text{C}$, as determined by DSC:

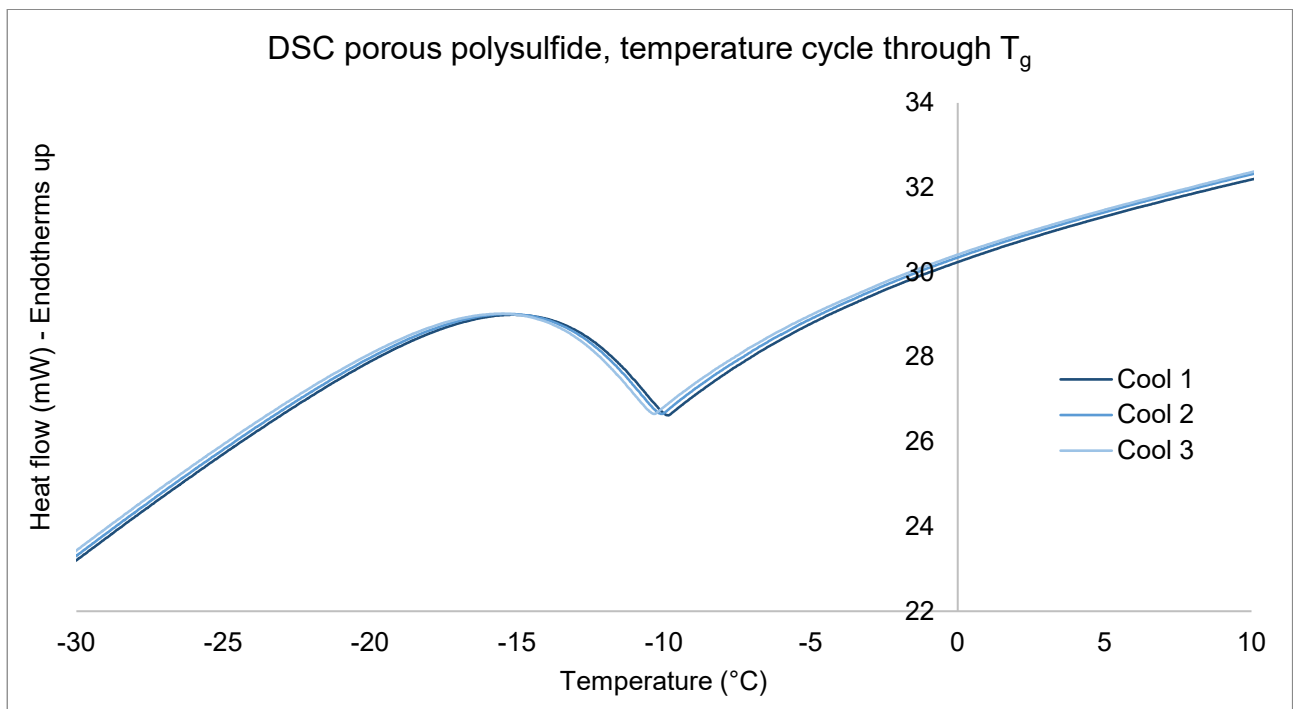
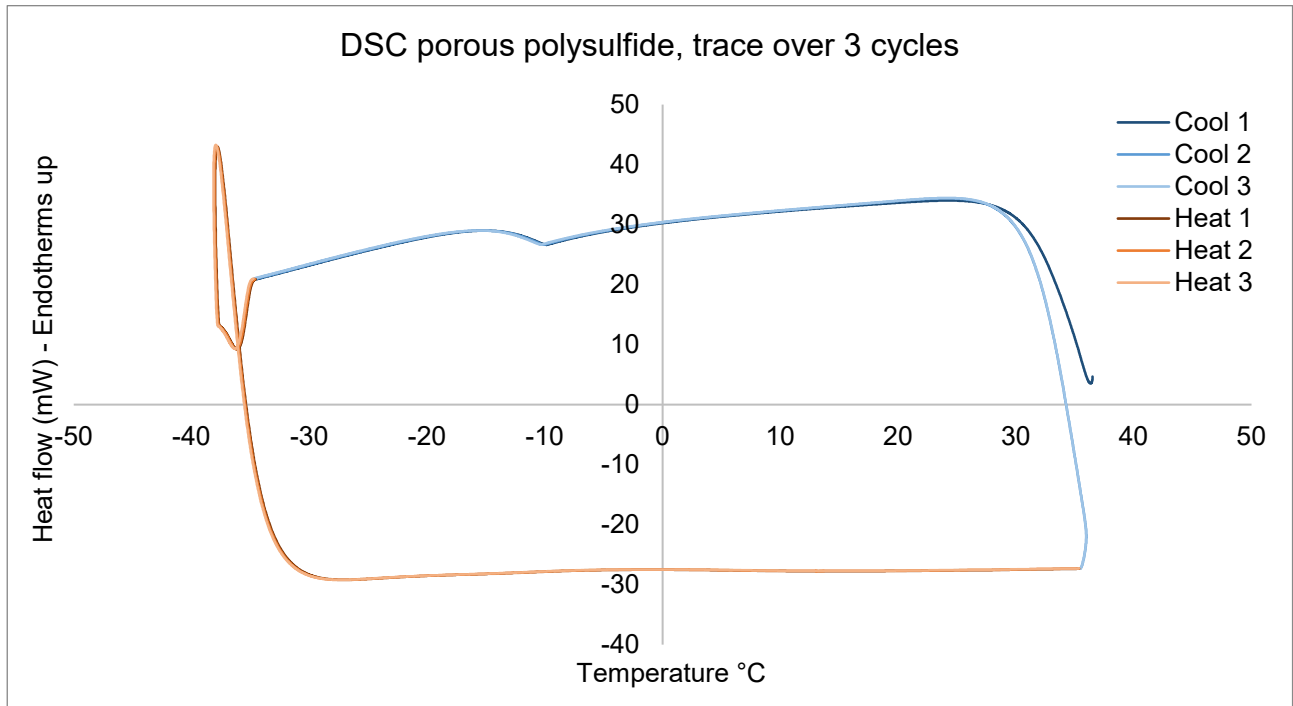


Figure 2.1.52 | Determination of T_g using DSC for the porous Canola Oil Polysulfide prepared at 50 wt. % sulfur. Polysulfide was heated to $35\text{ }^{\circ}\text{C}$ and cooled to $-35\text{ }^{\circ}\text{C}$ for 3 cycles. Top: whole spectra, bottom: focus on the glass transition.

Low density polysulfide up-scaled Synthesis (2.5 kg reaction mixture)

This procedure was optimised and written by Louisa Esdaile

The reaction apparatus was assembled in a fume hood as follows: an overhead mechanical stirrer (Heidolph Hei-TORQUE 200) was secured on an H-frame stand and equipped with a stainless steel impeller (15 cm square blade fig. 2.1.53). A stainless steel reaction vessel (4.7 L, 20 cm diameter) was placed on a hotplate equipped with temperature probe. The reactor handles were further secured to the H-frame stand with cable ties. Because the reaction vessel is magnetised, the reactor is further secured by attraction to the magnetic hotplate. The impeller blade was positioned several millimetres from the bottom of the reaction vessel and the temperature probe and a large plastic funnel were secured so that they would not come into contact with the rotating impeller. An image of the setup is shown below:

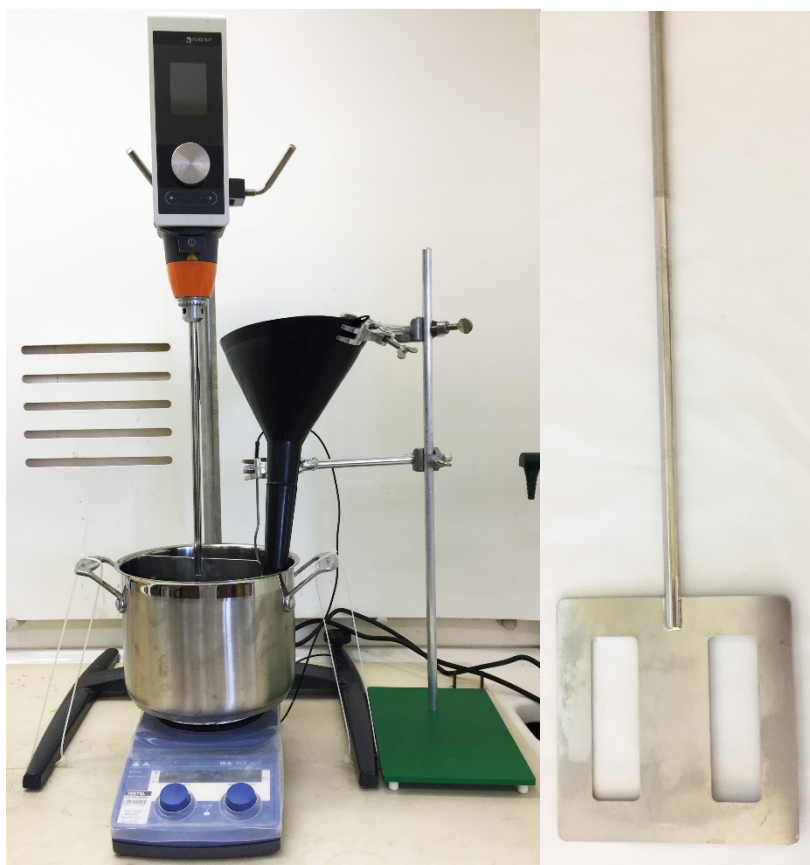


Figure 2.1.53 | Reactor apparatus (left) and impeller (right) used in large-scale synthesis of polymer

Canola oil (375.0 g, either pristine food grade or recycled used cooking oil) was added to the reaction vessel. The overhead stirrer was set to 90 rpm, and the oil was heated to 170 °C, with the temperature of the oil monitored and controlled directly with a temperature probe. Sulfur (375.0 g) was then added through the funnel at a rate such that the internal temperature did not fall below 155 °C. The addition of sulfur was carried out over approximately 5-10 min. The reaction initially appears

as two transparent liquid phases: the molten sulfur and sulfur pre-polymers from ring-opening polymerisation appear as an orange or red bottom layer and the canola oil forms a light yellow top layer. At this scale, the two phases begin to react and form an opaque mixture over the duration of the sulfur addition. Once the reaction mixture appears opaque and two distinct layers are not visible, the sodium chloride porogen was added. Accordingly, sodium chloride (1750 g, finely ground in a blender) was added through the funnel at a rate such that the internal temperature did not drop below 155 °C. Upon commencing the addition of the sodium chloride, the reaction temperature was set to 180 °C to compensate for the internal temperature drop. The full addition of sodium chloride was carried out over 15-20 min.

Upon completion of the salt addition, the reaction mixture was typically an orange, opaque and relatively free-flowing slurry. Upon continued heating at 180 °C, the mixture thickens and darkens to a brown colour. The reaction was stopped when the viscosity increases to a point at which the overhead stirrer registers a torque of 40 N•cm. This change typically occurs 10-15 minutes after the addition of the sodium chloride is complete. At this stage of the reaction, some gas may be evolved (H₂S) so operation in a fume hood is essential. Overheating or prolonged heating at 180 °C also leads to additional gas evolution, so the reaction was shut down immediately when the torque of the stirrer was 40 N•cm. To stop the reaction, the stirrer and the hotplate are turned off at the power source, the cable ties are cut, and the hot plate is removed, and the reaction vessel is placed on a trivet to prevent further heating. The polymer (a soft rubber) is friable, allowing straightforward removal of the impeller with a spatula. To remove the polymer from the reaction vessel, it was broken into large chunks with a large spatula or paint scraper (Fig. 2.1.54). The polymer was then processed with a mechanical grinder to provide particles between 0.5 and 3 mm. Typically >2.48 kg of the polymer salt composite was isolated at this stage (Fig. 2.1.55).



Figure 2.1.54 | The canola oil polysulfide and salt composite, after breaking down into large pieces with a spatula or paint scraper.



Figure 2.1.55 | The canola oil polysulfide salt composite is a friable rubber, easily processed into particles using a mechanical grinder.

To remove the sodium chloride progen, the polymer was washed repeatedly with DI water. In a representative procedure, the polymer (2.5 kg of the polymer salt composite) was added to a 20 L bucket along with 17 L of DI water. The mixture was stirred using an overhead stirrer (200 rpm, 30 min). The polymer was then isolated by filtration through a sieve (0.5 mm cut-off) and washed three more times in a similar manner. After the final wash, the polymer was filtered through a sieve (0.5 mm) and pressed with a piece of flat plastic to squeeze out excess water. The polymer was then dried in the sieve by passing warm air through the material (5-24 hours, 18 - 42 °C). A final drying step was carried out by placing the polymer in a plastic tray in a fume hood until the mass of the polymer was constant (1-3 days). The final mass of the product varies with water content, which can be up to 2% by mass). Typically, 750 g to 768 g of the final polymer are obtained (Fig. 2.1.56).



Figure 2.1.56 | Washed and dried porous canola oil polysulfide, prepared on a 750 g scale.

STA analysis of low density polysulfide

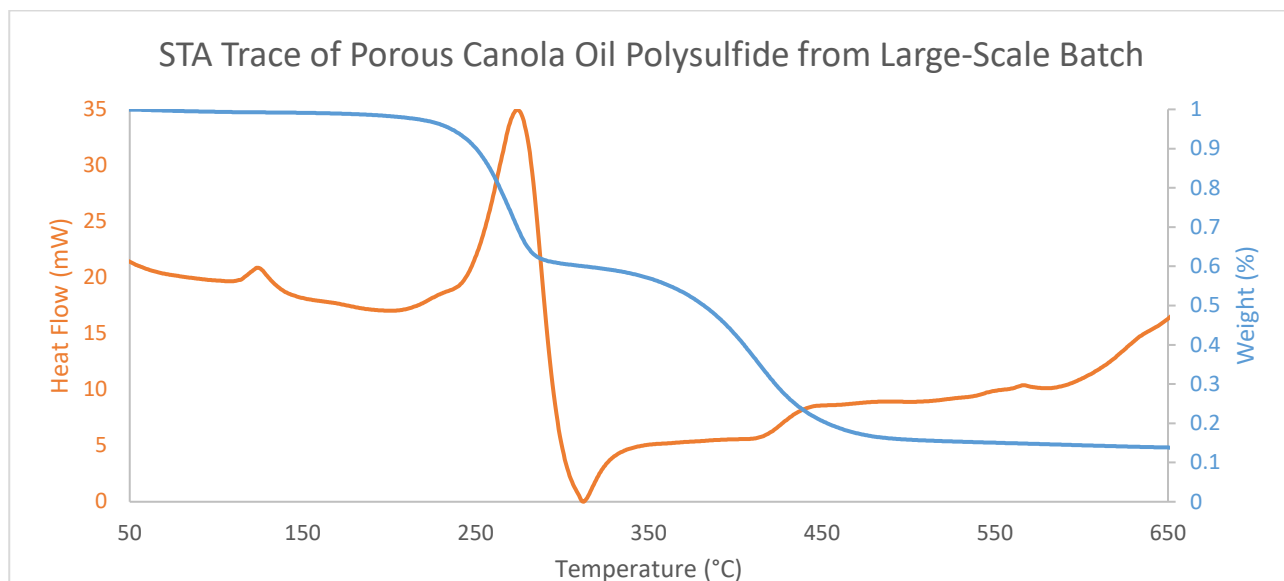


Figure 2.1.57 | Low-density polysulfide prepared using the large-scale method described above shows an identical STA trace to that of the material prepared using the previous method³. The first mass drop over 200–280 °C corresponds to the loss of the sulfur component, the second mass loss from 350–500 °C corresponds to degradation of the vitrified canola oil component. The polysulfide is most accurately described as a composite of sulfur and vitrified canola oil. The small peak in heat flow at 120 °C corresponds to the melting of free sulfur trapped within the composite. The area of this peak correlates to the mass of free, unreacted sulfur present.

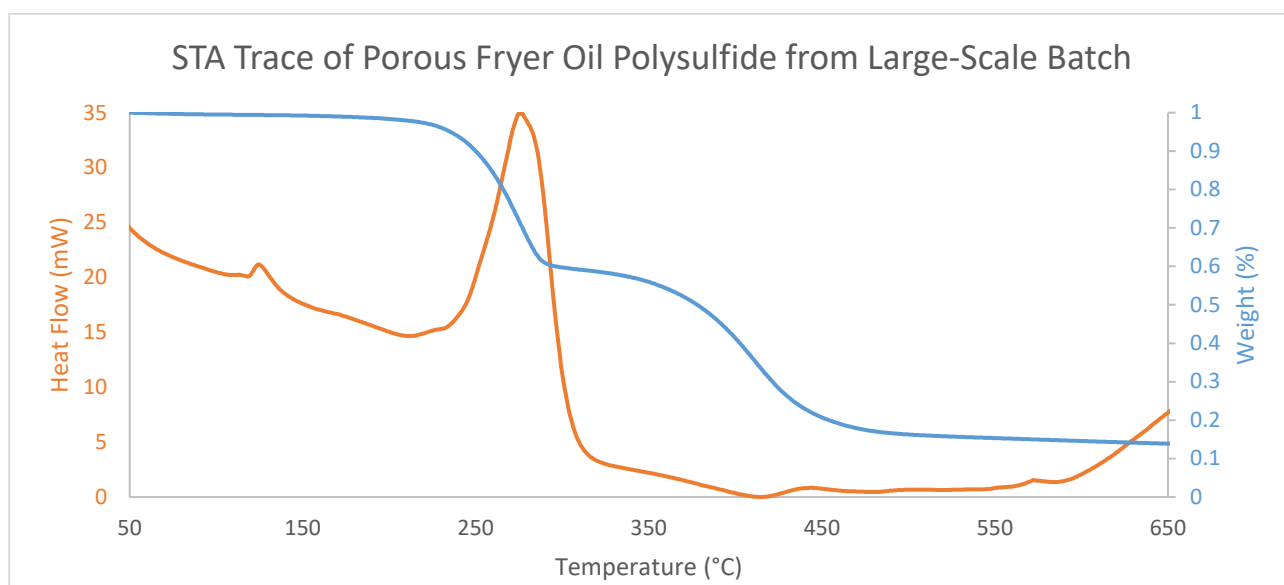


Figure 2.1.58 | The STA trace of low-density polysulfide formed with fryer oil is very similar to that of pristine canola oil. A standard curve correlating sulfur mass to the area of the heat flow peak at 120 °C (indicating the melting of free sulfur) was prepared previously³ and used here to determine the level of free sulfur present in the low-density polysulfides. The 120 °C peak in the canola oil sample corresponds to 16.1 % free sulfur and the fryer oil corresponds to 19.0 % free sulfur.

SEM Analysis of Low-Density Polysulfide

Samples were loaded onto aluminium SEM studs with adhesive carbon tape and sputter coated with platinum, achieving a surface coating of 5.0 nm Pt. Studs were then loaded on to the sample stage of an FEI Inspect 50 SEM with EDX analyser.

Canola Oil Polysulfide

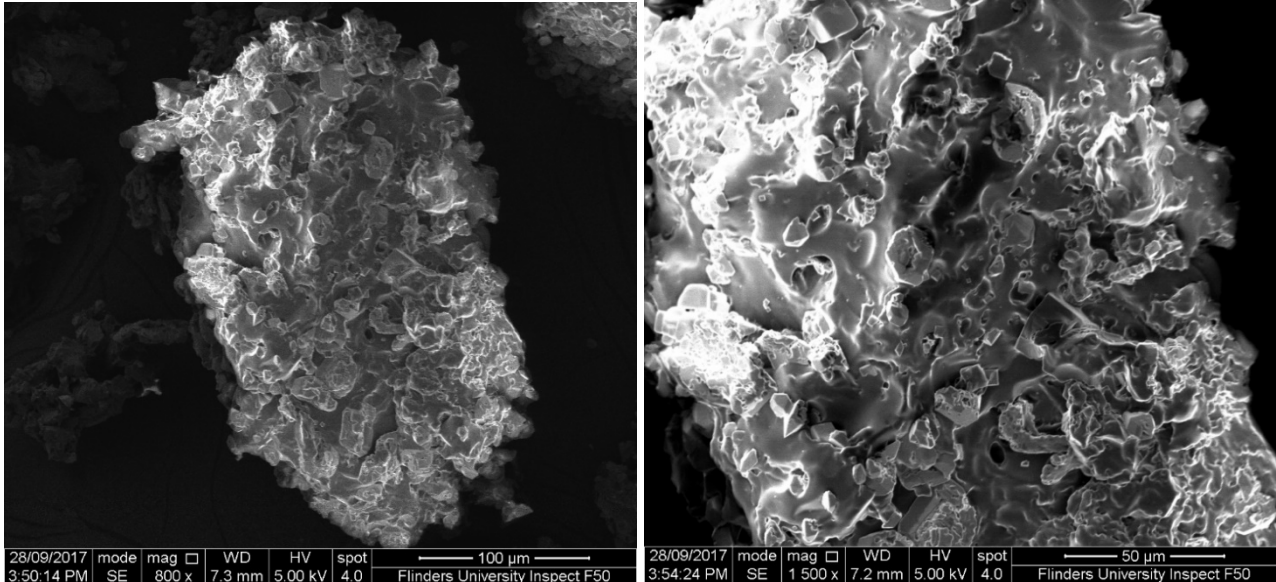


Figure 2.1.59 | Left: a single particle of low-density polysulfide; right: the same particle, at greater magnification.

Fryer Oil Polysulfide

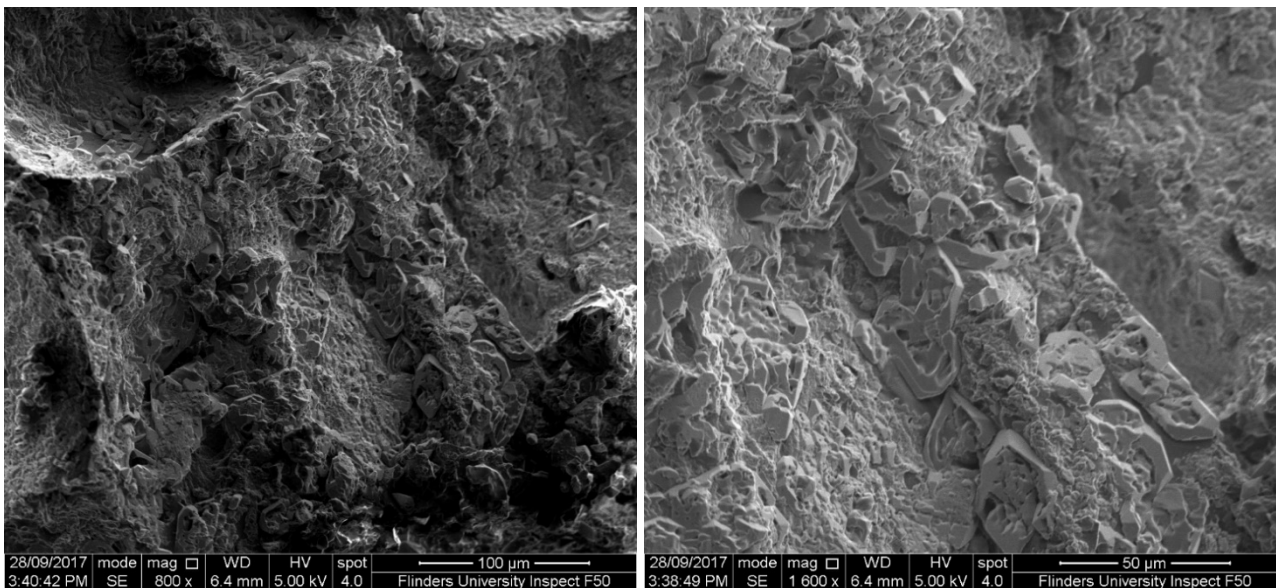


Figure 2.1.60 | Left: SEM image of low-density polysulfide prepared from fryer oil; right: the same location, at greater magnification.

Even with the inclusion of salt in the syntheses, porosity of the material is not immediately discernible. Despite this the material bears a lower density and performs more efficiently in oil removal than non-porous polysulfide. EDX analysis shows the presence of C, O and S peaks in both samples, consistent with previous EDX analysis of porous polysulfide³.

Canola Oil Polysulfide Analysis by GPC

Method

Polystyrene standards were prepared to 3 mg mL⁻¹ in a solvent mixture of 5 % pyridine and 95 % THF. Canola oil polysulfide was also prepared in solution to the same concentration by first dissolving in pyridine, then diluting with THF to the same solvent ratio.

Instrument Parameters

Shimadzu Prominence UPLC. Solvent: 5 % Pyridine in THF Flow Rate: 1.00 mL min⁻¹ Column: Phenomenex Linear(2) THF with guard column

Results

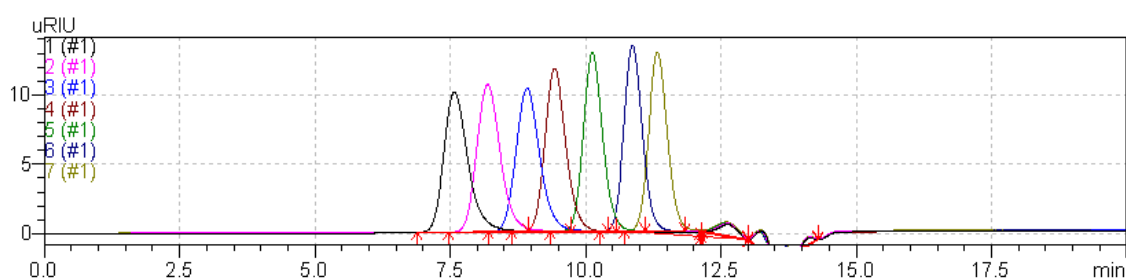


Figure 2.1.61 | Chromatogram of calibration standards

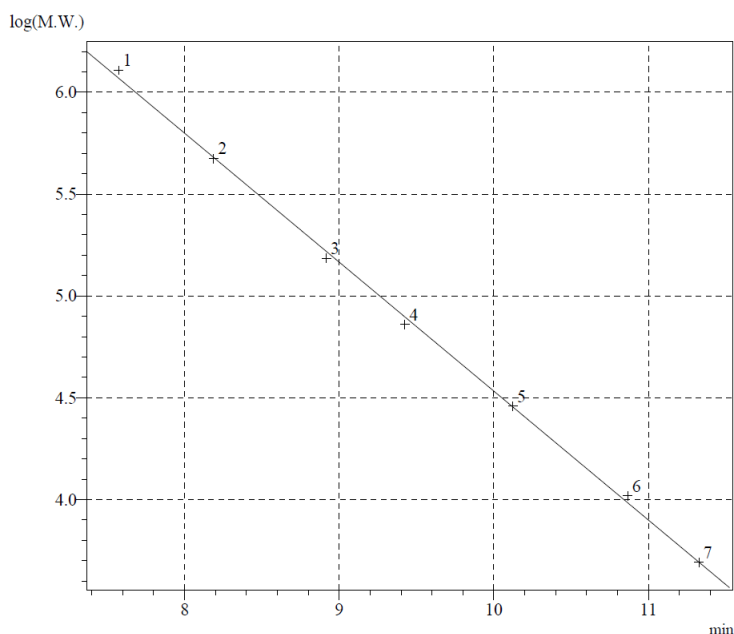


Figure 2.1.62 | Calibration curve – Log (MW) vs. retention time, $R^2 = 0.9988$

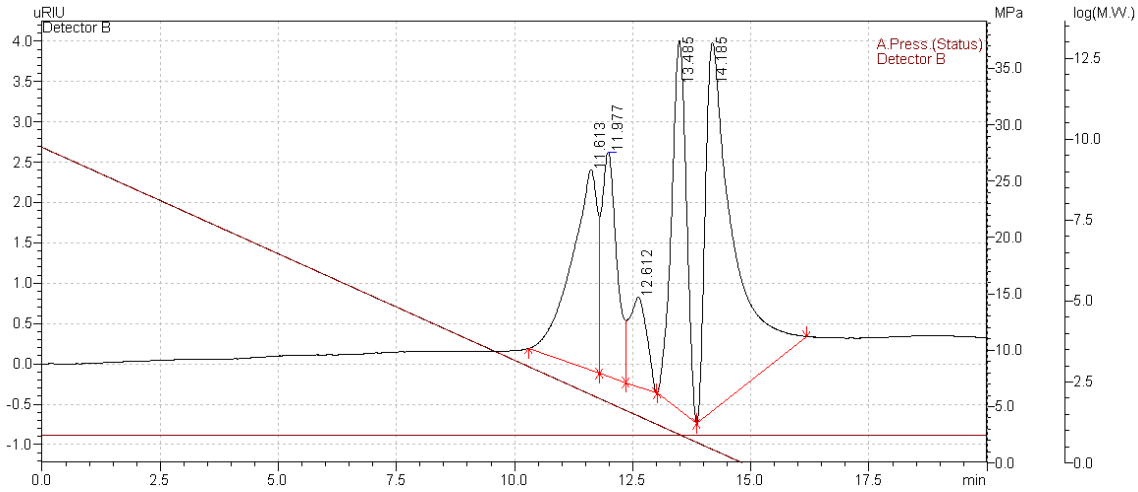


Figure 2.1.63 | Chromatogram of polymer sample

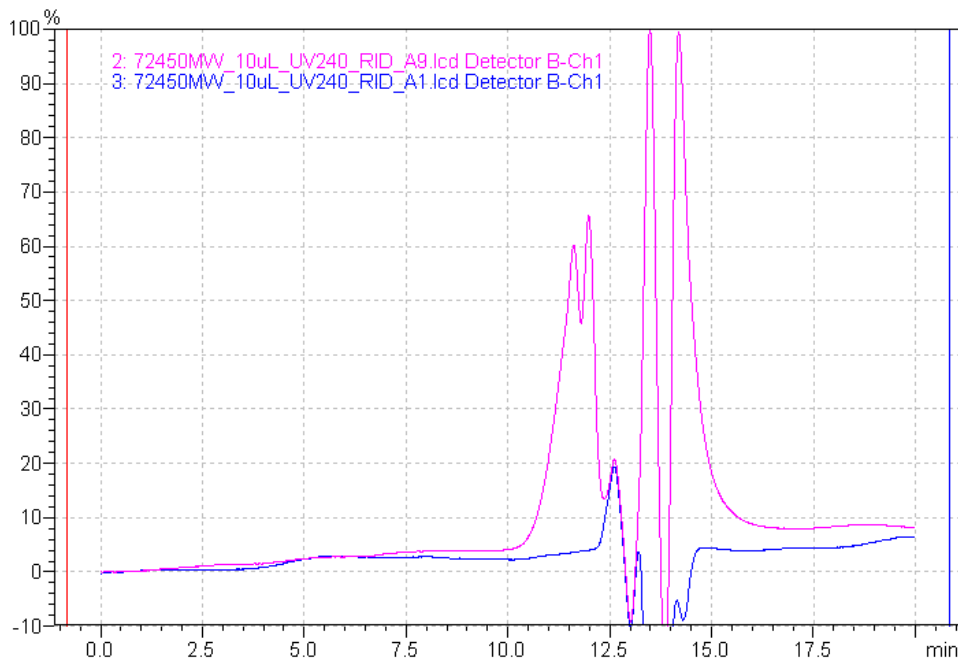


Figure 2.1.64 | Chromatogram of polymer sample (pink) against blank sample (blue) – The peak at 12.5 minutes present in all samples, including the blank, signifies the injection event and end of the run.

Analysis shows distinct elution of polystyrene standards and a strong correlation between retention time and molecular weight. The polymer sample exhibits two peaks, broad and blended together at 11.613 and 11.977 minutes, the former corresponds to a number average MW (Mn) of 4193 and weight average (Mw) of 5097. The latter a Mn 1735 of and an Mn of 1808, unfortunately falling just short of the lowest polystyrene standard and lying outside of the calibration curve.

Revised experiment

The experiment was run a second time with the following changes, addressing the shortcomings of the first:

- Flow rate changed to 0.75 mL min^{-1} to hopefully extend run time and achieve greater separation
- Lower MW polystyrene standards included in the analysis
- Canola oil (monomer) also ran to show differences between the reacted and unreacted material

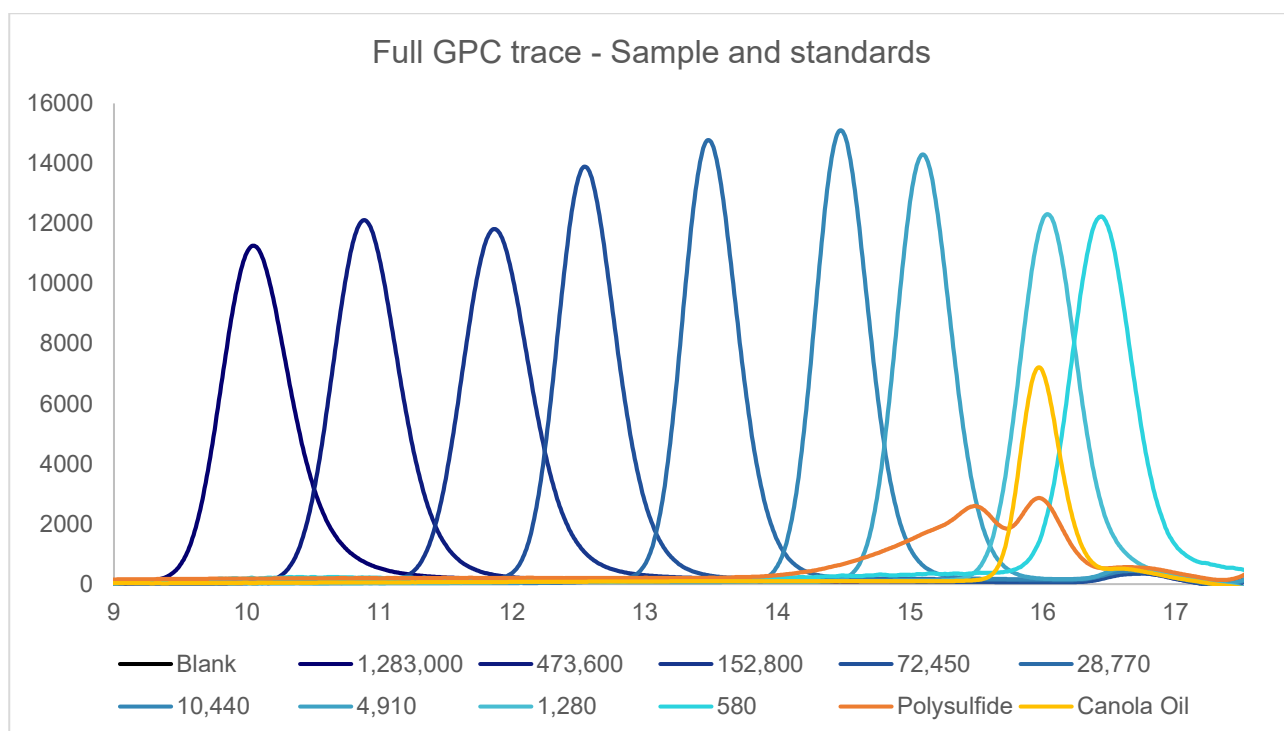


Figure 2.1.65 | Full GPC trace of canola oil polysulfide and pristine canola oil overlaid with a series of polystyrene standards of known molecular weight.

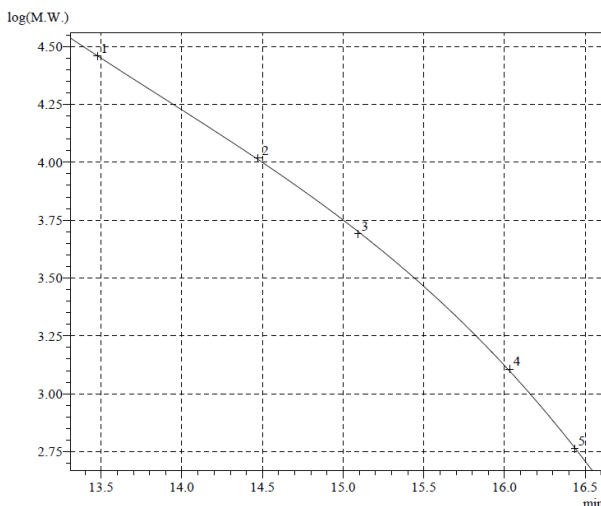
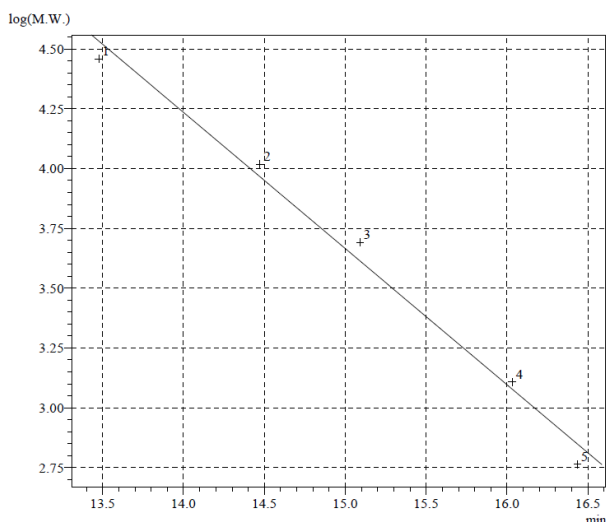
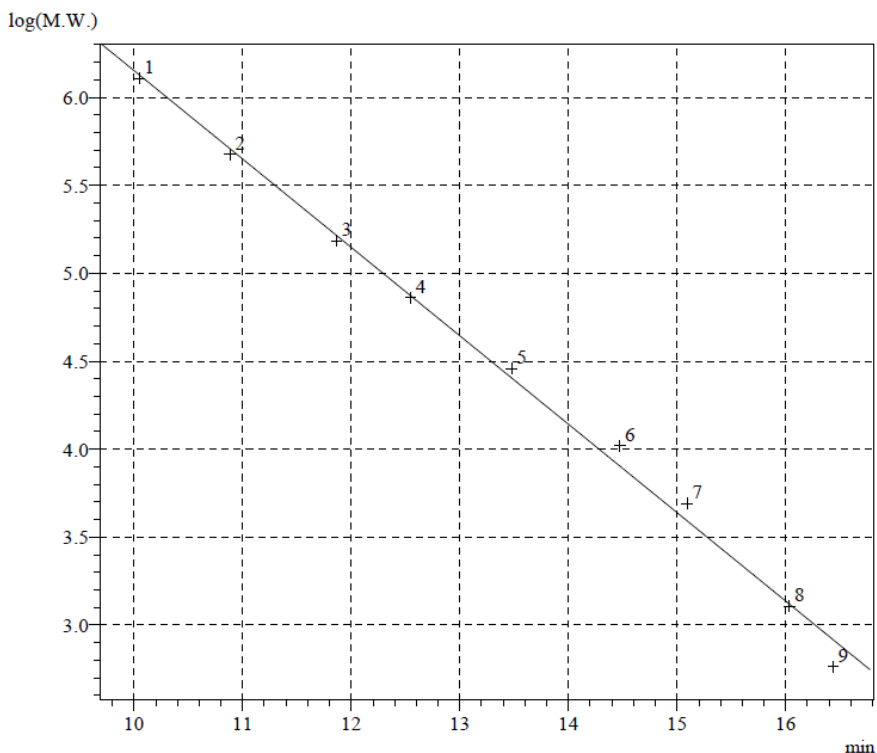


Figure 2.1.66 | Calibration curves – linear correlation to all data points $R^2 = 0.9949$ (top), linear fit on only those data points relevant to the sample ($R^2 = 0.9880$ (left), 3rd order fit to only the data points relevant to the sample ($R^2 = 0.9999$) (right).

Though the full spectrum of standards gave a strong linear correlation ($R^2 = 0.9949$), it did not hold so well when applied to only those data points at retention times relevant to the sample. When reducing the plotted points from the full 9 down to these 5 the R^2 value dropped below 0.99. Applying a 3rd order polynomial relationship raised this value back above 0.99 to 0.9999, a significant improvement.

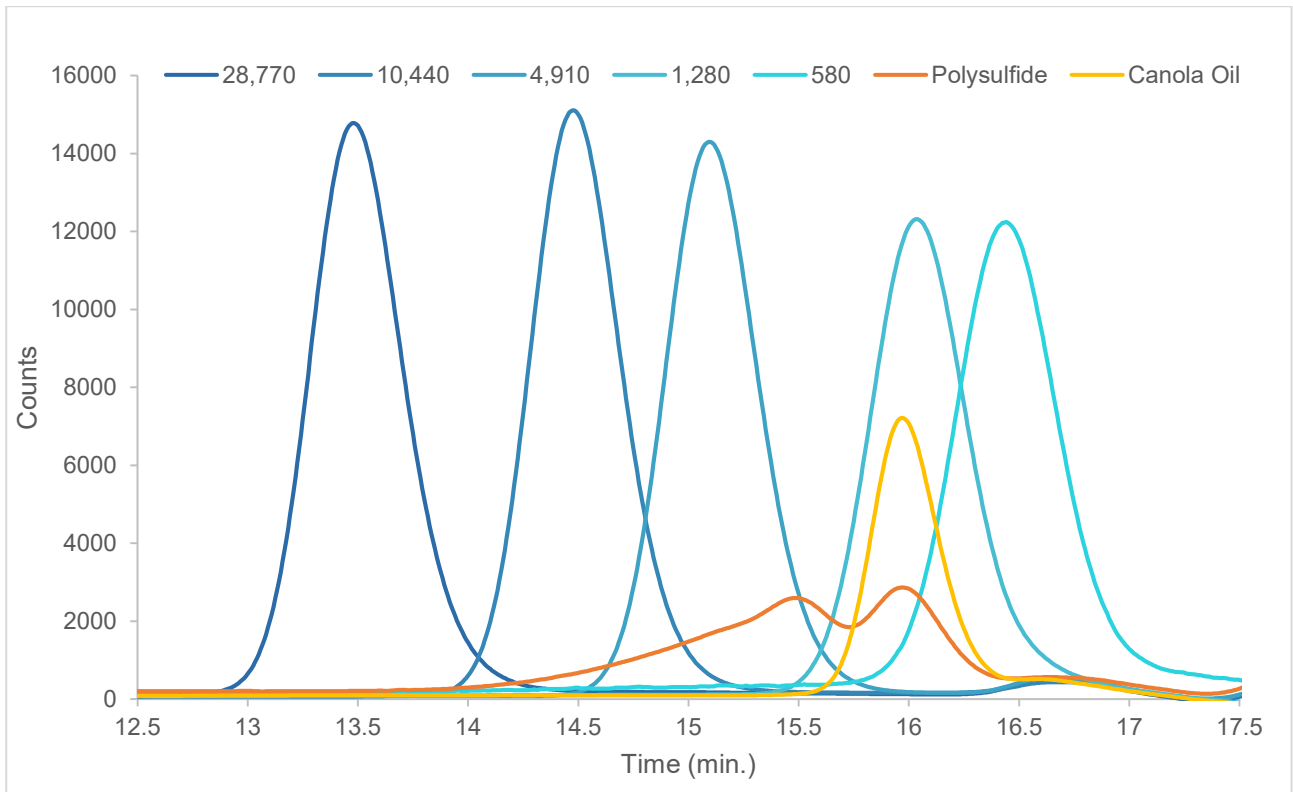


Figure 2.1.67 | GPC trace of canola oil polysulfide and pristine canola oil overlaid with polystyrene standards of known molecular weight.

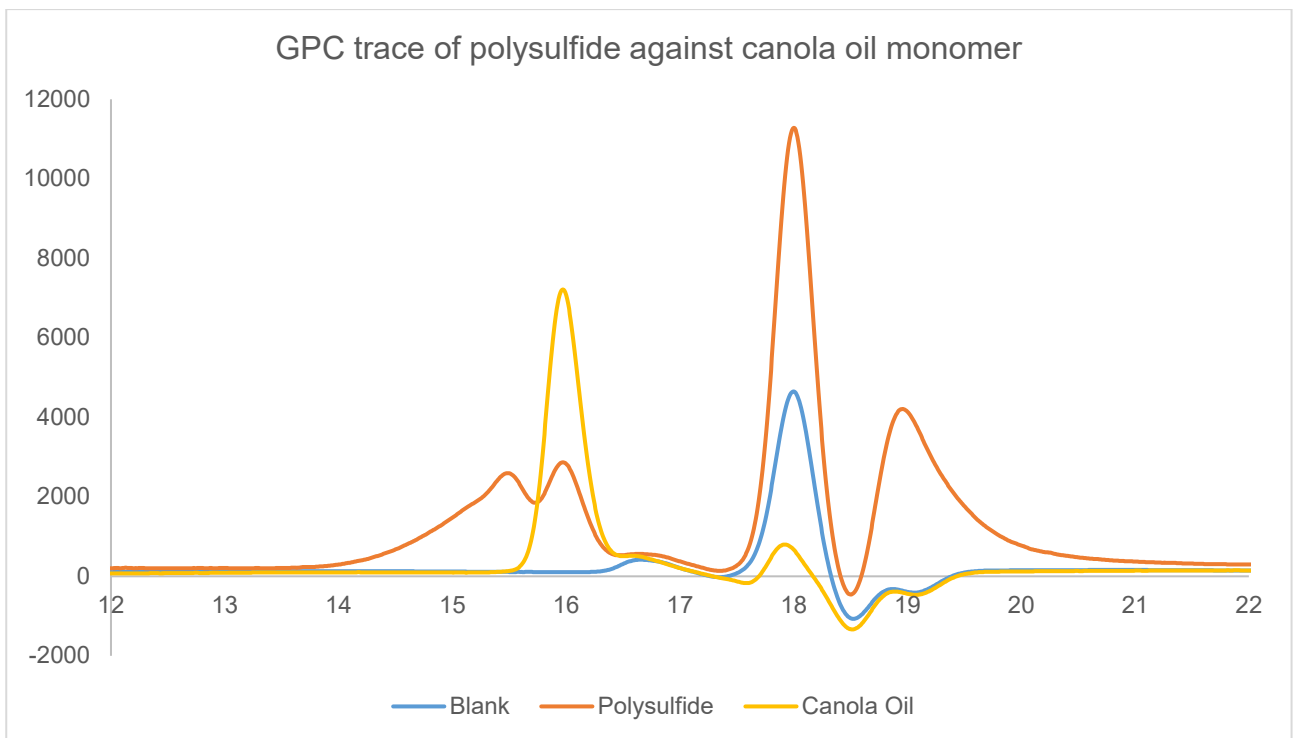


Figure 2.1.68 | GPC trace of canola oil polysulfide and pristine canola oil

The polysulfide sample exhibits two peaks, one broad, fronting peak, and the second overlapping the first but in the same location and same width as that of the pristine canola oil sample. Whether this represents unreacted canola oil within the sample or smaller polysulfide oligomers is not clear. It could also be due to the destruction of polymer in the process of analysis – perhaps even as early as the dissolution in pyridine, causing the appearance of lower molecular weight components. When compared to a series of polystyrene standards of known molecular weight, canola oil recorded a number average of 1215 and a weight average of 1362. The polysulfide showed number averages 3945 (broad first peak) and 1236, with weight averages of 5010 (broad peak) and 1350. For comparison, a single triglyceride molecule of canola oil should show an average molecular weight of 883 Da (biodieseleducation.org – find better source), 65% of the recorded value. If we assume this ratio is applicable to the polysulfide sample, this results in a modal molecular weight of 3248 over the first broad peak and 875 for the second peak. For reference, S₈ has a molecular weight of 256.5, if the polysulfide were breaking down to its constituent parts a sulfur peak might also be expected along with canola oil.

Effect of Mixing Duration on Final Product

Method

3 batches of Canola Oil Polysulfide were synthesised to standard procedure (20.0 g sulfur and 20.0 g canola oil) with each stirrer bar removed at different time interval during synthesis. The aim was to determine if there was a point during synthesis where stirring could be stopped without affecting the final product. 2 batches of polysulfide were also produced by classic vulcanisation to determine if order of addition of reactants played a role in the requirement for thorough mixing.

Results - Inverse Vulcanisation

Mass sulfur	Mass canola oil	Time stirrer removed*	Description at time	Product
20.21 g	20.13 g	8 min.	One phase, dark orange	Liquid, partial gel at reactant interface. Sulfur crystallising.
20.42 g	20.39 g	19 min.	One phase, dark brown	Two phases: gel-like and sticky top layer, hard lower
20.05 g	20.14 g	31 min.	One phase, dark brown, slightly more viscous	Two phases: gel-like and sticky top layer, hard lower.

*time after all reactants were combined

Results - Classic Vulcanisation

Mass sulfur	Mass canola oil	Time stirrer removed*	Description at time	Product
20.32 g	20.07 g	17 min.	One phase, red-brown	Two phases: liquid top layer, hard, solid lower
20.08 g	20.01 g	17 min.	One phase, dark brown	Two phases: gel-like and sticky top layer, hard lower

*time after all reactants were combined

Conclusion

In all cases where stirring was stopped early, the final product did not form correctly. From this it can be concluded that continuous stirring is required right up to gel point in order to form a homogenous canola oil polysulfide.

Lipid analysis of oils

Experiments performed by Renata Kucera as part of an undergraduate research project.

Vegetable oil (1.00 g) was mixed with methanol (100 mL) in a 250 mL round bottom flask and cooled to 0 °C. Sodium methoxide (100 mg) was then added to the stirred mixture. The reaction mixture was stoppered and stirred vigorously at room temperature for 24 hours. Vigorous stirring is important to ensure effective mixing of the two phases present at the start of the reaction. After 24 hours, the reaction was cooled to 0 °C and quenched with 0.1 M HCl (10 mL). The mixture was transferred to a separatory funnel and then diluted with ethyl acetate (150 mL) and water (150 mL). The organic layer was isolated and then washed with water (3 x 50 mL) and brine (3 x 50 mL) before drying (sodium sulfate), filtering and concentrating under reduced pressure. Analysis by ^1H NMR and GC-MS revealed clean conversion to the fatty acid methyl esters. Typical yields for fatty acid methyl esters from 1.00 g vegetable oil: Canola oil: 800 mg; Sunflower oil: 800 mg; Olive oil: 780 mg.

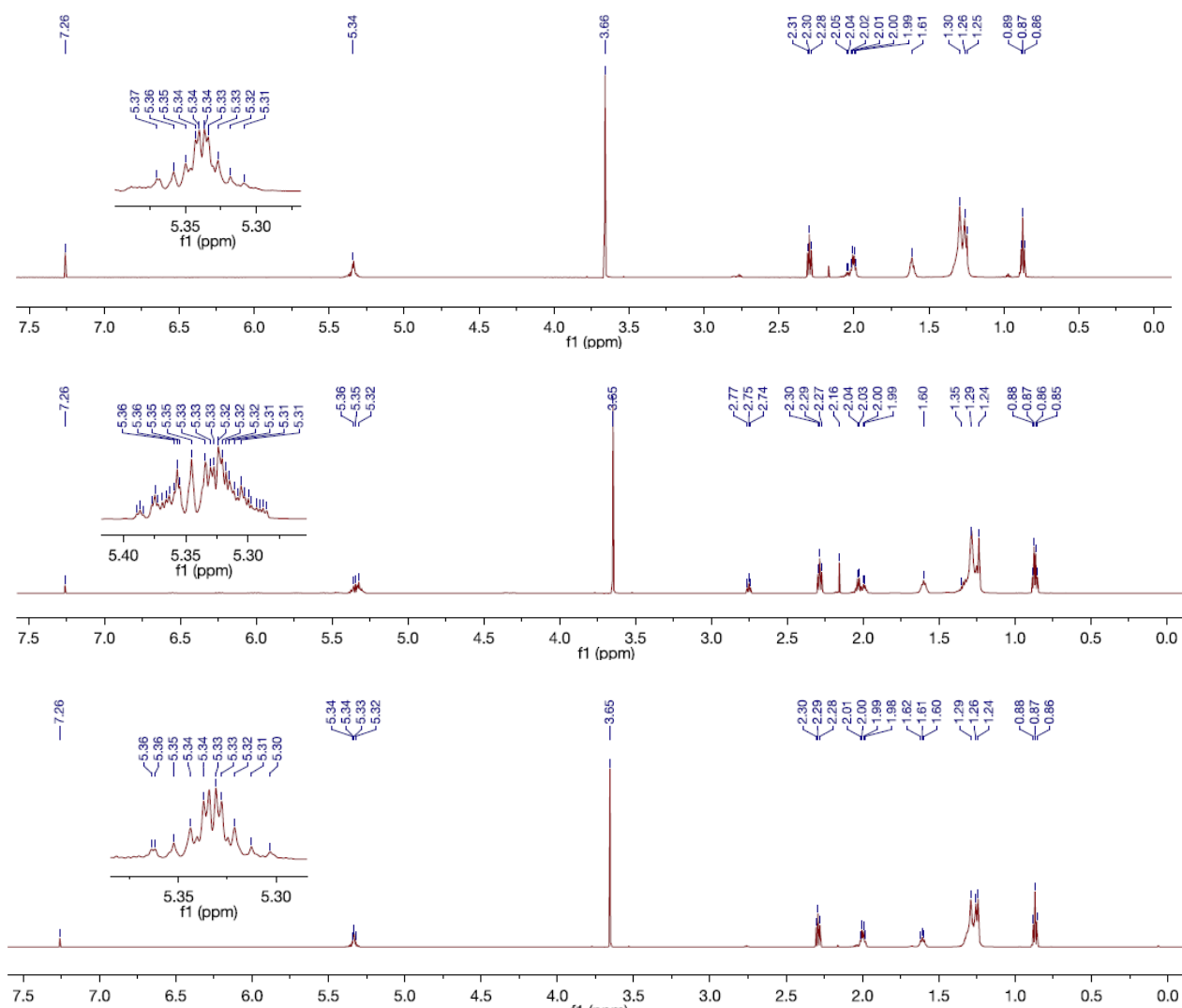


Figure 2.1.69 | ^1H NMR (600 MHz, CDCl_3) of fatty acid methyl esters derived from canola oil (top), sunflower oil (middle) and olive oil (bottom). The alkene region is expanded, showing differences in unsaturation.

Sulfur and fatty acid methyl ester obtained from canola oil

Sulfur (87 mg, 0.34 mmol S₈) was added to a 100 mL round bottom flask and then heated to 180 °C with stirring. The methyl ester prepared from transesterification of canola oil with sodium methoxide (100 mg) was then added to the sulfur. The reaction was stirred at 180 °C for 30 minutes and then cooled to room temperature to provide a viscous black oil. The mixture was analysed directly by ¹H NMR. All alkene peaks (5.0–5.5 ppm) were consumed in the reaction.

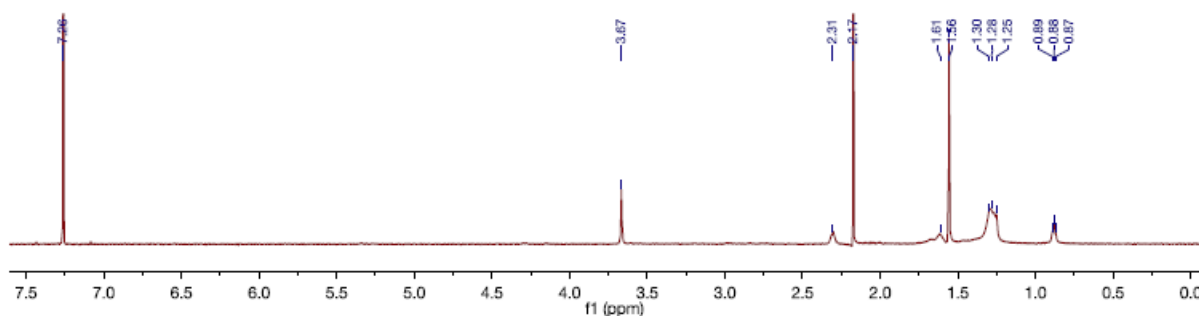


Figure 2.1.70 | | ¹H NMR (600 MHz, CDCl₃) of the dissolvable fraction of the reaction of sulfur and fatty acid methyl esters derived from canola oil.

Sulfur and fatty acid methyl ester obtained from sunflower oil

Sulfur (404 mg, 1.56 mmol S₈) was added to a 100 mL round bottom flask and then heated to 180 °C with stirring. The methyl ester prepared from transesterification of sunflower oil with sodium methoxide (500 mg) was then added to the sulfur. The reaction was stirred at 180 °C for 30 minutes and then cooled to room temperature to provide a viscous black oil. The mixture was analysed directly by ¹H NMR. All alkene peaks (5.0–5.5 ppm) were consumed in the reaction.

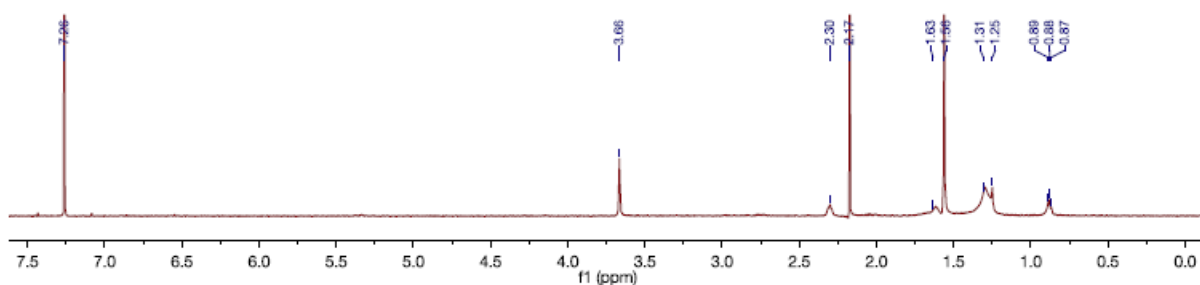


Figure 2.1.71 | | ¹H NMR (600 MHz, CDCl₃) of the dissolvable fraction of the reaction of sulfur and fatty acid methyl esters derived from sunflower oil.

Sulfur and fatty acid methyl ester obtained from olive oil.

Sulfur (440 mg, 1.72 mmol S₈) was added to a 100 mL round bottom flask and then heated to 180 °C with stirring. The methyl ester prepared from transesterification of olive oil with sodium methoxide (Fig S3) (500 mg) was then added to the sulfur. The reaction was stirred at 180 °C for 30 minutes and then cooled to room temperature to provide a viscous black oil. The mixture was analysed directly by ¹H NMR. All alkene peaks (5.0–5.5 ppm) were consumed in the reaction.

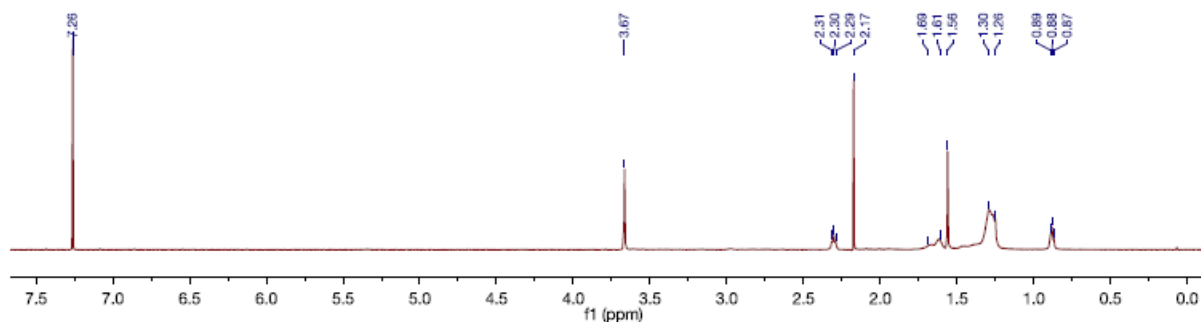


Figure 2.1.72 | ¹H NMR (600 MHz, CDCl₃) of the dissolvable fraction of the reaction of sulfur and fatty acid methyl esters derived from olive oil.

To confirm that sulfur reacts at the alkenes present in the vegetable oils, the reaction between elemental sulfur and the methyl ester derived from each oil was studied. NMR analysis of the polymer formed from the triglyceride and sulfur was not pursued because the product was insoluble in chloroform at room temperature.

Scanning Auger Electron Spectromicroscopy of canola oil polysulfide

Auger experimental performed by Alex Sibley

The non-conductive nature of the samples meant that for a useful Auger Electron Spectrum to be obtained, a 2 nm layer of platinum was needed to provide conductivity to the surface of the sample. The elemental maps of carbon and sulfur show that the carbon-sulfur ratio varies spatially.

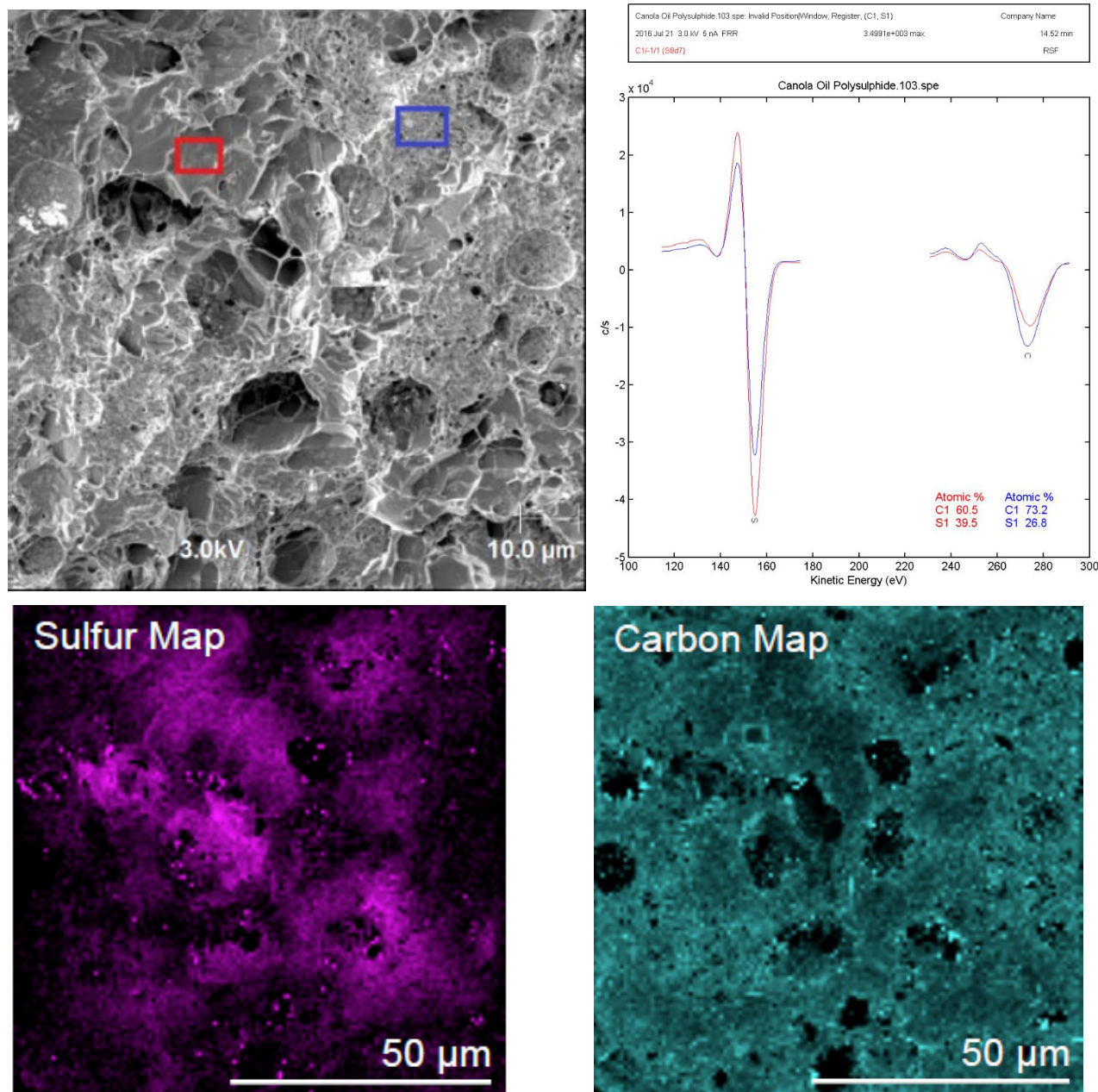


Figure 2.1.73 | Top: Auger spectroscopy of the canola oil polysulfide (50 wt. % sulfur) revealed strong signals for carbon and sulfur, consistent with the proposed structure. Bottom: Auger imaging of representative sections of the canola oil polysulfide (50 wt. % sulfur), with atomic mapping of sulfur and carbon.

Confocal Raman images of Canola Oil Polysulfide (50 wt. % sulfur)

Experiments performed by Christopher Gibson

Confocal Raman images were acquired for the canola oil polysulfide and are displayed in Figure 2.1.74. Figure 2.1.74a is an optical image of the sample with figures 2.1.74b and c representing confocal Raman images ($30 \times 30 \mu\text{m}$) of exactly the same area of the sample. Figures 2.1.74d and e are zoomed in Raman images ($15 \times 15 \mu\text{m}$) of the same area with the centre of each image corresponding to the white and black crosses in figures 2.1.74b and c. The data in figures 2.1.74b and d were generated by plotting the intensity of the 470 cm^{-1} region of each Raman spectrum while the data in figures 2.1.74c and e were generated by plotting the intensity of the 2900 cm^{-1} region of each Raman spectrum. The Raman spectra that are present in the brighter regions of figures 2.1.74b and d typically have the appearance of the sulfur starting material and the Raman spectra that are present in the brighter regions of figure 2.1.74b and e typically have the appearance of the canola oil polysulfide copolymer (50 wt.% sulfur). It is apparent from figure 2.1.74b that there are regions of free sulphur embedded in the polysulfide matrix that form what appear to be small microparticles (5 to $15 \mu\text{m}$ in size). This data supports the SEM/EDS analysis as well as other results recently reported in the literature on related composites.

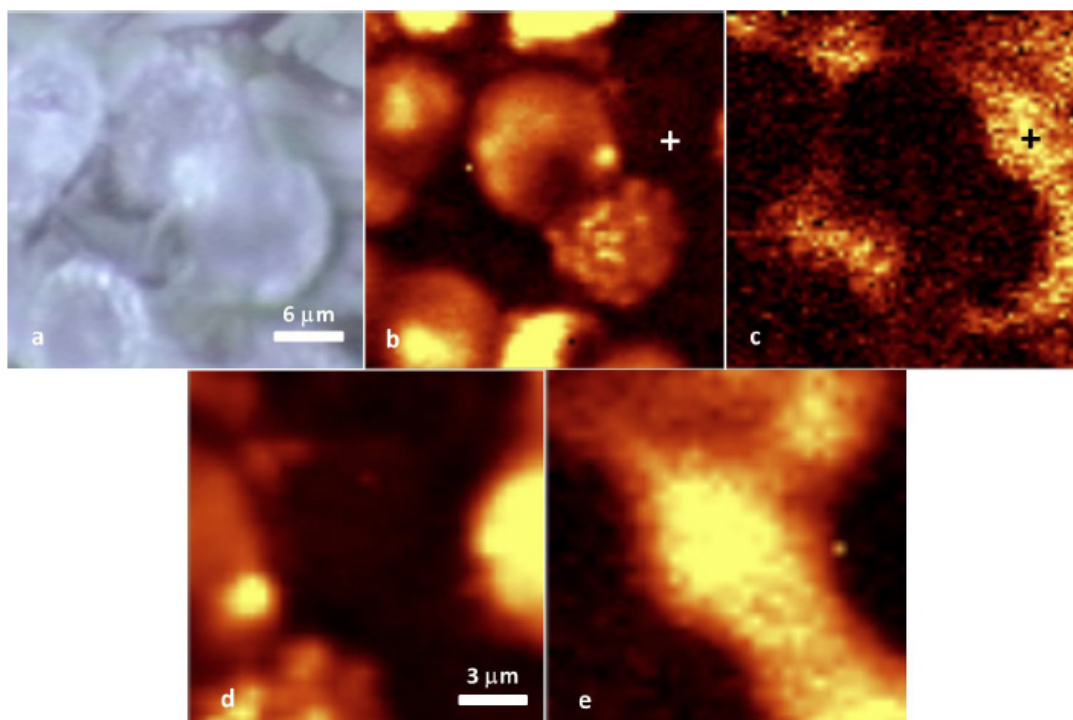


Figure 2.1.74 | Optical image (a) of a section of the canola polysulfide with corresponding confocal Raman images of the same region (b and c). The number of pixels in b and c is 70×70 (4900) with the integration time per pixel equal to 1 second. The confocal Raman images in d and e are zoomed in areas of b and c and correspond to exactly the same area of the sample. The centre of each image in d and e is denoted by the white and black crosses displayed in b and c. The number of pixels in d and e is 35×35 (1225) with the integration time per pixel equal to 6 seconds.

Toxicity Studies

Experiments performed by Ines Albuquerque

Cell culture

Huh7 and HepG2 (ATCC® HB-8065™) cells were routinely grown in a humidified incubator at 37 °C under 5% CO₂ and split before reaching confluence using TrypLE™ Express. Both cell lines were grown on DMEM medium supplemented with 10% heat-inactivated FBS, 2 mM GlutaMAX™, 10 mM HEPES, 1% NEAA, 1 mM sodium pyruvate, 100 units/mL penicillin and 100 µg mL⁻¹ streptomycin. All reagents were bought from Gibco, Life Technologies (USA), unless otherwise stated.

Cytotoxicity and estimation of IC₅₀ of HgCl₂ in HepG2 and Huh7 cells.

Cytotoxicity of HgCl₂ was assessed using a CellTiter-Blue® Cell Viability Assay (Promega, USA), a fluorescent dye approach based on the ability of metabolically active cells to convert the dye resazurin to the fluorescent resorufin product. Briefly, cells were seeded at a concentration of 10,000 cells per well (100 µL) in flat-bottom 96 well-plates and allowed to adhere and adapt to the plates for 24 h. At this point, culture medium was exchanged to complete medium supplemented with increasing concentrations of HgCl₂ in technical triplicates (1, 5, 10, 30, 60, 80, 100 µM). Plates were incubated for 22 h 30 min, at which time cell viability was assessed by exchanging the culture medium to medium supplemented with CellTiter-Blue Reagent (dilution 1:20 from commercial stock) and incubated for another 1 h 30 min, before analysis of fluorescence on an Infinite M200 (Tecan, USA) plate-reader ($\lambda_{exc}=530$, $\lambda_{em}=590$). Relative fluorescence units (R.L.U.) were normalized to the values obtained for the appropriate vehicle controls. Results are shown as average of 3 independent experiments. A sigmoidal curve (variable slope) was fitted to each dataset, using GraphPad Prism v5 software, and used to calculate the half maximal inhibitory concentration (IC₅₀) of HgCl₂ on both cell-lines. The average IC₅₀ was 40 µM for HepG2 cells and 34 µM for Huh7 cells.

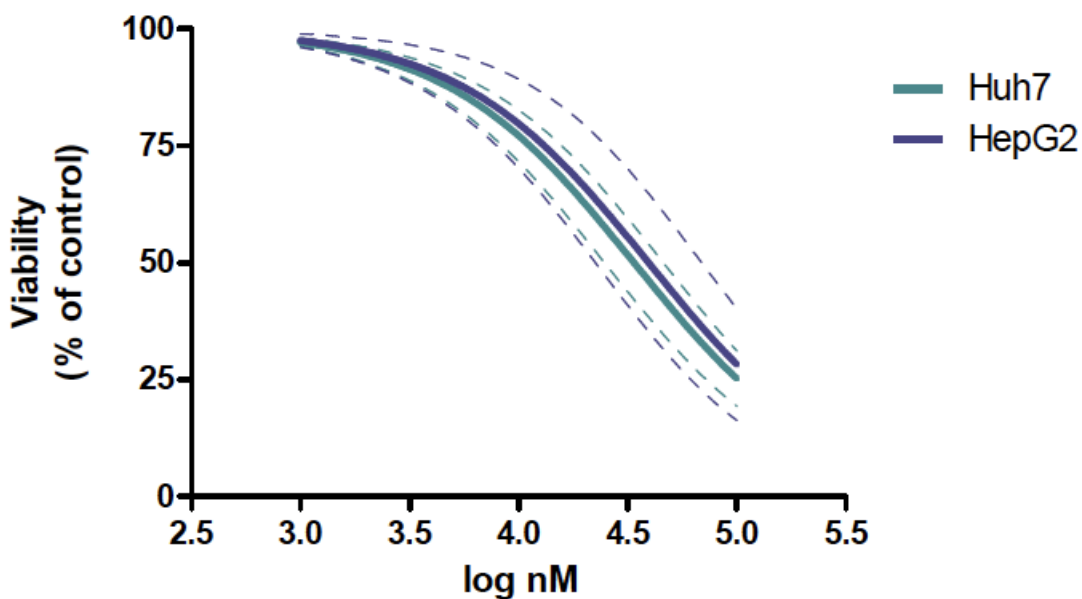


Figure 2.1.75 | Dose-response curve and IC_{50} measurement of $HgCl_2$ in HepG2 and Huh7 cells. The average IC_{50} was 40 μM for HepG2 cells and 34 μM for Huh7 cells.

Cytotoxicity of mercury-treated and untreated polysulfides in HepG2 and Huh7 cells.

Cells were cultivated as described above and seeded in 24 well-Transwell® plates at a concentration of 30,000 cells/well (300 μL) and allowed to adhere to the bottom of the well for 24 h. At this point, culture medium was removed and 200 μL of fresh complete medium was added to the bottom layer. Also, 3.75 mg or 37.5 mg of treated or untreated polysulfide was added to each insert in technical duplicates, and 100 μL of complete medium was added on top of the polysulfide, thus creating a continuous layer of medium on top of the cells and the polysulfides. Cells were incubated for another 22 h 30, at which time cell viability was assessed as described above. Results are shown as average of 3 independent experiments (bars), and error bars represent standard error of the mean. There was no difference in cell viability for the cells treated with polymer and cells treated with the polymer bound mercury. Under these conditions, neither the polymer nor the polymer-bound mercury exhibit significant toxicity.

Notes for figures 2.1.76 and 2.1.77:

Dose 1 = 37.5 mg of polymer in 300 mL of culture medium

Dose 2 = 3.75 mg of polymer in 300 mL of culture medium

The polymer treated with HgCl_2 contained 2.2 mg HgCl_2 per gram of polymer

The polymer treated with Hg_0 contained 79 mg mercury per gram of polymer

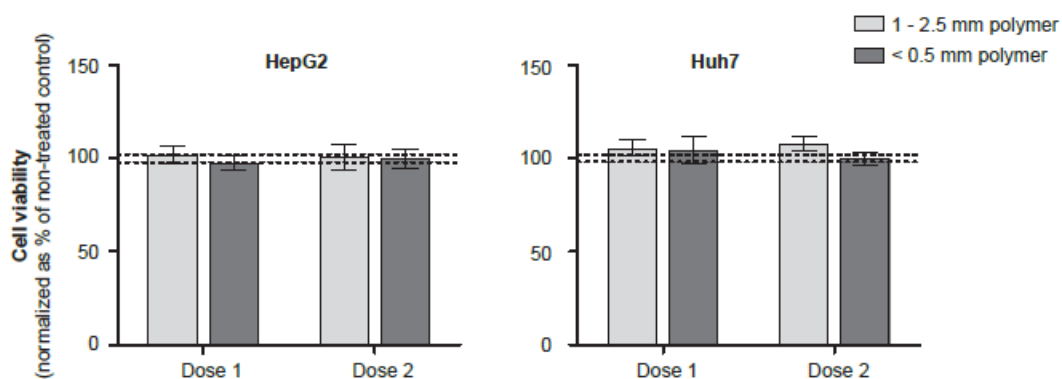


Figure 2.1.76 | Cell viability of HepG2 and Huh7 cell lines grown in presence of canola oil polysulfide (50 wt.% sulfur). There was no difference in cell viability for the cells treated with polymer and cells that were untreated. This experiment demonstrates that the polysulfide is not toxic.

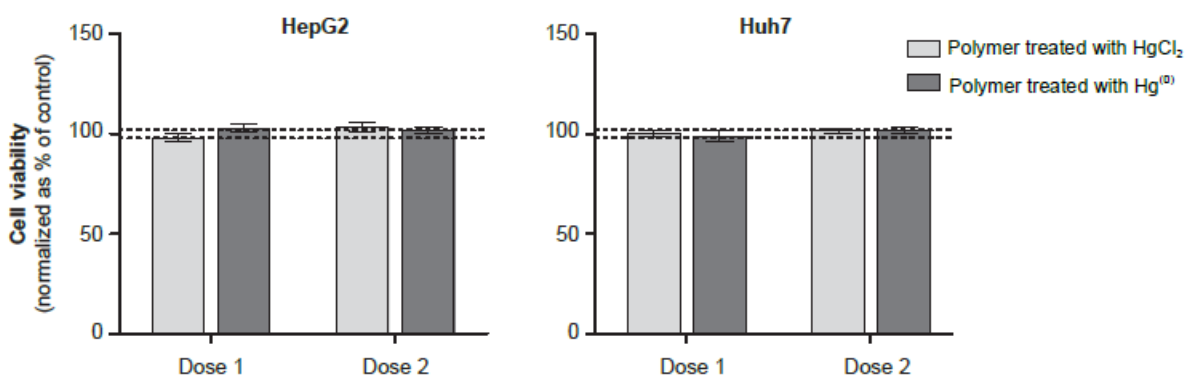


Figure 2.1.77 | Cell viability of HepG2 and Huh7 cell lines grown in presence of polymer-bound mercury. There was no difference in cell viability for the cells treated with polymer and cells treated with the polymer-bound mercury. Under these conditions, neither the polymer nor the polymer-bound mercury exhibit significant toxicity.

References

1. Crockett, M. P.; Evans, A. M.; Worthington, M. J. H.; Albuquerque, I. S.; Slattery, A. D.; Gibson, C. T.; Campbell, J. A.; Lewis, D. A.; Bernardes, G. J. L.; Chalker, J. M., Sulfur-Limonene Polysulfide: A Material Synthesized Entirely from Industrial By-Products and Its Use in Removing Toxic Metals from Water and Soil. *Angew. Chem. Int. Ed.* **2016**, 55, 1714-1718.
2. Agilent Technologies, Determination of Fatty Acid Methyl Esters (FAMES) in Milk Matrix Using an Agilent 5977E GC/MS. **2014**. <<https://www.agilent.com/cs/library/applications/5991-4867EN-D2.pdf>> Accessed September 2016
3. Worthington, M. J. H.; Kucera, R. L.; Albuquerque, I. S.; Gibson, C. T.; Sibley, A.; Slattery, A. D.; Campbell, J. A.; Alboaiji, S. F. K.; Muller, K. A.; Young, J.; Adamson, N.; Gascooke, J. R.; Jampaiah, D.; Sabri, Y. M.; Bhargava, S. K.; Ippolito, S. J.; Lewis, D. A.; Quinton, J. S.; Ellis, A. V.; Johs, A.; Bernardes, G. J. L.; Chalker, J. M., Laying Waste to Mercury: Inexpensive Sorbents Made from Sulfur and Recycled Cooking Oils. *Chem. Eur. J.* **2017**, 23 (64), 16219-16230.

3. SULFUR POLYMERS FOR MERCURY CAPTURE

Acknowledgements

Inês Albuquerque for cytotoxicity testing of mercury treated polysulfides

Christopher Gibson and Jason Gascooke for Raman analysis of polysulfides

Alexander Sibley for Auger and XPS analysis of mercury treated polysulfides

Ashley Slattery for aid and training in finding discrete structures under the SEM

Katherine Muller and Alexander Johs for sulfate leaching and Hg-NOM binding experiments

Jason Young for aid and training in ICPMS analysis of aqueous mercury solutions

Nick Adamson for XRD analysis of mercury treated polysulfides

Dehetti Jampaiah, Ylias Sabri and Suresh Bhargava for mercury vapour testing

Initial Experiments

The starting point for exploring the applications of the canola oil polysulfide was this question: Did the canola oil polysulfide, like the sulfur-limonene polysulfide, capture mercury? And if it did, what advantages did it have over other sorbents? To answer the first questions, 2.0 g polysulfide was submerged in a 5 mL aqueous solution of 20 mg mL⁻¹ HgCl₂ for 24 hours. The polymer was removed, washed with DI water and the filtrate combined and dried to determine remaining mercury chloride. Of an average of triplicate measurements, 45.5 mg of the initial 100 mg remained in solution with 54.5 % removed over the 24 hours. Not only was this an excellent start for a preliminary experiment, but it revealed something unexpected about the polysulfide—after being subject to the mercury-spiked water the polysulfide had turned grey. Scanning electron microscopy (SEM) and energy-dispersive x-ray spectroscopy (EDX) revealed nano-sized particles of mercury chloride were bound to the surface (Fig. 3.1d). Auger spectroscopy was also able to detect the presence of mercury, but an accurate surface map was not possible to produce due to excessive charging of the sample. X-ray photoelectron spectroscopy (XPS) imparted significant detail on the chemistry of the binding event, revealing a binding energy associated with mercury-sulfur bonding. The adsorption of mercury chloride from solution is not just due to physical interaction but a chemical bond-forming reaction is occurring to bring the two together.

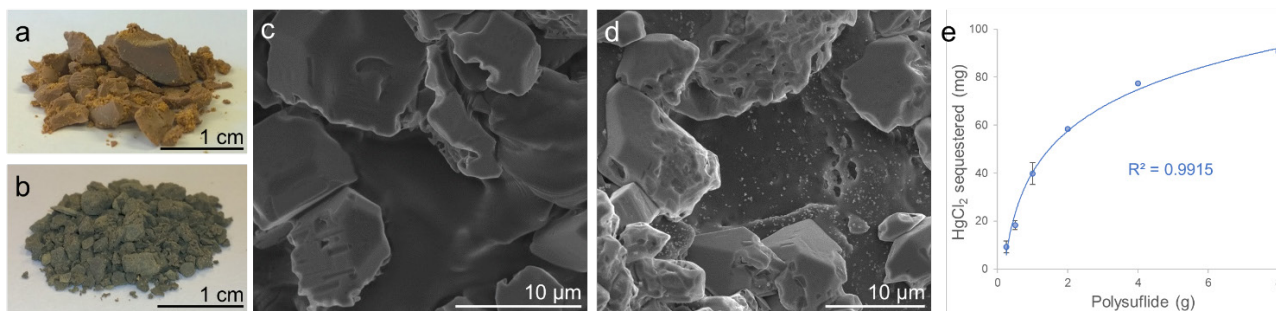


Figure 3.1 | a. Canola oil polysulfide, as synthesised; b. canola oil polysulfide after reaction with HgCl_2 ; c. SEM image of canola oil polysulfide; d. SEM image canola oil polysulfide after reaction with HgCl_2 , nanoparticles of mercury are visible as bright dots along the polysulfide surface; e. HgCl_2 removed from 10 mL of a 10 mg mL^{-1} solution by increasing amounts of polysulfide. A log curve has been fitted to model the trend.

The colour-changing result was particularly interesting because of the prospect for mercury sensing, or perhaps self-indicating when the sorbent would need to be replaced if used in a filter. Varying the mass of polymer to the same mass of mercury as the previous experiment (100 mg as a 10 mL aqueous solution at 10 mg mL^{-1}) found that with 8.0 g of polysulfide, over 90% of the mercury chloride present in solution could be removed in 24 hours. Varying the concentration of HgCl_2 in solution, 2.0 g polysulfide seemed to remove a similar percentage of mercury at 5, 10, and 20 mg mL^{-1} : 75.8, 63.2 and 61.9 %, respectively over 24 hours. At higher concentrations the polysulfide removes a higher mass of mercury chloride from solution but becomes increasingly less capable of lowering the concentration to the same extent. It should be noted at this point that the concentrations tested are far greater than is relevant to environmental remediation and were chosen first to facilitate simple gravimetric analysis—environmentally relevant mercury will be addressed further on.

To determine efficacy as a mercury sensor, polysulfide was incubated in a series of 10-fold dilutions of aqueous HgCl_2 from 10.0 to 0.001 mg mL^{-1} and monitored every 24 hours for 4 days. After the first day, polymer incubated at the highest concentration of 10 mg mL^{-1} mercury had undergone a change in colour from brown to grey. The same change was visible in the first dilution of 1.0 mg mL^{-1} , though to a lesser extent. No colour change was visible in the lower concentrations over the full time-course, and the colour of those that changed did not change further with continued exposure.

The simplest form of mercury to test due to its solubility, mercury chloride poses a good initial target for mercury remediation efforts. It is however neither the most prevalent form of mercury pollution encountered in the environment or the most toxic¹. To pose any use in clean-up or capture of mercury pollution our polymer would ideally need to be able to bind elemental mercury, organo-mercury (methyl mercury for example) and/or Hg-NOM (mercury bound to natural organic matter). The latter often poses a significant problem to deal with as mercury can be present in secluded pockets of organic macromolecules that hinder displacement by competing chemicals², in this case the reactive sites of canola oil polysulfide. The least toxic of these to start with was elemental mercury. 2.0 g

polysulfide and a bead of mercury weighing 170 mg were placed together with 7 mL DI water (to aid in mixing and mass transfer) in a glass vial and stirred magnetically at 1,500 rpm for 24 hours. As in the HgCl_2 experiment before, the polysulfide once again changed colour; its whole surface had turned black. XRD analysis revealed the product to be a spectral match for metacinnabar, or mercury sulfide, a common mercury ore. Essentially the polysulfide had reacted with the liquid mercury and immobilised it as a (non-toxic) solid. This is an important aspect of the polymer that is distinct from other sorbents: the polymer reacts with mercury and does not merely bind physically. After drying, no further mercury was visible, and the mass balance indicated over 99 % yield of the two starting materials in the black product. In the case of mercury metal, the chromogenic response was always seen across the experiments undertaken. In an experiment to specifically test the conditions under which the polymer would change colour, canola oil polysulfide and mercury were mixed together in an end-over-end mixer for 24 hours at ratios from 3.5 to 20.7 mg mercury per gram polymer, in every case all polysulfide involved had turned black. No mercury nanostructures could be identified along the surface as in the inorganic mercury test purely by SEM, but EDX mapping revealed a consistent spread of Hg signatures. Breaking open a single particle to analyse a cross section, the black colour change seemed isolated purely to the surface of the polymer, affirmed by EDX mapping that showed no penetration of Hg into the core of the polymer. Auger electron spectroscopy, a sensitive elemental analysis technique with a penetration depth under 100 angstroms, did not suffer the same charging issues as with the HgCl_2 -treated polysulfide and was also able to detect and map mercury on the polysulfide. The very shallow penetration depth of this technique shows that the binding is indeed occurring at the surface. XPS revealed the same binding signal as in the HgCl_2 treated polysulfide, that of an HgS species, corroborating the XRD findings. Interestingly this XPS signal for both HgCl_2 and Hg^0 bound to the surface was that of mercury in the 2+ oxidation state. For the former this indicates no change, but for Hg^0 this represents a change in speciation and thus perhaps a different binding mechanism.

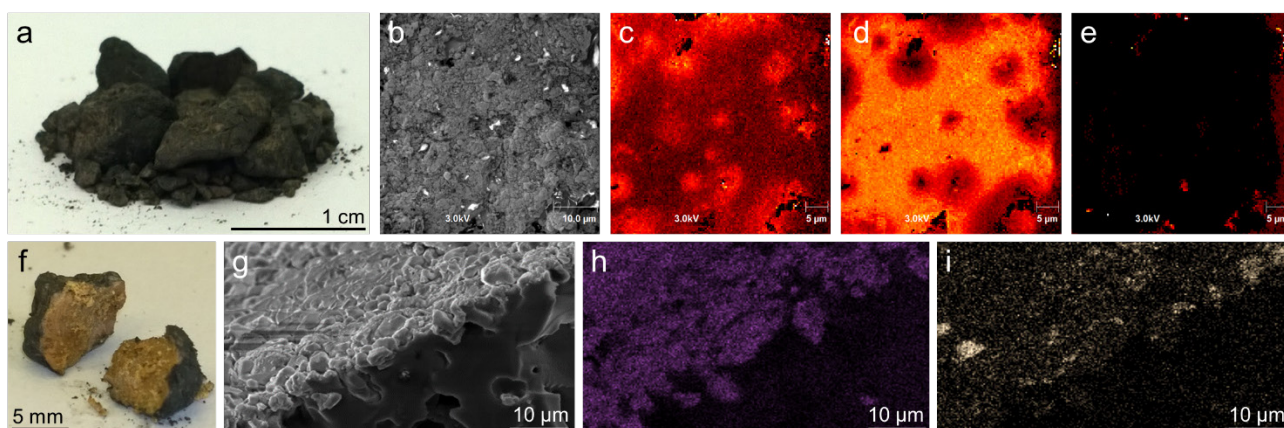


Figure 3.2 | a. Canola oil polysulfide after reaction with elemental mercury; b–e. SEM image of Hg^0 -treated polysulfide (b) and corresponding Auger maps of carbon (c), sulfur (d) and mercury (e); f. Hg^0 -treated polysulfide split for SEM analysis of the cross section g-i. SEM image of cross-section - surface is upper region, inner is lower (g) and EDX maps of sulfur (h) and mercury (i), both more prominent at the surface.

Stability of the polysulfide-mercury product

It would be of little use to sequester mercury contamination if the polysulfide did not also retain it over time. Polysulfide previously used to bind mercury chloride (79.42 mg g^{-1}) and elemental mercury (2.16 mg g^{-1}) were incubated separately in milliQ water for 24 hours to determine if bound mercury would leach. By inductively coupled plasma mass spectrometry (ICP-MS), the concentration of mercury in the incubation medium was 0.57 ppb for the Hg^{2+} treated polymer and 46.99 ppb for the Hg^0 treated. If all mercury had leached the concentration would reach 6,942,000 ppb Hg^{2+} and 216,000 ppb Hg^0 and so the quantity leached represents $< 0.00001\%$ of the inorganic and 0.02% of the elemental mercury bound. The discrepancy between the two mercury species may be explained by difficulties in separation of unreacted mercury from the polysulfide. Between the sequestration and leaching experiments both samples were washed in milliQ water to remove excess unbound mercury—efficient in the case of water-soluble mercury chloride but likely not with metal mercury. Regardless, mercury was found to be bound securely to the polysulfide, with very little leaching into pure milliQ water.

It would similarly be of little use to sequester mercury contamination if the mercury-polysulfide product continued to exhibit toxicity. Cytotoxicity was examined through a collaboration with the Bernardes group at the Instituto de Medicina Molecular, Lisbon. HepG2 and Huh7 (immortal hepatic cancer cell lines commonly used in toxicity studies) cells were cultivated and seeded in 24-well Transwell plates for 24 hours. After seeding, medium was exchanged for a fresh solution and HgCl_2 and Hg^0 - treated polysulfides (2.2 mg g^{-1} and 79 mg g^{-1} bound mercury respectively) were submerged using inserts that held the material in solution but out of contact with cells. After a 23 hour incubation, no difference in cell viability was observed—neither the mercury chloride or elemental mercury-treated polysulfides exhibited significant toxicity to cells.

As detailed in the previous chapter, factice is a commercially available plasticising agent of vulcanised canola oil, similar to canola oil polysulfide but prepared with lesser sulfur content (under 25 wt. %) and often as a formulation containing more than just sulfur and cooking oil. Given the similarities it was expected it too might have an affinity for mercury, and so samples provided by D.O.G. Chemie were tested in similar experiments. F10, F17 and F25 grade factices (containing 12.6 %, 17.7 % and 22.9 % sulfur respectively) were incubated in 5 mL of an aqueous 20 mg mL^{-1} HgCl_2 solution (100 mg total HgCl_2). Factices were portioned such that the amount of sulfur used in synthesis was equal to that of the polysulfide used for comparison in the same experiment: 0.50 g. In this way the experiment would both indicate if factice had an affinity for inorganic mercury but also elucidate the role reacted sulfur plays in binding. 3.96 g F10, 2.92 g F17 and 2.18 g F25 were used. On average, the indicated masses of F10 removed 91.2 %, F17 removed 88.2 % and F25 removed 84.6 %, all more so than the same mass of canola oil polysulfide had previously been shown to remove. This result also seems to indicate that the total sulfur content does have a bearing on HgCl_2 uptake as the amounts removed in each case were all within 6.6% of one another despite the

difference in total mass. Increased mass of factice, despite the difference in sulfur content, does lead to an increase in mercury uptake though. The triglyceride component also contributing to binding could explain this, as more than just the sulfur appears to have a bearing on mercury removal. In regard to elemental mercury, 2.8 g F17 (0.50 g total sulfur content) was mixed with a magnetic stirrer with 217 mg Hg^0 in 10 mL DI water for 24 hours. 117 mg mercury was removed by factice, 100 mg remained. Even with minimal (1.15 ± 0.25 % as determined by the manufacturer) free sulfur present, factice was capable of binding mercury, indicating that free sulfur is not required—a concern that had arisen from the revelation that up to 9 % free sulfur was incorporated into canola oil polysulfide. To align with our goals of producing functional materials from waste- or by-products, it is insufficient for any function of the canola oil polysulfide to not be applicable when it is synthesised from used cooking oils. Initial tests with pristine canola oil minimise the influence of impurities but observations must then be replicable in the waste-oil variant. To this end experiments were repeated with polysulfide prepared from used fryer oil as characterised in the previous chapter. 1.0 g of this recycled-oil polysulfide was able to remove 26.9 % total HgCl_2 from a 5 mL solution containing 100 mg over 24 hours, less than the same mass of canola oil polysulfide. The trend seen previously in factice that the amount of mercury chloride removed was proportional to the sulfur content of the polysulfide is not repeated here, indicating some other factor between factice and inverse vulcanised polysulfides that seems to be affecting uptake. It may be that additives used in the production of D.O.G. Chemie's factice are contributing in some way, or that the method of synthesis bears more reactive sites on the surface of the material, or that the canola oil or vegetable oil cross-linker also binds to mercury. Testing elemental mercury, 1.0 g polysulfide from recycled cooking oil (0.50 g total sulfur content) was mixed with a magnetic stirrer with 171 mg Hg^0 in 10 mL DI water for 24 hours. 116 mg mercury was removed by the polysulfide, 55 mg remained. Fryer oil polysulfide is capable of binding mercury as with pristine canola oil polysulfide. Interestingly factice and fryer oil polysulfide removed the same mass of elemental mercury, containing the same total mass of sulfur, despite the previous observation that this wasn't a trend for mercury chloride.

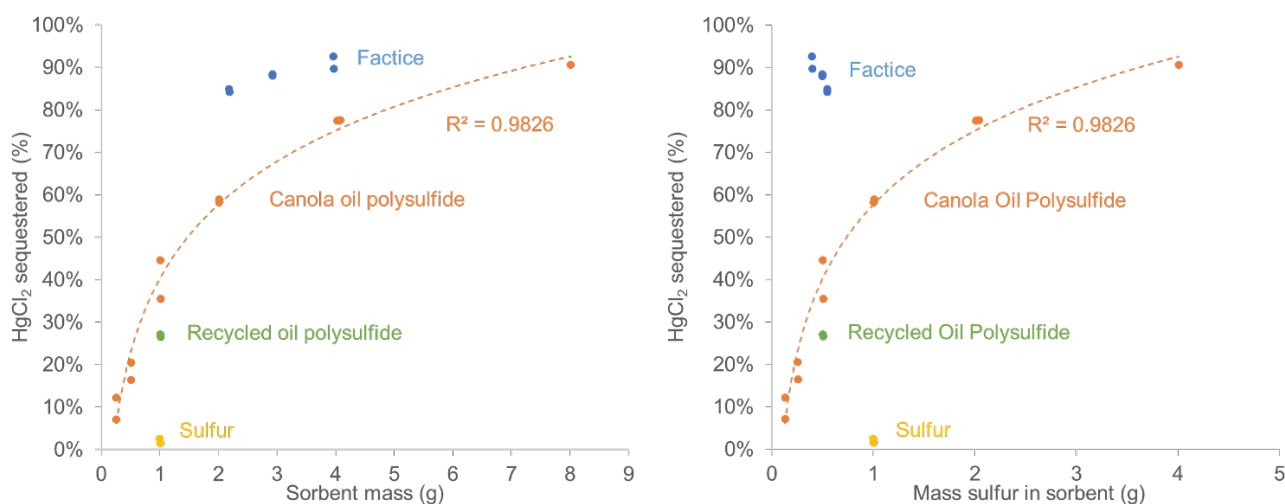


Figure 3.3 | Mercury chloride removal efficiency of multiple materials over multiple experiments. In each case material was incubated in 5 mL of a 20 mg mL⁻¹ aqueous solution for 24 hours. Left: Percentage of HgCl₂ sequestered increases as mass of canola oil polysulfide (non-porous) increases, a log curve is fitted to demonstrate the trend. Recycled canola oil polysulfide is less efficient at the same mass as canola oil polysulfide, factice is more efficient. Powdered sulfur alone is far less efficient at HgCl₂ removal than the polysulfides. Right: The same graph normalised to the mass of sulfur present in each sorbent. For canola and recycled oil polysulfides this is 50 % but varies with factice grade. Higher masses of lower grade factice removed more mercury from solution, indicating there is more influencing uptake than the percentage of sulfur incorporated.

Sulfur polymers are not wholly unique in their chromogenic response to mercury, this appears to be a feature inherited from the large amount of sulfur present within them. In mixing (1,500 rpm with a magnetic stirrer bar) powdered sulfur with a bead of elemental mercury in water, the sulfur turned from yellow to grey, much like canola oil polysulfide in the presence of inorganic mercury. Interestingly, when the experiment was repeated with crystalline sulfur (formed by the melting and then rapid cooling of powdered orthorhombic sulfur), the sulfur turned from yellow to black. Binding of mercury by sulfur is a known phenomenon but is subject to several disadvantages that prompted us to take this investigation further. Firstly, there is the mechanical aspect of using sulfur as a filter. Powdered sulfur is generally too fine to pack, which would result in clogging for any flowthrough process, and crystallised sulfur is very brittle, breaking easily under pressure. Polymeric sulfur too also has its own disadvantages, mainly in that it is unstable and breaks back down to S₈ and so has little use as a reliable, long-term device. Sulfur alone is also inefficient at binding inorganic mercury without significant heat and/or pressure applied, demonstrated in Fig. 3.3. Inverse vulcanisation offers an alternative method of polymerising sulfur that could address these shortcomings.

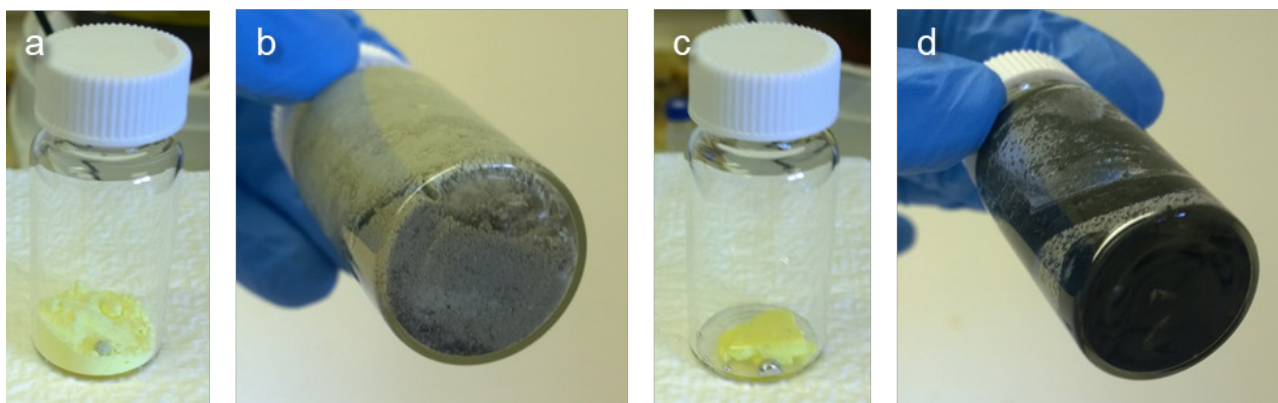


Figure 3.4 | a-b. Powdered sulfur and elemental mercury before (a) and after (b) mixing in water for 24 hours; c-d. Crystal sulfur and elemental mercury before (a) and after (b) mixing in water for 24 hours.

Environmental mercury

The most arduous form of mercury to remediate is that bound to natural organic matter (Hg-NOM). We did not have the facilities available locally to test the polysulfide's efficacy in this regard, but through a collaboration with Oak Ridge National Laboratory we were able to export samples to test. Suwannee River aquatic natural organic matter (SR-NOM), a standard reference material was mixed with $\text{Hg}(\text{NO}_3)_2$ to prepare Hg-NOM complexes with a molar mercury-carbon ratio of 1.8×10^{-5} in 10 mM pH 7.8 sodium phosphate buffer. 30 mL dilutions of this solution to a series of concentrations from 0.2 to $7.7 \mu\text{g L}^{-1}$ Hg-NOM were each added to 100 mg polysulfide in 40 mL amber borosilicate glass vials and mixed for 48 hours on a rotary shaker. Three variations of the polysulfide were tested: non-porous canola oil polysulfide, porous polysulfide, and partially reduced porous polysulfide. Solutions of $\text{Hg}(\text{NO}_3)_2$ were also prepared as a NOM-free control. Hg-NOM adsorbed by the polysulfide was plotted against the equilibrium concentration of each experiment to determine correlation. A non-linear relationship was observed, and a Langmuir isotherm determined as a good fit to describe the data. For the $\text{Hg}(\text{NO}_3)_2$ -only control, a linear correlation was observed and plotted in each case. A simpler method of quickly determining the comparable efficiency of the polysulfides in adsorbing Hg-NOM can be determined by expressing the results as the percentage of sorbate removed at a given concentration. At the lowest initial concentration of $0.2 \mu\text{g L}^{-1}$ Hg (1/300 sorbent/solution ratio), non-porous polysulfide had a 36 % removal efficiency, porous polysulfide: 79 %, and the partially reduced porous polysulfide: 81 %. The lower end of the Hg-NOM concentrations tested better represents a real-world contamination scenario and so provides the most relevant point of comparison. From the Langmuir plots we can read for the non-porous, porous, and partially reduced polysulfides equilibrium constants of 1.35, 0.46 and $1.29 \text{ L } \mu\text{g}^{-1}$, and sorption capacities of 0.21, 1.11 and $0.44 \mu\text{g g}^{-1}$ respectively. This demonstrates, over the full range of concentrations tested, more rapid uptake of Hg-NOM by the non-porous and surface treated polysulfide, but a greater capacity for Hg-NOM adsorption by the marginally slower porous polysulfide. Overall a very promising result for a notoriously challenging contaminant.

In an experiment also undertaken at Oak Ridge National Laboratory, sulfate release into water by canola oil polysulfide was measured. Sulfate-reducing bacteria have been linked to mercury methylation in marine environments and so the formation of from sulfur polymers has the potential to feed into methyl mercury synthesis³. During the previously described batch sorption experiment, final Hg-NOM and Hg(NO₃)₂ solutions were also tested for the presence of sulfate ions by ion chromatography. It was discovered that sulfates were present in the Hg-NOM solutions, with a linear relationship between the initial concentration of mercury with the concentration of sulfate. In the samples containing no NOM however, sulfate concentrations were negligible (<100 µg per g polysulfide). We can conclude that the sulfate present is derived almost entirely from those naturally occurring in the NOM and that the polysulfide (porous or partially reduced porous) does not significantly contribute to the sulfate present.

After our limonene polysulfide paper was published, our lab was contacted by many people concerned with and looking for solutions to mercury pollution. Many were individuals concerned with high levels of bioaccumulated mercury in the fish they were eating, an issue perhaps best tackled at the source of pollution rather than by the end user. Among them though were environmental agencies, included the United Nations Environment Programme, keen to assess the feasibility of mercury-binding sulfur polymers in an industry we hadn't been made aware of before: Artisanal and small-scale gold mining (ASGM). An overview is given in chapter 1 but in short, ASGM accounts for approximately 25 % of the worlds gold and occurs throughout South America, Africa and South-East Asia. In the process, mercury is used intentionally to remove gold from ore and then volatized by hand to recover the gold. There are two key waste streams of mercury that result from this process. The first is mercury vapour released in gold recovery. The second is mercury lost among waste ore and loam deposited in rivers, polluting drinking and irrigation water. To tackle the first issue, canola oil polysulfide would need to be able to capture mercury from the air. In a collaboration with RMIT in Melbourne, 300 mg porous canola oil polysulfide was loaded into a fixed bed-reactor and mercury vapour at 586.4 µg Nm⁻³ (N₂ carrier gas) flowed through at 0.1 L min⁻¹. Residence time under these parameters was 0.24 seconds, a demanding test of the polysulfide's capability. Reactor temperature was increased in increments of 25 °C from 25 °C to 100 °C for a total of four tests. In all tests the polysulfide captured a portion of the mercury passed through the reactor, but it was most efficient in doing so at 75 °C, removing 66.5 %. Sequestered mercury was determined by cold vapour atomic fluorescence spectroscopy of mercury captured in traps at the end of the flow channel. A negligible amount (<<1%) was oxidised to mercury(II), most trapped was mercury(0). Not all mercury vapour was captured during the experiment, but for such a short residence time this was a very promising result that we can take forward into developing air filters using sulfur polymers.

Tackling the second source of environmental mercury pollution from ASGM first required us to determine the nature of the mercury lost—mercury flour is the term used for unreacted mercury that remains trapped in fine loam after the amalgamation process that floats along the top of waste water

outlets to settle on banks down-river or pollute waterways. A bead of mercury was dropped into a sample fine loam sourced from the author's garden and mixed in a centrifuge tube on an end-over-end mixer for 24 hours. After this time there were no visible traces of mercury remaining, the loam looked indistinguishable from a sample that had not been subjected to mercury. SEM/EDX analysis revealed the mercury to be present as microbeads, coated in fine soil particles inhibiting aggregation. It is in this state, induced by mixing in trommels with earth and ore that mercury is lost in waste streams. Not only is this damaging to the health of those in the area but also represents a substantial loss of an expensive commodity miners could otherwise be feeding back into the amalgamation process. In a test to determine the efficacy of canola oil polysulfide in capturing this type of mercury, 5.0 g of the soil previously spiked with mercury and mixed to simulate mercury flour was further mixed for 24 hours in a 50 mL centrifuge tube with 5.0 g canola oil polysulfide of a controlled particle range of over 2.5 mm and under 5.0 mm. After this time the whole mixture had turned black. Polysulfide particles were simple to isolate with the use of a 2.5 mm mesh sieve, all of which had turned from brown to black during mixing, indicating binding of mercury and the formation of metacinnabar. The polysulfide itself was not all that appeared black though, the abrasion of the mixing process seemed to have powdered enough of the reacted polysulfide and dispersed it throughout the soil that it all appeared to be black. SEM/EDX analysis revealed that microbeads of mercury still remained in the mercury flour sample after treatment with polysulfide, and so despite the colour change indicating a reaction between mercury and the polysulfide, under the conditions tested not all had been removed.

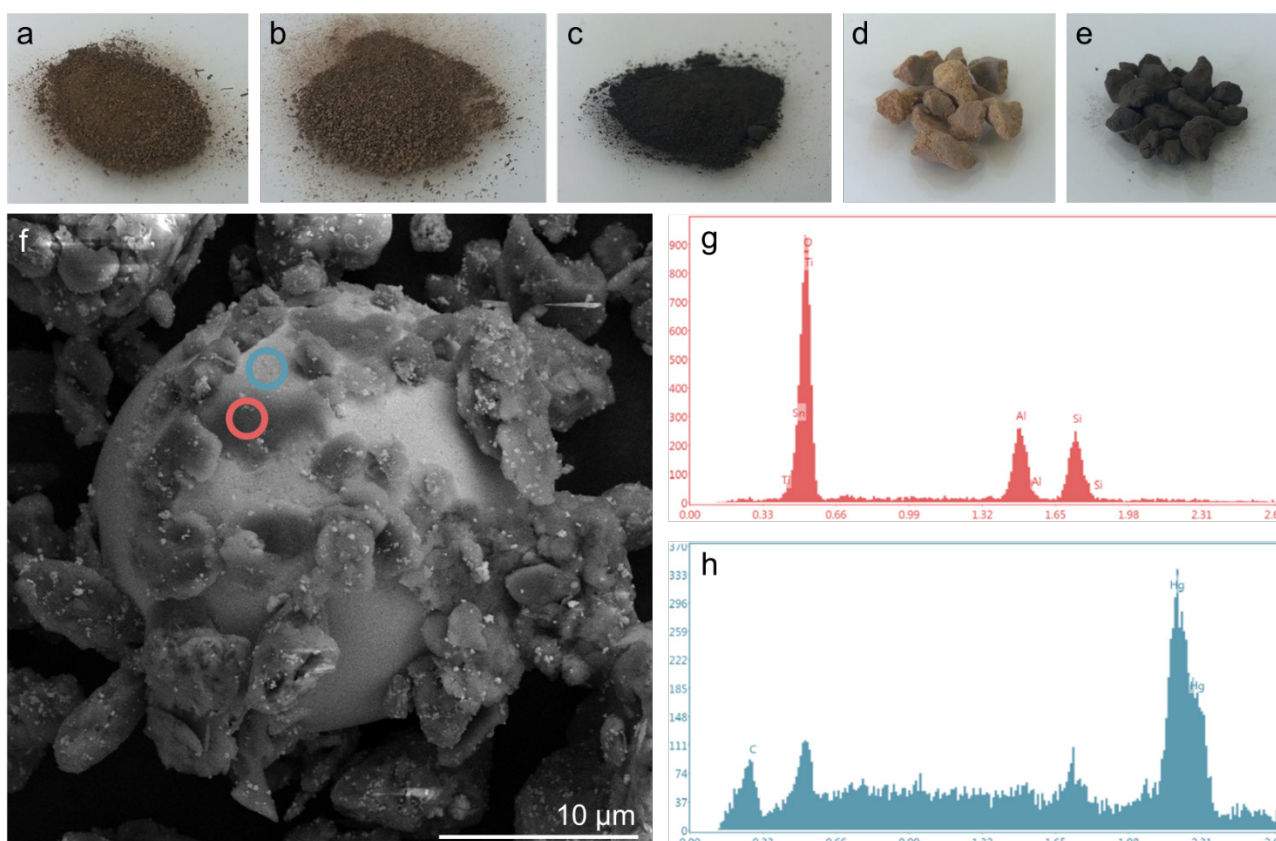


Figure 3.5 | a. Fine loam; b. Fine loam after 24 hours in an end-over-end mixer with elemental mercury, the mercury is no longer visible; c. Hg⁰-treated loam after 24 hours in an end-over-end mixer with canola oil polysulfide, the bulk of the loam has changed colour from brown to black; d-e. Canola oil polysulfide particles 2.5 – 5.0 mm in diameter before (d) and after (e) mixing with Hg⁰-treated loam, the polysulfide has changed colour from brown to black, indicating Hg uptake and HgS formation; f-h. SEM image of a concealed microparticle of mercury after 24 hours mixing with soil. Elemental analysis by EDX confirms the sphere to be mercury (h) and the flakes coating it to be aluminium and silicon oxides present in the soil (g).

Methoxyethyl mercury chloride (MEMC) is an organomercury compound used as a fungicide to prevent pineapple disease on sugar cane crops here in Australia. A ChemWatch Review MSDS provided by the US Environmental Protection Agency assigns the chemical a Hazard Alert Code of 4, the highest possible, assigning corrosive, toxic, health and environmental hazard GSH labels. MEMC is described as toxic if swallowed, and fatal in contact with skin or if inhaled with an LD₅₀ of 22 mg kg⁻¹ in rats via ingestion. The manufacturer's safety data sheet⁴ and directions for use⁵ do not fail to mention this information, but their handling instructions are alarming in that it instructs the user to "dispose of the discarded dip and spray solutions by combining with sand/soil mixture and bury under 500 mm of soil away from water sources and homes" and to "not contaminate streams, rivers or waterways with the chemical or used containers". Our primary concern, and that of the National Environmental Science Program's, the organisation that approached us about the use of MEMC in Australia, was the fate of this mercury being sprayed on crops along the Queensland coast. Given the molecule's hydrophilicity, irrigation was quite likely to dilute and carry it away into local waterways, and so our first thought was to develop canola oil polysulfide as a filter for irrigation

water. In a first test, to see if our polysulfide was capable of sequestering the organomercury compound, a solution of aqueous MEMC as store-bought commercial fungicide was diluted down from 120 g L^{-1} to the recommended operating concentration of 0.15 g L^{-1} in milliQ water. 10 mL of this solution was incubated in a 50 mL centrifuge tube with 2.0 g porous polysulfide without agitation for 24 hours. The incubation was prepared in triplicate. After this time the solution's prominent clear pink colour had reduced in intensity, and ICP-MS analysis revealed a drop in concentration from $0.149 \pm 0.008 \text{ g L}^{-1}$ to $0.03 \pm 0.00007 \text{ g L}^{-1}$, a 98% reduction in mercury. Not only did our polysulfide sequester MEMC from a commercial formulation, but even in this initial test it removed a significant amount. This was a useful first step in confirming this, but the greater challenge would be to adapt the polymer to a continuous filtration process where irrigation water is flowed through directly, rather than collected for treatment.

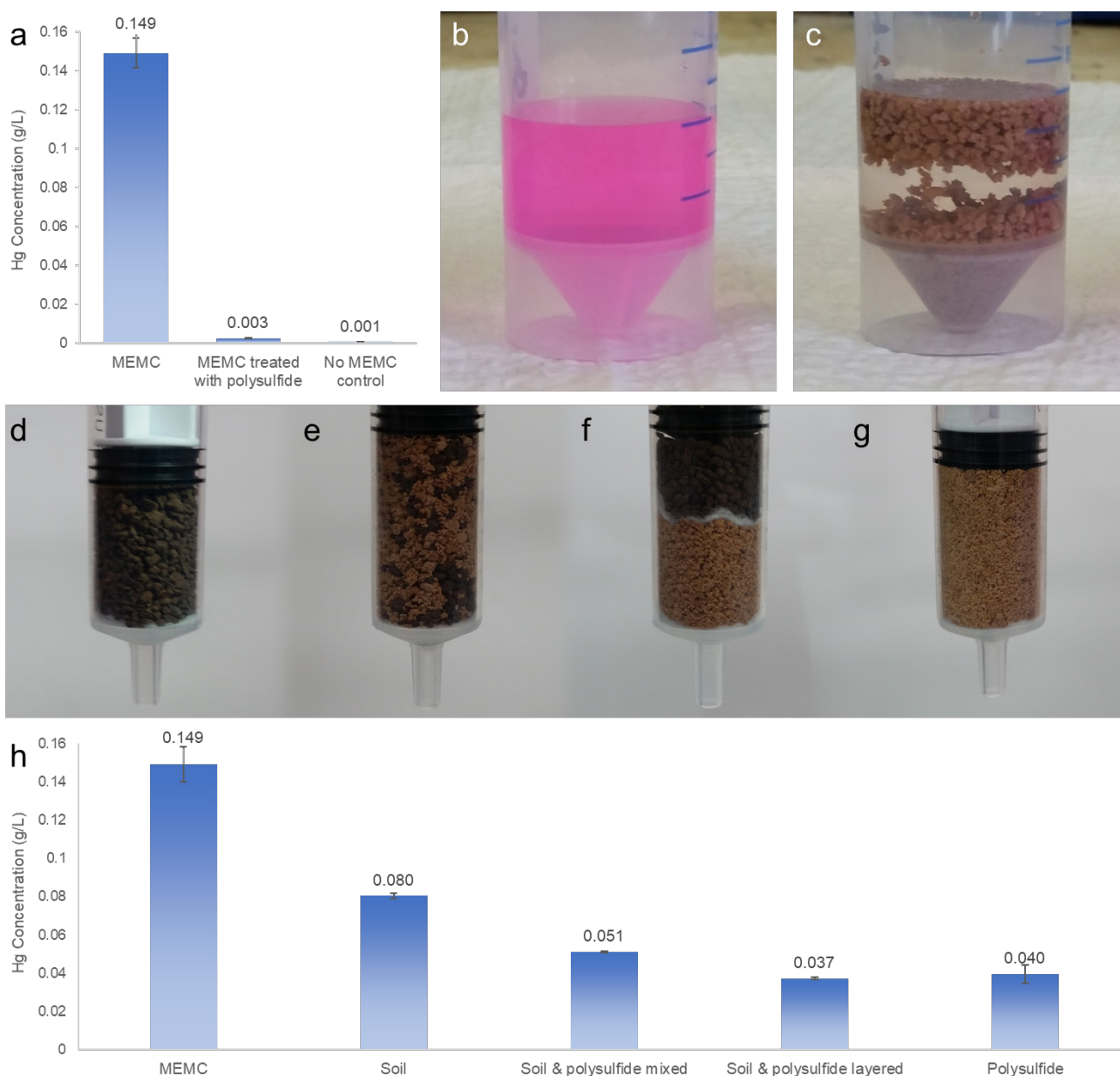


Figure 3.6 | a-c. Concentration of mercury remaining in a solution of MEMC prepared to working concentration before (b) and after treatment with canola oil polysulfide (c). Either the compound is coloured or commercial MEMC contains a coloured compound, either way a decrease in colour intensity accompanies a decrease in MEMC concentration; d-h. Concentration of mercury remaining in a solution of MEMC prepared to working concentration after passing through syringe filters packed with soil (d), canola oil polysulfide mixed with soil (e), soil layered on canola oil polysulfide (f) and polysulfide only (g).

10 mL syringe columns were prepared containing 3.0 g porous canola oil polysulfide. We were also interested to see how soil might interact with MEMC solution, and so syringe columns were prepared containing 3.0 g of soil, a mixture of 1.5 g soil and 1.5 g polysulfide representing polymer administered to soil, and layered variant with 1.5 g soil atop 1.5 g polysulfide separated with cotton wool, representing a barrier of polysulfide in soil. 3 mL MEMC at operating concentration was added to the top of the column by pipette, and the plunger carefully re-inserted with gentle pressure to elute the solution over approximately 2.5 minutes. Eluted solutions were prepared for ICP-MS analysis to determine remaining mercury content. The column containing soil alone reduced the mercury

present from 0.149 to 0.080 g L⁻¹, a 46 % reduction where porous polysulfide of the same mass reduced the concentration to 0.40 g L⁻¹, 73 % less. The mixed samples gave interesting results: The layered sample saw a reduction of 75 % mercury, marginally better than just polysulfide alone, and the mixed sample only removed 66 %. Though soil itself was capable of retaining MEMC, this difference can likely be attributed to the aqueous solution taking the preferred path through the soil, avoiding the hydrophobic polysulfide to an extent. We have determined with this experiment that soil alone is capable of removing nearly half of the mercury from an operating solution of MEMC at a ratio of 1 mL g⁻¹ with a residence time of under 3 minutes. How long this mercury remains bound we do not know, whether it becomes bound to natural organic matter or is washed away with subsequent irrigations to become lost to waterways. Either way it is clear that the use of MEMC is introducing mercury to the environment and the use of absorbent materials to minimise the run-off is far less preferable to the alternative of simply not introducing the mercury in the first place.

References

1. United Nations Environment Programme, Global Mercury Assessment 2018, **2019**. <<http://www.unep.org/PDF/PressReleases/GlobalMercuryAssessment2013.pdf>> Accessed March 2019.
2. Fitzgerald, W. F.; Lamborg, C. H.; Hammerschmidt, C. R., Marine biogeochemical cycling of mercury. *Chem. Rev.* **2007**, *107*, 641-662.
3. Gilmour, C. C.; Henry, E. A.; Mitchell, R., Sulfate Stimulation of Mercury Methylation in Freshwater Sediments. *Environ. Sci. Technol.* **1992**, *26*, 2281-2287.
4. Nufarm Australia Limited, SHIRTAN Liquid Fungicide Safety Data Sheet. **2017**. <https://cdn.nufarm.com/wp-content/uploads/sites/22/2018/05/06182459/ShirtanSDS5113_0717.pdf> Accessed July 2019.
5. Nufarm Australia Limited, SHIRTAN® LIQUID FUNGICIDE. **2017**. <<https://cdn.nufarm.com/wp-content/uploads/sites/22/2018/05/06182459/5113-Shirtan-24Sept2017.pdf>> Accessed July 2019.

APPENDICES

Publications that resulted from the research in this chapter:

M. J. H. Worthington, R. L. Kucera, I. S. Albuquerque, C. T. Gibson, A. Sibley, A. D. Slattery, J. A. Campbell, S. F. K. Alboajji, K. A. Muller, J. Young, N. Adamson, J. R. Gascooke, D. Jampaiah, Y. M. Sabri, S. K. Bhargava, S. J. Ippolito, D. A. Lewis, J. S. Quinton, A. V. Ellis, A. Johs, G. J. L. Bernardes, and J. M. Chalker, Laying Waste to Mercury: Inexpensive Sorbents Made from Sulfur and Recycled Cooking Oils. *Chem. Eur. J.* **2017**, 23, 16219 published by Wiley-VCH Verlag GmbH & Co. KGaA and reproduced below under a Creative Commons Attribution License.

CHEMISTRY

A **European** Journal

www.chemeurj.org

A Journal of



2017-23/64



Cover Feature:

J. M. Chalker et al.

Laying Waste to Mercury: Inexpensive Sorbents Made from Sulfur and Recycled Cooking Oils

Supported by



WILEY-VCH

Mercury Removal | Hot Paper |

Laying Waste to Mercury: Inexpensive Sorbents Made from Sulfur and Recycled Cooking Oils

Max J. H. Worthington,^[a, b] Renata L. Kucera,^[a] Inês S. Albuquerque,^[c] Christopher T. Gibson,^[a, b] Alexander Sibley,^[a, b] Ashley D. Slattery,^[a, b] Jonathan A. Campbell,^[a, b] Salah F. K. Alboaiji,^[a, b] Katherine A. Muller,^[d] Jason Young,^[a, e] Nick Adamson,^[a, b, h] Jason R. Gascooke,^[a, b] Deshetti Jampaiah,^[f] Ylias M. Sabri,^[f] Suresh K. Bhargava,^[f] Samuel J. Ippolito,^[f, g] David A. Lewis,^[a, b] Jamie S. Quinton,^[a, b] Amanda V. Ellis,^[a, b, h] Alexander Johs,^[d] Gonçalo J. L. Bernardes,^[c, i] and Justin M. Chalker*^[a, b]

This paper is dedicated to Prof. Theodore Cohen with gratitude for his mentorship and inspiring contributions to organosulfur chemistry.

Abstract: Mercury pollution threatens the environment and human health across the globe. This neurotoxic substance is encountered in artisanal gold mining, coal combustion, oil and gas refining, waste incineration, chloralkali plant operation, metallurgy, and areas of agriculture in which mercury-rich fungicides are used. Thousands of tonnes of mercury are emitted annually through these activities. With the Minamata Convention on Mercury entering force this year, increasing regulation of mercury pollution is imminent. It is therefore critical to provide inexpensive and scalable mercury sorbents. The research herein addresses this need by introducing low-cost mercury sorbents made solely from sulfur and unsaturated cooking oils. A porous version of the

polymer was prepared by simply synthesising the polymer in the presence of a sodium chloride porogen. The resulting material is a rubber that captures liquid mercury metal, mercury vapour, inorganic mercury bound to organic matter, and highly toxic alkylmercury compounds. Mercury removal from air, water and soil was demonstrated. Because sulfur is a by-product of petroleum refining and spent cooking oils from the food industry are suitable starting materials, these mercury-capturing polymers can be synthesised entirely from waste and supplied on multi-kilogram scales. This study is therefore an advance in waste valorisation and environmental chemistry.

[a] M. J. H. Worthington, R. L. Kucera, Dr. C. T. Gibson, A. Sibley, Dr. A. D. Slattery, Dr. J. A. Campbell, S. F. K. Alboaiji, J. Young, N. Adamson, Dr. J. R. Gascooke, Prof. D. A. Lewis, Prof. J. S. Quinton, Prof. A. V. Ellis, Dr. J. M. Chalker
School of Chemical and Physical Sciences
Flinders University, Bedford Park
South Australia (Australia)
E-mail: justin.chalker@flinders.edu.au
Homepage: <http://www.chalkerlab.com>

[b] M. J. H. Worthington, Dr. C. T. Gibson, A. Sibley, Dr. A. D. Slattery, Dr. J. A. Campbell, S. F. K. Alboaiji, N. Adamson, Dr. J. R. Gascooke, Prof. D. A. Lewis, Prof. J. S. Quinton, Prof. A. V. Ellis, Dr. J. M. Chalker
Centre for NanoScale Science and Technology
Flinders University, Bedford Park
South Australia (Australia)

[c] I. S. Albuquerque, Dr. G. J. L. Bernardes
Instituto de Medicina Molecular
Faculdade de Medicina da Universidade de Lisboa
Lisbon (Portugal)

[d] K. A. Muller, Dr. A. Johs
Environmental Sciences Division
Oak Ridge National Laboratory
Oak Ridge, Tennessee (USA)

[e] J. Young
Flinders Analytical, School of Chemical and Physical Sciences
Flinders University, Bedford Park
South Australia (Australia)

[f] Dr. D. Jampaiah, Dr. Y. M. Sabri, Prof. S. K. Bhargava, Dr. S. J. Ippolito
Centre for Advanced Materials & Industrial Chemistry (CAMIC), School of Science, RMIT University, Melbourne, Victoria (Australia)

[g] Dr. S. J. Ippolito
School of Engineering, RMIT University, Melbourne, Victoria (Australia)

[h] N. Adamson, Prof. A. V. Ellis
School of Chemical and Biomedical Engineering, University of Melbourne, Parkville, Victoria (Australia)

[i] Dr. G. J. L. Bernardes
Department of Chemistry, University of Cambridge, Cambridge (United Kingdom)

Supporting information and the ORCID identification number(s) for the author(s) of this article can be found under <https://doi.org/10.1002/chem.201702871>.

© 2017 The Authors. Published by Wiley-VCH Verlag GmbH & Co. KGaA. This is an open access article under the terms of the Creative Commons Attribution License, which permits use, distribution and reproduction in any medium, provided the original work is properly cited.

Introduction

Mercury pollution threatens the health and safety of millions of humans across the globe.^[1] This neurotoxic metal is encountered in many industrial activities including coal combustion, oil and natural gas refining, waste incineration, chloralkali plant operation and waste discharge, and various metallurgical processes.^[2] Mercury is used intentionally in artisanal and small-scale gold mining (ASGM)^[1a] and in agricultural practices that still rely on fungicides that contain highly toxic alkylmercury derivatives.^[3] ASGM is especially problematic, with widespread and increasing incidence in developing nations due to rising gold prices.^[4] In this practice, liquid mercury is mixed with crushed ore in order to extract gold as an amalgam. The amalgam is then isolated by hand and then heated with a torch to vaporise the mercury and separate it from the gold.^[5] About 12–15% of the world's gold is generated in this way through the efforts of approximately 15 million miners, many of whom are children.^[4a] It is estimated that, each year, up to 1400 tonnes of mercury are released to land and water due to ASGM alone,^[4a] with devastating effects on the health of miners and children in these communities.^[6] Because mercury pollution from ASGM occurs primarily in low-income nations, cost-effective and technologically simple methods for remediation are urgently needed. These crises have been highlighted in news reports in recent years,^[7] and at least one national emergency has been declared in response to mercury pollution due to gold mining.^[7d]

Increasing regulation of mercury emissions is on the horizon, with the Minamata Convention entering full force this year.^[8] In order to comply with these regulations, it is imperative that versatile and inexpensive mercury sorbents be introduced.^[2a,9] Additionally, sorbents that can be deployed across large geographic areas are important in remediation efforts associated with practices such as ASGM that may result in the contamination of thousands of acres of land.^[7d] Currently, high performance activated carbons and silver impregnated zeolites are widely used as mercury sorbents in the petroleum and waste sectors.^[2b] While these sorbents are effective in continuous industrial processes, the cost is still too-often prohibitive in non-commercial efforts to remediate contaminated ecosystems of large area.^[9,10] Additionally, activated carbon is highly flammable^[11] and often requires an oxidant additive (e.g. immobilised sulfur, bromine, or chlorine) to convert mercury metal to an immobilised mercury(II).^[12] And while the investigation of economical sorbents such as used vehicle tires,^[13] clays,^[14] and various forms of biomass^[14] is encouraging, these materials act primarily as a ligands for Hg²⁺. A general sorbent for mercury must accommodate the many forms commonly encountered in remediation including liquid mercury metal, matrix-bound mercury metal, mercury vapour, organomercury compounds and inorganic mercury complexed to organic ligands such as humic matter.^[2a,9] In an effort to address these problems, we herein introduce sulfur polymers, made through the co-polymerisation of sulfur and cooking oils (including waste cooking oils), that capture diverse forms of mercury pollution in air, water and soil.

Elemental sulfur is a readily available and inexpensive material produced in excess of 50 million tonnes each year as a by-product of petroleum refining.^[15] Elemental sulfur can capture and stabilise mercury,^[16] but it suffers from several chemical and physical limitations that make it inconvenient to use directly in remediation. For example, elemental sulfur is flammable with a low ignition temperature (190 °C), it readily sublimes, it is prone to caking and increases hydraulic resistance during filtration, it does not wet and mix well in batch processing of waste fluids, and it is difficult to prepare as durable particles of a desired size.^[15a,17] Furthermore, sulfur may decompose in the environment to sulfate, which can increase the abundance of sulfate-reducing bacteria that are the primary producers of the highly toxic methylmercury in soils and sediments.^[18] There is therefore an interest to discover new forms of sulfur that benefit from the high affinity of this chalcogen for mercury, but do not suffer from the limitations of elemental sulfur noted here.

Recently, the synthesis of polysulfides by inverse vulcanisation^[19] has ushered in a new class of materials with high sulfur content. Pioneered by Pyun, Char, and co-workers,^[19,20] this process involves melting elemental sulfur and then heating it above its floor temperature of 159 °C. Thermal homolysis of S–S bonds in S₈ leads to radical ring-opening polymerisation.^[17,19] Subsequent trapping of the thiyl radical end groups of the sulfur polymers with a polyene provides a cross-linked polysulfide.^[19] The polymers formed by inverse vulcanisation have been explored in a variety of contexts due to their interesting optical, electrochemical and self-healing properties.^[20,21] Our laboratory recently introduced a polysulfide prepared by the inverse vulcanisation of the renewable plant oil limonene, and explored its use in the remediation and sensing of Hg²⁺ in water.^[22] Further studies lead by Hasell^[23] and Theato^[24] revealed effective ways to increase the surface area of polymers prepared by inverse vulcanisation (by foaming or electrospinning, respectively) in order to increase performance in Hg²⁺ capture. While these studies motivate deployment of polysulfides for mercury remediation, the cost, scalability, and ease of use are issues that must be addressed before uptake is feasible.^[4b] Additionally, these preliminary reports^[22–24] only studied the purification of water containing inorganic HgCl₂, so it is not yet established whether these sulfur polymers are effective in capturing mercury metal, inorganic mercury bound to natural organic matter (Hg-NOM),^[25] or organomercury compounds—forms of mercury pollution commonly encountered in the field. We therefore set out to identify polysulfides made from feedstocks that are highly abundant, very inexpensive and easy to handle, and then tested them on diverse forms of mercury pollution in air, water and soil.

Unsaturated oils from rapeseed, sunflower, and olive plants are attractive as chemical building blocks because they are renewable and can be produced on all inhabited continents.^[26] The alkene functional groups in these triglycerides also provide the requisite points for cross-linking during inverse vulcanisation. It was anticipated that the Z stereochemistry of these alkenes, imparting strain to the olefin, would facilitate rapid reaction with sulfur radicals produced in inverse vulcanisation

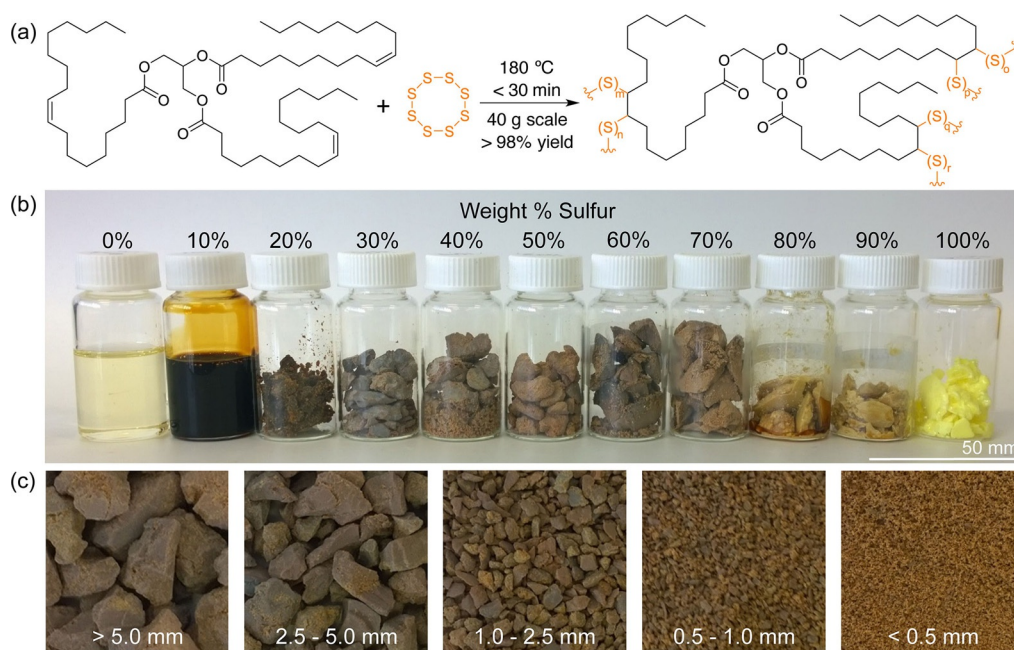


Figure 1. A polysulfide rubber with high sulfur content was formed by the reaction of elemental sulfur with canola oil, sunflower oil, or olive oil. (a) General structure of a plant oil triglyceride (oleic acid is shown here as the major fatty acid component) and the product formed by co-polymerisation with sulfur. (b) Photograph of the product formed by the reaction of canola oil and sulfur, with varying weight percentages of sulfur. (c) Photographs of the canola oil polysulfide (50% sulfur) after passing through sieves.

(Figure 1 a). Historically, the reaction of sulfur and unsaturated plant oils has been used to make factice and ebonite. Factice is a gel-like modifier used in the manufacture of various rubbers and pencil erasers, typically prepared with up to 25% sulfur by weight.^[27] Ebonite is a hard and durable building material formed by the prolonged heating of sulfur (≈ 30 –50 wt%) with natural rubber, often in the presence of unsaturated additives such as linseed oil.^[28] We reasoned that inverse vulcanisation of unsaturated plant oils would provide a variant of these materials with very high sulfur content (50% or more sulfur by mass). Following similar logic, Theato and co-workers also explored the inverse vulcanisation of linseed, sunflower, and olive oils, and used these polymers as cathode materials.^[29] Here we considered that *used* cooking oils (often comprised of canola and sunflower oils) could be recycled and employed as a starting material. Both sulfur and cooking oils are produced in multi-million tonnes each year, so the large-scale supply of raw materials would be addressed at the outset.^[26,30] Additionally, the high levels of sulfur in the proposed co-polymer were anticipated to impart high affinity for various forms of mercury. Finally, because sulfur is a by-product of petroleum refining^[15b] and used cooking oils are a by-product of the food industry,^[31] there is the intriguing prospect of making a mercury-binding polymer, in a single, solvent-free step, in which every atom in the product is derived from industrial waste.^[21d]

Results and Discussion

Polymer synthesis

As a starting point, the reaction between sulfur and food grade canola oil was investigated. In the event, sulfur was first

melted and then heated further to 180 °C to initiate ring-opening polymerisation. An equal mass of canola oil was then added slowly to maintain an internal temperature of approximately 180 °C. The reaction was initially two phases, so rapid stirring was used to ensure efficient mixing (Figure S1). After 10 minutes the mixture appeared to form one phase and within 20 minutes of total reaction time, a solid brown rubber formed (Figure 1). Essentially quantitative yields were obtained and no solvents or exogenous reagents were required in the synthesis. A similar material was produced using both sunflower and olive oil (Figure S2), though sunflower oil typically reached its gel point within 10 minutes of total reaction time at 180 °C. We attributed this difference in time required to reach the gel point to the variation in unsaturation between the plant oils. These differences were determined by conversion of the vegetable oils to their fatty acid methyl esters by treatment with sodium methoxide in methanol (Figure S3). Analysis of these esters by GC-MS revealed a far higher percentage of polyunsaturated linoleic acid in sunflower oil (50%) compared to canola oil (14%) and olive oil (9%). Oleic acid was the major fatty acid component in the canola oil and olive oil triglyceride, making up about 78% of the fatty acids in both oils (Figure S4–S5).

Subsequent experiments focused on canola oil because of its widespread use in the food industry.^[26b,31] The amount of sulfur that could be incorporated into the polymer was therefore investigated (Figure 1 b). At 10% sulfur by weight, a viscous oil was obtained. From 20% to 70% sulfur by weight, a rubber was obtained. With increasing sulfur content, the product became more brittle (Figure S6). The polymer prepared at 50% sulfur by weight and 50% canola by weight was selected for subsequent experiments in mercury binding. At this

composition, substantial sulfur would be available to capture mercury, and the particles would not be too brittle for use in applications that require filtration or sieving. This composition also ensured that a substantial amount of both sulfur and cooking oil were used to synthesise the polymer—an important consideration in waste valorisation.

The inverse vulcanisation reaction using canola oil was easily scaled to 40 g total polymer without incident. Larger batches are likely possible, but this scale allowed for relatively uniform mixing and temperature control. Running these reactions in parallel batch reactors allowed us to make more than 10 kg of this polymer to date. To prepare the polymer as particles, the rubber was milled in a blender to give particles less than 12 mm in diameter. These particles could be further partitioned according to size by passing through sieves (Figure 1c). Finally, when waste cooking oil obtained from a local café was used in the synthesis, there was no substantial difference in the polymerisation when compared to pure canola oil purchased from a supermarket (Figure S7). In this way, the polysulfide polymer was derived entirely from industrial waste.

Polymer characterisation

Reaction of sulfur at the alkenes in the canola oil was consistent with the disappearance of the C=C stretch at 1613 cm^{-1} and the alkene C-H stretch at 3035 cm^{-1} in the IR spectrum of the polymer (Figure S8). While the product had limited solubility in CDCl_3 , $^1\text{H NMR}$ of the soluble fraction indicated that alkenes were consumed in the reaction, though the gel point was reached before all alkenes were consumed (Figure S9). The ability of sulfur to react efficiently at the alkene of the fatty acid esters was also inferred by $^1\text{H NMR}$ spectroscopic analysis of the product formed when the methyl ester derived from each of the plant oils was treated with sulfur under the polymerisation conditions (Figure S10). Notably, the products obtained from the inverse vulcanisation of the fatty acid methyl esters were viscous oils rather than solid polymers, indicating the key structural role the triglycerides play in cross-linking.

Analysis of the milled polymer by SEM revealed a locally smooth surface yet a high level of microscale features that imparted high surface area (Figure 2a and Figure S11). The surface was rich in sulfur and carbon, as indicated by elemental mapping via EDS (Figure S12) and Auger spectroscopy (Figure 2b and Figures S13–14) and fully consistent with the sulfur and canola oil building blocks. The presence of polysulfides was inferred by confocal Raman microscopy with S–S stretching detected at 432 and 470 cm^{-1} (Figure S15).^[22,32] Interestingly, confocal Raman microscopy also revealed domains of very high sulfur, some of which appeared as sulfur particles embedded in the polymer and on the surface of the polymer (Figure S16). EDS of these domains also indicated very high levels of sulfur (Figure S12). No thiols were detected on the surface, as inferred by the lack of reactivity with thiol-specific Ellman's reagent (Figure S17).

Thermal analysis (TGA and DSC) of the canola oil polysulfide revealed several important properties of the polymer. First,

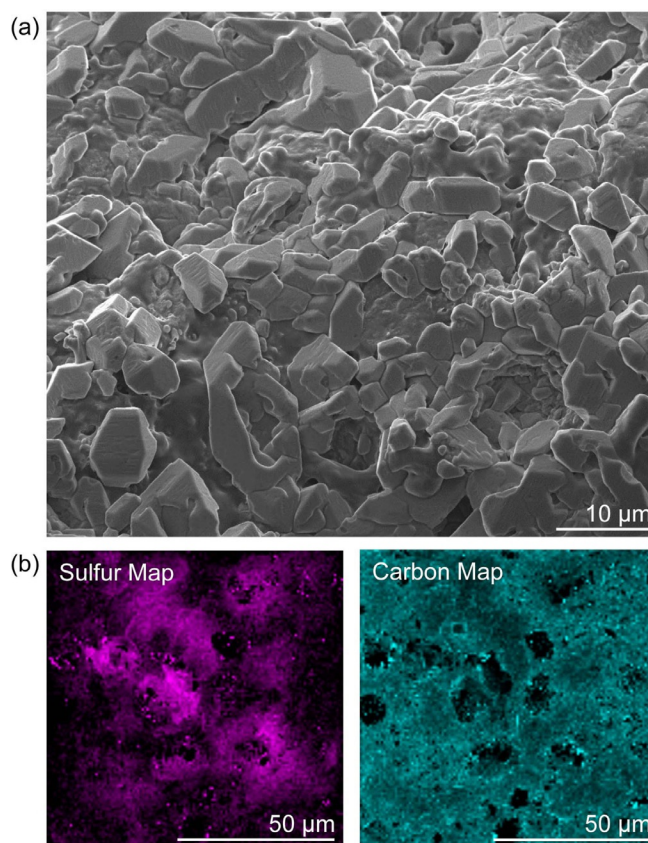


Figure 2. Surface analysis of the canola oil polysulfide. (a) Scanning electron microscopy revealed a locally smooth surface and microscale features. (b) Auger spectroscopic imaging revealed high carbon and sulfur content on the polymer surface, consistent with the canola oil and sulfur monomers used in the synthesis. Representative images are shown.

thermal degradation featured two major mass losses, with the first onset at $230\text{ }^\circ\text{C}$ and the second at $340\text{ }^\circ\text{C}$ (Figure 3a and Figure S18). The first mass loss was due to decomposition of polysulfide domains, as increasing sulfur content was correlated with greater mass loss in the first decomposition at $230\text{ }^\circ\text{C}$ (Figure 3a). The second mass loss was therefore the thermal decomposition of the canola oil domain of the polymer. (Thermal analyses of the unmodified cooking oils and elemental sulfur were also carried out for comparison, Figure S19–S20). DSC revealed that above 30% sulfur by mass, there was an endotherm between 100 and $150\text{ }^\circ\text{C}$ (Figure 3b). This transition was attributed to the melting range of free sulfur. By integrating each area of these endotherms, an estimate of free sulfur was made (Figure S20–S23). The polysulfide made from 50% canola oil and 50% sulfur, for instance, was estimated to contain about 9% free sulfur by mass. The polysulfides made from 60 and 70% sulfur, in comparison, were estimated to contain 23% and 38% free sulfur, respectively. Considered with the SEM, EDS and Raman data, these results suggested that sulfur reacted with canola oil up to a composition of 30% sulfur by mass. Above this level, the excess sulfur is trapped in the polymer matrix as microparticles. Similar thermal analyses were observed for polysulfides prepared from sunflower oil, olive oil and used cooking oil (Figures S24–S26). The interpretation of

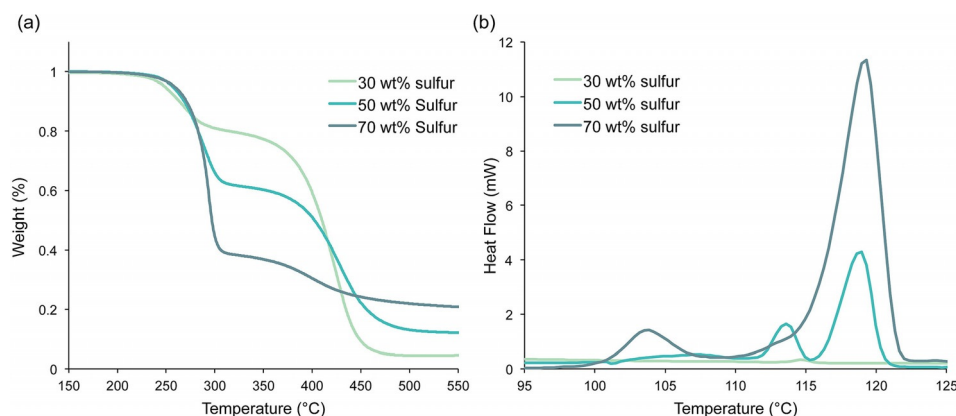


Figure 3. Thermal analysis of the canola oil polysulfide. (a) Thermogravimetric analysis (TGA) of the canola oil polysulfide prepared by inverse vulcanisation at 30, 50, and 70% sulfur by mass. (b) Differential scanning calorimetry (DSC) of the canola oil polysulfide between 100 and 125 °C revealed that when more than 30% sulfur was used in the synthesis, free sulfur was detected. For full thermal analysis of the polymers, including comparison to unreacted vegetable oils and elemental sulfur, see pages S24–S31.

these results was consistent with the characterisation of related polymer composites formed from vegetable oils and sulfur, as reported by Theato and co-workers.^[29]

It was noteworthy that while the IR and Raman spectra of the canola oil polysulfide and commercial factice were similar (Figure S27–S28), the TGA profiles were slightly different. For instance, commercial factice with the highest percentage of sulfur (25%) had a higher onset of degradation of the sulfur domain (280 °C) compared to the polysulfide prepared by inverse vulcanisation (230 °C) (Figure S29–S30). We therefore wondered if there was a difference in the material formed by inverse vulcanisation (where canola oil is added to a sulfur prepolymer at 180 °C) and classic vulcanisation (where sulfur is added portionwise to canola oil at 180 °C—a method of factice production). Executing both protocols with equal masses of canola oil and sulfur on a 40 g reaction scale provided essentially the same rubber material, as indicated by physical appearance, TGA and DSC (Figure S31). Only a very minor difference in endotherm of free sulfur was observed (Figure S32). Therefore, the order of addition of the sulfur and canola oil did not appear to make a major difference in the product obtained on this time scale and temperature. We suspect that the reaction mixture equilibrated to a similar composition of sulfur and polysulfide polymers in both reactions before reaching the gel point. With that said, there may be subtle differences in the products of inverse and classic vulcanisation (such as the number and length of sulfur chains), that are not revealed by the TGA and DSC experiments.

Dynamic mechanical analysis (DMA, Figure S33) was carried out at variable temperature to estimate the glass transition temperature (T_g) of the canola oil polysulfide. To accomplish this, the polymer was synthesised as previously described, except a beaker was used as the reaction vessel. After the synthesis, the rubber was carefully cut into a bar (1.4 cm × 0.8 cm × 0.2 cm) suitable for DMA. Subsequent DMA analysis revealed the peak of the tangent delta (T_t), an estimate of the T_g , at −9 °C. Independently, a T_g of −12.2 °C was inferred by DSC (Figure S34).

Mercury capture from water

Because the polysulfide surfaces were rich in sulfur, affinity for mercury was anticipated. Indeed inorganic polysulfides have been explored to some extent for mercury capture in water, though these materials have limited shelf-life and need to be prepared as needed.^[33] Before the canola oil polysulfide was tested, the polymer was briefly washed with aqueous NaOH (0.1 M) to ensure no small molecule thiols such as trace H₂S were present that might confound the mercury binding experiments. This control measure was taken in light of a report by Char, Pyun and co-workers that H₂S may be produced during some inverse vulcanisation reactions.^[34] After washing further with water and drying in air, the polymer was then tested for mercury binding. In an initial test, 2.0 g of the canola oil polysulfide (50% sulfur by weight) was simply incubated, without stirring, in a 5.0 mL aqueous solution of HgCl₂ (3.5 ppm in Hg²⁺). After 24 hours, the polymer was removed by filtration and the concentration of mercury in the water was quantified by ICP-MS. Typically 90% of the soluble mercury was captured after this single treatment, with the treated water containing 0.35 ± 0.1 ppm Hg²⁺ (the average of triplicate experiments). At higher concentrations of HgCl₂, the polymer performed similarly, with a single treatment of 8.0 g of the polysulfide removing 91% of Hg²⁺ from a 5.0 mL sample of 74 mM HgCl₂ after 24 hours (Figures S35–S37). Surprisingly, the polysulfide changed colour in this experiment, from brown to grey (Figure 4a). This result suggested that the polysulfide might self-indicate when bound to a specific amount of Hg²⁺. Because this chromogenic response was only obvious above 5 mM HgCl₂, it is unlikely to be useful in sensing low levels of Hg²⁺. However, it might be useful in monitoring the lifetime of a filter or other remediation device containing the polymer, where the colour change is observable after binding sufficient mercury.

After washing the Hg²⁺-treated polymer extensively with water, SEM and EDS analysis of the surface indicated the presence of mercury-rich nanoparticles (Figure S38–S39)—a result

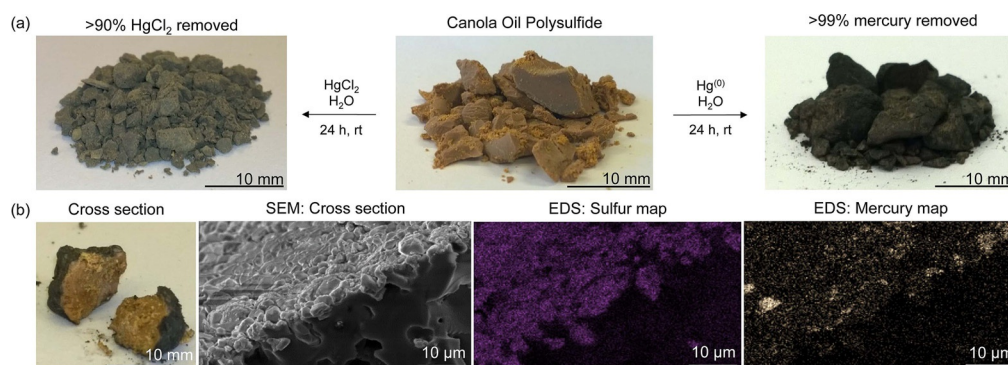


Figure 4. Mercury capture from water. (a) The canola oil polysulfide was effective in capturing both Hg^{2+} and Hg^0 from water. The polymer changes colour to grey when it binds to Hg^{2+} and to black when it reacts with liquid Hg^0 . (b) EDS analysis confirmed mercury was bound to the surface of the polymer.

consistent with our previous studies on the interaction of Hg^{2+} with polysulfides.^[22] It was also encouraging to note that the mercury was strongly bound to the polymer and minimal leaching was observed when the polymer-bound mercury was incubated in pure water. For example, after 1.0 g of the polysulfide captured 79 mg of HgCl_2 , the polymer was transferred to a 10 mL sample of milliQ-purified water and incubated for 24 hours. The concentration of mercury in the water was measured by ICP-MS to be 0.57 ppb, a level that is within regulatory limits for drinking water (Figure S40).^[35] Because Hg^{2+} is highly soluble in water, these low levels of leaching are a testament to the high affinity of the polymer to inorganic mercury.

The most prevalent form of mercury encountered in ASGM is mercury metal. It was therefore critical to assess how the polysulfides interacted with liquid mercury. In the first instance, 1.00 g of the canola oil polysulfide (50% sulfur by weight) was added to a vial of water containing 100 mg of elemental mercury. The three-phase mixture was stirred vigorously at room temperature. After 4 hours, no mercury was visible and the polymer had undergone a dramatic colour change from brown to black (Figure 4a and Figure S41). After 24 hours of total treatment, the polymer was isolated by filtration, washed thoroughly with water and then dried to a constant mass of 1.099 g. By mass balance, this result indicated that 99% of the mercury metal was captured by the polymer. EDS imaging (Figure 4b and Figure S42) confirmed the surface of the polymer to be rich in mercury, as did Auger and XPS spectroscopic analysis (Figures S43–S44).

Characterisation by XRD revealed that the major product was metacinnabar, a form of mercury sulfide (Figure S45). Importantly, because metacinnabar is non-toxic and insoluble in water, it has been proposed as a form in which mercury could be immobilised safely.^[16,36] Additionally, the oxidation of mercury metal to metacinnabar provides an essentially non-volatile form of mercury, thereby lowering the risk of inhalation and transmission of the pollution through air.^[16] Gratifyingly, the polysulfide prepared from used cooking oil behaved similarly in the capture of mercury metal, so there is no requirement to use pristine vegetable oils in the polysulfide synthesis (Figure S46).

It is important to note that the mechanism of mercury metal capture was distinct from that of HgCl_2 . In the case of liquid

mercury metal (Hg^0), the metal was oxidised by the polysulfide. The oxidant (S–S) could be derived either from free sulfur embedded in the polymer or the polysulfide cross-links, as the amount of total mercury captured was correlated with total sulfur content (Figure S46). Because of this, factice containing as little as 1% free sulfur by mass was also effective in capturing mercury metal, though a higher mass of total factice was required because of its lower total sulfur content (17% total sulfur, Figure S46). For Hg^{2+} , the sulfur of the polysulfide acted as a ligand to sequester the salt. In both cases, the final oxidation state of the mercury bound to the polysulfide was mercury(II). This result was consistent with XPS analysis in which the 4f photoelectron peak after capture of either HgCl_2 or Hg^0 had a binding energy consistent with that of a mercury(II) sulfide (Figure S44). At the same time, the structure of the mercury(II) product was different, as the HgCl_2 presented as surface-bound nanoparticles and the mercury metal was converted to metacinnabar. The greater sensitivity in the chromogenic response for mercury metal perhaps owed its origins to this structural difference. For instance, when 20 g of the polysulfide was exposed to 72 mg of mercury metal, the entire surface polymer sample appeared black (Figure S47). This result encourages future exploration of the canola oil polysulfide as a sensor for metallic mercury.

Mercury capture from soil

Arguably the most challenging pollution to remedy in ASGM communities is mercury-contaminated soil. When mercury metal is mixed with ore to form gold amalgams, the mercury is dispersed as microbeads that are covered with particles of soil and other debris. This soil-bound mercury does not coalesce and, despite the high density of mercury, it can float on water. This so-called “mercury flour” can be carried by waterways and threaten the environment and human health beyond the location of the mine.^[5a] A simple and cost-effective method for treating floured mercury is currently an outstanding problem for ASGM communities.^[5] We therefore turned to mercury-contaminated soil and studied how the canola oil polysulfide might be used in its remediation.

We first prepared mercury flour by using an end-over-end mixer to mill liquid mercury (200 mg) and 5 g fine loam

comprised of soil particles less than 0.5 mm. While the characteristic silver coloured mercury was visible to the naked eye at the start of the mixing, it gradually dispersed into the soil as very fine beads over the course of several hours. After 24 hours, the mercury-soil mixture was indistinguishable from the untreated soil (Figure S48). The floured mercury was analysed by SEM and EDS (Figure S49–S51), revealing microscale beads of mercury, with smaller soil particles adhered to the surface (Figure S50–S51). Figure 5a shows a representative

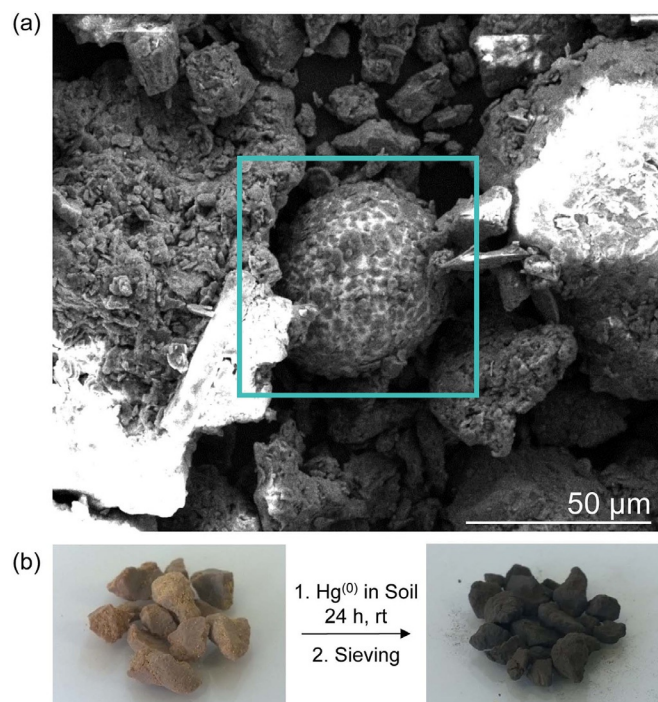


Figure 5. Remediation of simulated mercury flour. (a) SEM analysis of mercury flour showing a microbead of elemental mercury with soil particles bound to the surface. (b) Milling the simulated mercury flour with the canola oil polysulfide led to capture of the mercury. The polymer particles, bound to mercury, could be separated from the soil with sieves.

mercury bead, about 50 μm in diameter. To determine if the canola oil polysulfide could capture this floured mercury, the soil (5.0 g) was then treated with the canola oil polysulfide (5.0 g) containing 50% sulfur by weight. Polymer particles of 2.5–5.0 mm were used so that they could be separated from the soil using a sieve. The solid mixture was milled using an end-over-end mixer. After 24 hours of treatment the polymer had clearly turned black (Figure 5b), as observed in previous reactions with mercury metal. Separating the polymer from the soil using a sieve allowed analysis by EDS that verified mercury bound to the polymer (Figure S52–S53). Notably, the ability to isolate the polymer particles from soil provided a distinct advantage of the canola oil polysulfide over elemental sulfur. Additionally, while the amount of milling time and mass of polymer required for full remediation will need to be optimised for each type of soil and sediment, this initial demonstration of mercury removal from contaminated soil was an encouraging advance in dealing with mercury flour.

Toxicity studies and prospects for in situ mercury remediation

In any remediation effort, the lifetime of the mercury-binding material must be considered. Because of our interest in mercury pollution relevant to ASGM, we realised that the limited resources in these regions might prohibit separation of the polymer from soil and tailings post-treatment. Furthermore, areas of contaminated soil can span several thousand acres,^[7d] so complicated remediation protocols are simply not practical. We therefore considered whether in situ remediation or immobilisation would be appropriate—a practice where the polymer would be milled into the contaminated area and left in the environment after treatment.^[9] Decreased mobility of mercury and low-toxicity would be required for this to be a viable strategy. The formation of metacinnabar in the reaction of mercury metal with the polymer was therefore encouraging, given its low propensity for leaching and low toxicity.^[16,36] These properties notwithstanding, we thought it would be useful to carry out our own assessment of toxicity of the polymer and the polymer-bound mercury.

To assess toxicity, HepG2 and Huh7 human liver cells were cultured in the presence of both the unmodified canola oil polysulfide and the mercury treated polysulfide. In these experiments, the polymer samples were added to the permeable insert of Transwell cell culture plates. The insert effectively acted like a “teabag” where any mercury or other toxic materials leached into the growth media would be available to the cells (Figure 6a). There was no difference in cell viability between the untreated cells and the cells treated with polymer, so the canola polysulfide itself exhibited no cytotoxicity in this assay (Figure S54). More impressively, neither the polysulfide used to capture HgCl_2 nor the polysulfide used to capture mercury metal exhibited cytotoxicity in this experiment, as measured by cell viability (Figure 6b–c and Figure S55). The polymer used to capture mercury chloride contained 2.2 mg of mercury per gram of polymer. The polymer used to capture mercury metal contained 79 mg of mercury per gram of polymer. Neither sample leached sufficient mercury to affect liver cell viability when 37.5 mg of polymer was added to the 300 μL well in the culture medium. In contrast, the addition of an aqueous solution of mercury chloride to the cells, in the absence of polymer, resulted in rapid cell death with an IC_{50} of 34 and 40 μM for Huh7 and HepG2 cells, respectively (Figure S56). For the polymer bearing captured mercury chloride, if all mercury were released into the growth medium, the concentration of mercury would be 1 mM Hg^{2+} , more than 30 times the measured IC_{50} for HgCl_2 . For the polymer that oxidised and captured mercury metal, if all of this mercury were released into the growth medium, the concentration of mercury would be approximately 50 mM. Therefore, both mercury chloride and the oxidised mercury metal adhered to the polymer and were non-toxic to the cells.

These results encourage consideration of the canola oil polysulfide as a material for in situ remediation where the polymer is mixed into mine tailings and contaminated soil to capture mercury and render it far less toxic, less volatile, and insoluble

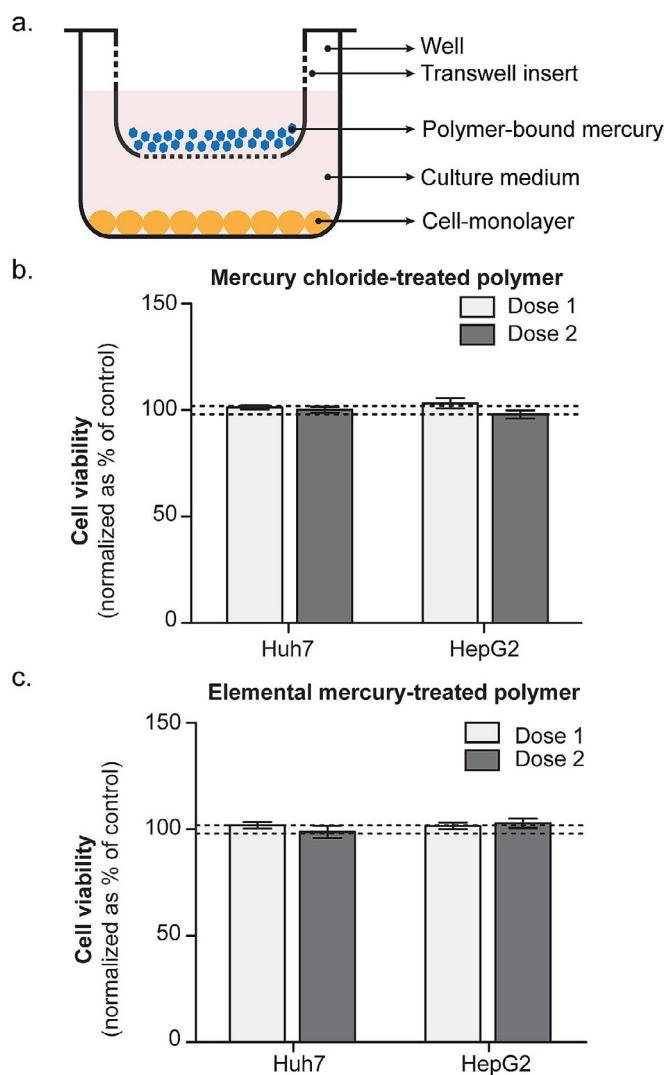


Figure 6. Toxicity assays of polysulfide after capturing mercury chloride or mercury metal. Cell viability was assessed using the CellTiter-Blue Cell Viability Assay, and values obtained for cells exposed to mercury-treated polymers were compared to values obtained for untreated polymers. (a) Cells were seeded in a 24-well plate and the polymers were added to the bottom of a Transwell insert, submerged in the cell culture medium. (b) Cytotoxicity analysis for the mercury chloride-treated polymer, in Huh7 and HepG2 cells. The polymer treated with HgCl_2 contained 2.2 mg HgCl_2 per gram of polymer. (c) Cytotoxicity for the elemental mercury-treated polymer, in Huh7 and HepG2 cells. The polymer treated with Hg^0 contained 79 mg mercury per gram of polymer. Bars represent average of biological triplicates, and error bars represent standard error of the mean. "Dose 1": 3.75 mg polymer/300 μL of culture medium. "Dose 2": 37.5 mg polymer/300 μL of culture medium. Under these conditions, no evidence of toxicity was revealed for any sample of the polymer-bound mercury.

in water. We propose, in the first instance, that the product of this process could be left at the site of contamination. While ultimately mercury will need to be phased out in ASGM practice, and it is ideal to remove all mercury from the site of contamination, in situ remediation using the canola oil polysulfide is a relatively simple measure to address the extensive mercury pollution these communities face in the short-term.

Synthesis of a porous canola oil polysulfide

The reaction of elemental mercury with the canola oil polysulfide was relatively slow, taking several hours in the experiments described in Figure 4 and Figure 5. For mercury vapour capture after coal combustion or during oil and natural gas refining, the process must be very rapid and continuous. We reasoned that increasing the surface area of the canola oil polysulfide would help the rate of mercury binding and reaction by increasing the amount of available sulfur. A porous version of the polysulfide was therefore prepared by synthesising the polymer in the presence of a sodium chloride porogen—a tactic inspired by a salt templating protocol recently reported by Hasell.^[37] In the synthesis, sulfur and canola oil were reacted directly as before and then sodium chloride (previously ground in a mortar and pestle) was added slowly to the reaction mixture. After reaching the gel point, the polymer-salt mixture was removed from the reaction vessel and milled into particles approximately 0.1–1.0 cm in diameter (Figure S57). These particles were then washed twice in water to leach the sodium chloride from the polymer. The resulting polymer—obtained in quantitative yield—was sponge-like and contained micron-scale pores and channels, as revealed by SEM analysis (Figure 7

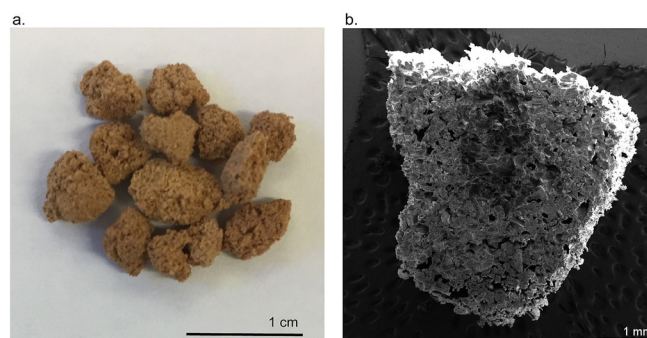


Figure 7. A porous version of the canola oil polysulfide. (a) Canola oil and sulfur were co-polymerised in the presence of a sodium chloride porogen. Removing the sodium chloride was achieved by soaking the milled polymer in water. The product is a sponge-like material. (b) SEM analysis of a cross-section of a particle revealed the presence of pores and channels on the order of 100–200 microns in diameter.

and Figure S58). During the optimisation of this protocol, it was found that a large excess of sodium chloride was required (70% of the total mass of the reaction mixture was sodium chloride). If less sodium chloride were used, substantial amounts of salt particles remain trapped in the polymer matrix. At the higher levels of sodium chloride, >99% of the porogen can be leached from the polymer. The Raman spectrum (Figure S59) of the porous polysulfide was similar to the non-porous polymer, as was the thermal stability and T_g (-12.9°C) (see TGA and DSC analysis, Figure S60–S61). ^1H NMR analysis of the CDCl_3 soluble fraction of the polymer was also similar to the non-porous variant (Figure S62). One notable difference in the porous polysulfide was absence of sulfur micro-particles that were prominent in the non-porous version. Though free sulfur was detected in the DSC analysis of the

porous polymer (13% by mass, Figure S60), the sodium chloride porogen apparently restricted the formation of larger sulfur particles.

Removal of mercury from gas streams

With a porous version of the canola oil polysulfide in hand, its ability to react with and capture elemental mercury gas was assessed. A 300 mg sample of the polymer was loaded in a quartz glass reactor, with the polymer occupying a volume of approximately 0.4 cm³. A stream of nitrogen containing mercury vapour was passed through the reactor, with the flow rate (0.1 L min⁻¹) and level of mercury (586.4 µg Nm⁻³) precisely maintained using a mass flow controller (Figure S63). Mercury capture was determined by measuring the difference in the amount of mercury delivered to the reactor and that detected in downstream KMnO₄ traps (Figure S63). At 25 °C, the polymer removed 7% of the mercury from the gas stream. Reasoning that the reaction between the polysulfide and mercury would increase by heating the reactor, the experiment was repeated at 50, 75 and 100 °C (Figure 8 and Figure S64). Of these tem-

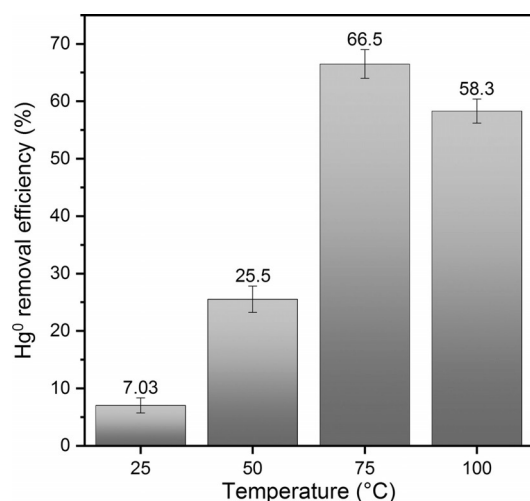


Figure 8. Mercury vapour capture using the porous canola oil polysulfide. 75 °C was found to be an optimal temperature for capturing mercury in a continuous process, with 67% of the mercury removed from the gas stream over a residence time of approximately 0.24 seconds. The higher temperature increases the rate at which the polymer oxidises the mercury gas.

peratures, 75 °C resulted in the highest mercury capture, enabling the canola oil polysulfide to react with and sequester 67% of the mercury. This unoptimised mercury removal efficiency is quite remarkable considering the residence time for this experimental setup is a mere 0.24 seconds, a timeframe compatible for typical waste incineration and fossil fuel processing. This feasibility study should therefore encourage consideration of these polysulfides as inexpensive mercury sorbents for gas streams contaminated with mercury.^[38]

Removing mercury bound to organic matter (Hg-NOM) from water

Mercury bound to natural organic matter (NOM) is often considered a recalcitrant form of pollution because humic matter, regularly containing thiols and sulfides, binds tightly to mercury. In natural and contaminated aquatic systems, mercury predominantly has an oxidation state of +2, but Hg²⁺ does not occur as a free, monatomic ion complexed only by water molecules. In freshwater streams and sediments, Hg²⁺ is typically bound by nucleophilic functional groups, which are present at high abundance in NOM. This complexation of mercury and methylmercury with NOM is known to affect its mobility, as well as chemical and biological transformation in aquatic environments.^[25]

For the polysulfide polymer to capture this mercury, a ligand exchange would need to occur. In addition to testing the non-porous and porous polysulfide for its ability to displace NOM, some of the porous polymer was partially reduced with sodium borohydride to install thiols that could perhaps facilitate this process and bind mercury (Figure S65). Testing this hypothesis, sorption isotherms for Hg(NO₃)₂ and a Hg-NOM complex were determined at environmentally relevant mercury concentrations between 0.2 and 16 µg L⁻¹. Over this concentration range, sorption of Hg(NO₃)₂ was found to follow a linear isotherm, confirming that in the absence of NOM all three forms of the polysulfide removed >90% of the mercury in solution and the sorbent did not approach saturation or Hg binding capacity (Figure S66). By comparison, when mercury is associated with NOM (i.e., Hg-NOM), functional groups on NOM compete with the polysulfide for mercury binding. Nevertheless, the removal efficiency at low Hg-NOM concentrations for the porous and the reduced porous polysulfide reached 79 and 81%, respectively (Figure S66). The removal efficiency of the non-porous polysulfide, in contrast, was only 36%.

As Hg-NOM concentrations increased, the removal efficiency decreased, as indicated by a fit of the equilibrium data to the Langmuir sorption isotherm. The sorption capacity for the porous polysulfide reached a value of 1.11 µg-Hg/g-sorbent under the experimental conditions (Figure S66). The results clearly show that the porous polysulfide material can effectively outcompete NOM, particularly at concentrations typically encountered in mercury contaminated freshwater systems. Partial reduction of the polymer surface to install thiols had only a small impact on removal efficiency in the presence of Hg-NOM and resulted in a lower sorption capacity compared to the porous polysulfide.

Additionally, we investigated whether sulfates were released from the porous polysulfide and its partially reduced derivative. Sulfate release from sulfur-based sorbents may enhance mercury methylation by promoting sulfate-reducing bacteria, which are considered the primary methylators in marine and estuarine environments.^[18b,c] The assessment of sulfate release was accomplished in batch experiments by combining 30 mL of phosphate-buffered Hg(NO₃)₂ or Hg-NOM complex with 100 mg of the porous canola oil polysulfides followed by

equilibration over 48 hours. The sulfate concentration in the filtered sample was then analysed by ion chromatography and normalised to the mass of the sample. The results indicated that sulfate release was typically below $100 \mu\text{g g}^{-1}$ and did not significantly elevate sulfate naturally present in the NOM used in the experiments (Figure S67). Therefore, the deployment of the polysulfide sorbent is not expected to enhance mercury methylation by stimulating sulfate reducing bacteria in the system.

Sequestering an organomercury fungicide

Organomercury compounds have long been used as fungicides to protect grain seeds, sugarcane setts and other crops.^[3] While some of these fungicides have been restricted or banned, their continued use in both industrialised and developing nations is cause for concern.^[2a] These mercury derivatives are highly toxic because they can be absorbed through the skin and enter and damage the central nervous system.^[1b] These fungicides are known to compromise the health of marine life^[39] and accidental ingestion by humans has led to death, with the most infamous episode occurring in Iraq in 1971, where wheat seeds coated with mercury-based fungicides were mistakenly consumed as food by thousands of people.^[40] Sorbents that are effective at capturing these fungicides could find use in preventing harmful runoff from fields to which they are applied. Accordingly, the porous canola oil polysulfide was tested in its ability to capture a representative mercury-derived fungicide, 2-methoxyethylmercury chloride (MEMC)-a fungicide that is still used by sugarcane, rice and potato growers in several countries.^[39]

To test whether the porous canola oil polysulfide could remove this compound from water, an aqueous solution of MEMC was prepared at 0.15 g L^{-1} (a typical operating concentration for the fungicide) and then 10 mL of this solution was

incubated with 2.00 g of the porous polymer for 24 hours. After this time, the concentration of mercury was determined by ICP-MS. Remarkably, 98% of the mercury was removed from solution, whereas the mercury concentration did not change in solutions not treated with the polymer (Figure 9 and Figure S68). To determine if this remediation could be translated to a continuous process, a series of columns were prepared in which the porous polysulfide and soil were used as filtration media (Figure 9 and Figure S69). Next, 3 mL of the 0.15 g L^{-1} MEMC solution was passed through each column and the mercury concentration of the flowthrough was determined by ICP-MS. Soil alone (3.0 g) retained 46% of the mercury; soil and polymer (1.5 g each) mixed randomly together retained 66% of the mercury; soil (1.5 g) layered on top of the polymer (1.5 g) retained 75% of the mercury; and polymer alone (3.0 g) retained 73% of the mercury. The total elution time for each column was approximately 2.5 minutes, so the mercury retention process is relatively fast. These results suggest the porous polysulfide might be useful as a soil additive that can reduce the levels of mercury-based fungicides that leach into agricultural wastewater.

Conclusion

Sulfur and unsaturated cooking oils were co-polymerised to form a polysulfide rubber that captured mercury from air, water, and soil. Because sulfur is a by-product of the petroleum industry and recycled cooking oil was a suitable starting material, the novel polymer can be made entirely from repurposed waste. This research is therefore an addition to the growing body of literature dedicated to preparing sulfur polymers with sustainable and low-cost cross-linkers.^[21d,22,29,37,41] The synthesis required a single, operationally simple chemical reaction. No purification was required and the transformation featured complete atom economy. A porous version of the material was

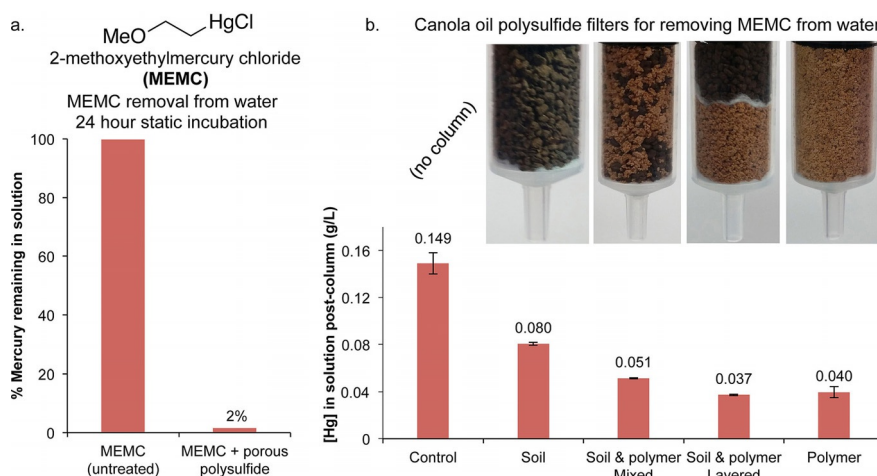


Figure 9. Trapping an organomercury fungicide, (2-methoxyethylmercury chloride, MEMC), using the porous canola oil polysulfide. (a) Incubating a 0.15 g L^{-1} aqueous solution of MEMC with 2.0 g of the porous canola oil polysulfide for 24 hours resulted in the removal of 98% of the mercury in solution. (b) Filters were constructed in the barrel of 10 mL syringes using soil (3.0 g), a random mixture of soil (1.5 g) and porous polysulfide (1.5 g), layers of soil (1.5 g) and polymer (1.5 g) separated by cotton, and solely porous polysulfide (3.0 g). Cotton plugs were used at the base of each column. Passing 3 mL of the MEMC solution (0.15 g L^{-1}) resulted in reduction of mercury in the flowthrough. The soil layered on the polymer and the polymer alone were most effective, removing 75 and 73% of the mercury, respectively.

also prepared using a sodium chloride porogen. The materials were demonstrated to be effective in capturing common forms of mercury pollution including liquid mercury metal, mercury vapour, inorganic mercury and organomercury compounds. The rapid reaction between the porous version of the polymer and mercury bode well for multiple industrial applications. The low-cost will also motivate uptake in developing nations struggling to control mercury pollution associated with gold mining. Neither the polymer nor the mercury-bound polymer were toxic to human cells, which prompts consideration of the polysulfide for in situ remediation of mine tailings, soil and agricultural wastewater. Currently, we are working with a variety of industrial partners, environmental agencies, and other non-profit firms to deploy this technology at sites plagued with mercury pollution.

Acknowledgements

We thank Flinders University, The Australian Government National Environmental Science Programme Emerging Priorities Funding (J.M.C.), the Australian Research Council (DE150101863, J.M.C.), FCT Portugal (I.S.A and G.J.L.B.), The Royal Society (University Research Fellowship, G.J.L.B), the EPSRC (G.J.L.B) and the European Research Council (Starting Grant, G.J.L.B.) for financial support. This research was also supported in part by the Mercury Technology Development Program at Oak Ridge National Laboratory (ORNL) with funding by the Office of Environmental Management, U.S. Department of Energy (DOE). We thank Ji Won Moon and Tonia Mehlhorn for assistance with ion chromatography and mercury analyses. We also acknowledge the support of the Australian Microscopy and Microanalysis Research Facility at Flinders University. This work was performed in part at the South Australian node of the Australian National Fabrication Facility under the National Collaborative Research Infrastructure Strategy to provide nano and microfabrication facilities for Australia's researchers. We are grateful to McHugh's café at Flinders University for supplying used cooking oil and to D.O.G. Chemie for samples of factice. We also thank Richard Fuller, Andrew McCartor, and Budi Susilorini of Pure Earth for helpful discussions regarding mercury pollution due to artisanal and small-scale gold mining. ORNL is managed by UT-Battelle, LLC, for DOE under Contract No. DE-AC05-00OR22725.

Conflict of interest

Two authors (J.M.C. and M.J.H.W.) are inventors on a provisional patent application filed in Australia on April 20, 2016 (Application number 2016901470). Among the claims in this patent application is the preparation of polysulfides from sulfur and vegetable oils and their use in mercury capture. The canola oil polysulfide featured in this study is licensed for sale by Kerfast.

Keywords: inverse vulcanisation · mercury · sulfur · sulfur polymer · waste valorisation

- [1] a) *Global Mercury Assessment 2013. Sources, Emissions, Releases and Environmental Transport*. United Nations Environment Programme, Chemicals Branch, Geneva, Switzerland, **2013**; b) P. B. Tchounwou, W. K. Ayensu, N. Ninashvili, D. Sutton, *Environ. Toxicol.* **2003**, *18*, 149–175; c) J.-D. Park, W. Zheng, *J. Prev. Med. Public Health* **2012**, *45*, 344–352.
- [2] a) Q. Wang, D. Kim, D. D. Dionysiou, G. A. Sorial, D. Timberlake, *Environ. Pollut.* **2004**, *131*, 323–336; b) S. M. Wilhelm, *Mercury in Petroleum and Natural Gas: Estimation of Emissions from Production, Processing and Combustion*. United States Environmental Protection Agency, **2001**.
- [3] N. A. Smart, *Residue Rev.* **1968**, *23*, 1–36.
- [4] a) Reducing Mercury in Artisanal and Small-Scale Gold Mining (ASGM). United Nations Environment Programme. Accessed 21 May 2017 from <http://www.unep.org/chemicalsandwaste/chemicalsandwaste/global-mercury-partnership/reducing-mercury-artisanal-and-small-scale-gold-mining-asgm>; b) G. Hilson, *Sci. Total Environ.* **2006**, *362*, 1–14.
- [5] a) P. W. U. Appel, L. D. Na-Oy, *J. Environ. Prot.* **2014**, *5*, 493–499; b) R. Vieira, *J. Cleaner Prod.* **2006**, *14*, 448–454.
- [6] a) H. Gibb, K. G. O'Leary, *Environ. Health Perspect.* **2014**, *122*, 667–672; b) S. Bose-O'Reilly, B. Lettmeier, R. M. Gothe, C. Beinhoff, U. Siebert, G. Drasch, *Environ. Res.* **2008**, *107*, 89–97.
- [7] a) Extracting gold with mercury exacts a lethal toll. *PBS Newshour*. Broadcast 9 Oct 2016. Accessed 20 October 2016 from <http://www.pbs.org/newshour/bb/extracting-gold-mercury-exacts-lethal-toll/>; b) Unearthing toxic conditions for impoverished gold miners. *PBS Newshour*. Broadcast 17 February 2015. Accessed 20 October 2016 from <http://www.pbs.org/newshour/bb/unearthing-toxic-conditions-impoverished-gold-miners/>; c) R. C. Paddock, (24 May 2016). The Toxic Toll of Indonesia's Gold Mines. *Nat. Geo.* Accessed 24 Sept 2016 from <http://news.nationalgeographic.com/2016/05/160524-indonesia-toxic-toll/>; d) S. Daley, (26 July 2016). Peru Scrambles to Drive Out Illegal Gold Mining and Save Precious Land. *The New York Times*. Accessed 27 July 2016 from <https://www.nytimes.com/2016/07/26/world/americas/peru-illegal-gold-mining-latin-america.html>; e) N. Notman, *Chem. World* **2016**, *13*, 54–57.
- [8] *Minamata Convention on Mercury*, United Nations Environment Programme. Accessed 23 May 2017 from <http://www.mercuryconvention.org>.
- [9] J. Wang, X. Feng, C. W. N. Anderson, Y. Xing, L. Shang, *J. Hazard. Mater.* **2012**, *221–222*, 1–18.
- [10] *Mercury Study Report to Congress. Volume VIII: An Evaluation of Mercury Control Technologies and Costs*. United States Environmental Protection Agency. EPA-452/R-97-010 December 1997.
- [11] L. C. Buettner, C. A. LeDuc, T. G. Glover, *Ind. Eng. Chem. Chem. Res.* **2014**, *53*, 15793–15797.
- [12] S. R. Shewchuk, R. Azargohar, A. K. Dalai, *J. Environ. Anal. Toxicol.* **2016**, *6*, 379.
- [13] X. Meng, Z. Hua, D. Dermatas, W. Wang, H. Y. Kuo, *J. Hazard. Mater.* **1998**, *57*, 231–241.
- [14] S. E. Bailey, T. J. Olin, R. M. Bricka, D. D. Adrian, *Wat. Res.* **1999**, *33*, 2469–2479.
- [15] a) B. Meyer, N. Kharasch, *Elemental Sulfur—Chemistry and Physics*, Interscience Publishers, **1965**; b) G. Kutney, *Sulfur: History, Technology, Applications & Industry*, 2nd ed., ChemTec Publishing, Toronto, **2013**.
- [16] F. A. López, A. López-Delgado, I. Padilla, H. Tayibi, F. J. Alguacil, *Sci. Total Environ.* **2010**, *408*, 4341–4345.
- [17] B. Meyer, *Chem. Rev.* **1976**, *76*, 367–388.
- [18] a) G. C. Compeau, R. Bartha, *Appl. Environ. Microbiol.* **1985**, *50*, 498–502; b) C. C. Gilmour, E. A. Henry, R. Mitchell, *Environ. Sci. Technol.* **1992**, *26*, 2281–2287; c) W. F. Fitzgerald, C. H. Lamborg, C. R. Hammerschmidt, *Chem. Rev.* **2007**, *107*, 641–662.
- [19] W. J. Chung, J. J. Griebel, E. T. Kim, H. Yoon, A. G. Simmonds, H. J. Ji, P. T. Dirlam, R. S. Glass, J. J. Wie, N. A. Nguyen, B. W. Guralnick, J. Park, Á. Somogyi, P. Theato, M. E. Mackay, Y.-E. Sung, K. Char, J. Pyun, *Nat. Chem.* **2013**, *5*, 518–524.
- [20] J. Lim, J. Pyun, K. Char, *Angew. Chem. Int. Ed.* **2015**, *54*, 3249–3258; *Angew. Chem.* **2015**, *127*, 3298–3308.

- [21] a) J. J. Griebel, R. S. Glass, K. Char, J. Pyun, *Prog. Polym. Sci.* **2016**, *58*, 90–125; b) A. Hoefling, P. Theato, *Nachr. Chem.* **2016**, *64*, 9–12; c) D. A. Boyd, *Angew. Chem. Int. Ed.* **2016**, *55*, 15486–15502; *Angew. Chem.* **2016**, *128*, 15712–15729; d) M. J. H. Worthington, R. L. Kucera, J. M. Chalker, *Green Chem.* **2017**, *19*, 2748–2761.
- [22] M. P. Crockett, A. M. Evans, M. J. H. Worthington, I. S. Albuquerque, A. D. Slattery, C. T. Gibson, J. A. Campbell, D. A. Lewis, G. J. L. Bernardes, J. M. Chalker, *Angew. Chem. Int. Ed.* **2016**, *55*, 1714–1718; *Angew. Chem.* **2016**, *128*, 1746–1750.
- [23] T. Hasell, D. J. Parker, H. A. Jones, T. McAllister, S. M. Howdle, *Chem. Commun.* **2016**, *52*, 5383–5386.
- [24] M. W. Thielke, L. A. Bultema, D. D. Brauer, B. Richter, M. Fischer, P. Theato, *Polymers* **2016**, *8*, 266.
- [25] a) M. Haitzer, G. R. Aiken, J. N. Ryan, *Environ. Sci. Technol.* **2002**, *36*, 3564–3570; b) G. R. Aiken, H. Hsu-Kim, J. N. Ryan, *Environ. Sci. Technol.* **2011**, *45*, 3196–3201; c) A. L.-T. Pham, A. Morris, T. Zhang, J. Ticknor, C. Levard, H. Hsu-Kim, *Geochim. Cosmochim. Acta* **2014**, *133*, 204–215.
- [26] a) M. A. R. Meier, J. O. Metzger, U. S. Schubert, *Chem. Soc. Rev.* **2007**, *36*, 1788–1802; b) L. Lin, H. Allemekinders, A. Dansby, L. Campbell, S. Durance-Tod, A. Berger, P. J. H. Jones, *Nutr. Rev.* **2013**, *71*, 370–385; c) *Food Uses of Sunflower Oils*. J. J. Salas, M. A. Bootello, R. Garcés in *Sunflower Chemistry, Production, Processing, and Utilization*, AOCS Press, **2015**, pp. 441–464.
- [27] *Rubber Basics* (Ed.: R. B. Simpson), Rapra Technology Ltd., Shawbury, **2002**, pp. 19, 133.
- [28] A. R. Kemp, F. S. Malm, *Ind. Eng. Chem.* **1935**, *27*, 141–146.
- [29] A. Hoefling, Y. J. Lee, P. Theato, *Macromol. Chem. Phys.* **2017**, *218*, 1600303.
- [30] N. G. Lordkipanidze, J. E. Epperson, G. C. W. Ames, *J. Int. Food Agribus. Mark.* **1998**, *9*, 23–34.
- [31] M. G. Kulkarni, A. K. Dalai, *Ind. Eng. Chem. Res.* **2006**, *45*, 2901–2913.
- [32] S. N. Talapaneni, T. H. Hwang, S. H. Je, O. Buyukcakir, J. W. Choi, A. Coskun, *Angew. Chem. Int. Ed.* **2016**, *55*, 3106–3111; *Angew. Chem.* **2016**, *128*, 3158–3163.
- [33] D. M. Findlay, R. A. N. McLean, *Environ. Sci. Technol.* **1981**, *15*, 1388–1390.
- [34] J. J. Griebel, G. Li, R. S. Glass, K. Char, J. Pyun, *J. Polym. Sci. Part A* **2015**, *53*, 173–177.
- [35] Table of Regulated Drinking Water Contaminants. United States Environmental Protection Agency. Accessed 20 Oct 2016 from <https://www.epa.gov/ground-water-and-drinking-water/table-regulated-drinking-water-contaminant>.
- [36] J. Liu, J.-Z. Shi, L.-M. Yu, R. A. Goyer, M. P. Waalkes, *Exp. Biol. Med.* **2008**, *233*, 810–817.
- [37] D. J. Parker, H. A. Jones, S. Petcher, L. Cervini, J. M. Griffin, R. Akhtar, T. Hasell, *J. Mater. Chem. A* **2017**, *5*, 11682–11692.
- [38] As discussed in reference [11], activated carbon is highly flammable. We have experienced no indication that the canola oil polysulfide is prone to spontaneous combustion, so it is likely a safer sorbent than activated carbon in this respect.
- [39] K. L. Markey, A. H. Baird, C. Humphrey, A. P. Negri, *Mar. Ecol. Prog. Ser.* **2007**, *330*, 127–137.
- [40] S. B. Skerfving, J. F. Copplestone, *Bull. World Health Organ.* **1976**, *54*, 101–112.
- [41] a) I. Gomez, O. Leonet, J. Alberto Blazquez, D. Mecerreyes, *ChemSusChem* **2016**, *9*, 3419–3425; b) S. Shukla, A. Ghosh, P. K. Roy, S. Mitra, B. Lochab, *Polymer* **2016**, *99*, 349–357; c) A. Ghosh, S. Shukla, G. S. Khosla, B. Lochab, S. Mitra, *Sci. Rep.* **2016**, *6*, 25207; d) A. Hoefling, D. T. Nguyen, Y. J. Lee, S.-W. Song, P. Theato, *Mater. Chem. Front.* **2017**, In press. <https://doi.org/10.1039/C7QM00083A>.

Manuscript received: June 22, 2017

Accepted manuscript online: August 1, 2017

Version of record online: August 30, 2017

3.1 SULFUR POLYMERS FOR MERCURY CAPTURE

EXPERIMENTAL

Hg(II)

2.0 g Canola Oil Polysulfide was left in a glass vial with 5 mL of a 20 mg mL⁻¹ aqueous HgCl₂ solution (100 mg HgCl₂) for 24 hours. A control sample containing just water and no HgCl₂ was also produced. After the 24 hours, the aqueous solution was washed from the polysulfide by vacuum filtration with 3 aliquots of 5 mL deionised water. The aqueous solution was then transferred to a pre-weighed 50 mL round bottom flask and the water removed by rotary evaporation. The white precipitate that formed within the round bottom flask was then weighed as remaining HgCl₂. Three replicates were tested, and an average taken.

On average 45.5 mg HgCl₂ (with a range of 7.3 mg) remained in solution, with 54.5 mg removed by the 2 g polysulfide. The polysulfide also underwent a change in colour during the incubation, from brown to grey (fig. 1).



Figure 3.1.1 | Canola Oil Polysulfide. Left: as synthesised using standard procedure, right: after treatment with HgCl₂ (20 mg mL⁻¹, 24 hours). The material has turned from brown to grey.

Effect of canola oil polysulfide mass on mercury(II) capture

The general procedure above was repeated with different quantities of canola oil polysulfide: 250 mg, 500 mg, 1.0 g, 2.0 g, 4.0 g and 8.0 g. The volume and concentration of aqueous HgCl_2 remained the same for each sample. The incubation time, 24 hours, also remained the same. Two replicates were prepared for each sample and an average taken, except in the case of the 8.0 g sample.

Polysulfide (g)	HgCl_2 remaining (mg)	HgCl_2 sequestered (mg)	Range (mg)
0.25	90.7	9.3	5.1
0.5	81.7	18.3	2.8
1	60.2	39.8	9.2
2	41.6	58.4	0.7
4	22.5	77.5	0.1
8	9.4	90.6	-

As the mass of polysulfide increases, the mass of HgCl_2 remaining in solution after the 24 hour incubation decreases.

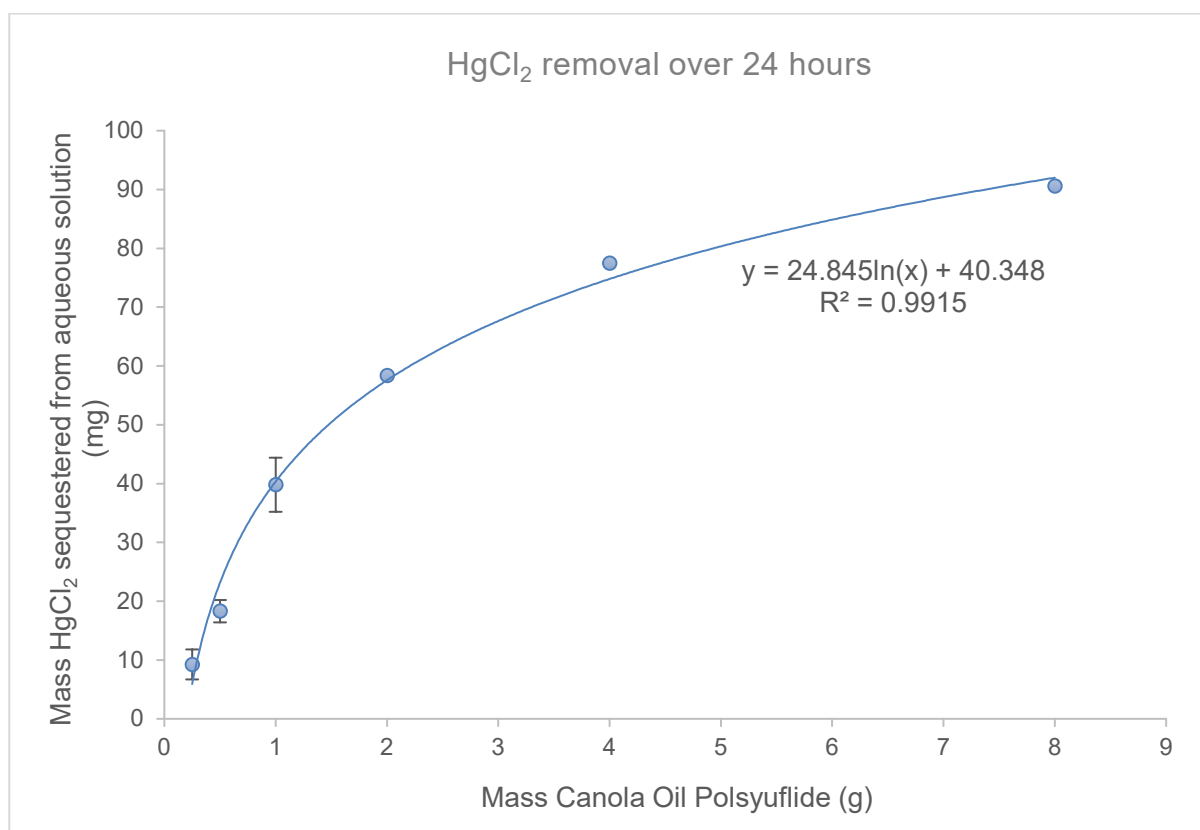


Figure 3.1.2 | Effect of canola oil polysulfide mass on aqueous HgCl_2 capture. A log curve seems to accurately describe the correlation between mass of polysulfide and mass of mercury sequestered.

Effect of Hg(II) concentration on mercury(II) capture

The general procedure above was repeated with different concentrations of mercury chloride: 20, 10 and 5 mg mL⁻¹. The volume (5 mL) and mass of polysulfide (2 g) remained the same for each sample. The incubation time, 24 hours, also remained the same. Two replicates were prepared for each sample and an average taken.

HgCl ₂ (mg mL ⁻¹)	Total HgCl ₂ (mg)	HgCl ₂ remaining (mg)	HgCl ₂ sequestered (mg)	Range (mg)	% HgCl ₂ sequestered
5	25	6.0	19.0	2.3	75.8
10	50	18.4	31.6	1.0	63.2
20	100	38.1	61.9	1.7	61.9

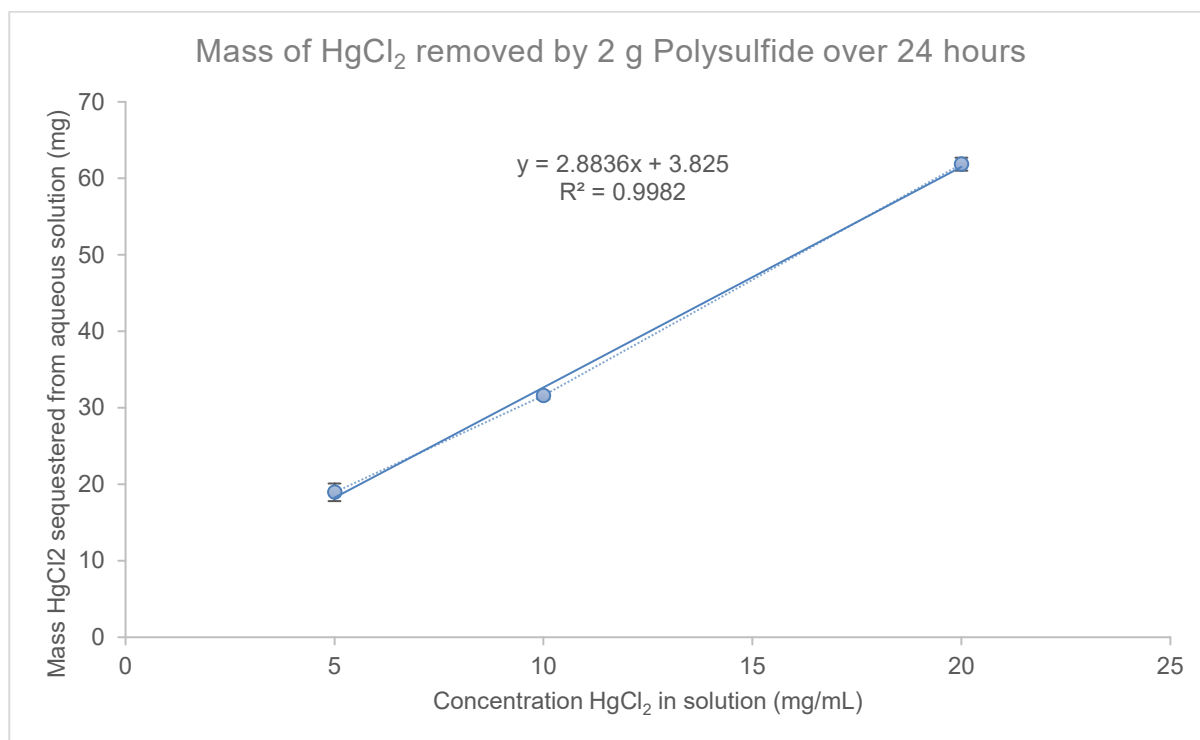


Figure 3.1.3 | Effect of HgCl₂ concentration on aqueous HgCl₂ capture

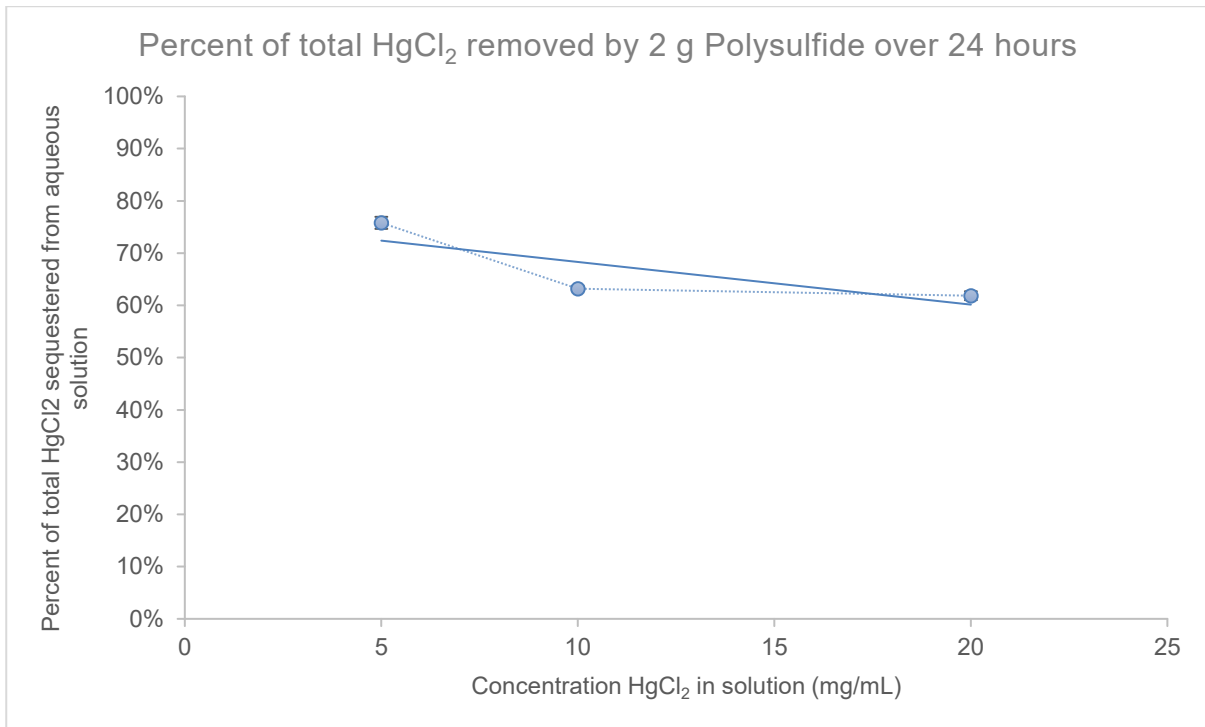


Figure 3.1.4 | Effect of HgCl₂ concentration on percentage of aqueous HgCl₂ captured

Hg(0)

2.0 g canola oil polysulfide prepared to standard procedure and 170 mg elemental mercury were added with a stirrer bar to a glass vial with 7 mL DI water. The solution was spun at 1,500 rpm for 24 hours. After this time no elemental mercury was visible and the polysulfide had changed colour from brown to black (Fig. 3.1.5)



Figure 3.1.5 | Canola oil polysulfide. Left: as synthesised using standard procedure, right: after treatment with Hg⁰ (170 mg mercury, 2.0 g polysulfide, 24 hours). The material has turned from brown to black.



Figure 3.1.6 | Canola oil polysulfide. Left: single pellet after treatment with Hg⁰, right: same pellet cracked open. The polysulfide only alters colour at the surface.

Control 1: Powdered sulfur with mercury(0)

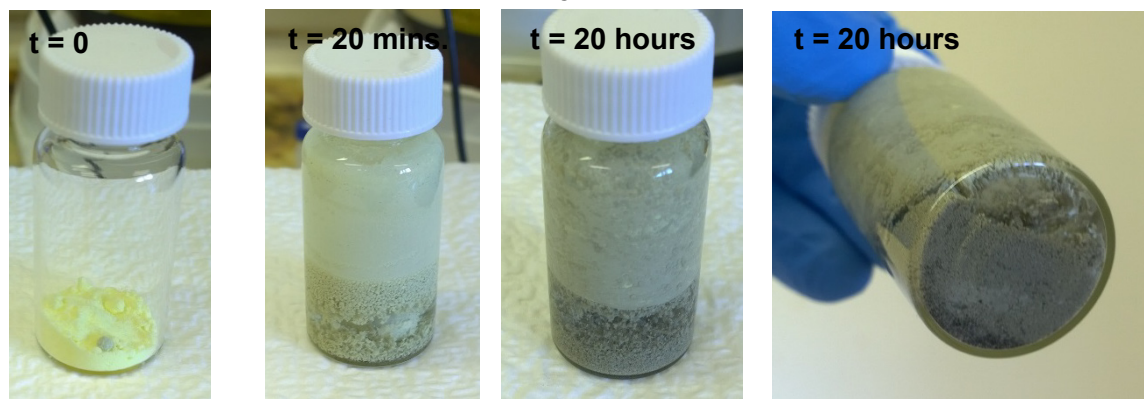


Figure 3.1.7 | Powdered sulfur and elemental mercury spun at 1,500 rpm for 20 hours. After 24 hours the bead of mercury had disappeared and the powdered sulfur had turned from yellow to grey, similar to the colour of the polysulfide on binding to mercury chloride.

Control 2: Crystal Sulfur with mercury(0)

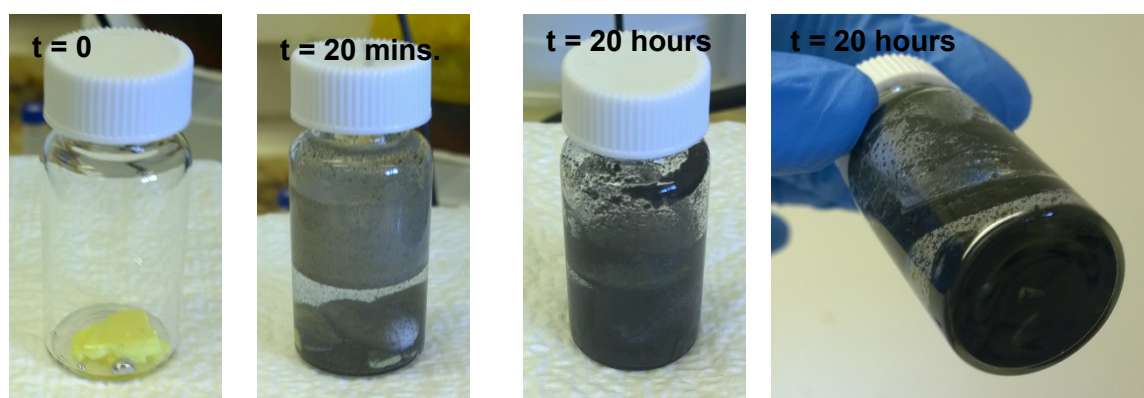


Figure 3.1.8 | Crystal sulfur and elemental mercury spun at 1,500 rpm for 20 hours. After 24 hours the bead of mercury had disappeared and the crystalline sulfur had turned from yellow to black, similar to the colour of the polysulfide on binding to elemental mercury.

Control 3: Canola Oil Polysulfide without mercury(0)

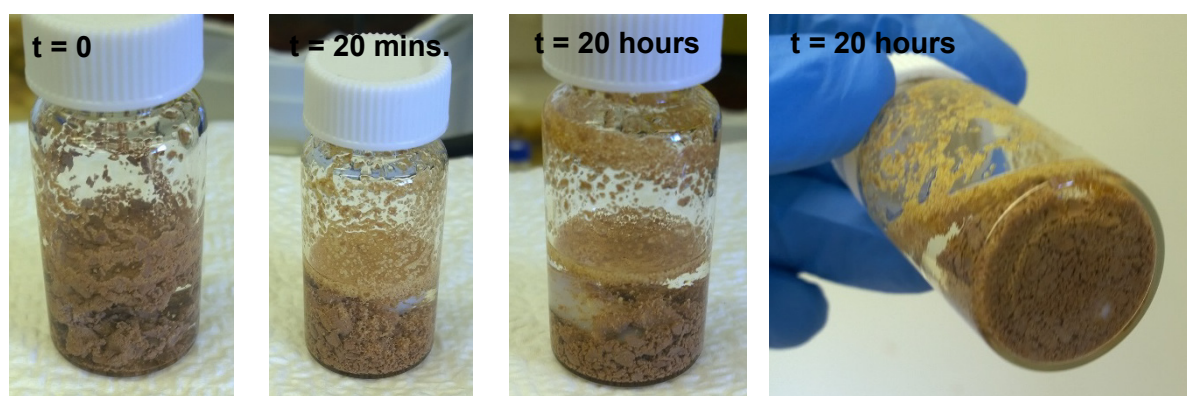
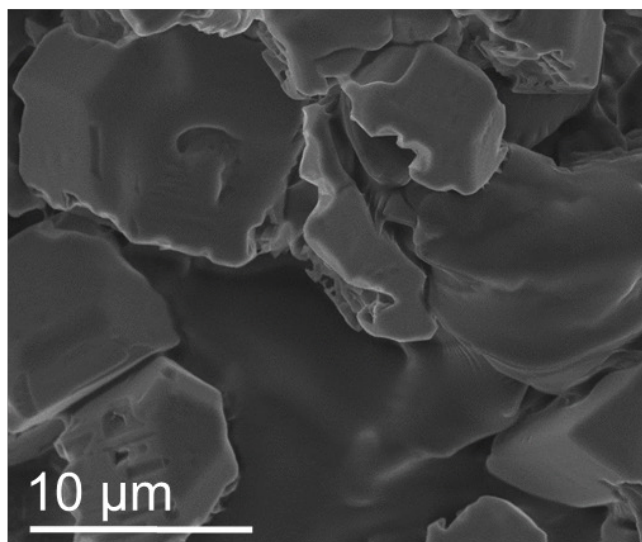
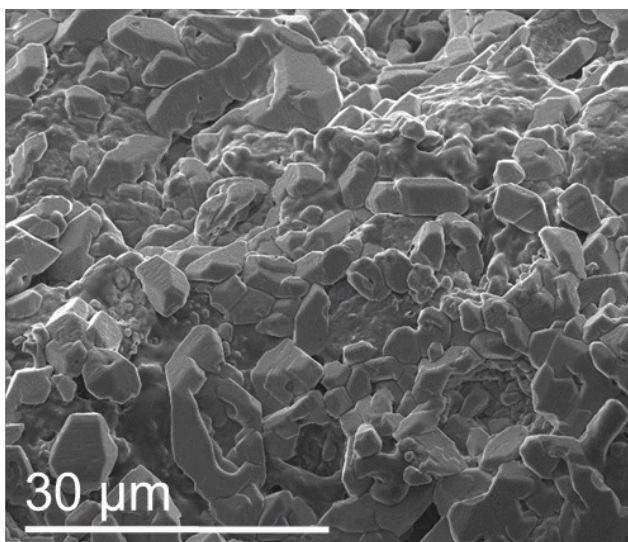
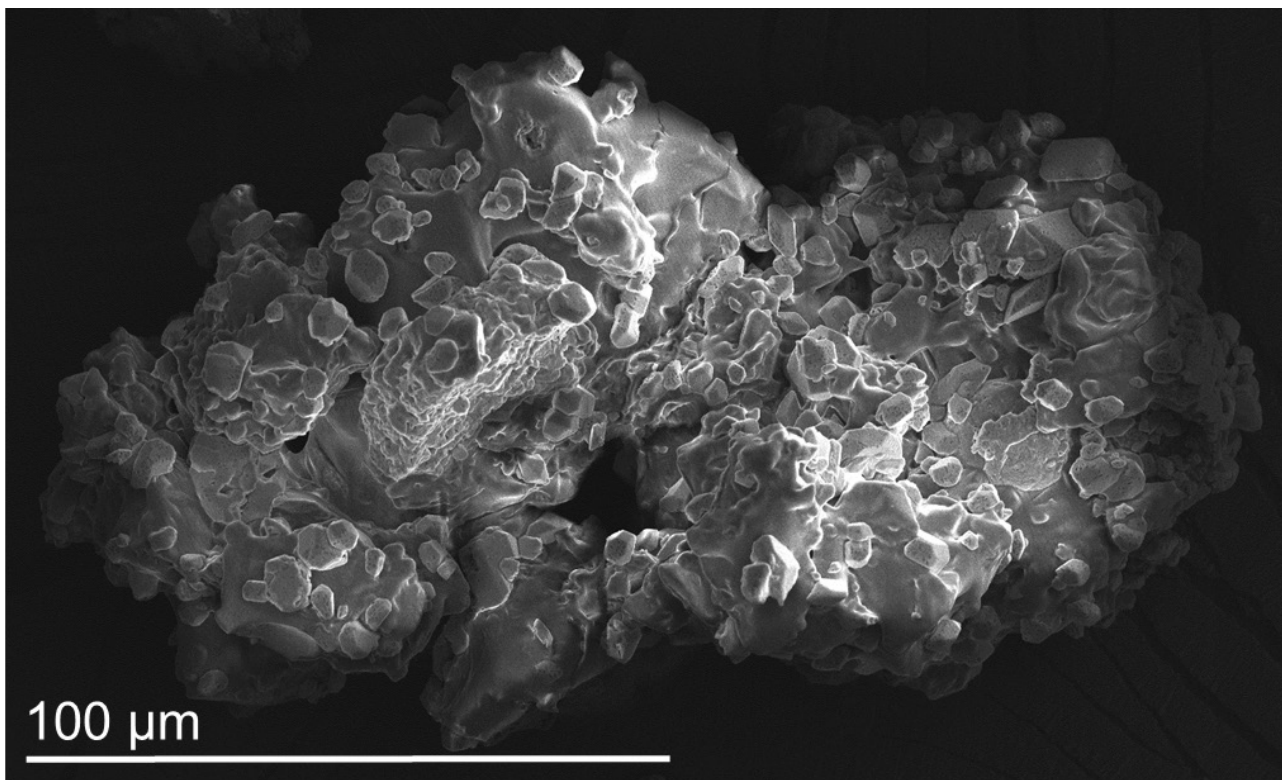


Figure 3.1.9 | Canola Oil Polysulfide spun at 1,500 rpm for 20 hours. After 24 hours no change had occurred, indicating long periods of high-rpm stirring was not responsible for the colour change.

SEM Analysis

The untreated Canola Oil Polysulfide above was prepared to standard procedure and then ground and filtered to give particle sizes between 0.5 and 1 mm in diameter. To prepare the mercury chloride-treated sample these particles were incubated with an aqueous mercury chloride solution for 24 hours resulting in a grey material calculated to consist of 3.5 % mercury chloride.



Mercury chloride-treated canola oil polysulfide

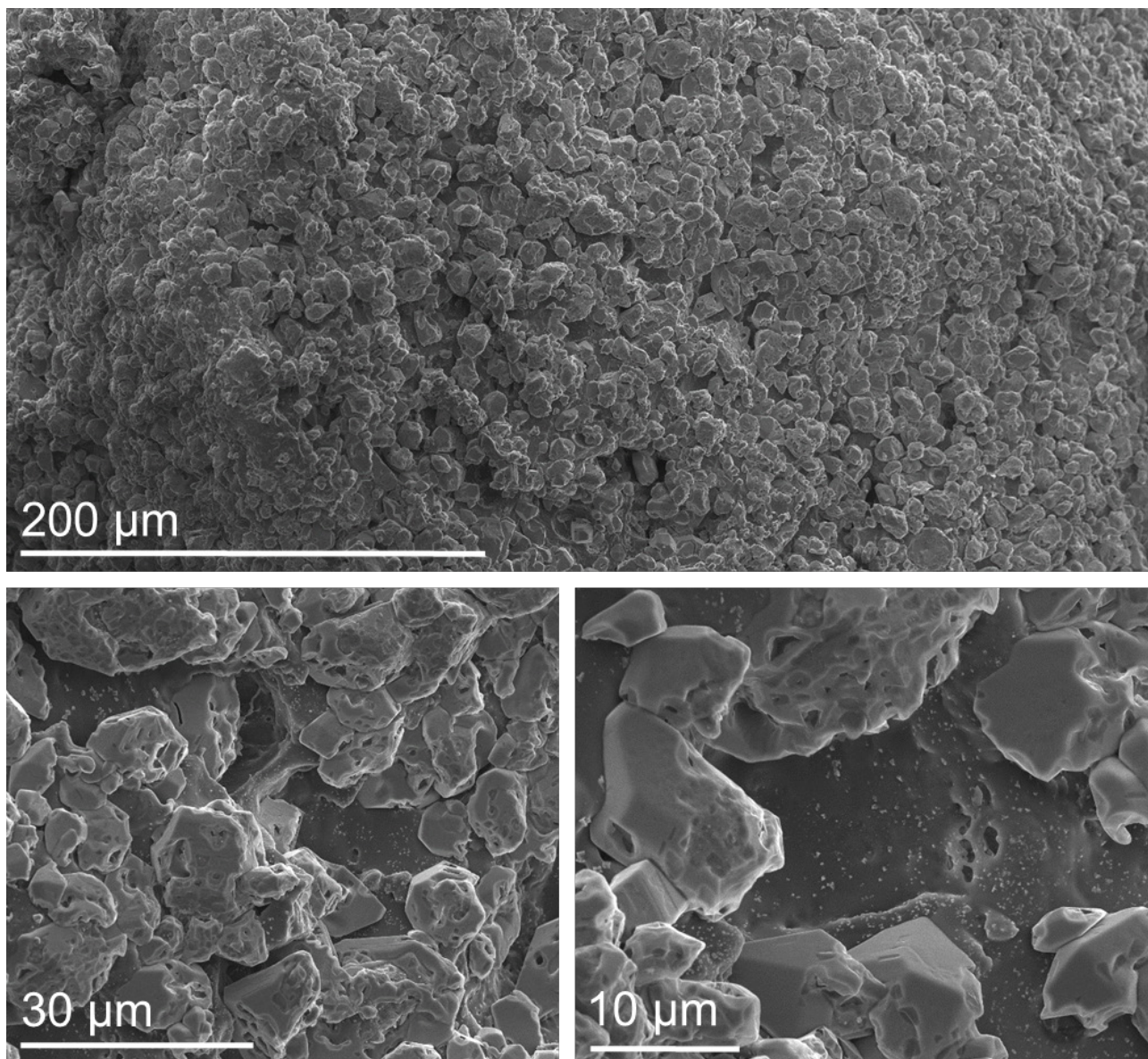


Figure 3.1.11 | SEM images of polysulfide surface after treatment with mercury chloride

Canola oil polysulfide seems to consist of two components: nano-to-micrometre sized crystalline regions and an amorphous region that forms the base structure of the material. The only major difference in morphology (beyond the optical colour change) visible by SEM analysis are the presence of nanometre-sized particles dotted across the outer amorphous regions of the polysulfide. This can be seen most clearly in comparing figures 3.1.10 (bottom right) and 3.1.11 (bottom right).

EDX analysis of mercury chloride-treated polysulfide surface

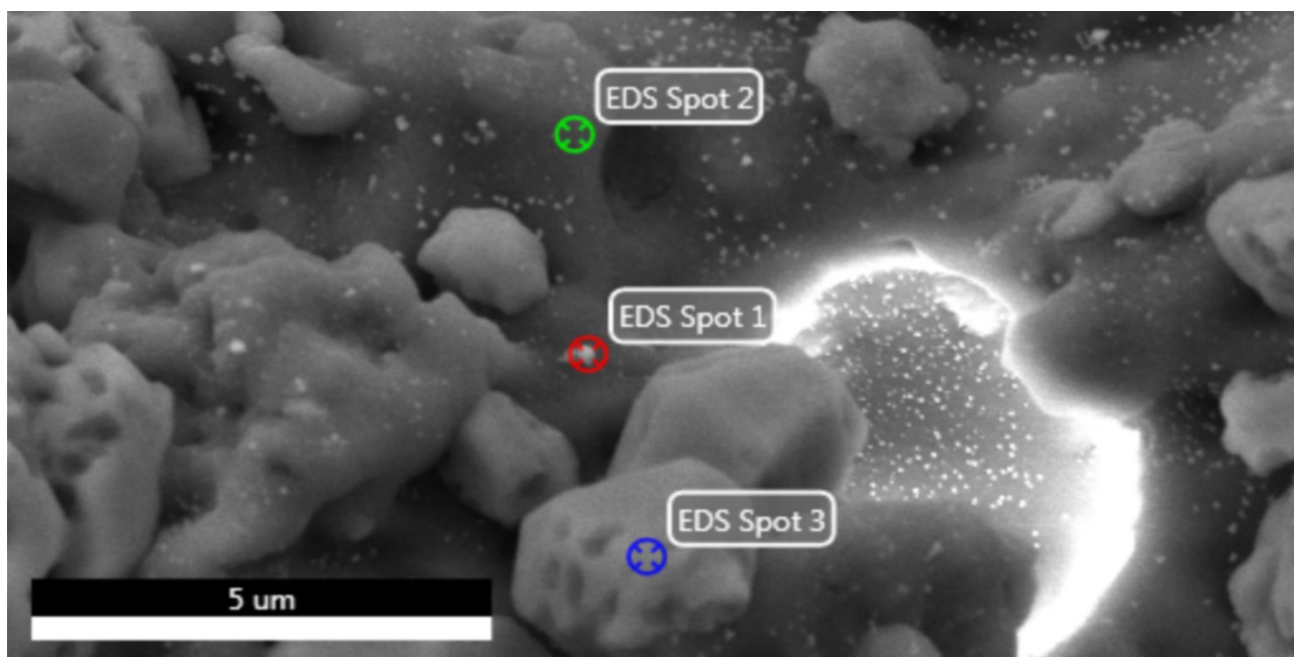
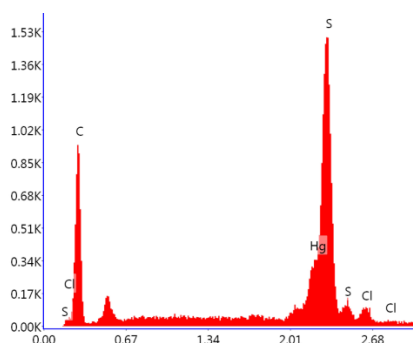


Figure 3.1.12 | SEM image indicating spots for EDX analysis

EDS Spot 1

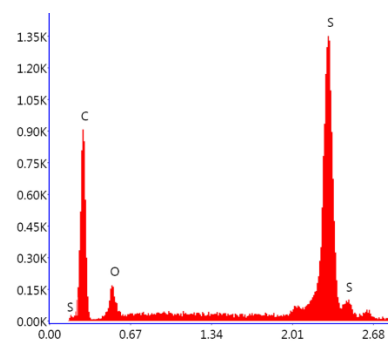
HgCl₂ nanoparticle



Mercury shoulder visible to the left of the major sulfur peak. Characteristic X-rays for chlorine also present.

EDS Spot 2

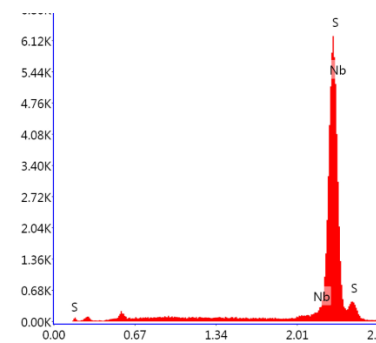
Amorphous section



Both sulfur and carbon present in high quantity. Oxygen also present; consistent with a sulfur-canola oil mixture.

EDS Spot 3

Crystal section



Sulfur peak very prominent. Carbon and oxygen peaks present but with minimal signal.

The Polysulfide seems to consist of two regions: Firstly, an amorphous component that makes up the vast majority of the material, strong peaks for carbon, oxygen and sulfur are all present from EDX analysis, consistent with a polysulfide material consisting of the starting materials sulfur and canola oil. Also present are crystalline segments with very high sulfur content and minimal canola oil-affiliated peaks. These crystal segments coat the surface of the polysulfide and can also be found dispersed throughout. Raman data indicates the presence of pure S₈ within the sample, these

crystalline regions are potentially either pure S₈ or exist as a different, high-sulfur-content polysulfide network to the amorphous regions.

EDX analysis of elemental mercury-treated polysulfide surface

A particle of the polysulfide 10 mm in diameter having been treated with elemental mercury was cut open and imaged by SEM with elemental composition given by EDX analysis.

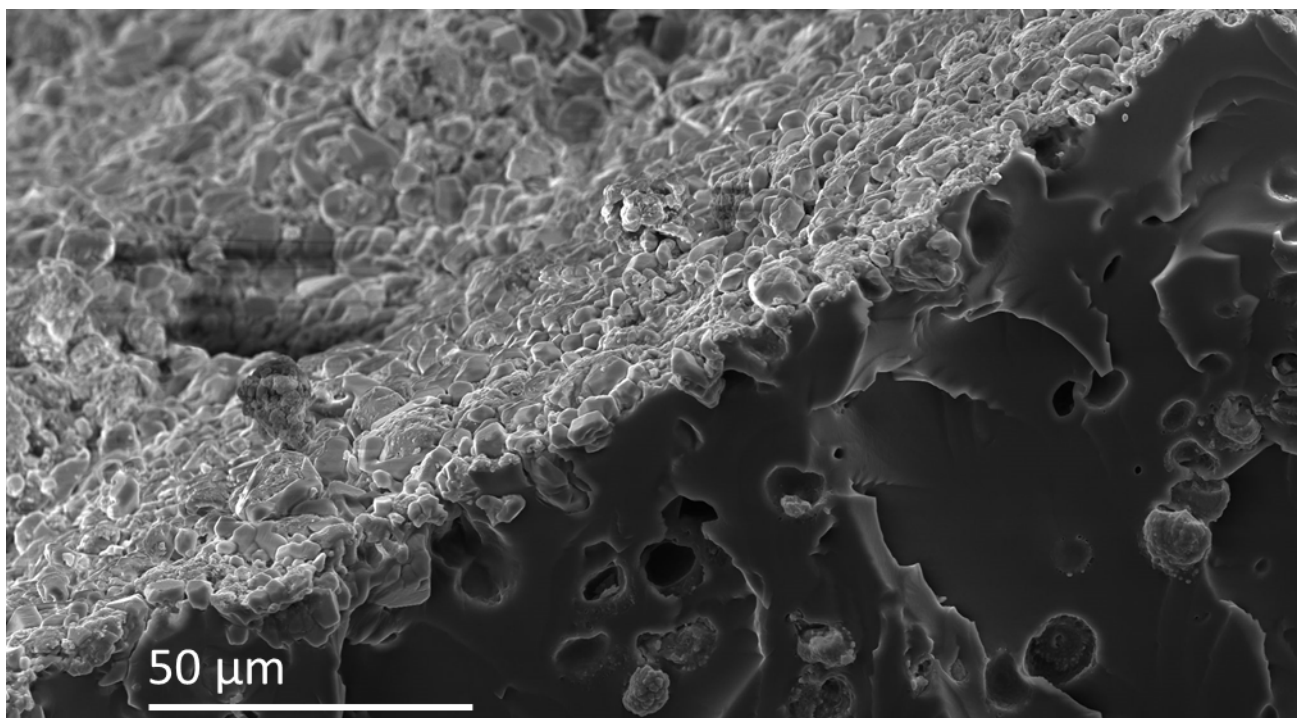


Figure 3.1.13 | SEM image of polysulfide cross-section. Upper left: surface, lower right: interior

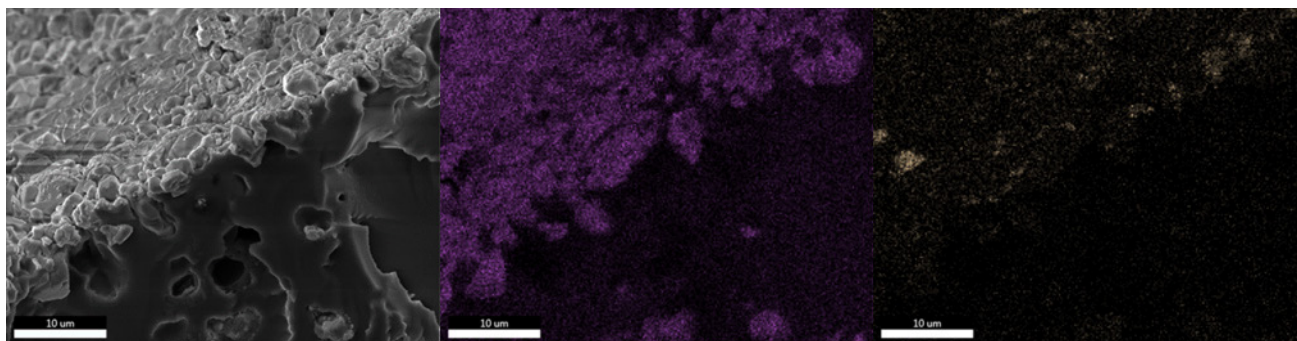


Figure 3.1.14 | SEM image (left) and EDX map of sulfur (middle) and mercury (right) distribution. Mercury is primarily adhered to the surface of the polysulfide, with very little, if any, permeating the polymer.

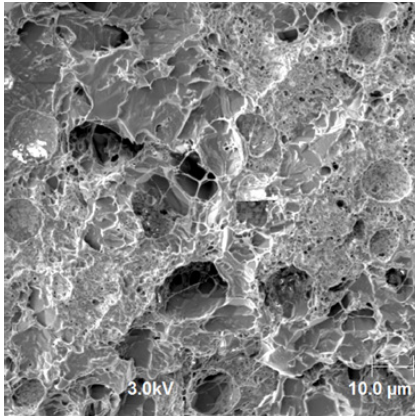


Figure 3.1.15 | The surface of the canola oil polysulfide (50 % sulfur) reacts with mercury metal, forming a black product. EDS analysis verifies mercury is found on the surface of the material.

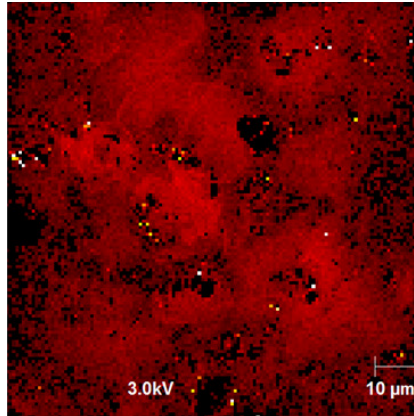
Auger Analysis

Experiments performed by Alex Sibley

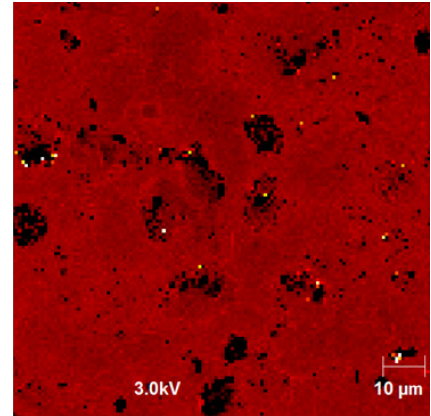
Canola oil polysulfide



SEM image

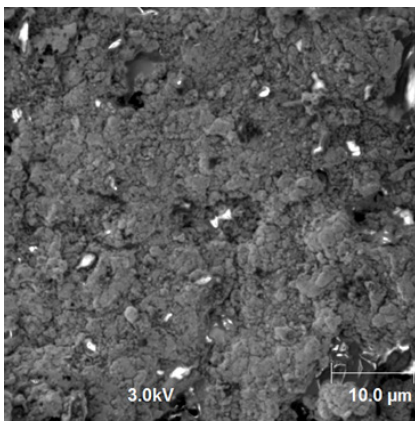


Sulfur map

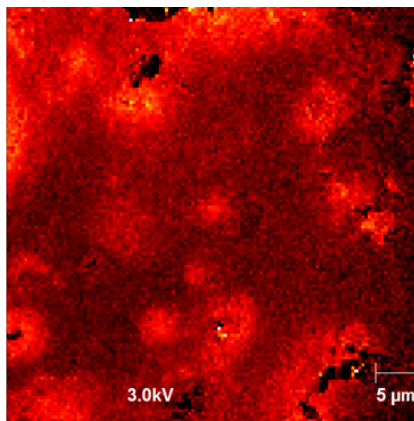


Carbon map

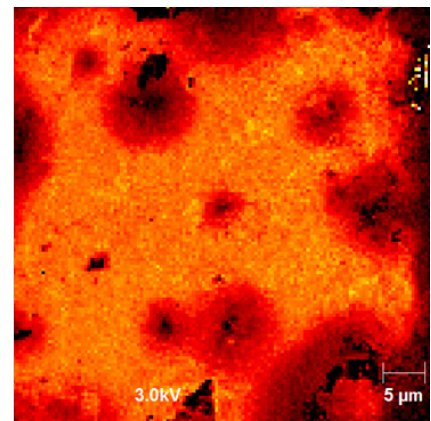
Elemental Hg treated polysulfide



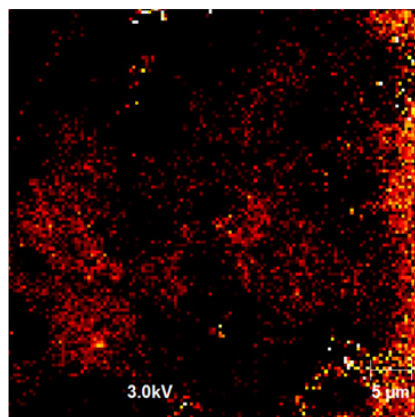
SEM image



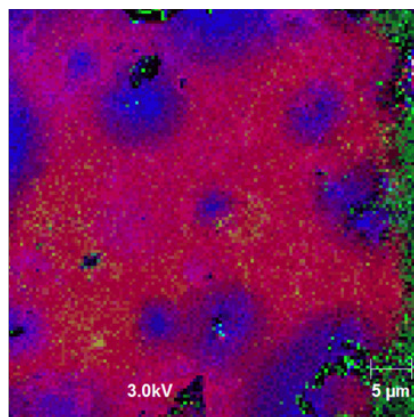
Sulfur map



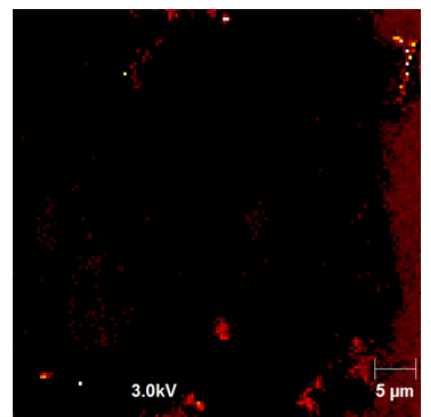
Carbon map



Oxygen image



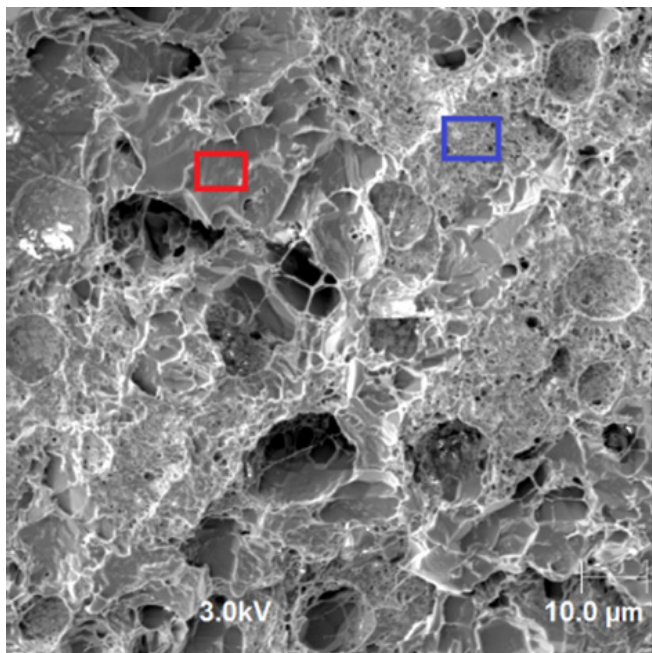
Sulfur, oxygen and carbon map



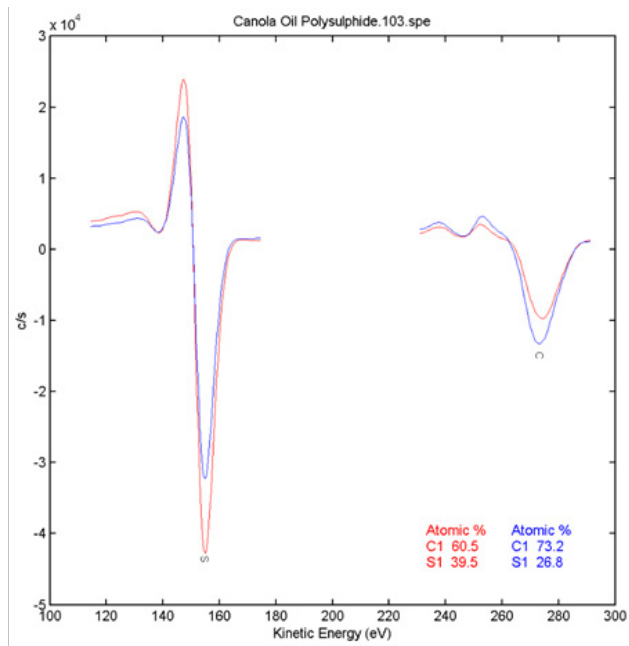
Mercury map

Signal was too poor to acquire an accurate elemental map of the HgCl_2 -treated polysulfide due to significant charging

Canola oil polysulfide

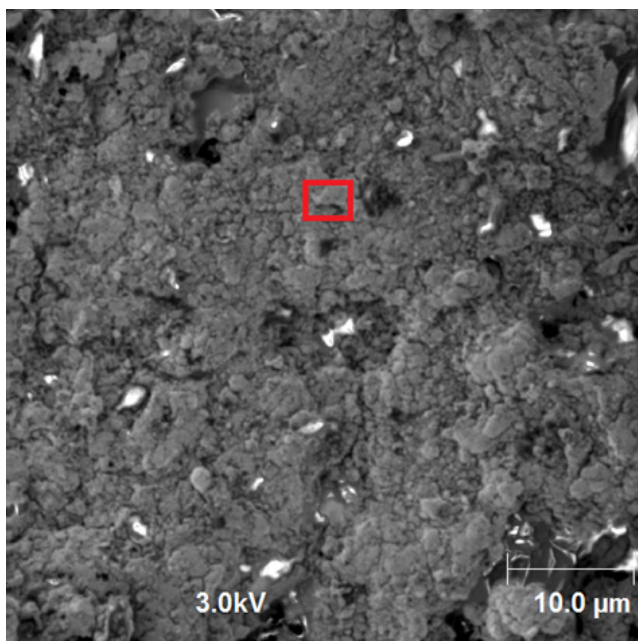


SEM image

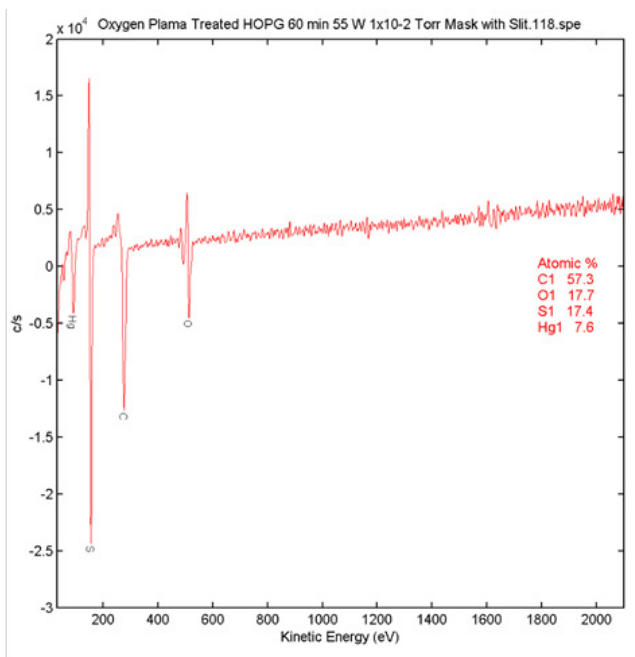


Auger response

Elemental Hg treated canola oil polysulfide (region 1)

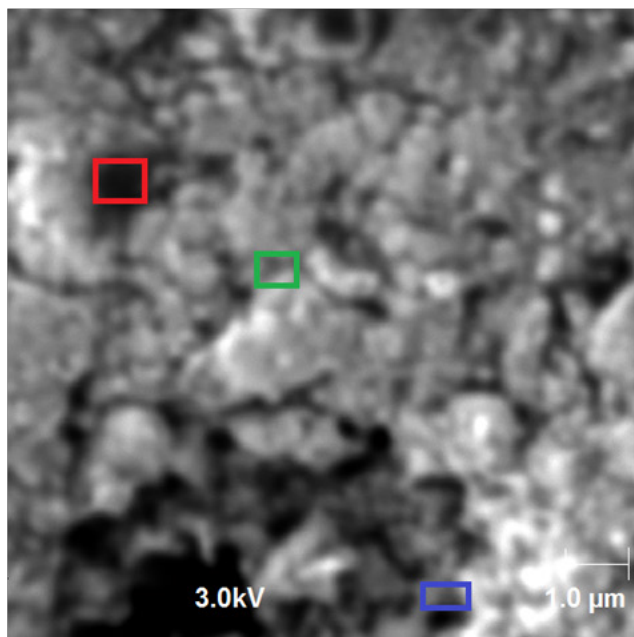


SEM image

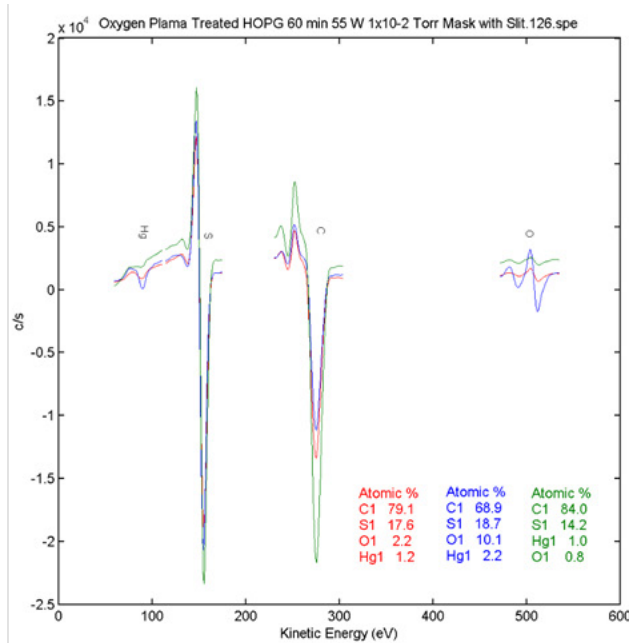


Auger response

Elemental Hg treated canola oil polysulfide (region 2)

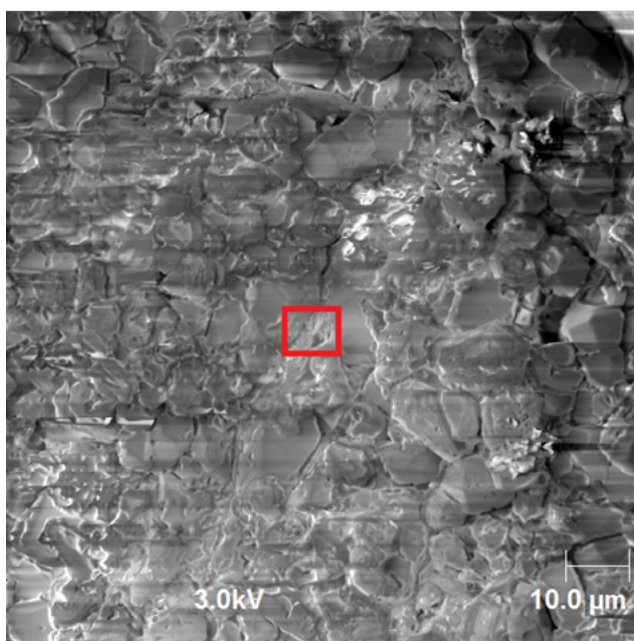


SEM image

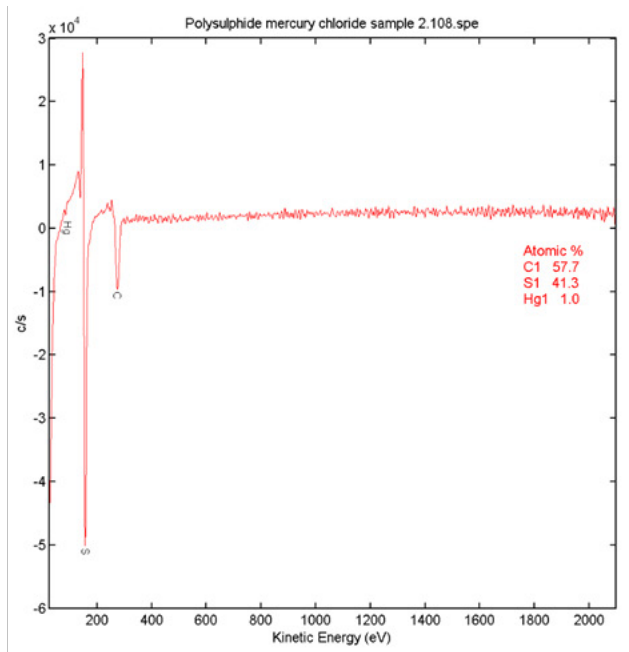


Auger response

HgCl₂ treated canola oil polysulfide



SEM image



Auger response

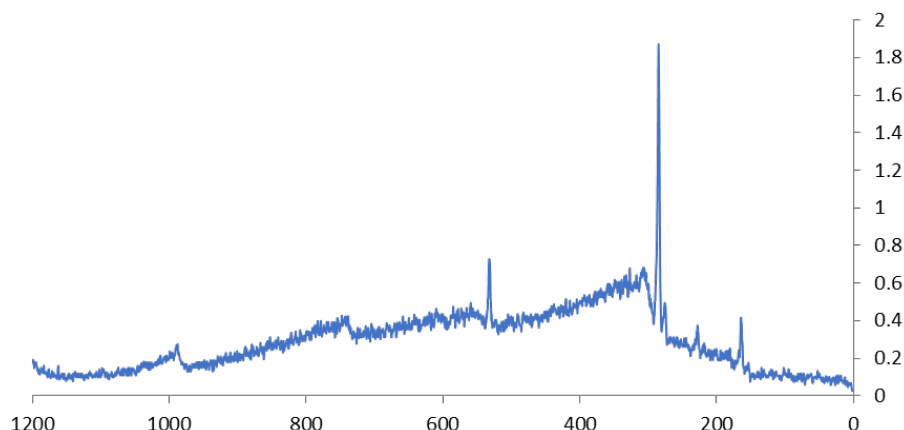
Figure 3.1.16 | Auger analysis of canola oil polysulfide before and after exposure to elemental mercury or mercury chloride. Mercury is detected on the surface of the polysulfide after exposure to both mercury species.

XPS analysis of mercury-treated canola oil polysulfide before and after mercury capture

Experiments performed by Alex Sibley

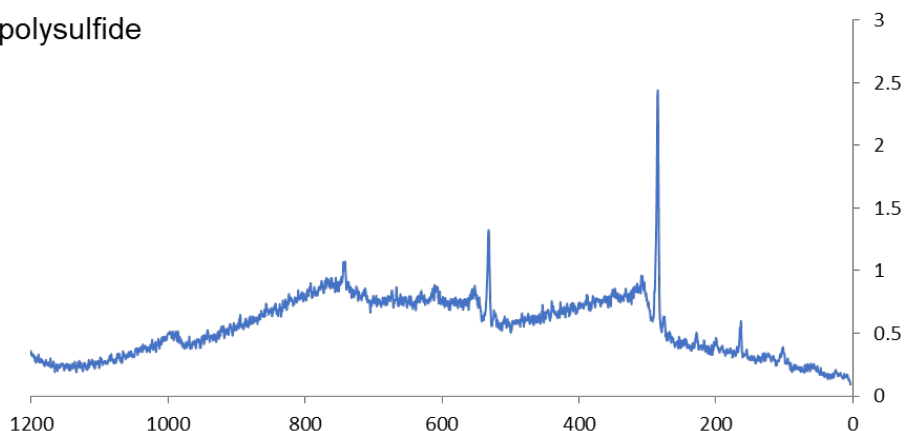
a. Canola oil polysulfide

Name	Position	% Conc.
O 1s	532.5	8.777
C 1s	285	83.431
S 2p	164.5	7.792



b. HgCl₂-treated canola oil polysulfide

Name	Position	% Conc.
C 1s	285	79.393
S 2p	163.5	4.505
Hg 4f	102	0.312
Cl 2p	200	1.886
O 1s	532	13.904



c. Hg⁰-treated canola oil polysulfide

Name	Position	% Conc.
O 1s	533	8.458
C 1s	285	86.992
S 2p	164	4.383
Hg 4f	101	0.167

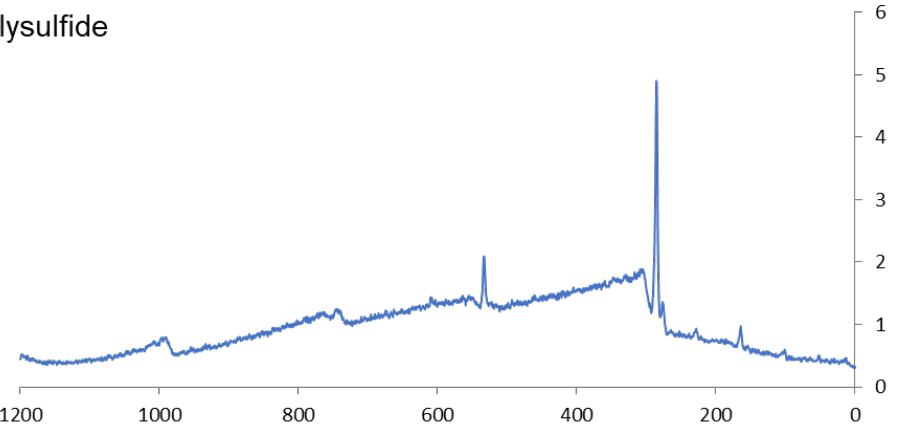


Figure 3.1.17 | XPS analysis of the canola oil polysulfide revealed the mercury '4f' photoelectron peak for both the mercury chloride capture (b) and mercury metal capture (c). The observed binding energy is associated with mercury bound to sulphur (~101eV for HgS) for both samples. In the case of Hg⁰ capture, this is consistent with oxidation of mercury to metacinnabar.

XRD Sample Preparation

XRD data acquired by Nick Adamson

1.24 g elemental mercury was added to a 50 mL centrifuge tube containing 2.47 g sulfur and mixed for 24 hours using an end-over-end mixer. Similarly, 2.47 g of canola oil polysulfide (50 wt. % sulfur, < 0.5 mm particle size) was mixed with 1.52 g elemental mercury in an end-over-end mixer for 24 hours. Unreacted sulfur, unreacted polysulfide, as well as those samples reacted with elemental mercury, were all ground to a fine powder using a mortar and pestle in preparation for loading on an XRD sample stage. The XRD spectra obtained for both reactions was metacinnabar, as it was identical to previously published XRD spectra.² It can therefore be concluded that the black material that results from the reaction of mercury metal and the S-S bonds of the canola oil polysulfide is metacinnabar

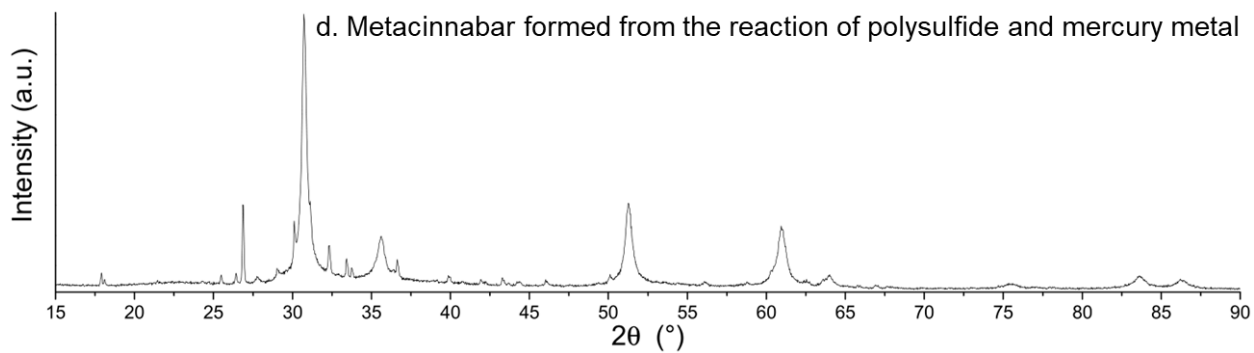
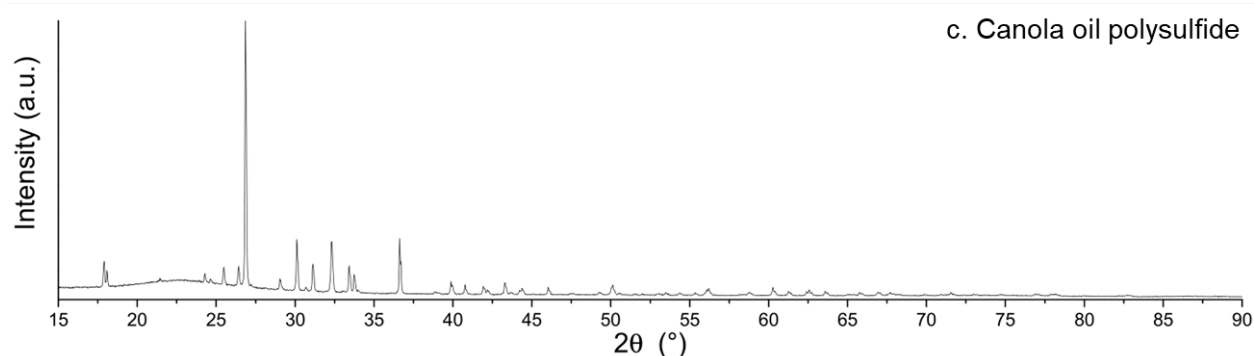
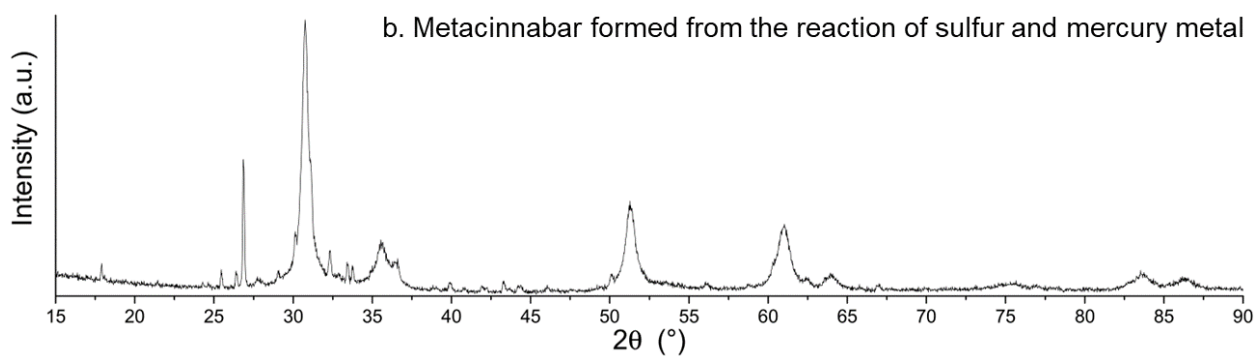
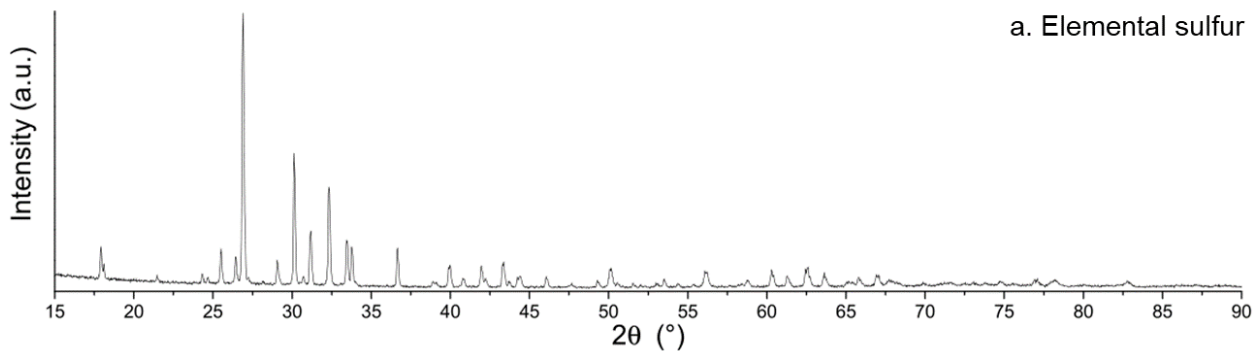


Figure 3.1.18 | XRD scans of a, elemental sulfur, b, metacinnabar prepared by the reaction of sulfur and mercury metal c, canola oil polysulfide (50 % sulfur) and d, metacinnabar formed by reaction of polysulfide and mercury metal.

Mercury capture using polysulfide prepared from recycled cooking oil

1.0 g of the polysulfide (50 % sulfur) prepared from recycled cooking oil was placed in a 25 mL round bottom flask equipped with a stirrer bar, along with elemental mercury (171 mg) and 10 mL DI water. The flask was sealed and the mixture stirred for 24 hours. During this time the polysulfide turned black, and some unreacted elemental mercury was still visible. The polymer and mercury were separated by mixing with equal volumes of hexane and water. The polymer remained at the phase boundary and the mercury settled to the bottom of the aqueous phase. The water and mercury were isolated and separated from the polymer. The mercury was then separated from the water by transferring to a separatory funnel and diluting with dichloromethane. The mercury-dichloromethane mixture was then isolated, and the dichloromethane evaporated in a fume hood. The mass of the unreacted mercury was recorded.

Mercury capture using Factice F17 (D.O.G.)

2.8 g of F17 grade D.O.G. Factice was placed in a 25 mL round bottom flask equipped with a stirrer bar, along with elemental mercury (217 mg) and 10 mL DI water. The flask was sealed and the mixture stirred for 24 hours. During this time the factice darkened in colour, and some unreacted elemental mercury was still visible. The factice and unreacted mercury were separated by mixing with equal volumes of hexane and water. The polymer remained at the phase boundary and the mercury settled to the bottom of the aqueous phase. The water and mercury were isolated, and separated from the polymer. The mercury was then separated from the water by transferring to a separatory funnel and diluting with dichloromethane. The mercury-dichloromethane mixture was then isolated and the dichloromethane evaporated in a fume hood. The mass of the unreacted mercury was recorded.

Sample	F17 factice	Polysulfide from recycled cooking oil
Polymer (g)	2.8	1.0
Sulfur (g)	0.50	0.50
Hg ⁰ (mg)	217	171
Hg ⁰ removed (mg)	117	116
% Hg ⁰ removed	49	70
Hg ⁰ removed per gram polymer (mg)	40.9 ± 2.8	114.5 ± 28.9

Factice F17 (17 % sulfur) and a polysulfide prepared from recycled cooking oil (50 % sulfur) were compared in their reaction with mercury metal. An amount of polymer was added such that the mass of sulfur was the same. Both samples captured virtually the same amount of mercury metal, suggesting that the amount of mercury that can react corresponds to the amount of sulfur in the polysulfide. This result also suggests that the polysulfides in factice can react with mercury metal and that free sulfur is not required.

Point of Colour Change

1.0 g Canola Oil Polysulfide was left to incubate for 24 hours in 5 mL solutions of Hg in 2% HNO₃ ICP standard solution and aqueous HgCl₂ over a range of concentrations.

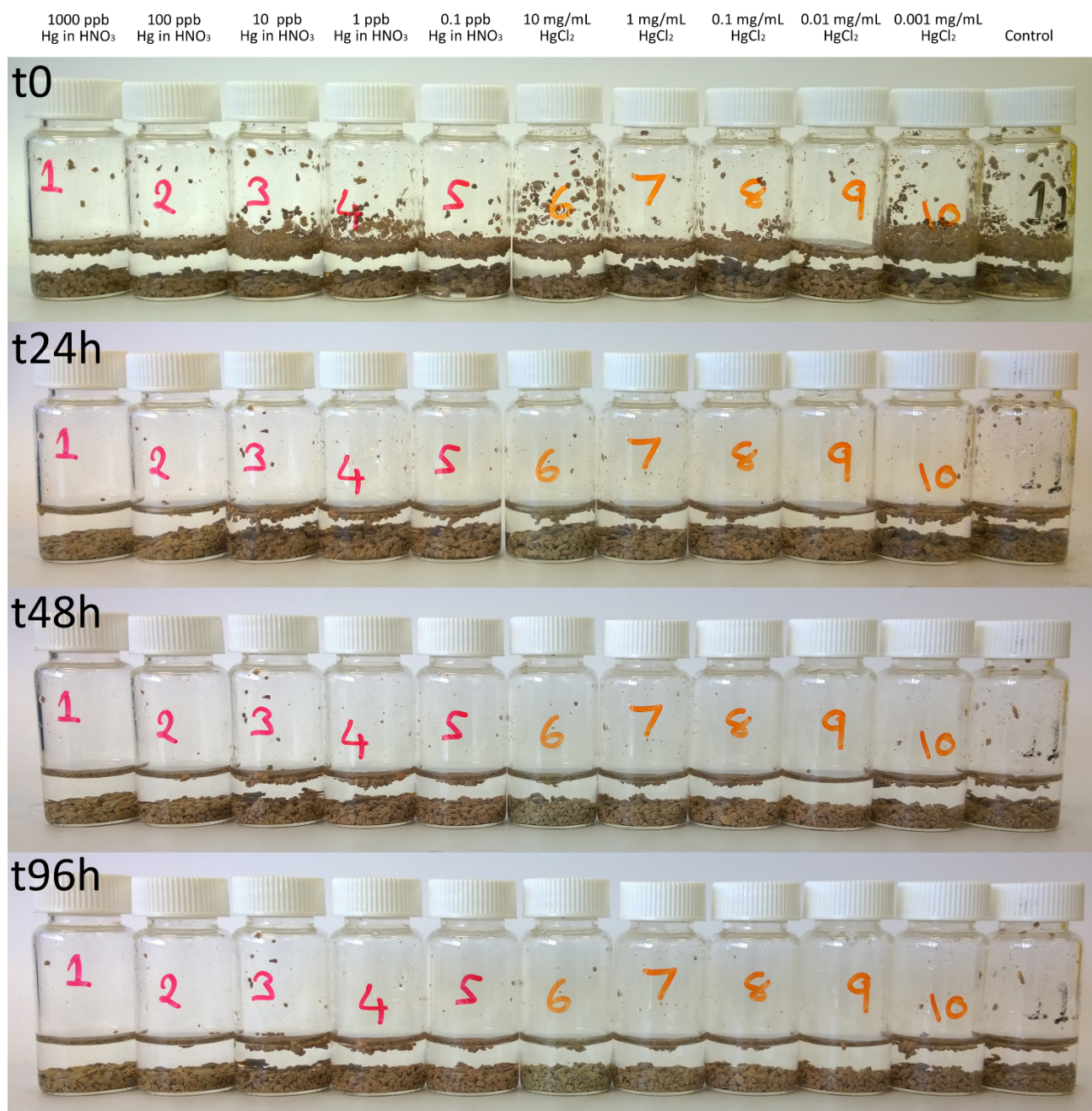


Figure 3.1.19 | After 24 hours, a colour change of brown to grey was observed in the 10 mg mL⁻¹ HgCl₂ sample, with a slight colour change also visible in the 1 mg mL⁻¹ sample. No other samples (0.1 ppb – 1000 ppb Hg in 2% HNO₃ ICP standard solution or 0.001 – 0.1 aqueous HgCl₂) showed a visible colour change. No further change was observed passed the first 24 hours.

Sensitivity of chromogenic response of canola oil polysulfide to mercury metal

In order to test the sensitivity of the polysulfide's response to elemental mercury, quantities of mercury ranging from 72 to 285 mg were added to 10 and 20 g quantities of polysulfide in separate 50 mL centrifuge tubes (Fig. 3.1.20). The polymer-mercury mixtures were rotated on a lab rotisserie for 24 hours and any changes to the mixture recorded. In all cases the polymer turned black, indicating reaction of mercury with the polysulfide. Given the intensity of the colour change, it is presumed that the polymer may also turn black when exposed to lesser quantities of elemental mercury than shown here. Because of the difficulties in measuring small quantities of metallic mercury, this experiment was not pursued further. From these results we can conclude that mercury can be detected by visual inspection after the reaction of mercury and the canola oil polysulfide at ratios of 3.6 mg of mercury per gram of polymer or lower.

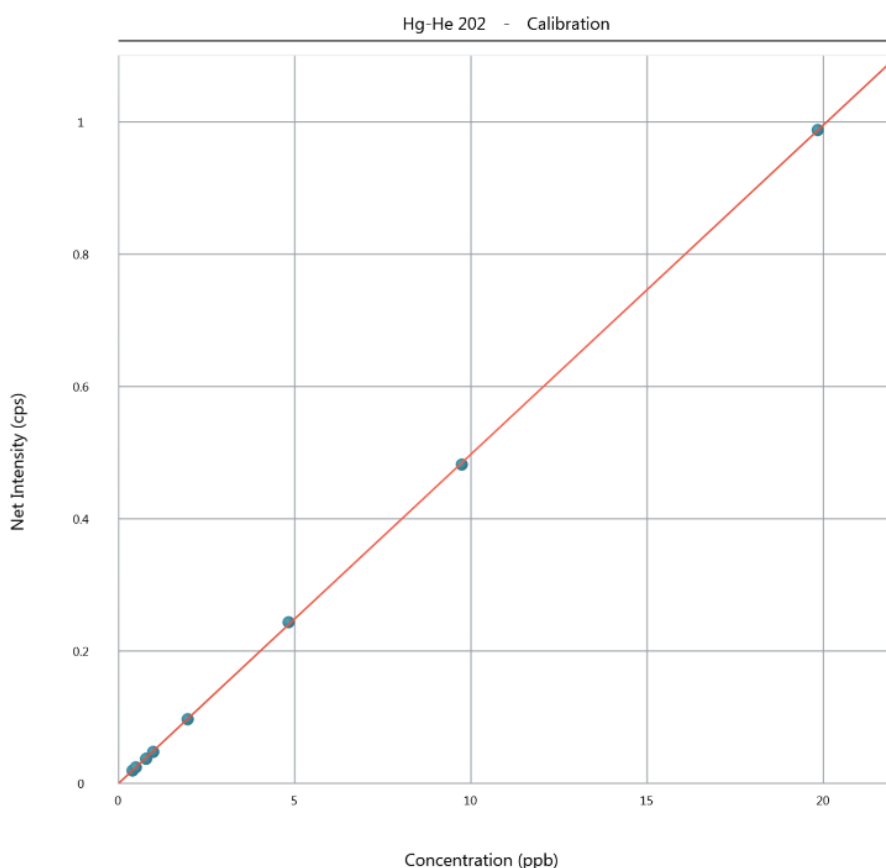
Polymer (g)	10.0	10.0	10.0	20.0	20.0	20.0	10.0
Hg ⁰ (mg)	285	207	75	121	72	216	0
Result							

Figure 3.1.20 | Preliminary study of the sensitivity of the canola oil polysulfide in its detection of metallic mercury

Mercury leaching by ICP-MS

1.0 g samples of mercury chloride-treated and elemental mercury-treated polysulfides were incubated in 10 mL milliQ water for 24 hours. The water was then tested by ICP-MS against an ICP standard of Hg in 2 % HNO₃ (1 % HNO₃ and 1 % HCl in water used as a diluent) to determine the concentration of mercury that had leached from the polymer over this time. Tests were run in duplicate, an untreated sample of canola oil polysulfide was also incubated in water and tested as a control. All samples were diluted 1/10 in a 1 % HNO₃ and 1 % HCl in water matrix. Samples were run in He mode to ensure ions flew monatomically (for example Hg ions, not HgCl₂). Mercury chloride-treated polysulfide contained 79.42 mg HgCl₂ per gram polysulfide. Elemental mercury-treated polysulfide contained 2.16 mg Hg per gram polysulfide.

Calibration curve



Statistics

Eqn. : $y = 0.050x + 0.000$
 Cor.Coeff. : 0.999991
 BEC : -0.012797 ppb
 DL : 0.004680 ppb

Calibration Table

	Net Intensity Hg-He 202 (cps)	Apparent Conc. Hg-He 202 (ppb)
Blank	11.000	
Cal. Std.1	0.019	0.392
Cal. Std.2	0.024	0.489
Cal. Std.3	0.037	0.749
Cal. Std.4	0.048	0.959
Cal. Std.5	0.097	1.950
Cal. Std.6	0.244	4.897
Cal. Std.7	0.482	9.687
Cal. Std.8	0.988	19.849

Figure 3.1.21 | Calibration standards of 0.4, 0.5, 0.8, 1, 2, 5, 10, 20 and 50 ppb Hg in 2 % HNO₃ gave an accurate calibration curve with high linearity.

Results

Sample	Conc. Hg (ppb)	Description
Hg (1)	61.52	Elemental mercury treated polysulfide 24hr incubation water
Hg (2)	32.46	
Average	46.99	
HgCl ₂ (1)	0.51	Mercury chloride treated polysulfide 24hr incubation water
HgCl ₂ (2)	0.64	
Average	0.57	
Water	0.24	milliQ water (control)
Polysulfide	0.30	Untreated Canola Oil Polysulfide 24hr incubation water (control)

Spike Recovery (QC)

Samples were diluted 10-fold and spiked with 2 mL 20 ppb Hg stock (4 ppb mercury). The solution was then made up to volume with 1 % HNO₃ and 1 % HCl in water. Values below have been multiplied by 10 to account for the 1/10 dilution.

Sample	Spike conc. (ppb)	Neat sample conc. (ppb)	Measured conc. (ppb)	Expected conc. (ppb)	Difference (Recovery)
Hg Spike	39.60	61.52	106.97	101.12	105.79%
HgCl ₂ Spike	39.60	0.51	40.65	40.11	101.35%
Water Spike	39.60	0.24	40.23	39.84	100.98%

A spike recovery within 80–120 % is considered accurate, these results do not deviate higher than 106 %.

Internal Standard Recovery (Matrix Effects)

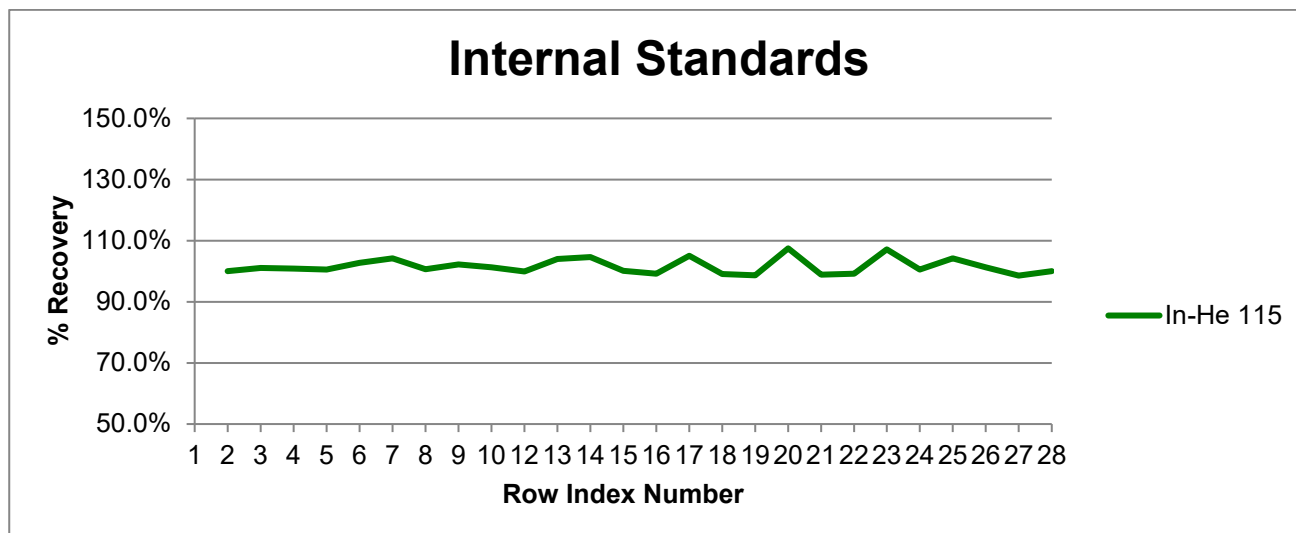


Figure 3.1.22 | Internal standard (Indium) recovery indicates a uniform acid matrix across all samples.

Conclusion

Of a maximum 79.42 mg HgCl_2 with 69.42 mg as Hg^{2+} (6,942 ppm in 10 mL water) bound to the mercury chloride treated polysulfide, an average of 0.57 ppb leached into milliQ water over 24 hours. Of a maximum 2.16 mg Hg (216 ppm in 10 mL water) bound to the elemental mercury treated polysulfide, an average of 46.99 ppb leached into milliQ water over 24 hours. This could potentially be due to the difficulty in separating residual elemental Hg from the polysulfide after reacting the two together to form the treated polymer, resulting in residual unreacted Hg.

Mercury flour simulation

Introduction

The process of ASGM produces multiple waste streams, the most difficult to tackle is the product of mercury beads struck into ore and soil formed during the amalgamation procedure. This material is very difficult to separate into its component parts and is commonly lost in mine tailings, floating off on the surface of waste streams. This leads to significant loss of gold and further environmental pollution as mercury too is lost, beaten into the dirt and milled ore. The tainted ore lost this way is referred to as mercury flour¹. We proposed to simulate the formation of this material by spinning elemental mercury with fine dirt and then treating the contaminated dirt with canola oil polysulfide. Both soil and polymer will be tested for traces of Hg by SEM/EDX analysis before and after treatment.

Results

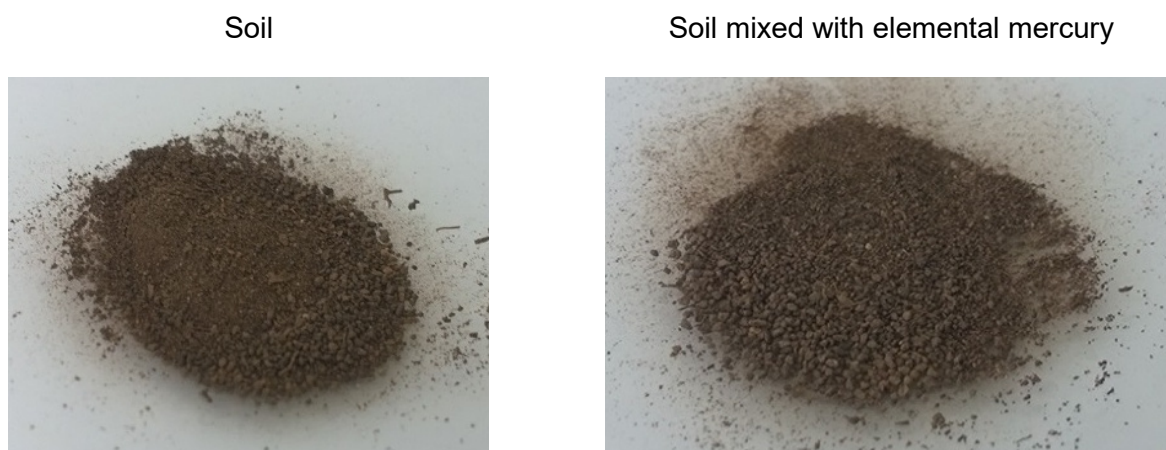


Figure 3.1.23 | Soil mixed with mercury appears no different to the eye than soil without mercury.

SEM and EDX analysis of simulated mercury flour

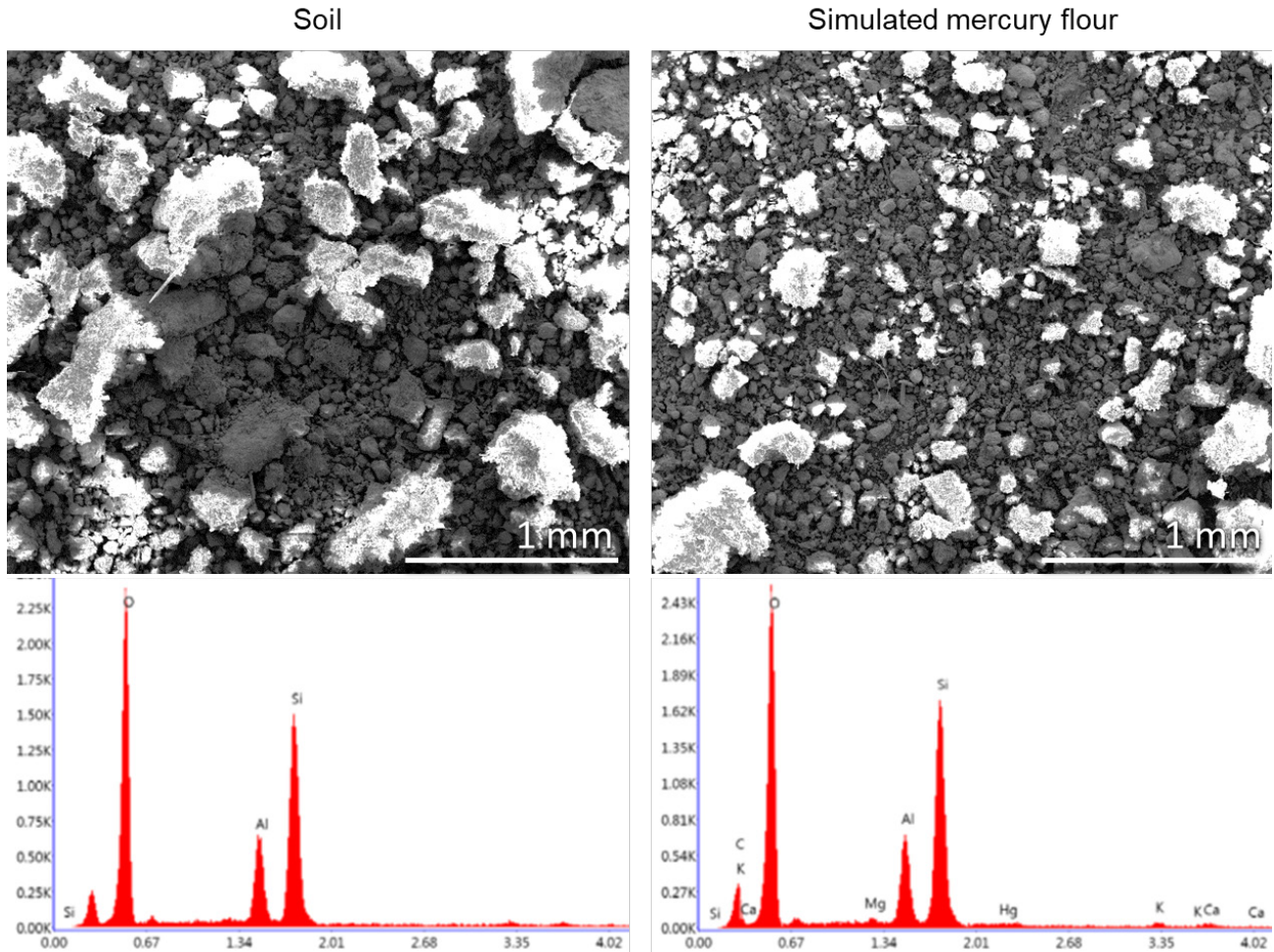


Figure 3.1.24 | In a cursory SEM and EDS scan, it is difficult to detect mercury in the simulated mercury flour. Left: Soil sieved to fine particles no greater than 0.50 mm in diameter. Right: EDX scans over an area approximately 10 mm² did not return a clear indication of mercury due to the formation of mercury microspheres that are difficult to detect.

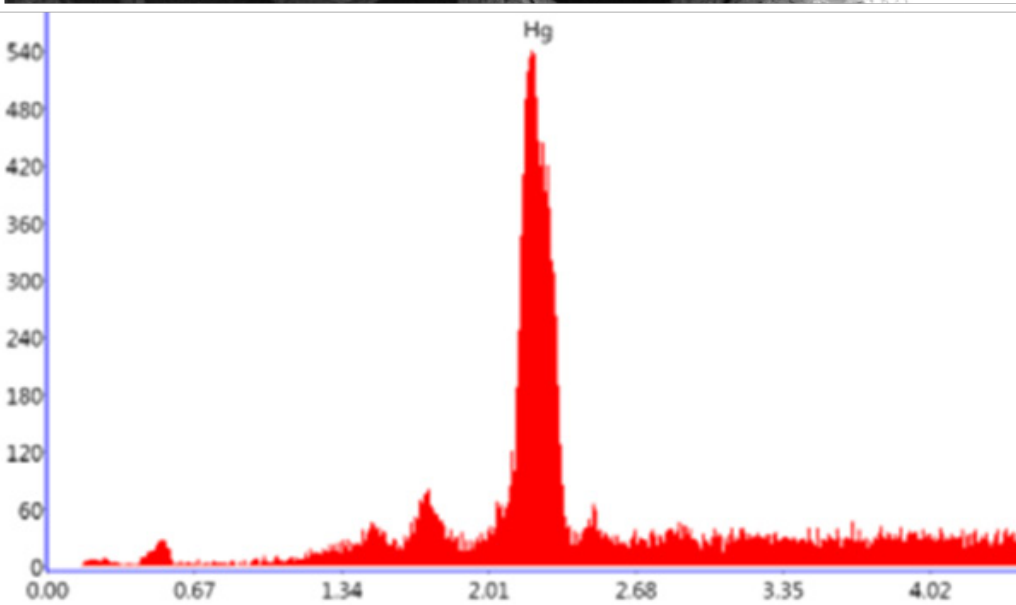
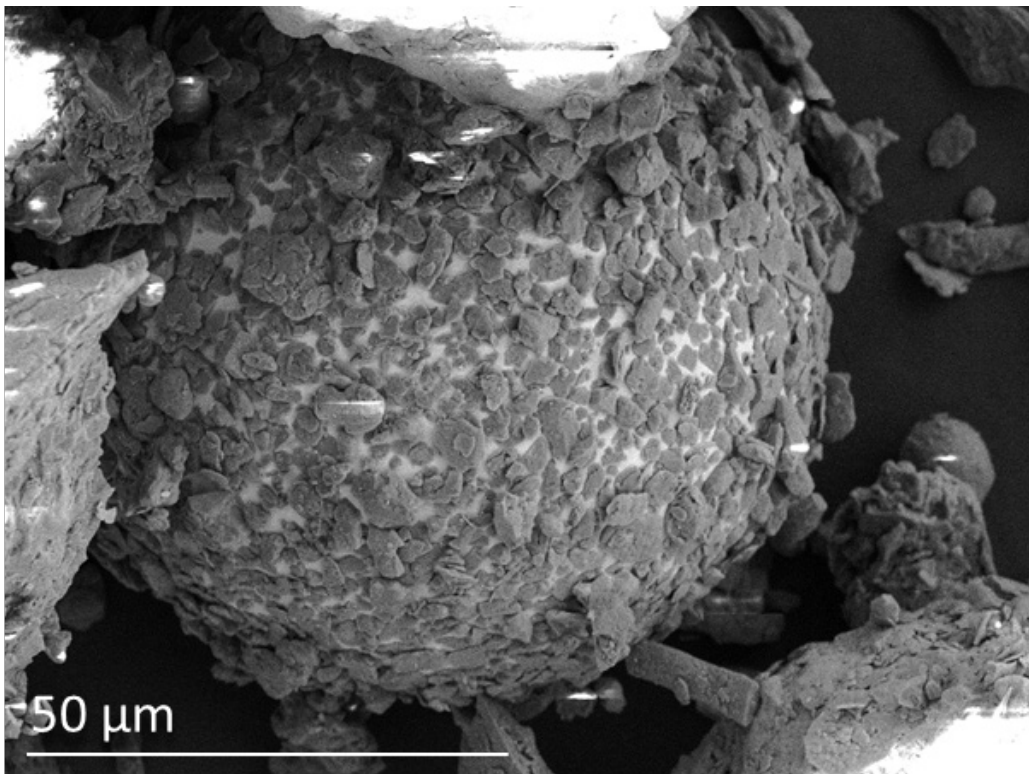


Figure 3.1.25 | SEM and EDS analysis of mercury flour. After thorough searching, mercury was detected as microspheres dispersed in the soil. This floured mercury is covered in micro- and nano-particles of soil. The soil prevents the mercury from coalescing.

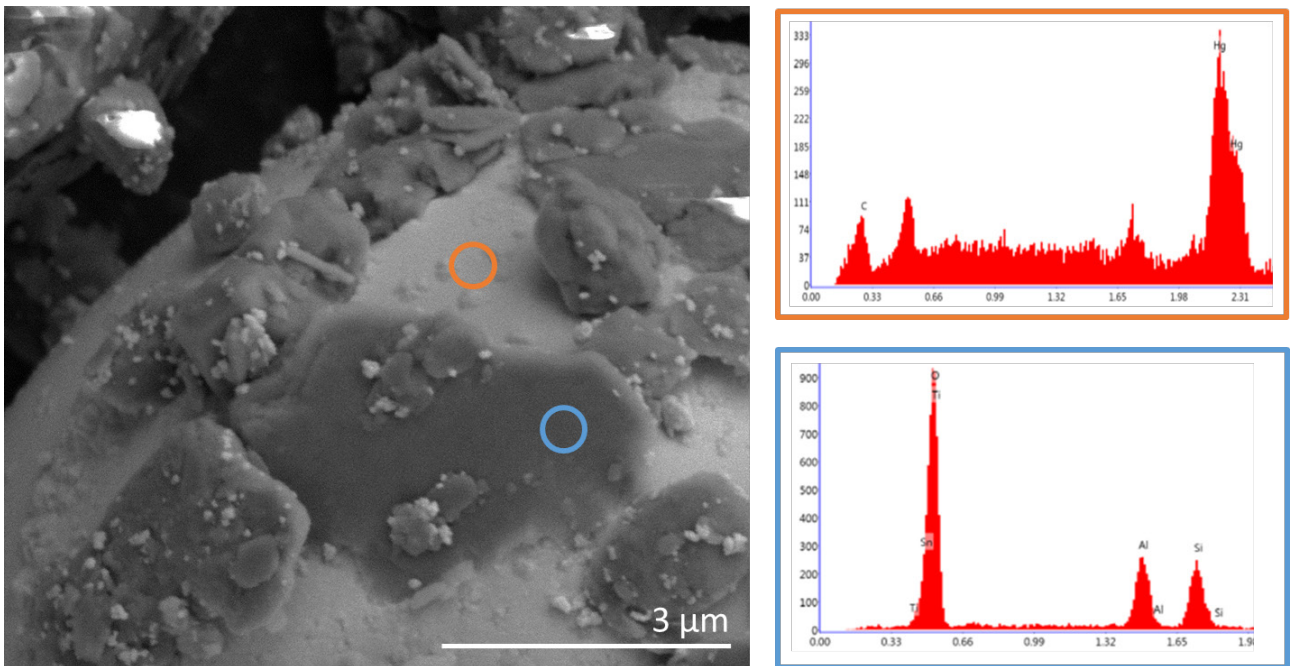


Figure 3.1.26 | SEM and EDS analysis of mercury flour. The SEM image reveals micro- and nano-particles of soil adhering to the surface of the mercury microsphere. Orange: Microparticle of mercury, coated in nanoscale soil particles. Blue: Soil particle, adsorbed to the surface of a mercury microparticle.

Capturing mercury flour using the non-porous canola oil polysulfide

5.0 g canola oil polysulfide (50 % sulfur) of a particle range of 2.5 – 5.0 mm was isolated using a sieve. These particles were added to 5.0 g of the simulated mercury flour and mixed in a 50 mL centrifuge tube on an end-over-end mixer for 24 hours. A control sample treated identically but without the addition of mercury was also prepared for comparison. Over this time, the polymer in the presence of mercury turned black, indicating reaction with the mercury flour. The polymer in the soil in which no mercury was added remained brown. The polymer particles were then separated from the bulk of the soil using a sieve. EDS analysis clearly indicated that mercury was bound to the polymer. This experiment demonstrates that the canola oil polysulfide, prepared as a particle, can capture mercury from soil and then be isolated using a sieve.

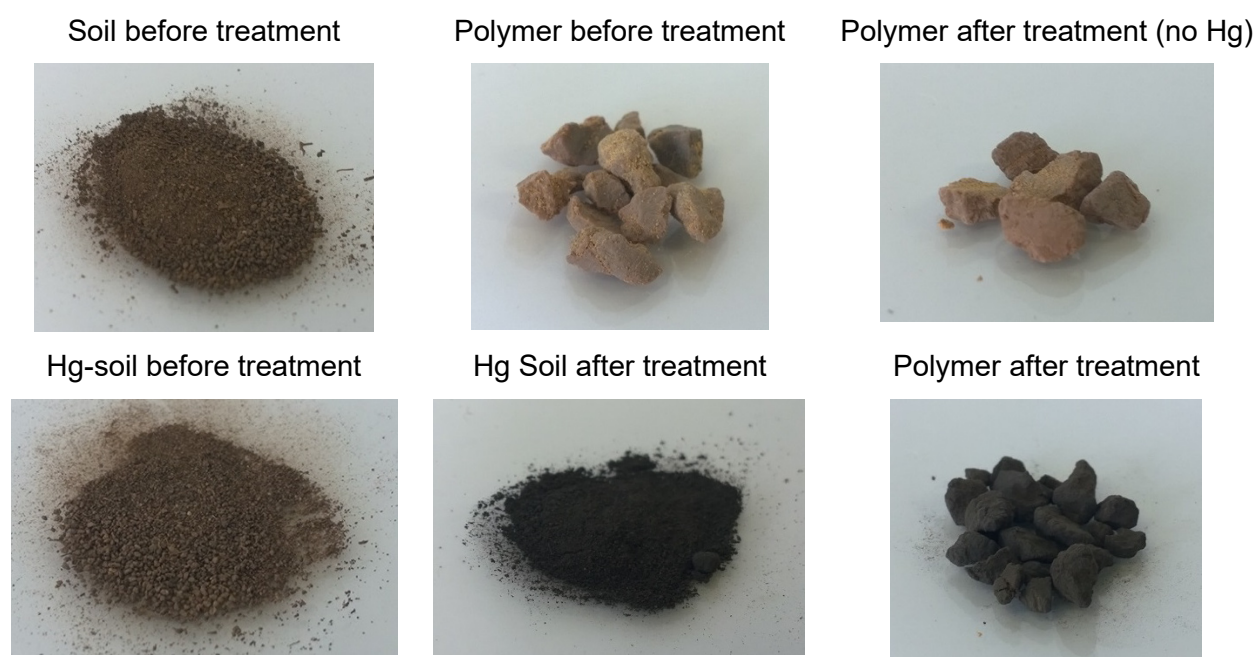
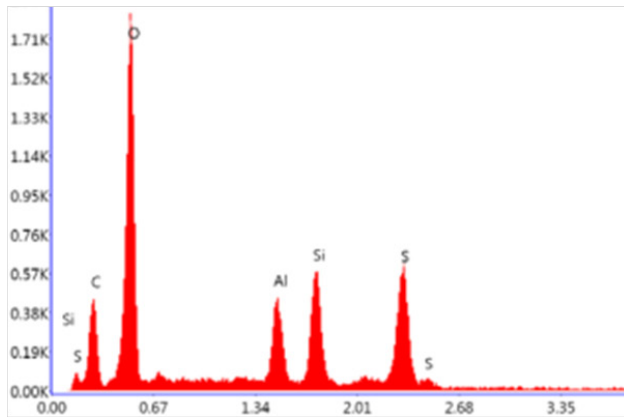
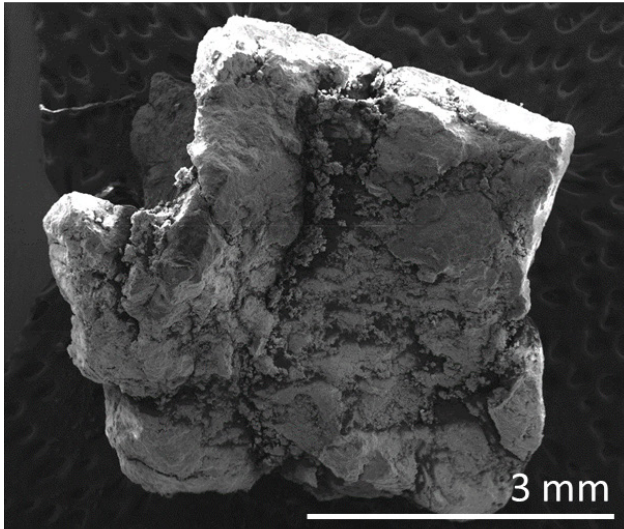


Figure 3.1.27 | Mixing polysulfide with soil containing mercury results in a colour change in the polymer from brown to black, indicating mercury capture and HgS formation. The soil also changes colour to black during this process, as fine particles of polymer that has reacted with mercury are mixed throughout and difficult to recover by separating by particle size. Mixing soil containing no mercury with the polysulfide results in no colour change to the polymer or soil.

Polysulfide isolated from soil with no mercury (control)



Polysulfide isolated from simulated mercury flour

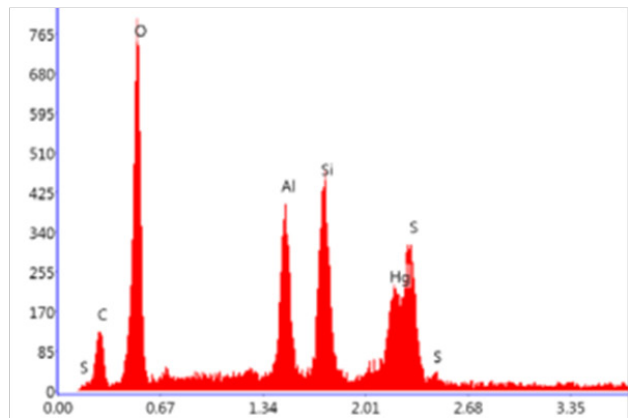
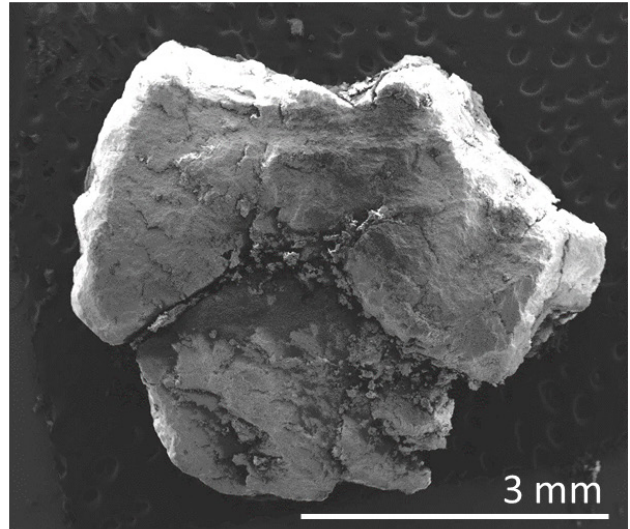


Figure 3.1.28 | Left: Polymer mixed with soil for 24 hours and separated by sieving and washed with 3×10 mL water to remove some of the soil particles.. Right: Polymer mixed with simulated mercury flour, separated by sieving and washed with 3×10 mL water to remove some of the soil particles. For both, the upper image is an SEM micrograph, the lower an EDX spectra from an area of the imaged polymer particle. The canola oil polysulfide reacts with mercury flour. SEM and EDS analysis of the particles isolated from the soil after treatment are shown. The particle isolated from the mercury flour clearly trapped mercury.

Mercury flour leaching by ICP-MS

Soil from the author's garden in Glenalta, SA was crushed and run through a 0.5 mm gauge sieve to achieve a fine particle size. Aliquots of 5.0 g each were distributed among three 50 mL centrifuge tubes. To two tubes, approximately 200 mg elemental mercury was added. All centrifuge tubes were rotated on a lab rotisserie (30 rpm) for 3 days to ensure thorough mixing. After this time, 5.0 g of polysulfide (0.5–1.0 mm diameter particles, 50 wt. % sulfur) was added to one of the tubes containing elemental mercury and all centrifuge tubes were rotated again for 3 days. 20 mL pure milliQ water was added to each sample and left to incubate for 24 hours. 5 mL of each sample was filtered through a 20 µm filter to remove excess soil and polymer. All samples were prepared in duplicate. All samples were diluted 100-fold in a 1 % HNO₃ and 1 % HCl in water matrix and run in KED mode against calibration standards prepared from a stock solution of Hg in 2 % HNO₃ (diluted with a 1 % HNO₃ and 1 % HCl water matrix).

Calibration curve

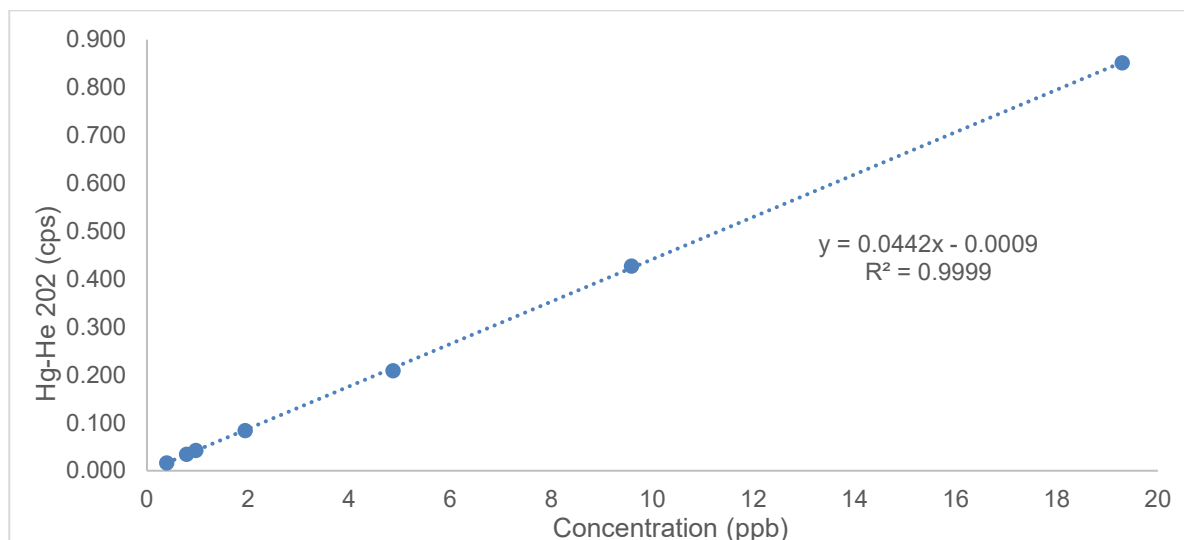


Figure 3.1.29 | Calibration standards display a linear relationship with high confidence

Internal Standard Recovery (Matrix Effects)

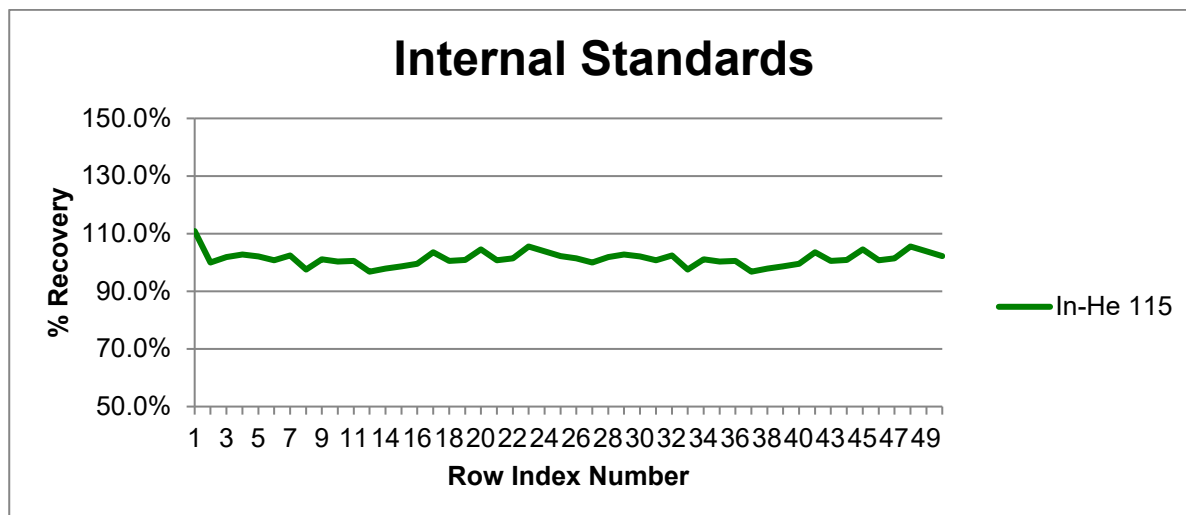


Figure 3.1.30 | Internal standard (Indium) recovery indicates a uniform acid matrix across all samples.

Results

Note: Polysulfide sample did not turn black (indicating binding to mercury) as expected.

Sample	Conc. Hg (ppb)	Description
Mercury flour, polymer treated (1)	583.4	Water incubated in Soil, mixed with mercury for 3 days, then mixed with polysulfide for 3 days.
Mercury flour, polymer treated (2)	558.4	Water incubated in Soil, mixed with mercury for 3 days, then mixed with polysulfide for 3 days.
Average	570.9	
Mercury flour (1)	68.85	Water incubated in Soil, mixed with mercury for 3 days.
Mercury flour (2)	89.50	Water incubated in Soil, mixed with mercury for 3 days.
Average	79.18	
Soil (1)	0.607	Water incubated in Soil.
Soil (2)	0.644	Water incubated in Soil.
Average	0.626	

Sample	Hg ⁰ (g)	Maximum possible Hg ⁰ concentration (ppb)	Measured Hg ⁰ concentration (ppb)	Percentage Leached
Mercury-laden soil, polymer treated (1)	0.2219	11,040	583.4	5.28%
Mercury-laden soil, polymer treated (2)	0.1865	9,295	558.4	6.01%
Average				5.65%
Mercury-laden soil (1)	0.3499	17,469	68.85	0.39%
Mercury-laden soil (2)	0.2497	12,495	89.50	0.72%
Average				0.56%
Soil (control) (1)	0	0	0.607	-
Soil (control) (2)	0	0	0.644	-

Spike Recovery (QC)

Samples were diluted 1/10 and spiked with 0.050 mL 100 ppb Hg stock (5 ppb mercury). The solution was then made up to volume with 1% HNO₃ and 1% HCl in water. Values below have been multiplied by 10 to account for the 1/10 dilution.

Sample	Spike conc. (ppb)	Sample conc. (ppb)	Measured conc. (ppb)	Expected conc. (ppb)	Recovery
Mercury flour, polymer treated spike	4.782	0.572	5.269	5.355	98.41%
Mercury-laden soil spike	4.796	0.0670	4.696	4.863	96.56%
Soil (control) spike	4.854	0.0006	4.690	4.855	96.61%

Conclusion

With the inclusion of polysulfide, more mercury was found to leach from mercury-laden soil and into the incubation water than without. As the polysulfide has previously shown to bind to elemental mercury bound within soil, this was an unexpected result. This may be explained in the reaction mechanism that binds mercury to the polysulfide. Oxidation of elemental mercury, followed by oxidative addition into the polysulfide domains of the polymer may not occur in one concerted step, with oxidated Hg²⁺ being lost into the incubation medium before having a chance to bind to the polysulfide. This may explain why, by ICP-MS, far more (an average of 570.9 ppb versus an average of 0.0670 ppb mercury) leached from the polymer treated sample than the untreated mercury-laden soil sample.

Raman

Raman spectra acquired by Christopher Gibson

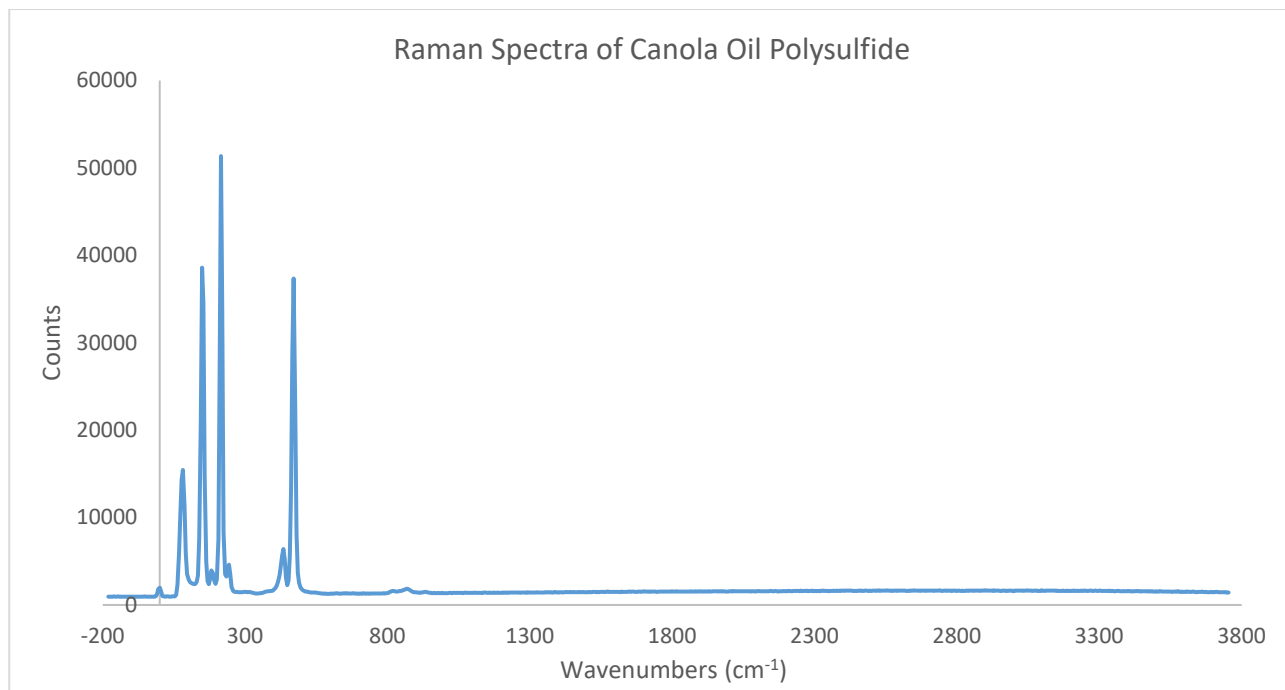


Figure 3.1.31 | Raman spectra of Canola Oil Polysulfide

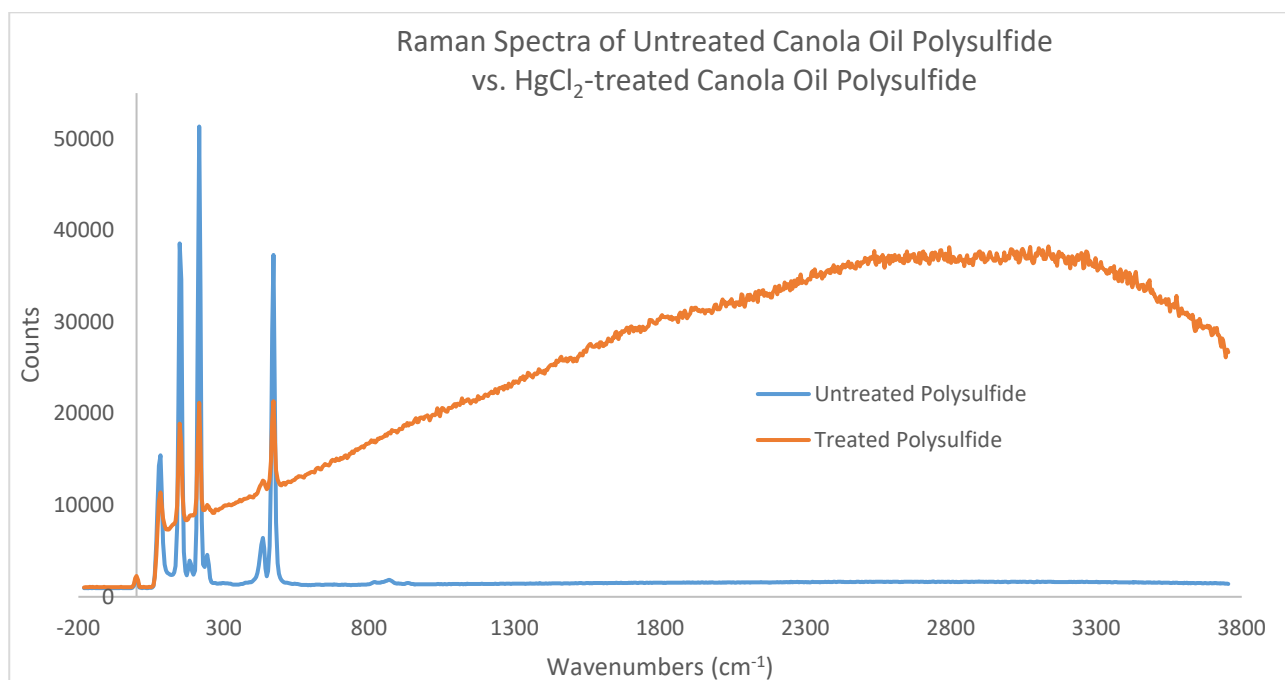


Figure 3.1.32 | Raman spectra of HgCl₂-treated canola oil polysulfide overlaid on spectra of untreated sample.

Raman analysis shows stretches at 343 cm⁻¹ and 471 cm⁻¹, consistent with S-S stretching modes, consistent with a polysulfide material. After treatment with HgCl₂, fluorescence is present across the whole spectrum.

Mercury vapour experiments using the porous canola oil polysulfide

Hg⁰ vapour tests performed by Deshetti Jampaiah, Ylias Sabri and Suresh Bhargava.

Hg⁰ removal tests were performed using a fixed bed-reactor as shown in Fig. 3.1.33. The inlet Hg⁰ vapour was generated using a mercury permeation device (VICI metronics), which was operated at 60 °C. The porous canola oil polysulfide (300 mg) was placed in the quartz glass reactor (1 cm internal diameter), occupying a volume of approximately 0.4 cm³. N₂ gas with a flow rate of 0.1 L min⁻¹, which contained 586.4 µg Nm⁻³ Hg⁰, was introduced to the reactor using mass flow controllers. At this volume of sorbent and flow rate, the residence time is 0.24 seconds—a challenging test for the polysulfide sorbent. All elemental and oxidised mercury exiting the reactor were measured quantitatively using a modified Ontario Hydro Method (OHM), in which KCl (0.01 M) and KMnO₄/H₂SO₄ (20 mg L⁻¹) impinger solutions were used in the train of traps as mercury absorbing media. Elemental mercury (Hg⁰) is captured by the KMnO₄ solution, whereas any oxidised mercury (Hg₂⁺) is trapped by the KCl solution. The remaining adsorbed mercury was retained on the canola oil polysulfide. Cold vapour atomic fluorescence spectroscopy (CV-AFS) was used to measure the collected Hg from the system after the Hg⁰ removal experiments. In all experiments, the amount of oxidised mercury (Hg₂⁺) collected from the KCl traps was negligible (<< 1% of total Hg). Hg⁰ removal efficiency of material was determined by the following equation:

$$Hg^0 \text{ removal efficiency (\%)} = \frac{Hg_{in}^0 - Hg_{out}^0}{Hg_{in}^0} \times 100 (\%)$$

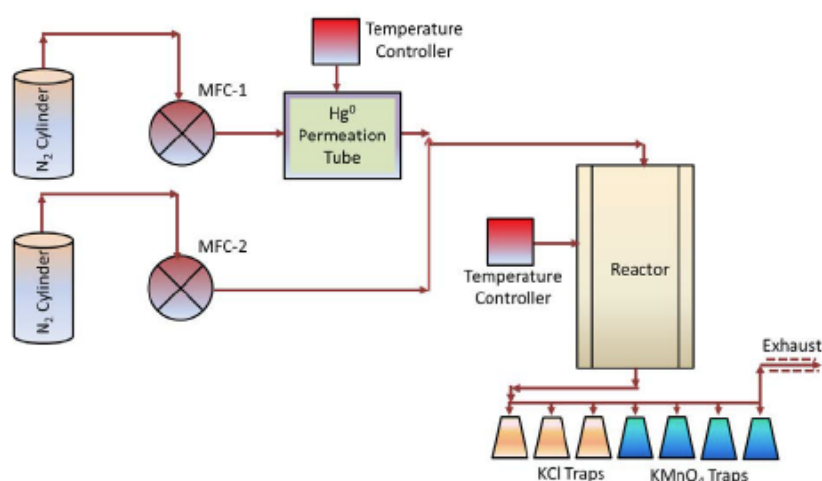


Figure 3.1.33 | Schematic diagram of the experimental setup for testing the canola oil polysulfide as a sorbent for mercury vapour

The effect of operating temperature on mercury removal efficiencies of the developed material was tested by varying the reactor temperature from 25–100 °C. It was hypothesised that the rate of reaction between the mercury vapour and the polysulfide would increase with temperature—a requirement for continuous processes with short residence times such as those in this experiment. It was found that the material had highest Hg^0 removal efficiency of 66.5 % at 75 °C.

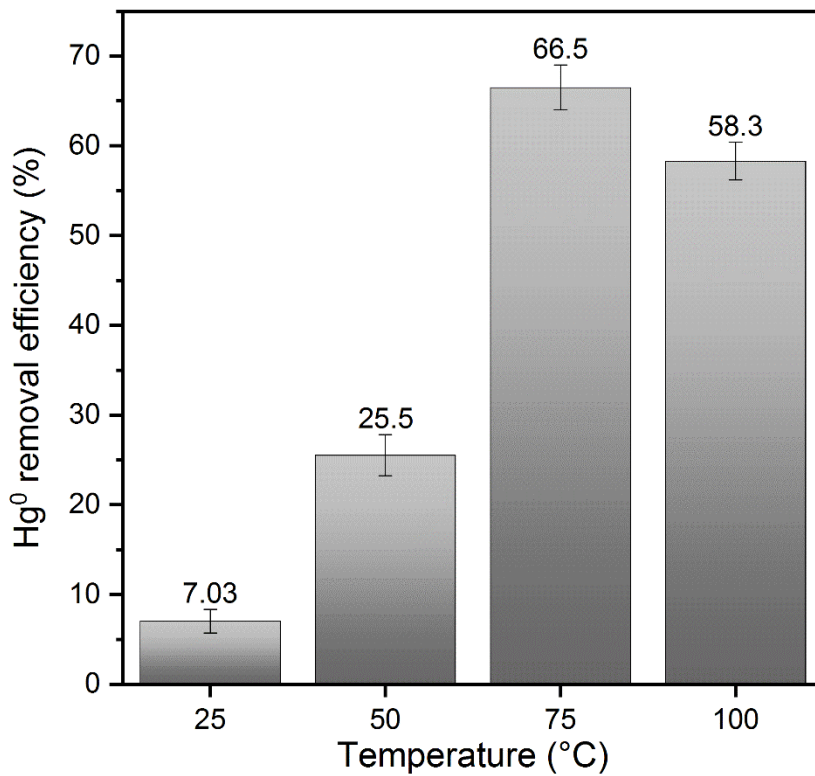


Figure 3.1.34 | 75 °C was found to be an optimal temperature for capturing mercury in a continuous process, with 66.5 % of the mercury removed from the gas stream over a residence time of approximately 0.24 seconds.

Experiments on mercury bound to natural organic matter (NOM)

NOM and sulfate release experiments performed by Katherine Muller and Alexander Johs

Materials and Methods

Mercury speciation can significantly affect reactivity of mercury and its interaction with sorbent materials. The speciation of mercury in aquatic ecosystems is typically dominated by association with natural organic matter (NOM). Suwannee River aquatic natural organic matter (SR-NOM), reference material 2R101N (International Humic Substance Society) and a 1 ppm $\text{Hg}(\text{NO}_3)_2$ standard (Brooks Rand Instruments, Seattle, WA, USA) were used to prepare Hg-NOM complexes containing $40 \mu\text{g L}^{-1}$ Hg and $2400 \mu\text{g L}^{-1}$ total carbon (C_{NOM}) equivalent to a molar Hg: C_{NOM} ratio of 1.8×10^{-5} . SR-NOM was dissolved in 10 mM sodium phosphate buffer (pH 7.8) and filtered through a $0.2 \mu\text{m}$ syringe filter to remove residual particulates. $\text{Hg}(\text{NO}_3)_2$ was added and the pH was re-adjusted to 7.8 and allowed to age at $4 \text{ }^\circ\text{C}$ for at least 5 days. The Hg-NOM stock solution was diluted with 10 mM sodium phosphate buffer to obtain working solutions with Hg concentrations from 0.2 to $7.7 \mu\text{g L}^{-1}$. A dilution series of the 1 ppm $\text{Hg}(\text{NO}_3)_2$ standard in 10 mM sodium phosphate buffer was prepared as an NOM-free control.

Sorption isotherms were determined in triplicate batch experiments by adding 30 mL Hg-NOM complex at Hg concentrations of 0.2, 0.4, 0.7, 1.5, 3.6 and $7.7 \mu\text{g L}^{-1}$ or $\text{Hg}(\text{NO}_3)_2$ in phosphate buffer at concentrations of 0.2, 0.5, 0.8, 1.6, 4.0 and $16 \mu\text{g L}^{-1}$ to 40 mL amber borosilicate glass vials containing approximately 100 mg of canola oil polysulfide (COP), porous COP or partially reduced porous COP after equilibration for 48 hours on a rotary shaker. The suspensions were filtered through a $0.2 \mu\text{m}$ polyethersulfone (Supor[®]) syringe filter for total mercury and sulfate analyses by ion chromatography. To determine Hg equilibrium concentrations, 5 mL of the filtered samples were oxidized by addition of $150 \mu\text{L}$ BrCl. An aliquot of this solution was added to an excess of 20% (w/v) stannous chloride and purged with ultrahigh purity N_2 . The amount of emerging Hg^0 was determined by a cold vapor atomic absorption spectroscopy (CV-AAS) Zeeman effect mercury analyzer (Lumex RA-915+, Ohio Lumex Company, Inc., Twinsburg, OH, USA). The concentration of sorbed Hg was determined by difference between the known initial amount of Hg added and the equilibrium aqueous Hg concentrations, which also included Hg sorbed to the wall of the amber glass vials

Results & Discussion

Within the tested concentration ranges, a linear correlation was obtained for the sorption to all COP variants when Hg was added as $\text{Hg}(\text{NO}_3)_2$. The sorption isotherms with Hg added as Hg-NOM show a nonlinear characteristic, which was approximated by the Langmuir isotherm model. The Langmuir adsorption isotherm assumes monolayer adsorption onto a surface containing a finite number of uniform adsorption sites. The surface reaches a saturation point, where maximum sorption of

adsorbate on a monolayer is reached. The relationship between adsorbed and solution concentrations for the Langmuir isotherm is as follows.

$$Y = \frac{Y_{max} \times K_L \times C_{eq}}{1 + K_L \times C_{eq}}$$

Where Y is the concentration of the adsorbate on the sorbent, Y_{max} is the sorption capacity, C_{eq} is the solution concentration at equilibrium and K_L is the Langmuir adsorption equilibrium constant. The isotherm fits for all COP variants are shown in Fig. 3.1.35. The results show that all tested COP samples removed >90 % of Hg when added as $Hg(NO_3)_2$. The strong complexation of mercury with functional groups on NOM competes with the sorption of Hg to any sorbent, thus presenting a unique challenge for the removal of Hg from contaminated ecosystems. Under the conditions of the isotherm experiments, a dilution series was prepared from a concentrated Hg-NOM stock solution. Thus, the concentration of Hg is coupled the concentration of NOM. In a freshwater creek ecosystem, the level of NOM can span a wide range of concentrations, while the level of Hg typically corresponds to the low end of the experimental range, even in contaminated systems². Efficient removal of Hg from solutions containing strong Hg-NOM complexes is achievable as it is determined by the sorbent to solution ratio and the concentration of Hg-NOM. A measure of how efficient the sorbent can remove the contaminant at a specific concentration can be obtained as follows:

$$R(\%) = \frac{C_0 - C_{eq}}{C_0} \times 100$$

Where R is the removal efficiency, C_0 is the initial Hg concentration and C_{eq} is the Hg concentration after equilibration with the sorbent. Surface modification of canola polysulfide had a significant impact on Hg removal, with the higher surface area of the porous versions significantly improving removal efficiency. At the lowest initial Hg-NOM concentrations ($0.2 \mu g L^{-1}$ Hg) and a sorbent to solution ratio of 1/300, R was 36 % for non-porous canola oil polysulfide, 79 % for porous canola oil polysulfide, and 81 % for the partially reduced porous polysulfide. The results show that the surface modification of COP, particularly the increased surface area in porous COP, results in a highly effective sorbent which can sorb Hg in the presence of competing ligands such as NOM.

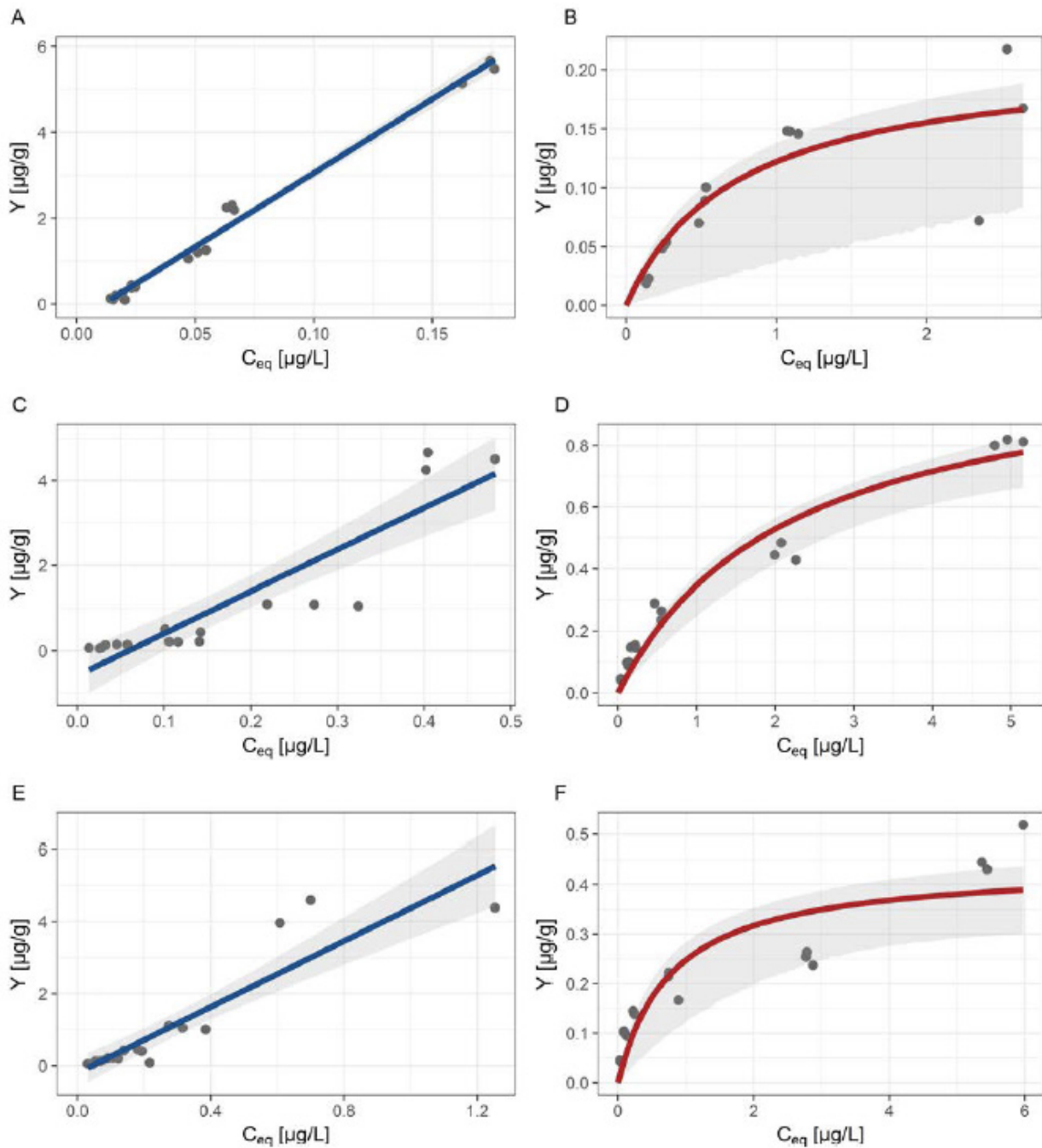


Figure 3.1.35 | Equilibrium sorption data (dots) and fits to isotherm models for the sorption of Hg at low mercury concentrations. 95% confidence bands are shown in gray. A. Unmodified COP with Hg added as $\text{Hg}(\text{NO}_3)_2$ and linear fit (blue), residual standard error of the fit: $0.21 \mu\text{g g}^{-1}$; B. Unmodified COP with Hg added as Hg-NOM complex and model fit to the Langmuir isotherm model (red). Langmuir fit parameters: $K_L = 1.35 \text{ L } \mu\text{g}^{-1}$, $Y_{max} = 0.21 \mu\text{g g}^{-1}$, residual standard error of the fit: $0.032 \mu\text{g g}^{-1}$; C. Porous COP with Hg added as $\text{Hg}(\text{NO}_3)_2$ and linear fit (blue), residual standard error of the fit: $0.71 \mu\text{g g}^{-1}$; D. Porous COP with Hg added as Hg-NOM complex and model fit to the Langmuir isotherm model (red). Langmuir fit parameters: $K_L = 0.46 \text{ L } \mu\text{g}^{-1}$, $Y_{max} = 1.11 \mu\text{g g}^{-1}$, residual standard error of the fit: $0.061 \mu\text{g g}^{-1}$; E. Partially reduced porous COP with Hg added as $\text{Hg}(\text{NO}_3)_2$ and linear fit (blue), residual standard error of the fit: $0.65 \mu\text{g g}^{-1}$; F. Partially reduced porous COP

with Hg added as Hg-NOM complex and model fit to the Langmuir isotherm model (red). Langmuir fit parameters: $K_L = 1.29 \text{ L } \mu\text{g}^{-1}$, $Y_{max} = 0.44 \text{ } \mu\text{g g}^{-1}$, residual standard error of the fit: $0.065 \text{ } \mu\text{g g}^{-1}$.

Sulfate release from the porous canola oil polysulfide

High sulfate concentrations in low oxygen subsurface environments can result in increased production of methylmercury. Sulfate-reducing bacteria have been associated with mercury methylation and are considered the primary methylators in marine and estuarine environments^{3,4}. We therefore determined sulfate concentrations in solutions obtained from batch sorption studies (see Fig. 3.1.36). Briefly, 30 mL Hg-NOM complex dissolved in 10 mM sodium phosphate buffer (pH 7.8) at various concentrations were added to amber glass vials containing approximately 100 mg of canola oil polysulfide and equilibrated for 48 hours on a rotary shaker. The solid to solution ratio was constant for all samples. Sulfate concentrations were determined by ion chromatography with a Dionex ICS 2100 AS9HC9 (Dionex Instruments Corporation, Sunnyvale, CA, USA) from filtered sample solutions using 9 mM K_2CO_3 as the eluent. The amount of sulfate released was normalised to the mass of the polysulfide for each sample. The amount of sulfate released correlated with the concentration of Hg-NOM initially added to the sample (Fig. 3.1.36). In the absence NOM, sulfate concentrations were typically $<100 \text{ } \mu\text{g}$ per g of sorbent. For samples containing NOM, the sulfate concentration was proportional to the NOM concentration.

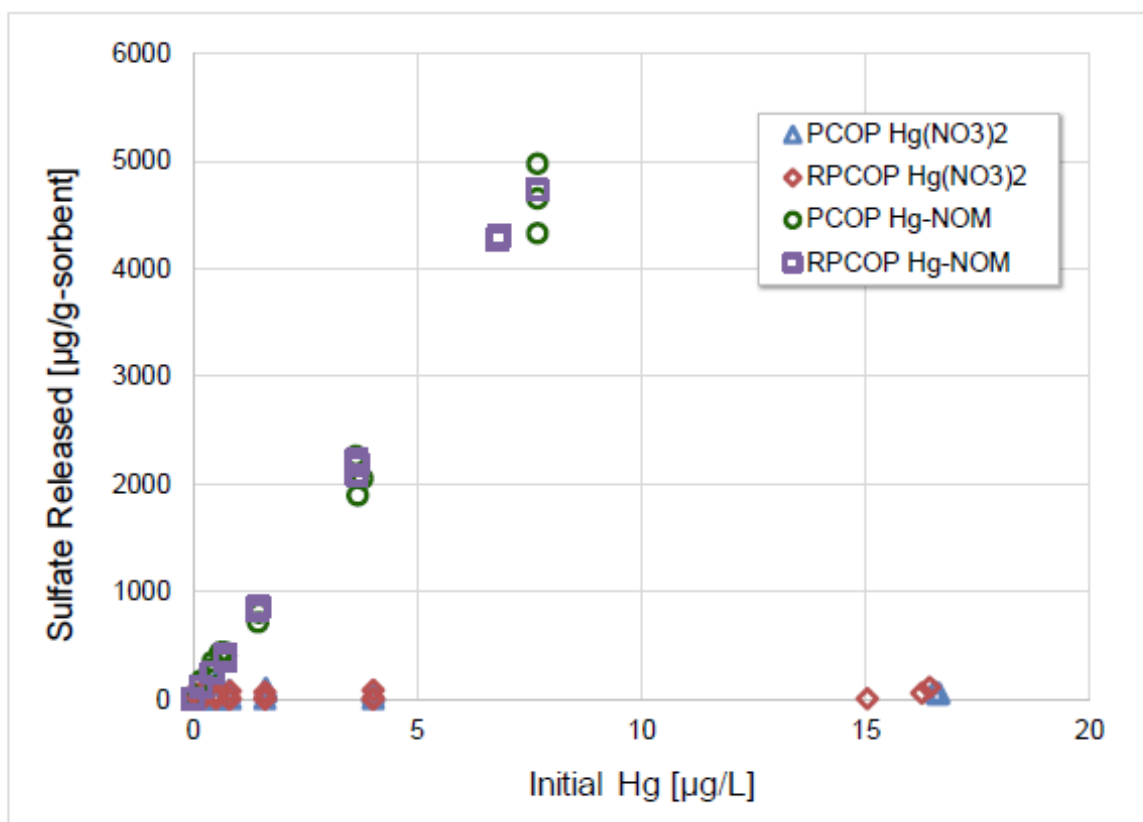


Figure 3.1.36 | Sulfate concentrations normalized to mass of sorbent in 48 h batch equilibrium experiments for porous canola oil polysulfide (PCOP) and the partially reduced porous canola oil polysulfide (RPCOP).

MEMC Fungicide ICPMS Experiment

Method

2.00 g porous canola oil polysulfide was incubated with 10 mL MEMC fungicide diluted to a typical operating concentration (0.15 g L^{-1} Hg as methoxyethyl mercuric chloride) for 24 hours. Commercial MEMC contains a pink dye as a visual indicator of spillage and contamination, even after the 800-fold dilution down to working concentration the colour is quite pronounced (Fig. 3.1.17). During the incubation however, after just 4 hours the solution had become clear, indicating perhaps that the polysulfide had sequestered the dye from solution – an unexpected side effect. Notably during and after incubation the polysulfide itself did not change colour, remaining light-brown. This is in line with previous experiments with lower concentrations of mercury, but also shows the dye has not simply bound to the surface but somehow has become inactive (colourless).



Figure 3.1.37 | Photo of samples after 24 hour incubation. Left to right: MEMC after treatment with polysulfide, MEMC, polysulfide.

Samples were diluted 100,000 fold in a 2 % HNO_3 acid matrix and analysed for Hg content on a Perkin Elmer NexION ICPMS in KED mode (Flinders Analytical, South Australia). Calibration standards were prepared from a stock solution of 1,000 ppm Hg in 2 % HNO_3 (Chem-Supply, South Australia).

Results

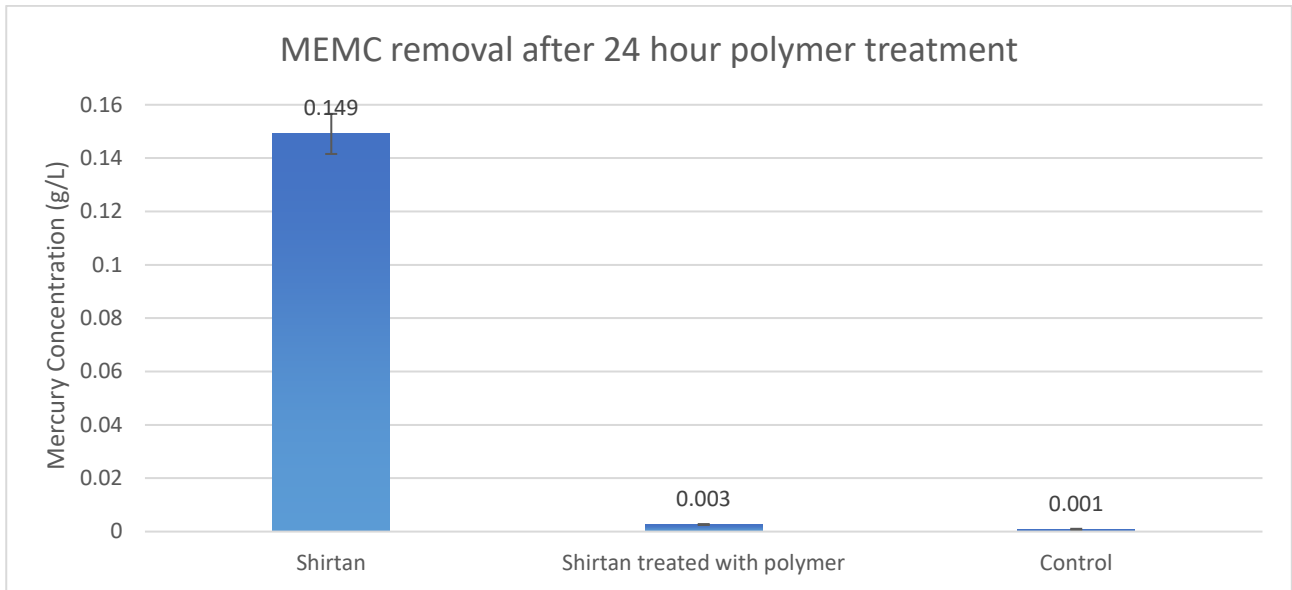


Figure 3.1.38 | Hg concentration as measured by ICPMS, averages of triplicate samples.

After incubation with porous polysulfide (0.20 g per mL MEMC), the Hg concentration in MEMC fungicide was significantly reduced. Treated samples contained only 2.0 % of the mercury present in the untreated samples on average.

Quality Control - Calibration Curve

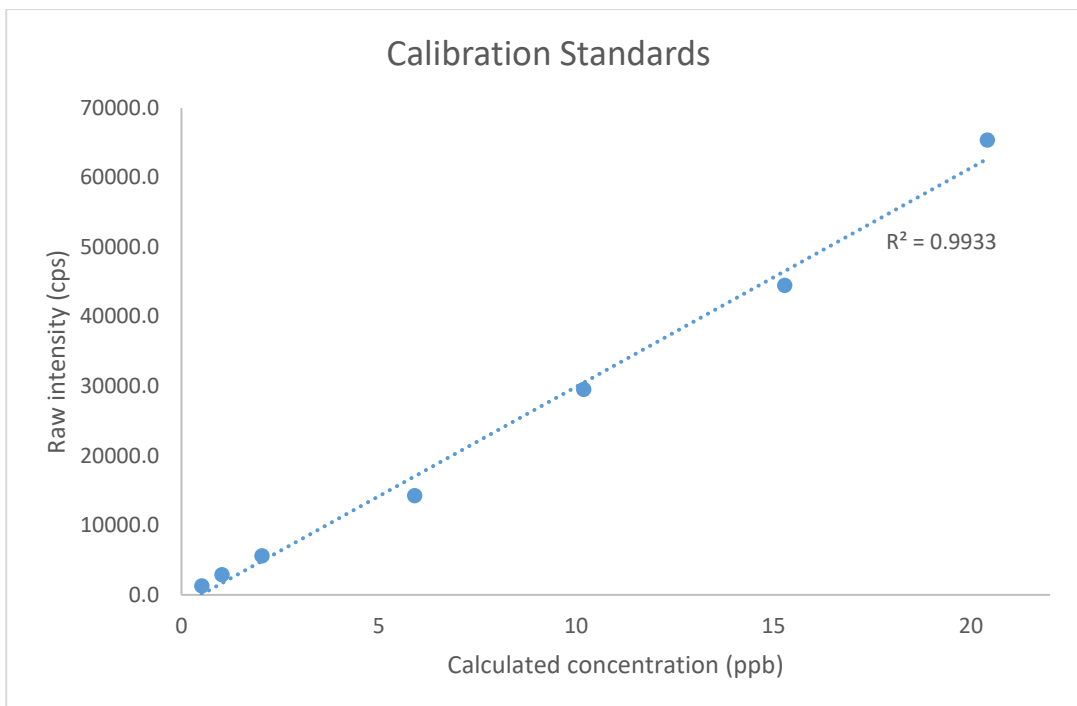


Figure 3.1.39 | Calibration standards graphed as raw detector intensity against prepared Hg concentration

Internal Standard (Matrix effects, sampling consistency)

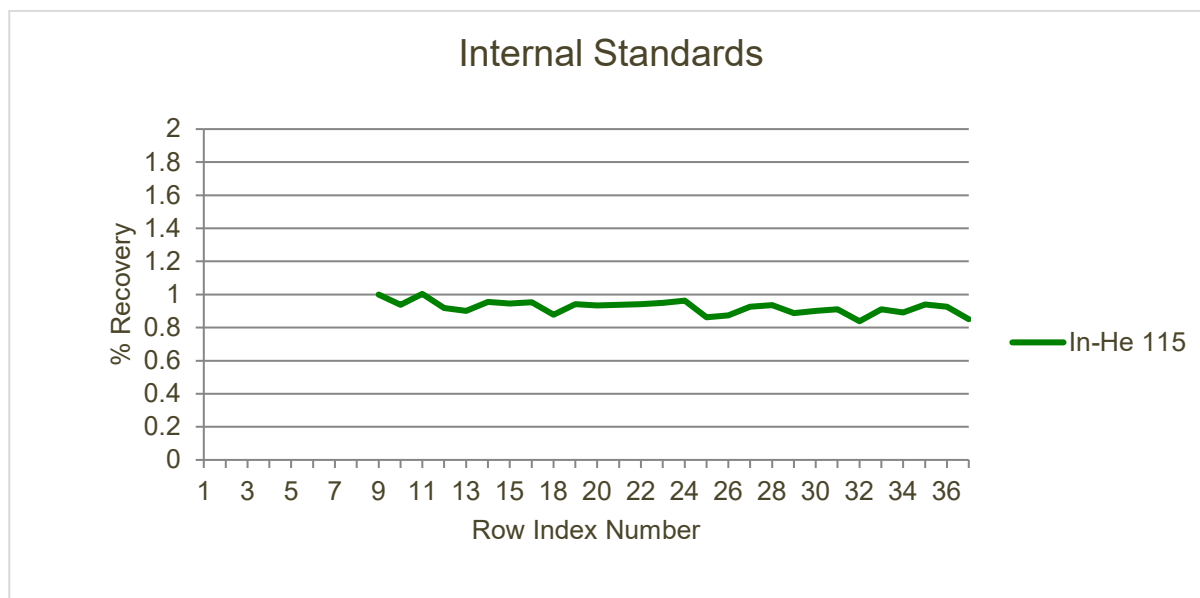


Figure 3.1.40 | Internal standard (indium) recovery – fluctuations in concentration generally remained consistent between 90 and 100%, indicating Hg readings may also have drifted similarly. This drift is taken into consideration when reporting concentrations by the ICP-MS Syngistix software package.

Spike Recovery

Sample	Conc. from sample (ppb)	Conc. from spike (ppb)	Total conc. (ppb)	Measured conc. (ppb)	Recovery
Treated	0.135	4.968	5.103	4.186	82.02 %
Untreated	6.923	5.072	11.996	12.418	103.52 %
Control	0.055	5.083	5.138	4.271	83.12 %

Samples were spiked with a known concentration of Hg from a calibration standard and the calculated and measured concentrations compared to determine the recovery. For the untreated MEMC sample containing a higher concentration of mercury, only a 3.52 % difference is observed. In the samples containing less mercury however the difference is as high as 17.98 %. This may in part be due to inaccuracies in measuring very small masses, only 50 mg of sample was used in each case.

Polysulfide Column - Shirtan Fungicide ICPMS Experiment

Method

4 syringe columns were prepared containing a) 3.00 g soil b) 1.50 g soil and 1.50 g porous canola oil polysulfide (polymer) mixed together c) 1.50 g soil and 1.50 g polymer separated into layers by cotton wool and d) 3.00 g polymer. Syringes were prepared in triplicate. To each column, 3 mL MEMC fungicide at operating concentration (0.15 g L^{-1} Hg as methoxyethyl mercuric chloride) was carefully pipetted into the opening and allowed to soak for 2 minutes. After this time the syringe plunger was used to force elution of the solution over 30 seconds. In the case of the soil sample, solution soaked into the column by gravity. For the sample containing the hydrophobic polymer however, slight pressure (from the syringe plunger) was applied in order to saturate the column. MEMC fungicide solutions that had passed through polymer appeared a paler pink than the intensely coloured solution at operating concentration. The solution that had only passed through soil remained strongly coloured.



Figure 3.1.42 | Photo of columns before use. Left to right: Soil only, soil and polymer mixed together, soil and polymer layered with cotton wool, polymer only.

Samples were diluted 100,000 fold in a 2 % HNO_3 acid matrix and analysed for Hg content on a Perkin Elmer NexION ICPMS in KED mode (Flinders Analytical, South Australia). Calibration standards were prepared from a stock solution of 1,000 ppm Hg in 2 % HNO_3 (Chem-Supply, South Australia).

Results

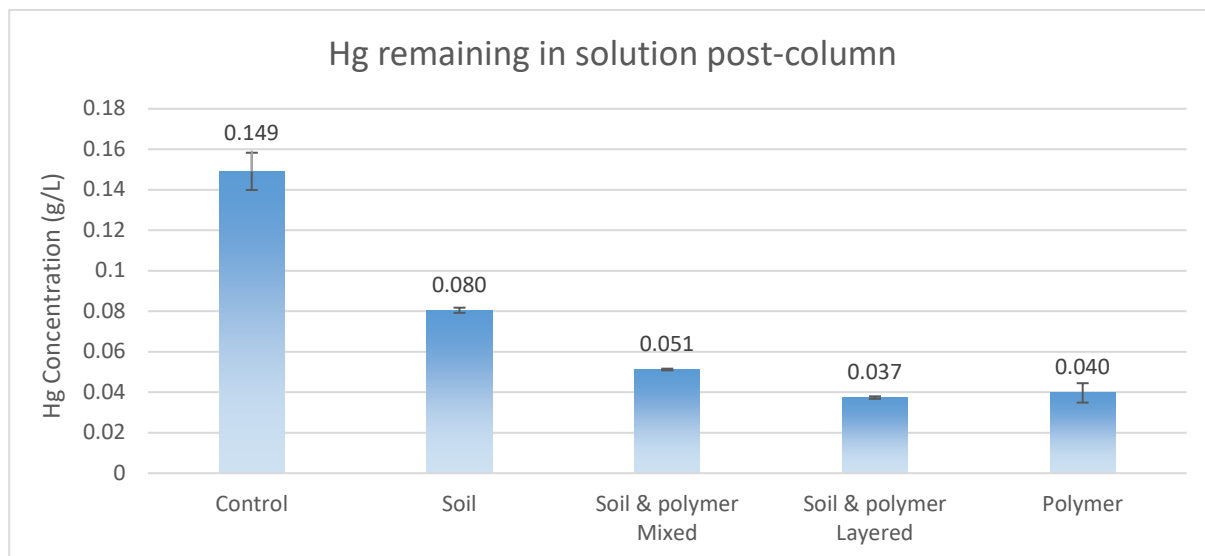


Figure 3.1.43 | Hg concentration after passing through soil and/or polymer columns as measured by ICP-MS.

After passing through the column, mercury concentration had decreased in all samples. With only soil in the column, only 54.0 % of the initial mercury remained. This number is improved however by the presence of the polymer, where a mixture of soil and polymer leaves only 34.4 % of mercury. Where the solution is forced to pass directly through polymer this value is decreased again, with a soil; polymer layered mixture and a column of only polymer leaving 25.1 % and 26.6 % mercury respectively: A single 2 minute pass at a ratio of 1 g polymer per 1 mL MEMC fungicide at operating concentration (0.15 g L^{-1}) removed 73.4 % mercury.

Quality Control

Calibration Curve

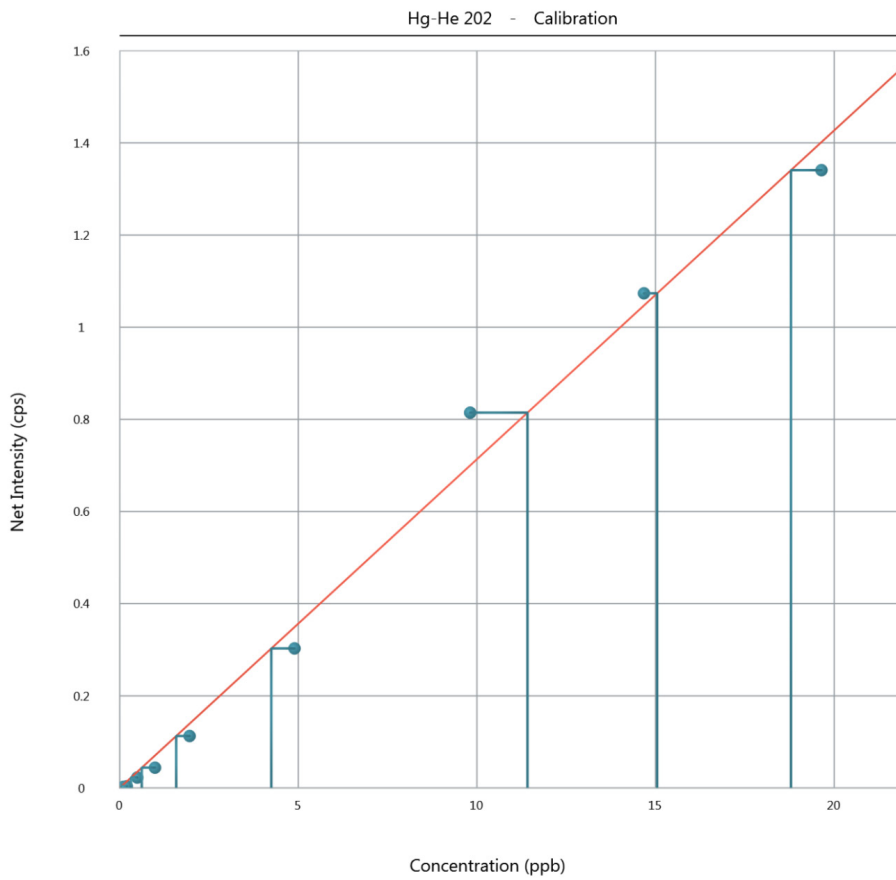


Figure 3.1.44 | Calibration standards graphed as detector intensity (counts per second) against prepared Hg concentration (ppb)

Internal Standard (Matrix effects, sampling consistency)

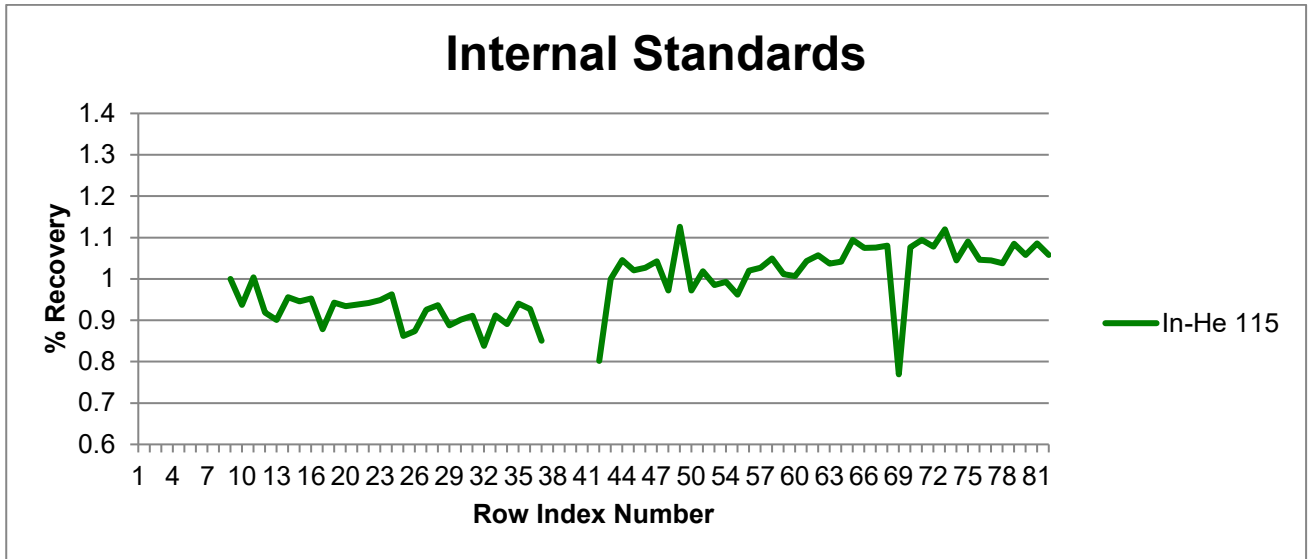
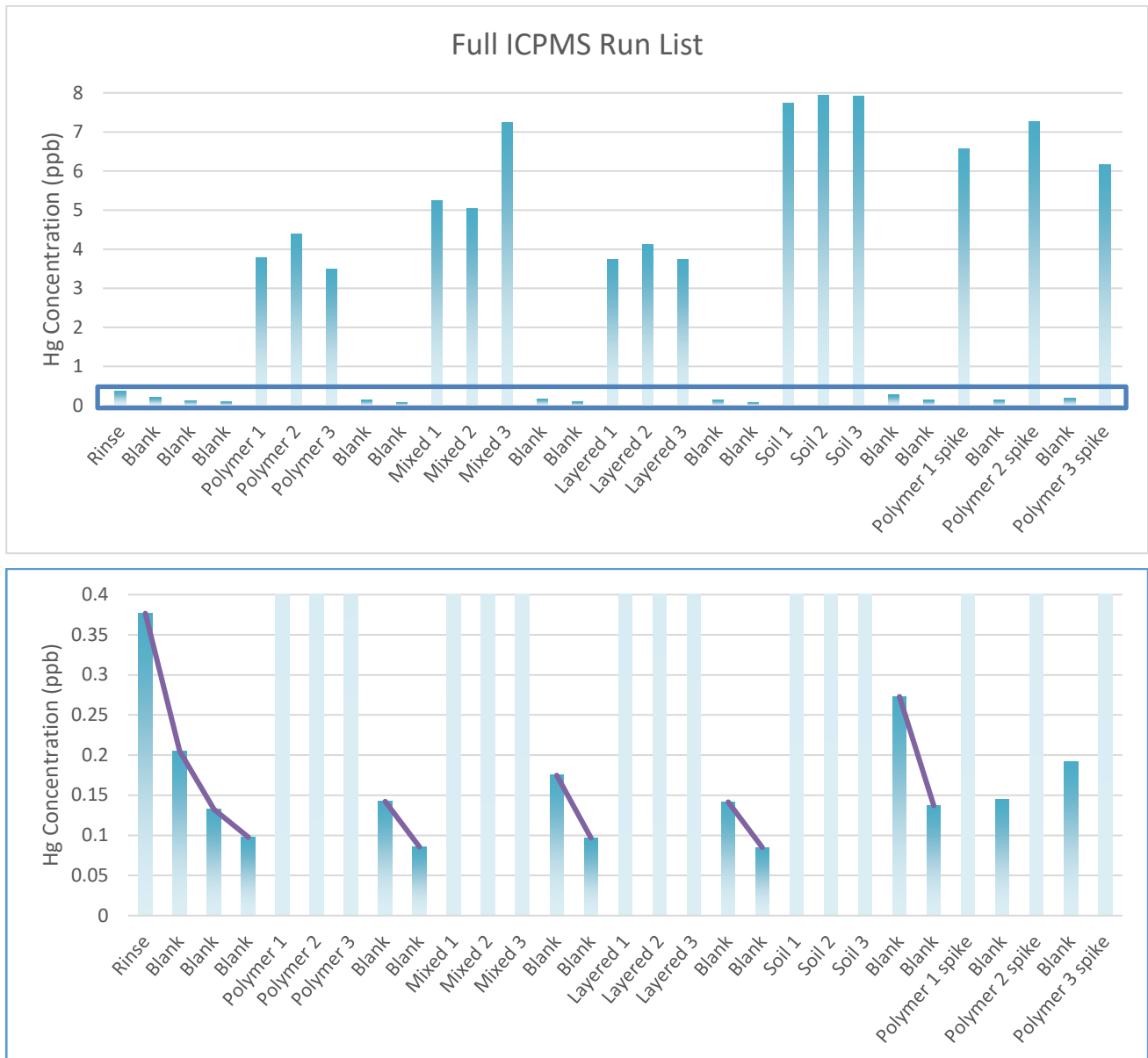


Figure 3.1.45 | Internal standard (indium) recovery – fluctuations in concentration generally remained consistent between 90 and 110 %, indicating Hg readings may also have drifted similarly. This drift is taken into consideration when reporting concentrations by the ICP-MS Syngistix software package. The anomalous sharp drop at sample 69 corresponds to a replicate of “soil and polymer layered” and was not included when calculating averages. Argon bottles were switched during the run, it may have been at this position. This sample was excluded from averaged measurements.

Mercury run-over



References

1. Appel, P. W. U.; Na-Oy, L. D. Mercury-Free Gold Extraction Using Borax for Small-Scale Gold Miners. *J. Environ. Prot.* **2014**, *5*, 493-499.
2. Southworth, G. et al. Sources of mercury in contaminated streams-implications for the timescale of recovery. *Environ. Toxicol. Chem.* **2013**, *32*, 764-772.
3. Gilmour, C.C., Henry, E. A. & Mitchell, R. Sulfate Stimulation of Mercury Methylation in Freshwater Sediments. *Environ. Sci. Technol.* **1992**, *26*, 2281-2287.
4. Fitzgerald, W. F., Lamborg, C. H. & Hammerschmidt, C. R. Marine biogeochemical cycling of mercury. *Chem Rev.* **2007**, *107*, 641-662.

4. SULFUR POLYMERS FOR OIL REMEDIATION

Acknowledgements

Cameron Shearer for help with contact angle measurements and analysis.

Louisa Esdaile and Stephanie Legg for synthesis of large batches of low density polysulfide as well as the building and testing of the continuous flow device.

Jonathan Campbell for dynamic mechanical analysis of polysulfide compressibility.

Christopher Gibson and Jason Gascooke for Raman analysis.

Ocean oil spills

For as long as petrochemicals remain a crucial component of human society, the threat of oil spills remains an enduring threat to human health and marine life. In 2015, an average of over 58 million barrels of crude oil and petroleum products were transported by sea every day, amounting to 61 % of the world's total production for the year¹. Accidental oil spills at sea have significant detrimental impacts on marine and coastal habitats²⁻⁵ and the health and wellbeing of humans who rely on those habitats for their livelihood. Destruction of fisheries through the killing or poisoning of sea life is one clear economic impact, but the release of toxic chemicals to the local environment can pose severe, chronic health effects for inhabitants living near the spill⁶.

The fate of spilled oil is quite complex. In the initial event, volatile components are lost quickly to the atmosphere. In two such cases, the Exxon Valdez and Amoco Cadiz, as much as 30 and 40 % of the total mass of spilled material was lost to evaporation². Thicker crude oils often contain a mixture of components that will react differently to conditions of open weather in turbulent seas. Oil will initially form a slick at the surface only a few millimetres thick, spreading out from the source, from there it is at the mercy of wave, wind and weather action. Dispersion of oil microparticles through wave action is one method that oil can be lost from the slick into the ocean. Conversely, sub-millimetre particles of water can become trapped in the slick, forming an emulsion and increasing its size and thus the difficulty of remediation². Slicks that reach the shore result in immediate harm to wildlife that come into contact.

One such case, the Deepwater Horizon oil spill in 2010, saw some 4.9 million barrels⁷ released from a deep-sea wellhead that suffered a blowout when a series of automated safety procedures failed to halt a kick event. The blowout led to an explosion on the rig that resulted in the death of 11 crewmen and the destruction of the drilling pipe mining the seabed, stretching over 9 km below sea level^{7, 8}. The Deepwater Horizon spill represents a unique scenario in which oil was not spilt directly on the surface, as in the case of a damaged tanker for example, but was the result of an open well stretching up from the sea floor, releasing oil up into the ocean. The depth of the spill meant response efforts took 3 months to seal the isolated wellhead, over a kilometre below sea level⁷. The response to oil

spills differs by case but often employs a mixture of techniques to remove or recover the oil. In the case of the Deepwater spill, 5 % was burned, 3 % was skimmed and 17 % was recovered through the riser pipe⁹. Of the oil that was released, about 5 % evaporated, 10 % reached the surface to form the slicks that at their largest covered over 40,000 km² and the remainder dissolved or dispersed forming plumes in the water column^{5, 9}. A controversial approach to the deep-sea release saw 7,000 m³ of oil-dispersants applied intended to break up the slick and promote bio-remediation. During a previous major oil spill, these Corexit oil dispersants were implicated in health problems experienced by clean-up workers leading to their ban in the UK⁷. Approximately 40 % of these dispersants were applied directly at the wellhead and the remainder sprayed at the surface, covering less than 0.1 % of the cumulative area where slicks were detected⁵. The result of the Deepwater event was a slick that covered a cumulative area of 112,000 km², the oiling of 2,100 km of shoreline in the Gulf of Mexico and damage to deep-sea and shoreline ecosystems⁵. Most fisheries in the affected areas closed leading to income loss and adverse physical and mental health effects were recorded in the human population⁷.

The impacts and responses to such spills demonstrate a need for methods that can be deployed rapidly and on a large scale. The response portfolio from recent spills would benefit greatly from a solution that meets these targets and also removes the spilled oil from the environment. Currently dispersion into the environment, and not recovery, is the leading solution to act quickly and reduce environmental harm. Collection also carries the economic potential of recovering the lost oil on top of the environmental benefits. Canola oil polysulfide is a material prepared through a relatively simple synthesis from waste and renewable materials available worldwide. By including table salt as a porogen in synthesis the result is an oleophilic, porous and sponge-like rubber that we posit may be utilisable as a tool for oil recovery on a large scale. The validation of large quantities of waste sulfur—from the petroleum industry—also represents a serendipitous, though ironic, case of a circular economy in which petroleum waste products would be used to reduce petroleum waste.

Conventional oil spill response methods can be categorised into three distinct groups: mechanical control and recovery through barriers, skimmers or sorbents, chemical treatment such as dispersants, emulsion breakers gelling or sinking agents, and natural degradation - monitoring only with no countermeasure actions taken. In addition to these primary methods are more advanced or specialised responses, such as the promotion of bioremediation, or in-situ controlled ignition¹⁰. Sea state as well as oil type (viscosity and tendency to emulsify)¹¹ both need to be considered when considering the appropriate response to a spill, with larger and more complex spills requiring an array of techniques, as seen in the response to the Deep Water Horizon and Exxon Valdez spills. In such cases, even the use of several conventional techniques at once cannot address the entirety of the spill, and so new and novel approaches are highly desirable.

Current conventional sorbents include three distinct types: Natural organics such as peat moss, vegetable fibres and straw typically absorb 3–15 times their weight, are inexpensive and readily available but lack selectivity, absorbing water along with oil leading to difficult recovery and sinking. Natural inorganics including clay, sand and volcanic ash typically absorb 4–20 times their weight, are also inexpensive and readily available but are difficult to apply as loose material and carry potential inhalation risks. The most widely used are synthetic sorbents; Hydrophobic polypropylene, polystyrene and polyester foams, with 70–100 times adsorption capacities, some of which can be re-used several times, suffer mainly from their fate after use as they lack biodegradability¹². With a promising outlook for canola oil polysulfide's biodegradability¹³, we hypothesised it could overcome this major shortcoming of other synthetic approaches.

Also notable are the impressive advances made in the development of superhydrophobic/oleophilic and superhydrophilic/oleophobic materials for water/oil separation. These materials can exhibit absorption capacities hundreds of times their mass, but often suffer from difficult synthetic procedures, use of costly components or contain fragile nanostructures key to their effectiveness¹⁴. For an oil clean-up operation on turbulent seas a sorbent should ideally be inexpensive to produce, robust and deployable at scale, limiting the applicability of these advanced materials.

Porous polysulfide as a sorbent for oil

The first experiment was to simply float oil on water, apply the polysulfide and see if and how much it could absorb. Motor oil was floated atop DI water in a 20 mL glass vial, and polysulfide poured in. On contact with the oil, the polysulfide began to aggregate, drawing the oil in and forming a gel, all the while remaining floating on top of the water (Fig. 4.1b). For the cleaning of oil spills these are important and useful properties; Aggregation into a single location and buoyancy facilitate simple recovery of the polymer once it has reached capacity. The next property to test was simply how much oil the polysulfide could absorb: In a series of 20 mL glass vials, crude oil (Nockatunga, Australia) at volumes from 0.5 to 2.0 mL at 0.25 mL increments was carefully pipetted on to 5.0 mL DI water. 1.00 g porous canola oil polysulfide was added to each vial and left for 5 minutes to collect the oil. Polysulfide aggregated as before, absorbing the oil. After removal of the oil-loaded polysulfide with forceps, a thin layer of oil still remained visible in the vials previously holding 1.25 mL oil or more. Those containing 0.5, 0.75 and 1.0 mL however seemed to have been cleared of oil. Unfortunately, this experiment was not as useful as we had hoped in determining a precise capacity, but it did show that we were testing at the right volume, hinting at a capacity for this particular variety of crude oil of 1 mL per gram polysulfide. A complimentary experiment was devised to determine a precise capacity and carried out with a variety of industrial oils that may be involved in spills: Two varieties of crude oil, one thin from an Australian wellhead in Nockatunga, and a thick sludge-like oil from a Texan wellhead. Motor oil (Castrol Magnatec 10W40) and Diesel were also included. In the experiment, porous polysulfide was cut into 5.0 mm cubes (Fig. 4.1d) using a scalpel and placed in

a glass petri dish containing a thin layer of oil such that the polymer was partially submerged. Time taken for the oil to wick up through the polysulfide block was monitored and once saturated, the block was lifted with forceps and excess liquid removed by dabbing on a separate glass dish. Absorbed oil mass was determined gravimetrically and capacity averaged over 5 replicates. Wicking time varied from 30 seconds to 5 minutes, but capacity remained quite close among the oils. The thinner Nockatunga crude oil absorbed into the polysulfide fastest with a 30 second wicking time at a capacity of 0.95 ± 0.15 mL per gram polysulfide. Diesel, also a thin oil saturated the polymer within a minute with the greatest capacity of 1.36 ± 0.39 mL g^{-1} . The two thicker oils, motor oil and the Texan crude oil both required 5 minutes to soak up to the apex of the polymer with capacities of 0.86 ± 0.14 and 0.95 ± 0.14 mL g^{-1} respectively. Canola oil polysulfide exhibited the same capacity for both crude oil samples, despite the differences in viscosity and density. As a control to determine specificity of the polysulfide to absorb oil exclusively, polymer cubes were partially submerged in DI water. After 5 minutes the mass difference was recorded, accounting for an equivalent capacity of 0.056 ± 0.012 mL g^{-1} for water, 5.9 % of that of the crude oils. Water was not observed to wick up through the polysulfide and so the experiment was halted at the maximum time needed for all oils to absorb: 5 minutes. Water in this case is simply adhering to the polysulfide and a clear preference for oils is observed.

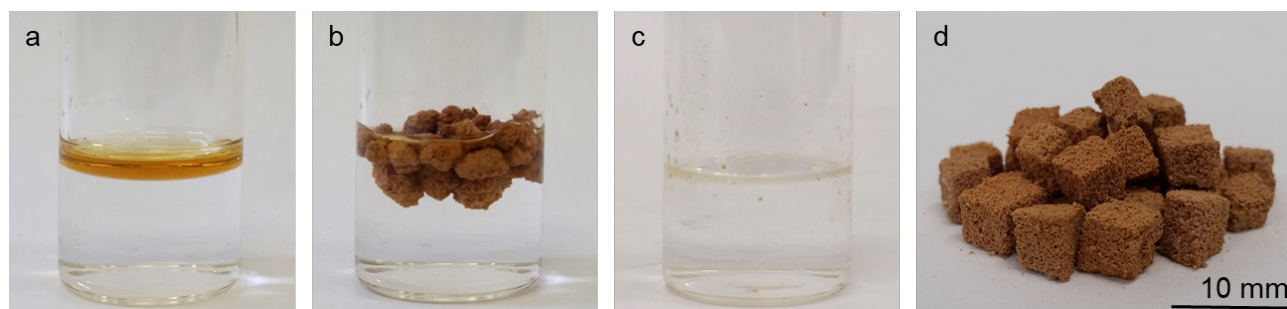


Figure 4.1 | a-c: Motor oil on water before (a), during (b) and after (c) application of porous polysulfide to recover the oil. d: Porous canola oil polysulfide prepared as 5 mm cubes for use in wicking experiments.

Contact angle measurements were able to further describe oleophilicity and quantify hydrophobicity. Across 15 different measurements, water contact angle of a 10 μ L droplet averaged $130^\circ \pm 10.5^\circ$ with a minimum of 111° and maximum of 156° (Fig. 4.2e). Surface roughness or inhomogeneity of the porous polymer surface may influence this value, but the polymer is clearly hydrophobic. Repeating the same procedure with oil, carefully applying a 5 μ L droplet of liquid to the surface of a 5 mm cube of polysulfide, resulted in absorption of the oil over a short period of time. The thicker oils took the longest to absorb, 50 seconds for the motor and a full minute for the Texas crude. The thinner oils were significantly quicker, at 3 seconds for the diesel and only 600 ms (measured from a video recording of the absorption process) for the Australian crude (Fig. 4.2). Contact angle over time for each oil was plotted to visualise the absorption process (Fig. 4.2f). This experiment clearly

demonstrates the hydrophobicity (perhaps to be expected of a polymer of sulfur chains and fatty acids) of the polysulfide and affinity for petroleum oils of a variety of viscosities, from crude to refined.

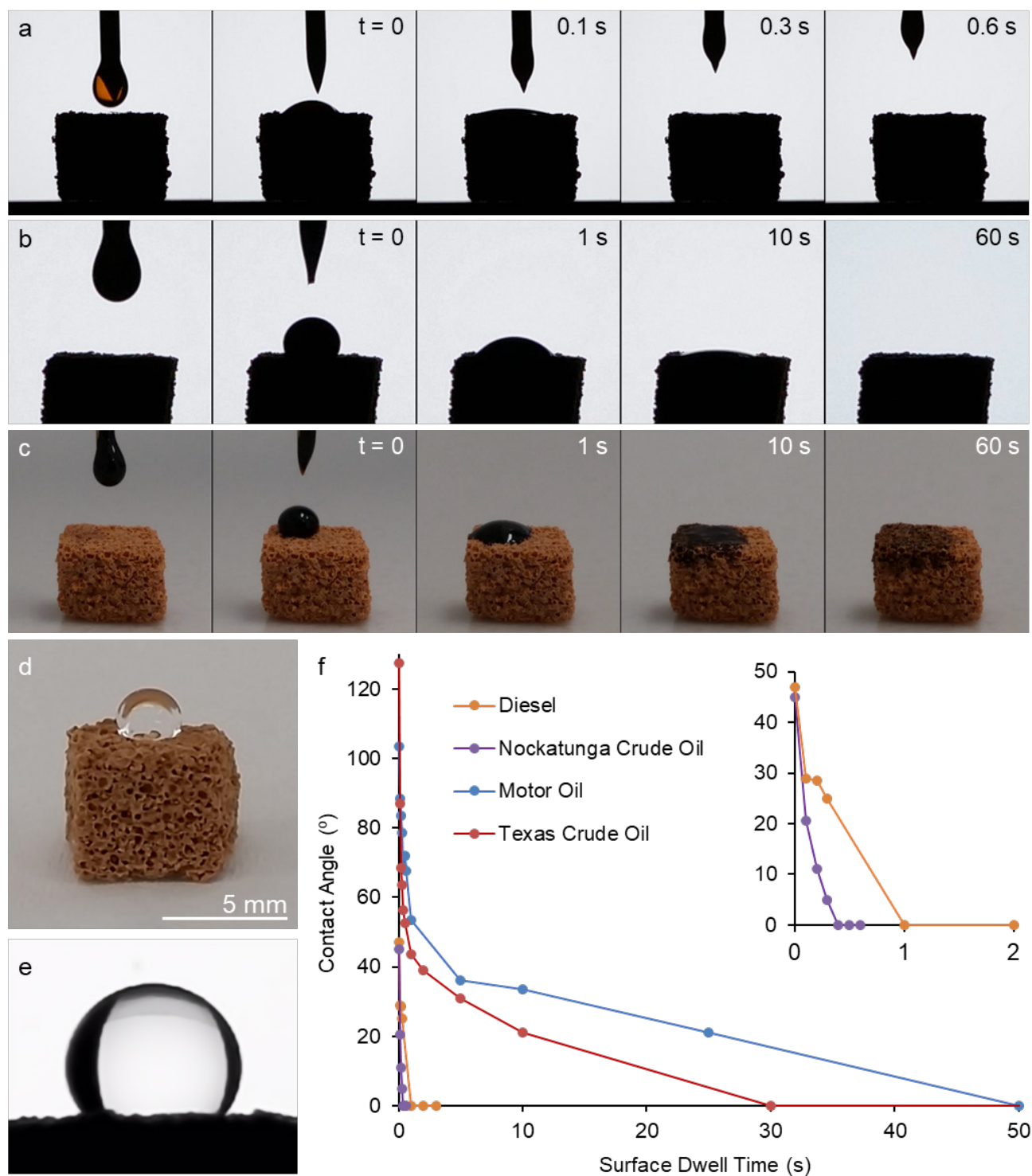


Figure 4.2 | a-b: Screen-captures from a video recording of applying a droplet (approx. 5 μ L) of Nockatunga crude oil (a) or Texan crude oil (b) to a 5 mm porous polysulfide cube in a contact angle goniometer c: As b, outside of the goniometer to demonstrate in colour. d-e: A droplet of water on a cube of porous polysulfide outside (d) and inside (e) the goniometer, where the latter was used to determine water contact angle. f: Graph of droplet contact angle over time.

Once captured, an obvious question is what is the final fate of the used sorbent? Given the compressibility of porous canola oil polysulfide, we thought it might be feasible to recollect oil after use by simple mechanical compression. By taking porous polysulfide saturated with motor oil and squeezing it between glass slides, oil could be recovered, though not without small portions of the polymer breaking under the stress in this initial crude test. With the recovery of absorbed oil, the fate of recovered polysulfide is the next to be brought into question. Given the separation of oil from polymer, could it simply be used again? To test, 1.00 g polysulfide was added to 1.00 mL motor oil floating on 5.00 mL water in a 20 mL glass vial. The polysulfide absorbed the oil and aggregated as before. This time however the polysulfide was removed after 5 minutes, compressed to recover the oil, and added back into a fresh vial of oil and water. The polysulfide acted as before, absorbing the oil and aggregating. It was removed and compressed, and the oil and polymer separated once more. The same batch of polymer was used a total of 5 times, visibly removing all oil for a total of 5.00 mL recovered by 1.00 g (Fig. 4.3), more than 5 times greater than the capacity reported in the wicking experiment. Polysulfide could feasibly be used over many more cycles, but each recovery step employed non-uniform, by-hand compression between two glass slides that led to deformation of the polysulfide. The test was stopped at 5 cycles because recovery of the polysulfide became difficult. SEM imaging, and FTIR and Raman analysis showed that after compression, some oil still remained on the surface of the polymer. SEM was also used to investigate the deformation of polysulfide that had not been in contact with motor oil; crushing of polysulfide particles leads to loss of equable pores and channels visible in un-crushed polysulfide, but the fracturing of the polymer particles seems to impart new void-space as oil capacity is not negatively impacted with each re-use.

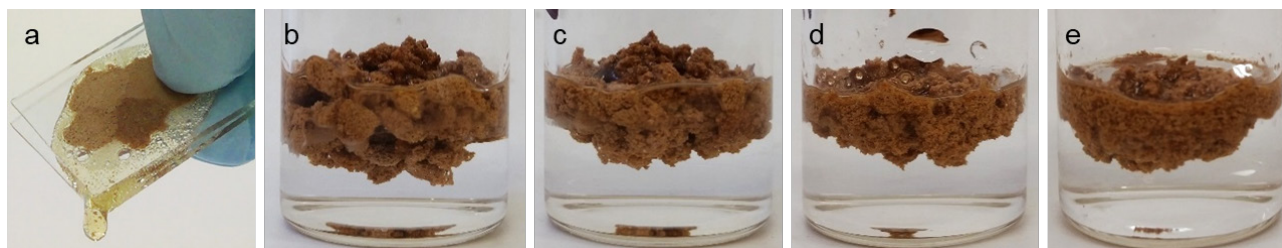


Figure 4.3 | a: Porous polysulfide compressed between glass slides after being used to absorb motor oil to separate and recover the oil and polysulfide. b-e: 1.0 g recovered polysulfide used for a second (b), third (c), fourth (d) and fifth (e) time to collect 1.0 mL motor oil with recovery by compression repeated between each re-use. Compression damage becomes more prominent with each recovery cycle.

Deployment inside a semi-permeable membrane (a teabag-like bag for example) where particle deformation would not be a detriment to recovery or controlled compression that might not lead to deformation could result in vastly increased recyclability. To test the latter proposition, we undertook a collaboration with Jonathan Campbell of the Flinders Institute for Nanoscale Science and Technology. Over a series of experiments either sourced from literature or devised for dynamic mechanical analysis (DMA) we discovered that porous polysulfide could recover fully after

compression under a certain strain threshold. At 20 and 40 % strain, recovery was instantaneous. Deformation began to occur at 60 % strain with slight compression set but still instantaneous recovery. At 80 % strain compression set was far more noticeable and the polymer cube continued to decompress for up to 5 minutes after relieving compression (Fig. 4.4b). Compressing the polymer to such a thorough extent results in permanent damage. In a separate experiment, continued compression and decompression from 0 to 35 % strain was performed on a single polymer cube. Over 20 cycles permanent deformation of only 5.6 % was observed (Fig. 4.4c). The polymer soaked with oil was found to require slightly more force to compress to the same extent as the pristine polymer, but both followed a similar profile, compressing linearly with pressure up to approximately 40 % strain but rapidly requiring more force to continue compression approaching the strain levels that result in deformation ($\geq 60\%$).

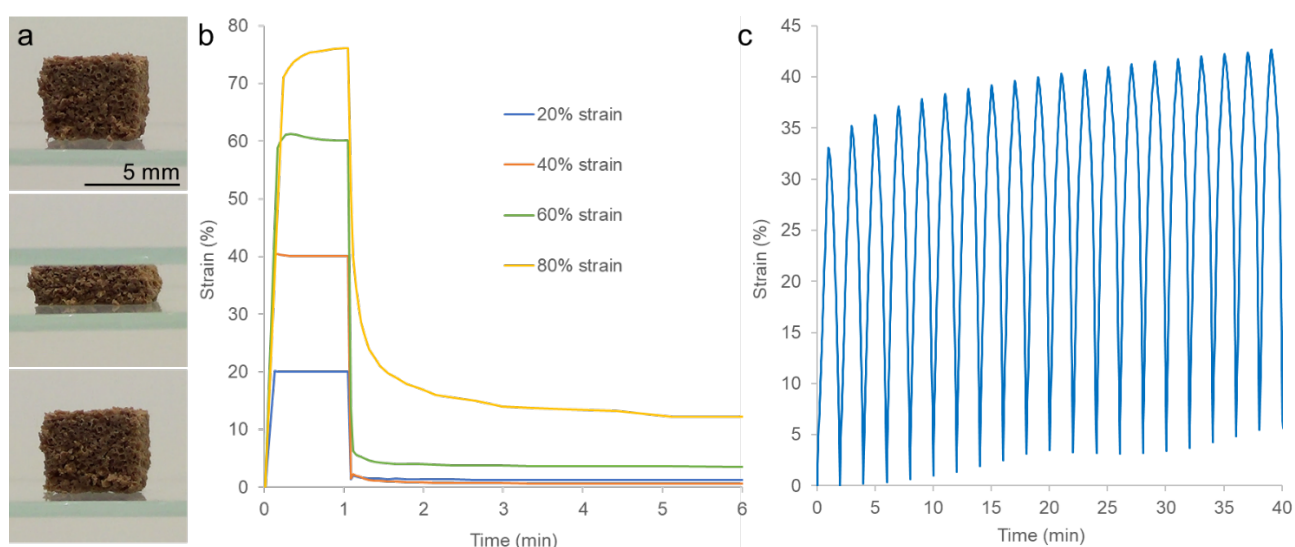


Figure 4.4 | a: 5 mm cube of porous polysulfide before (top), during (middle), and after (bottom) compression between two glass slides. b: Cubes of porous polysulfide were compressed to 20, 40, 60 and 80 % strain for 1 minute. Compression set (permanent deformation) begins to occur at 60 % strain and is far more prominent at 80 %. c: Force was applied to compress a porous polysulfide cube to 35 % strain over 1 minute and the ramped back down over 1 minute. This was repeated for 40 minutes to demonstrate compression set from a weaker force (as per b) over multiple compressions.

To validate the need for porosity in the polysulfide, oil recovery was attempted with non-porous polysulfide. Hypothetically, if the mechanism of action was dependent primarily on the polysulfide's hydrophobicity and not void space, it could result that non-porous polysulfide would be as efficient as the porous. Thus, the extra steps and reagents required in synthesis to impart porosity would simply be a waste of salt and water. To validate the green metrics of the polysulfide's synthesis it was necessary to take a step back and test the simpler material. To a 20 mL glass vial was added 8.0 mL DI water and 1.0 g Nockatunga crude oil (more water was required than in previous experiments to avoid the oil colliding with and remaining at the base of the glassware under gravity on addition). To this, powdered porous (low density polysulfide) or non-porous polysulfide was added

with swirling until no free oil was observed. Both porous and non-porous polymers aggregated with the oil as it was absorbed. On average of triplicate measurements, 0.50 g porous polysulfide was required for no oil to remain visible, whereas 1.19 g was required of the non-porous (Fig. 4.5). In one replicate the non-porous polysulfide-oil agglomerate sank in the vial. Not only was more than double the mass of non-porous polysulfide required to collect the same mass of oil, but it runs the risk of sinking, taking the oil with it and preventing recovery. In an identical experiment using 2.0 g motor oil on 25 mL water, 1.15 g porous polymer was required and 2.96 g non-porous. The latter again sinking to the bottom. These shortcomings together encourage the use of porous over non-porous polysulfide. Given the hydrophobicity of sulfur we also thought to repeat the experiment with just powdered S_8 . Initial addition followed a similar pattern to the polysulfides, aggregation with the oil, but with the addition of approximately 0.5 g sulfur the bulk began to clump and sink (Fig. 4.5d). The sunken sulfur-paste that formed sat at the bottom of the glass with a bubble of oil adhered to the surface having been dragged down with it. In total 1.23 g was added to agglomerate all oil, but in all cases the material sank, proving ineffective for recovery. Despite this it is still interesting to note that sulfur contributes to oil-binding, not just the triglyceride component of the polymer.

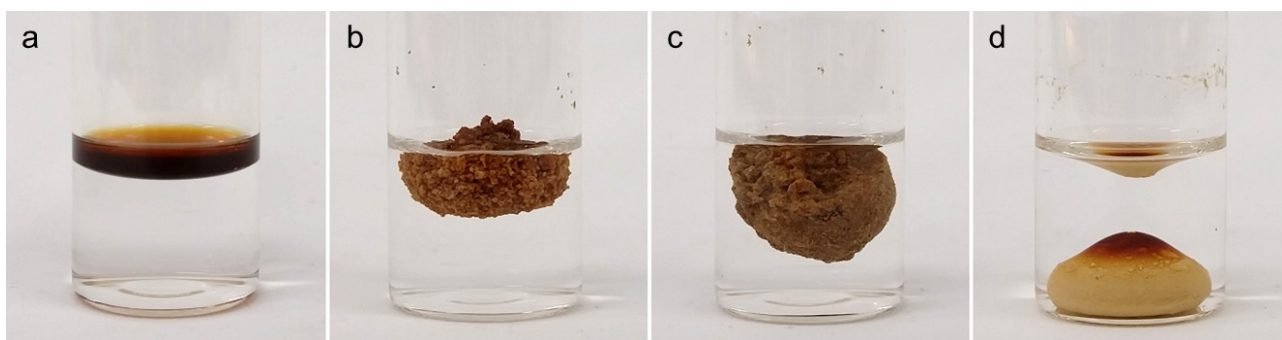


Figure 4.5 | a-d: Nockatunga crude oil on water before (a) and after the addition of enough low density polysulfide (b), non-porous polysulfide (c) or powdered sulfur (d) to absorb the oil. More than double the mass of non-porous polysulfide compared to low-density was required to absorb the same volume of oil. Powdered sulfur agglomerated and sank on contact with crude oil.

Experiments on a larger scale

With the ambition of applying porous sulfur polymers as sorbents for large-scale oil spills, we would need to demonstrate effectiveness on a much larger scale. To a 3.0 L pyrex dish was added first 500 mL deionised water, and then 100 mL motor oil that sat as two phases. To the oil was added 100 g low density polysulfide (i.e. powdered porous polysulfide). Over 5 minutes the polysulfide visibly soaked up the oil and began to gel. Removal of the polymer from the surface was made simple with only a net, leaving clear water behind—all motor oil had been removed. Even at this scale the polysulfide continues to function as an oil sorbent with at least the same capacity as tested on the gram scale. However, more impressive would be something closer to a real-world scenario. DI water was replaced with sea water from Brighton beach, SA, a short drive from the lab, processed motor oil was replaced with the far more unpleasant Texan crude oil, and importantly the polysulfide

used was prepared from waste vegetable oil. Though not at the scale of a disastrous oil spill, this experiment would at least replicate crude oil on seawater with a sorbent prepared from waste materials. 100 mL crude oil was poured onto 1.50 L water (more water was required as the heavy oil would sink on addition and stick to the base) and 100 g waste-oil polysulfide was spread along the oil. Recovery of the polysulfide occurred after only 1 minute this time, proving to be sufficient as the polysulfide gelled, discoloured by the oil, and was equally simple to extract with a net (Fig. 4.6)¹⁵.

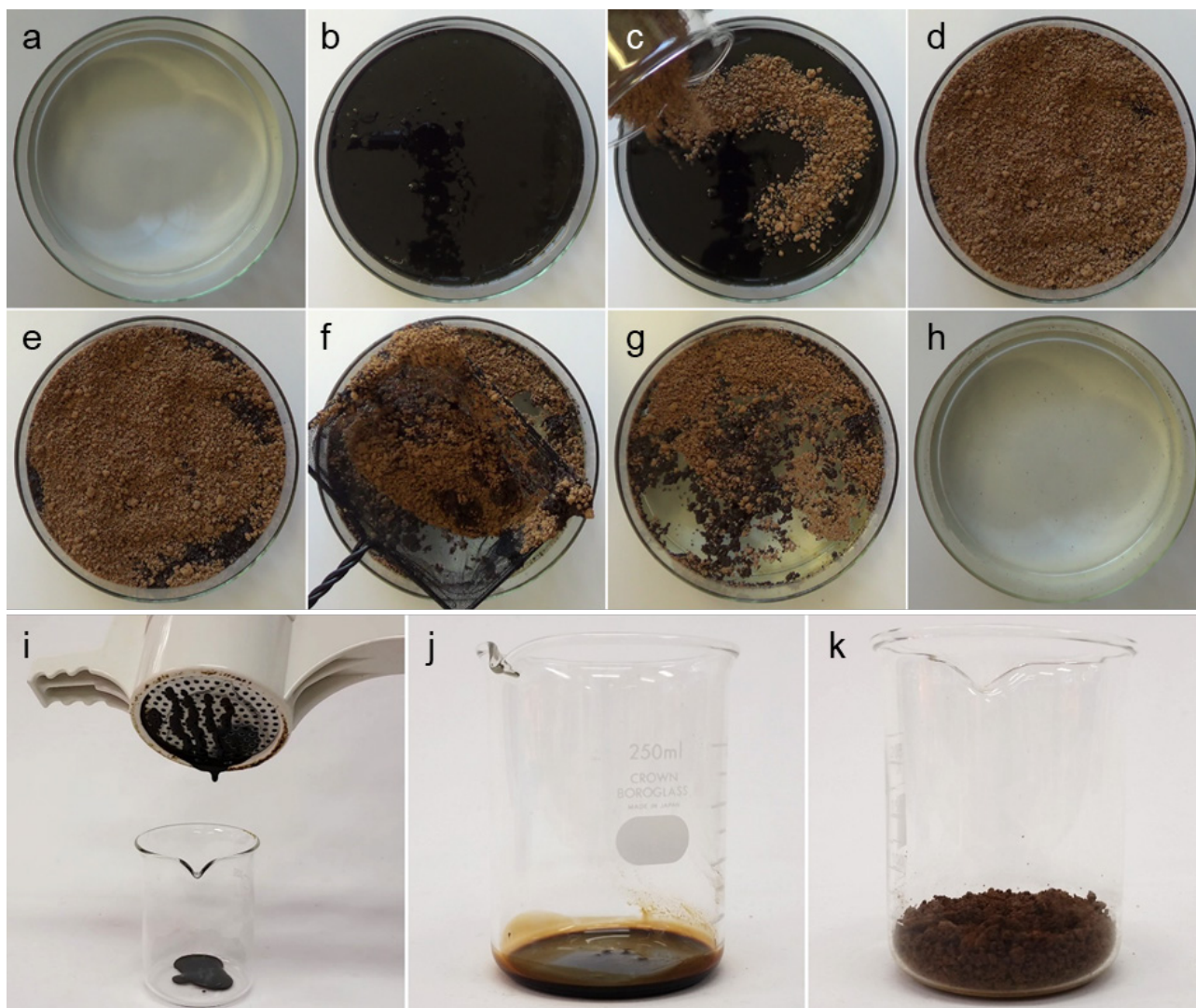


Figure 4.6 | a-h: To 1.5 L seawater (a) 100 mL Texan crude oil was added (b) and then 100 g low density polysulfide prepared from waste cooking oil was applied (c). The polysulfide was spread across the surface (d) and left for 1 minute, during which time the oil migrated into the mass of the polymer, seen as a change in colour (e). The resultant polymer-oil gel was removed with a simple net (f) revealing no free oil beneath (g). Once all polymer had been recovered only water remained (h). i-k: Compression of polymer-crude oil gel by household kitchen apparatus (a potato ricer) (i) facilitated separation of the oil (j) from the polysulfide (k).

In a more complex scenario such as turbulent open water contaminated with oil, simply applying polysulfide to the contaminant may not be so easy. The final task for this project was to address this concern by transforming the procedure to a continuous filtration process. A filtration device could also provide the added benefit of an isolated sorbent chamber in which saturated sorbent would be

pre-collected without the need for manual recovery. The pilot design involved the sealing of 30.0 g low density polysulfide inside PVC pipe with PVC-coated fibreglass yarn mesh at the inlet and cotton fabric at the outlet. A mix of 100 mL sea water and 10.0 mL Texas crude oil was passed through the assembled filter, it initially collected at the inlet but as it slowly passed through the column all that remained was water flowing out of the device into the collection beaker (Fig. 4.7)¹⁵.

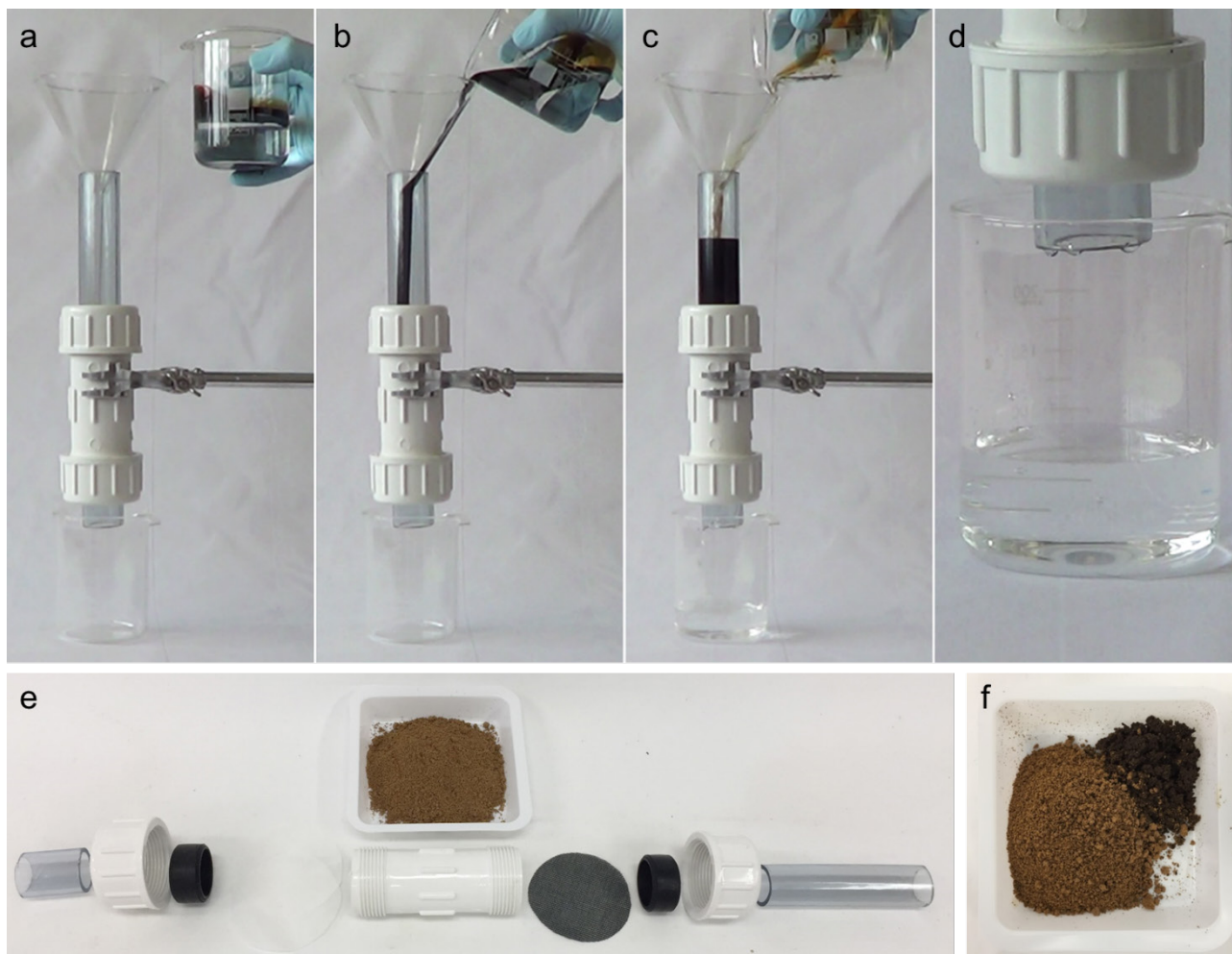


Figure 4.7 | a-d: A layered mixture of 10 mL crude oil on 100 mL seawater was passed through a gravity filtration device containing low density polysulfide. Crude oil is trapped by the polysulfide and only clear water elutes. e: Components of the polysulfide filtration device before use. f: Polysulfide collected after filtration of water from oil, some polysulfide has turned black indicating capture of crude oil.

In conclusion, low density and porous canola oil polysulfide has been demonstrated to absorb petroleum oils: diesel, motor oil as well as thin and viscous crude oils on a short (< 1 min) timescale with a capacity that varies slightly based on experimental design but averages close to 1 mL g⁻¹. Oil can be recovered from the polysulfide by compression and recovered polymer can be re-used to soak up oil to a similar capacity. This recycling process can be repeated multiple times to recover larger quantities of oil with the same supply of polysulfide. Low density polysulfide retains its oleophilic and hydrophobic properties at the 100 mL scale and remains floating on collection, facilitating simple recovery. And by incorporation of low density polysulfide in a simple filtration column, water-oil mixtures can be passed through to separate the two by absorption of the oil layer.

Further investigation is planned to demonstrate the use of canola oil polysulfide as an oil sorbent on even larger scales, incorporating the effects of wave action and open weather as well as the stability of the polysulfide itself under such conditions on a longer time scale.

Biodegradation studies of the polymer and oil-polymer aggregate are planned for the future of this project. The Australian Maritime Safety Authority has expressed an interest in the polymer and its development into an oil-remediation device, prompting the need for details on the final fate and stability of the material. As a tool to be used alongside a panel of oil spill response mechanisms, we foresee the polymer as a tool for use in wetland and coastal areas where access is severely restricted, and where control of slicks is paramount in the case of an oil spill emergency. The porous polysulfide may fit an important niche in this area, where traditional sorbents are difficult to apply by air and dispersants are not applicable as they run the risk of dissolving natural plant waxes and damaging the environment.

References

1. U.S. Energy Information Administration, World Oil Transit Chokepoints. **2017**. <<https://www.eia.gov/beta/international/regions-topics.php?RegionTopicID=WOTC>> Accessed June 2019.
2. Kingston, P. F., Long-term Environmental Impact of Oil Spills. *Spill Sci. Technol. Bull.* **2002**, 7 (1-2), 53-61.
3. Rogowska, J.; Namieśnik, J., Environmental Implications of Oil Spills from Shipping Accidents. In *Reviews of Environmental Contamination and Toxicology Volume 206*, Whitacre, D. M., Ed. Springer New York, NY. **2010**, 95-114.
4. National Wildlife Federation, Five Years & Counting: Gulf Wildlife in the Aftermath of the Deepwater Horizon Disaster. **2015**. <<https://www.nwf.org/Educational-Resources/Reports/2015/03-30-2015-Five-Years-and-Counting>> Accessed March 2019
5. Beyer, J.; Trannum, H. C.; Bakke, T.; Hodson, P. V.; Collier, T. K., Environmental effects of the Deepwater Horizon oil spill: A review. *Marine Pollution Bulletin* **2016**, 110 (1), 28-51.
6. Chang, S. E.; Stone, J.; Demes, K.; Piscitelli, M., Consequences of oil spills: a review and framework for informing planning. *Ecology and Society* **2014**, 19 (2) 26.
7. Nyankson, E.; Rodene, D.; Gupta, R. B., Advancements in Crude Oil Spill Remediation Research After the Deepwater Horizon Oil Spill. *Water, Air, & Soil Pollution* **2015**, 227 (1), 29.
8. Kaufman, L., Search Ends for Missing Oil Rig Workers. *New York Times*, **2010**. <<https://www.nytimes.com/2010/04/24/us/24spill.html>> Accessed October 2019.
9. Lubchenco, J.; McNutt, M. K.; Dreyfus, G.; Murawski, S. A.; Kennedy, D. M.; Anastas, P. T.; Chu, S.; Hunter, T., Science in support of the Deepwater Horizon response. *Proc. Natl. Acad. Sci. U. S. A.* **2012**, 109 (50), 20212-20221.
10. Ventikos, N. P.; Vergetis, E.; Psaraftis, H. N.; Triantafyllou, G., A high-level synthesis of oil spill response equipment and countermeasures. *J. Hazard. Mater.* **2004**, 107 (1), 51-58.
11. Prendergast, D. P.; Gschwend, P. M., Assessing the performance and cost of oil spill remediation technologies. *J. Cleaner Prod.* **2014**, 78, 233-242.
12. Dave, D. and Ghaly, A. E. Remediation Technologies for Marine Oil Spills: A Critical Review and Comparative Analysis. *Am. J. Environ. Sci.* **2011**, 7 (5), 423-440.

13. Mann, M.; Kruger, J. E.; Andari, F.; McErlean, J.; Gascooke, J. R.; Smith, J. A.; Worthington, M. J. H.; McKinley, C. C. C.; Campbell, J. A.; Lewis, D. A.; Hasell, T.; Perkins, M. V.; Chalker, J. M., Sulfur polymer composites as controlled-release fertilizers. *Org. Biomol. Chem.* **2019**, *17*, 1929-1936.
14. Ma, Q.; Cheng, H.; Fane, A. G.; Wang, R.; Zhang, H., Recent Development of Advanced Materials with Special Wettability for Selective Oil/Water Separation. *Small* **2016**, *12* (16), 2186-2202.
15. Worthington, M. J. H.; Shearer, C. J.; Esdaile, L. J.; Campbell, J. A.; Gibson, C. T.; Legg, S. K.; Yin, Y.; Lundquist, N. A.; Gascooke, J. R.; Albuquerque, I. S.; Shapter, J. G.; Andersson, G. G.; Lewis, D. A.; Bernardes, G. J. L.; Chalker, J. M., Sustainable Polysulfides for Oil Spill Remediation: Repurposing Industrial Waste for Environmental Benefit. *Advanced Sustainable Systems*, **2018**, *2* (6), 1800024.

APPENDICES

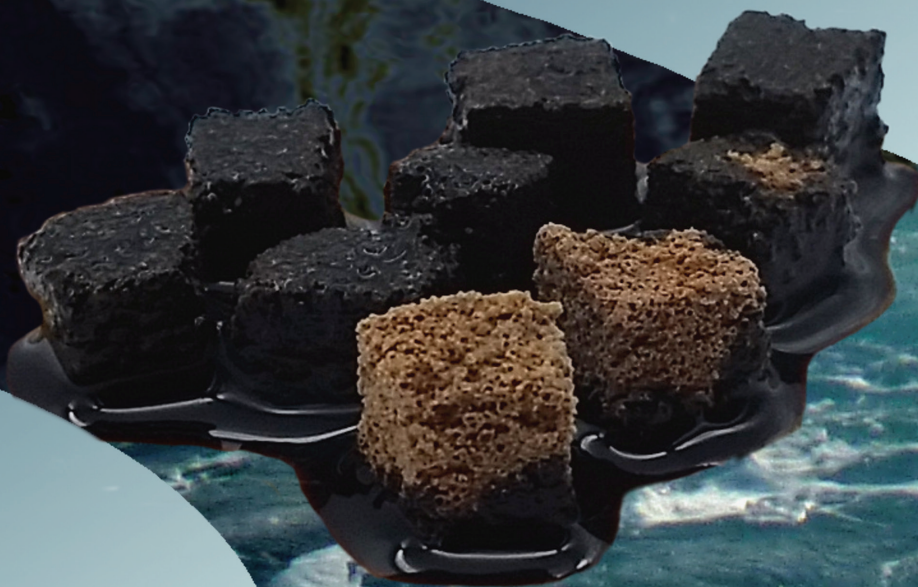
Publications that resulted from the research in this chapter:

Worthington, M. J. H., Shearer, C. J., Esdaile, L. J., Campbell, J. A., Gibson, C. T., Legg, S. K., Yin, Y., Lundquist, N. A., Gascooke, J. R., Albuquerque, I. S., Shapter, J. G., Andersson, G. G., Lewis, D. A., Bernardes, G. J. L., Chalker, J. M., *Adv. Sustainable Syst.* **2018**, 2, 1800024. published by WILEY - VCH Verlag GmbH & Co. KGaA, Weinheim and reproduced below under a Creative Commons Attribution License.

Vol. 2 • No. 6 • June • 2018

www.advsustainsys.com

ADVANCED SUSTAINABLE SYSTEMS



WILEY-VCH

Sustainable Polysulfides for Oil Spill Remediation: Repurposing Industrial Waste for Environmental Benefit

Max J. H. Worthington, Cameron J. Shearer, Louisa J. Esdaile, Jonathan A. Campbell, Christopher T. Gibson, Stephanie K. Legg, Yanting Yin, Nicholas A. Lundquist, Jason R. Gascooke, Inês S. Albuquerque, Joseph G. Shapter, Gunther G. Andersson, David A. Lewis, Gonçalo J. L. Bernardes, and Justin M. Chalker*

Crude oil and hydrocarbon fuel spills are a perennial threat to aquatic environments. Inexpensive and sustainable sorbents are needed to mitigate the ecological harm of this pollution. To address this need, this study features a low-density polysulfide polymer that is prepared by the direct reaction of sulfur and used cooking oils. Because both sulfur and cooking oils are hydrophobic, the polymer has an affinity for hydrocarbons such as crude oil and diesel fuel and can rapidly remove them from seawater. Through simple mechanical compression, the oil can be recovered and the polymer can be reused in oil spill remediation. The polysulfide is unique because it is prepared entirely from repurposed waste: sulfur is a by-product of the petroleum industry and used cooking oil can be used as a comonomer. In this way, sulfur waste from the oil industry is used to make an effective sorbent for combatting pollution from that same sector.

Oil and hydrocarbon fuel spills continue to threaten both terrestrial and aquatic ecosystems, with adverse effects on the environment,^[1] economy,^[1d] and human health.^[2] The explosion on the *Deepwater Horizon* offshore drilling rig in 2010 and subsequent release of ≈4.9 million barrels of crude oil into the Gulf of Mexico is a reminder of the catastrophic scale on which these events can occur.^[3] In addition to such large-scale oil releases, there are hundreds of smaller spills each year in which diesel fuel is a common form of hydrocarbon pollution.^[4] Oil pollution is also a serious concern in developing regions where limited resources hamper the response to spills that threaten ground water, drinking water, and food staples such as fish and other aquatic organisms. The

extensive oil pollution in the Niger Delta^[5] and the Amazon basin of Ecuador^[6] are prominent examples in this regard.

Because of these ongoing challenges with oil and fuel spills, there have been calls for research into cost-effective technologies that can facilitate the response to this pollution.^[3a,7] Accordingly, there is wide interest in skimming technology and sorbents that can be produced and deployed on an immense and economically viable scale.^[7,8] Regarding sorbents, these materials are typically most effective in oil capture if they are hydrophobic and have high surface area, low specific gravity and high buoyancy in water.^[7,8] Mechanical recovery of the oil and sorbent reuse are also desirable features,^[7,8] and low cost is critical for uptake in the field.^[9] Impressive advances have been made for both sorbents and membranes, with highly effective materials reported for oil separation and recovery from water.^[7,8] Nevertheless, the majority of these high-performance materials are not economically viable on the scale required for many remediation needs and most commercial sorbents are made from nonrenewable polypropylene fibers^[10] or polyurethane foams.^[8d] Additionally, while natural biomass and fibrous vegetation have been investigated as low-cost and sustainable sorbents,^[11] these typically suffer from low buoyancy, high water sorption, or limited means by which to recover the oil.

In this report we introduce a new class of oil sorbents that is low-cost, scalable, and enable the efficient removal and recovery of oil from water. The key material is an elastic and porous copolymer made from the direct reaction of sulfur and unsaturated seed

M. J. H. Worthington, Dr. C. J. Shearer, Dr. L. J. Esdaile, Dr. J. A. Campbell, Dr. C. T. Gibson, S. K. Legg, Y. Yin, N. A. Lundquist, Dr. J. R. Gascooke, Prof. J. G. Shapter, Prof. G. G. Andersson, Prof. D. A. Lewis, Dr. J. M. Chalker

Centre for NanoScale Science and Technology
College of Science and Engineering
Flinders University

Sturt Road, Bedford Park, South Australia 5042, Australia
E-mail: justin.chalker@flinders.edu.au

I. S. Albuquerque, Dr. G. J. L. Bernardes
Instituto de Medicina Molecular
Faculdade de Medicina da Universidade de Lisboa
Av. Prof. Egas Moniz 1649-028, Lisboa, Portugal

Prof. J. G. Shapter
Australian Institute of Bioengineering and Nanotechnology (AIBN)
University of Queensland
St. Lucia, Queensland 4072, Australia

Dr. G. J. L. Bernardes
Department of Chemistry
University of Cambridge
Lensfield Road, Cambridge CB2 1EW, UK

 The ORCID identification number(s) for the author(s) of this article can be found under <https://doi.org/10.1002/adsu.201800024>.

© 2018 The Authors. Published by WILEY-VCH Verlag GmbH & Co. KGaA, Weinheim. This is an open access article under the terms of the Creative Commons Attribution License, which permits use, distribution and reproduction in any medium, provided the original work is properly cited.

DOI: 10.1002/adsu.201800024

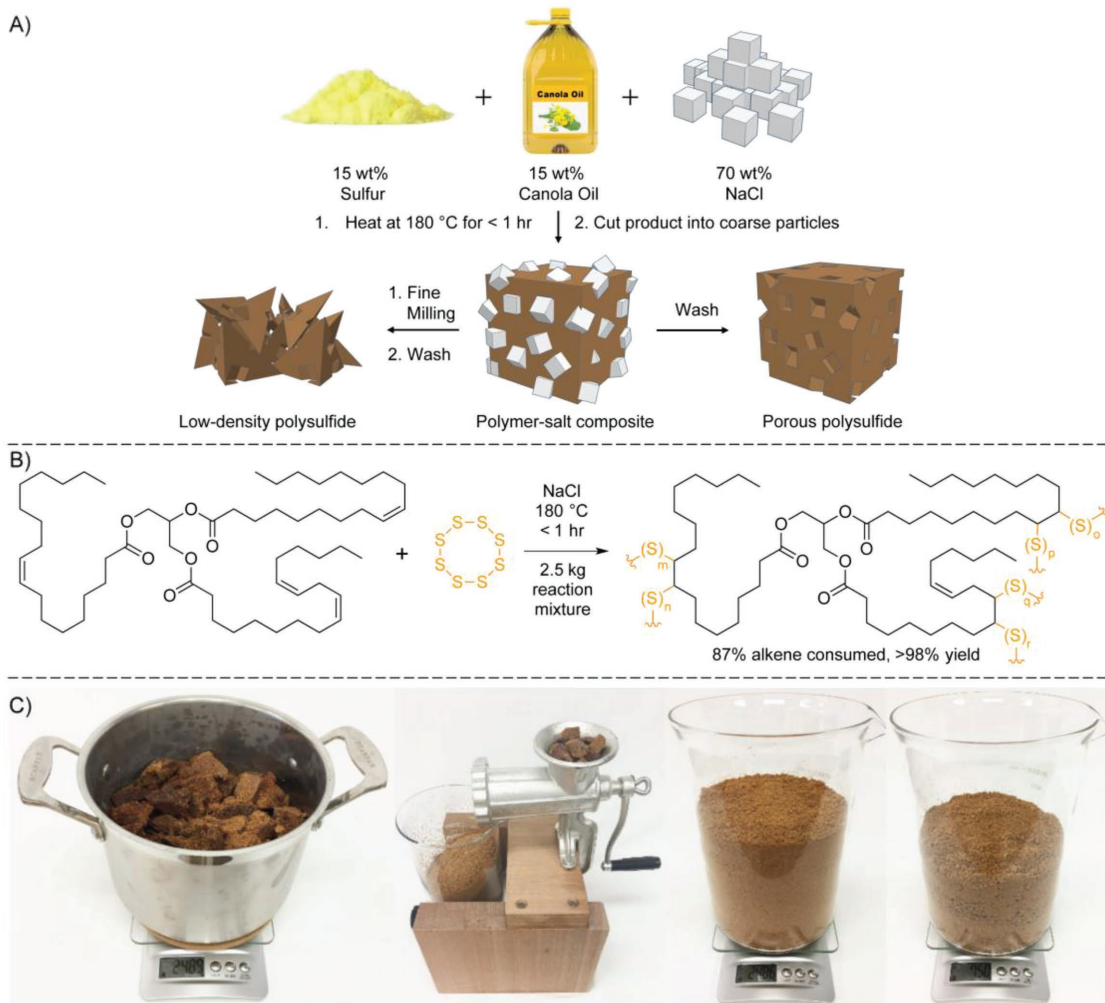


Figure 1. A) Elemental sulfur and canola oil (or used cooking oil) react directly to form a polysulfide copolymer. The polymer, equal mass in sulfur and canola oil, is a friable rubber. The inclusion of sodium chloride in the reaction mixture results in a polymer–salt composite. The sodium chloride can be removed with a water wash to introduce pores into the polymer. If the polymer is ground finely (0.5–3.0 mm particle size) and then washed with water, the void spaces formed after sodium chloride removal no longer appear as pores. In this case, the polymer tears at the salt interface where a pore would otherwise form. This finely milled polymer is referred to as a “low-density polysulfide” rather than a “porous polysulfide.” B) The polysulfide copolymer is formed by ring-opening polymerization of elemental sulfur and reaction of the resulting thiol-radical end groups with the Z-alkene of the unsaturated cooking oil triglyceride (primarily oleate and linoleate in the oils used in this study) 87% of the alkenes are consumed in the polymerization, as determined by 1H NMR spectroscopy. C) Left to right: The polymer–salt composite was prepared on a 2.5 kg scale and ground finely before washing with water. After washing with water and drying, 750 g of the low-density polysulfide was obtained (far right image).

oils such as canola oil, with inexpensive sodium chloride crystals serving as a porogen to impart higher surface area to the polymer (Figure 1). Because sulfur is a by-product of the petroleum industry^[12] and used cooking oils are suitable starting materials, this oil sorbent can be made entirely from industrial waste that is inherently low in cost. Furthermore, because both sulfur^[12,13] and canola oil^[14] are produced in millions of tonnes each year, the starting materials are sustainable and available on the scale required for addressing the oil spill problem.^[15] Additionally, this advance would constitute a valuable use for sulfur polymers^[16] that is distinct from recent applications of high-sulfur materials in battery technology,^[16a,c] optics equipment,^[16c,17] and heavy-metal remediation.^[18] Importantly, a polysulfide made from sulfur and canola might also be effective in oil spill remediation because both

comonomers are hydrophobic. Furthermore, a porous and flexible version of this material might enable recovery of bound oil by simple mechanical compression. We therefore set out to test the hypothesis that hydrophobic, porous, and compressible sulfur polymers will enable the separation and recovery of oil from water.

The porous canola oil polysulfide was first prepared using either pristine, food-grade canola oil, or used unsaturated cooking oils obtained directly from a restaurant (Figures S1–S9, Supporting Information). We aimed for kilogram-scale batch processes at the outset to demonstrate scalability—an important consideration for use in oil spill remediation. Accordingly, the optimized polymerization was carried out in 4 L reactors using an overhead stirrer with torque control to account for changes in viscosity (Figure S3, Supporting Information). The unsaturated

cooking oil (375 g) was first added to the reactor and heated to 170 °C, with the internal reaction temperature monitored directly throughout the synthesis. Elemental sulfur (375 g) was then added over 10 min, with the slow addition ensuring the reaction temperature did not fall below 155 °C. The reaction mixture appears as two transparent liquid phases at this stage: the sulfur appears orange or red on the bottom phase, while the yellow cooking oil resides in the top phase. Thermal homolysis of S–S bonds in elemental sulfur under these conditions generates thiyl radicals that initiate ring-opening polymerization of sulfur. The thiyl radical end groups contained in the resulting polysulfide intermediates also react with the alkenes of the cooking oil to form a crosslinked polysulfide (Figure 1).^[16e,18b] As this copolymerization occurs, the reaction mixture gradually becomes opaque and appears as one phase. At this stage, the reaction temperature was increased to 180 °C and the sodium chloride porogen (1.75 kg) was added over 15–20 min. As the copolymerization continues, the reaction mixture gradually forms a paste. Approximately 10–15 min after the addition of sodium chloride was complete, the viscosity increased such that the torque of the overhead stirrer registered 40 N cm. At this point, the synthesis was complete so the stirring was stopped and the reactor was removed from the heating source. After cooling the reaction to room temperature, the solid polymer–salt composite was broken into smaller pieces (Figure 1) and then washed with water to remove the sodium chloride porogen.

After removing the porogen from coarse particles (e.g., >2.5 mm diameter) of the salt–polysulfide composite, the resulting polymer contains pores measuring $119 \pm 53 \mu\text{m}$ diameter (Figure 1 and Figure 2A). We refer to material prepared in this way as a “porous polysulfide.” The salt–polymer composite can also be cut into a desired shape such as a cube and then converted into the porous polysulfide through a simple water wash as shown in Figure 2A. If the polymer is ground more finely (<2.5 mm particle diameter, Figure 1C), the friable polysulfide tears at the salt interface where a pore would otherwise form. After removing the salt from these smaller particles, a textured surface results, instead of pores (Figures S10 and S11, Supporting Information). We refer to this material as a “low-density polysulfide” rather than a porous polysulfide. Both the porous polysulfide and low-density polysulfides were dried to a constant mass by passing warm air (<45 °C) over the polymer for several hours.

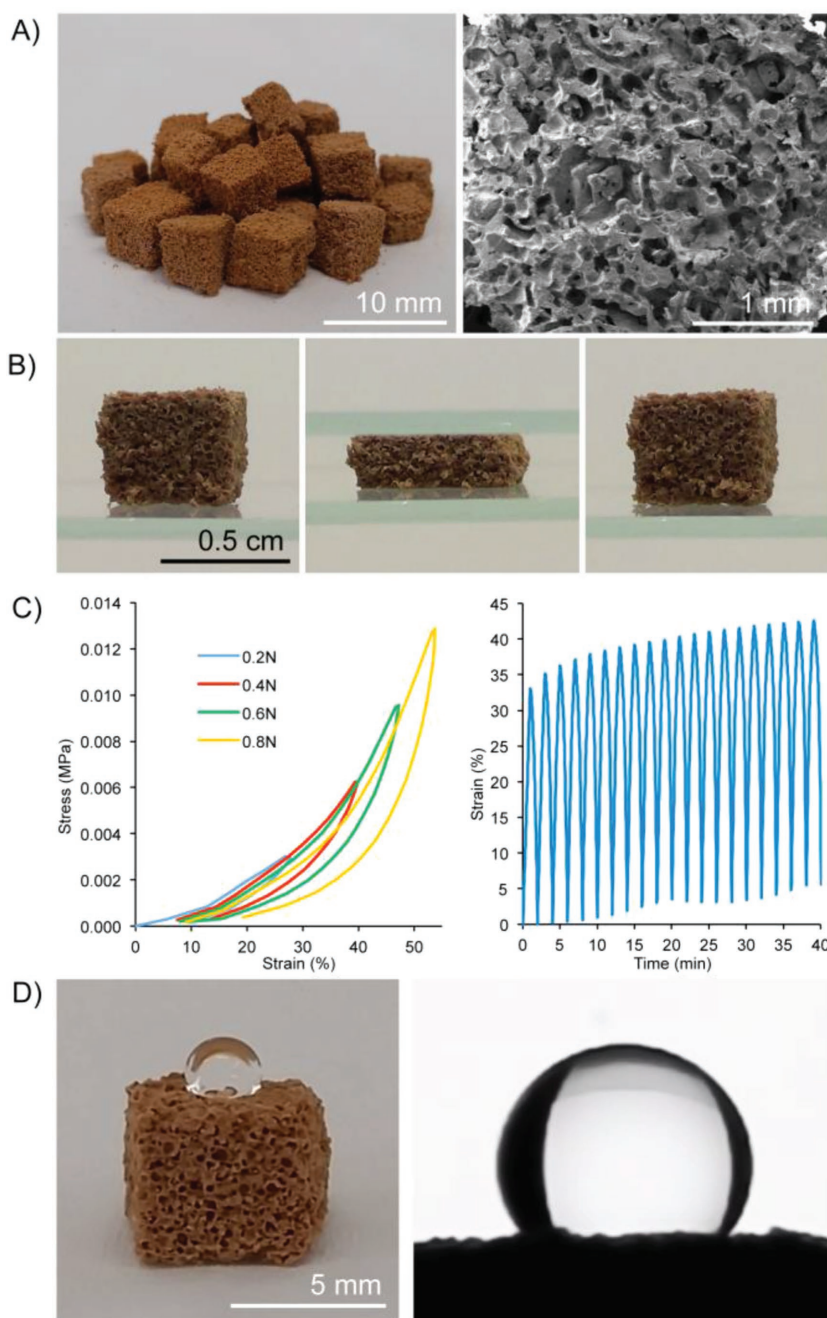


Figure 2. A) Blocks (5 mm × 5 mm × 5 mm) of the porous canola oil polysulfide and an SEM image of a polymer cross section showing the micrometer-scale pores ($119 \pm 53 \mu\text{m}$ diameter, measured for 50 randomly sampled pores in SEM images of the cross-section). B) The porous polysulfide is compressible. C) Left: Stress–strain curve of porous polysulfide when stress of 0.5 N is applied at 1 N min^{-1} up to 0.2, 0.4, 0.6, and 0.8 N force, with a relaxation of 1 N min^{-1} in between each compression step. The polymer can be compressed to increasing amounts of strain and recover, but there is an offset to a fixed strain (polymer deformation) that increased after each cycle. Right: Strain of the porous polysulfide when a stress of 0.5 N is applied at 0.5 N min^{-1} , followed by a return to zero force at 0.5 N min^{-1} , repeated over 20 cycles. This analysis shows that there is good repeatability of the compression and relaxation cycle. The polymer can be squeezed to 35% strain (0.5 N force) repeatedly. At this strain, there is only a small increase in compression set (the permanent deformation that remains after the cycle). D) The porous polysulfide is hydrophobic, with a water contact angle of $130^\circ \pm 10.5^\circ$, with a minimum observed angle of 111° and a maximum of 156° over 15 individual measurements. The photographs show a bead of water on the polymer and a representative image used to calculate water contact angles.

^1H NMR spectroscopy of the canola oil polysulfide in perdeuterated pyridine indicated 87% of the alkenes were consumed in the copolymerization for both pristine canola oil and used cooking oil (Figures S12–S15, Supporting Information). Pyridine was used in this analysis as it was the only solvent identified that could fully dissolve the canola oil polysulfide. The density of the canola oil polysulfide was 0.5 g cm^{-3} , which was anticipated to aid in buoyancy during oil spill remediation on water (Figure S16, Supporting Information). The surface area of the polymer was calculated to be in the range of $0.02\text{--}0.04\text{ m}^2\text{ g}^{-1}$, using the measured surface area of the sodium chloride porogen as a proxy for this feature (Figure S13, Supporting Information). It should be noted that no effort was made to optimize the surface area (for instance by preparing smaller porogen crystals), so that the sodium chloride could be used as received and not require laborious recrystallization. Thermogravimetric analysis indicated stability up to $200\text{ }^\circ\text{C}$. Above this temperature two major mass losses are observed at (≈ 230 and $\approx 340\text{ }^\circ\text{C}$).^[18b] The first mass loss is attributed to degradation of the more labile polysulfide domain (regions of the material containing S–S bonds) and the mass loss at higher temperature corresponds to degradation of remaining organic matter. The thermal analysis also revealed that there is typically 10–15% free sulfur in the final polymer product, as determined by integration of the endotherm detected through differential scanning calorimetry upon the melting of free sulfur. Similar thermal profiles were observed for polymer made from pristine canola oil and polymer made from used cooking oil (Figures S17 and S18, Supporting Information).

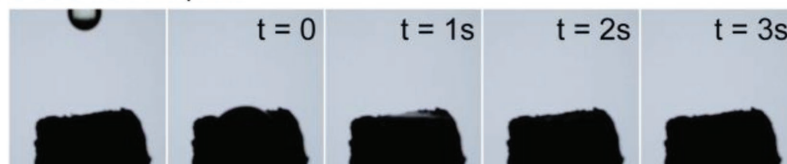
The formation of the polysulfide structure (S–S bonds) in the polymer was consistent with X-ray photoelectron spectroscopy (XPS) signals for S $2p_{3/2}$ at 163.8 eV (Figure S19, Supporting Information) as well as a signal at 463 cm^{-1} in the Raman spectrum. Angle resolved XPS also indicated residual sodium chloride (<3% fractional composition) is retained in the polymer even after extensive water washing (Figure S19, Supporting Information). Angle resolved XPS and neutral impact collision ion scattering spectroscopy were also used to profile the surface composition of the polysulfide, revealing a higher relative amount of carbon to sulfur down to 4 nm , and a constant ratio of carbon to sulfur in the bulk of the polymer at depths greater than 4 nm (Figures S19 and S20, Supporting Information).

Mechanical properties of the porous polysulfide were investigated through dynamic mechanical analysis (Figure 2C and Figures S21–S24, Supporting Information). Stress–strain curves indicate that polymer can be compressed repeatedly to 30% strain and can return to its original shape. Above 40% strain, polymer deformation is substantial (Figure S24, Supporting Information). The flexibility of the polysulfide gives it a sponge-like consistency

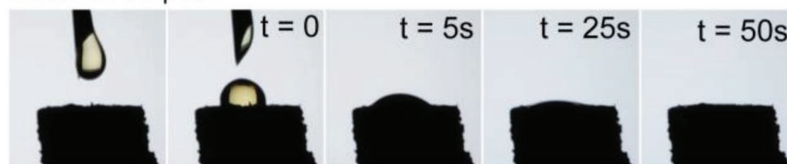
(Figure 2B) anticipated to be important in recovering bound oil through mechanical compression. The polymer was also hydrophobic, with a water contact angle of $130^\circ \pm 10^\circ$ (Figure 2D and Figure S25, Supporting Information). This property was expected for a material comprised of a hydrophobic triglyceride crosslinked with low-polarity polysulfide groups. The uptake of water is also relatively low, with only 56 mg of water sorbed per gram of polymer after 5 min of complete immersion in water.

Next, the porous polysulfide was tested in oil sorption experiments. The uptake of diesel fuel, motor oil (10W-30), and crude oil were all evaluated (Figure 3 and Figures S26–S30, Supporting Information). Diesel fuel uptake into the porous polysulfide was rapid, with complete sorption of a $5\text{ }\mu\text{L}$ drop within 3 s (Figure 3A). The more viscous motor oil was somewhat slower to permeate the polymer, but complete sorption was observed within 50 s (Figure 3B). Similar rates of uptake were observed for crude oil obtained directly from wellheads at multiple locations (Figures S28 and S29, Supporting Information). The sorption capacity for each of these oils was determined by partially immersing a $5.0\text{ mm} \times 5.0\text{ mm} \times 5.0\text{ mm}$ cube of the porous polysulfide into each respective oil. After the oil was visible at the top of the cube (transported through capillary action), the cube was removed and weighed after removing unbound oil. One gram of porous polymer typically absorbed 0.9 mL motor oil, 1 mL crude oil, and 1.4 mL of diesel fuel in this experiment (Figure S31, Supporting Information). The polymer was also effective at removing oil from water (Figure 3C). When the polymer particles ($2.5\text{--}5.0\text{ mm}$) were added to the oil–water mixture, the oil

A) Diesel fuel sorption



B) Motor oil sorption



C) Motor oil removal from water and recovery by compression



Figure 3. A) Sorption of $5\text{ }\mu\text{L}$ of diesel fuel into the porous polysulfide occurs within 3 s. B) Sorption of viscous motor oil (10-W30) into the porous polysulfide occurs over 50 s. C) 1.00 g of the porous polysulfide ($2.5\text{--}5.0\text{ mm}$ diameter particles) was added to a mixture of motor oil (1.00 mL) and water (5.00 mL). The polymer rapidly absorbs the oil and forms an oil–polymer aggregate, which can be easily removed from the water. The oil–polymer aggregate can be mechanically compressed to recover the oil (compression between two glass slides is shown). The polymer can be reused in oil–water separation.

was bound to the polymer within seconds. Additionally, the polymer particles aggregated upon oil sorption thereby facilitating recovery of the polymer-bound oil. Gratifyingly, both the oil and the polysulfide could be recovered by simply compressing the sorbent (Figure 3D). Imaging the surface of the bound oil by scanning electron microscopy (SEM) revealed that the pores were filled with oil (Figure S32, Supporting Information). After recovering the oil by compression, a film of oil remains on the surface of the polymer, as indicated by SEM analysis and infrared and Raman spectroscopy (Figures S33–S38, Supporting Information). Fortunately, this retained oil had minimal impact on the reuse of the polymer and the same oil sorption performance was observed for five sorption and oil recovery cycles (Figure S39, Supporting Information).

Further investigation of the low-density polysulfide (prepared as finer particles varying in size from 0.5 to 2.5 mm in diameter) revealed a similar behavior of binding to crude oil and forming an oil–polymer aggregate (Figure S40, Supporting Information). These particles could typically bind twice their mass in crude oil. In a control experiment in which the polysulfide was prepared without using the sodium chloride porogen, crude oil sorption was still observed but the oil capacity was 2.4 times lower than the low-density polysulfide (Figure S40, Supporting Information). Additionally, preparing the polysulfide without the porogen leads to a denser polymer that is less buoyant in water after binding to oil. Similarly, elemental sulfur can bind to crude oil and aggregate, but its binding sorption capacity is ≈ 2.5 times lower than the low-density polysulfide and the sulfur–crude oil aggregate sinks in water (Figure S40, Supporting Information). Buoyancy of the polymer-bound oil is a critical feature of a sorbent because it facilitates removal from the surface of contaminated water by skimming.

With these encouraging oil sorption and recovery results, we were motivated to assess the low-density polysulfide's ability to remove crude oil from seawater (Figure 4). For this experiment, the low-density polysulfide was first prepared from unsaturated waste cooking oil obtained from a restaurant (Figures S5–S9, Supporting Information). Next, 100 mL of crude oil was added to a glass dish containing 1.5 L of seawater. The low-density polysulfide (100 g) was added to the oil–water mixture and rapid uptake of oil was observed over a few seconds with simultaneous aggregation of the oil-soaked polymer particles. After 1 min of total treatment time, the oil–polysulfide aggregate was removed from the water using a net (Figure 4A) and the crude oil

could be recovered by compressing the oil–polymer aggregate (Figure 4B). A video of the oil sorption and removal from water is provided in Movie S1 in the Supporting Information. The protocol is fast, technically simple, and fully compatible with seawater (Figures S41 and S42, Supporting Information). Similar results were also observed in a similar experiment with motor oil (Figure S41, Supporting Information).

Due to the rapid sorption of the oil, the oil water separation could also be completed in a continuous process (Figure 4C and Movie S2, Supporting Information). In this experiment,

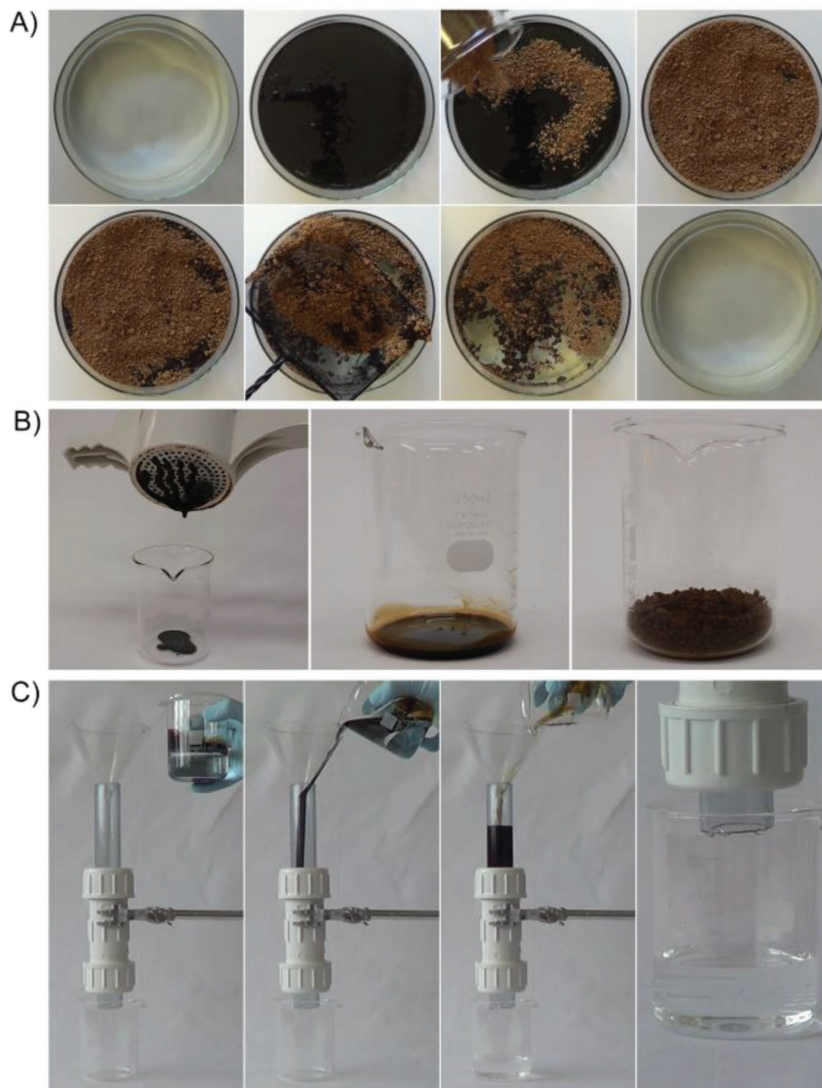


Figure 4. A) Crude oil (100 mL) was added to 1.50 L of seawater. The low-density polysulfide (100 g) was then added to the oil–water mixture. In less than 1 min, the oil and polymer form an aggregate that can be removed from the water by skimming with a net. A video of this process is provided in Movie S1 in the Supporting Information. B) The crude oil can be recovered from the low-density polysulfide by mechanical compression and the recovered polymer can be reused in oil sorption. C) A filter was constructed in which 30 g of the low-density polysulfide was packed into polyvinyl chloride (PVC) pipe. The polymer was immobilized using PVC mesh on the inflow end and cotton fabric on the outflow end (Figure S39, Supporting Information). A mixture of crude oil (10 g) and seawater (100 g) was poured through the filter. The oil remained bound to the polymer while the purified seawater passed through the filter. A video of this process is provided in Movie S2 in the Supporting Information.

the low-density polysulfide (30 g) was used as filtration media (Figures S43 and S44, Supporting Information). Pouring a mixture of seawater (100 g) and crude oil (10 g) through the filter resulted in efficient capture of the oil and purification of the seawater. We anticipate that the continuous process will be useful in cases where it is more convenient to pump oil and water mixtures through a filter, rather than depositing the sorbent directly on the oil spill.

In summary, a polysulfide was prepared by the copolymerization of sulfur and unsaturated cooking oils. This material binds oil and aggregates upon contact, allowing straightforward separation from water. Because of the unique material properties of the featured sulfur polymer, the bound oil can be recovered by mechanical compression and the polymer can be reused in oil sorption. The material can also serve as filtration media for the separation of oil and water in a continuous process. All starting materials are available in megaton quantities at low cost, so the prospect for using this material in large-scale oil spill remediation is promising. The sorbent was also prepared from sulfur and used cooking oil, meaning that every atom of the sorbent, in principle, can be derived from industrial waste. In the case of sulfur, it is a by-product of the petroleum sector—an industry closely tied to oil spills. Therefore, this study represents an intriguing way to extend industrial chemical life-cycles: a by-product from the petroleum industry was used to make a polymer that could remediate oil pollution directly associated with that same industry. We also note that the use of canola oil aligns with a growing interest in identifying low-cost and sustainable crosslinkers for sulfur polymers.^[16e,18a,d,19] The use of such polysulfides in oil spill remediation is an entirely new and environmentally beneficial application for polymers made from sulfur. This application consumes excess waste sulfur that is stockpiled around the globe and may help mitigate the perennial problem of oil spills in aquatic environments.

Supporting Information

Supporting Information is available from the Wiley Online Library or from the author.

Acknowledgements

This research was supported financially by Flinders University, the Australian Government National Environmental Science Programme Emerging Priorities Funding (J.M.C.), FCT Portugal (I.S.A. and G.J.L.B.), The Royal Society (University Research Fellowship, G.J.L.B.), the Engineering and Physical Sciences Research Council (G.J.L.B.), and the European Research Council (Starting Grant, G.J.L.B.). J.M.C. also acknowledges support from the Australian Research Council Discovery Early Career Research Award (DE150101863) and the Royal Australian Chemical Institute David Solomon Award. The authors are also grateful for the support of the Australian Microscopy and Microanalysis Research Facility (AMMRF) at Flinders University. Additionally, this work was performed in part at the South Australian node of the Australian National Fabrication Facility (ANFF) under the National Collaborative Research Infrastructure Strategy to provide nano and microfabrication facilities for Australia's researchers. The authors thank McHugh's cafe at Flinders University for supplying used cooking oil and the Australian School of Petroleum at the University of Adelaide for providing crude oil samples.

Conflict of Interest

Two authors (M.J.H.W. and J.M.C.) are inventors on a patent associated with the synthesis and applications of the canola oil polysulfide material (Patent No. WO 2017181217).

Keywords

inverse vulcanization, oil spills, polysulfides, sulfur, waste valorization

Received: February 16, 2018

Revised: March 6, 2018

Published online: April 18, 2018

- [1] a) P. F. Kingston, *Spill Sci. Technol. Bull.* **2002**, *7*, 53; b) J. Rogowska, J. Namieśnik, *Environmental Implications of Oil Spills from Shipping Accidents*, Vol. 206, Springer, New York **2010**, p. 95; c) Y. Gong, X. Zhao, Z. Cai, S. E. O'Reilly, X. Hao, D. Zhao, *Marine Pollut. Bull.* **2014**, *79*, 16; d) S. E. Chang, J. Stone, K. Demes, M. Piscitelli, *Ecol. Soc.* **2014**, *19*, 26; e) J. Coleman, J. Baker, C. Cooper, M. Fingas, G. Hunt, K. Kvenvolden, K. Michel, J. Michel, J. McDowell, J. Phinney, R. Pond, N. Rabalais, L. Roesner, R. B. Spies, *Oil in the Sea III. Inputs, Fates, and Effects*, The National Academies Press, Washington, D.C. **2003**.
- [2] B. D. Goldstein, H. J. Osofsky, M. Y. Lichtveld, *N. Engl. J. Med.* **2011**, *364*, 1334.
- [3] a) J. Lubchenco, M. K. McNutt, G. Dreyfus, S. A. Murawski, D. M. Kennedy, P. T. Anastas, S. Chu, T. Hunter, *Proc. Natl. Acad. Sci. USA* **2012**, *109*, 20212; b) J. Beyer, H. C. Trannum, T. Bakke, P. V. Hodson, T. K. Collier, *Mar. Pollut. Bull.* **2016**, *110*, 28.
- [4] *Summary of West Coast Oil Spill Data, Pacific States/British Columbia Oil Spill Task Force*, <http://oilspilltaskforce.org/ourwork/data-project/> (accessed: November 2017).
- [5] Environmental Assessment of Ogoniland, *United Nations Environment Programme*, https://postconflict.unep.ch/publications/OEA/UNEP_OEA.pdf (accessed: November 2017).
- [6] a) M. San Sebastián, B. Armstrong, J. A. Córdoba, C. Stephens, *Occup. Environ. Med.* **2001**, *58*, 517; b) M. San Sebastián, A.-K. Hurtig, *Pan Am. J. Public Health* **2004**, *15*, 205.
- [7] E. Nyankson, D. Rodene, R. B. Gupta, *Water, Air, Soil Pollut.* **2016**, *227*, 29.
- [8] a) M. O. Adebajo, R. L. Frost, J. T. Klopogge, O. Carmody, S. Kokot, *J. Porous Mater.* **2003**, *10*, 159; b) Q. Ma, H. Cheng, A. G. Fane, R. Wang, H. Zhang, *Small* **2016**, *12*, 2186; c) J. Ge, H.-Y. Zhao, H.-W. Zhu, J. Huang, L.-A. Shi, S.-H. Yu, *Adv. Mater.* **2016**, *28*, 10459; d) M. Fingas, *The Basics of Oil Spill Cleanup*, 3rd ed., CRC Press, New York **2013**.
- [9] D. P. Prendergast, P. M. Gschwend, *J. Cleaner Prod.* **2014**, *78*, 233.
- [10] Q. F. Wei, R. R. Mather, A. F. Fotheringham, R. D. Yang, *Mar. Pollut. Bull.* **2003**, *46*, 780.
- [11] a) H.-M. Choi, R. M. Cloud, *Environ. Sci. Technol.* **1992**, *26*, 772; b) T. R. Annunciado, T. H. D. Sydenstricker, S. C. Amico, *Mar. Pollut. Bull.* **2005**, *50*, 1340.
- [12] G. Kutney, *Sulfur: History, Technology, Applications and Industry*, 2nd ed., ChemTec Publishing, Toronto **2013**.
- [13] L. E. Apodaca, in *Mineral Commodity Summaries, U.S. Department of the Interior*, U.S. Geological Survey **2017**, pp. 162–163.
- [14] a) M. G. Kulkarni, A. K. Dalai, *Ind. Eng. Chem. Res.* **2006**, *45*, 2901; b) L. Lin, H. Allemekinders, A. Dansby, L. Campbell, S. Durance-Tod, A. Berger, P. J. H. Jones, *Nutr. Rev.* **2013**, *71*, 370.
- [15] M. A. R. Meier, J. O. Metzger, U. S. Schubert, *Chem. Soc. Rev.* **2007**, *36*, 1788.

- [16] a) W. J. Chung, J. J. Griebel, E. T. Kim, H. Yoon, A. G. Simmonds, H. J. Ji, P. T. Dirlam, R. S. Glass, J. J. Wie, N. A. Nguyen, B. W. Guralnick, J. Park, Á. Somogyi, P. Theato, M. E. Mackay, Y.-E. Sung, K. Char, J. Pyun, *Nat. Chem.* **2013**, *5*, 518; b) A. Hoefling, P. Theato, *Nachr. Chem.* **2016**, *64*, 9; c) J. J. Griebel, R. S. Glass, K. Char, J. Pyun, *Prog. Polym. Sci.* **2016**, *58*, 90; d) D. A. Boyd, *Angew. Chem., Int. Ed.* **2016**, *55*, 15486; e) M. J. H. Worthington, R. L. Kucera, J. M. Chalker, *Green Chem.* **2017**, *19*, 2748.
- [17] J. J. Griebel, S. Namnabat, E. T. Kim, R. Himmelhuber, D. H. Moronta, W. J. Chung, A. G. Simmonds, K.-J. Kim, J. van der Laan, N. A. Nguyen, E. L. Dereniak, M. E. Mackay, K. Char, R. S. Glass, R. A. Norwood, J. Pyun, *Adv. Mater.* **2014**, *26*, 3014.
- [18] a) M. P. Crockett, A. M. Evans, M. J. H. Worthington, I. S. Albuquerque, A. D. Slattery, C. T. Gibson, J. A. Campbell, D. A. Lewis, G. J. L. Bernardes, J. M. Chalker, *Angew. Chem., Int. Ed.* **2016**, *55*, 1714; b) M. J. H. Worthington, R. L. Kucera, I. S. Albuquerque, C. T. Gibson, A. Sibley, A. D. Slattery, J. A. Campbell, S. F. K. Alboaiji, K. A. Muller, J. Young, N. Adamson, J. R. Gascooke, D. Jampaiah, Y. M. Sabri, S. K. Bhargava, S. J. Ippolito, D. A. Lewis, J. S. Quinton, A. V. Ellis, A. Johs, G. J. L. Bernardes, J. M. Chalker, *Chem. Eur. J.* **2017**, *23*, 16219; c) T. Hasell, D. J. Parker, H. A. Jones, T. McAllister, S. M. Howdle, *Chem. Commun.* **2016**, *52*, 5383; d) D. J. Parker, H. A. Jones, S. Petcher, L. Cervini, J. M. Griffin, R. Akhtar, T. Hasell, *J. Mater. Chem. A* **2017**, *5*, 11682; e) M. W. Thielke, L. A. Bultema, D. D. Brauer, B. Richter, M. Fischer, P. Theato, *Polymers* **2016**, *8*, 266; f) N. A. Lundquist, M. J. H. Worthington, N. Adamson, C. T. Gibson, M. R. Johnston, A. V. Ellis, J. M. Chalker, *RSC Adv.* **2018**, *47*, 231; g) L. J. Esdaile, J. M. Chalker, *Chem. Eur. J.* **2018**, <https://doi.org/10.1002/chem.201704840>.
- [19] a) I. Gomez, O. Leonet, J. Alberto Blazquez, D. Mecerreyes, *ChemSusChem* **2016**, *9*, 3419; b) A. Hoefling, Y. J. Lee, P. Theato, *Macromol. Chem. Phys.* **2017**, *218*, 1600303; c) S. Shukla, A. Ghosh, P. K. Roy, S. Mitra, B. Lochab, *Polymer* **2016**, *99*, 349; d) A. Ghosh, S. Shukla, G. S. Khosla, B. Lochab, S. Mitra, *Sci. Rep.* **2016**, *6*, 25207.

4.1 SULFUR POLYMERS FOR OIL REMEDIATION

EXPERIMENTAL

General Experimental Considerations

IR Spectroscopy: Infrared (IR) spectra were recorded on a Fourier Transform spectrophotometer using the ATR method. Absorption maxima are reported in wavenumbers (cm^{-1}).

Raman Spectroscopy and Microscopy: Raman data was obtained using an XplorRA Horiba Scientific Confocal Raman microscope. Spectra were acquired using a 50X objective (numerical aperture 0.55) at an excitation wavelength of 638 nm. Typical integrations times for the spectra were 20 to 60 s and averaged from 1 to 3 repetitions.

SEM: Scanning Electron Microscopy (SEM) images were obtained using an FEI F50 Inspect system.

Materials

Porous polysulfide/polymer: Canola oil polysulfide prepared using the salt-inclusion method described in chapter 2. Where fryer oil is used instead of canola oil in the synthesis this will be noted.

Low-density polysulfide/polymer: Canola oil polysulfide prepared using the up-scaled method as described in chapter 2. The material is identical to the porous polysulfide however is milled to such a small particle size the individual particles no show visible pores or channels. Where fryer oil is used instead of canola oil in the synthesis this will be noted.

Non-porous polysulfide: Canola oil polysulfide as described in chapter 2. Synthesised without the use of an NaCl porogen. Where fryer oil is used instead of canola oil in the synthesis this will be noted.

Fryer oil: Used mixed-vegetable cooking oil donated by McHugh's Café, Flinders University SA.

Australian Crude Oil: A thin crude oil from Nockatunga Oil Fields, QLD, Australia

Texan Crude Oil: A thick crude Oil from Texas Crude, West Texas, USA

Motor Oil: Castrol Magnatec 10W40 motor oil

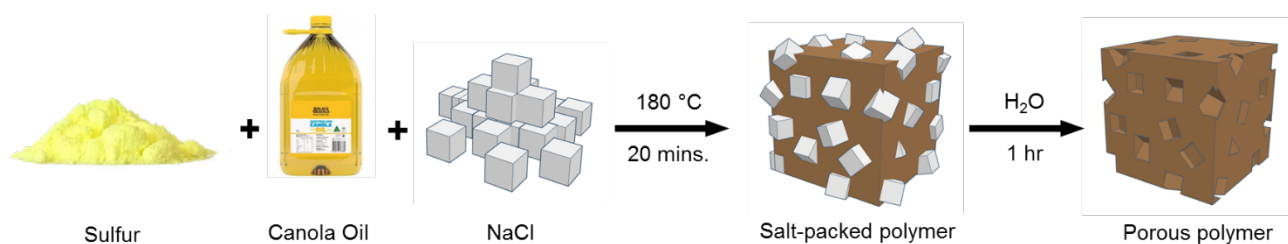


Figure 4.1.1 | Overview of synthesis procedure for porous polysulfide. An equal mass of sulfur and canola oil are heated with stirring to 180 °C with 70 wt. % salt until the material vitrifies (ca. 20 minutes). After cooling the material is washed with water to remove the salt, leaving a porous block of material.



Figure 4.1.2 | Cube of porous polysulfide, approximately 5.0 mm across on each side.

Crude Oil capacity of porous polysulfide

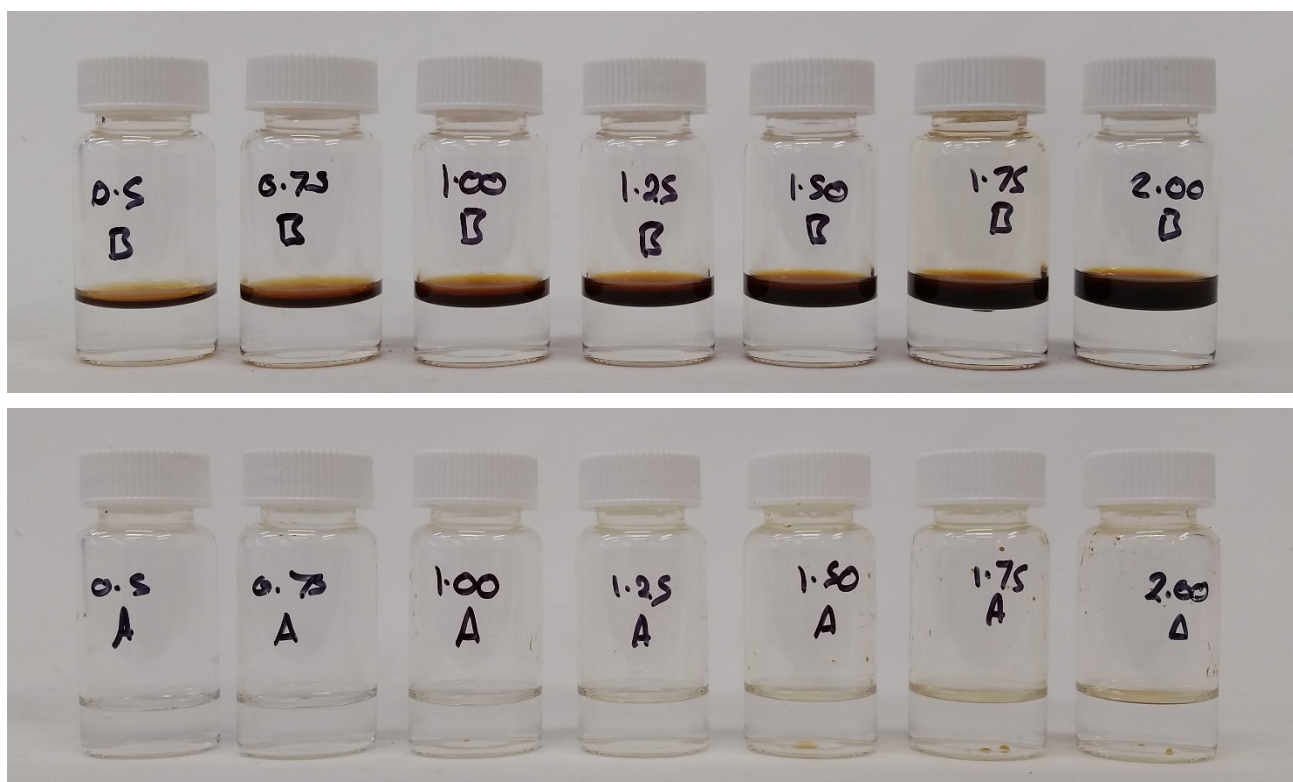


Figure 4.1.3 | Top: Left to right: 0.50, 0.75, 1.00, 1.25, 1.50, 1.75 and 2.00 mL Nockatunga crude oil suspended on DI water. Bottom: Crude oil suspensions after treatment with 1.00 g porous polymer for 5 min.

Oil is still visible from 1.25 mL oil and onwards. On measuring the mass of the polymer after absorption, the change in mass exceeded that of the oil available. Excess mass is likely to be water. Absorption experiments (see contact angle experiments below) show porous polysulfide absorbs its capacity in crude oil within seconds, so for the remainder of the 5-minute residence the polymer is exposed to the surface of the water below. As such weight measurements do not accurately represent the exact volume of oil sequestered. This experiment gives some idea as to the effectiveness of the polymer at sequestering oil however.

A follow-up experiment was devised to determine polymer capacity: Porous polymer was cut into manageable cubes of 0.5 cm diameter and placed in a glass dish of crude oil such that the polymer was partially submerged. After enough time had passed for the oil to wick up to the surface of the polymer cubes, they were removed from the oil, excess liquid dabbed off in a separate glass dish and the change in mass used to determine the amount of oil sequestered. Values are given as an average of 5 replicates per oil type.

Liquid	Density (g mL ⁻¹)	Wicking time (s)	Capacity (mL g ⁻¹)	Std. Dev.
Australian crude oil	0.76	30	0.95	± 0.15
Texan crude oil	0.89	300	0.95	± 0.14
Motor oil	0.75	300	0.86	± 0.14
Diesel	0.80	60	1.36	± 0.39
Water (control)	1.00	300	0.056	± 0.012

Note that water did not fully wick up into the polysulfide, but the experiment was stopped after 5 minutes to correspond with the longest time taken for the oils to wick.

The porous polysulfide exhibits the same capacity for both the thin and thick crude oils, with a significant difference in wicking time (0.5 vs. 5 minutes). Of the processed oils, motor also took 5 minutes to soak into the polymer but with a lower total capacity and diesel took twice as long as the thin crude oil but to a greater capacity, but also the highest deviation in individual measurements. Only 56 µL water was absorbed by the polymer over 5 minutes.

Re-use and recovery of porous polysulfide and motor oil

To a mixture of 5.00 mL water and 1.00 mL motor oil was added 1.00 g porous polymer (2.5–5.0 mm diameter particles). After 5 minutes the polymer was removed and compressed to remove the trapped oil. The recovered polymer was then re-used in a repeat experiment. This process was repeated until the polymer had been used 5 times.

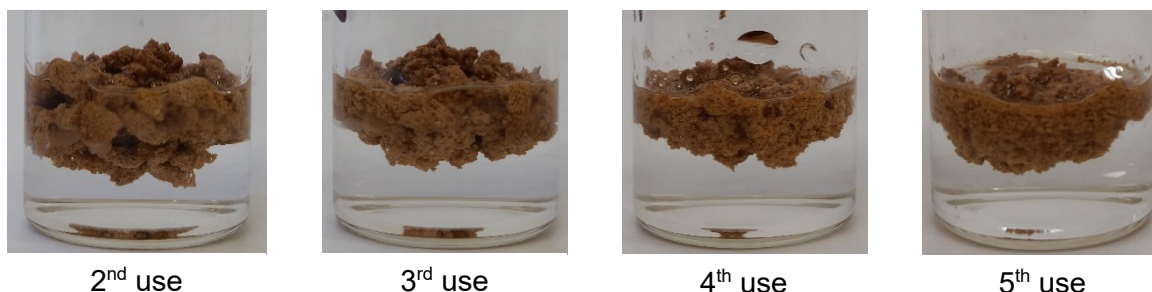


Figure 4.1.4 | 1.0 g porous polysulfide re-used multiple times to sequester a total of 5.0 mL oil in 1.0 mL batches

With increasing use, the porous polysulfide begins to break into smaller and smaller particles, partly from a weakening of the structure when saturated but also from the compression used in the recovery step. Despite the change in size, the polymer continues to show affinity for oil, with a single 1.00 g sample removing 1 mL oil 5 times for a total of 5 mL sequestered in this experiment. The polymer could theoretically be used more than 5 times but the degradation of structure after 5 tests made recovery difficult. Encased in a tea bag- or pillow-like membrane the polymer may continue to prove capable of recovering oil with a simplified recovery process.

SEM analysis of porous polysulfide before and after oil absorption

2.0 g porous polysulfide was incubated at room temperature in 10 mL motor oil (over capacity) for 10 minutes to ensure saturation. After removing the polymer particles from the oil with forceps, a portion of the saturated polymer was compressed to recover the absorbed oil. 4 samples were observed under the SEM from different points of this experiment: 1. Porous polysulfide, saturated with motor oil. 2. Porous polysulfide, saturated with motor oil after compression to remove oil. 3. Untreated, pristine porous polysulfide. 4. Pristine porous polysulfide, compressed similarly to sample 1 but with no oil treatment.

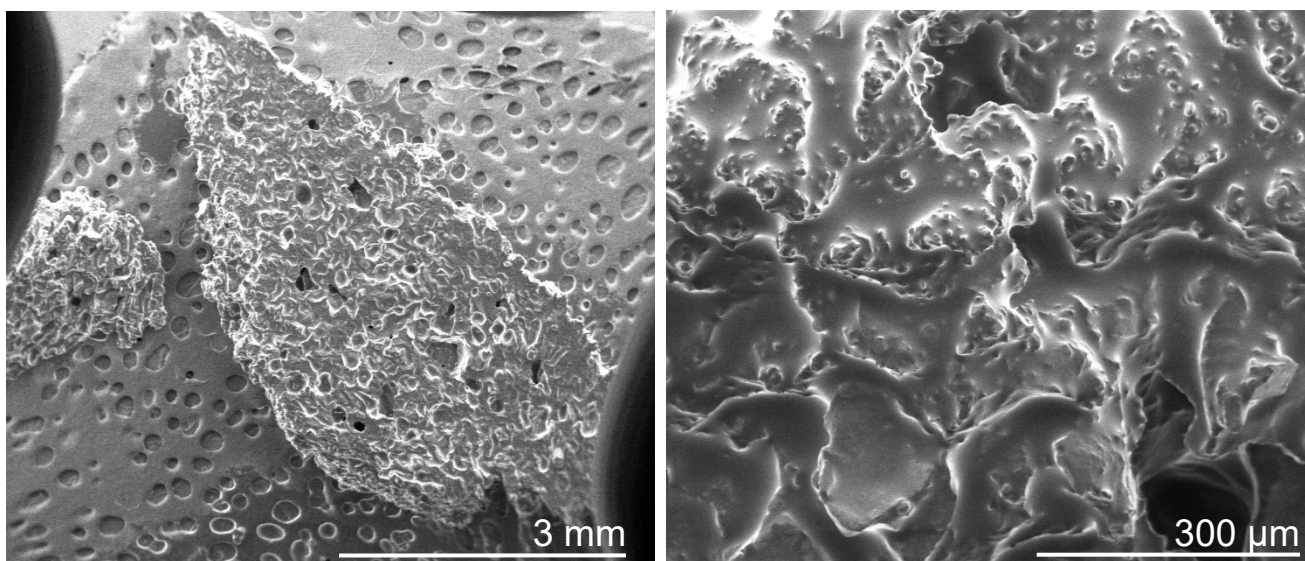


Figure 4.1.5 | Porous polysulfide, saturated with motor oil. Left: low magnification, right: high magnification.

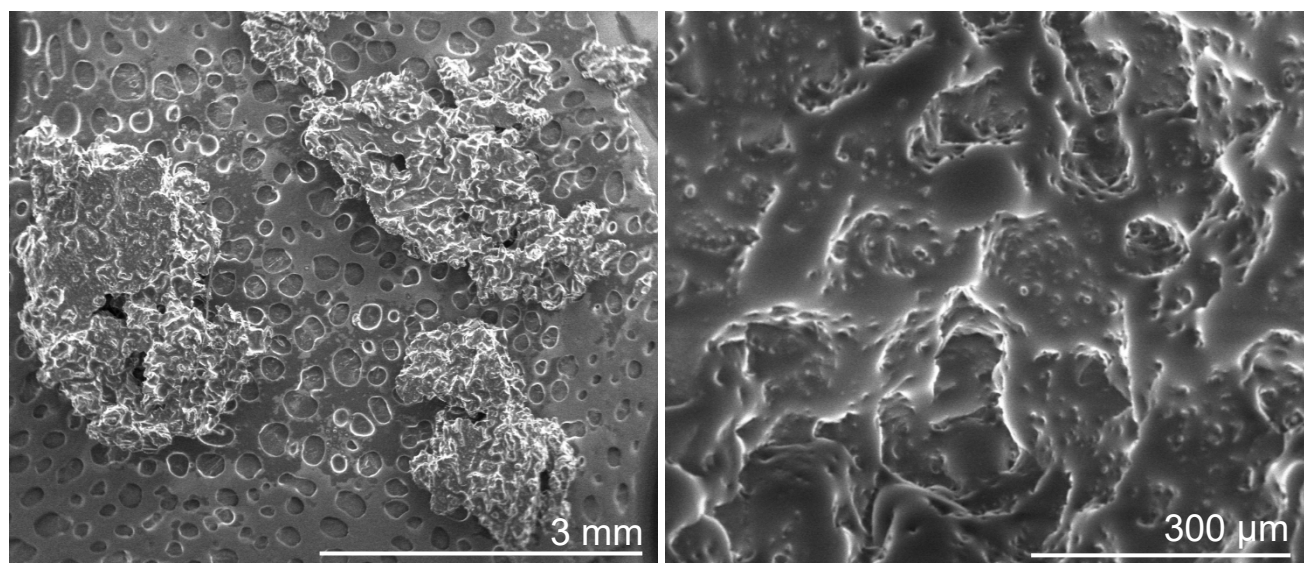


Figure 4.1.6 | Porous polysulfide, saturated with motor oil, pressed to recover oil. Left: low magnification, right: high magnification.

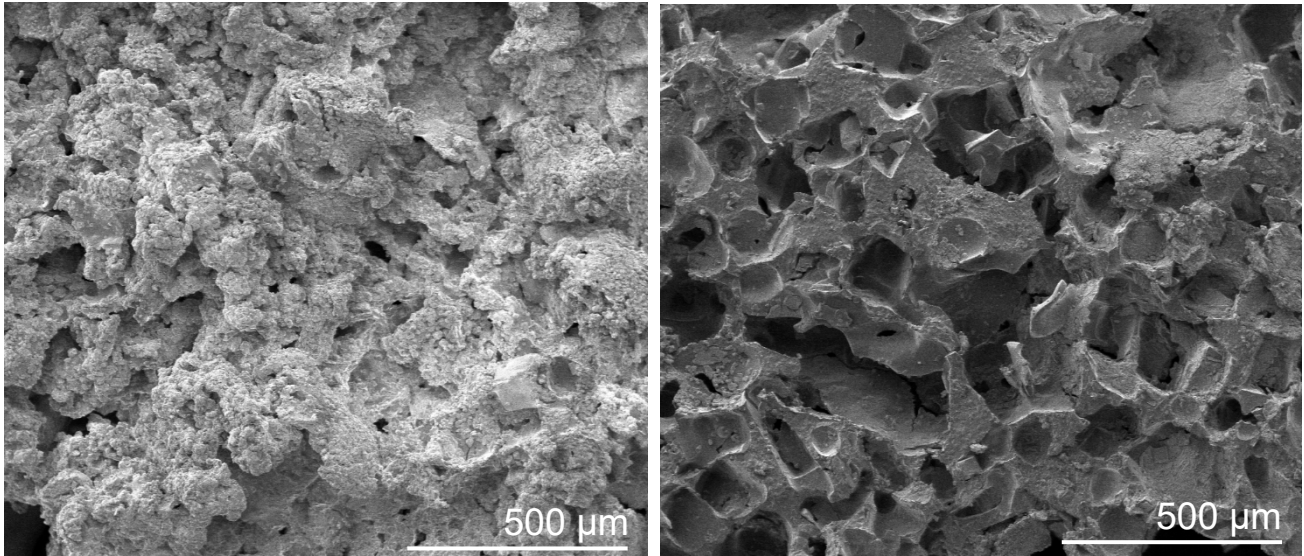


Figure 4.1.7 | Porous polysulfide. Left: high magnification image of the polymer surface, right: high magnification of internal cross section.

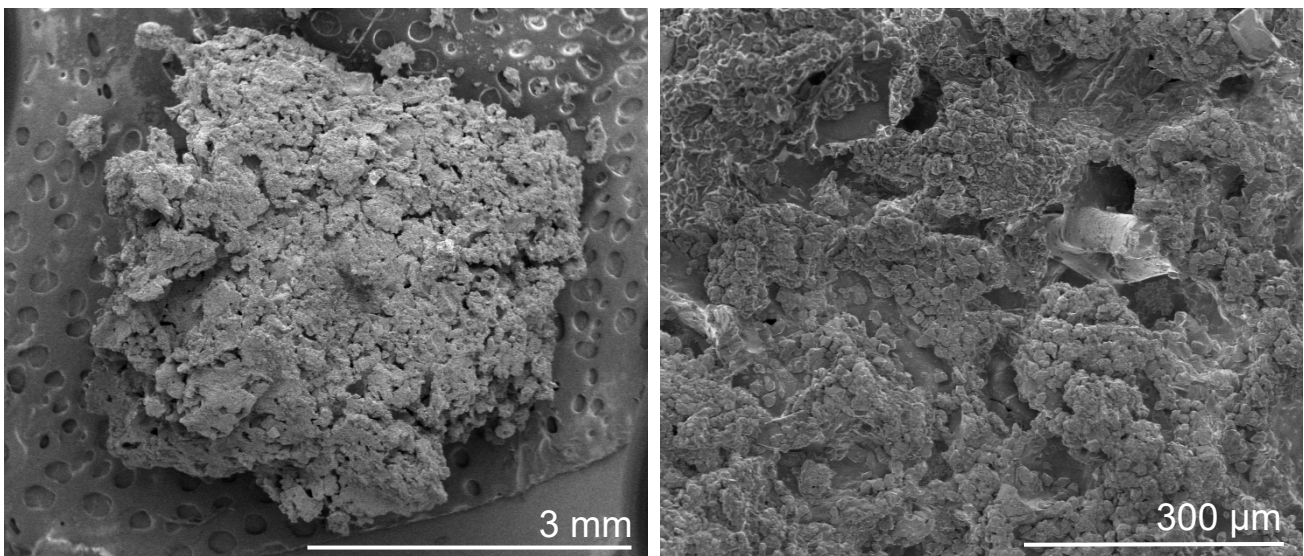


Figure 4.1.8 | Porous polysulfide, pressed similarly to sample 2 but without oil present. Top left: low magnification surface, right: high magnification surface, left: very high magnification surface.

IR analysis of porous polysulfide before and after oil absorption

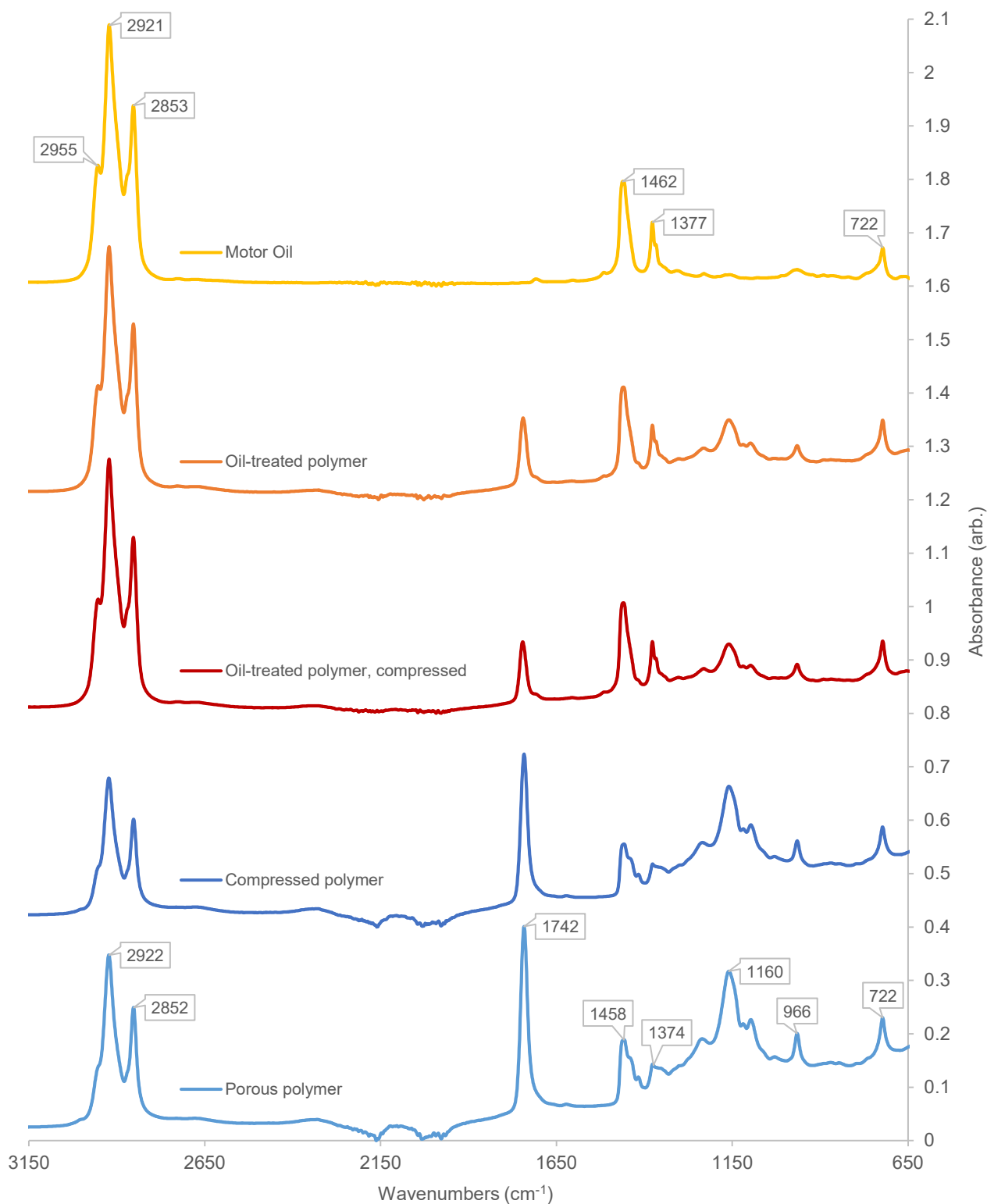


Figure 4.1.9 | IR spectra of porous polysulfide treated with motor oil, before and after compression to recover the oil. The porous polysulfide and motor oil samples share a few common peaks that overlap in the oil-treated polymer spectra. Shown here is that even after compression, motor oil is still present on the surface of the porous polysulfide (indicated by peaks at 1377 cm⁻¹ and 1462 cm⁻¹) as the IR trace of oil-treated polysulfide is no different before and after compression.

Raman analysis of porous polysulfide before and after oil absorption

Spectra acquired by Christopher Gibson

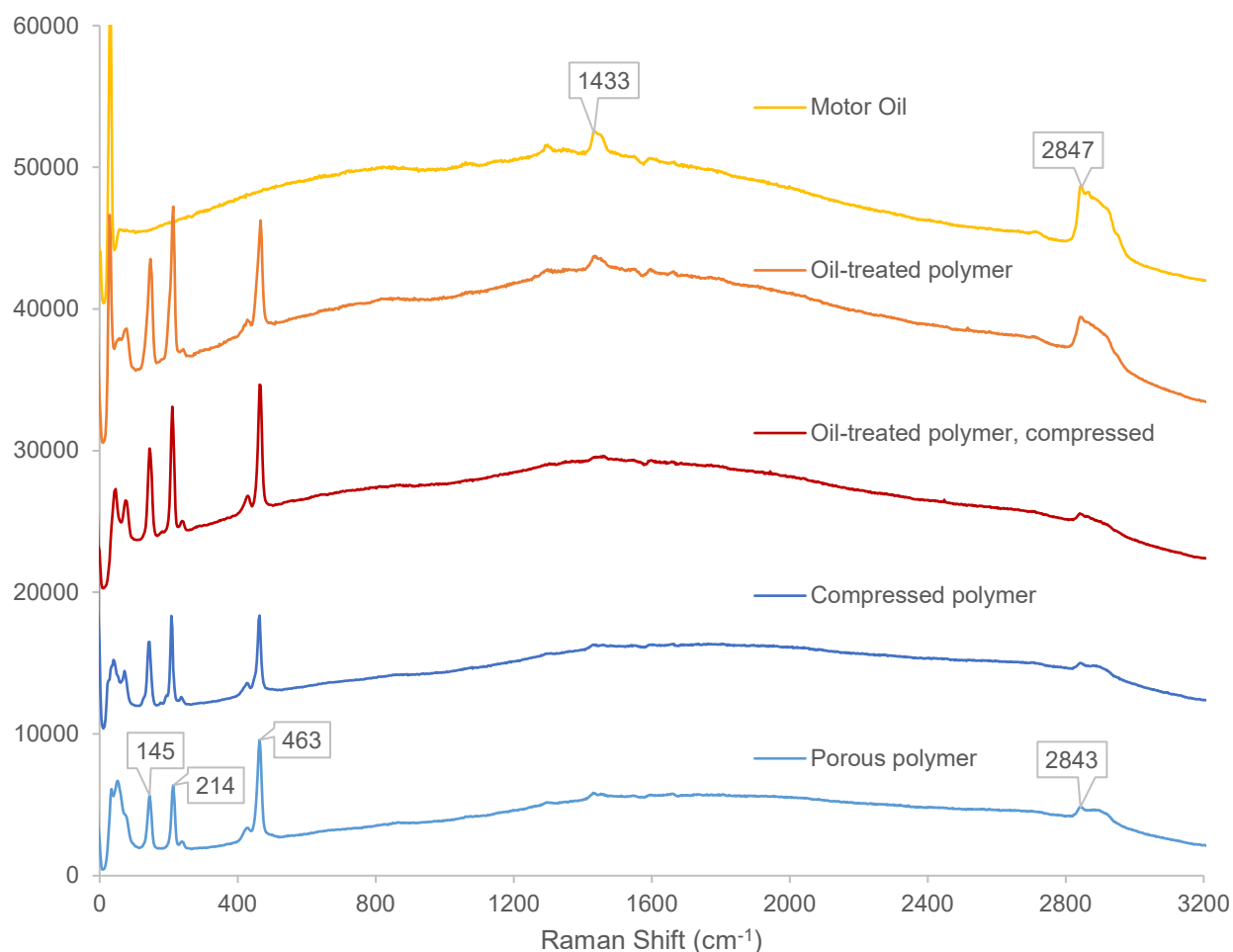


Figure 4.1.10 | Raman spectra of porous polysulfide treated with motor oil

Raman analysis provides information similar to that of the IR analysis. Major peaks for the polysulfide occur below 500 cm^{-1} , corresponding to sulfur stretches¹. A broad stretch also occurs at approximately 2900 cm^{-1} , from 2820 to 2950 cm^{-1} . This feature appears as a sharp bump at 2843 and a broad, secondary peak that stretches over to 2950 cm^{-1} . Motor oil shows a similar peak stretching over 2800 to 2990 cm^{-1} . The appearance is not quite the same however, after the initial peak there is not a second bump, but a slow descending slope that eventually drops off from 2930 to 2990 cm^{-1} . A similar motion is seen in the oil-treated polymer, indicating oil on the surface of the polymer. The oil-treated and then compressed polymer however also shows this slope rather than a second broad peak, this could be indicative of oil still being present and clinging to the surface of the polysulfide. Fig. 4.1.11 shows a focused view of these peaks for comparison.

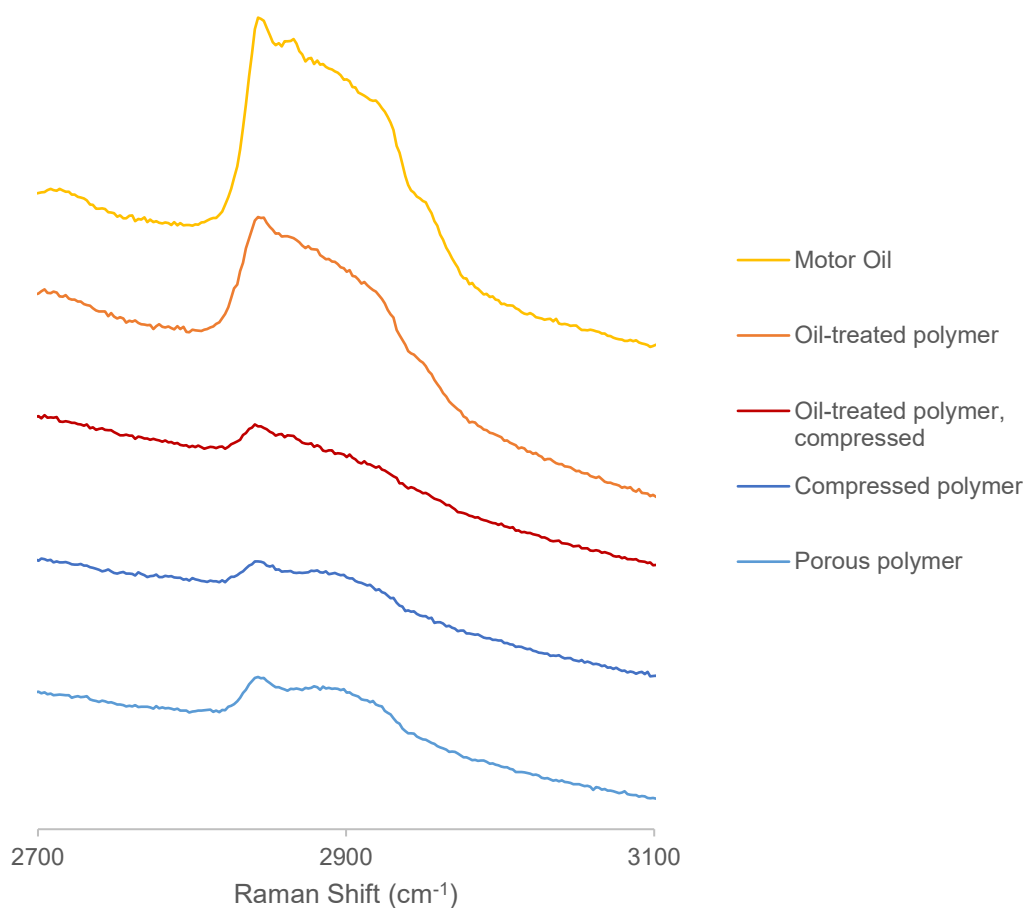


Figure 4.1.11 | Focused section of Fig. 4.1.10 (2700–3100 cm⁻¹). Note the downward slope across the top of the broad peak in the motor oil sample, but the presence of two distinct peaks in the polysulfide. The former is seen in the oil-treated and compressed post oil-treatment polysulfide, indicating oil is still present on the surface after compression.

Water and Oil Contact Angle Measurements

Experiments performed with and contact angle measurements determined by Cameron Shearer

The contact angle measurements of the polymer surface was determined with a contact angle goniometer (Sinterface PAT1). A droplet of Milli-Q water, diesel or motor oil was applied to the surface (approx. 5 μL) using a motor controlled syringe (water) or manual syringe (diesel, motor oil). Water contact angle (WCA) measurements were determined using low bond axisymmetric drop shape analysis from the plugin DropSnake² for ImageJ software (v1.48, NIH, USA).

Motor Oil

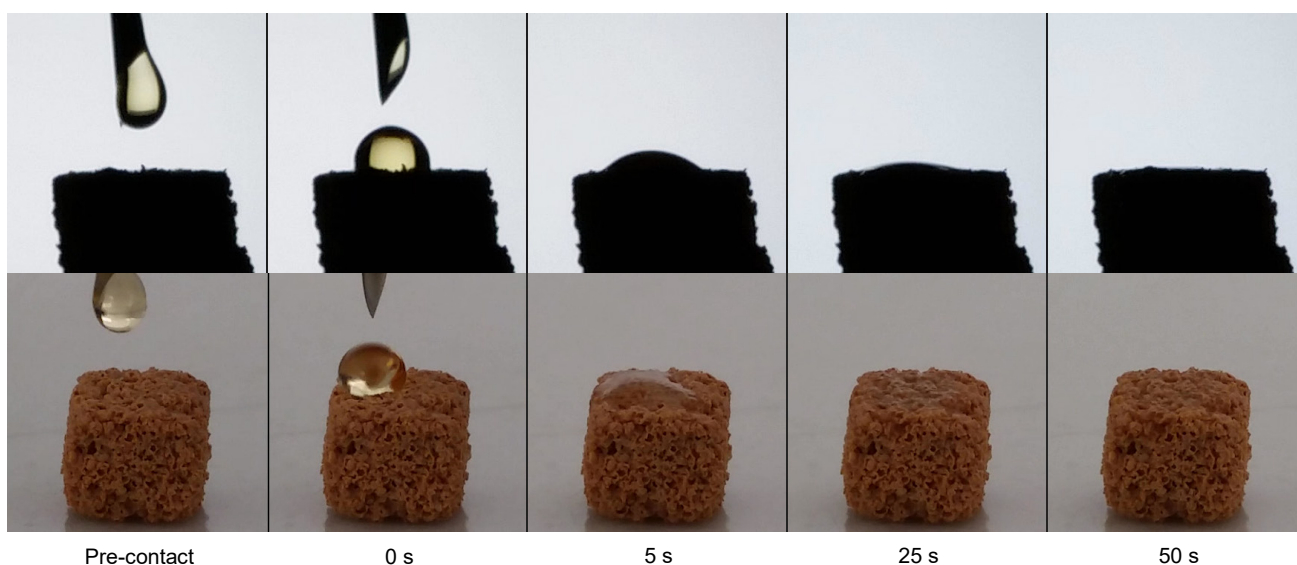


Figure 4.1.12 | Top: Experiment performed on the goniometer; Bottom: experiment performed on the desk to afford a colour image. A single drop of motor oil was dropped onto the surface of a 0.5 cm cube of porous polysulfide. Within 50 seconds the single motor oil bead was absorbed fully into the polymer. The same absorption rate was witnessed for multiple tests (each row of time-lapse images is a different experiment).

Diesel

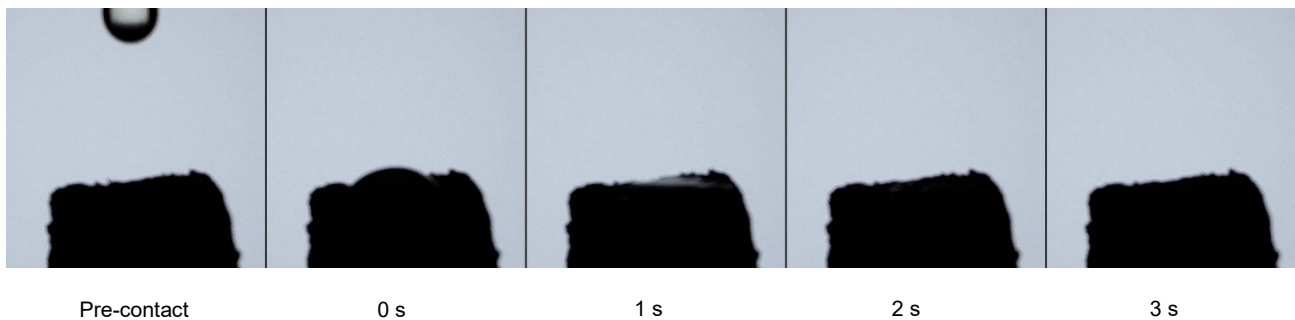


Figure 4.1.13 | Diesel, the thinner of the two processed oils, flowed very readily into the polymer. Within 3 seconds the bulk was absorbed into the polysulfide and residual traces were seen to evaporate from the surface.

Crude Oil (Australian)

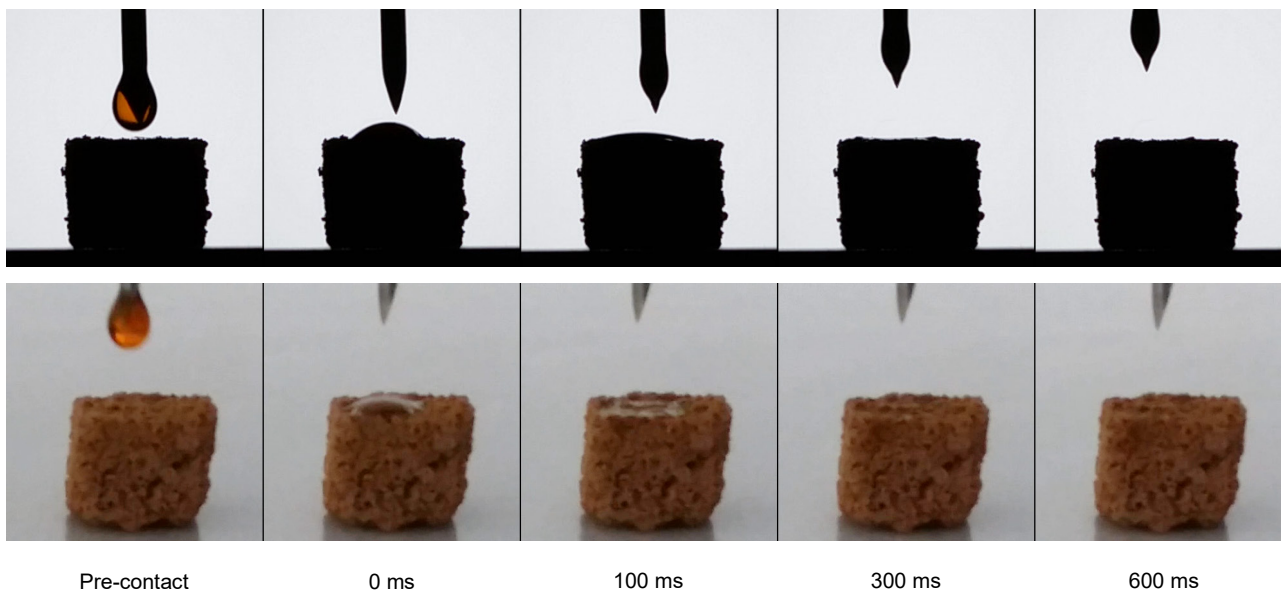


Figure 4.1.14 | Top: Experiment performed on the goniometer; Bottom: experiment performed on the desk to afford a colour image. The fastest absorption rate was observed for the Australian-sourced crude oil, the droplet soaking in in less than a second.

Crude Oil (Texas)

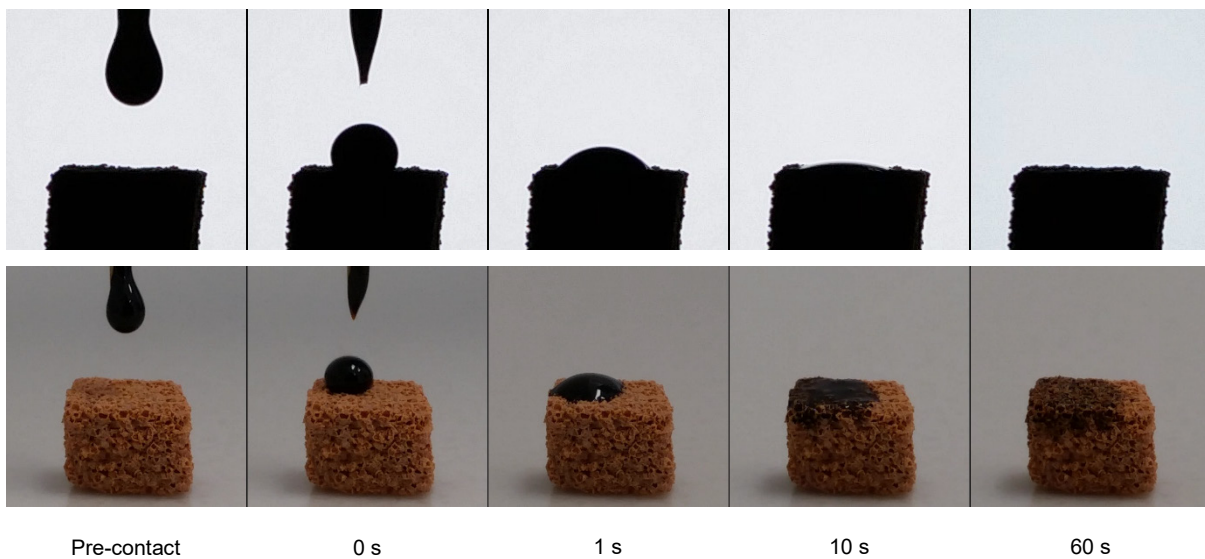


Figure 4.1.15 | Top: Experiment performed on the goniometer; Bottom: experiment performed on the desk to afford a colour image. In a first test, a droplet of the thicker, Texas-sourced crude oil fully permeated in under a minute, similar to the motor oil sample.

It was observed in this series of experiments that the inclusion of sodium chloride (remaining from synthesis having not been washed away fully) interfered with oil absorption, increased sorption times. For example, from 1 minutes to 5 minutes in the case of the Texan crude oil. This stresses the importance of thorough washing and removal of salt before the polysulfide is to be used in oil sorption.

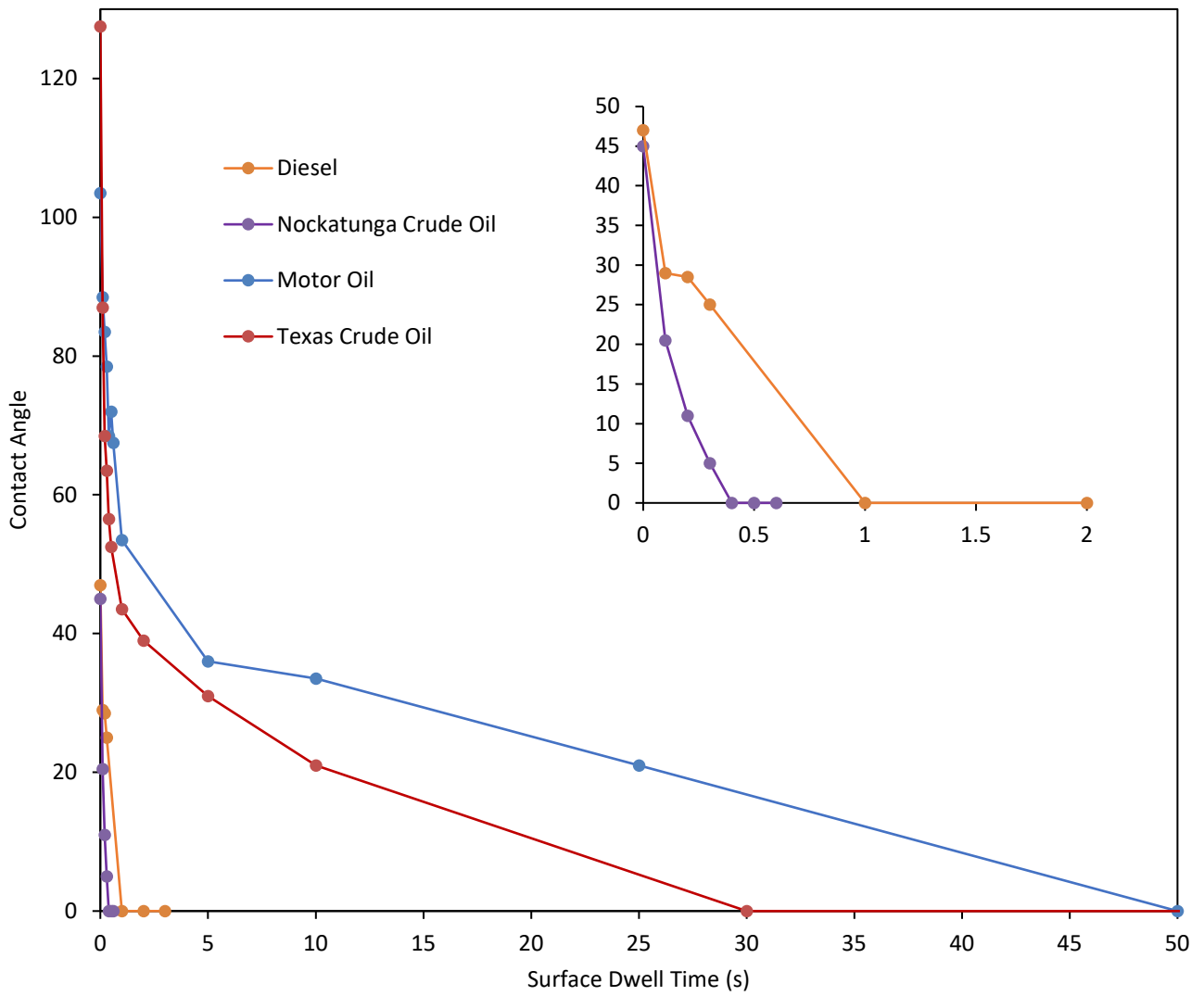
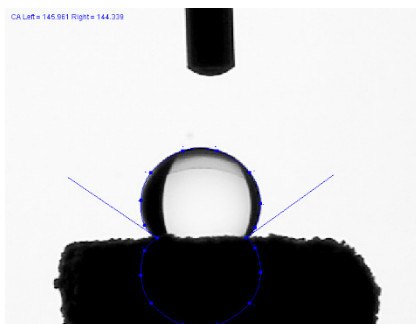


Figure 4.1.16 | Contact angle of a droplet of oil on the polymer surface as it changes over time for various oils. Values are an average of the left and right contact angles of a single droplet. Sorption is especially rapid for diesel and thin crude oil, but absorption of all oils is fast at under 1 minute in all cases.

Water contact angle



Water droplet on cube of porous polymer



Example contact angle measurement



10 μ L droplet on 0.5 cm-side cube of polysulfide

Figure 4.1.17 | Average water contact angle was measured to be $130^\circ \pm 10.5$, with a minimum observed angle of 111° and a maximum of 156° over 15 individual measurements. The porous polysulfide is both hydrophobic and oleophilic, ideal properties for an oil sorbent.

Large Scale Oil Clean-Up

Two tests were carried out on a large scale, the first removal of motor oil with porous polysulfide from deionised water over 5 minutes. The second was a little more ambitious and closer represents a real-world scenario – low-density polysulfide made from used cooking oil was used to remove crude oil from sea water over just one minute. Both tests were successful, videos of the processes are available³ to demonstrate with screen captures detailing the process below.

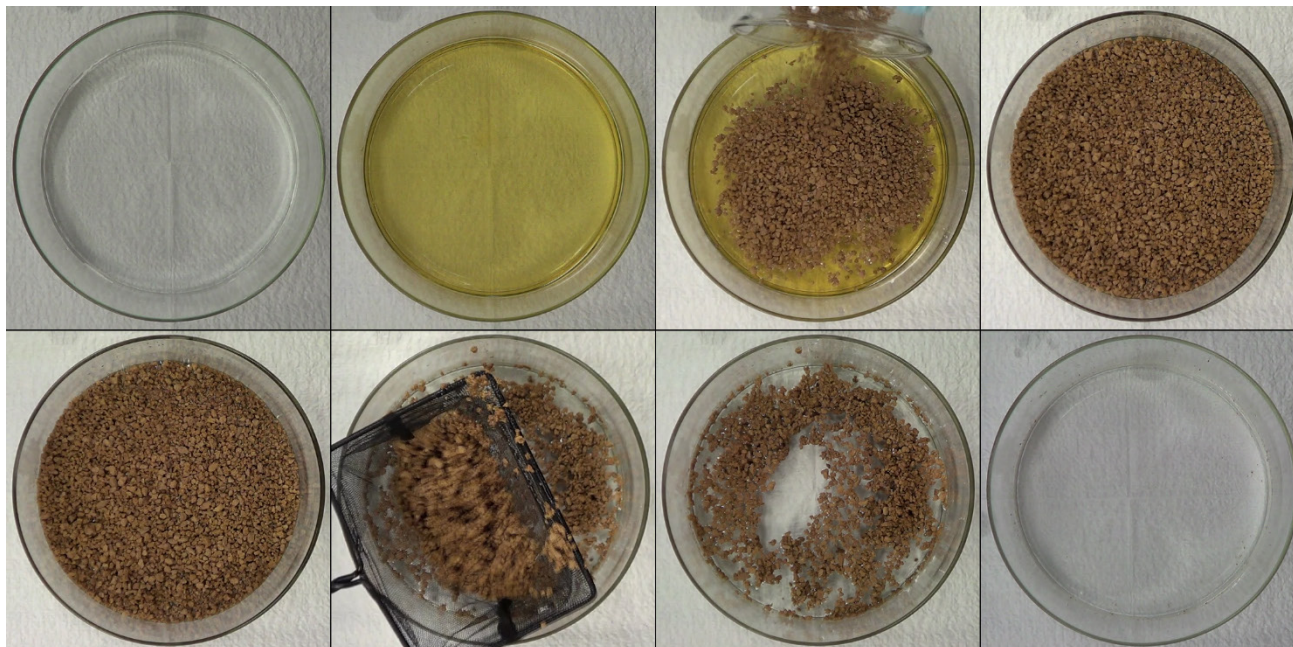


Figure 4.1.18 | Screenshots from video (top left to bottom right): 500 mL Deionised water; 100 mL motor oil added; 100.0 g porous polysulfide (canola oil) added; $t = 0$ of removal procedure; $t = 5$ minutes; polysulfide removed with net; motor oil no longer visible on surface; all polysulfide removed, the oil taken with it.

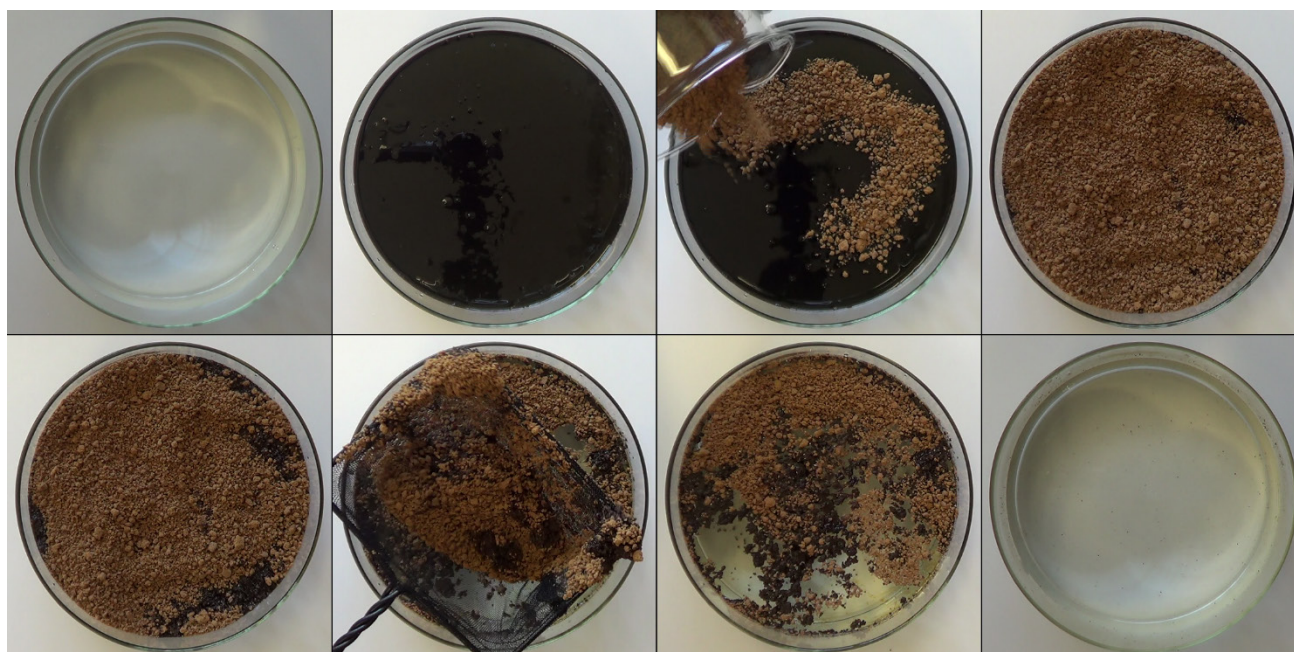


Figure 4.1.19 | Screenshots from video (top left to bottom right): 1.50 L sea water (Brighton beach, SA); 100 mL crude oil (Texas, USA) added; 100.0 g low-density polysulfide (used cooking oil) added; t = 0 of removal procedure; t = 1 minute; polysulfide removed with net; polysulfide has changed colour in absorbing oil; all polysulfide removed, the oil taken with it.

In the case of both the motor oil and crude oil, the mass of polymer used was sufficient to remove all oil. The 5 minutes allowed in the motor oil experiment appeared to be more than required as the crude oil experiment succeeded in only one minute. The ease of material recovery was dependent on the size of polymer particles relative to the net's mesh size. The porous canola oil polysulfide was processed to size using a food processor followed by sieving, as described in chapter 2. For this the removal step was quite simple. The low-density polysulfide prepared from waste oil however followed the large scale protocol described above, affording particles of a much smaller average size. Despite sieving, a number of particles finer than the net mesh were used in the experiment, making recovery more time consuming.

Removal of crude oil from seawater using a continuous process

Device designed and experiments performed by Louisa Esdaile and Stephanie Legg

Filtration apparatus

The low-density polysulfide (30.0 g, synthesised from used cooking oil) was packed into a PVC pipe (25 mm internal diameter PVC compression fitting). The polymer was enclosed using mesh (PVC coated fibreglass yarn; 0.25 mm diameter wire; 18 × 30 strands per inch) on the inflow end and cotton fabric (2 ply) at outflow end. Vinyl tubing (25 mm diameter) was affixed to both ends (all components are shown in Fig. 4.1.20 and the assembled filter is shown in Fig. 4.1.21).



Figure 4.1.20 | Components for a filtration apparatus used to separate crude oil and seawater.



Figure 4.1.21 | Assembled filtration apparatus used to separate crude oil and seawater.

Continuous separation of crude oil and seawater

A mixture of seawater (100.0 g, obtained from Brighton Beach, South Australia) and crude oil (10.00 g, Texas Raw Crude) was poured through the filter. The clear seawater eluted through the outflow end and the crude oil was retained on the filter. A video of this experiment is available as online³ to demonstrate. Screen shots of the experiment and images of the polymer before and after oil capture are shown in Figure 4.1.22.

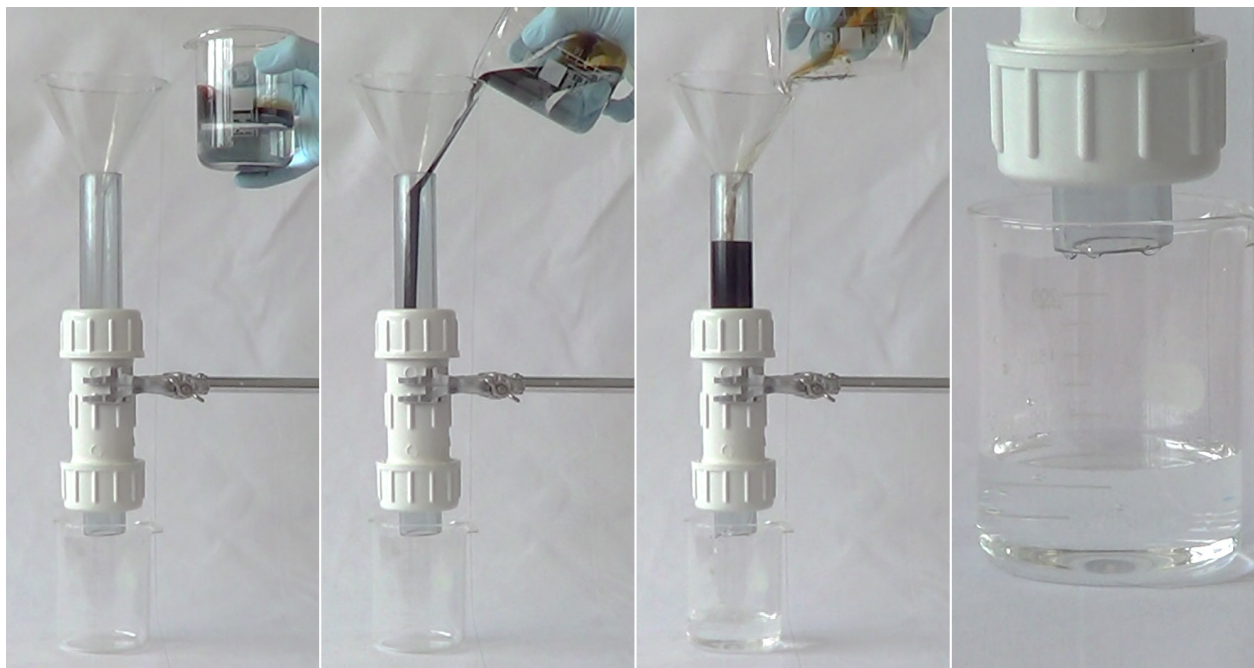


Figure 4.1.22 | Screen shots from a video of the continuous separation of crude oil and seawater using a filter containing the low-density polysulfide as the oil sorbent.

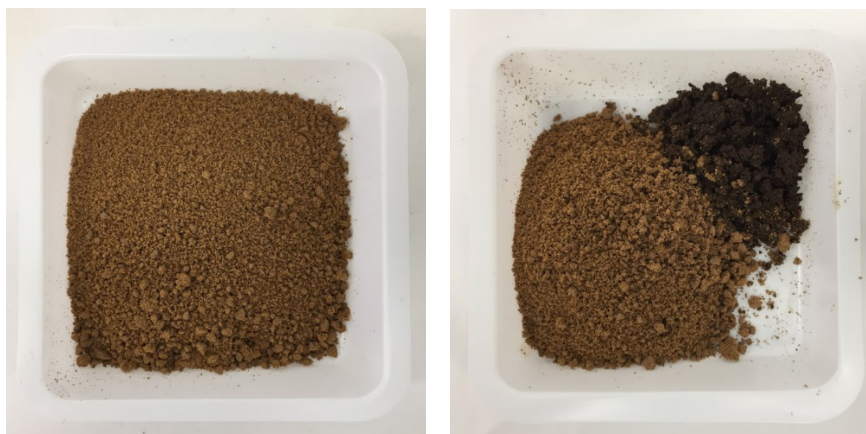


Figure 4.1.23 | Left: The low density polysulfide (prepared from used cooking oil) before the crude oil and seawater separation. Right: The porous polysulfide after oil capture. The darker material is polymer that captured the crude oil. Note that excess polymer was used in the filter.

Crude oil sorption using a non-porous canola oil polysulfide

Crude oil (1.00 g, Nockatunga oil field) was layered on to DI water (8.0 mL) in each of three 20 mL glass vials. The vials were swirled gently and then the canola oil polysulfide was added until no free crude oil was observed (typically a few seconds). To the first beaker, this experiment was carried out with the low density polysulfide, to the second beaker the non-porous polysulfide was used. To the third beaker was added sulfur. For the low density polysulfide, only 0.50 g of polymer was required to capture the oil. For non-porous polysulfide, 1.19 g of polymer was required to capture the oil. For sulfur, 1.23 g of the powder was required. The low density polysulfide aggregated efficiently and floated on the surface of the water. Non-porous polysulfide required more material and aggregated into a larger ball rather than the small island of the porous polymer. In one replicate a small ball of non-porous polymer that had absorbed oil sank to the bottom. Agitation of the vial also caused the polymer aggregate to partially sink and eventually float back to the surface over a couple of seconds in one case. The first few portions of sulfur soaked into the oil layer but as approximately half of the required sulfur was added, it began to clump and sink, remaining connected to the surface oil in cases. It is perhaps inaccurate to say the amount of sulfur added was sufficient to absorb all the oil, as in all cases the oil was simply dragged to the bottom along with the sulfur-paste as it sank, removing it from the surface.



Figure 4.1.24 | From left to right – Nockatunga crude oil on water; porous polymer added to oil; non-porous polymer added to oil; sulfur added to oil.

A second experiment was carried out on a slightly larger scale, with 2.00 g oil and 25.0 mL water. For the low density polysulfide, only 1.15 g of polymer was required to capture the oil. For non-porous polysulfide, 2.96 g of polymer was required to capture the oil. The low density polysulfide aggregated efficiently and floated on the surface of the water. In contrast the non-porous polysulfide did not aggregate as efficiently and, with a higher density, sank to the bottom of the beaker (Fig. 4.1.25). This experiment illustrates that the porosity is important for both oil sorption capacity and buoyancy in water.



Figure 4.1.25 | Left: Only 1.15 g of the low density canola oil polysulfide was required to capture the 2.00 g crude oil. The particles aggregate upon sorption of the oil and float on the water. Right: non-porous canola oil polysulfide particles still bind to crude oil and aggregate, with 2.96 g of polymer required to bind all oil. The non-porous polymer and oil product does not float on water.

DMA testing of mechanical properties of porous polysulfide

Experiments performed by Jonathan Campbell

For all mechanical analyses a $5.0 \times 5.0 \times 5.0$ mm cube of the porous polysulfide was used

Stress-strain curve with and without oil

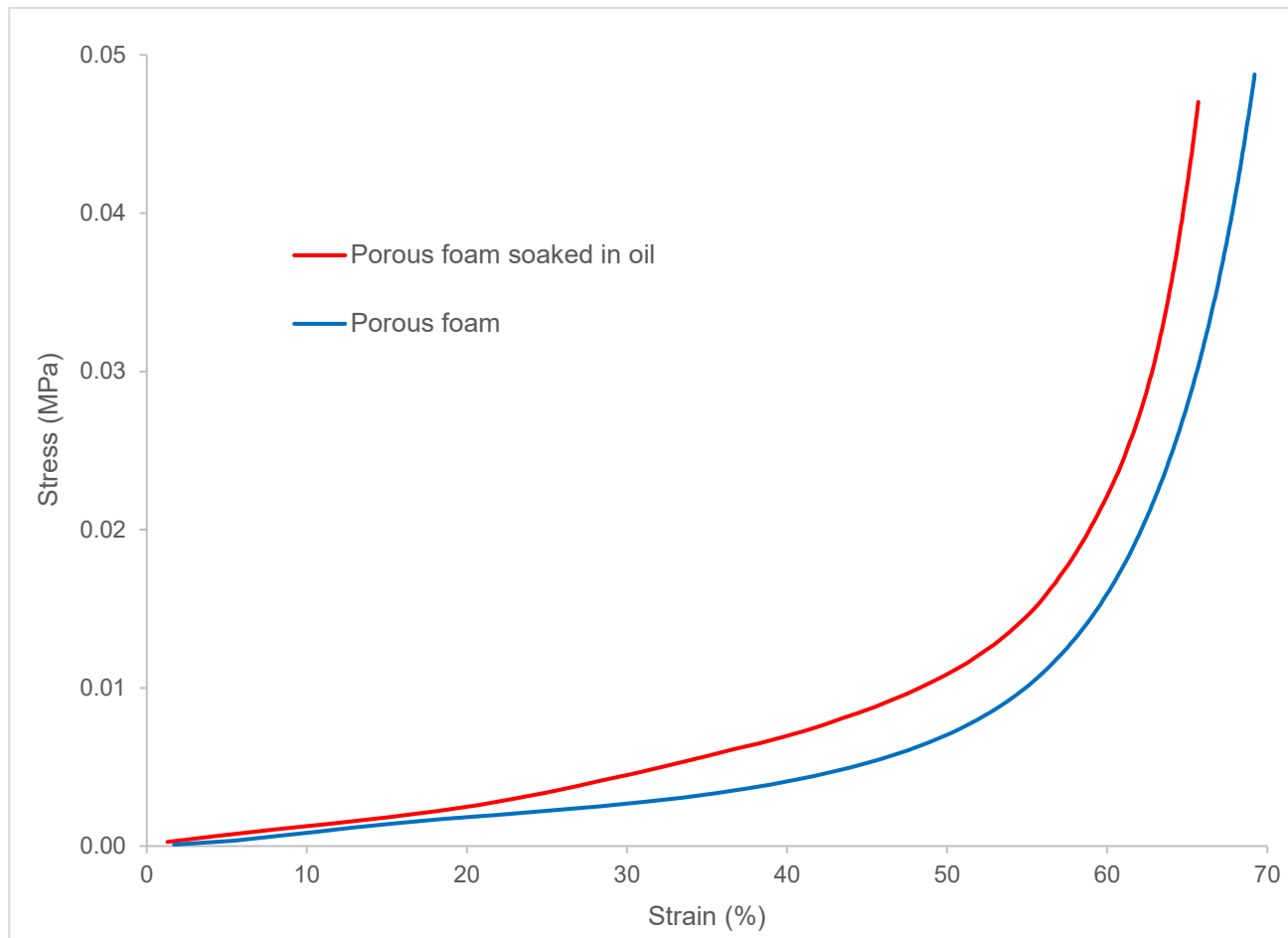


Figure 4.1.26 | Stress-strain curve in compression (force applied at 0.5 N min^{-1} up to 4 N) for porous polymer (blue) and porous polymer soaked in oil (red), measured by DMTA. This result shows that the compression-force curve for the foam with and without oil is similar. The foam with oil requires a bit more force to compress, but the difference is small. This indicates that the oil can be easily removed from the foam by squeezing. At 70 % strain the foam is compressed very flat and can be damaged if this is repeated.

Repeated strain over 20 cycles

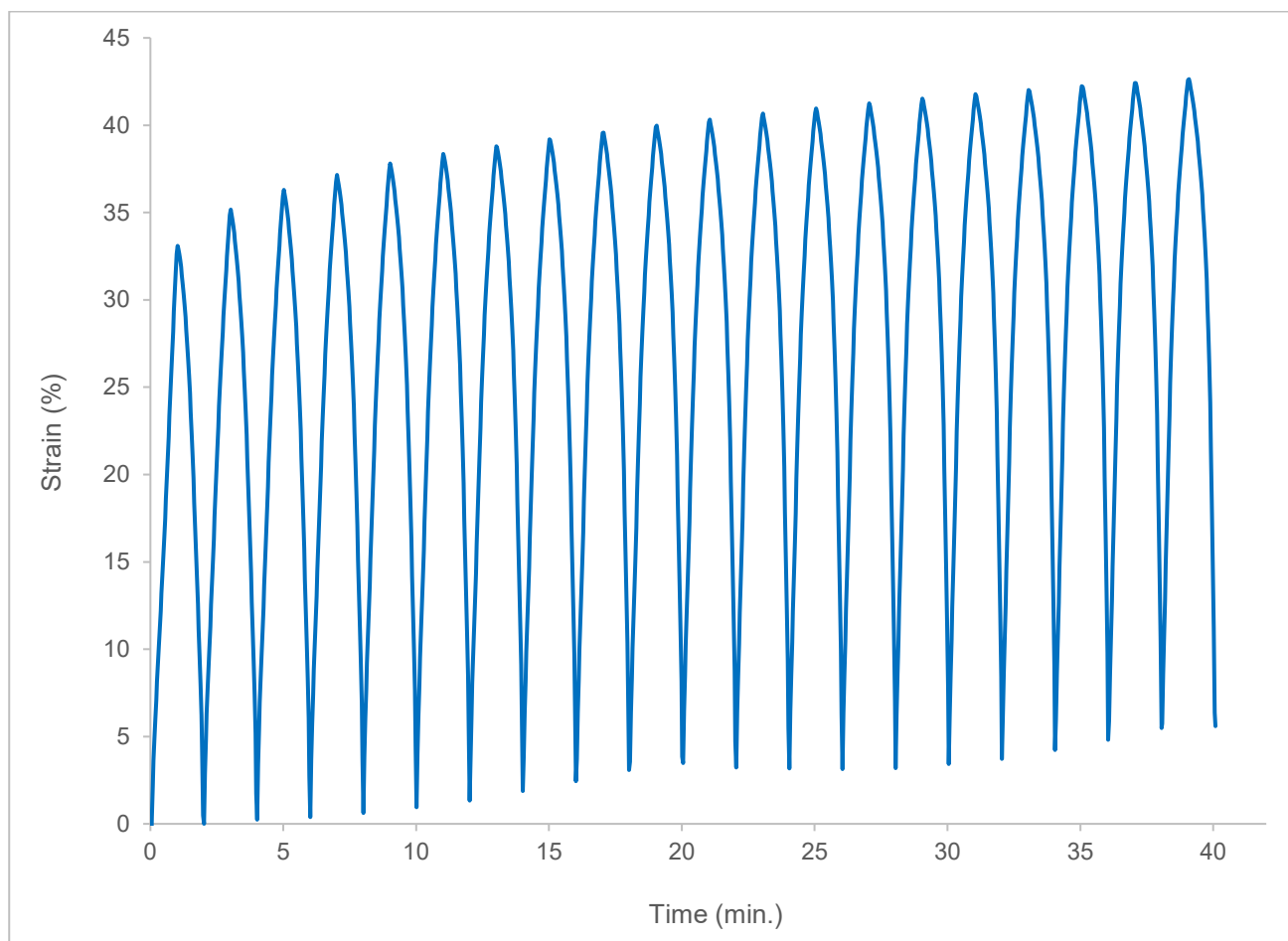


Figure 4.1.27 | Strain of porous foam when stress of 0.5 N (applied at 0.5 N min^{-1}) and then down to zero force (applied at 0.5 N min^{-1}) is repeated over 20 cycles. This shows that there is good repeatability of the strain (compression) and relaxation cycle – the foam can be squeezed to 35 % strain (0.5 N force) repeatedly. There is only a small increase in compression set observed - this is the permanent deformation that remains after the cycle. This experiment was performed using DMA in compression mode.

Stress-strain and recovery (hysteresis)

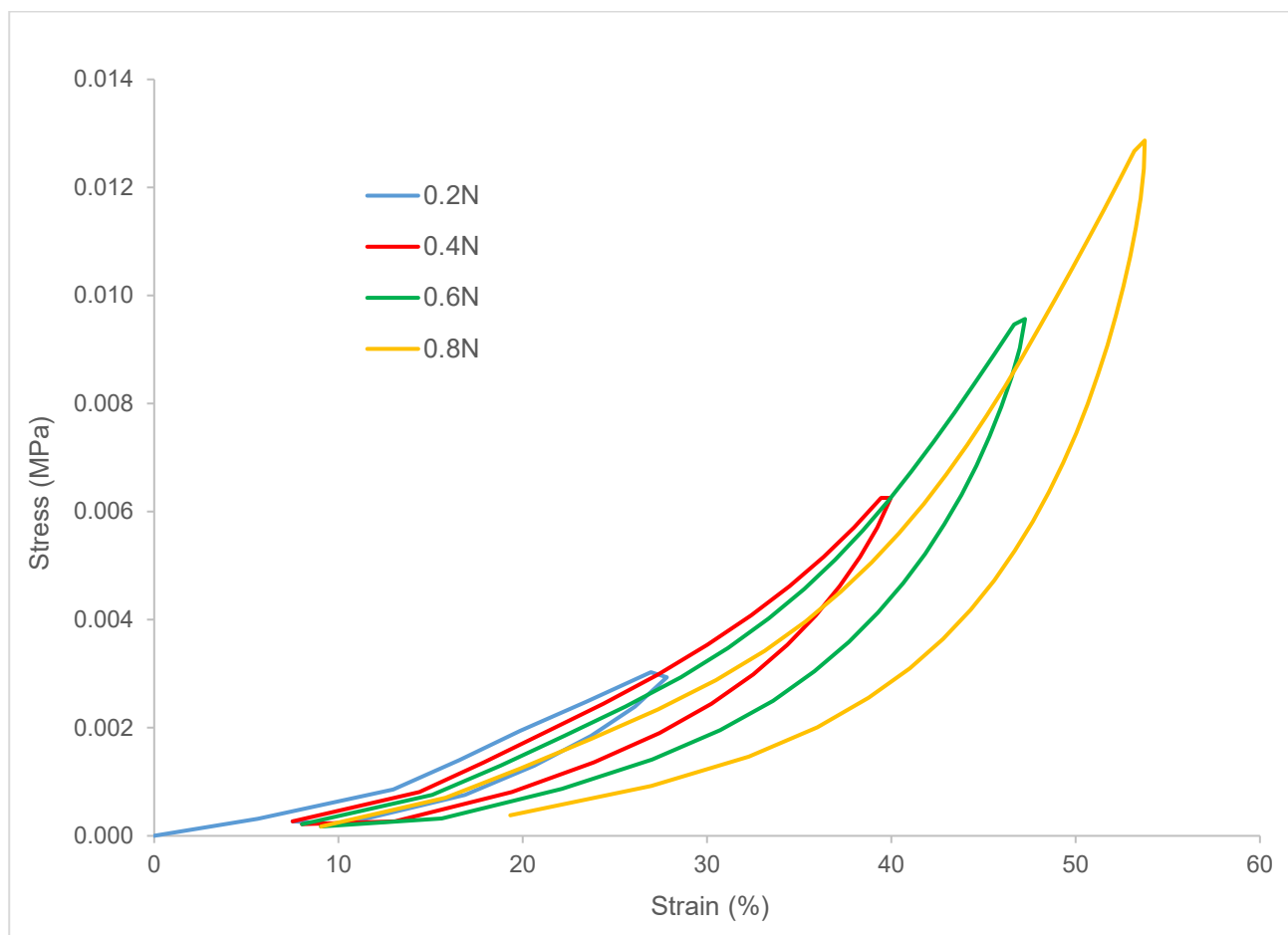


Figure 4.1.28 | Strain of porous foam when stress of 0.5 N (applied at 1 N min^{-1}) to 0.2, 0.4, 0.6 and 0.8 N force (with relaxation at 1 N min^{-1} in between each compression step). This experiment examines the repeated application of force at increasingly higher compression on the same sample run as a single experiment. This shows that the polymer can be compressed to increasing amounts of strain, and it springs back quite well, although there is an offset to a fixed strain (deformation), increasing after each cycle.

Stress relaxation

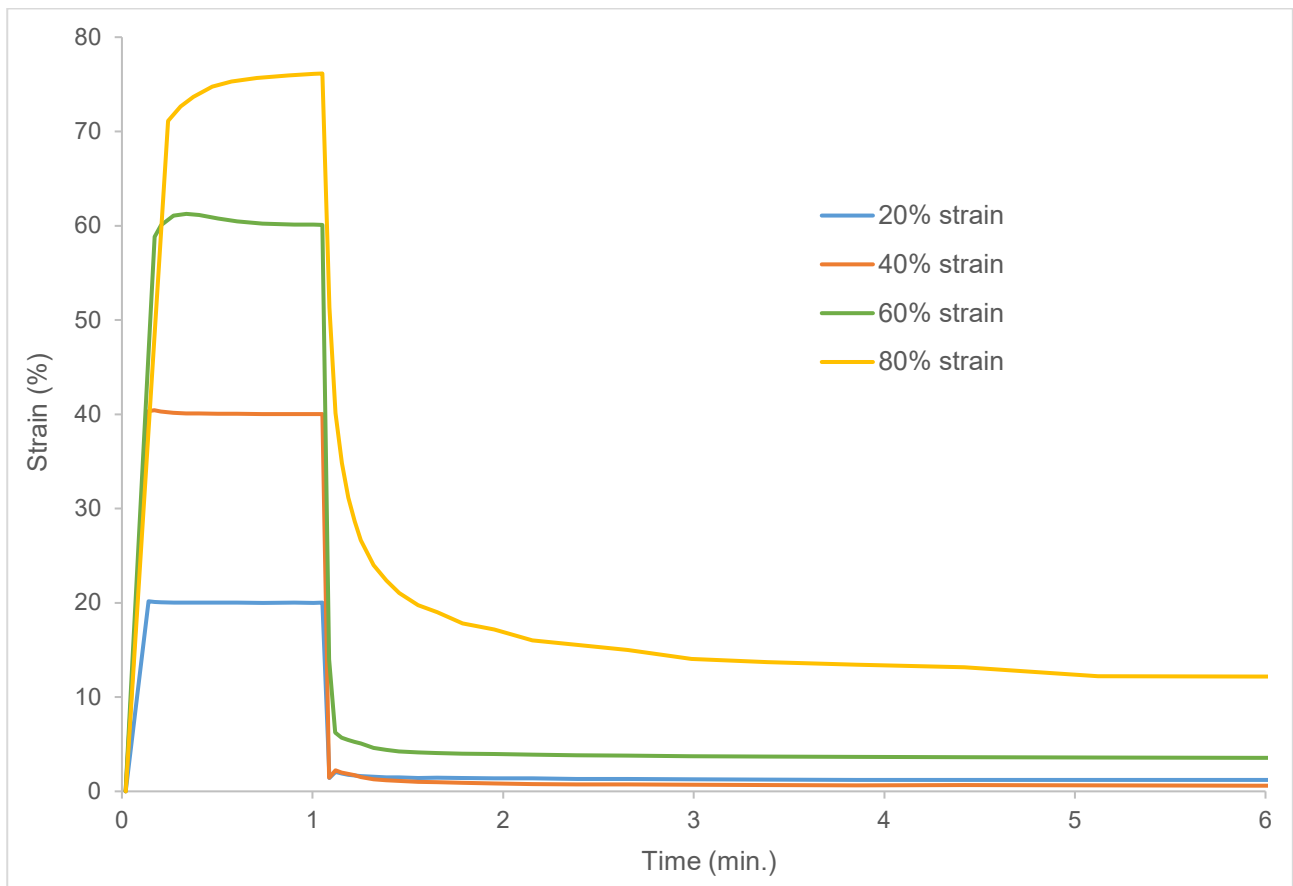


Figure 4.1.29 | Stress relaxation after application of various strains to the foam polymer. This experiment shows that the foam can recover over a short time after application of a strain (or a force). The recovery is instantaneous for strains up to 40 %, but at higher strain there is some compression set (permanent deformation) most likely due to damage of the foam structure. This is particularly noticeable at 80% strain; however, the amount of compression is very high at this value, and the polymer would be expected to be damaged to some degree because it has low strength. Note that the 80 % strain is the programmed target strain, but it only reaches 75 % strain, at which point it is pressed flat.

References

1. Crockett, M. P.; Evans, A. M.; Worthington, M. J. H.; Albuquerque, I. S.; Slattery, A. D.; Gibson, C. T.; Campbell, J. A.; Lewis, D. A.; Bernardes, G. J. L.; Chalker, J. M., Sulfur-Limonene Polysulfide: A Material Synthesized Entirely from Industrial By-Products and Its Use in Removing Toxic Metals from Water and Soil. *Angew. Chem. Int. Ed.* **2016**, *55*, 1714-1718.
2. Stalder, A. F.; Melchior, T.; Müller, M.; Sage, D.; Blu, T.; Unser, M. Low-Bond Axisymmetric Drop Shape Analysis for Surface Tension and Contact Angle Measurements of Sessile Drops. *Colloids Surf, A*, **2010**, *364*, (1-3), 72-81.
3. Worthington, M. J. H.; Kucera, R. L.; Albuquerque, I. S.; Gibson, C. T.; Sibley, A.; Slattery, A. D.; Campbell, J. A.; Alboaiji, S. F. K.; Muller, K. A.; Young, J.; Adamson, N.; Gascooke, J. R.; Jampaiah, D.; Sabri, Y. M.; Bhargava, S. K.; Ippolito, S. J.; Lewis, D. A.; Quinton, J. S.; Ellis, A. V.; Johs, A.; Bernardes, G. J. L.; Chalker, J. M., Laying Waste to Mercury: Inexpensive Sorbents Made from Sulfur and Recycled Cooking Oils. *Chem. Eur. J.* **2017**, *23* (64), 16219-16230.

5. SULFUR POLYMERS FOR GENE AND DRUG DELIVERY

Acknowledgments

Padma Akkapeddi for acquiring preliminary data before my visit and for instructing me on an appropriate procedure for gel electrophoresis for DNA uptake and release experiments.

Ana Guerreiro for helping with culturing and instruction on how to culture cells. Also for aiding in planning of toxicity experiments and helping with performing them, including providing access to the microplate plate reader. Ana also aided in method development for the CO release assay.,

Inês Albuquerque for provided access to the gel reader while waiting for training and providing training on the microplate reader. Inês also aided in method development for cell viability assays.

Annabel Kitowski for helping with access and running of the pH meter while waiting for training. Annabel also provided replacement HepG2 cells for use in cell viability testing.

Gonçalo Bernardes for kindly hosting me in his Lisbon laboratory at the Instituto de Medicina Molecular (iMM) for 3 months to undertake the following projects.

Overview of bioactive cargo delivery

The following project is made up of 3 distinct investigations, all of which focus on the attachment or incorporation of therapeutic agents into canola oil polysulfide. This was facilitated by a collaboration with the Bernardes research group in Lisbon, who hosted me for 3 months to allow me to learn techniques in cell biology and carry out experiments in a laboratory equipped to study medicinal biochemistry.

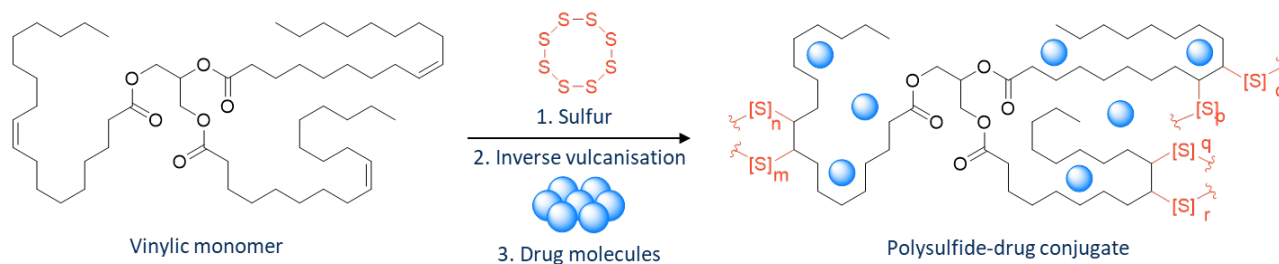


Figure 5.1 | Proposed principle mechanism for utilising sulfur polymers as drug delivery devices

DNA transfection

Polymers as DNA transfection tools

Conjugation of DNA with cationic polymers was first displayed in the late 1980s for targeted gene delivery¹. An ionic interaction between the negatively charged phosphate backbone of DNA and a cationic polymer is supplemented by hydrophobic interactions between the two long chain polymeric molecules to form a conjugate “polyplex”. Through chemical addition of cell-receptor targets to the polymer component, specific cell types can be targeted for uptake and release of bioactive cargo to be transcribed to modulate cellular activity¹. This forms the basis of polymers as DNA transfection agents and has since advanced considerably, with the synthesis of bespoke multi-functional polymers and expansion of transportable nucleic acid morphologies, as a promising technique in gene therapy. The aim of this project was to take the concept in its simplest form and apply it to sulfur polymers. Not only was this a novel new pathway to take sulfur polymers but also provided an opportunity for the author to expand training and experience in biomedical chemistry.

Discovery of DNA binding properties

This project stemmed from the serendipitous discovery of mercury-treated polysulfide’s capacity for DNA binding; at the same time as cell viability studies were being performed by Inês Albuquerque at the IMM, Padma Akkapeddi, at the time another PhD student in the Bernardes group, was investigating DNA transfection via carrier polymers. Padma carried out an experiment with the porous polysulfide to test its capability as a DNA carrier, but by accident used the HgCl₂-treated sample. She found that over a 4 hour incubation, the polysulfide was able to sequester a notable portion of plasmid DNA from aqueous solution. To follow up on this discovery and investigate further, and also to learn new biological techniques in DNA in cell handling and analysis, I travelled to the IMM in Lisbon for 3 month research visit in the last months of the third year of my candidature.

Preparation and characterisation of metal-treated polymers

The discovery that a mercury-treated polysulfide could absorb DNA was a welcome one, but despite the lack of cytotoxicity from Inês’ testing (see chapter 3), use of mercury intracellularly could potentially have long term negative effects. If the polysulfide were to break down under biological conditions, (as would be ideal for a drug delivery device – circumventing the need for later retrieval) it may be that free mercury becomes unbound in the process. Binding a more biocompatible metal to the polysulfide and seeing if this new conjugate also exhibited affinity for DNA was deemed a prudent initial set of experiments. A World Health Organisation report on trace metals² listed copper, zinc, magnesium, calcium and iron among the major essential minerals in human beings. All of these elements are known to undergo bond-forming interactions with DNA, also³. Replacing mercury with one of these less toxic elements would be ideal. Most likely these elements would not be sequestered as readily as mercury by the polymer, the interaction between the sulfur and mercury is that of a soft acid and base, and so the most likely candidate for a non-toxic mercury alternative would be

something with similar properties, most notably gold. It was this reasoning that informed a separate polysulfide-based project being undertaken in the Chalker laboratory at the time and so we also had early experiments indicating a strong affinity for gold from the polysulfide. Solutions of metal ions were prepared to 10 mg mL⁻¹ in pure milliQ water (5 mg mL⁻¹ gold was used because of limited supplies) and 1.0 g porous polysulfide incubated for 72 hours in 10 mL of each solution. Each incubation was performed in triplicate for a total of 3.0 g of treated polysulfide. Metal remaining in solution was determined by inductively coupled plasma mass spectroscopy (ICP-MS) against commercially available metal standards. From the remaining concentrations, it could be determined that 43 % of mercury was removed during the incubation, and >99 % of gold. Presuming the metals removed from solution had adhered to the polysulfide (no precipitate was visible to indicate another means of removal from solution) this results in 3.0 g each of polysulfides containing 43 mg per g mercury from HgCl₂ and 49 mg per g gold from AuCl₃. The other metals unfortunately were not sequestered to the same extent, with very little if any adhesion to the polysulfide occurring—none that could be accurately detected within the uncertainty of the ICP-MS measurements at least. Despite the negative result, all treated polysulfides were washed of excess metal solution with milliQ water, dried, packaged and posted to Lisbon.

DNA absorption experiments

Once in Lisbon, the first experiment performed was to simply repeat and verify Padma's preliminary observations. Porous polysulfide: gold-treated, mercury-treated and untreated was portioned out at 10, 30 and 50 mg into 2 mL centrifuge tubes. Plasmid DNA as provided by the Bernardes group was prepared to 100 ng mL⁻¹ in DNase and RNase free water (milliQ) and 200 µL added to each tube. All tubes were vortexed for 30 seconds to ensure wetting of the polymer and then centrifuged 30 seconds to ensure all was submerged. Polymer-DNA incubations were left for 2 hours at room temperature (26 °C) and then transferred to the fridge (4 °C) for 17 hours (overnight) to preserve until analysis. Gel was prepared from 500 mg agarose in 50 mL TAE buffer with microwave heating, once clear and cooled 5 µL RedSafe was added and the gel cast to set. To prepare each sample for gel electrophoresis, 20 µL of each incubation solution was transferred to a new 1.5 mL centrifuge tube and mixed with 4 µL DNA binding solution. Once the gel had set, each DNA solution was loaded and the gel run at 70 volts for approximately 50 minutes, during which time the voltage promotes separation of DNA down the gel relative to the size of the fragment. In the DNA solutions incubated only with porous polysulfide two broad bands are visible at approximately 10,000 and 5,000 bp. With 10 and 30 mg polysulfide these bands appear at high intensity, but at 50 mg this intensity is reduced, perhaps indicating that the polysulfide itself without any metal treatment has some affinity for DNA. It is possible that the hydrophobic nature of the polymer would interact with the hydrophobic segments of the DNA to facilitate such a reaction^{1,4}. The band intensity (and thus DNA concentration) in the solutions including metal-treated polymers show a much more obvious decrease from the starting concentration. The characteristic 10,000 bp band is still present at 10 mg (50 mg mL⁻¹)

Au-treated polysulfide (Au-PS), but with 30 mg (150 mg mL^{-1}) and 50 mg (250 mg mL^{-1}) present this band is entirely diminished. Similar results were achieved by the mercury-treated polysulfide (Hg-PS), seemingly more effective at drawing DNA from water at all concentrations. Even at the lowest concentration of 50 mg mL^{-1} the two major bands of 5,000 and 10,000 bp are not present. This is in line with Padma's initial experimental observations. Also to be noted is the apparent degradation of DNA in the presence of gold- and mercury-treated polysulfides. In the solutions treated with 30 and 50 mg Au-PS as well as 10 mg Hg-PS a broad smear down the lane is visible, the most likely explanation for this is plasmid DNA degrading to smaller fragments. Unfortunately, it is not clear how much of the total DNA is subject to this degradation (if it is the case), all that is clear is that with increasing concentration of Au-PS this smear is pushed further down the lane indicating increased degradation to smaller fragments.

Building on this first experiment focusing on differences in adsorption with polysulfide concentration, a follow up experiment was performed to test uptake over time. The first experiment had been allowed an incubation of 19 hours, observed to be sufficient time to remove the entirety of the two major DNA bands from solution. To test the speed of this adsorption, much shorter times would need to be tested. Solutions of DNA in DNase and RNase free water were prepared to 100 ng mL^{-1} as before and portioned into a series of 2 mL centrifuge tubes, 200 μL in each along with 50 mg polymer: untreated, Au-PS and Hg-PS. Four samples were prepared for each polymer type, one each to be incubated for 180, 60, 30 and 0 minutes, where the "0 minute" sample was centrifuged for 20 seconds to submerge the polymer in solution and then a 20 μL sample removed immediately for testing. Sampling and gel electrophoresis were performed identically to the previous experiment to investigate remaining DNA in solution after each incubation. Over 180 minutes no uptake was observed in the untreated polysulfide, despite using the same ratio of polymer to DNA as the previous experiment, indicating any action by the polysulfide alone takes longer than 3 hours to remove a noticeable quantity. Hg-PS similarly seemed to require more than the 3 hours tested to remove a significant quantity of DNA as only a faint decrease in band intensity is seen from 0 to 180 minutes. Au-PS was not so slow, with a clear difference in band intensity over time. In just 30 minutes the concentration of DNA is noticeably decreased, with a similar result at 60 minutes. After the full 180 minutes the bands are no longer distinct, but the lane is characterised by a streak of DNA down the length of the lane—again this may be indicative of DNA degradation.

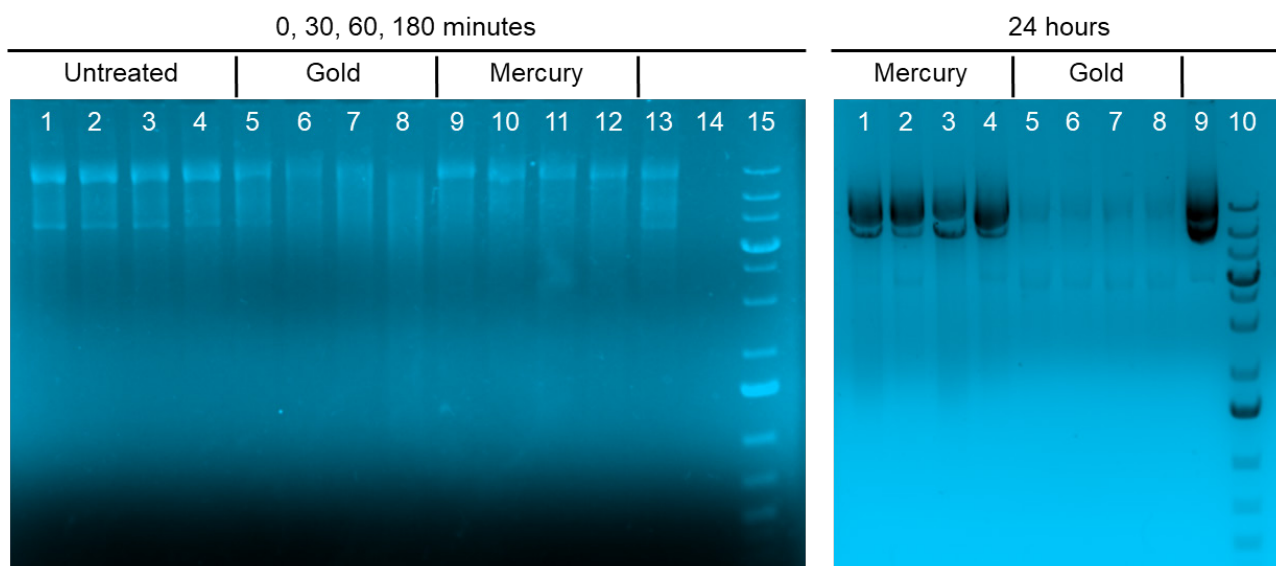


Figure 5.2 | Plasmid DNA uptake by untreated, gold- and mercury-treated polysulfides over time. Left: Uptake over 0 (lanes 1, 5, 9), 30 (lanes 2, 6, 10), 60 (lanes 3, 7, 11) and 180 (lanes 4, 8, 12) minutes by polymers with treatments as denoted above each lane. Lane 13 contains a control sample of the plasmid DNA in the absence of any polymer, lane 14 is empty and 15 contains a 1 kb DNA ladder for referencing fragment size. Right: Uptake over 24 hours (4 tests per treatment). Lane 9 contains a control sample of the plasmid DNA, and lane 10 contains a 1 kb DNA ladder.

The band pattern of the DNA control was elucidated with its inclusion in this experiment and was found to have some differences than even cases where seemingly nothing had occurred. For example, in the 0 minute (20 second centrifuge) incubation with untreated polysulfide. The pristine DNA displayed three distinct bands, approximately matching the 1 kb DNA ladder bands of 10,000, 8,000 and 5,000 bp. The bands are not different lengths of DNA, but a single form of plasmid DNA in three morphologies: supercoiled (standard in vivo formation), nicked (a relaxed coil formed by a break in the phosphor backbone of one strand) and open (a full break in the chain resulting in linear DNA). The shape of the molecule passing through the gel plays a key role in flow and thus travel distance. As DNA is damaged, the structure expands and loses motility, interacting more with the gel and inhibiting flow. What is likely being observed is, from top to bottom, the nicked, linear and lastly supercoiled plasmid DNA⁵. Vortexing and centrifuging of each sample could be contributing to the large amount of nicked DNA. Interestingly not all of these are present after incubation with the polysulfide—the linear DNA band, as faint as it is in the control, seems to be rapidly removed by the polysulfide. It may be that the linear form offers greater access to the otherwise obstructed nucleosides, facilitating rapid hydrophobic interaction with the polymer. The next band to disappear in uptake testing is the supercoiled, and lastly the broad nicked-DNA band, accompanied by degradation observed as smearing down the lane.

Incubations from the previous test were kept at 4 °C for 6 days, to see if simply more time would be sufficient in improving DNA adsorption. This seems to be the case as all bands in Au-PS and Hg-PS

incubated DNA solutions were no longer present. Linear and supercoiled plasmids are both absent in the untreated polysulfide sample, though the open form remains. This is an interesting result that may indicate selectivity for specific morphologies that is lost with the inclusion of surface metals.

Despite the negligible binding, it was not a complete waste to have brought along the polysulfides treated with other metals as the results when combined with plasmid DNA were far from expected: The general binding experiment was repeated with polysulfides incubated in iron, zinc, calcium, copper and magnesium salts. Further gold and mercury treated polysulfides were included for comparison. Little differed from the untreated-DNA control over a 24 hour incubation for most samples. Au-PS acted to remove nearly all DNA in this time, Hg-PS appears to have removed some (nicked and open) but the most unexpected result comes from the copper treated polysulfide (Cu-PS). The open and nicked bands, though blurred together in other samples, are very distinct with less of the nicked morphology present. Also visible though is a smear down the lane indicative of degradation, perhaps this explains the lack of nicked plasmid DNA – the small quantity of copper has in some way damaged it. A 7 day incubation of the same samples saw some change: The iron, zinc and calcium treated polysulfide solutions display more distinct bands for each plasmid morphology, but all appear the same as each other. Significant DNA loss can be seen in the Hg-PS sample given the extra time, and the Au-PS remains the same as before. The difference here is degradation has begun to occur in the magnesium-treated sample, leaving an open band of increased intensity and a faded nicked band. The Cu-PS that exhibited this behaviour after just 1 day is after the 7 days completely missing any distinct plasmid bands and only displays a faint smear that stretches from the open band location to the end of the lane. Very small quantities (unquantifiable by ICP-MS) of copper and magnesium on the polysulfide seem to be having the same effect, with the former acting much quicker than the latter. Nicked DNA is being further damaged to open fully and then degrading further to small fragments. It is not clear if anywhere in this process DNA is being adsorbed to the polysulfide surface but the exchange of DNA from one band to the other indicates some interaction that differs from those seen from the other polysulfides.

A cursory explanation for the gold-polymer's stronger affinity for plasmid DNA may be due to differences in electronegativity between gold and mercury. It may also be that the formation of gold nanoparticles on the surface of the polymer plays some role, as these have been demonstrated to bind plasmid DNA previously⁶. Further experiments to explore this observation could include monitoring the interaction of plasmid DNA with solitary mercury and gold nanoparticles, not adhered to a polymer surface. Scanning or transmission electron microscopy (SEM or TEM) techniques could prove useful in imaging the bound complex to gain further understanding of binding modes.

DNA release experiments

With promising results in binding, the following challenge was to discover conditions for release. The binding experiment described above was repeated over 48 hours to create a batch of untreated, gold treated, and mercury treated polysulfides that had each been incubated in 100 ng mL^{-1} plasmid DNA at a ratio of 250 mg polymer per mL DNA solution. Uptake was tested by gel electrophoresis 24 hours into each incubation to confirm before attempting to test release. The first series of experiments investigated release by pH control; 100 mM acetate buffers at pH 3.6, 4.6 and 5.6, 100 mM trizma buffers at pH 7 and 8, and 100 mM carbonate buffers at pH 9 and 10 were all prepared. 24 hours in the acidic buffers (below pH 7) resulted in blank lanes—no release. There was not a particularly strong chemically driven reason that this would work, other than that acid generally aids on solvation of metal ions and may have outcompeted polymer binding. The conditions of interest were the basic buffers, as it had previously been observed aqueous sodium hydroxide can attack and break down the polysulfide. Results were similar across pHs 7–9, however the pH 10 buffer saw some interaction with the gel matrix that destroyed those lanes leaving them unreadable. After 48 hours in buffer, no release was observed from Au-PS, from Hg-PS however very faint bands were present indicating open and nicked DNA. Between uptake and release each sample was washed with $2 \times 200 \mu\text{L}$ DNase and RNase free water with a 10 s vortex then 10 s centrifuge to ensure no plasmid incubation solution remained that would result in a false positive. This same washing procedure was carried out on an aliquot of 100 ng mL^{-1} plasmid DNA (effectively washing the centrifuge tube) and resulted in zero DNA by electrophoresis, validating the procedure. With this in mind the presence of even a very faint band of plasmid DNA is highly likely to have been released directly from the polysulfide. Uptake experiments had consistently shown Au-PS to take up DNA more rapidly than Hg-PS and this may translate into a stronger interaction between the DNA and polymer when it comes to release, an interaction that is not overcome by a 48 hour incubation in base. Left for one week in basic solutions, these faint nicked and open bands in the Hg-PS samples remain, but even with this extended incubation no release was observed from DNA-treated Au-PS.

In the final attempt to release DNA bound to the polymer, Au-PS and Hg-PS were first incubated for 24 hours in DNA as detailed earlier, then washed and added to aqueous solutions of either 92 mg mL^{-1} glutathione or 36 mg mL^{-1} cysteine. These concentrations correspond to roughly 5 equivalents of the metal atoms present on the polysulfide's surface. Given the strong affinity of gold and mercury to sulfur, it was postulated that sulfur-containing biomolecules might be able to disrupt the DNA-metal adherence with a ligand-exchange-like mechanism, resulting in DNA release. Au-PS and Hg-PS in cysteine or glutathione solutions were held at $37 \text{ }^\circ\text{C}$ for 3 hours and then tested for DNA release by gel electrophoresis. Unfortunately, this supposition did not hold and no release was observed, even after a further 6 day incubation at $4 \text{ }^\circ\text{C}$.

Conclusion

The summation of this first attempt to branch sulfur polymers into DNA transfection agents is that through treating the polysulfide surface with mercury(II) and gold(III), a brown rubber capable of adsorbing plasmid DNA from water can be produced. The gold-treated variant takes up DNA more rapidly than the mercury (removal from solution is visible over minutes for the former, hours for the latter), with the seeming consequence that reversing the binding becomes far more difficult. Incubation in buffered solution at pH 7 and above saw release of nicked and open plasmid DNA but not the native supercoiled from Hg-PS. As the basic buffers were balanced with NaOH this may also be a contributing factor to release.

Further experiments should look to explore further the fundamental science behind the interactions of sulfur polymers with DNA and how metals present on the polymer surface can modulate binding. Sulfur polymers able to bind DNA offer the opportunity for useful tools in gene delivery as well as DNA isolation. An essential next step for this will be the development of a reliable method for DNA release. From there understanding the oxidation and structural states of metals adhered to the polymer surface and how this affects binding will be key components in developing this chemistry further.

Drug encapsulation

Polymers as drug delivery tools

In a more traditional approach to polymer-based therapeutic delivery the loading of small molecule anti-cancer drugs was also considered. As opposed to the approach of producing a particulate polymer-drug complex intended for localisation via the EPR effect, the intention with a sulfur-polymer complex was to produce a drug-loaded implant that might be grafted to the patient post-surgery, for directly localised inhibition of tumour regrowth. For this reason, the investigation of uptake and release from the polymer can be undergone as a first step, as shape is imparted at synthesis and definition at the millimetre-scale is not a concern. Crizotinib, an ATP-blocking protein kinase inhibitor⁷ and doxorubicin, an intercalating agent that interferes with DNA⁸, were both chosen as candidate drugs. Both are FDA approved chemotherapeutics with the latter featured on the WHO's list of essential medicines and utilised previously in drug-polymer conjugate studies⁹.

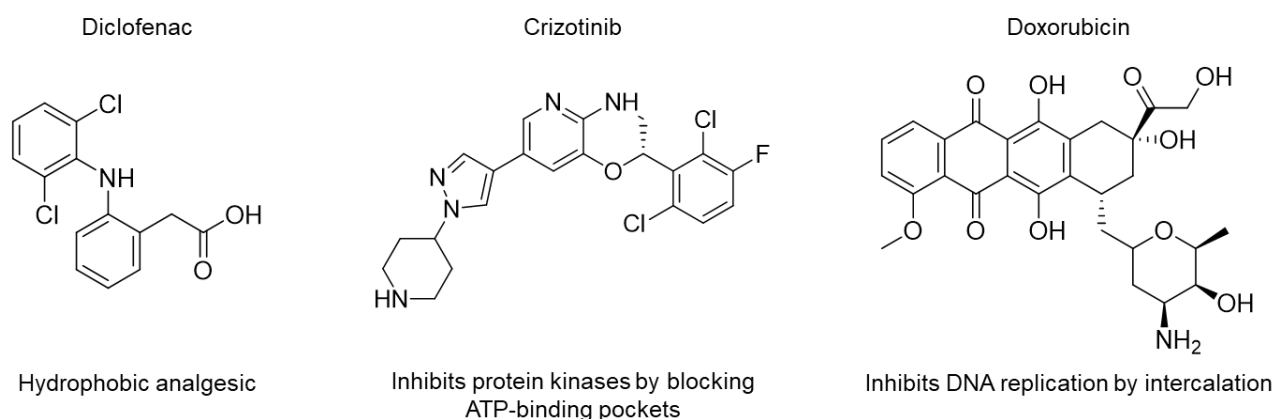


Figure 5.3 | Name and structure of drug molecules incorporated into the polysulfide, with therapeutic effect.

Preparation of drug-loaded polymers

To first validate experimental procedures before consuming the more costly anti-cancer compounds, diclofenac, a small molecule analgesic was used as a model, chosen because it was inexpensive, bioactive, hydrophobic and despite its smaller size exhibits the same ortho-substituted dichlorobenzene handle at one end as in crizotinib. Quantitative NMR was used to determine if a simple incubation of diclofenac and porous polysulfide in methanol could result in binding through hydrophobic interaction, but this was not the case. Incorporation in synthesis was the next method to be tested with diclofenac-loaded polymers prepared at 1 and 10 wt. % by first dissolving the drug in canola oil before synthesis. The product was not ideal though with mm-scale drug crystals distributed unevenly through the polymer. To combat this the drug was instead added into the polymer mixture shortly before it vitrified. In this way the drug powder is mixed through and set in place before crystal nucleation localises it to distinct crystals. It also confers the added benefit that the time the drug spends at reaction temperature is minimised in the event it may react or be

otherwise negatively affected by heat, should temperature-sensitive cargo be incorporated. The drug-loaded polymers were cut down to particles between 1 and 5 mm wide and release into water monitored by ^1H NMR. No release was observed over this time directly into D_2O , but 0.1 M phosphate buffered D_2O at pH 7 and 8 was enough to coerce the drug into solution, more so at the higher pH, presumably through ionisation under basic conditions. With the encapsulation method detailed, polysulfides were prepared with an equal mass of sulfur and canola oil, with 5 wt. % and 10 wt. % loading of diclofenac or crizotinib. Release was tested directly in a cell viability assay detailed later in this chapter.

Therapeutic CO distribution

CO as a therapeutic agent

Use of carbon monoxide as a therapeutic agent is a relatively recent development. Only in the mid-20th century was it discovered that CO was not just a toxic xenochemical but was in fact produced endogenously in humans as a by-product of heme degradation¹⁰, and then only at the end of the century did the literature arise questioning potential beneficial physiological roles¹⁰. Today several CO-releasing molecules (CORMs) have been developed to investigate the use of CO in vascular regulation and disease therapy. The primary concern with administration of CO is oral toxicity, when absorbed through the lungs CO binds irreversibly to red blood cells and starves the body of oxygen. CO-releasing molecules are designed to circumvent this mode of toxicity by limiting the concentration of gaseous CO to the site of interest. Early CORM candidates were metal carbonyl complexes, single or multiple metal atoms surrounded by carbonyl ligands that under certain conditions could dissociate to release CO. In the case of some metal carbonyls, such as dimanganese decacarbonyl, CO liberation was mediated by simply exposing it to light¹¹. With the goal of furthering the effectiveness of CORMs we embarked on a collaboration with the Bernardes Lab with experience in the field¹²⁻¹⁵ to encapsulate these molecules into sulfur polymers. By isolating CORMs into a malleable polymer, controlled, site-specific release could be achieved in the form of a CO-releasing implant.

Preparation and characterisation of metal carbonyl-treated polymers

Four pathways were considered to bind together the polysulfide and metal carbonyls: Incubation of polymer in metal carbonyl solutions, inclusion in synthesis, chemical tethering and co-elution from a mixture in solvent. As no metal carbonyls (MCs) were soluble in water and a harsh organic solvent might destroy the polysulfide over a long period, MCs were dissolved in ethanol (1 mM $\text{Fe}_3(\text{CO})_{12}$ and $\text{Mn}_2(\text{CO})_{10}$, 0.33 mM $\text{Ru}_3(\text{CO})_{12}$) and 1.0 g polysulfide added to 10.0 mL of each. After 1 hour polymer was recovered by gravity filtration, washed with ethanol to remove excess MC solution and left to dry in air. By FTIR, carbonyl peaks that would indicate the presence of MCs on the surface of the polymer were not detected. The experiment was repeated with a 19 hour incubation but gave the same result. It should be noted that the ATR-FTIR instrument available for this work introduces noise to all solid-phase spectra between 1900 and 2200 wavenumbers, precisely where a metal carbonyl peak should be expected¹⁵. With this in mind small concentrations of metal carbonyl on the surface may simply be under the limits of detection for the instrument and there may be some undiscernible quantity of MC on the surface of the polymer. However as will be shown later, larger concentrations do result in a noticeable signal in this region. With the limited analytical information available, combination by incubation was deemed inappropriate. Chemical tethering too was ruled out as too time-consuming to fit into a short project window, and inclusion in synthesis was ruled out due to toxicity of metal carbonyls and risks that may arise from heating. This left co-elution from

solvent as the safest and final method to test: Canola oil polysulfide was dissolved in pyridine to 100 mg mL^{-1} , and $\text{Fe}_3(\text{CO})_{12}$, $\text{Mn}_2(\text{CO})_{10}$ and $\text{Ru}_3(\text{CO})_{12}$ in the same solvent to 5 mg mL^{-1} . 4.0 mL polysulfide solution was mixed with 8.0 mL MC solution to afford a 12.0 mL mixture of 400 mg polysulfide and 40 mg MC – approximately 10% MC loading (9.1%). This mixture was cast into a petri dish and left in the fume hood to dry overnight. What resulted was a thin polysulfide film harbouring one of three metal carbonyls. The film was scraped from the petri dish and collected in a glass vial. It remained rubbery if somewhat sticky and did not appear to separate into its constituent parts, remaining a single material. FTIR shifts in the $2000\text{--}2100 \text{ cm}^{-1}$ region indicative of carbonyls from metal carbonyl complexes¹⁵ were present in the manganese- and ruthenium-polymer spectra. This shift did not seem to be present in the iron-polymer but a pattern of peaks present in the pristine $\text{Fe}_3(\text{CO})_{12}$ spectra from 1600 to 1800 cm^{-1} were. A small, sharp peak at 1605 cm^{-1} may also indicate the presence of carbonyls in the ruthenium treated sample other than those bound in the triruthenium complex as this peak is not present in the pristine MC spectra. EDX analysis of the polymer-MC mixed films revealed iron, manganese and ruthenium signals as supplementary evidence.

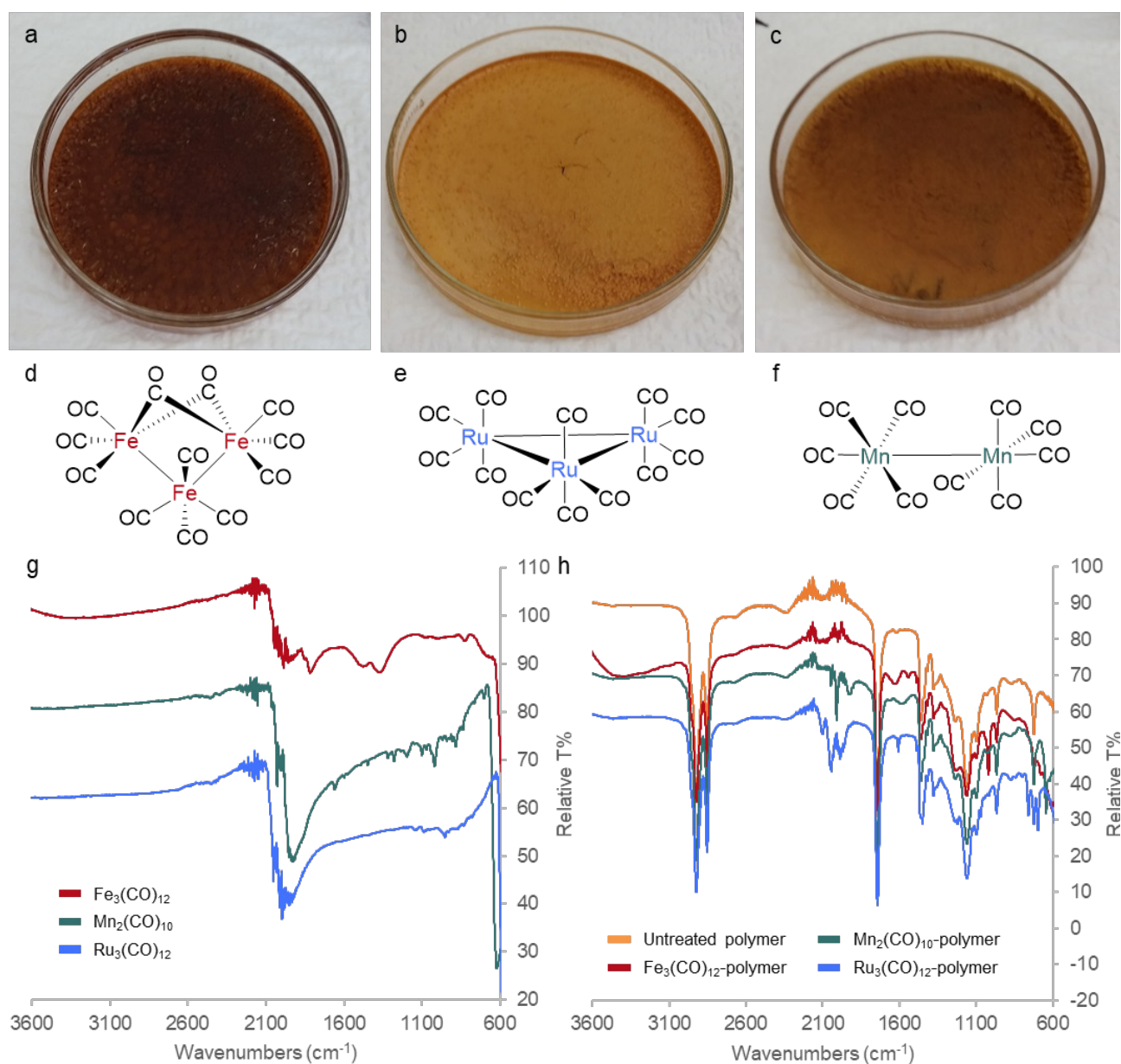


Figure 5.4 | a-c. Metal carbonyl-polysulfide films produced from iron (a), ruthenium (b) and manganese (c) carbonyls. d-f. Chemical structure of triiron dodecacarbonyl (d), triruthenium dodecacarbonyl (e) and dimanganese decacarbonyl (f) for reference. g. FTIR spectra of pristine metal carbonyls, the broad peak at 2000 cm⁻¹ can be attributed to CO stretching modes¹⁶ h: FTIR spectra of MC-polymers, the array of peaks at 2100 cm⁻¹ are present in the treated polymers but not the untreated.

CO release experiments

Measurement of CO release was informed by an established protocol¹⁷ in which a CO-reactive compound (COP-1) was dissolved in phosphate buffered saline and incubated with metal carbonyl-loaded polysulfides. If CO came into contact with COP-1, the two would react to form a fluorescent compound that can be measured spectroscopically. 10 mg of each polysulfide type ($\text{Fe}_3(\text{CO})_{12}$ -, $\text{Mn}_2(\text{CO})_{10}$ - and $\text{Ru}_3(\text{CO})_{12}$ -treated at 10 wt. % loading) were portioned into well plate inserts and submerged in 0.50 mL PBS for 20 minutes to wet the hydrophobic polymer and facilitate interaction with COP-1 in solution. 0.50 mL solution of 2 μM COP-1 in PBS was added to each well to yield a 1 μM concentration. Untreated polysulfide and a well containing only the COP-1 solution were also included as controls. Emission across 510–610 nm was measured at several intervals over 3 hours on a TECAN Infinite M200 Microplate reader. All samples were exposed to white light between each reading, a known promoter of CO release from certain CO-releasing molecules^{11, 18}.

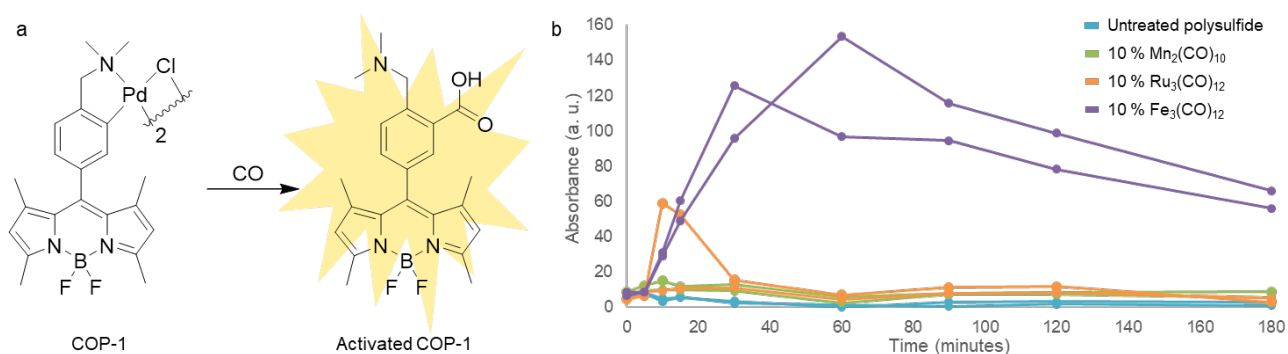


Figure 5.5 | a. Activation of COP-1 by CO to form a measurable fluorophore. b. Average fluorescent response metal carbonyl-treated polymers over 510–610 nm after incubation in 1 μM COP-1. Response from $\text{Fe}_3(\text{CO})_{12}$ was later confirmed to be a false positive and not indicative of CO release.

Of all polymers tested, only the iron-treated showed a continued fluorescence over time, rising over the first hour and then receding for the proceeding two. The same trend was not observed in any other MC-polymer. The well plate was left in sunlight (by a North-facing window in the lab) for 3 days, with further readings taken at 48 and 72 hours: measured fluorescence was consistently higher than the control-defined baseline in all cases after 2 days but fell slightly after the third. Even a full 3 days had not seen any further release of CO. In order to rule out false positive readings across the tested wavelength range, the experiment was repeated lacking COP-1. Unfortunately, the trends were the same: the 10% iron-loaded polymer continued to exhibit emission from 510–610 nm, contradicting the link between COP-1 reactivity and the observed response. Further control experiments confirmed the same response in the absence of light, and a delayed and lessened, but similar trend when the polymer was not pre-soaked in PBS before addition of COP-1. It would appear something other than COP-1 was emitting across the monitored wavelengths when submerged in PBS, interfering with the experiment. Beyond this one anomalous result though, no emission by COP-1 was observed, inferring no release of CO from the MC-polymers.

Cell viability studies

To determine cytotoxicity of the metal carbonyl-polymer composites, HepG2 and SKBR3 immortal cancer cell lines were cultured for several passages before seeding for 24 hours at approximately 30,000 cells per well into two separate 24-well transwell plates, one per cell line. Untreated, gold chloride-, mercury chloride-, triiron carbonyl-, triruthenium carbonyl-, dimanganese carbonyl-, crizotinib- and doxorubicin-treated polymers were each portioned into transwell plate inserts at masses of 6, 12 and 24 mg (12, 24 and 48 mg mL⁻¹) and submerged in 0.50 mL culture medium in all 24 wells. In this way the polymer was not in direct contact with the bed of cells, crushing or smothering them, but any cargo released into the matrix is free to interact. Cell viability was monitored with cell titre blue and a TECAN Infinite M200 microplate reader at 24 and 48 hours. It is to be noted before assessing the data that due to time and equipment pressures the cell viability studies were not carried out in triplicate, and so repeated experimentation is necessary to achieve conclusive results.

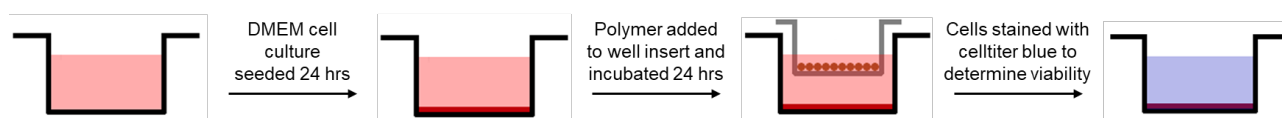


Figure 5.6 | Diagram of cell viability testing procedure.

There are two ways to consider the measured viability: either as an absolute measure of cell death, or as percentage normalised to the untreated polysulfide. That is, to consider the polysulfide only as a vessel for bioactive treatments. To fully appreciate the experiment in this instance it is necessary to assess from both approaches. Firstly, polymers intended for DNA transfection will be considered: For HepG2 cells, Hg-PS presence resulted in lower cell viability except at 48 mg mL⁻¹ where there was little difference compared to the control. In all cases viability dropped after the second 24 hours but trends remained the same. This assessment remains true in both the absolute and comparative sense, where data points are skewed from the observation that increasing concentration of untreated polysulfide resulted in increased cell viability. In some way the polysulfide had nourished the cancer cells (or perhaps interfered with the microplate reading, though this seems less likely) and led to an increased cell count. It is for this reason that both assessments should be considered, as higher quantities of polysulfide have a higher threshold for “100% viability” due to this secondary effect. Regardless, what is observed is an increase in cell viability at 12 mg mL⁻¹ Au-PS, a similar viability at 24 mg mL⁻¹ Au-PS, and decreased viability at 48 mg mL⁻¹ compared to the untreated polymer. At these concentrations the gold-treated polymer is not toxic to HepG2 hepatic cancer cells, but may also nourish them, a counterproductive circumstance that prompts further study. SKBR3 breast cancer cells, slower to propagate and fickle to work with, did not imitate the HepG2 cells’ reaction to the untreated polysulfide, remaining at a steady cell count at all concentrations and simplifying analysis. Similar to the HepG2 test, Hg-Ps and Au-PS were both detrimental to cell viability, but in this instance with greater sensitivity: 12 mg mL⁻¹ Au-PS saw no viability loss, but at increased

concentrations, and all concentrations of Hg-PS, viability dropped below 50 %. Overall this is a promising result in the use of gold-treated canola oil polysulfide as a DNA/RNA carrier polymer.

Metal carbonyl-polymer composites returned surprising results. 10% loadings of triruthenium dodecacarbonyl (Ru-PS) and dimanganese decacarbonyl (Mn-PS) increased HepG2 and SKBR3 cell viability over the untreated polysulfide at all concentrations except the highest Mn-PS where it dropped only slightly. The same trend holds at 48 hours as it does for 24 in HepG2 cells, with even increased viability at the later timepoint in the lowest concentration of Ru-PS. This trend is similar but not as pronounced in SKBR3 cells, where viability fell in all cases. The same cannot be said for the 10 % loaded triiron dodecacarbonyl polysulfide (Fe-PS), that saw similar viability at 12 mg mL⁻¹ to the untreated polysulfide, but cell losses with increased concentration. CO release studies detailed above revealed the release of some spectroscopically-active substance from Fe-PS that resulted in a false positive reading for CO release. It may be this leaking of compound into culture medium that has resulted in cytotoxicity.

Polymer-anticancer composites were also included in the same batch of experiments, but to a different end. The intention was explicitly to kill cells rather than limit toxicity. In short, the result was positive, at all concentrations cell viability dropped significantly. Doxorubicin was seen to accumulate as an orange solid in the well however, revealing an insecurity in the polymer packing. To continue towards the goal of sulfur polymers as drug delivery vessels the security of the drug within the polymer matrix will first need revision.

Future Experiments

The experiments contained in this chapter constitute a very preliminary and exploratory study of the use of sulfur polymers as drug delivery tools. We have discovered that canola oil polysulfide is capable of binding plasmid DNA after a simple incubation with mercury or gold chlorides, and the polymer itself has some binding capability even without metals present. Precise conditions for controlled release remain elusive, however some release was observed into basic buffered water. Metal carbonyls and small drug molecules can be incorporated into the polymer, but again precise conditions for release of the therapeutic agent in each case requires further investigation. Overall this work represents an interesting introductory study in taking this work in sulfur polymers in a new direction.

References

1. Zhang, P.; Wagner, E.; History of Polymeric Gene Delivery Systems. *Top. Curr. Chem.* **2017**, *375* (26), 39.
2. World Health Organisation, Vitamin and mineral requirements in human nutrition, 2nd ed. **2005**. <<https://www.who.int/nutrition/publications/micronutrients/9241546123/en/>> Accessed June 2018.
3. Anastassopoulou, J., Metal-DNA interactions. *J. Mol. Struct.* **2003**, *651-653* 19-26.
4. Xia, F.; Zuo, X.; Yang, R.; Xiao, Y.; Kang D.; Vallée-Bélisle, A.; Gong, X.; Heeger, A. J. and Plaxco, K. W. On the Binding of Cationic, Water-Soluble Conjugated Polymers to DNA: Electrostatic and Hydrophobic Interactions. *J. Am. Chem. Soc.* **2010**, *132*, 1252–1254.
5. Johnson, P.; Grossman, L. I., Electrophoresis of DNA in agarose gels. Optimizing separations of conformational isomers of double- and single-Stranded DNAs. *Biochemistry* **1977**, *16*, 4217-4225.
6. Raju, D.; Vishwakarma, R. K.; Khan, B. M.; Mehta, U. J.; Ahmad, A., Biological synthesis of cationic gold nanoparticles and binding of plasmid DNA. *Materials Letters* **2014**, *129*, 159-161.
7. Roskoski, R., Properties of FDA-approved small molecule protein kinase inhibitors. *Pharmacological Research* **2019**, *144*, 19-50.
8. Binaschi, M.; Bigioni, M.; Cipollone, A.; Rossi, C.; Goso, C.; Maggi, C.; Capranico, G.; Animati, F., Anthracyclines: Selected New Developments. Current medicinal chemistry. *Anti-cancer agents* **2001**, *1*, 113-30.
9. World Health Organisation, World Health Organization Model List of Essential Medicines, 21st List. **2019**. <<https://www.who.int/medicines/publications/essentialmedicines/en/>> Accessed September 2019
10. Durante, W.; Johnson, F. K.; Johnson, R. A., Role of carbon monoxide in cardiovascular function. *J. Cell. Mol. Med.* **2006**, *10* (3), 672-686.
11. Motterlini, R.; Clark, J. E.; Foresti, R.; Sarathchandra, P.; Mann, B. E.; Green, C. J., Carbon monoxide-releasing molecules: characterization of biochemical and vascular activities. *Circ. Res.* **2002**, *90* (2), 17-24.

12. Romao, C. C.; Blattler, W. A.; Seixas, J. D.; Bernardes, G. J. L., Developing drug molecules for therapy with carbon monoxide. *Chem. Soc. Rev.* **2012**, *41* (9), 3571-3583.
13. Chaves-Ferreira, M.; Albuquerque, I. S.; Matak-Vinkovic, D.; Coelho, A. C.; Carvalho, S. M.; Saraiva, L. M.; Romão, C. C.; Bernardes, G. J. L., Spontaneous CO Release from RuII(CO)₂-Protein Complexes in Aqueous Solution, Cells, and Mice. *Angewandte Chemie* **2015**, *127* (4), 1188-1191.
14. Garcia-Gallego, S.; Bernardes, G. J. L., Carbon-Monoxide-Releasing Molecules for the Delivery of Therapeutic CO In Vivo. *Angew. Chem., Int. Ed.* **2014**, *53* (37), 9712-9721.
15. Seixas, J. D.; Chaves-Ferreira, M.; Montes-Grajales, D.; Gonçalves, A. M.; Marques, A. R.; Saraiva, L. M.; Olivero-Verbel, J.; Romão, C. C. and Bernardes, G. J. L. An N-Acetyl Cysteine Ruthenium Tricarbonyl Conjugate Enables Simultaneous Release of CO and Ablation of Reactive Oxygen Species. *Chem. Eur J.* **2015**, *21*, 14708-14712
16. Bhatt, V., Chapter 8 - Metal Carbonyls. In *Essentials of Coordination Chemistry*, Academic Press: **2016**, 191-236.
17. Michel, B. W.; Lippert, A. R.; Chang, C. J., A Reaction-Based Fluorescent Probe for Selective Imaging of Carbon Monoxide in Living Cells Using a Palladium-Mediated Carbonylation. *J. Am. Chem. Soc.* **2012**, *134* (38), 15668-15671.
18. Gonzales, M. A.; Mascharak, P. K., Photoactive metal carbonyl complexes as potential agents for targeted CO delivery. *J. Inorg. Biochem.* **2014**, *133*, 127-35.

5.1 SULFUR POLYMERS FOR GENE AND DRUG DELIVERY EXPERIMENTAL

CO-Releasing polymer

Materials

Metal Carbonyl compounds and potential CO-releasing molecules (CORMs)

1. FeCO_5 - Iron pentacarbonyl
2. Fe_2CO_9 - Diiron nonacarbonyl
3. $\text{Fe}_3\text{CO}_{12}$ - Triiron dodecacarbonyl
4. $\text{Mn}_2\text{CO}_{10}$ - Dimanganese decacarbonyl
5. $\text{Ru}_3\text{CO}_{12}$ - Triruthenium dodecacarbonyl

Metal carbonyl solubility

Triiron dodecacarbonyl was left to incubate in a selection of solvents at room temperature to determine solubility and stability over time. Ethanol, THF, DCM, hexane as well as water were all tested. No metal carbonyls showed solubility in water and had similar (sparing) solubilities in the organic solvents tested. Ethanol was chosen to continue with due to its lesser toxicity and low vapour pressure, allowing quick and simple drying of the polymer after incubation.

Binding to porous polysulfide by incubation

To 1 mM solutions of metal carbonyls **3** and **4** and a 0.33 mM solution of **5** in ethanol in sealed glass vials, 1.0 g porous polysulfide (canola oil, 0.5–1.0 mm diameter particles) was added, agitated for 30 seconds and then left for 1 hour at room temperature. Polysulfide was recovered by gravity filtration, washed with 50 mL ethanol to ensure any CORM present was bound rather than a potential settled precipitate and then left to dry over 3 days. Treated polymers were tested by FTIR spectroscopy for traces of CO peaks that would indicate the presence of metal carbonyl molecules bound to the polymer.

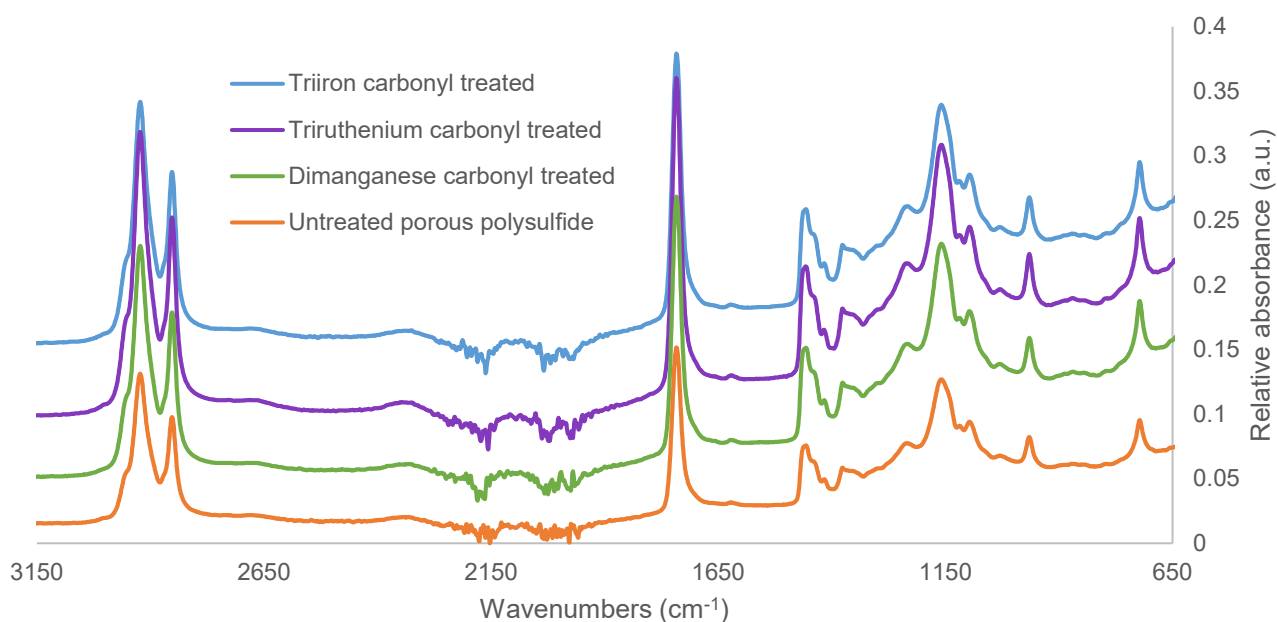


Figure 5.1.1 | FTIR trace of CORM treated porous polysulfide. No differences between the treated and control (untreated) sample were observed.

The experiment was repeated, with 1 mM solutions **2**, **3** and **4** and a 0.25 mM solution of **5**. To each, 200 mg porous polysulfide (canola oil, 1.0–2.5 mm diameter particles) was added and left to incubate at room temperature for 19 hours (overnight). Polymer was recovered by gravity filtration, washed with 10 mL ethanol to remove residual metal carbonyl solution and left to dry for 3 hours in the fume cupboard. Dry, treated polymer samples were tested by FTIR spectroscopy using the ATR method to determine any difference against an untreated sample.

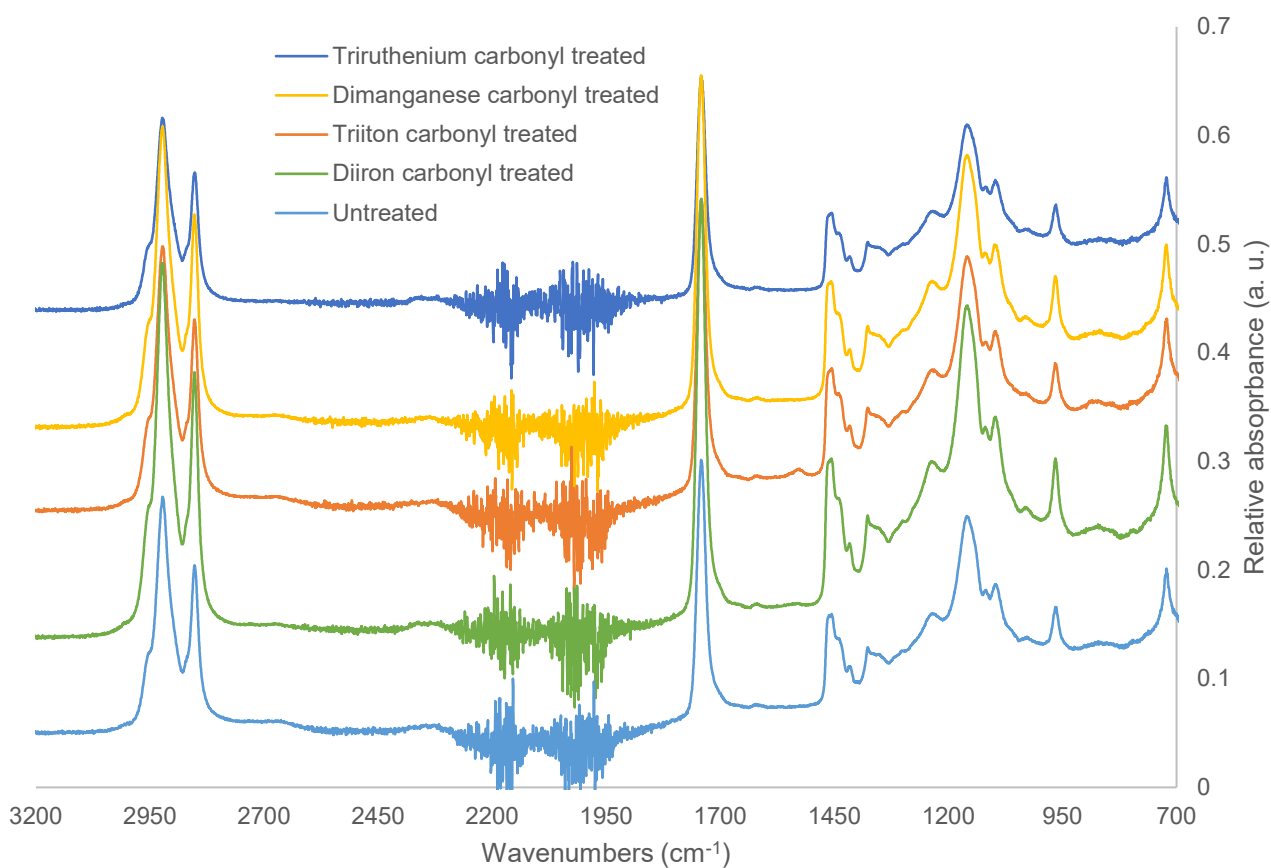


Figure 5.1.2 | FTIR spectra of metal carbonyl-treated polysulfides (19 hour incubation). No differences between the treated and control (untreated) sample were observed.

Metal carbonyls generally absorb in the region from 2000–2200 cm^{-1} . Unfortunately, this may prove FTIR to be an unsuitable method of determining the presence of metal carbonyls in conjunction with the polymer, as the analysis of solid samples by the ATR method appears to introduce significant noise in this region.

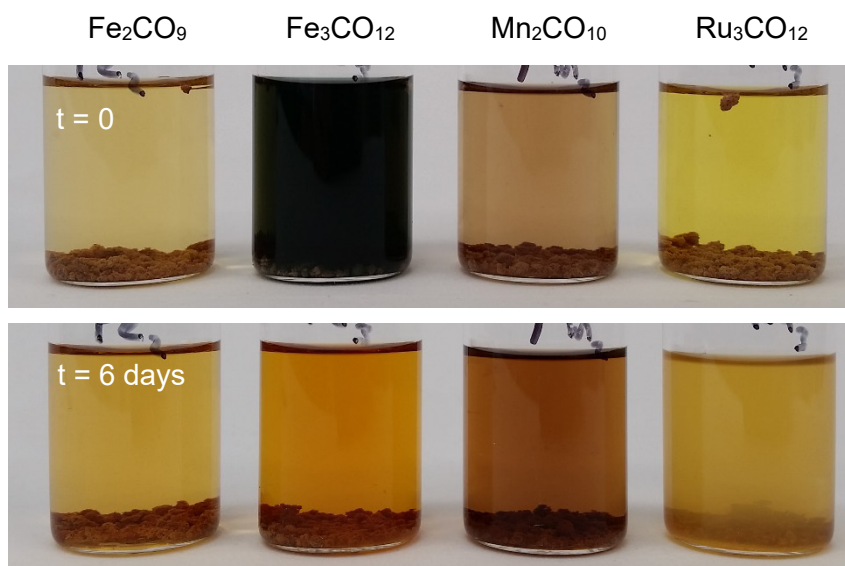


Figure 5.1.3 | Colour change in CORM solutions in ethanol over time. The most significant change is seen in $\text{Fe}_3\text{CO}_{12}$, changing from a deep green to orange over several days. Potential reasons for the colour change include the breaking down of the metal carbonyl complex to di or mono-iron carbonyl, or ligand exchange of CO with ethanol¹.

Metal carbonyl-polysulfide composites

Method: Canola oil polysulfide, prepared by reacting sulfur and canola oil at a 1:1 mass ratio at 180 °C for 20 minutes in the presence of sodium chloride followed by a washing step to remove the salt, was dissolved in pyridine to a concentration of 100 mg mL⁻¹. Triiron dodecacarbonyl, dimanganese decacarbonyl and triruthenium dodecacarbonyl were also dissolved separately in pyridine to a concentration of 5 mg mL⁻¹. All solutions were sonicated for 30 minutes to ensure dissolution, and then mixed in petri dishes at a ratio of 4.0 mL polysulfide solution to 8.0 mL metal carbonyl solution. Mixtures were stirred with a spatula and then left overnight to dry. The result is a single material, a film of reformed polysulfide harbouring a metal carbonyl. The iron polysulfide appeared red-brown, the manganese a light brown, and the ruthenium a yellow-brown. The film was scraped from the surface of the petri dishes using a spatula and collected in a glass vial. Over 3 replicates for each, an average of 137 mg iron-, 124 mg manganese- and 126 mg ruthenium-polymers

were collected, yields as low as 56 %. This can partly be attributed to loss in transfer as not all could be recovered from the petri dishes but might also indicate the loss of some component during drying, or perhaps a lesser inclusion of one component (most likely the polysulfide) from incomplete solvation.

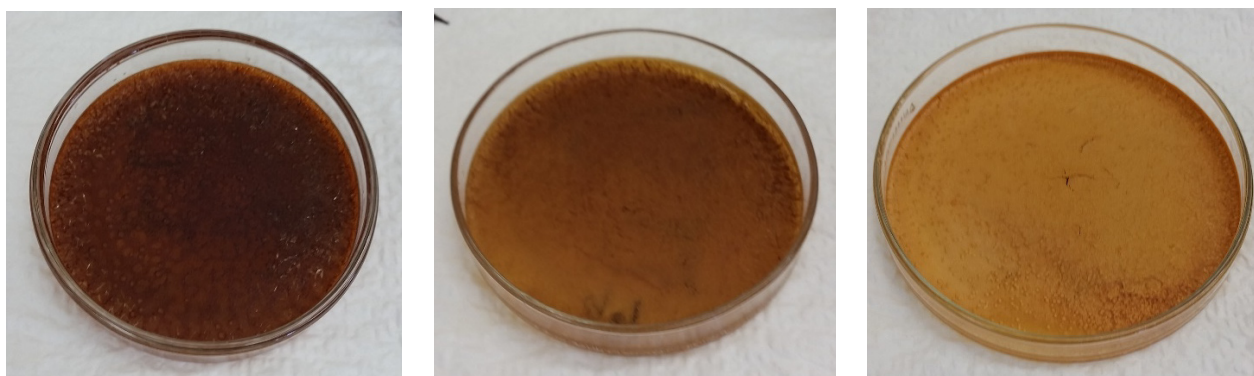


Figure 5.1.4 | Canola oil polysulfide co-precipitated with metal carbonyls. Left to right: Fe₃(CO)₁₂-polysulfide, Mn₂(CO)₁₀-polysulfide, Ru₃(CO)₁₂-polysulfide

In a repeat experiment to prepare more materials for analysis, 395 mg Ru-polymer, 398.8 mg Mn-polymer and 358.9 mg Fe-polymer were recovered with more rigorous collection of a total 440 mg for yields from 82 % to 91 %. Despite the more rigorous procedure some material still remained too difficult to remove with abrasion alone and so loss in transfer remains the most likely explanation for low yields in the first instance.

FTIR analysis

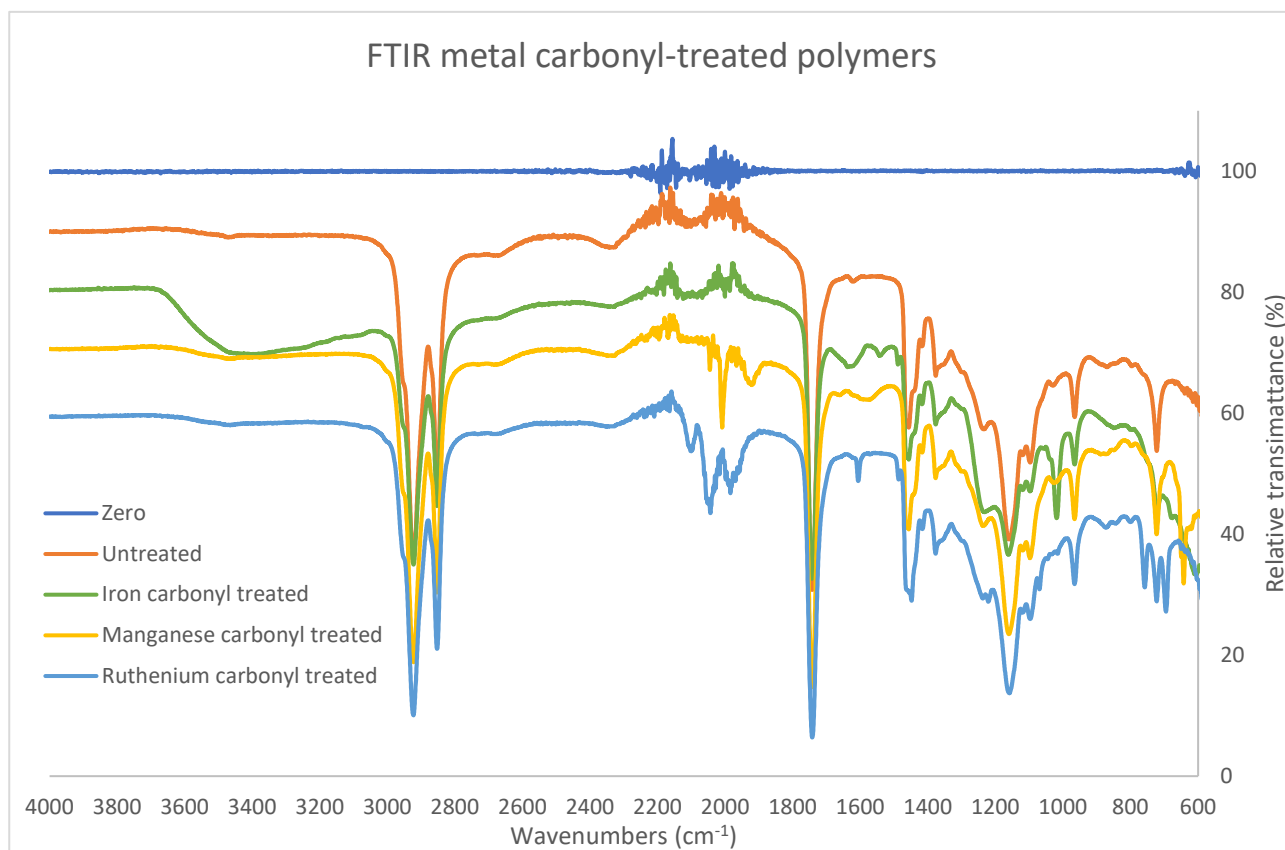


Figure 5.1.5 | Manganese and ruthenium-polymers exhibit peak distortions around 2000 cm⁻¹, as seen from pristine manganese and ruthenium carbonyls. A “zero” scan is included to demonstrate the noise introduced to the sample from the ATR instrument, prevalent in all scans.

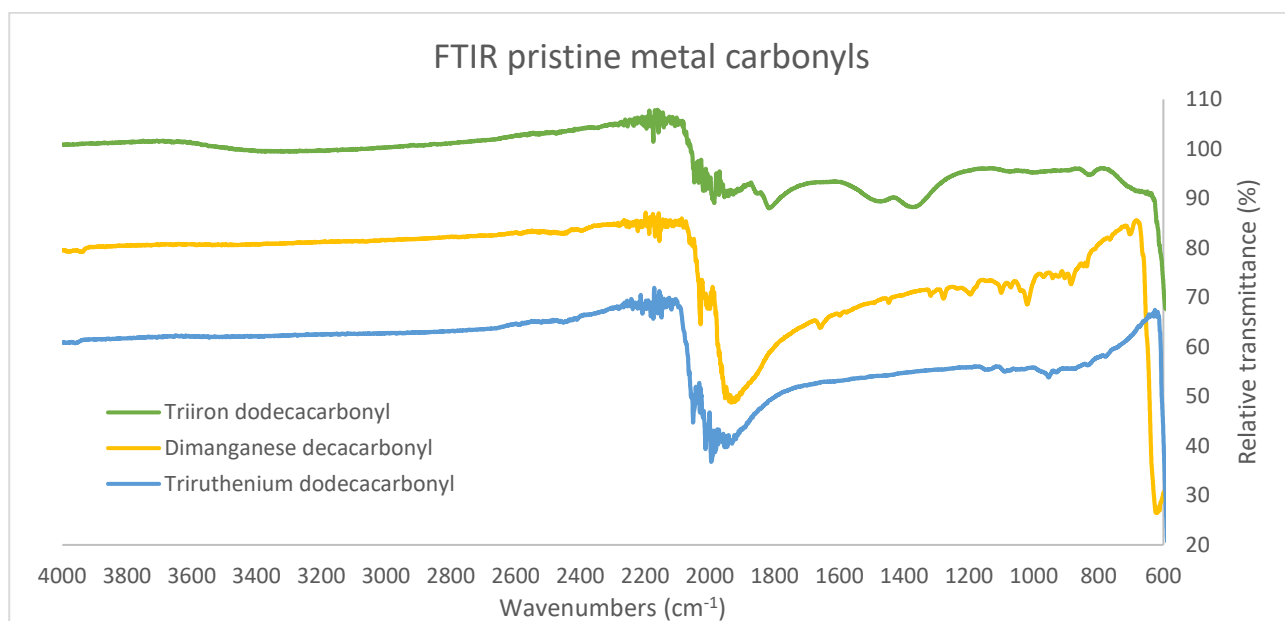


Figure 5.1.6 | All pristine metal carbonyls exhibit broad peaks at 2000 cm⁻¹, visible despite the noise in this region.

SEM analysis – Iron carbonyl treated canola oil polysulfide

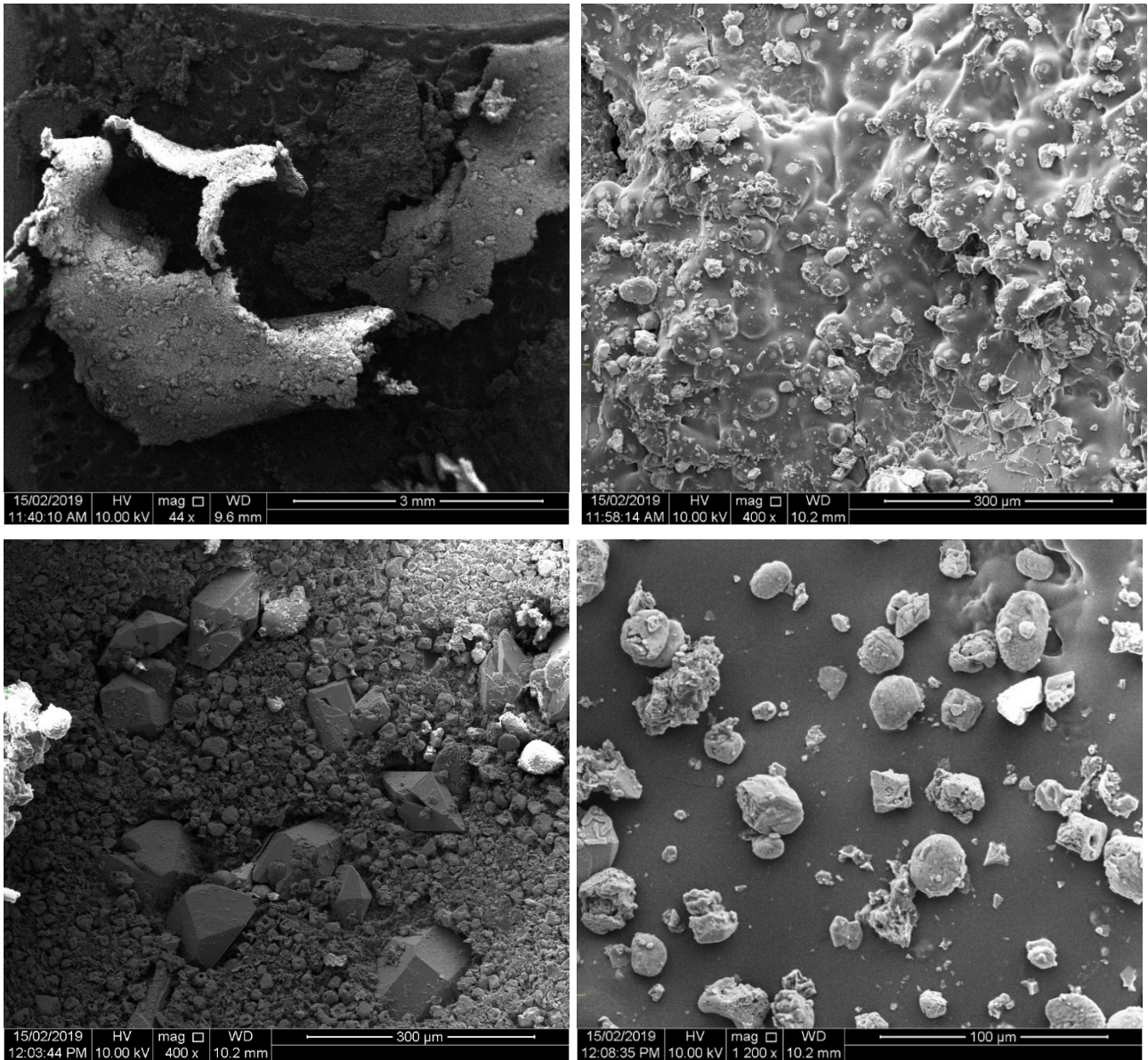


Figure 5.1.7 | SEM images of Fe-polymer indicating the different morphologies present

SEM analysis – Manganese carbonyl treated canola oil polysulfide

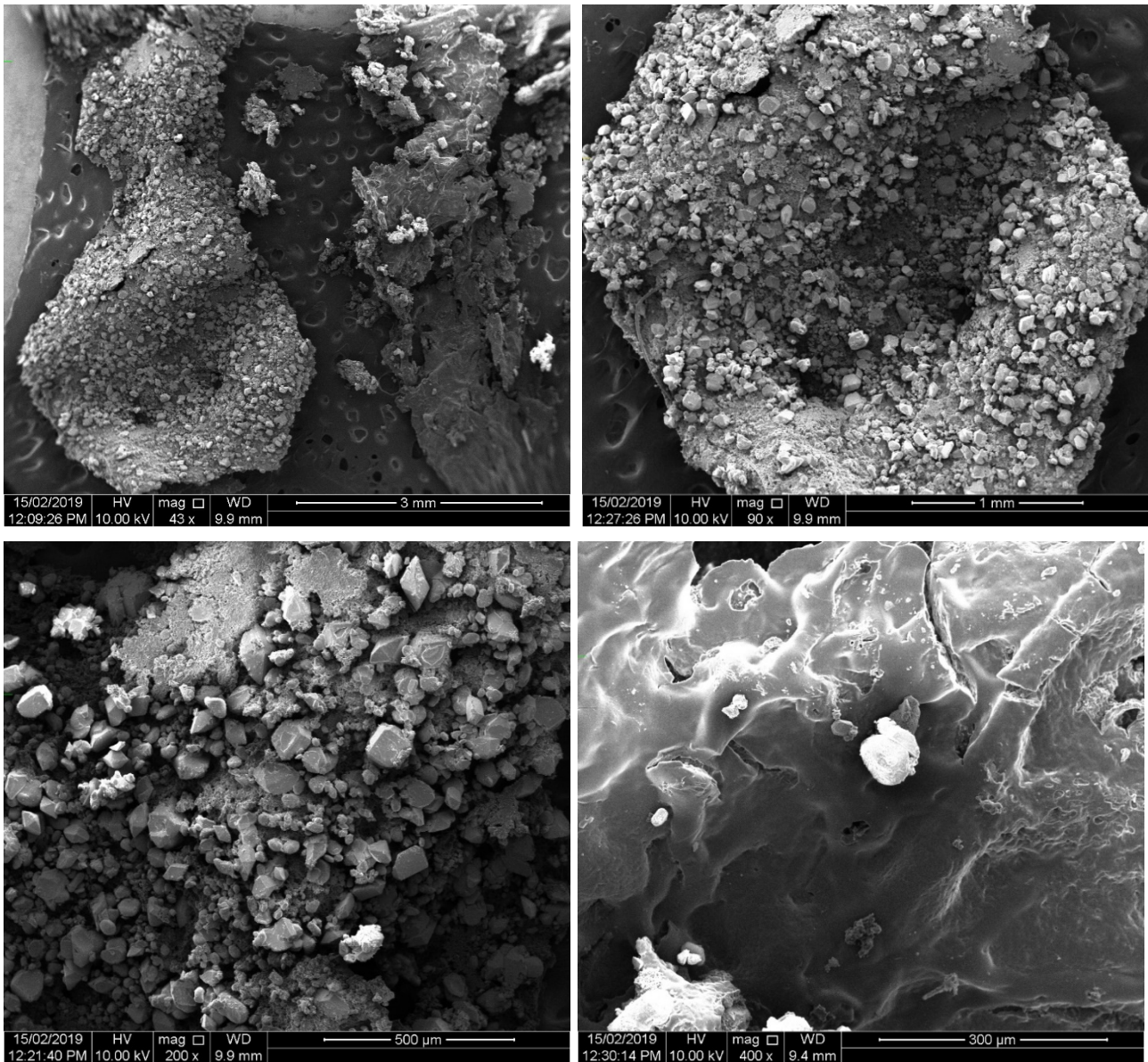


Figure 5.1.8 | SEM images of Mn-polymer indicating the different morphologies present

SEM analysis – Ruthenium carbonyl treated canola oil polysulfide

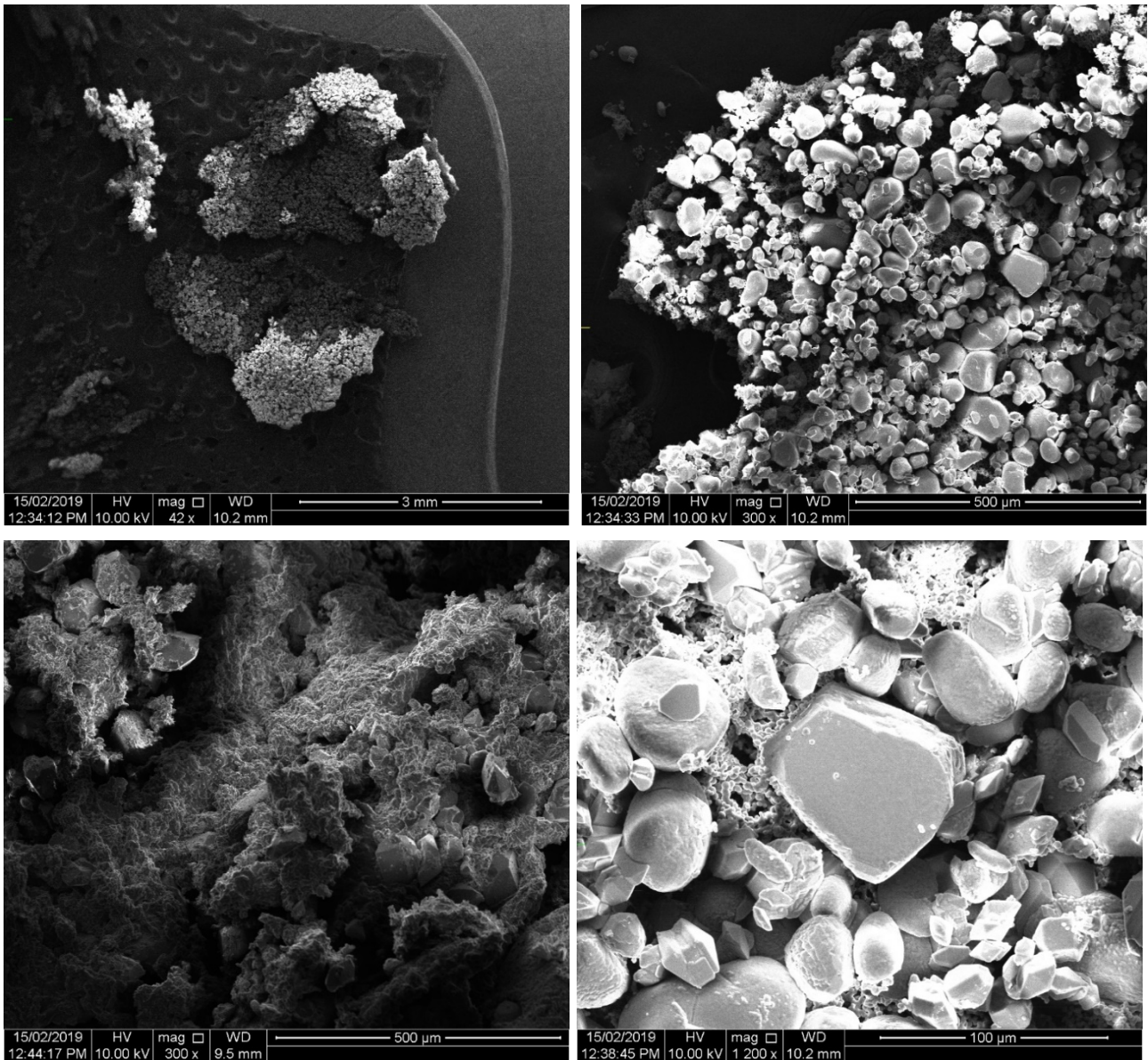
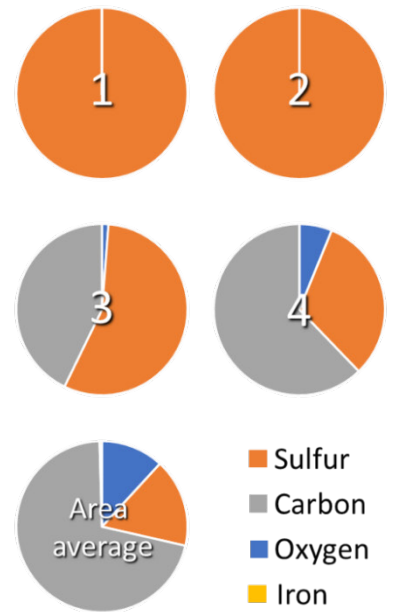
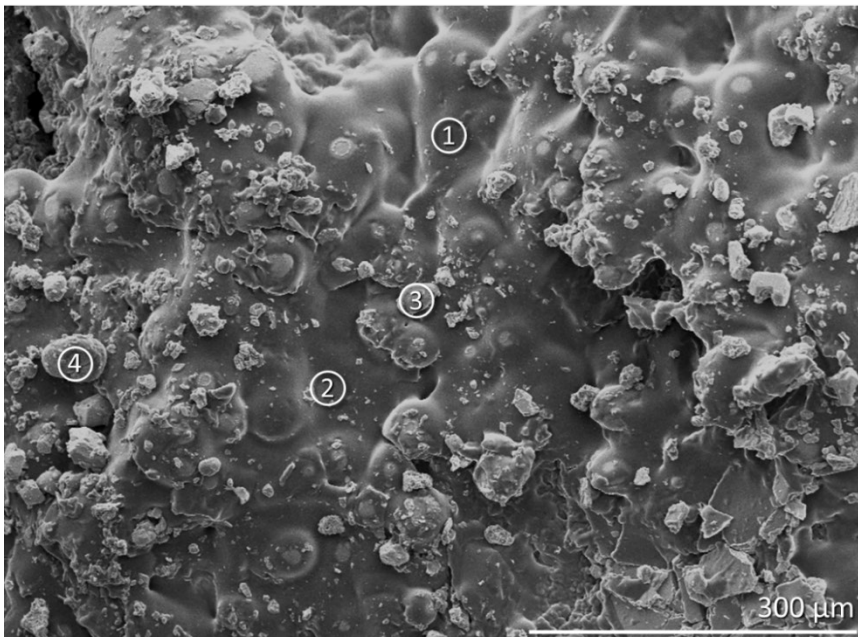
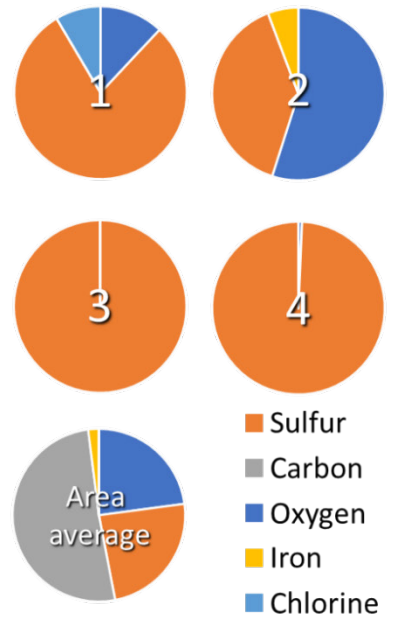
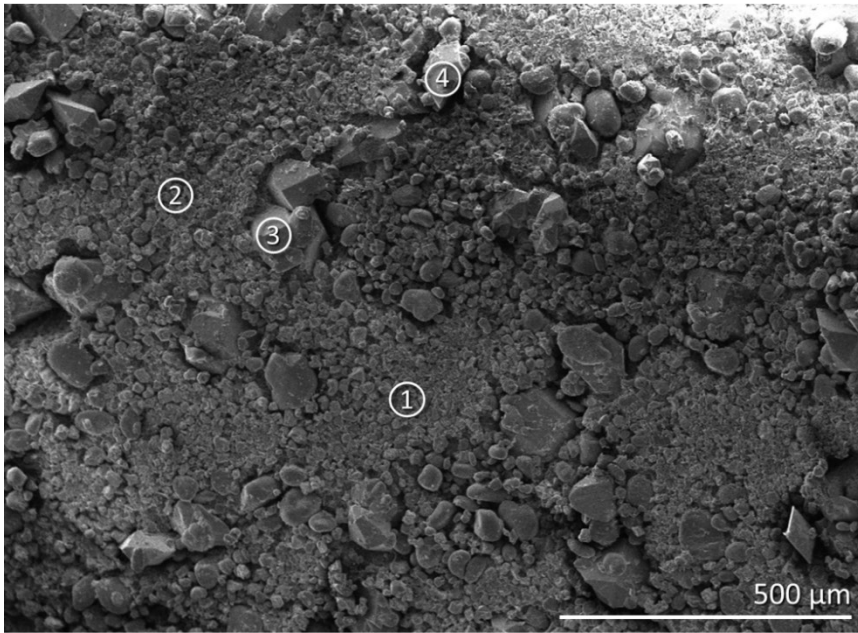


Figure 5.1.9 | SEM images of Ru-polymer indicating the different morphologies present

EDX analysis – Iron carbonyl treated canola oil polysulfide



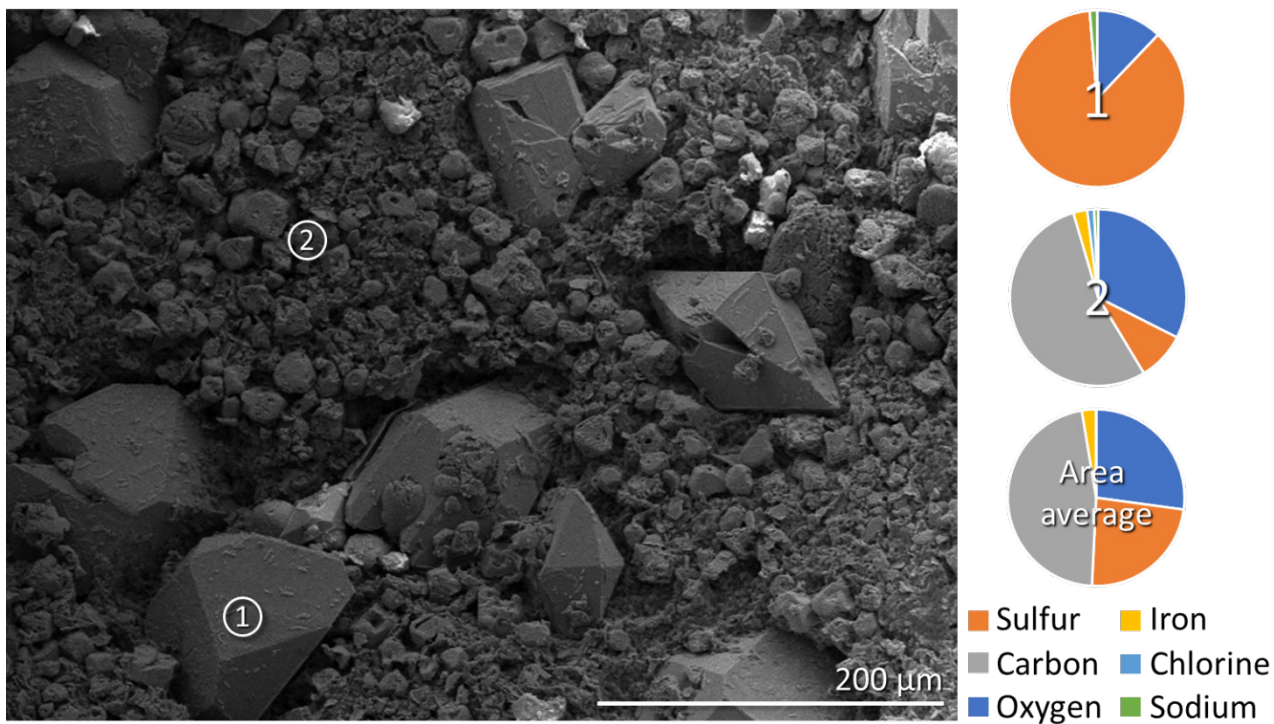
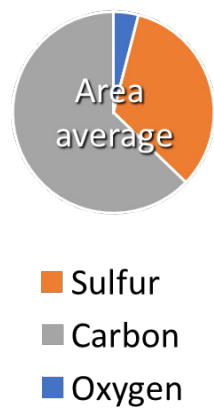
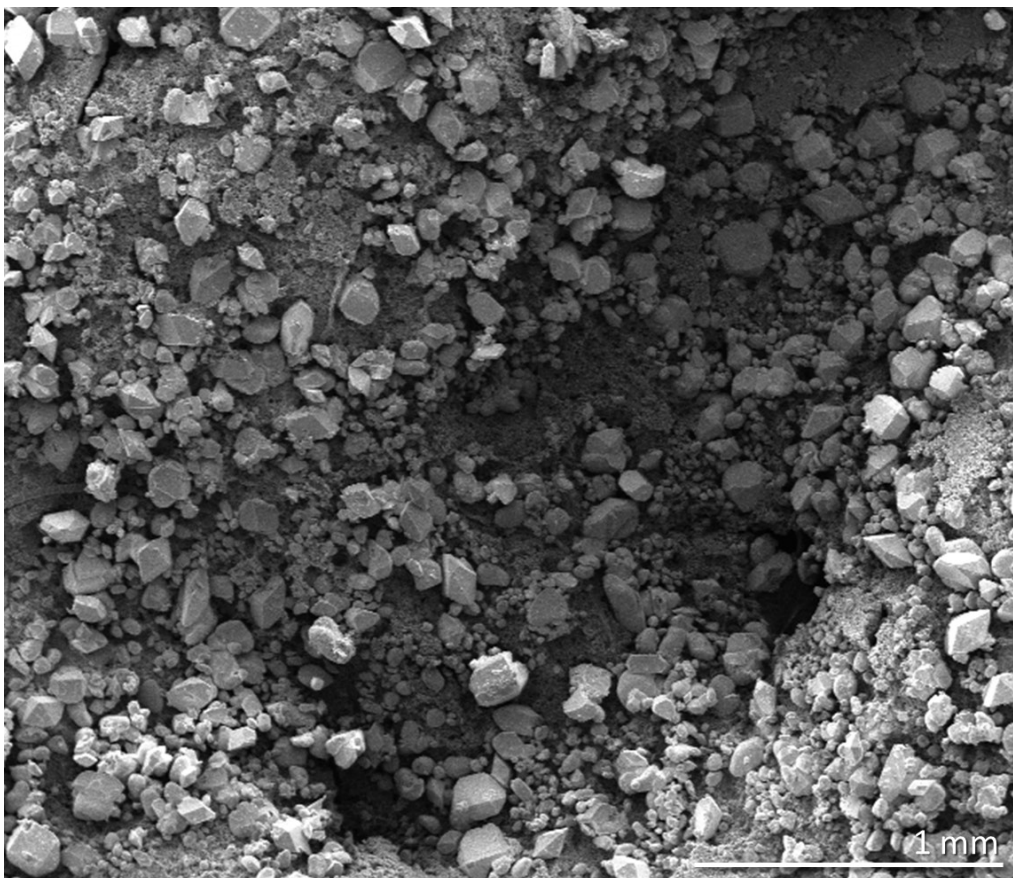
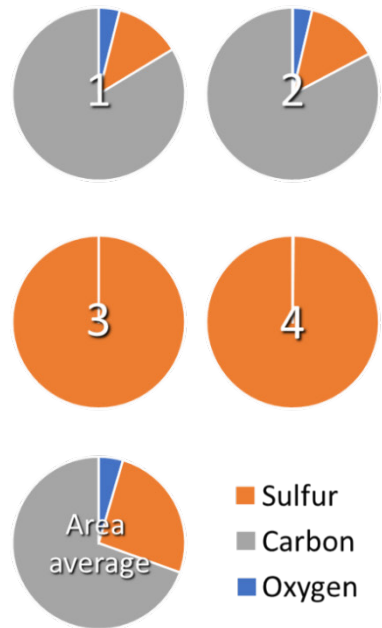
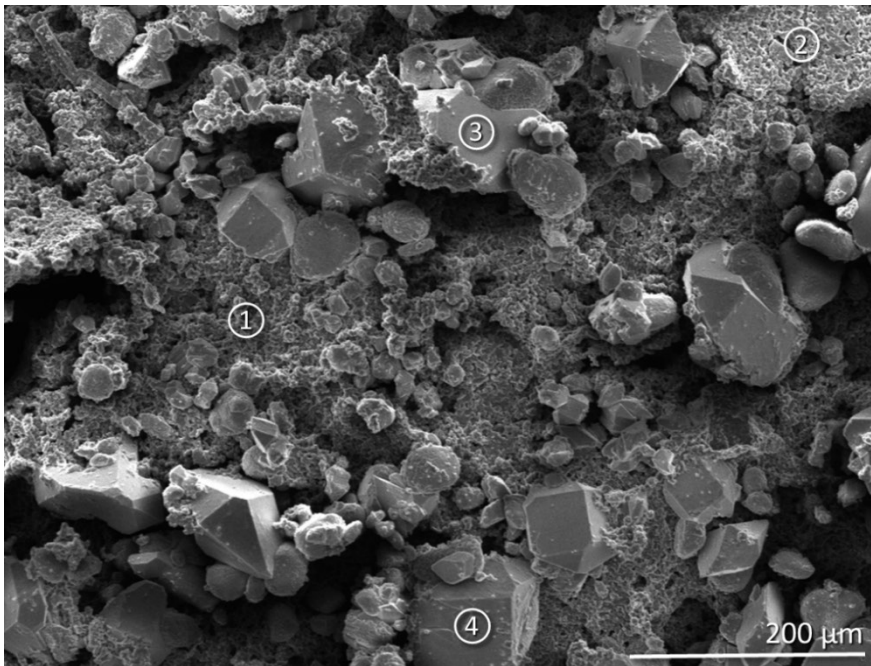


Figure 5.1.10 | SEM images of Fe-polymer with overlaid elemental analysis by EDX. Pie charts represent percent of atoms present. The area average represents an average across the full area shown in the SEM image. Iron can be detected along the surface though does not appear in or as a specific morphology.

EDX analysis – Manganese carbonyl treated canola oil polysulfide



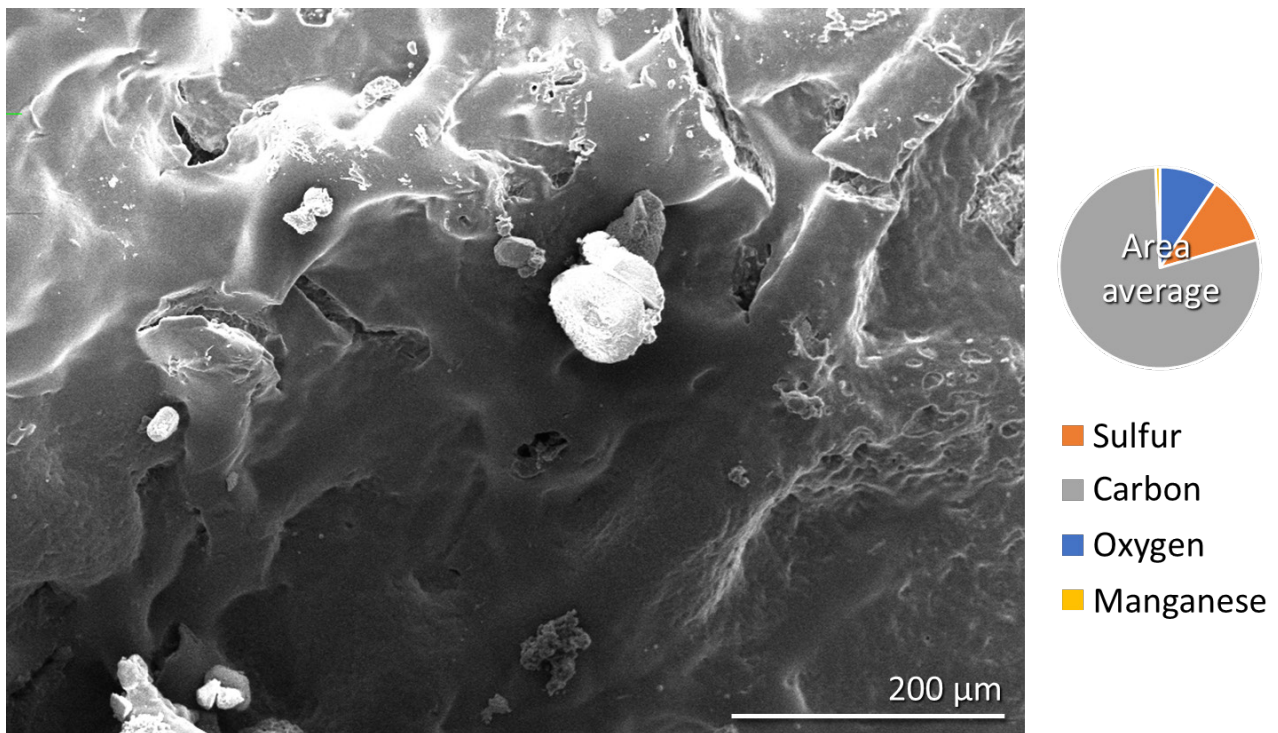


Figure 5.1.11 | SEM images of Mn-polymer with overlaid elemental analysis by EDX. Pie charts represent percent of atoms present. The area average represents an average across the full area shown in the SEM image. Manganese can be detected sparingly along the surface though does not appear in or as a specific morphology.

EDX analysis – Ruthenium carbonyl treated canola oil polysulfide

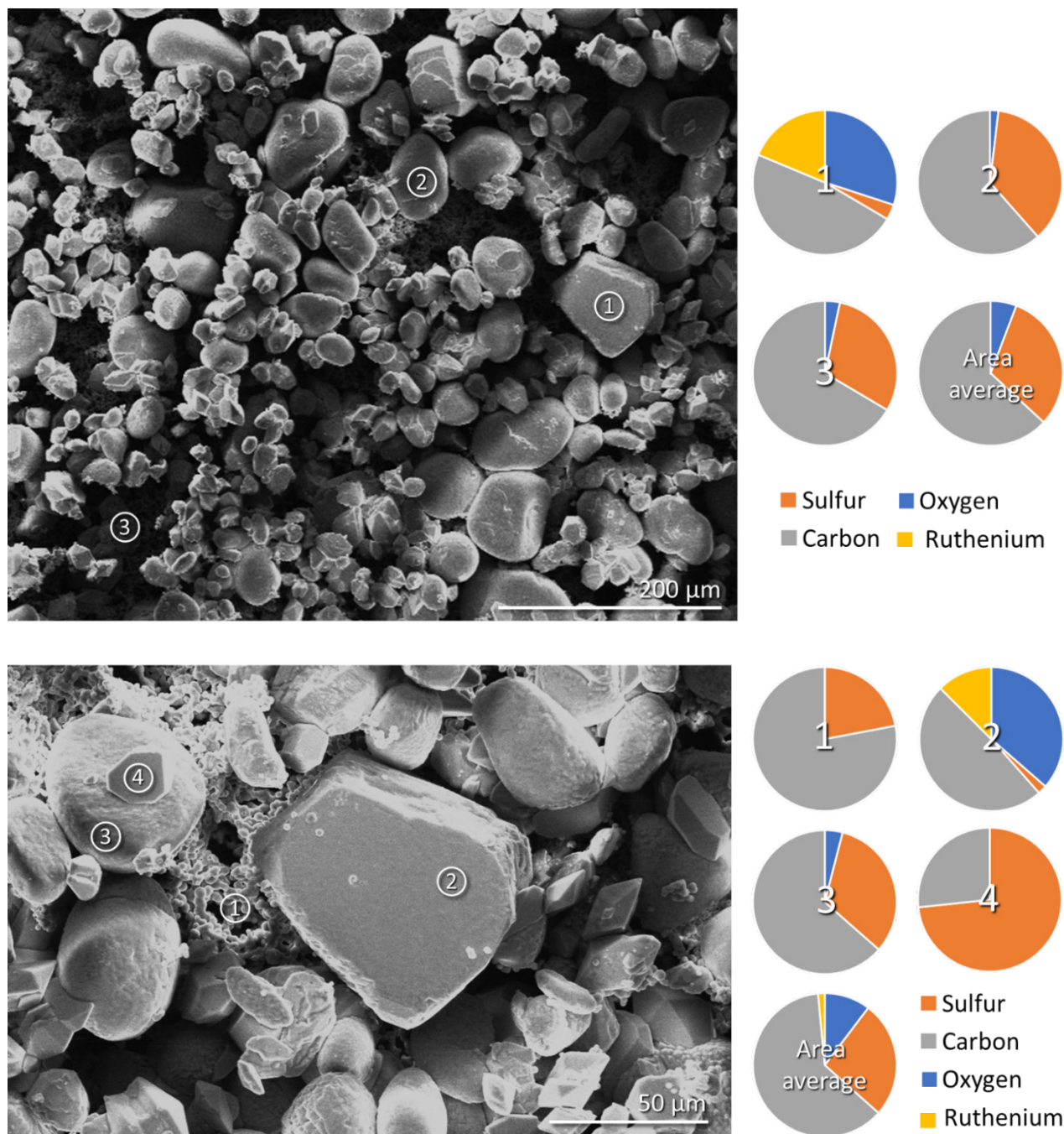


Figure 5.1.12 | SEM images of Ru-polymer with overlaid elemental analysis by EDX. Pie charts represent percent of atoms present. The area average represents an average across the full area shown in the SEM image. Ruthenium can be detected along the surface though does not appear in or as a specific morphology.

Drug-releasing polymer

Binding by incubation in solution

Method

A solution of diclofenac (analgesic) and dioxane (internal standard) was prepared in deuterated methanol and incubated with porous polymer for 24 hours. Proton NMR data was acquired for the solution as prepared and after incubation and compared to determine if diclofenac had been lost from solution while in contact with the polymer.

Results

¹H NMR trace of diclofenac before and after polymer incubation

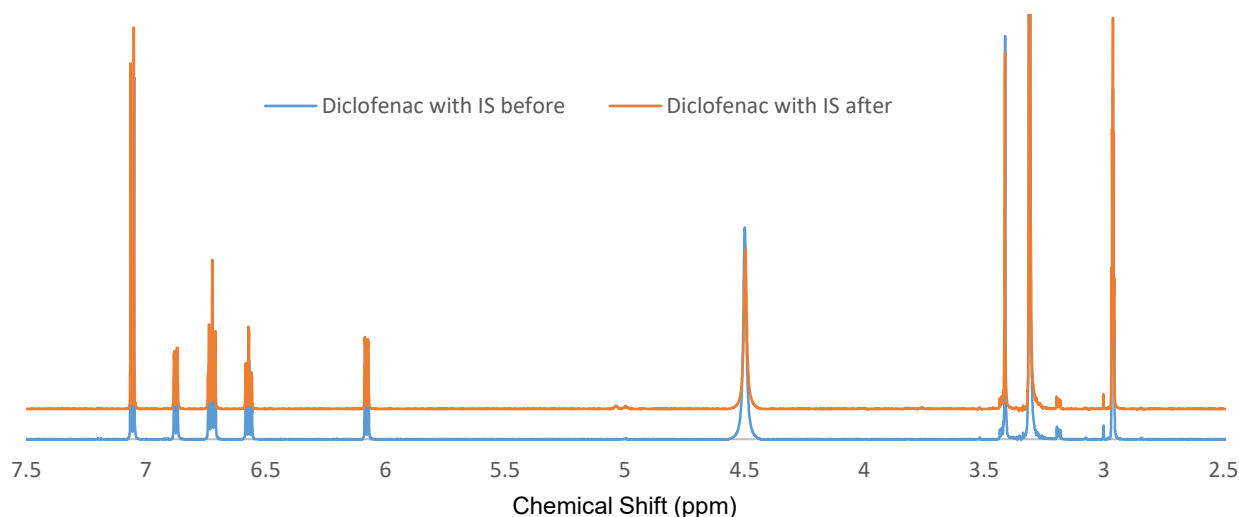


Figure 5.1.13 | NMR trace of diclofenac and dioxane (4.5 ppm singlet peak) in CD₄, before and after polymer incubation. All major peaks occur at the same instance in both samples.

The two traces show very little difference, indicating no native sorption of diclofenac by the polymer from methanol.

Encapsulation of drug in polymer synthesis

Method – 1 % diclofenac

20.0 g canola oil polysulfide (non-porous) was prepared to a 1:1 weight ratio of sulfur and canola oil, with the inclusion of 1.0 wt. % diclofenac (200 mg). The drug was initially mixed with the canola oil and heated (with stirring) to 180 °C, over which time the drug dissolved within the oil. After 5 minutes, the sulfur was added slowly over a period of a further 5 minutes. The mixture appeared at this stage as two phases: a clear, yellow canola oil upper and opaque, orange molten sulfur lower. Over the following 30 minutes, the mixture formed a single orange phase and then changed colour gradually through orange to dark brown before vitrifying. The solid product was left on the heat for a further 5 minutes and then removed to cool to room temperature.

Results

The solid polymer product contained interspersed regions of crystalline diclofenac rather than a consistent dispersion throughout. The material was cut to particles between 1.0 and 5.0 mm in diameter. 20.0 g starting material yielded 18.25 g 1 % diclofenac-loaded polysulfide due to loss of material in glassware transfer.

Method – 10 % diclofenac

20.0 g canola oil polysulfide (non-porous) was prepared to a 1:1 weight ratio of sulfur and canola oil, with the inclusion of 10.0 wt. % diclofenac (2.00 g). The drug was initially mixed with the canola oil and heated (with stirring) to 180 °C, over which time the drug dissolved within the oil. After 5 minutes, the sulfur was added slowly over a period of a further 5 minutes. The mixture appeared at this stage as two phases: a clear, yellow canola oil upper and opaque, orange molten sulfur lower. Over the following 40 minutes, the mixture formed a single orange phase and then changed colour gradually through orange to dark brown before vitrifying. The solid product was left on the heat for a further 5 minutes and then removed to cool to room temperature.

Results

After cooling the polymer had changed colour to dark red-brown with white powder visible along the surface. The solid polymer product contained interspersed regions of crystalline diclofenac rather than a consistent dispersion throughout. The material was cut to particles between 1.0 and 5.0 mm in diameter.

STA analysis of drug-loaded polymer

Method

18 mg polymer, prepared with inclusion of 1 or 10 wt% diclofenac, was weighed into an STA sample crucible and heated from 30 °C to 700 °C at 20 °C min⁻¹. Heat flow and sample weight were recorded during this time. The 10 wt. % sample was heated for longer, up to 900 °C.

Results

After both runs, a black crystalline (shiny) solid remained in the crucible, more of which was present after heating the 10 wt. % sample than the 1 wt. %. This is likely to be the thermal decomposition product diclofenac, as previous tests have left nothing in the crucible after heating untreated canola oil polysulfide up to this temperature. Up until 400 °C the STA trace appears no different to polysulfide with no diclofenac present, it is only from this temperature and up that a difference is observed, attributable to the thermal decomposition of the drug. It can be concluded from this that heating the drug to 180 °C as in synthesis should not result in thermal decomposition.

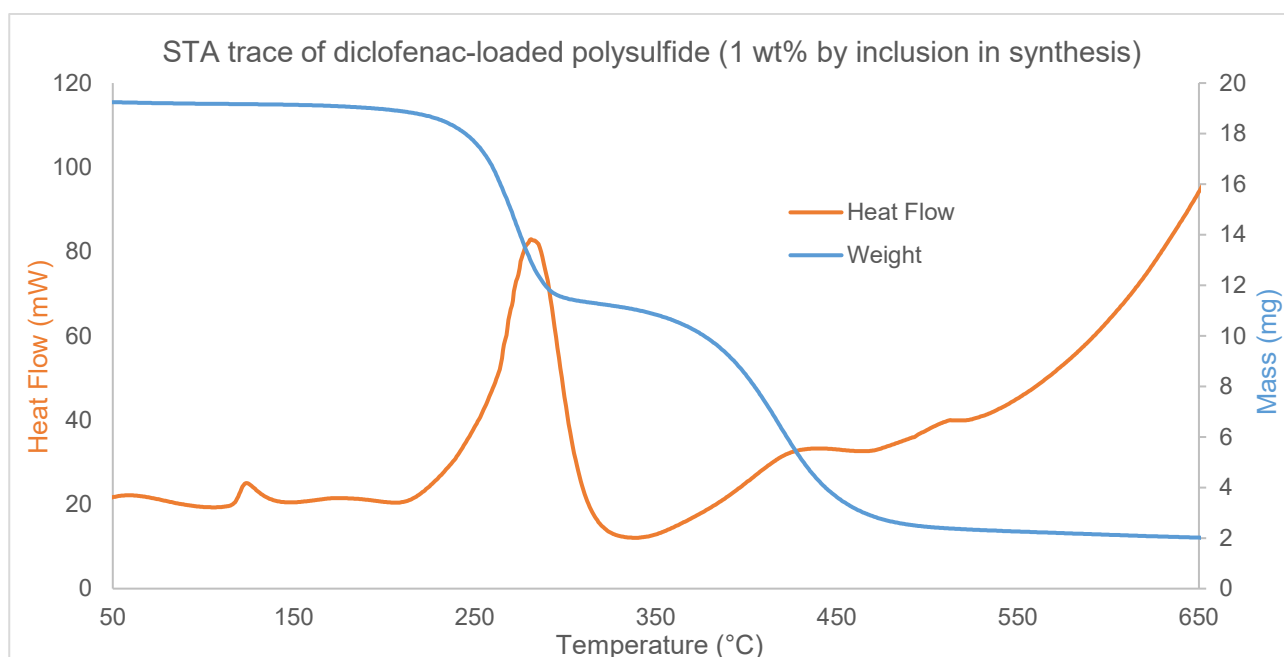


Figure 5.1.14 | STA trace of canola oil polysulfide synthesised to include 1 wt. % diclofenac

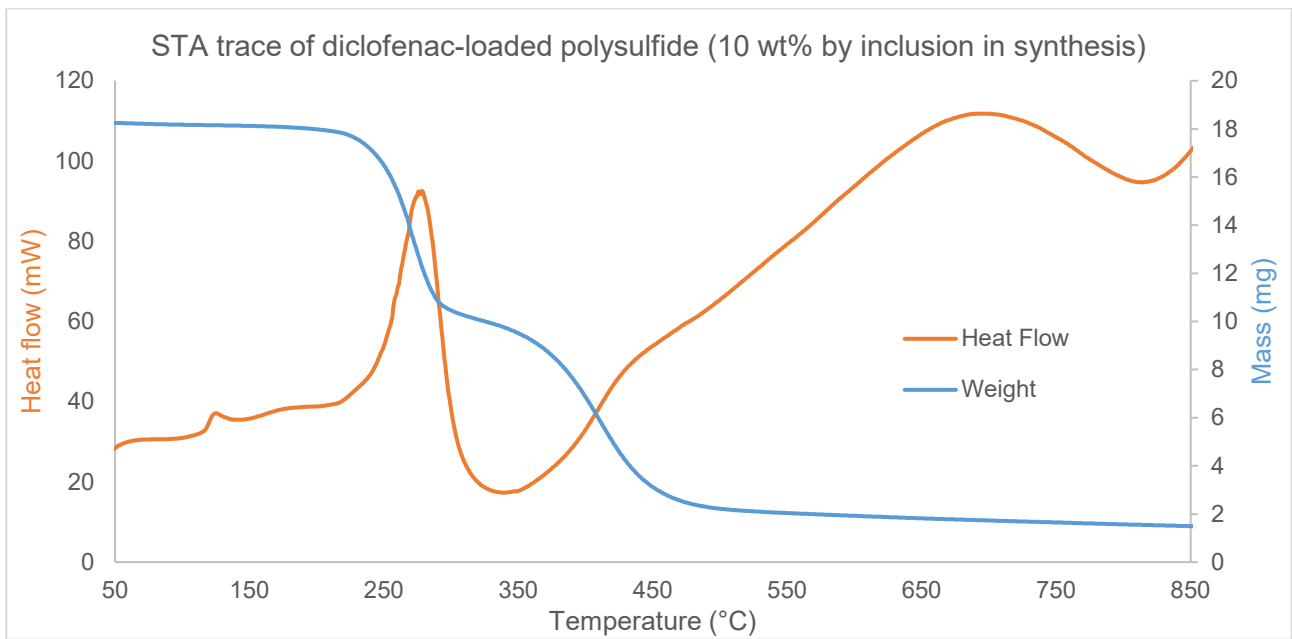


Figure 5.1.15 | STA trace of canola oil polysulfide synthesised to include 10 wt. % diclofenac

Drug release in water

Method

1.00 g drug-loaded polysulfide (10 wt% diclofenac) was measured into seven glass vials, 3 lots as synthesised, 2 having been washed with ethanol (3 x 10 mL) and dried, and 2 having been washed with deionised water (3 x 10 mL) and dried. This was to test if any drug released from the polymer was coming primarily from the surface or if drug would still be released after pre-washing. To a further two glass vials diclofenac was added: 100 mg to the first 10 mg to the second, as positive controls without polymer. To each vial, 3 mL D₂O was added, all were lightly stirred for 30 seconds and left for 22 hours. D₂O was removed from each sample by syringe and filtered through 0.20 µm filters. To 1 mL of the resulting solutions, 15 µL of dioxane was added as an internal standard for NMR analysis. All samples were analysed by ¹H NMR spectroscopy to look for the presence of diclofenac. Diclofenac has previously been dissolved in methanol-d₄ to achieve a ¹H NMR spectrum for comparison.

Results

In no samples were peaks indicative of diclofenac seen. In all samples peaks at 3.70 ppm (dioxane) and 4.70 ppm (water) were present. In the samples pre-washed with ethanol, a very weak triplet peak was observed at 1.15 ppm. In the water-washed samples, the water peak height was greater than that of dioxane and integrated for 82 and 96 % of the internal standard. In all other samples the dioxane peak height was greater and the water peak integrated for between 30 and 50 %.

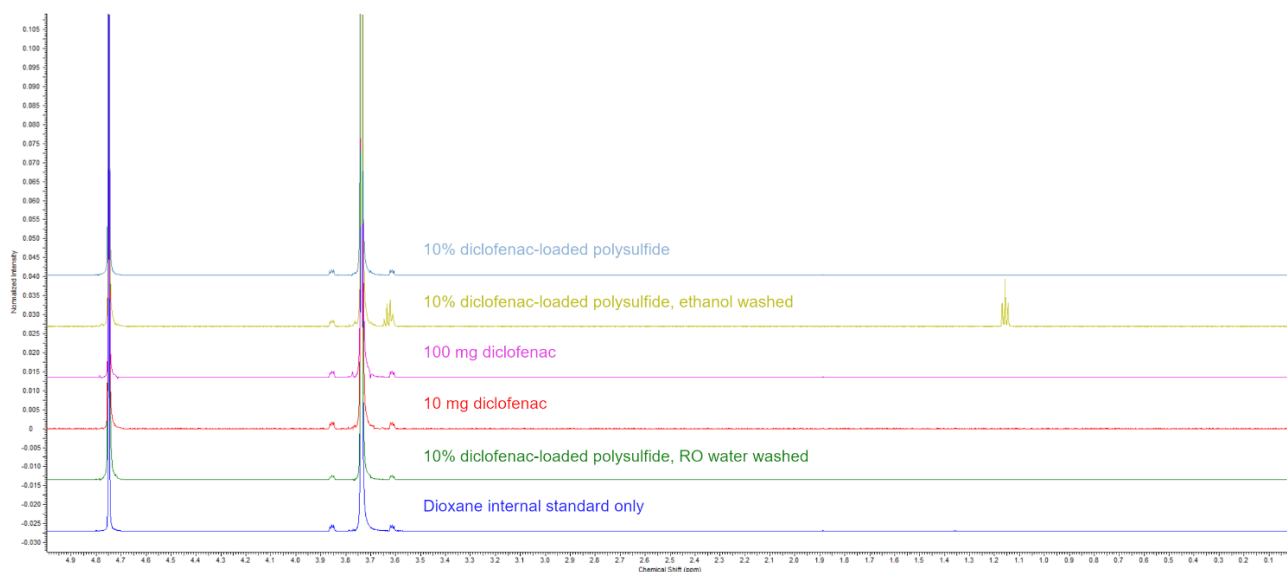


Figure 5.1.16 | ¹H NMR spectra shows no solvation of diclofenac in D₂O

Conclusion

Diclofenac is not soluble in water and may require a buffer to deprotonate prior to testing. Residual ethanol is present in the sample washed with the solvent. A repeat experiment with deuterated chloroform (in which diclofenac does dissolve) as an NMR solvent was attempted but interaction with the polymer led to decolouration of solvent and ultimately was not considered worth perusing further as such conditions were not biologically relevant.

Drug release in buffer

Method

0.1 M phosphate buffers were prepared to pH 8, 7 and 6 and a 0.1 M acetate buffer to pH 5 all in D₂O. 500 mg 10 wt. % diclofenac-loaded polymer (50 mg drug) was portioned into a 2 mL aliquot of each buffer and left for 7 days. 50 mg diclofenac was added also to 2 mL D₂O and left for the same time as a no-polymer positive control. Each was prepared in triplicate. After this time the D₂O was removed from each sample by syringe and filtered through 0.20 µm filters for ¹H NMR analysis. Dioxane was included as an internal standard.

Results

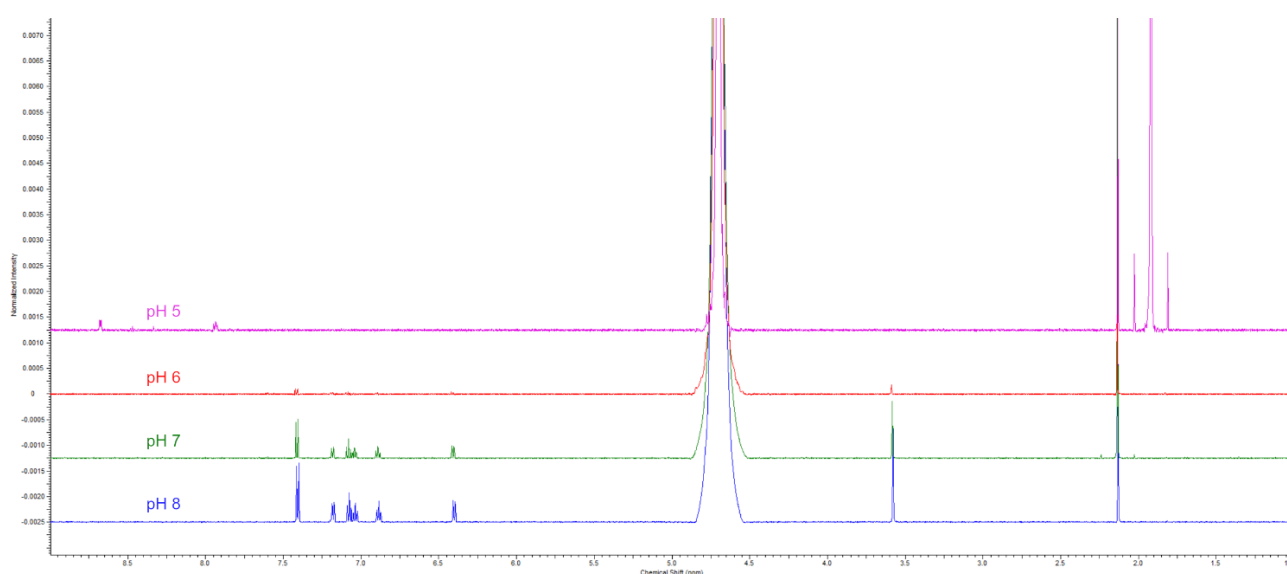


Figure 5.1.17 | ¹H NMR spectra of 10 wt. % diclofenac-polymer incubated in buffered D₂O for 1 week.

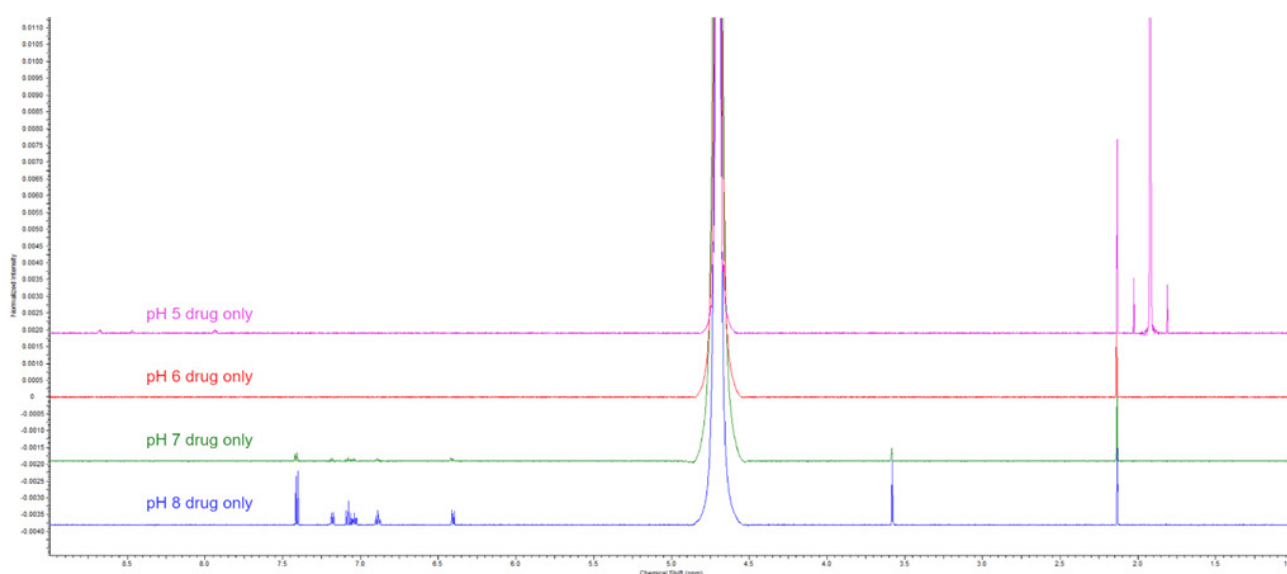


Figure 5.1.18 | ¹H NMR spectra of diclofenac incubated in buffered D₂O for 1 week.

Encapsulation of drug in polymer synthesis (drug added near end of synthesis)

Method

20.0 g canola oil polysulfide (non-porous) was prepared to a 1:1 weight ratio of sulfur and canola oil, with the inclusion of 10.0 wt. % diclofenac (2.0 mg). After 5 minutes of preheating the canola oil to 180 °C in a round bottom flask, the sulfur was added slowly over a period of a further 5 minutes with magnetic stirring. The mixture appeared at this stage as two phases: a clear, yellow canola oil upper and opaque, orange molten sulfur lower. Over the following 16 minutes, the mixture formed a single orange phase and then changed colour gradually through orange to dark brown and began to thicken. At this point the diclofenac was added to the round bottom flask to be mixed in with the quickly thickening pre-polymer. 3 minutes later the polymer became too thick to stir and 6 minutes after that it was removed from the heat to cool.

Results

The solid polymer product appeared as a brown rubber, indistinguishable from canola oil polysulfide as prepared without the inclusion of diclofenac. The material was cut to particles between 1.0 and 5.0 mm in diameter. 20.0 g starting material yielded 19.0 g 10 wt. % diclofenac-loaded polysulfide due to loss of material in glassware transfer.

Drug release in buffer (polymer prepared with drug added near end of synthesis)

Method

0.1 M phosphate buffers were prepared to pH 8, 7 and 6 and a 0.1 M acetate buffer to pH 5 all in D₂O. 500 mg 10 wt. % diclofenac-loaded polymer (drug added at end of synthesis) was portioned into a 2 mL aliquot of each buffer and left for 7 days. Each was prepared in triplicate. After this time the D₂O was removed from each sample by syringe and filtered through 0.20 µm filters for ¹H NMR analysis.

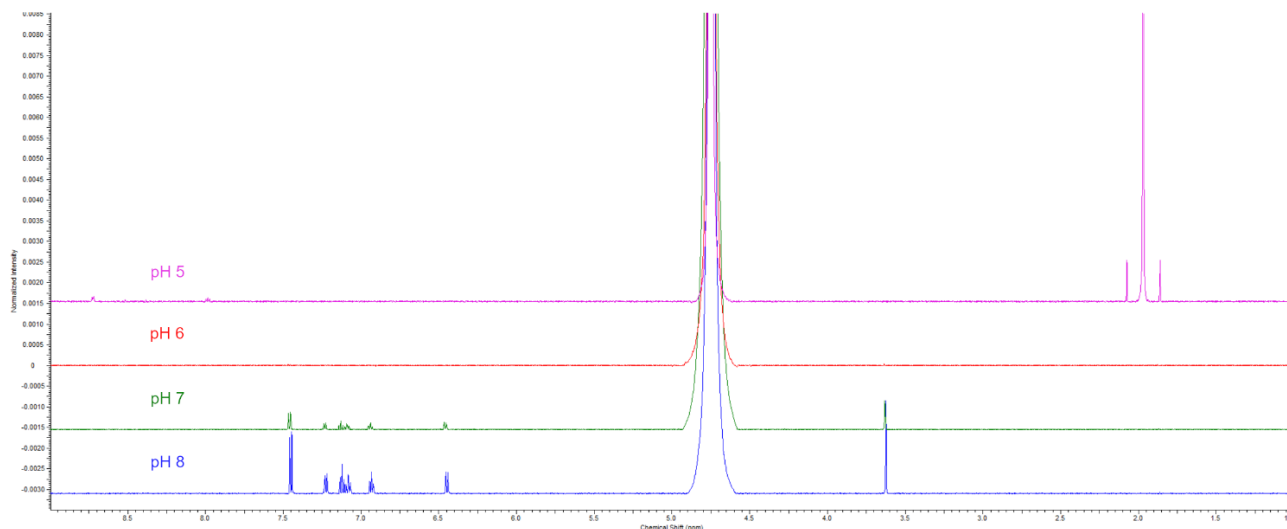


Figure 5.1.19 | Though signals are weak, the manipulation of pH above 7 results in an increase in diclofenac signal. This both confirms solvation at pH 8 and the release of the drug from the polymer matrix under these conditions.

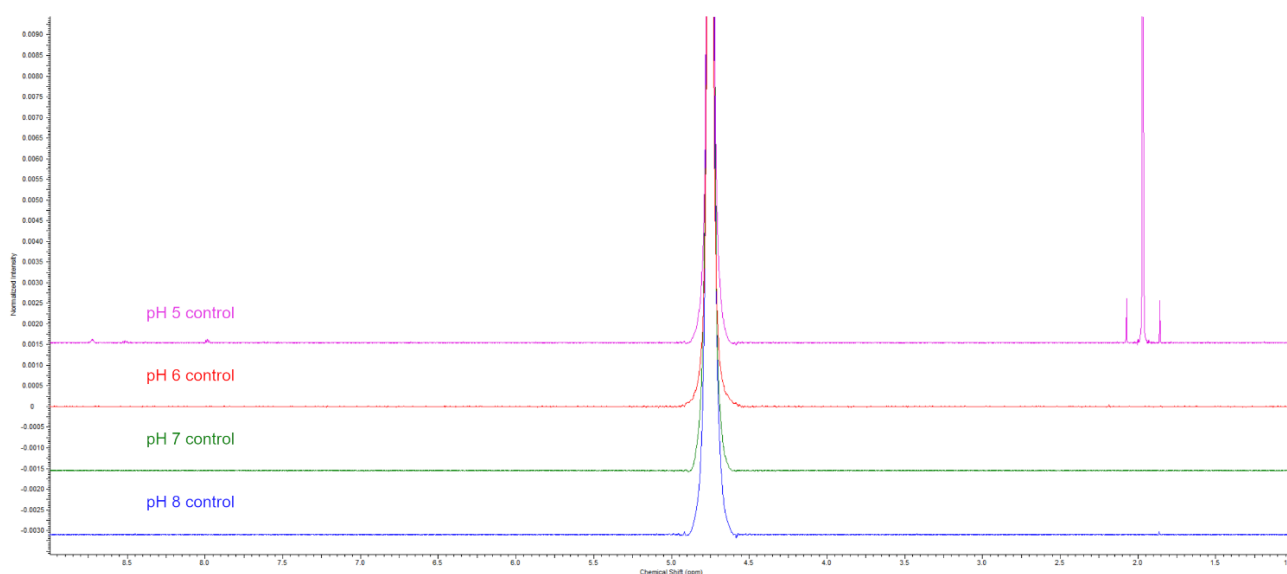


Figure 5.1.20 | ¹H analysis of the buffer solutions only reveals the peak at ca. 1.8 ppm at pH 5 to be a buffered solvent artefact and not relevant to the polysulfide.

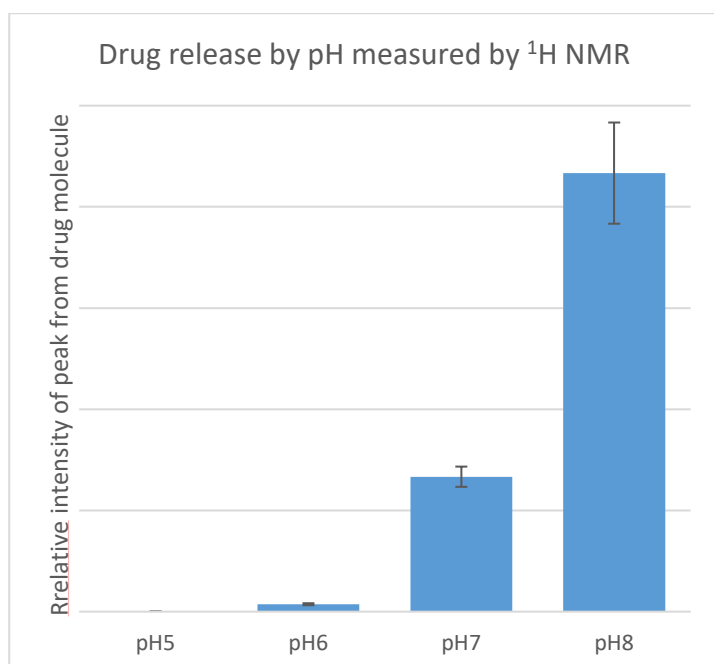


Figure 5.1.21 | Monitoring the area under the peak at 3.7 ppm shows how release into solution increases with pH

Conclusion

Given that with inclusion of diclofenac at the end of synthesis appeared to provide more consistent mixing, and release at high pH occurred in both instances, this was the method chosen to incorporate drug molecules for subsequent studies.

Maximum drug capacity of canola oil polysulfide

25 wt. % diclofenac

8.0 g canola oil polysulfide (non-porous) was prepared to a 1:1 weight ratio of sulfur and canola oil, with the inclusion of 25.0 wt. % diclofenac (2.0 g). After first melting the sulfur at 180 °C in a glass vial on an aluminium heating block, the canola oil was added slowly over a period of 2 minutes with magnetic stirring. The mixture appeared at this stage as two phases: a clear, yellow canola oil upper and opaque, orange molten sulfur lower. Over the following 15 minutes, the mixture formed a single orange phase and then changed colour gradually after a further 6 minutes through orange to dark brown and began to thicken. At this point the diclofenac was added to the mixture. 3 minutes later the polymer became too thick to stir and 6 minutes after that it was removed from the heat to cool. After 2 minutes of mixing the mixture began to bubble and after a further 6 minutes had doubled in size, filling the volume of the glass vial whilst solidifying.

After allowing the polymer to cool the mass appeared hollow, indicating gas formation or entrapment of gas during synthesis, following bubbling and expansion. Crystalline diclofenac was visible in pockets throughout the polymer, that itself was rather weak and sticky as if it had not reacted to completion.

50 wt. % diclofenac

8.0 g canola oil polysulfide (non-porous) was prepared to a 1:1 weight ratio of sulfur and canola oil, with the inclusion of 50.0 wt. % diclofenac (4.0 g). After first melting the sulfur at 180 °C in a glass vial on an aluminium heating block, the canola oil was added slowly over a period of 2 minutes with magnetic stirring. The mixture appeared at this stage as two phases: a clear, yellow canola oil upper and opaque, orange molten sulfur lower. Over the following 15 minutes, the mixture formed a single orange phase and then changed colour gradually after a further 6 minutes through orange to dark brown and began to thicken. At this point the diclofenac was added to the mixture. Addition of such a large quantity of the solid resulted in a paste-like mixture that became difficult for the magnetic stirrer bar to mix. Over 10 minutes the mixture changed colour to a black-brown with a red-brown layer at the top and began to bubble. After a further 45 minutes at temperature the mixture had not vitrified and so the experiment was stopped.

After leaving to cool and sit for 48 hours the mixture remained the two-phase red-brown and black-brown but had increased in viscosity to a sticky elastic, able to be pulled from the vial as a long string. The mixture had no shape consistency however and flowed back into a formless puddle after 20 minutes.

Conclusion

Inclusion of 25 wt. % diclofenac results in bubbling and deformation and inclusion of 50 wt. % hinders polymerisation. With this in mind drugs should not be incorporated into the polymer in this manner at proportions over the previously tested 10 wt. %.

Encapsulation of anti-cancer drugs in polymer synthesis

Doxorubicin – 5 wt. %

To a 3 mL glass vial was added 170 mg sulfur, heated to 180 °C with stirring. After 5 minutes 170 mg canola oil was added by first warming on the heating block to increase flow. After 11 minutes the polymer mixture began to thicken, at this point 18 mg doxorubicin was added via a funnel. The doxorubicin was mixed into the polymer, vitrifying 2 minutes after addition to afford 368 mg of a 5 wt. % doxorubicin polysulfide, red-brown in appearance.

Doxorubicin – 10 wt. %

To a 3 mL glass vial was added 180 mg sulfur, heated to 180 °C with stirring. After 2 minutes 180 mg canola oil was added by first warming on the heating block to increase flow. After 7 minutes the polymer mixture began to thicken, at this point 40 mg doxorubicin was added via a funnel. The doxorubicin was mixed into the polymer, vitrifying 3 minutes after addition to yield 400 mg of a 10 wt. % doxorubicin polysulfide, red-brown in appearance.

Crizotinib – 5 wt. %

To a 3 mL glass vial was added 350 mg sulfur, heated to 180 °C with stirring. After 2 minutes 350 mg canola oil was added by first warming on the heating block to increase flow. After 12 minutes the polymer mixture began to thicken, at this point 37 mg crizotinib was added via a funnel. The crizotinib was mixed into the polymer, bubbling and expanding and then vitrifying 5 minutes after addition to yield a 5 wt. % crizotinib polysulfide, brown in appearance with visible crystals of the drug trapped within.

Crizotinib – 10 wt. %

To a 3 mL glass vial was added 180 mg sulfur, heated to 180 °C with stirring. After 2 minutes 180 mg canola oil was added by first warming on the heating block to increase flow. After 19 minutes the polymer mixture began to thicken, at this point 40 mg crizotinib was added via a funnel. The crizotinib was mixed into the polymer, vitrifying 6 minutes after addition to yield 400 mg of a 10 wt. % crizotinib polysulfide, brown in appearance with visible crystals of the drug trapped within.

DNA-releasing polymer

Method

Aqueous solutions of metal salts were prepared to 10 mg mL⁻¹ of metal ions for copper nitrate, magnesium nitrate, zinc nitrate, calcium nitrate, iron nitrate and mercury chloride. An aqueous solution of gold chloride was also prepared to 5 mg mL⁻¹. Mercury and gold chloride solutions were sonicated for 10 minutes to aid in dissolution, and after allowing all solutions to settle for 1 hour, 10 mL of each was portioned into a series of 20 mL glass vials and 1.0 g porous polysulfide added to each. Each mixture of polysulfide and metal solution was prepared in triplicate. After 72 hours, 10 µL of each sample was diluted 1,000,000 fold in a 1 % HNO₃, 1 % HCl acid matrix in pure milliQ water for ICP-MS analysis against standard metal stock solutions of known concentration.

Results

Analysis of metal solutions incubated with polysulfide by ICP-MS reiterated previous results for mercury and gold: both were sequestered from solution by porous canola oil polysulfide. The pre-incubation solution of mercury chloride contained 10.154 mg mL⁻¹ mercury and the gold chloride solution 4.901 mg mL⁻¹ gold. The post-incubation solutions contained, on average of triplicate individual incubations, 5.80 mg mL⁻¹ mercury and 0.010 mg mL⁻¹ gold. This corresponds to removal of 42.9 % of the mercury and 99.8% of the gold from solution.

	Magnesium	Iron	Copper	Zinc	Mercury	Gold
Replicate 1 (mg mL ⁻¹)	8.093	9.410	9.646	8.879	5.957	0.010
Replicate 2 (mg mL ⁻¹)	8.015	8.989	10.410	9.392	5.674	0.006
Replicate 3 (mg mL ⁻¹)	7.717	8.887	9.713	9.787	5.757	0.007
Average (mg mL ⁻¹)	7.94	9.10	9.92	9.35	5.80	0.008
Standard deviation	0.162	0.226	0.345	0.372	0.118	0.002
Initial conc. (mg mL ⁻¹)	7.464	8.689	9.607	9.209	10.154	4.901
Percentage remaining	106.40%	104.67%	103.29%	101.55%	57.08%	0.16%
Percentage removed	-6.40%	-4.67%	-3.29%	-1.55%	42.92%	99.84%

Sequestration of other metals did not seem to occur under these conditions. Post-incubation magnesium, iron, copper and zinc nitrate solutions all read as concentrations very close to their initial concentrations – oddly showing concentrations above the initial in all cases. For the case of calcium (atomic mass 40.078 Da), all results unfortunately displayed interference from competing species, likely due to the carrier gas argon (atomic mass 39.948 Da).

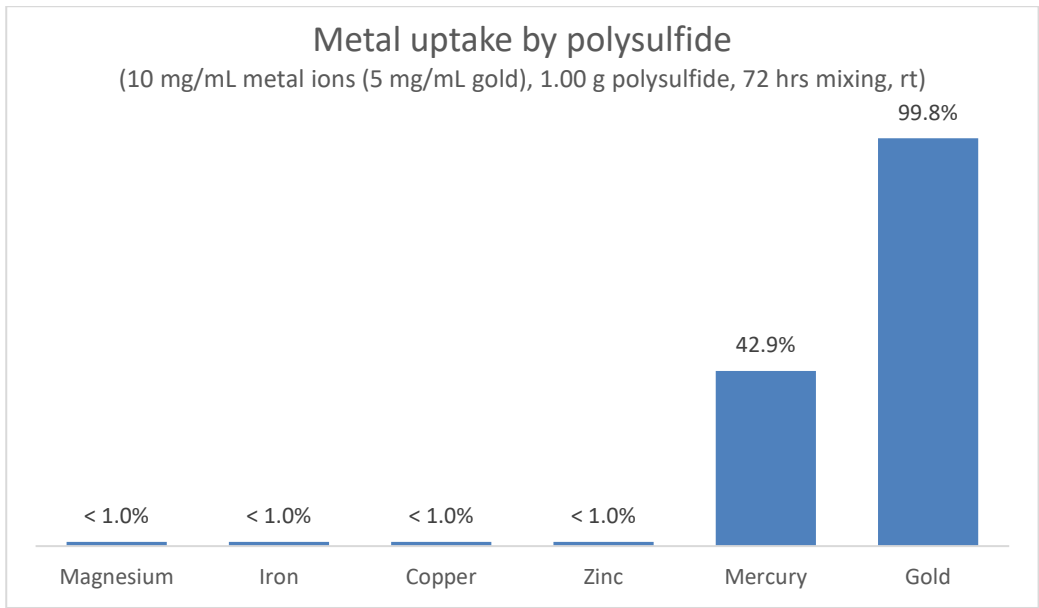


Figure 5.1.22 | Comparison of metal salt uptake by canola oil polysulfide

Internal standard recovery was within 5 % of 100 % for the majority of samples, straying outside of the ± 5 % window on only 4 of 41 occasions, though only to as low as 94.1 %. This level of indium recovery imparts strong confidence in the data obtained having little interference from carrier matrix or flow disturbances.

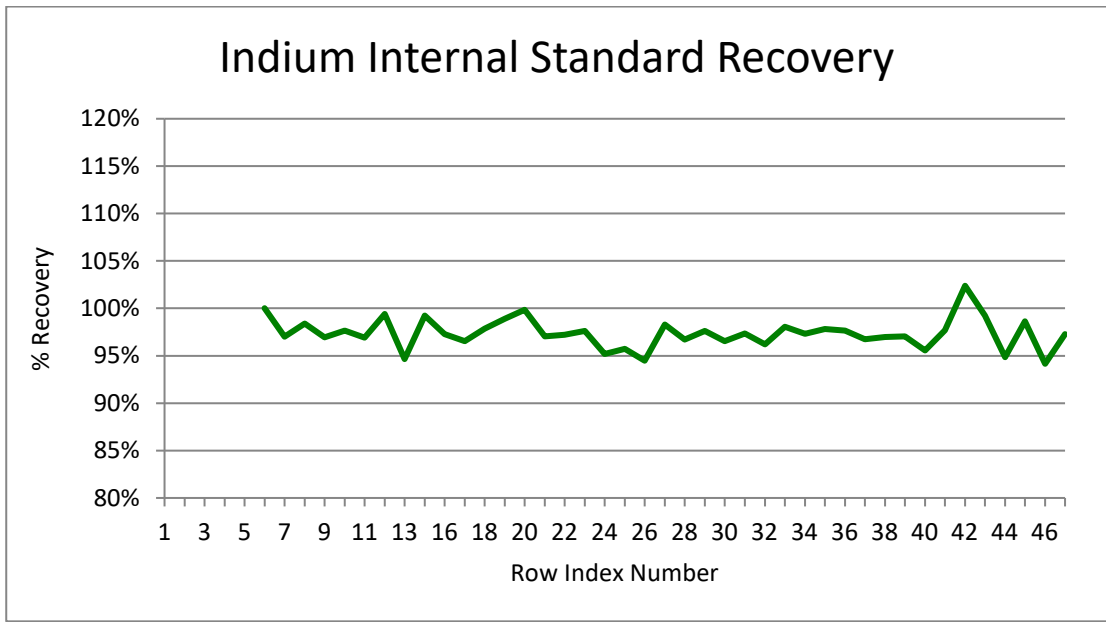


Figure 5.1.23 | Internal standard recovery is an indicator of measurement consistency across an ICP-MS experiment.

Binding DNA to metal treated polymers – varying polymer mass

Materials

Untreated polymer: Porous canola oil polysulfide, particles of 1.0–2.5 mm diameter

Au-treated polymer: 48.80 mg gold (from Au₂Cl₆) per g polymer

Hg-treated polymer: 42.59 mg mercury (from HgCl₂) per g polymer

Method

Polymers treated with gold chloride and mercury chloride were added to 2 mL centrifuge tubes at masses of 50, 30 and 10 mg. Untreated polymer was portioned out similarly as a control to a further 3 tubes to prepare a total of 9 samples. Plasmid DNA was prepared to 100 ng μL^{-1} in DNase and RNase free water and 200 μL added to each centrifuge tube. Each tube was vortexed for 30 seconds to ensure thorough wetting of the polymer and then centrifuged for a further 30 seconds and to ensure all was submerged (metal-treated polymers had adhered to the walls due to static during transfer). Samples were left at room temperature (26 °C) for 2 hours, and then left in the fridge at 4 °C overnight (17 hours).

Sample	Mass (mg)	Treatment	Metal (μg)	DNA (μg)	Metal/DNA (wt/wt)
Untreated 10	10.20	None	-	20	0
Untreated 30	30.31	None	-	20	0
Untreated 50	50.01	None	-	20	0
Au-treated 10	10.36	Au ₂ Cl ₆	505.6	20	25.3
Au-treated 30	30.53	Au ₂ Cl ₆	1,489.9	20	74.5
Au-treated 50	49.92	Au ₂ Cl ₆	2,436.1	20	121.8
Hg-treated 10	10.66	HgCl ₂	454.0	20	22.7
Hg-treated 30	30.36	HgCl ₂	1,293.0	20	64.65
Hg-treated 50	50.34	HgCl ₂	2,144.0	20	107.2

A gel solution was prepared from 500 mg agarose in 50 mL TAE buffer, microwaved for 5 lots of 30 seconds, checking and stirring each time to see if the solution had turned clear. Once clear, 5 μL RedSafe was added and the solution was cast into a mould to set. While being let to set, samples were prepared to run: 20 μL DNA solution, from each batch of DNA solution incubating with polymer, was transferred to a 1.5 mL centrifuge tube along with 4 μL 6x DNA binding solution. In doing so the DNA binding solution was diluted 6-fold to working concentration (1x). Once set the gel was mounted within [the instrument] and DNA solutions loaded into the wells as follows:

1	Untreated 10 mg	6	Au-treated 30 mg	11	Hg-treated 30 mg
2	Untreated 30 mg	7	Au-treated 50 mg	12	Hg-treated 50 mg
3	Untreated 50 mg	8	Ignore results, spillage from 7	13	Empty
4	Empty	9	Empty	14	DNA Ladder
5	Au-treated 10 mg	10	Hg-treated 10 mg	15	Empty

The gel was then run at 70 volts for approximately 50 minutes.

Results

DNA bands were visible in rows 1, 2, 3 and 5. None in the other rows. This may indicate that during the incubation with the polymer samples treated with heavy metals, the DNA had been pulled from solution to become bound to the solid polymer. The bands present in row 3 (50 mg untreated polymer) was slightly thinner/brighter than the lower masses of untreated polymer. This may indicate that at higher loadings, untreated polymer has some DNA-capturing capability. Similarly, the bands in lane 5 (10 mg Au-treated polymer) were thinner/brighter than the control, indicating that a portion of the DNA from solution had been bound but not all. In comparison to the Hg-treated polymers, the Au-treated requires a higher mass to achieve the same capture efficiency. That said the Au-treated has the advantage of being synthesised from a non-toxic metal, which carries environmental (and psychological) implications even if the Hg-treated polymer is not explicitly toxic to cells.

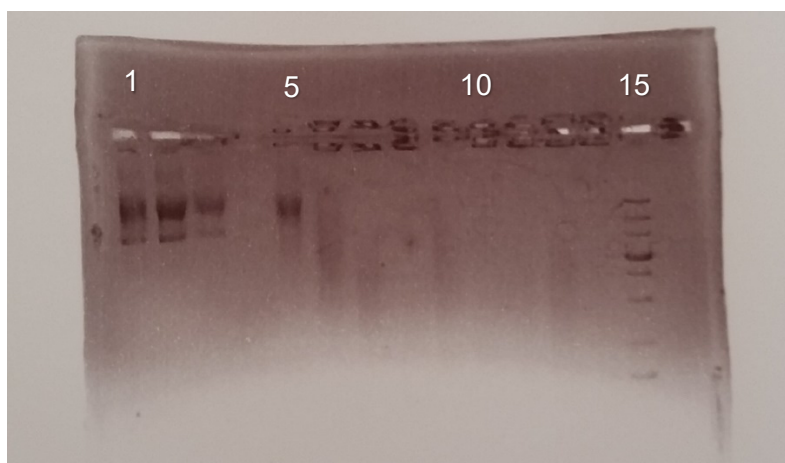


Figure 5.1.24 | Image of gel post-electrophoresis, samples as in table 2

Binding DNA to metal treated polymers – varying time

Materials

Untreated polymer: Porous canola oil polysulfide, particles of 1.0 - 2.5 mm diameter

Au-treated polymer: 48.80 mg gold (from Au₂Cl₆) per g polymer

Hg-treated polymer: 42.59 mg mercury (from HgCl₂) per g polymer

Method

50 mg polymers treated with gold chloride and mercury chloride were added to four 2 mL centrifuge tubes. Untreated polymer was portioned out similarly as a control to a further 4 tubes to prepare a total of 12 samples. DNA (type? – plasmid?) was prepared to 100 ng μL^{-1} in DNase and RNase free water and 200 μL added to each centrifuge tube. Each tube was vortexed for 30 seconds and then centrifuged for a further 30 seconds to ensure thorough mixing of the polymer and to ensure all was submerged (the metal-treated polymers exhibited movement and adherence to the walls due to static). Samples were left at room temperature (26 °C) for 0, 30, 60 and 180 minutes, one sample per polymer treatment, after which time 20 μL of the DNA solution was transferred to a new 1.5 mL centrifuge tube and left in the fridge at 4 °C. The 0-minute sample was centrifuged to submerge the polymer in the DNA solution and then 20 μL immediately removed.

Sample	Mass (mg)	Treatment	Metal (μg)	DNA mass (μg)	Metal/DNA (wt/wt)
Untreated 0	50.19	None	-	20	-
Untreated 30	50.62	None	-	20	-
Untreated 60	50.78	None	-	20	-
Untreated 180	50.75	None	-	20	-
Au-treated 10	50.68	Au ₂ Cl ₆	2473	20	124
Au-treated 30	50.78	Au ₂ Cl ₆	2478	20	124
Au-treated 60	49.86	Au ₂ Cl ₆	2433	20	122
Au-treated 180	50.02	Au ₂ Cl ₆	2441	20	122
Hg-treated 10	49.80	HgCl ₂	2121	20	106
Hg-treated 30	49.86	HgCl ₂	2124	20	106
Hg-treated 60	50.78	HgCl ₂	2163	20	108
Hg-treated 180	49.99	HgCl ₂	2129	20	106
No polymer	None	None	-	20	-
No DNA	49.90	-	-	0	-

A gel solution was prepared from 500 mg agarose in 50 mL TAE buffer, microwaved for 3 lots of 30 seconds, checking and stirring each time to see if the solution had turned clear. Once clear 5 μL

GelRed was added and the solution was cast into a mould to set. While being left to set, the samples were prepared to run: 20 μL DNA solution was transferred to a 1.5 mL centrifuge tube along with 4 μL 6x DNA binding solution. In doing so the DNA binding solution was diluted 6-fold to working concentration (1x). Once set the gel was mounted within [the instrument] and DNA solutions loaded (10 μL each) into the wells as follows:

1	Untreated 0 min	6	Au-treated 30 min	11	Hg-treated 60 min
2	Untreated 30 min	7	Au-treated 60 min	12	Hg-treated 180 min
3	Untreated 60 min	8	Au-treated 180 min	13	No DNA control
4	Untreated 180 min	9	Hg-treated 0 min	14	Stock DNA solution
5	Au-treated 0 min	10	Hg-treated 30 min	15	DNA ladder

The gel was then run at 70 volts for approximately 1 hour.

Results

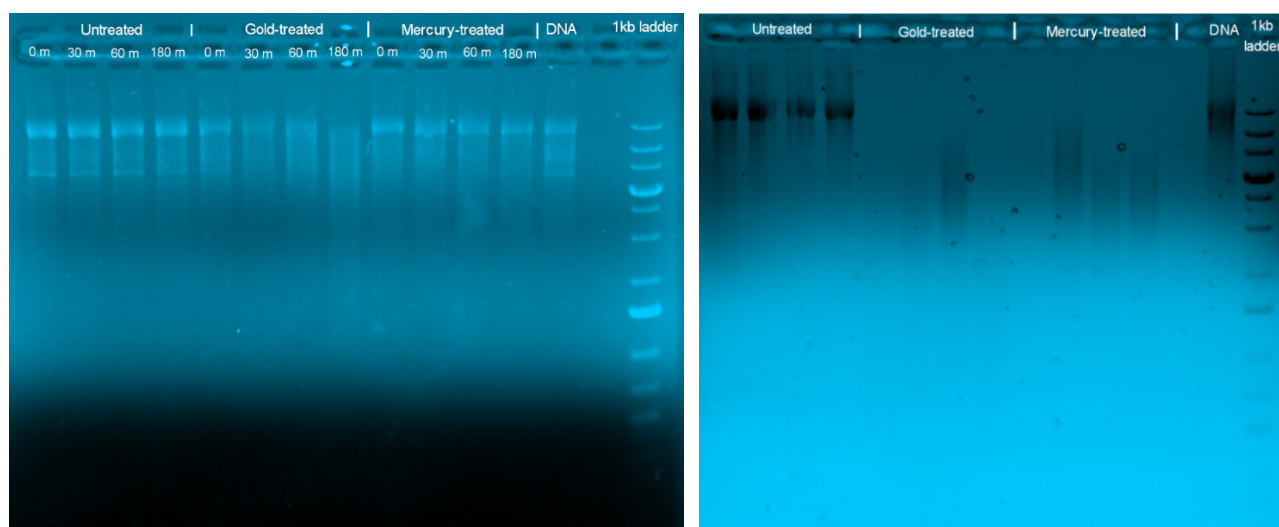


Figure 5.1.25 | Left: DNA uptake over up to 180 minutes. This short time frame does not seem sufficient for the mercury treated polymer to bind to DNA, however the amount of DNA present with the gold-treated polymer decreases steadily over time. The presence of degraded DNA also increases with time however. Right: DNA uptake over 6 days. No DNA remains of the same length as was initially added incubating with gold and mercury treated polymers. There is some evidence of degradation as stretched bands appear further down the lane.

Notes:

- 3 bands in plasmid DNA indicate: supercoiled, nicked and open, bp length is the same but molecule shape influences flow.
- Vertical gradient along the gel is due to flowthrough of dyes used to visualise the DNA (Redsafe in agarose preparation and 2 blue dyes present in the DNA loading dye). Unfortunately, the presence of a gradient impacts the baseline in ImageLab making it impossible to accurately quantify the DNA in each lane.

Binding DNA to metal treated polymers – polymers with low metal loading

Canola oil polysulfide had been previously incubated with salts of more metals than just mercury and gold, however their uptake had been so inefficient as to be difficult to quantify by ICP-MS. They were tested for DNA uptake regardless to see if even very small quantities of these metals had some effect.

Method

50 mg of each polymer (see table) was added to a 2 mL centrifuge tube along with 200 μ L of DNA in DNase/RNase free water (100 ng μ L⁻¹). Gold and mercury treated polymers were included for comparison, other polymers were included in duplicate. Samples were vortexed for 10 seconds to mix and then centrifuged 10 seconds to submerge the polymer in solution. After 24 hours solutions were analysed for presence of DNA by gel electrophoresis. Samples were tested again after 7 days.

Sample	Mass (mg)	Treatment	Metal (μ g)	DNA mass (μ g)
Iron treated	50.86	Fe(NO ₃) ₃	LOD	20
Iron treated	50.68	Fe(NO ₃) ₃	LOD	20
Zinc treated	49.23	Zn(NO ₃) ₂	LOD	20
Zinc treated	50.26	Zn(NO ₃) ₂	LOD	20
Calcium treated	49.15	Ca(NO ₃) ₂	LOD	20
Calcium treated	50.07	Ca(NO ₃) ₂	LOD	20
Copper treated	49.41	Cu(NO ₃) ₂	LOD	20
Copper treated	50.90	Cu(NO ₃) ₂	LOD	20
Magnesium treated	50.85	Mg(NO ₃) ₂	LOD	20
Magnesium treated	49.60	Mg(NO ₃) ₂	LOD	20
Gold treated	49.44	Au ₂ Cl ₆	2,413	20
Mercury treated	49.32	HgCl ₂	2,101	20
No polymer	None	None	None	20

Results

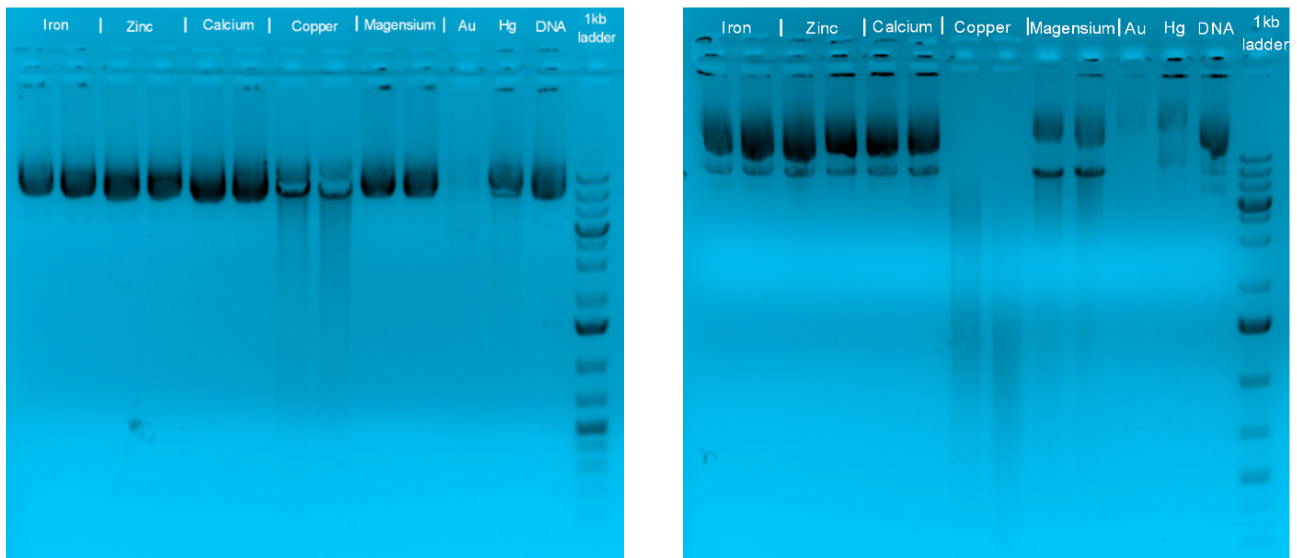


Figure 5.1.26 | Left: 24 hour incubation. For most metals, no difference to the control was observed, but the copper-treated polymer seemed to degrade the DNA. Right: 7 day incubation. DNA bands have shifted in all samples since the test 6 days prior. The copper polymer had either adhered or degraded DNA to the point there was none left at the initial band length and the magnesium treated polymer seemed to exhibit some loss of DNA over the longer period.

Release of DNA after binding – Release by pH control

Method

Polymers (mercury and gold treated) were incubated in DNA solutions for at least 24 hours to allow DNA to bind and then washed and dried to be used in varying treatments in an attempt to subsequently release the bound DNA.

Results

Low pH

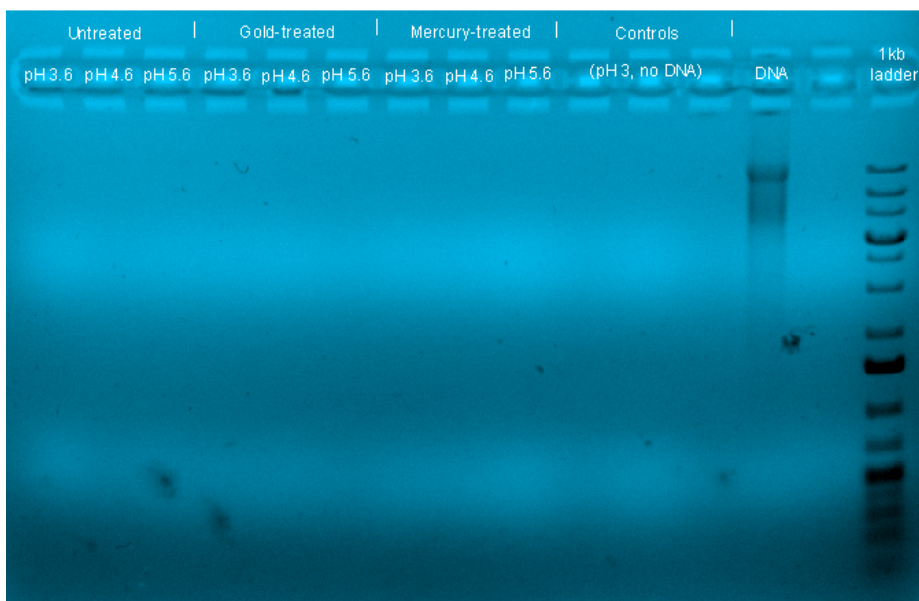


Figure 5.1.27 | Polymers from the previous uptake experiment were washed and incubated for 24 hours in aqueous acetate buffers at pH 3.6, 4.6 or 5.6. No release was observed.

High pH

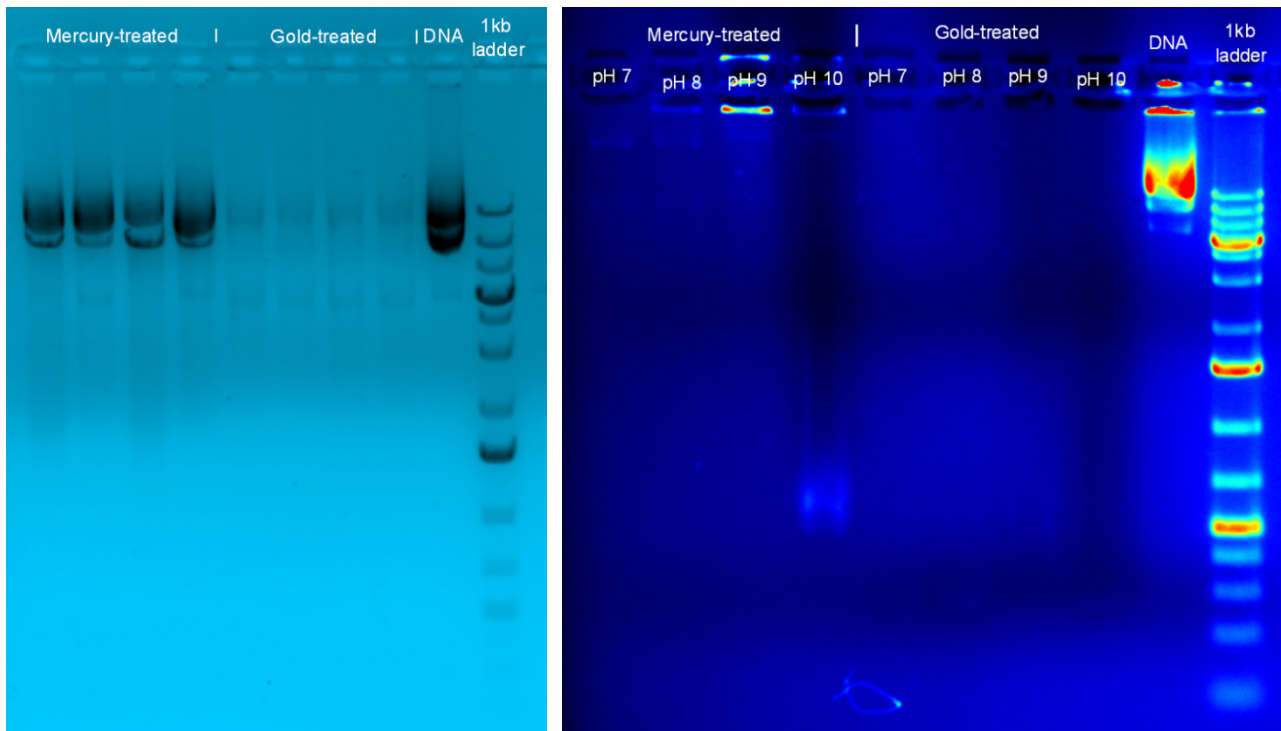


Figure 5.1.28 | Polymers were incubated in 200 μL of a 100 $\text{ng } \mu\text{L}^{-1}$ DNA solution for 48 hours (24 hour uptake test shown on left) and then washed and incubated in trizma (pH 7 and 8) or carbonate (pH 9 and 10) buffers for 24 hours. High pH buffer has interacted with the gel causing the artefacts seen in lanes 4, 7 and 8. There are very faint bands present in all Hg-treated samples corresponding to the same weight as the control DNA. This may be due to excess DNA that was not removed during the washing step but it is odd that the same does not appear in the gold-treated polymer's lanes. This may be evidence that DNA can be removed from the Hg-treated polymer as perhaps the bond is weaker, making uptake less efficient but allowing for easier release.

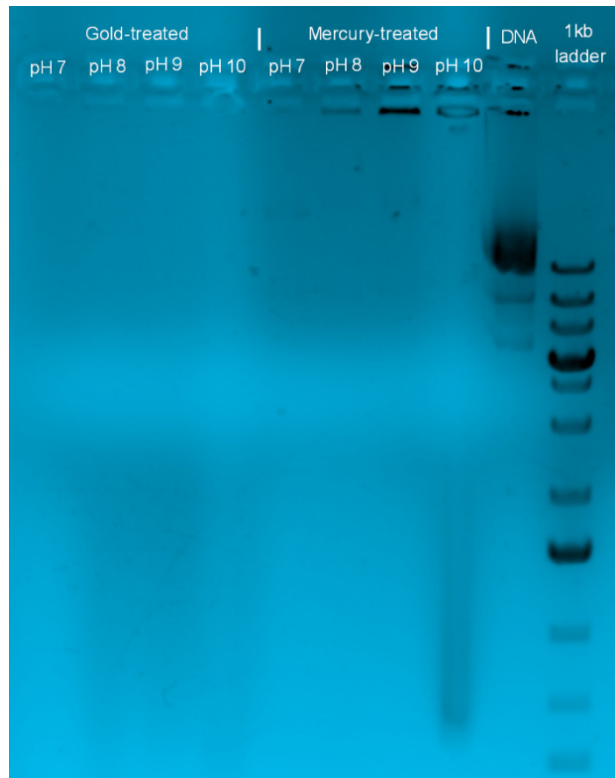


Figure 5.1.29 | The experiment shown in fig. 4 was continued for 7 days, no further release of DNA was observed over this time.

Thiols

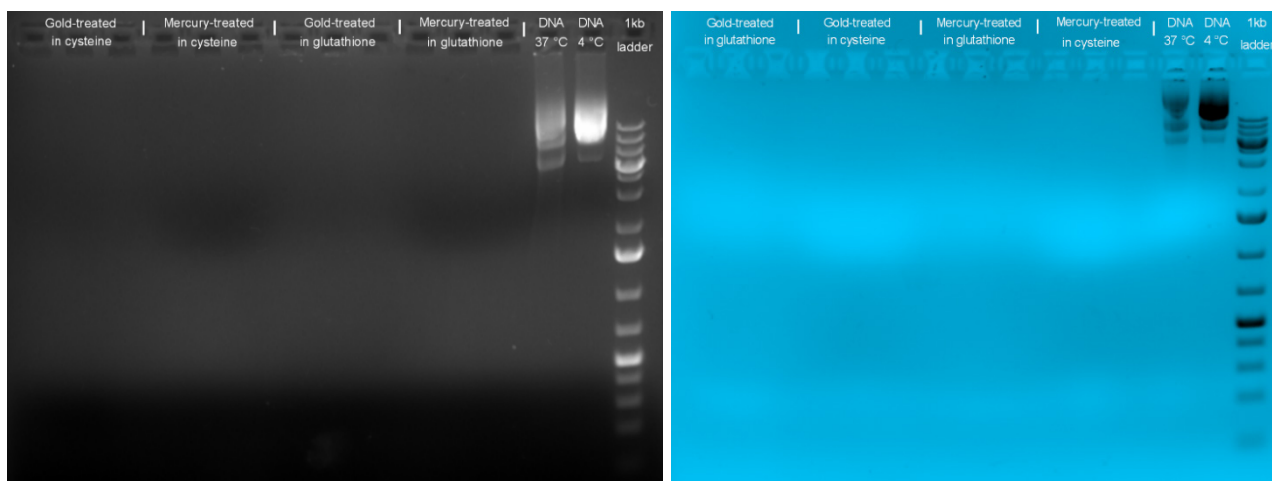
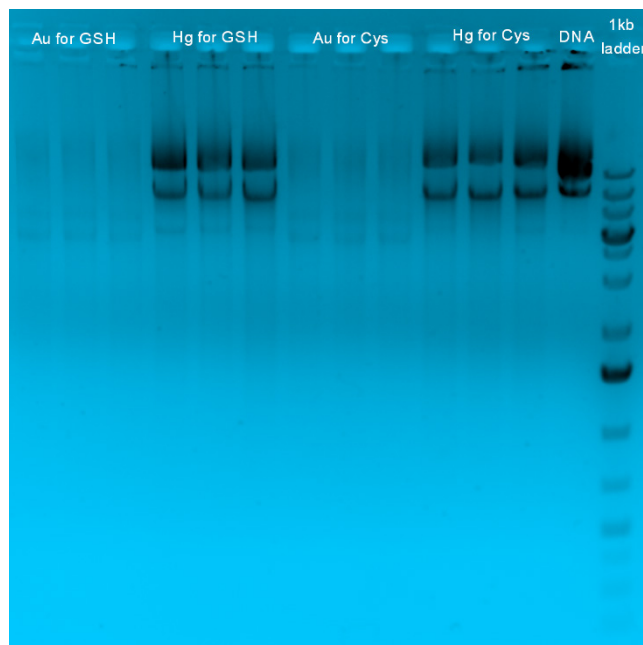


Figure 5.1.30 | Gold and mercury-treated polymers were incubated in 200 μL of a 100 $\text{ng } \mu\text{L}^{-1}$ DNA solution for 24 hours (top) and then washed and added to solutions of either glutathione (92 mg mL^{-1}) or cysteine (36 mg mL^{-1}) prepared at 5 molar equivalents of the metal atoms present on the polymer surface. Samples were held at 37 $^{\circ}\text{C}$ for 3 hours and then tested for release. Both untreated DNA kept at 37 $^{\circ}\text{C}$ for the 3-hour incubation and 4 $^{\circ}\text{C}$ are shown as controls to determine the effects of temperature. Left: After 3 hours, right: after 7 days at 4 $^{\circ}\text{C}$. No release was observed in either case.

DNA Delivery Summary

Gold and mercury-treated polymers both remove DNA from solution whereas the polymer alone does not appear to be as effective. Likely the DNA is adhering to the polymer in most part due to the presence of the metal. The polymer is hydrophobic, and the metal provides a counter charge for the positive phosphor backbone of DNA, offering two potential modes of interaction with the polymer and DNA. Uptake is fast by the gold treated polymer (200 μL , 100 $\text{ng } \mu\text{L}^{-1}$, 3 hours with 50 mg polymer), slow in the mercury (between 1 and 6 days under same conditions). There is evidence to suggest degradation of DNA during the binding incubation.

Once bound, DNA is difficult to remove from the polymer. 100 mM buffers of several types were prepared at pH 4, 5, 6, 7, 8, 9 and 10, and polymer with DNA bound incubated for 24 hours in each. Alkaline pH also has the potential to degrade the polymer, however no release was seen. Release was also tested in the presence of thiols. Aqueous solutions of cysteine and glutathione were prepared at approximately 5 molar equivalents of metal atoms present on the polymers. DNA-bound polymer (Au and Hg-treated) was incubated in both solutions, no release was observed.

Cell Viability

Method

HepG2 and SKBR3 cells were cultured for several passages before seeding 500 μL at 60 cells μL^{-1} into the wells of 24-well transwell plates, 1 plate for each cell line. Polymers were measured out into 1.5 mL centrifuge tubes and then transferred into well-inserts under a sterile environment. 24 hours after transferring cells to plates, polymers loaded in well-inserts were submerged in wells and left for 24 hours. To measure the effect the presence the polymers had on cell viability, the well-inserts were removed, and cell medium exchanged for fresh medium containing a 1/20 dilution of stock cell titre blue. After 90 minutes, cell viability was measured using a TECAN Infinite M200 microplate reader. After measuring, cell titre blue was trashed, the wells were washed with 200 PBS μL and then 500 μL fresh DMEM medium added back in. The previous well-plates containing polymer were also added back into each well. This measurement process was repeated after a further 24 hours to determine cell viability after 48 hours of exposure.

Results

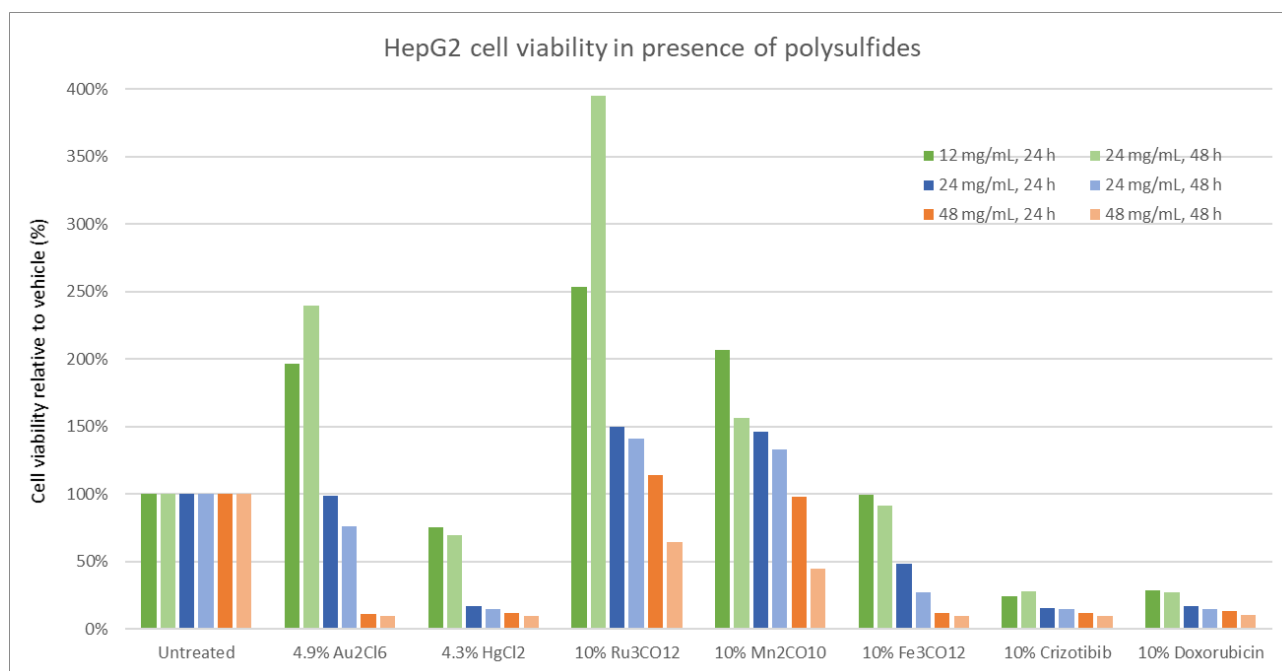


Figure 5.1.31 | HepG2 Cell viability relative to the corresponding concentration of untreated polysulfide

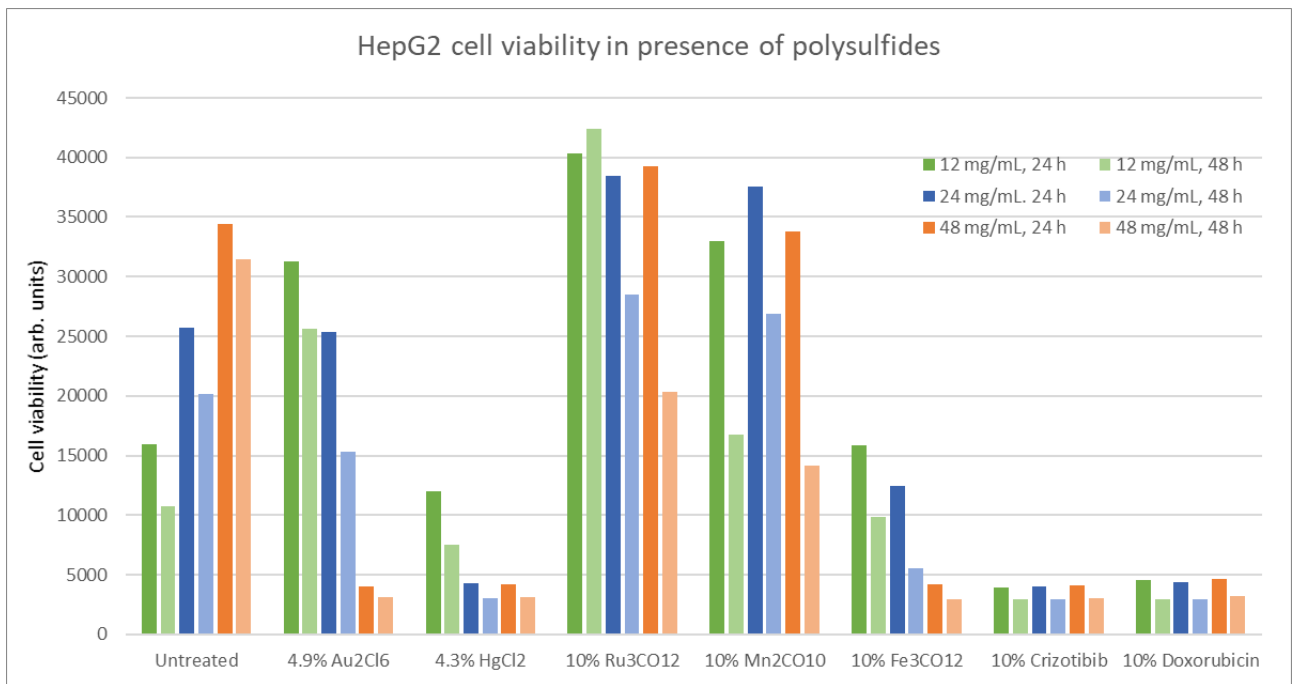


Figure 5.1.32 | HepG2 absolute cell viability

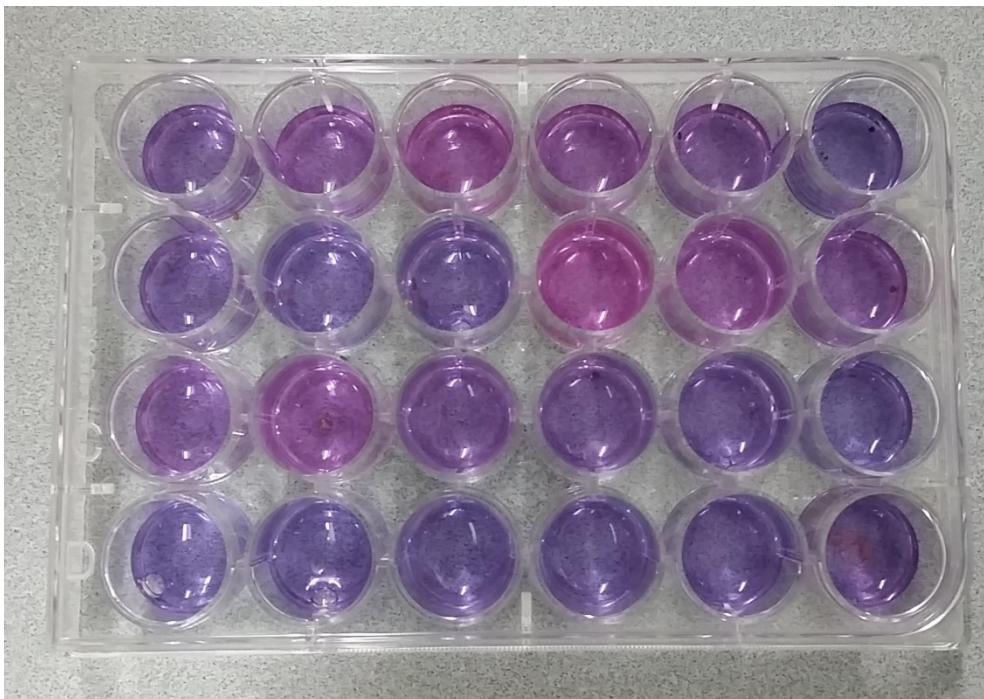


Figure 5.1.33 | HepG2 plate after 48 hours. Intensity of red colouration in cell titre blue solution corresponds to cell viability: Viability is highest with low concentrations of Ru₃CO₁₂ and Mn₂CO₁₀, higher even than with all concentrations of untreated polymer.

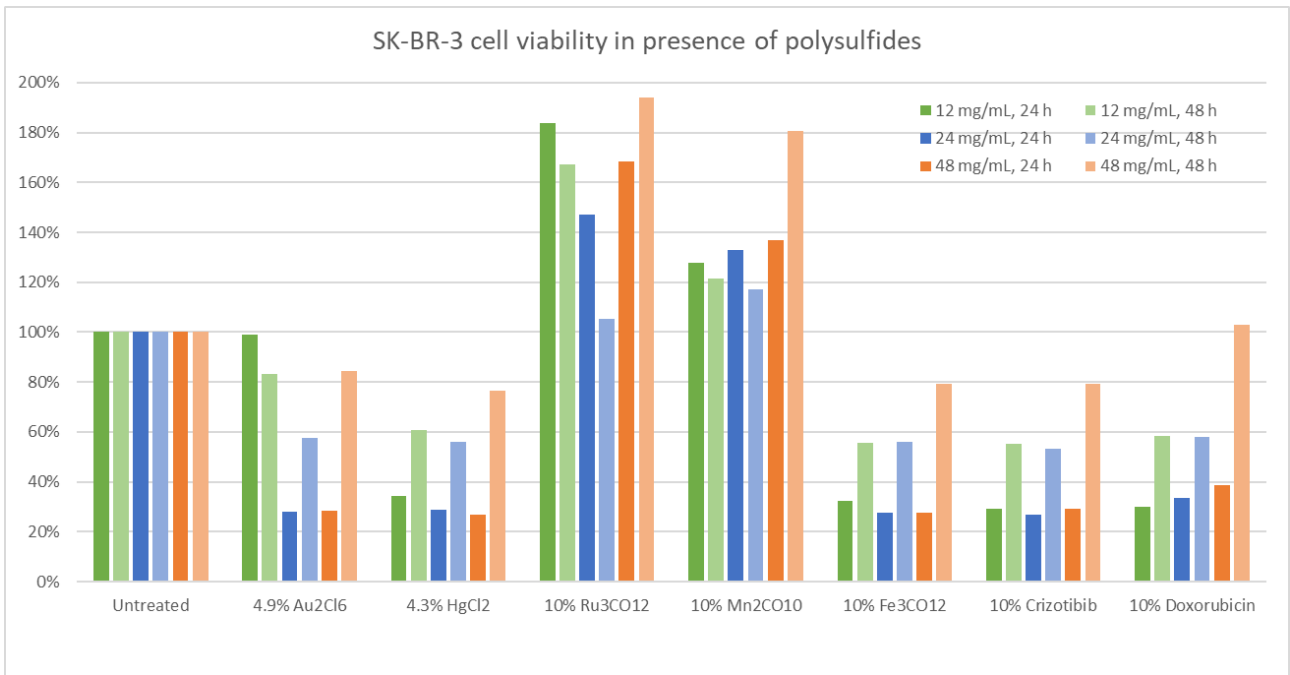


Figure 5.1.34 | SKBR3 cell viability relative to the corresponding concentration of untreated polysulfide

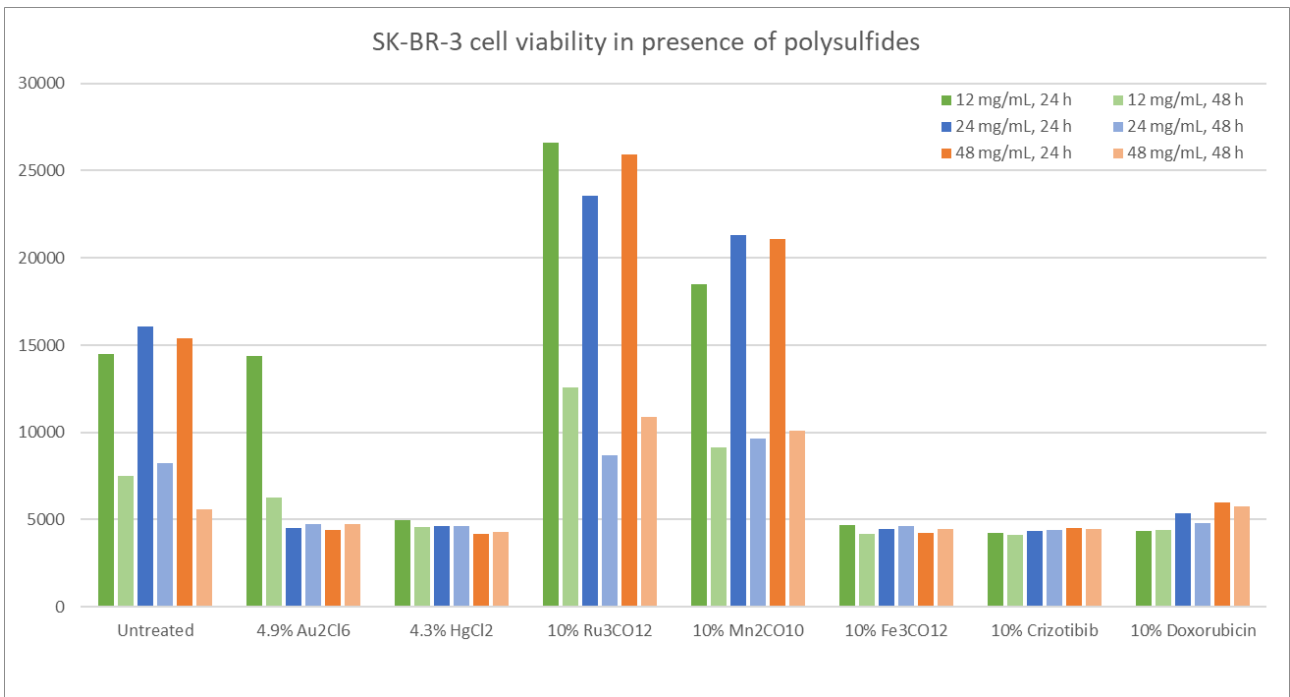


Figure 5.1.35 | SKBR 3 absolute cell viability



Figure 5.1.36 | SKBR3 plate after 48 hours. Intensity of red colouration in cell titre blue solution corresponds to cell viability: Viability was low in all cases.

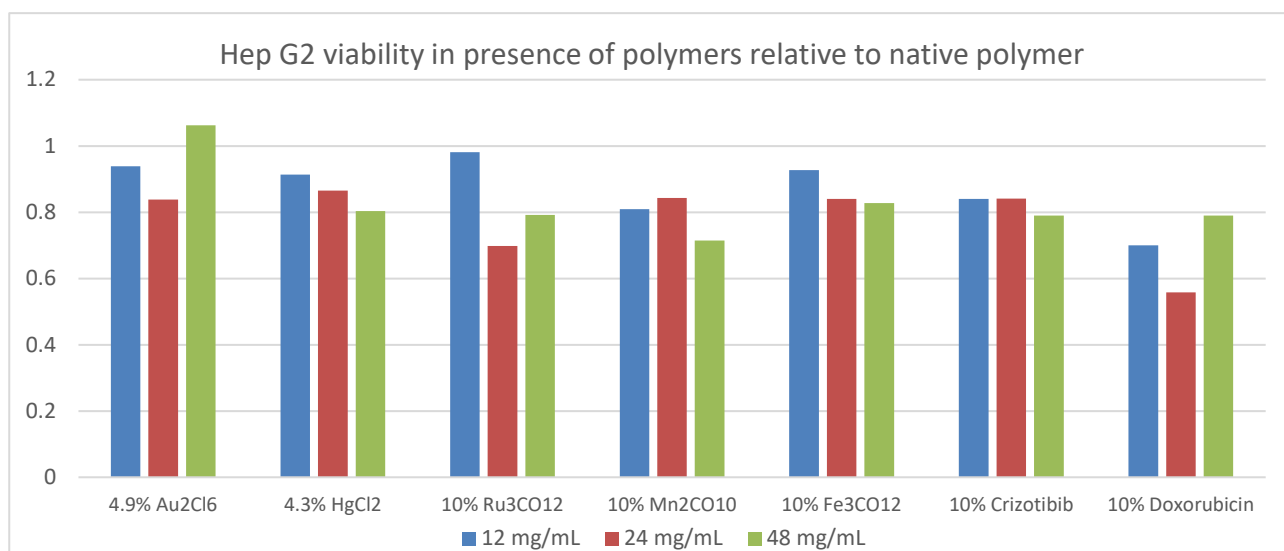
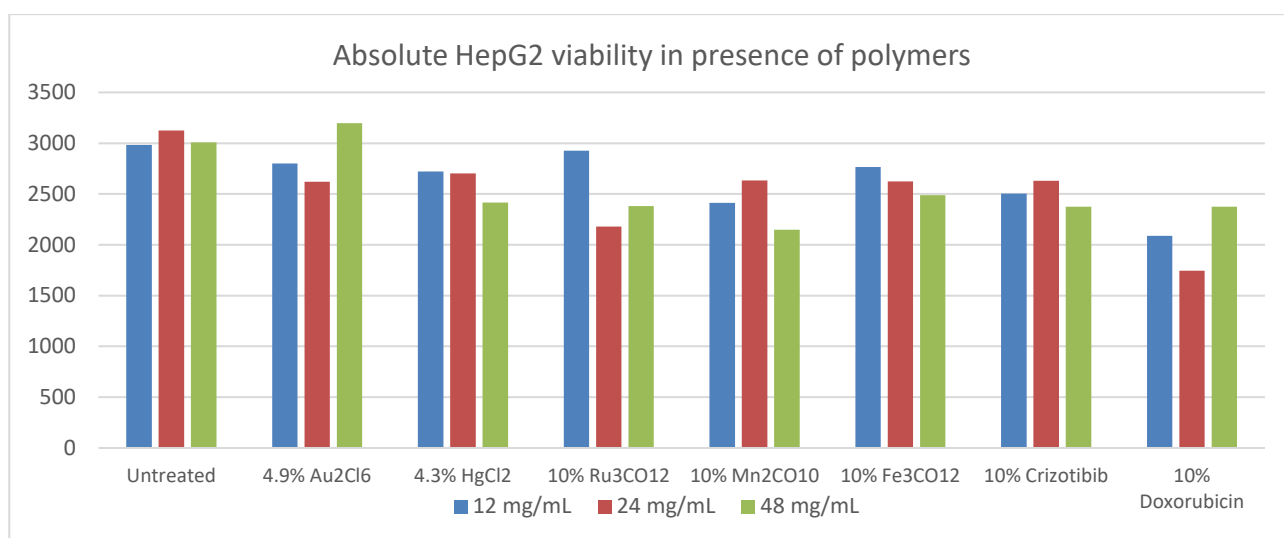
Second Replicate

Initial cell lines died and there was not enough time to thaw and grow SKBR3 to experiment. Annabel offered HepG2 cells to at least run a duplicate of that line.

Method

HepG2 cells were dispersed as acquired into 15 mL fresh DMEM culture medium and diluted 10-fold to count. After determining concentration, the culture was diluted to afford 30,000 cells per well. The polymer incubation experiment detailed above was repeated with these new cells.

Results



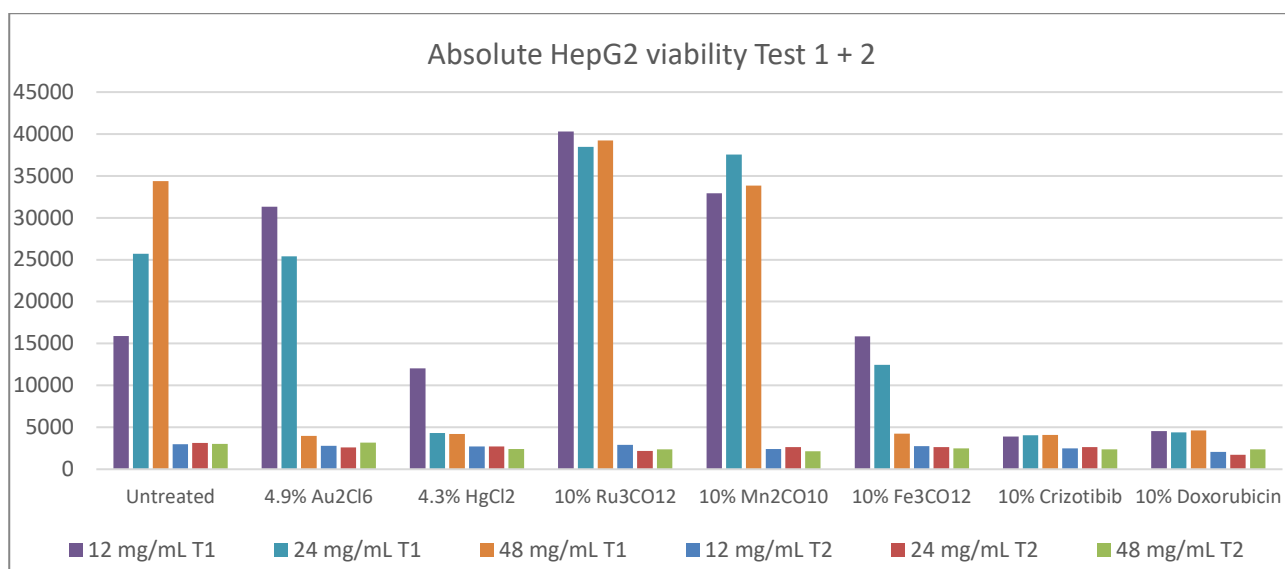


Figure 5.1.37 | Cells are dead, or otherwise not present. All wells are the same blue-purple colour at time of testing. Under the microscope there are very few cells visible, no more than 20 circular cells in each well. Some wells contain different shaped bacteria, two rod cells were visible in one. Cells in the flask appear larger than the few circular cells in the wells. Cells are present at about 30 % coating of the flask base in the source container so where the issue has arisen is not clear. Perhaps the cells had not seeded and were washed away with the medium exchange for cell titre blue or were they simply not present from the start and the issue lies in the handling and dilution beforehand. Either way there was neither the time nor supplies available to repeat the experiment.

Cell Viability Summary

HepG2 (hepatoma) and SKBR3 (breast cancer) cell lines were grown over the month and transferred to 24-well Transwell plates. After leaving 24 hours to settle, Transwell inserts containing polysulfides of various treatments were added at different concentrations: Gold chloride, mercury chloride, triruthenium dodecacarbonyl, dimanganese decacarbonyl, triiron dodecacarbonyl, crizotinib and doxorubicin-treated, as well as an untreated control, each at 6, 12 and 24 mg in 500 μ L medium. Polymers were incubated with cells for 24 hours, culture media (DMEM) exchanged for a solution of cell titre blue in DMEM to measure viability, then exchanged back to medium to repeat the reading after 48 hours.

For HepG2 cells, after 24 hours, increased concentration of polysulfide resulted in increased cell viability whereas increasing concentrations of the Au_2Cl_6 , HgCl_2 and $\text{Fe}_3\text{CO}_{12}$ treated polysulfides decreased cell viability. All concentrations of $\text{Ru}_3\text{CO}_{12}$ and $\text{Mn}_2\text{CO}_{10}$ seemed to increase cell count, though not in the same fashion as the untreated polysulfide. This is an interesting result if during the incubation no CO was released, as it would mean the material itself is non-toxic until activated and CO is released (presumably). The third metal carbonyl, $\text{Fe}_3\text{CO}_{12}$, did not show the same trend. All concentrations of crizotinib and doxorubicin killed cells, which is not unexpected but in the case of doxorubicin, the medium had been stained a deep red and a red precipitate had formed in the wells. This likely indicates very fast leaching of the drug from the polymer into solution and so may render the material inviable for slow release. Solids were not visible in the crizotinib wells, though it could be that crizotinib dissolves better in DMEM culture medium. When plotted relative to the increase in viability afforded by the untreated polysulfide, it appears that all treatments resulted in increased cell death as concentration increased (fig. 5.1.31). I do not believe this provides a completely accurate picture however, due to interference of the polysulfide itself, so I have provided both plots of the absolute amounts (fig. 5.1.32) and the amounts "relative to the vehicle" (fig. 5.1.31) as is considered standard for reporting to demonstrate the difference.

In the case of SKBR3 cells, 12 mg mL^{-1} Au_2Cl_6 resulted in some loss of viability, but 24 mg mL^{-1} onwards and all concentrations of HgCl_2 resulted in a much starker loss. $\text{Ru}_3\text{CO}_{12}$ and $\text{Mn}_2\text{CO}_{10}$ again seemed to increase cell viability, where $\text{Fe}_3\text{CO}_{12}$ did the opposite. Crizotinib and Doxorubicin both killed cancer cells down to near the same level as in the HepG2 experiment.

At 48 hours, cell viability followed the same trend in HepG2 cells, with decreased cell count in all cases. SKRBR3 cells suffered over the second day, with all cases of high viability dropping to about half, and cases where cell count was already low dropping only marginally.

A second replicate was attempted. With only one transwell plate remaining it was not possible to do both cell lines, so only HepG2 was tested. An issue with cell seeding was identified late into the experiment and neither the time nor supplies were available to repeat the experiment.

CO Release

Instrument details

TECAN Infinite M200 Microplate reader, CORING 24 well plate with transwell inserts

Method

10 mg MC-Polysulfides, prepared by co-precipitation of canola oil polysulfide and metal carbonyls from pyridine, were portioned into plate inserts and added to wells containing 500 μL PBS buffer (biology standard, 1x concentration). After 20 minutes wetting, in the absence of light, plate inserts were removed and absorbance from 490 to 610 nm read in each well on a TECAN Infinite M200 Microplate reader (to define a $t=0$ zero reading for each well). COP-1 was prepared to 2 μM in PBS from a frozen ($-80\text{ }^\circ\text{C}$) stock of 50 mM in DMSO. 500 μL COP-1 solution was added to each well to afford a 1 μM concentration, and well inserts were replaced. At 5, 10, 15, 30, 60, 90, 120 and 180 minutes, the reading was repeated to determine if CO had been released and subsequently reacted with COP-1 in solution to form a fluorescent product. Between readings the plate was left under a 10 W 1000 lumen LED (lights in the plate reader room) as $\text{Mn}_2\text{CO}_{10}$ specifically is known to release CO photolytically under cold light.

A1	Untreated polymer	A5	$\text{Ru}_3\text{CO}_{12}$ treated polymer (10%)	B3	$\text{Mn}_2\text{CO}_{10}$ treated polymer (50%)
A2	Untreated polymer	A6	$\text{Ru}_3\text{CO}_{12}$ treated polymer (10%)	B4	$\text{Ru}_3\text{CO}_{12}$ treated polymer (50%)
A3	$\text{Mn}_2\text{CO}_{10}$ treated polymer (10%)	B1	$\text{Fe}_3\text{CO}_{12}$ treated polymer (10%)	B5	$\text{Fe}_3\text{CO}_{12}$ treated polymer (50%)
A4	$\text{Mn}_2\text{CO}_{10}$ treated polymer (10%)	B2	$\text{Fe}_3\text{CO}_{12}$ treated polymer (10%)	B6	Blank

Table 1: Contents of well inserts

After testing the plate was sealed and left by the window in the lab for 48 hours (approximately 20 hours sunshine – sunrise to sunset over 2 days).

Results

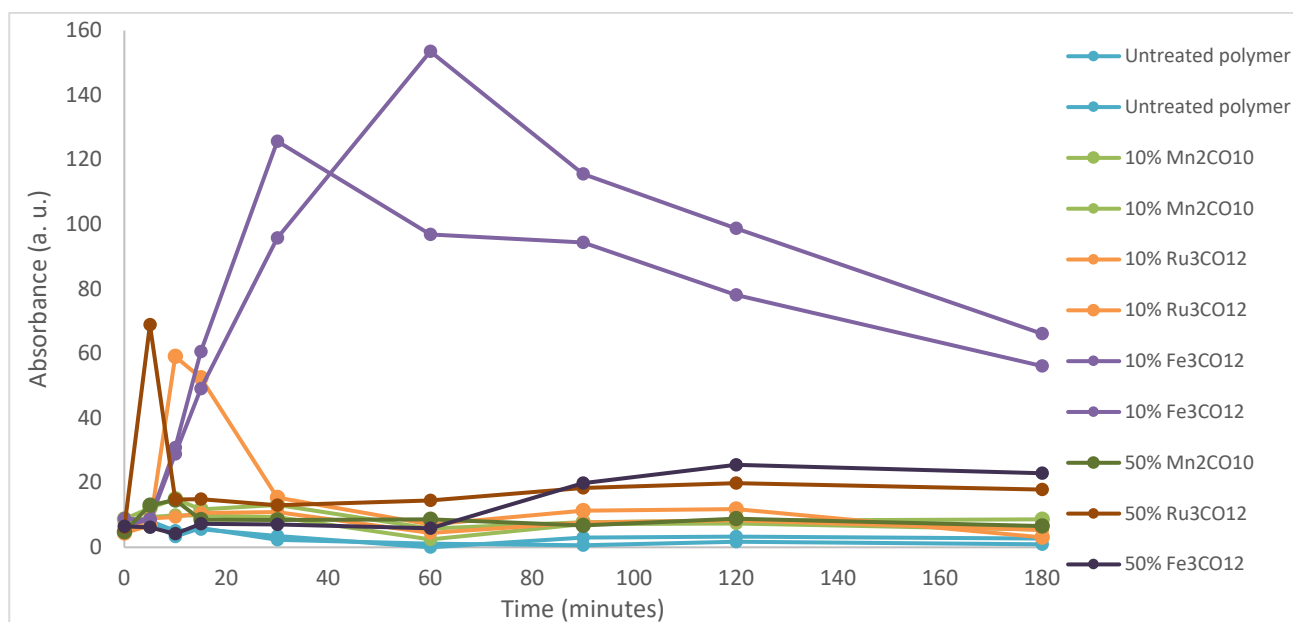


Figure 5.1.38 | Average absorbance from 510–610 nm (11 data points) up to 180 minutes after incubation of metal carbonyl-treated polymers in COP-1. Higher absorbance is attributed to higher concentration of the reaction product of carbon monoxide and COP-1, indicating CO release. Absorbance over time of a COP-1-only control was used to define the baseline. Polymers at 10 % metal carbonyl loading and an untreated control were run in duplicate, polymers at 50 % loading were run only once due to limited available plate wells.

Fe₃CO₁₂ treated polymers with a 10 % metal carbonyl loading give the clearest indication of CO release, peaking at 30 minutes in one replicate and 60 in the other, then trailing off gradually for the remainder of the experiment. Oddly no change in absorbance was witnessed in the sample at higher MC loading. One of the two 10 % Ru₃CO₁₂ replicates showed a brief increase in absorbance at 10 and 15 minutes, quickly diminishing back to the baseline level afterwards, similarly the 50 % Ru₃CO₁₂ sample increased to a similar height in the first 5 minutes, but quickly dropped back down before 10 minutes had passed.

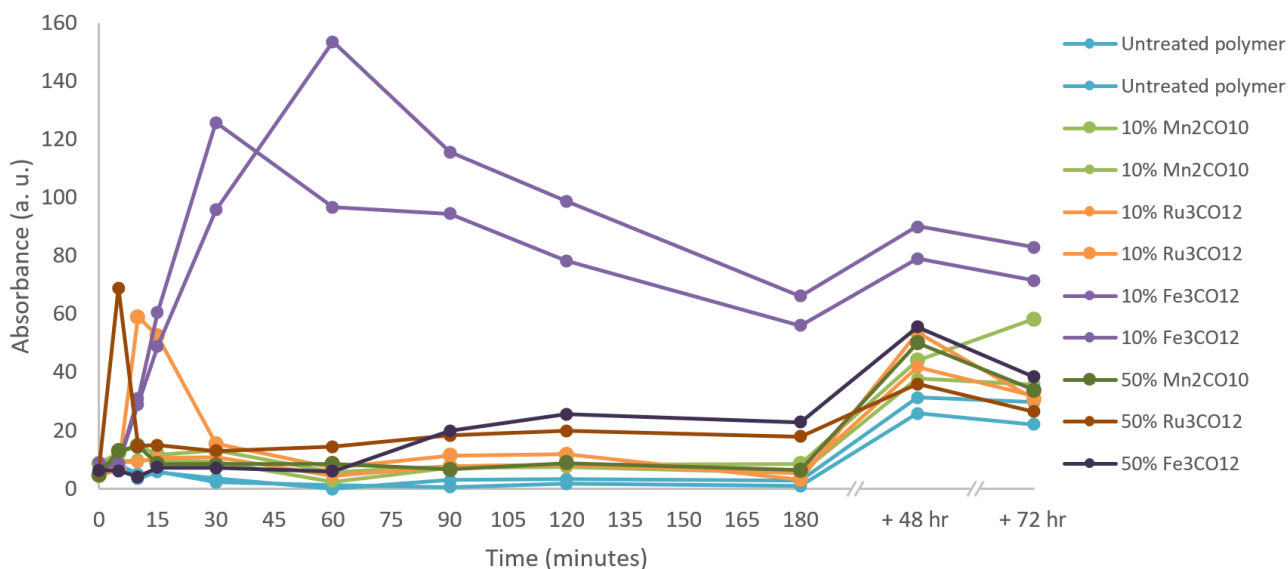


Figure 5.1.39 | The experiment was continued for 72 hours, with measurements taken at 48 and 72 hours. Changes in the signal were consistent in all samples. No further release was measured.

No COP-1 Control

Method: Weighed out 10 mg of each polymer as in previous experiment, wet in 500 mL PBS 15 minutes, took t_0 , then added a further 500 mL PBS (no COP-1) and measured absorbance over the same time.

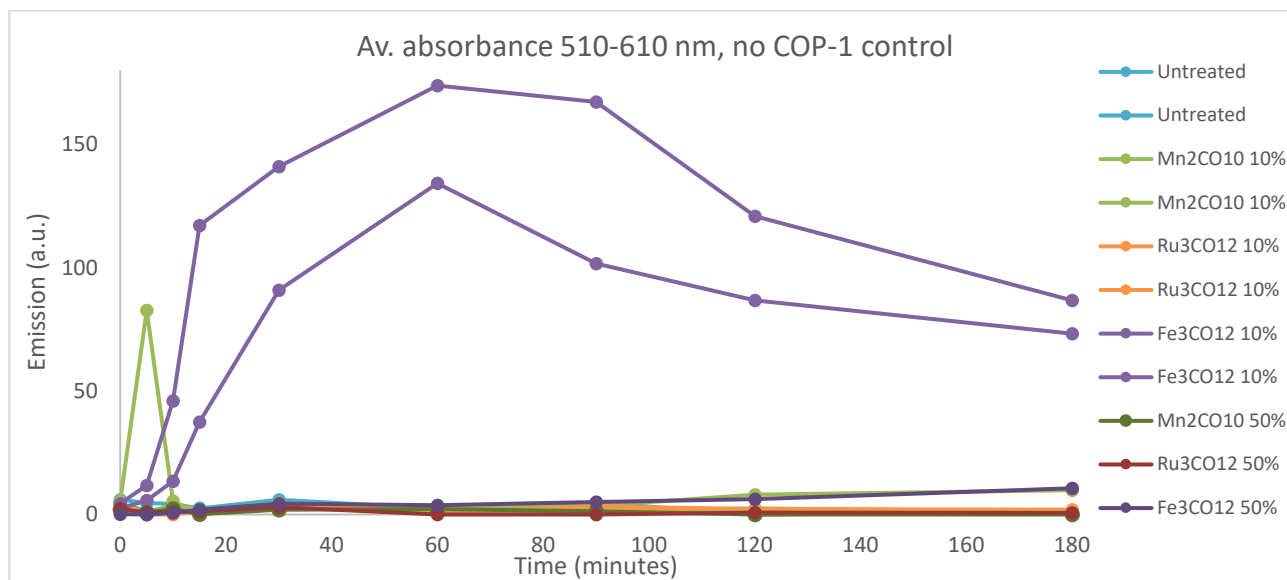


Figure 5.1.40 | $\text{Fe}_3\text{CO}_{12}$ absorbance is still present with lack of COP-1 and so cannot correlate with presence of a COP-1/CO reaction product.

In dark and without pre-soaking control

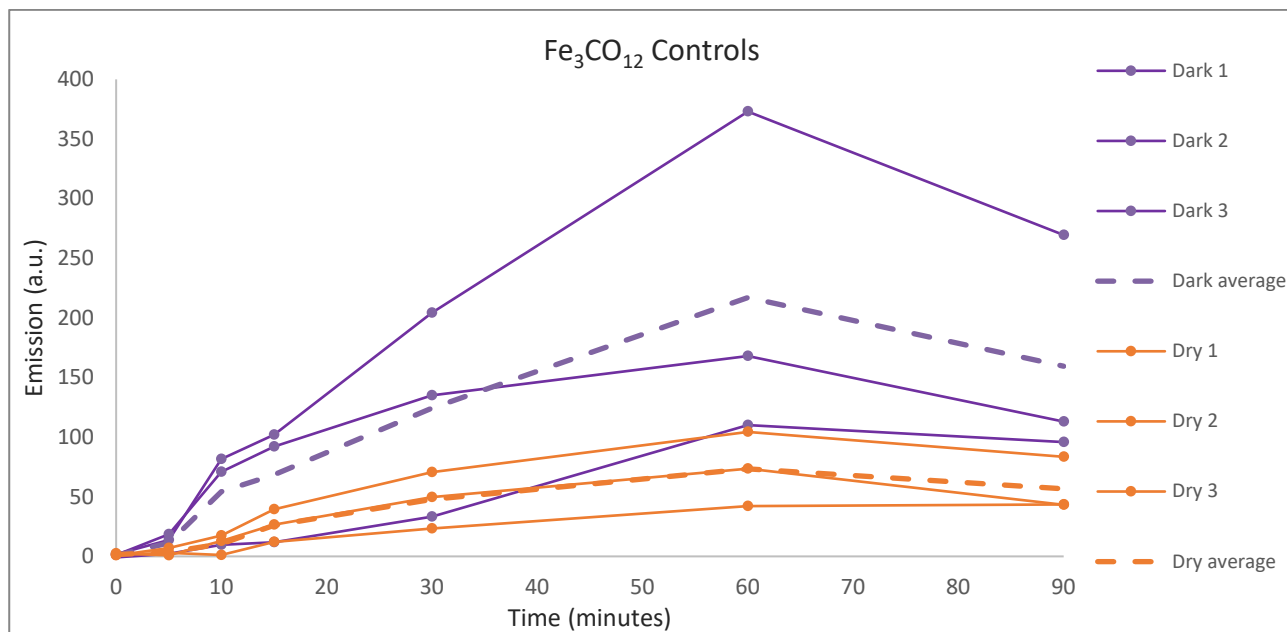


Figure 5.1.41 | Control experiments to investigate emission from Fe₃CO₁₂ incubation (note different scales on both axes to previous tests).

Emission is not affected by lack of light and shows the same profile as in light apart from a single experiment that reached double the emission units. Wetting of the polymer beforehand did influence release of the coloured agent, delaying the initial spike and resulting in lower emission overall.

CO Release Summary

No release observed into PBS for Fe₃CO₁₂, Ru₃CO₁₂ or Mn₂CO₁₀ treated polymers over 24 hours at 10 % and 50 % metal carbonyl (MC) loading. No difference was observed in light or dark conditions. COP-1 was used to visualise release. COP-1 and CO react to form a fluorescent product that can be monitored from 490–610 nm². Some visual response was seen in the Fe₃CO₁₂ but was due leaking of a coloured compound (the MC) into solution as a control without COP-1 gave the same result.

References

1. Bhatt, V. Chapter 8 - Metal Carbonyls. *Essentials of Coordination Chemistry*, *Academic Press*. **2016**, 191-236.
2. Michel, B. W.; Lippert, A. R.; Chang, C. J., A Reaction-Based Fluorescent Probe for Selective Imaging of Carbon Monoxide in Living Cells Using a Palladium-Mediated Carbonylation. *J. Am. Chem. Soc.* **2012**, *134* (38), 15668-15671.